

Vol. 45 - N. 2 SUPPLEMENT

# **Bollettino di Geofisica** teorica ed applicata

*An International Journal of Earth Sciences*

Guest Editors: J. Carcione, F. Donda, E. Lodolo

## **International Symposium on the Geology and Geophysics of the Southernmost Andes, the Scotia Arc and the Antarctic Peninsula**

Extended Abstracts of the  
GeoSur2004 International Symposium

22-23 November, 2004  
Buenos Aires, Argentina



Istituto Nazionale di Oceanografia  
e di Geofisica Sperimentale

ISSN 0006-6729

*Responsibility for all statements made in B.G.T.A. lies with the authors*

Cover design and typesetting: Nino Bon – OGS  
Printing: Centro Box SRL – Buenos Aires, Argentina  
Authorized by the Tribunale di Trieste, n. 242, September 17, 1960

INTERNATIONAL SYMPOSIUM



**International Symposium on the  
Geology and Geophysics of the  
Southernmost Andes, the Scotia Arc  
and the Antarctic Peninsula**

**22-23 November 2004**

**Buenos Aires, Argentina**

**EXTENDED ABSTRACTS**

**ORGANIZERS**

---

ISTITUTO NAZIONALE DI OCEANOGRAFIA E DI GEOFISICA  
SPERIMENTALE - OGS, TRIESTE, ITALY

INSTITUTO DE GEOFÍSICA “DANIEL A. VALENCIO”,  
DEPARTAMENTO DE GEOLOGÍA,  
UNIVERSIDAD DE BUENOS AIRES, ARGENTINA

**SPONSORS**

---

ITALIAN EMBASSY IN ARGENTINA

PROGRAMMA NAZIONALE DI RICERCHE IN ANTARTIDE (P.N.R.A.)

EAGE-SEG Italian Section

---

**SCIENTIFIC COMMITTEE**

---

G. BRANCOLINI - OGS, Trieste  
A. CAMERLENGHI - OGS, Trieste  
M. CANALS - University of Barcelona  
J.M. CARCIONE - OGS, Trieste  
A.H. COMÍNGUEZ - CONICET, University of La Plata  
I.W.D. DALZIEL - University of Texas at Austin  
E. DOMACK - Hamilton College, New York  
F. HERVÉ - University of Santiago  
R. LARTER - British Antarctic Survey  
S. MARENSSI - IAA, Buenos Aires  
G. PANZA - University of Trieste  
C. PARICA - CONICET, University of Buenos Aires  
V. RAMOS - University of Buenos Aires  
A. RAPALINI - INGEODAV, University of Buenos Aires  
G. RÉ - INGEODAV, University of Buenos Aires  
C. RODA - University of Udine  
M. RUSSI - OGS, Trieste  
D. VELIS - University of La Plata

---

**ORGANIZING COMMITTEE**

---

J.L. HORMAECHEA - EARG, Rio Grande  
H. LIPPAI - INGEODAV, University of Buenos Aires  
E. LODOLO - OGS, Trieste  
M. MENICHETTI - University of Urbino  
S. PERSOGLIA - OGS, Trieste  
J. RABASSA - CADIC, Ushuaia  
R. SEMENZATO - Italian Embassy, Buenos Aires  
A. TASSONE - INGEODAV, University of Buenos Aires  
J.F. VILAS - INGEODAV, University of Buenos Aires

---

**CONFERENCE SECRETARIAT**

---

ANGELA MARCHETTO - EAGE-SEG Italian Section



# CONTENTS

---

## **Session 1 - Regional Geology**

LATE JURASSIC BIRTH OF THE ROCAS VERDES BASIN AT THE SARMIENTO OPHIOLITIC COMPLEX: EVIDENCE FROM ZIRCON U-PB SHRIMP GEOCHRONOLOGY .....	1-01
<i>M. Calderón, F. Hervé, C.M. Fanning</i>	
THE ITALIAN CONTRIBUTION TO THE DEVELOPMENT OF THE GEOLOGIC KNOWLEDGE OF ARGENTINA .....	1-02
<i>H.H. Camacho</i>	
DEEP-SEISMIC IMAGING ACROSS LOS CHIHUIDOS ARCH, NEUQUEN BASIN, ARGENTINA (38° SL) .....	1-03
<i>A.H. Comínguez, J.R. Franzese</i>	
REFLECTIONS ON THE SCOTIA ARC AT ITS CENTENNIAL .....	1-04
<i>I.W.D. Dalziel</i>	
AEROGEOPHYSICAL IMAGING REVEALS A COMPOSITE TERRANE OVER PALMER LAND (ANTARCTIC PENINSULA) .....	1-05
<i>F. Ferraccioli, P. Jones, A.P.M. Vaughan, A. Dean, P.T. Leat</i>	
THE CARIBBEAN PLATE CURRENT PROBLEMS: AN EXAMPLE FOR EVOLUTION OF SMALL PLATES .....	1-06
<i>G. Giunta</i>	
THE WEST-DIRECTED SUBDUCTION ZONES OUTSIDE OF THE PACIFIC: SCOTIA, CARIBBEAN, TYRRHENIAN AND CARPATHIANS DOMAIN .....	1-07
<i>M. Guidarelli, O. Gonzalez, R. Raykova, T. Pinat, G.F. Panza</i>	
NORTHERN ANTARCTIC PENINSULA – SOUTHERN PATAGONIA: A PRELIMINARY STRATIGRAPHIC FRAMEWORK FOR COMPARISON OF PALEOGENE EVENTS .....	1-08
<i>S.A. Marensi</i>	
GEOMETRIES, DEFORMATION STYLES AND KINEMATICS OF THE FUEGINAN ANDES AND MAGALLANES FOLD-AND-THRUST BELT (TIERRA DEL FUEGO ISLAND) .....	1-09
<i>M. Menichetti, M. Cenni, D. Gattini, A. Gaudio, M. Mattioli</i>	
TECTONICS OF THE SOUTHERNMOST ANDES: A COMPARISON BETWEEN THE PATAGONIAN AND THE FUEGIAN CORDILLERAS .....	1-10
<i>V.A. Ramos</i>	
SEISMIC IMAGING OF THE MAGALLANES-FAGNANO FAULT SYSTEM (TIERRA DEL FUEGO REGION) .....	1-11
<i>D. Yagupsky, A. Tassone, E. Lodolo, M. Menichetti, J.F. Vilas</i>	

## **Session 2 - Geodynamic and Tectonics**

DEVELOPMENT OF ASYMMETRIC BASINS ALONG THE MAGALLANES-FAGNANO FAULT AND OTHER CONTINENTAL TRANSFORM FAULTS .....	2-01
<i>Z. Ben-Avraham, E. Lodolo</i>	
PLATE KINEMATICS OF THE ANTARCTIC PENINSULA .....	2-02
<i>R. Dietrich, A. Rülke</i>	
BREAKUP OF GONDWANA AND OPENING OF THE SOUTH ATLANTIC: REASSESSMENT BASED ON MAGNETIC ANOMALIES .....	2-03
<i>M.E. Ghidella, L.A. Lawver, L.M. Gahagan</i>	
CRONOLOGY OF OROGENIC FRONT PROPAGATION IN THE FUEGIAN FOLD-THRUST BELT .....	2-04
<i>M.C. Ghiglione, V.A. Ramos, E.B. Olivero</i>	

TECTONIC AND GEODYNAMIC EVOLUTION OF THE SOUTH SANDWICH ARC AND EAST SCOTIA SEA .....	2-05
<b>R.D. Larter</b>	
AGULHAS PLATEAU, MAUD RISE AND NE GEORGIA RISE, PRODUCTS OF A TRIPLE JUNCTION? .....	2-06
<b>L.A. Lawver, L.M. Gahagan</b>	
SOUTH AMERICA - ANTARCTICA PLATE MOTION AND TECTONICS OF THE SOUTHERNMOST ANDES, SCOTIA SEA AND ANTARCTIC PENINSULA .....	2-07
<b>R. Livermore, G. Eagles, P. Morris, A. Nankivell</b>	
SPREADING REGIME AND TECTONICS IN THE WESTERNMOST SCOTIA SEA .....	2-08
<b>E. Lodolo, A.A. Schreider</b>	
GEOLOGICAL CROSS-SECTION ACROSS THE FUEGINAN ANDES IN THE TIERRA DEL FUEGO ISLAND .....	2-09
<b>M. Menichetti</b>	
DIFFERENT STYLES OF CONTINENTAL GROWTH AT THE CONVERGENCE ZONE OF SOUTHERN CHILE .....	2-10
<b>A. Polonia, M.-F. Loreto, L. Torelli, E. Vera</b>	
NORTHWARD MOTION OF SOUTH AMERICA, SCOTIA SEA DEVELOPMENT, AND CARIBBEAN CONVERGENCE .....	2-11
<b>R. Somoza</b>	
PALEOMAGNETISM FROM UPPER TRIASSIC-LOWER JURASSIC ROCKS IN THE DESEADO MASSIF: NEW INSIGHTS ON THE BEHAVIOR OF PATAGONIA DURING THE BREAKUP OF GONDWANA .....	2-12
<b>H. Vizán, R. Somoza, G. Taylor</b>	

### **Session 3 - Earthquake Seismology**

EARTHQUAKE EPICENTRES IN TIERRA DEL FUEGO FROM MAY 1999 TO MARCH 2004 .....	3-01
<b>G. Connon, L. Barbero, C. Ferrer, J.L. Hormaechea, N. Sabbione, R. Pincioli, C. Rastelli, M.P. Plasencia Linares</b>	
LITHOSPHERIC STRUCTURES AND REGIONAL SEISMICITY IN THE SCOTIA SEA AREA: A REVIEW .....	3-02
<b>M. Guidarelli, M.P. Plasencia Linares, M. Russi, G.F. Panza</b>	
THE 4 AUGUST 2003 EARTHQUAKE RECORDED BY ASAIN NETWORK IN ANTARCTICA AND TIERRA DEL FUEGO .....	3-03
<b>M.P. Plasencia Linares, B.G. Bukchin, M. Guidarelli, M. Russi, G.F. Panza</b>	
FURTHER DEVELOPMENTS OF THE ASAIN NETWORK IN ANTARCTICA AND TIERRA DEL FUEGO .....	3-04
<b>M. Russi, M.P. Plasencia Linares, M. Guidarelli</b>	

### **Session 4 - Magmatic Processes**

DISCOVERY OF ALKALI-BASALTS IN TIERRA DEL FUEGO .....	4-01
<b>R.D. Acevedo</b>	
LITHOLOGIC TYPES OF THE JEU-JEPEN DIORITE ISLA GRANDE DE TIERRA DEL FUEGO .....	4-02
<b>R.D. Acevedo, C. Roig, M.L. Valín-Alberdi</b>	
IRON SULFIDES RELATED TO FUMAROLIC VENTS IN DECEPTION ISLAND, ANTARCTICA .....	4-03
<b>A.T. Caselli, S.M. Tourn, C. Bengoa</b>	



EMPLACEMENT FABRICS OF THE CONCÓN DYKE SWARM, CENTRAL CHILE .....	4-04
<i>C. Creixell, M.A. Parada, P. Roperch, C. Arriagada, D. Morata</i>	
METAMORPHIC P-T CONDITIONS OF RHYOLITES IN THE MAGALLANES FOLD AND THRUST BELT, PATAGONIAN ANDES .....	4-05
<i>F. Hervé, H.-J. Massonne, T. Theye, M. Calderón</i>	
MONITORING MAGMATISM OF THE PATAGONIAN BATHOLITH THROUGH THE U-PB SHRIMP DATING OF DETRITAL ZIRCONS IN SEDIMENTARY UNITS OF THE MAGALLANES BASIN .....	4-06
<i>F. Hervé, E. Godoy, C. Mpodozis, M. Fanning</i>	
THE PALEOCENE–EOCENE SEJONG FORMATION, BARTON PENINSULA, KING GEORGE ISLAND, ANTARCTICA: ERUPTIVE AND DEPOSITIONAL PROCESSES AND ENVIRONMENTS .....	4-07
<i>S.B. Kim, Y.K. Sohn, M.Y. Choe, J.I. Lee, S.D. Hur</i>	
IMPLICANCES OF THE ACTIVITY OF FLUOR-RICH FLUIDS ON BASALTS AFFECTED BY VERY LOW GRADE METAMORPHISM IN CHAPELCO HILLS, NEUQUÉN, ARGENTINA .....	4-08
<i>C.I. Martínez Dopico, E. Gallegos, M.E. Vattuone</i>	
MAGMATIC MUSCOVITE AND GARNET IN GRANITES OF THE SOUTHERN PATAGONIAN BATHOLITH .....	4-09
<i>H-J. Massonne, M. Calderon, F. Hervé</i>	
EFFECTS OF METAMORPHISM ON MAGNETIC SUSCEPTIBILITY AND FERROMAGNETIC MINERALS IN THE SARMIENTO OPHIOLITE COMPLEX, SOUTHERN CHILE .....	4-10
<i>S. Singer, A. Rapalini, M. Calderón, F. Hervé</i>	
THE ORIGIN OF PLATINUM IN TIERRA DEL FUEGO: GEOLOGICAL EVIDENCE .....	4-11
<i>E. Zappettini, L. Villar, S. Segal, A. Celeda, A. Romano, D. Acevedo</i>	

### **Session 5 - Geomorphology and Geodesy**

REGIONAL GEOID DETERMINATION IN TIERRA DEL FUEGO INCLUDING GPS LEVELLING .....	5-01
<i>D. Del Cogliano, R. Dietrich, A. Richter, R. Perdomo, J.L. Hormaechea, G. Liebsch, M. Fritsche</i>	
HORIZONTAL DISPLACEMENTS IN THE MAGALLANES-FAGNANO FAULT ZONE DETERMINED BY REPEATED GPS OBSERVATIONS .....	5-02
<i>J.L. Hormaechea, D. Del Cogliano, R. Perdomo, R. Dietrich, G. Liebsch, A. Richter, M. Fritsche</i>	
GEOID UNDULATION ON THE ANDEAN CORDILLERA .....	5-03
<i>A. Introcaso, L.E. Lenzano, A.M. Robin, M.V. Mackern</i>	
MORPHO-STRUCTURE OF LAGO FAGNANO (TIERRA DEL FUEGO) AND ADJACENT AREAS .....	5-04
<i>H. Lippai, E. Lodolo, A. Tassone, J.L. Hormaechea, M. Menichetti, J.F. Vilas, TESAC Party</i>	
GEODETTIC DETERMINATION OF RELATIVE PLATE MOTIONS AND CRUSTAL DEFORMATIONS DUE TO SOUTH AMERICA, SCOTIA AND ANTARCTIC PLATE INTERACTIONS .....	5-05
<i>R. Smalley Jr., E. Kendrick, M.G. Bevis, I.W.D. Dalziel, F. Taylor, E. Lauría, R. Barriga, G. Casassa, E. Olivero, E. Piana, A. Zakrajsek</i>	

### **Session 6 - Marine Geology and Geophysics**

MORPHOLOGY AND SEDIMENTARY PROCESSES ON THE TERRACED ACCRETIONARY PRISM OF SOUTHERNMOST SOUTH AMERICA .....	6-01
<i>R. Bartole, D. Morelli, A. Cuppari</i>	
SEISMOSTRATIGRAPHY AND RECENT SEDIMENTARY EVOLUTION OF AN ASYMMETRIC EXTENSIONAL BASIN AT THE WESTERN ARM OF THE MAGALLANES-FAGNANO TRANSFORM SYSTEM .....	6-02
<i>R. Bartole, W. Colautti, E. Colizza, C. Salvi, F. Tosoratti</i>	

MARINE GEOLOGY OF THE EREBUS AND TERROR GULF REGION, NW WEDDELL SEA .....	6-03
<b>E.W. Domack, E. Backman</b>	
A GEOPHYSICAL STUDY ALONG THE EASTERN MARGIN OF THE ANTARCTIC PENINSULA .....	6-04
<b>W. Jokat, V. Helm, R. Krockner</b>	
SEISMIC EXPRESSION OF THE WESTERN SCOTIA SEA CONTINENTAL MARGINS .....	6-05
<b>C. Sauli, E. Lodolo, N. Wardell, A. Tassone, A. Polonia</b>	
3D CRUSTAL VARIATIONS IN THE PHOENIX-ANTARCTIC RIDGE (P2 SEGMENT) .....	6-06
<b>E. Suriñach, E.L. Flores-Márquez, J. Galindo-Zaldivar, A. Maldonado</b>	
3D MODELLING OF THE SOUTH SCOTIA RIDGE PLATE BOUNDARY (ANTARCTICA) .....	6-07
<b>S. Susini, M. De Donatis, N. Zitellini</b>	
GAS HYDRATES AND ACTIVE FLUID OUTFLOW NE OF THE SOUTH SHETLAND ISLANDS, ANTARCTIC PENINSULA .....	6-08
<b>U. Tinivella, F. Accaino, R. Geletti, B. Della Vedova</b>	

### **Session 7 - Sedimentary Processes**

RARE-EARTH ELEMENTS SIGNATURE OF PATAGONIAN MARINE SEDIMENTS PHOSPHATES, ARGENTINA .....	7-01
<b>L.N. Castro, A.M. Fazio</b>	
GEOPHYSICAL RECONSTRUCTION OF THE SEDIMENTARY INFILL OF LAGO ICALMA (39°S, CHILEAN LAKE DISTRICT) SINCE THE LAST DEGLACIATION .....	7-02
<b>F. Charlet, C. Marchand, S. Bertrand, E. Chapron, M. Pino, R. Urrutia, M. De Batist</b>	
HOLOCENE CARBONATE SEDIMENTATION IN THE NORTH WESTERN SECTOR OF THE MAGELLAN STRAIT: TEXTURAL, GEOCHEMICAL AND MICROPALAEONTOLOGICAL PRELIMINARY RESULTS .....	7-03
<b>E. Colizza, F.O. Amore, S. Morabito, C. Salvi, R. Bartole</b>	
MAJOR SEDIMENTARY CHANGES RELATED TO THE BEGINNING OF A GLACIALLY-DOMINATED MARGIN STAGE WEST OF ADELAIDE ISLAND, ON THE ANTARCTIC PENINSULA PACIFIC MARGIN .....	7-04
<b>F.J. Hernández-Molina, R.D. Larter, A. Maldonado</b>	
LATE CRETACEOUS CONGLOMERATES FROM THE CHILEAN MAGALLANES BASIN, AND THEIR RELATION WITH BASIN CLOSURE .....	7-05
<b>A. Sánchez, F. Hervé, E. Gogoy, M. Solari, J. Fuentealba</b>	
SEDIMENTARY CHARACTERISTICS AND FLUVIAL ARCHITECTURE OF A GIGANTIC GRAVELLY SUBMARINE CHANNEL: THE CRETACEOUS LAGO SOFIA CONGLOMERATE, SOUTHERN CHILE .....	7-06
<b>Y.K. Sohn, M.Y. Choe, Y.K. Jin, J.I. Lee, S.D. Hur, Y. Kim, H.R. Jo</b>	

### **Session 8 - Ice-sheet Dynamics**

THE IMPRINT OF ICE MASSES ON THE CONTINENTAL MARGIN DURING GLACIAL MAXIMA: THE SEA FLOOR RECORD WEST OF THE NORTHERN ANTARCTIC PENINSULA .....	8-01
<b>M. Canals</b>	
THE RESPONSE OF THE WARSZAWA ICEFIELD, KING GEORGE ISLAND TO RECENT AND PREDICTED FUTURE CLIMATE CHANGE .....	8-02
<b>A. Hubbard, A. le Broq</b>	
PLIO-PLEISTOCENE ORBITAL PERIODICITIES IN GLACIALLY INFLUENCED SEDIMENTS FROM WESTERN PACIFIC MARGIN OF ANTARCTIC PENINSULA .....	8-03
<b>M. Iorio, E. Marsella, G. Nardi, E. Petruccione</b>	

PERIGLACIAL FEATURES IN NORTHERN TIERRA DEL FUEGO, THE ARGENTINE FUEGIAN ANDES AND NORTHERN JAMES ROSS ISLAND, ANTARCTIC PENINSULA: A COMPARISON . . . . .	8-04
<i>J. Rabassa, P. Carrera Gómez, M. Valcárcel Díaz, A. Coronato, A. Pérez Alberti, G.G. Bujalesky, J.M. Redondo Vega</i>	

### **Session 9 - Geophysical Methodologies**

IMPLEMENTATION OF BIO-TECHNOLOGY FOR EARTHQUAKE PREDICTION . . . . .	9-01
<i>S. Agarwal, S. Tiwari</i>	
SIMULATION OF SEISMOGRAMS USING THE KELVIN-VOIGT STRESS-STRAIN RELATION . . . . .	9-02
<i>J.M. Carcione, F. Poletto, D. Gei, M.A.B. Botelho</i>	
COMBINED USE OF THE GGSFT DATA BASE AND ON BOARD MARINE COLLECTED DATA TO MODEL THE CRUST-MANTLE INTERFACE BENEATH THE POWELL BASIN, ANTARCTICA . . . . .	9-03
<i>R.E. Chávez, E.L. Flores-Marquez, E. Suriñach, J. Galindo-Zaldivar, J. Rodríguez-Fernández, A. Maldonado</i>	
DEPTH-MIGRATED SEISMIC IMAGING NORTH OF 'ISLA DE LOS ESTADOS', ARGENTINA (54° 25' S) . . . . .	9-04
<i>A.H. Comínguez, A. Tassone, E. Lodolo</i>	
CRUSTAL STRUCTURE OF THE CHILEAN FOREARC BETWEEN 36° AND 40°S FROM COMBINED OFFSHORE AND ONSHORE SEISMIC WIDE-ANGLE MEASUREMENTS - SPOC 2001 . . . . .	9-05
<i>S. Lüth, P. Wigger, J. Mechie, M. Stiller, C. Krawczyk, K. Bataille, C. Reichert, E. Flüh, SPOC Research Group</i>	
INNOVATION IN SEISMIC SURVEY ON SUBGLACIAL LAKES . . . . .	9-06
<i>D. Nieto Yabar, A. Bratus, E. Del Negro, R. Geletti</i>	

### **Session 10 - Paleomagnetism, Paleoenvironments and Paleoclimatic Reconstructions**

COASTAL MAPPING OF THE QUATERNARY MARINE DEPOSITS IN THE STRAIT OF MAGELLAN (CHILE) . . . . .	10-01
<i>S. DeMuro, A. Brambati</i>	
HOLOCENE DIFFERENTIAL TECTONIC MOVEMENTS ALONG THE ARGENTINE SECTOR OF THE BEAGLE CHANNEL (TIERRA DEL FUEGO) INFERRED FROM MARINE PALAEOENVIRONMENTS . . . . .	10-02
<i>G. Bujalesky, A. Coronato, C. Roig, J. Rabassa</i>	
SEDIMENTARY PROCESSES IN LAKE PUYEHUE OVER THE LAST 500 YEARS: IMPLICATIONS FOR PALEOENVIRONMENTAL RECONSTRUCTIONS IN THE CHILEAN LAKE DISTRICT (41°S) . . . . .	10-03
<i>E. Chapron, S. Bertrand, F. Charlet, X. Boes, M. De Batist, N. Fagel, O. Magand, F. Arnaud, M.A. Mélières, M. Pino, R. Urrutia</i>	
EOCENE COOLING RECORDED IN THE CHEMISTRY OF LA MESETA FORMATION MOLLUSKS, SEYMOUR ISLAND, ANTARCTIC PENINSULA . . . . .	10-04
<i>L.C. Ivany, D.B. Blake, K.C. Lohmann, R.B. Aronson</i>	
FIRST PALEOMAGNETIC RESULTS ON THE SARMIENTO OPHIOLITE, SOUTHERN CHILE: IMPLICATIONS FOR THE PATAGONIAN OROCLINE . . . . .	10-05
<i>A.E. Rapalini, M. Calderón, F. Hervé, U. Cordani, S. Singer</i>	
VOLCANIC ERUPTION IMPACTS ON PALEOENVIRONMENTAL RECONSTRUCTION: A HIGH-RESOLUTION STUDY OF SEDIMENTOLOGY, GEOCHEMISTRY AND PALEOECOLOGY FROM TWO LAKES OF THE CHILEAN LAKE DISTRICT (SOUTH CENTRAL CHILE) . . . . .	10-06
<i>S. Volland, J. Müller, M. Pino, M. Sturm</i>	

**Session 11 - Paleontology and Paleoecology**

- MESOZOIC CALCAREOUS NANNOFOSSILS FROM LARSEN BASIN,  
SOUTHERN ANTARCTIC PENINSULA ..... 11-01  
**A. Concheyro**
- EOCENE-PLIOCENE ECOSYSTEMS OF SOUTH SHETLANDS AND ANTARCTIC PENINSULA ..... 11-02  
**A. Gazdzicki**
- SOUTHERN OCEAN EOCENE-OLIGOCENE CALCAREOUS NANNOFOSSIL:  
PALAEOECOLOGY AND PALAEOCEANOGRAPHIC IMPLICATIONS ..... 11-03  
**G. Villa, D. Persico, S.M. Bohaty, F. Florindo**
- EFFECTS OF LATE EOCENE COOLING ON ANTARCTIC MARINE COMMUNITIES ..... 11-04  
**J.E. Werner, D.B. Blake, R.B. Aronson**

**Session 12 - Hydrodynamics**

- HYDROLOGICAL MEASUREMENTS COLLECTED ON BOARD THE  
R/V OGS-EXPLORA IN THE WESTERN SECTOR OF THE STRAIT  
OF MAGELLAN AND IN THE PACIFIC MARGIN DURING APRIL 2004 ..... 12-01  
**A. Giorgetti, R. Laterza**
- HYDRODYNAMICS OF LAGO FAGNANO, TIERRA DEL FUEGO ..... 12-02  
**A. Richter, R. Dietrich, J.L. Hormaechea, D. Del Cogliano,  
R. Perdomo, G. Liebsch, M. Fritsche**
- HYDROLOGIC CHARACTERISTICS OF MELTING CREEKS IN POTTER COVE,  
(KING GEORGE ISLAND, ANTARCTICA) ..... 12-03  
**L. Varela, E. Kruse, M. Bonardi, L. Tosi, A. Mazzoldi**

# **Session 1**

---

## **REGIONAL GEOLOGY**



## LATE JURASSIC BIRTH OF THE ROCAS VERDES BASIN AT THE SARMIENTO OPHIOLITIC COMPLEX: EVIDENCE FROM ZIRCON U-PB SHRIMP GEOCHRONOLOGY

1-01

M. Calderón(\*), F. Hervé(\*), C.M. Fanning(\*\*)

(\*) *Departamento de Geología, Universidad de Chile, Casilla 13518, Correo 21, Santiago, Chile*

(\*\*) *Research School of Earth Sciences, The Australian National University, Canberra ACT 0200, Australia*

### Introduction

The formation of the Late Jurassic to Early Cretaceous Rocas Verdes backarc marginal basin (RVB; Dalziel, 1981; Stern et al. 1992; Mukasa & Dalziel, 1996) was preceded by ~20 My of lithospheric thinning, continental rifting and widespread silicic volcanism of the Middle to Late Jurassic Tobífera Formation (e.g. Bruhn et al., 1978; Fuenzalida and Covacevich, 1988; Pankhurst et al. 2000; Stern & de Wit, 2003). The opening of the RVB has been considered diachronous from south (Late Jurassic) to north (Early Cretaceous) suggesting a northward unzipping mode of opening (Stern et al. 1992; Mukasa & Dalziel, 1996; Stern & de Wit, 2003). The Rocas Verdes basin (RVB), separates two continental blocks over a diffuse zone dominated by the interaction between mafic magmas and continental rocks (e.g. Stern & de Wit, 2003). The RVB closure and subsequent obduction of ocean-floor rocks onto the cratonic margin has been postulated to have begun in mid-Cretaceous (e.g. Dalziel, 1981), and the maximum age of initiation of the orogenic deformation and Magallanes foreland basin is constrained at ~92 Ma (Fildani et al., 2003). A minimum orogenic shortening of 300 km, during four stages that represent the main events of compressive deformation (mid-Cretaceous, Late Cretaceous, Paleogene to Neogene events), was calculated for the southernmost part of the Patagonian Andes orocline (Kraemer, 2003).

The Sarmiento ophiolitic complex (SOC; Fig. 1), the northern ocean mafic-floor remnant of the Rocas Verdes marginal basin, comprises massive gabbros, plagiogranites, sheeted dikes and a thick extrusive unit composed of pillow basalts, pillow breccias with intercalation of radiolarian bearing cherts and siltstones (Allen, 1982; Stern and de Wit, 2003). Igneous zircons from a dacitic dike, that intrudes pillow basalts, were dated with SHRIMP U-Pb analysis which help to establish a minimum age for the oceanic-type basaltic rocks generation. The procedures followed for zircon age determinations carried out at the University of Canberra are outlined by Williams (1998), and data were processed using Squid and Isoplot/Ex (Ludwing, 1999).

### Geological Background

The studied area comprises four main N-S trending and east-verging thrust sheets (Fig. 1), in which three of them form elongated mountain belts of supracrustal rocks and shallow intrusives. The westernmost thrust slice comprises Paleozoic metamorphic rocks of the Staines Complex (SC; Forsythe and Allen, 1980; Hervé et al., 2003) which to the north at Seno Yussef are unconformably overlain by volcanosedimentary rocks of the Tobífera Formation (TF). The base member comprises a monolithic basal breccia with centimetre- to metre sized boulders of polydeformed metamorphic rocks assigned to the SC, overlain by mudstones, sandstones and conglomerates, and by pyroclastic flow deposits and rhyolitic lava flows (Allen, 1982). Part of the TF was deposited under relatively deep marine conditions (Allen, 1982; Wilson, 1991) and has an estimated minimum thickness of 1000 m (Allen, 1982).

Along the western side of the Peninsula Taraba and Isla Young, mafic pillow lavas and dikes are intruded by several felsic dikes (Fig. 1 and 2). Mafic and felsic rocks from the Peninsula Taraba have mean  $\epsilon Nd_{150}$  values of +2 and -4, respectively, indicating mantelic and crustal magmatic sources (Calderón et al., 2003). This tectonic slice, which is under the scope of this contribution, is overthrust to the east over the shaly Zapata Formation (ZF), consisting of ammonite, belemnite and radiolarian bearing succession of siltstones and mudstones which reach a minimum thickness of 2000 m and which conformably overlie pillowed basaltic rocks (Fig. 1; e.g. Allen, 1982). At the Cordillera Sarmiento a thick pile of mafic pillowed and massive lavas and dikes crops out with gentle apparent south-dipping structure. Finally, the Cordillera Riesco is made up by several N-S trending and east-

verging thrust sheets of foliated volcanosedimentary rocks assigned to the TF. Although at Canal Morla Vicuña the TF has yielded crystallization ages of ~172Ma (Pankhurst et al., 2000), recent zircon SHRIMP analysis of ~149 Ma, obtained from a foliated metarhyolite at the same area are considered more reliable crystallization ages (M. Calderón and A. Fildani, unpublished data).

The studied area is flanked to the west by the calcalkaline composite South Patagonian batholith (SPB), in which the oldest plutons occur on the eastern margin (ca. 151-141 Ma), with earliest Cretaceous units in the west (ca. 137 Ma), and Late-Cretaceous to Tertiary granitoids concentrated near the central axis of the batholith (U-Pb conventional and SHRIMP zircon ages; Martin et al., 2001). At the Peninsula Staines, close to the contact with hornfelsic metasedimentary rocks of the SC, a biotite granite with Late Jurassic crystallization age crops out (F. Hervé and M. Fanning, unpublished data).

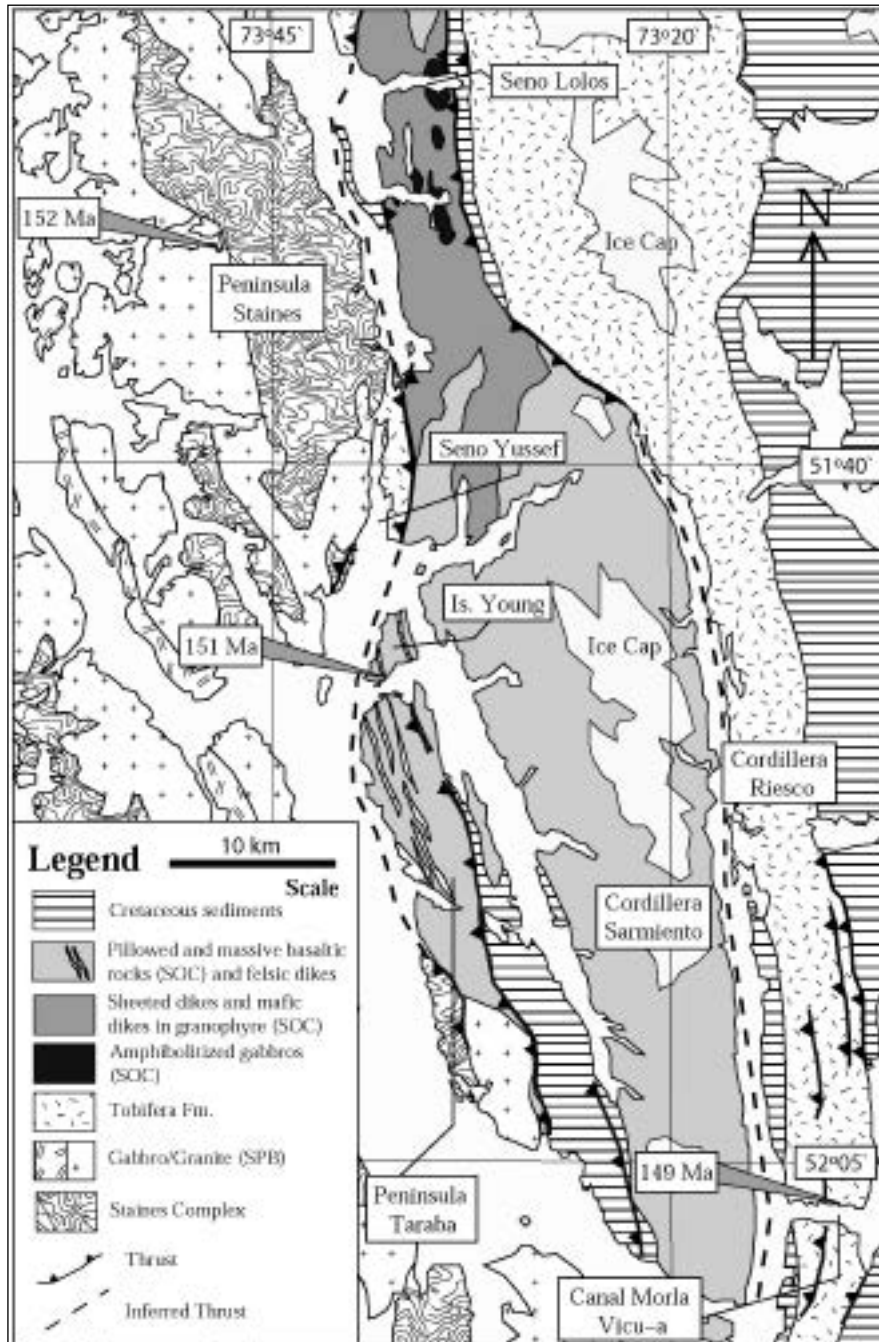


Fig. 1 - Geological units at the Sarmiento ophiolite (after Allen, 1982).

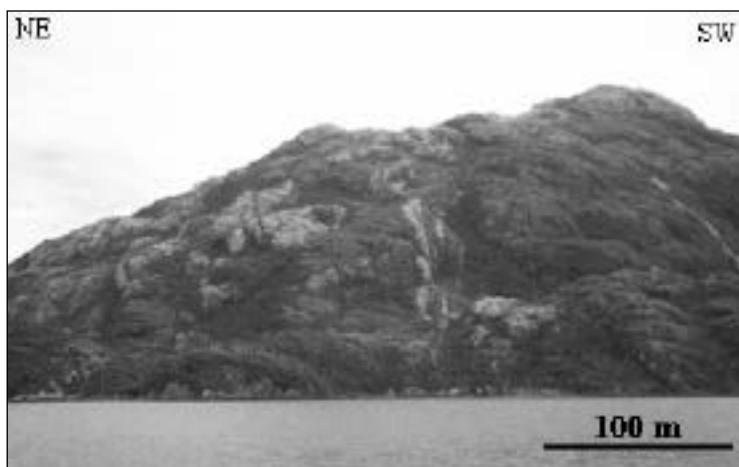


## Geochronology of the Sarmiento Ophiolitic Complex

The dating of plagiogranites, interpreted as fractionated liquids derived from the differentiation of basic magmas within the spreading center, yielded an age range between 141-136 Ma, considered as formation ages for the SOC (conventional zircon U-Pb ages; Stern et al., 1992). This age range is coincident with the fossil record in the ZF which indicate Tithonian-Neocomian age of deposition (Fuenzalida & Covacevich, 1988), ie. between 144 – 121 Ma (according to the GSA 1999 Geologic Time Scale; Palmer & Geissman, 1999). Lower concordia intercept ages of  $147 \pm 10$  Ma, from coarse-grained granophyre in the gabbro unit (Seno Lolos), reflect inherited zircon components (probably of Proterozoic age), and were therefore interpreted as remobilized fragments of country rocks entrapped within the essentially mantle-derived rocks of the ophiolite complex (Stern et al., 1992).

The analysed sample in this study, is a subvertical porphyritic dacitic dike with horizontal columnar joints against surrounding undeformed pillowed basalts, collected at a small island to the south of Isla Young (Fig. 1). This rock with quartz and plagioclase phenocrysts in a fine grained quartz-feldspathic groundmass with spherulitic texture, contains minor euhedral allanite and garnet pseudomorphosed by chlorite. The zircon crystallization age of this dike is ~151 Ma. This is a clear indication that mafic volcanism was already taking place 10 to 15 My before than the crystallization of the plagiogranites.

Fig. 2 - Panoramic view of the northern edge of the Península Taraba, where several porphyritic quartz-feldspathic dikes, with miarolitic cavities, intrude massive and pillow basalts. Leucocratic rocks with embayed quartz phenocrysts and a microgranophyric and spherulitic texture in the groundmass, indicate hypabisal or sub-volcanic depths during crystallization. The pillow lavas show a quenching plumose texture with relict clinopyroxene in the groundmass and abundant chloritized pseudomorphs of olivine phenocrysts.



## Discussion

The Late Jurassic age of the garnet-bearing dacitic dike does constrain the minimum age for the submarine mafic volcanism occurring probably over a partially melted continental crust in the continental-oceanic crust transition. The bimodal magmatism may occur close to the spreading center from which mantelic magmas were injected/accreted to the long-term attenuated continental crust, in which partial melting processes migrate from the lower crust to the upper crustal rock assemblages, affecting the metasedimentary rocks of the SC and/or the buried pre-Late Jurassic volcanic rocks or their plutonic equivalents.

In the SOC a large relative volume of mafic extrusives to extensional mafic dikes suggests that in the narrow northern extreme of the RVB, with an estimated maximum width of ~25 km, extension was slow relative to magma supply (e.g. Stern & de Wit, 2003). However, even considering very low orthogonal-spreading rates of 1 cm/yr, the oceanic-type RVB could have reached a width of 200 or 400 km after activity periods of 10 or 20 My, respectively. The extension of the oceanic crust was thus greatly shortened and maybe partially consumed by a short episode of reverse subduction during the mid-Cretaceous compressive event as proposed by Kraemer (2003).

## Acknowledgements

This work was supported by the Conicyt BAPRTD to M. Calderón and the Fondecyt 1010412 grant to F. Hervé. The authors are grateful to the aid of colleagues and cruise crew during the field work.

## REFERENCES

- Allen, R.B., 1982, Servicio Nacional de Geología y Minería, Boletín no. 38, p. 1-46.
- Bruhn, R.L. et al., 1978, Earth and Planetary Science Letters, v. 41, p. 32-46.
- Calderón, M. et al., 2003, International Workshop on Subduction Zone Processes in Southern Chile, a post-Congress event of the X Congreso Geológico Chileno, Abstract Volume, p.42.
- Dalziel, I.W.D., 1981, Royal Society of London Philosophical Transactions, ser. A, v. 300, p. 319-335.
- Fildani, A. et al., 2003, Geology, v. 31, no. 12, p. 1081-1084.
- Forsythe, R. & Allen, R.B., 1980, Revista Geológica de Chile, no.10, p. 3-15.
- Fuenzalida, R. & Covacevich, V., 1988, V Congreso Geológico Chileno, 3, p. H159-H183.
- Hervé, F. et al., 2003, Journal of South American Earth Science, v. 16, p. 107-123.
- Kraemer, P.E., 2003, Journal of South American Earth Sciences, v. 15, p. 731-748.
- Ludwig, K., 1999, Berkeley Geochronological Center Special Publication 1.
- Martin, M. et al., 2001, Third South American Symposium on Isotope Geology, Pucón, Chile, CD-ROM, SERNAGEOMIN, p. 580-585.
- Mukasa, S.B. & Dalziel, I.W.D., 1996, Journal of South American Earth Sciences, v. 9, p. 349-365.
- Palmer, A.R., & Geissman, J., 1999, GSA geologic time scale: Geological Society of America CTS004.
- Pankhurst, R.J. et al., 2000, Journal of Petrology, v. 41, p. 605-625.
- Stern, C.R. et al., 1992, Journal of South American Earth Sciences, v. 6, p. 97-104.
- Stern, C.R. & de Wit, M.J., 2004, Geological Society of London, Special Publication (in press).
- Williams, I.S., 1998, Reviews in Economic Geology, v. 107, p. 1-35.
- Wilson, T.J., 1991, Geological Society of America Bulletin, v. 103, p. 98-111.

## THE ITALIAN CONTRIBUTION TO THE DEVELOPMENT OF THE GEOLOGIC KNOWLEDGE OF ARGENTINA

1-02

Horacio H. Camacho

*Museo Argentino de Ciencias Naturales "Bernardino Rivadavia"*  
 Av. Angel Gallardo 470 - (C1405DJR) Buenos Aires  
 E-Mail: hcamacho@macn.gov.ar

### Introduction

The historical and cultural development of the Argentina shows a permanent and active italian presence, in which the birth of our nationality can be found. Throughout the years, many of the italian characteristics and thoughts have been incorporated to the life of the argentine society, strongly influencing it.

The italians that arrived in these lands not only populated them but also integrated in the local community, also taking part in its principal political activities, both social and cultural. Hence, it can be stated that there is no ground in our culture, and there are not times in our history untied from the italian presence.

The first italians who arrived at the River Plate were part of the crew of Juan Díaz de Solís (1516), Hernando de Magallanes (1519), Sebastián Caboto (1526), Pedro de Mendoza (1535) and Alvar Nuñez Cabeza de Vaca (1540), but the radicación process began in 1810, when in Buenos Aires there already lived some 64 italians (Caraffa, 1926) and they definitively began to live here since 1838, when the official relations were established between the two countries.

It is not our purpose to talk about the italian influence in the argentine culture (this subject was discussed in many important works), but we consider it useful and necessary to briefly refer to it in order to better comprise the italian scientific contributions in the development of Natural Sciences of our country, particularly Geology. It was framed in a major cultural process which involved and made brothers of both countries.

Now we will refer to the most outstanding italian personalities which, during the XIX centuries and first part of the XX, influenced scientific thought of our country, specially linked to Geological Sciences. All of them came from the highest scientific stratum of their period and were gifted with a

spirit willing to give itself in benefit of the River Plate society. They provided to this community the first lesson of Natural Sciences and its significance. After some years, in the XX century, they were called to collaborate in the development of the petroleum research, and responded with the same enthusiasm and dedication.

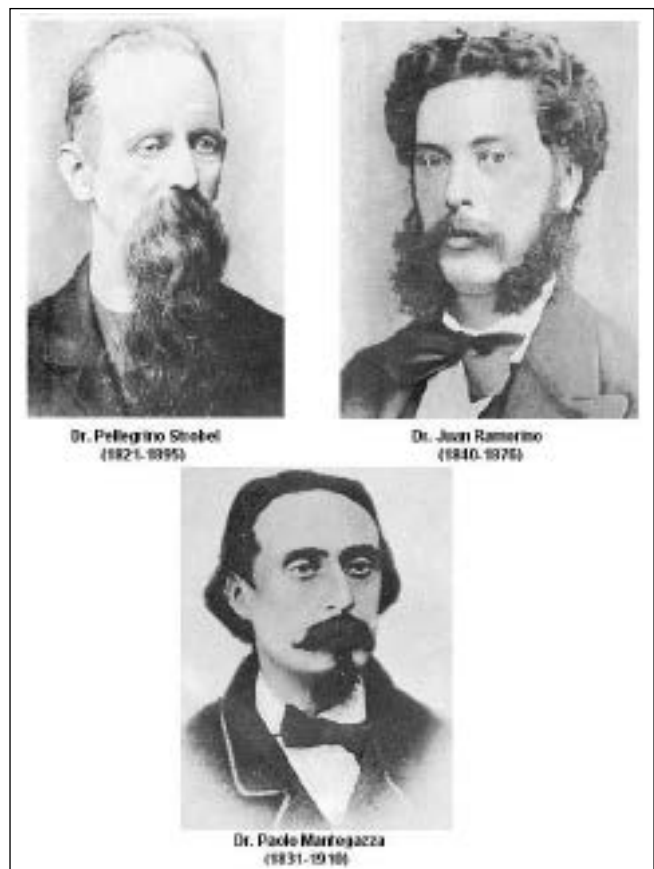
### The Italian contribution in the XIX century

Just after the May Revolution (1810), the new authorities had to face serious problems which required the help of people knowing about Mathematics, Medicine and Natural Sciences. A great statesman of that time, Bernardino Rivadavia (1780-1845) was the author of important initiatives trying to improve this situation, which included the founding of a Natural History Museum (June 27<sup>th</sup> 1812), of a University (August 9<sup>th</sup> 1821) and other institutions dedicated to the study of Mathematics, Medical subjects, Pharmacy, Mineralogy, Geology, Botany, Zoology and Meteorology. In Europe books and laboratories were purchased, but these efforts were insufficient, mainly related to the Natural Sciences, seeing that the main problem was the fact to don't teach them.

This circumstance imposed to contract (December 21, 1824) Dr. Pedro Carta Molino, who Rivadavia had met in London. Carta Molino was a political emigrant, Doctor in Medicine of the University of Turin and professor in this institution. Before travelling to Argentina, Carta Molino improved his knowledge of Physics, Chemistry, Medicine, Mineralogy and Geology, attending classes of famous European naturalists, seeing that in Buenos Aires he had to take charge of the Physics Laboratory, installed in the Public Museum of Natural History, (reestablished on December 31, 1823) and especially of teaching Physics, Chemistry and Natural History. Carta Molino was named Professor of Experimental Physics on April 10, 1826 and on June 17<sup>th</sup>, 1827 he inaugurated his Chair with a talk that constituted the first public expression made in Buenos Aires on the importance and usefulness of the Natural Sciences and their different branches, according to the criteria of the time. On June 14<sup>th</sup> 1826, Carta was also named Professor of the Medical Matter and Pharmacy, which position he held until 1833. He resigned from teaching Experimental Physics at the end of 1827 or beginning of 1828, and was replaced by another excellent Italian scientist, Octavio Fabricio Mossotti (1791-1863), who installed the first astronomical observatory in Buenos Aires.

A great collaborator of Carta Molino was Carlos José Ferraris (1793-1859), known as Cadmo, a political emigrant. They arrived together in Buenos Aires and Rivadavia named him Incharged of the Cabinet of Physics and Chemistry and Curator of the objects of the Hall of Natural History. He also helped together with Carta in the first installation of the observatory that would be directed by Mossotti.

As chief of the Museum, Ferraris did very good work which was praised by those who knew him, such as Alcide d'Orbigny (1802-1857), who on passing through Buenos Aires in 1827, visited the institution and had such a good impression of it, that he dedicated him one species (*Ostrea ferrarisi*). Also Pedro de Angelis



(1784-1859) an Italian most notable contractee living in Buenos Aires since 1826, praised the work of Ferraris, while Juan M. Gutiérrez (1837-1878), considered him the true founder of the Museum. Ferraris played an outstanding part in the life of Buenos Aires, since when he arrived, as is shown by his help in what was happenings of 1829, when he enlisted as Lieutenant in the battalion "Friends of Order" commanded by Colonel Ramón Larrea. In August of the same year he inaugurated his pharmacy, which he himself attended as he had a degree of Pharmacist approved by the Buenos Aires School of Medicine. In 1835 he sold it to Antonio Demarchi, a chemist and first Swiss Councillor in Argentina, who also took his place in the Museum, seeing that Ferraris had resigned from it on March 29, 1836, due to the fact that the Rosas government did not attend to his initiatives. Nevertheless, his resignation was only accepted on February 3<sup>th</sup> 1842, which allowed him to return to Italy where he died in 1859.

Between 1835 and 1852, the Rosas government imposed a cloak of darkness in the cultural progress of Buenos Aires. Once this had been overcome, a scientific rebirth took place and the interest in investigation of the Natural Sciences was renewed. On a higher level, these studies were renewed in the School of Medicine, with a Chair of Natural History for pharmacists headed by Carlos Imperiale, an Italian, chemist and pharmacist who, around 1860, opened a pharmacy. Imperiale started his course on June 1<sup>st</sup> 1864 and his classes included the first notions of geology given in our country.

At that time other actions destined to reactivate the studies and investigations of the Natural Sciences were executed. Among these, in 1862, the reorganization of the Museum of Natural History headed by Germán Burmeister (1807-1892) and in the University of Buenos Aires the re-establishment of the Department of Exact Sciences (June 16, 1865), which comprised the teaching of the Natural History, Mineralogy and Geology took place. Nevertheless the problem caused by the absence of professors of Natural Sciences still subsisted. Then the Chancellor Juan M. Gutiérrez asked for the help of an Italian outstanding personality, Dr. Paolo Mantegazza (1831-1910) recommending him as specialist able to teach this knowledge. Mantegazza had made these studies in Milan and was a Medical Doctor, anthropologist and traveller. He arrived in Argentina around 1854, worked as a Medical Doctor in Nogoyá (Province of Entre Ríos) and went back to Italy in 1858. Being a great friend of Gutiérrez, he came back to Buenos Aires in 1861 and in 1863 and he travelled through the interior of the country, gathering much data that earned him popularity in the scientific world. In 1865 he returned to Italy, dedicating himself to politics. He published important papers where he discussed diverse aspects of the life of our country and its culture. He was the creator of the Italian Anthropology and in 1866 he published also on Tierra del Fuego skulls.

Replying to the request of Gutiérrez for teaching Natural Sciences in the University of Buenos Aires, Mantegazza recommended Dr. Pellegrino Strobel (1821-1895) who arrived to Argentina at the beginning of 1865. Although he has been highly praised (in Jurisprudence in the University of Pavia, 1842), his deep vocation of naturalist led him to outstand in Paleoethnology, Biogeography and Malacology. He founded in 1853 the Journal of Malacology (*Giornale de Malacologia*), in the University of Parma he was Professor of Natural History (1859) and Professor of Mineralogy, Geology and Zoology (1863), which he left in 1864 to come to Argentina. By then he was very well known for his scientific works.

According to the contract signed with the University of Buenos Aires, as Professor of Natural History, Strobel had to teach Natural Sciences in general and especially Geology including Mineralogy, the study of metals and the classification of lands. Furthermore he had to teach special courses on Mineralogy and Geology for students of engineering, as well as making scientific excursions during the vacations.

In the inauguration talk of his Chair of Natural History (July 7, 1865), Strobel gave the definition of this science and his ideas on Geology and the way to teach it. To illustrate his course he asked for the purchase, in Paris, of texts, instruments and natural samples. So, thanks also to the zoological and mineralogical collections, the Cabinet of Natural History of the University was created. Unfortunately for family reasons, Strobel decided to go back to Italy and resigned in April of 1866, but he continued to work, accomplishing also study journeys. Thus he travelled to Bahía Blanca and Carmen de Patagones gathering material for publication and, between the 14<sup>th</sup> and 22<sup>nd</sup> of February of 1866 he crossed the high mountains range of Mendoza, uniting the Paso del Planchón with the town of San Rafael. It was a memorable but very sacrificed journey which gave him a great quantity of material

and during which he made tidy geologic, botanical and zoological observations; he discovered liassic fossils and he even wrote notes regarding the clothing of the town dwellers. He distributed the material he collected during his scarce 10 months in Argentina, among several specialists keeping for himself the geologic, geographic and palaeontologic materials together with seeds of the natural plants of Argentina and Chile, successfully cultivated in Italy. Therefore many of his specialized publications talked about Malacology, Zoology, Ethnology, Archeology and fossil man.

On June 1<sup>st</sup> 1866, Strobel donated to the University the amount of \$ 400 to be dedicated to a prize to the student having the most merit in Natural Sciences. This was the beginning of the present Strobel Prize.

Replacing Strobel and also by means of Mantegazza, Dr. Juan Ramorino (1840-1876), genovees, doctored in Sciences in the Royal University and in which Museum of Natural History he worked as Assistant up to 1866, when he travelled to Argentina. He had a great vocation for Archaeology and Anthropology. He started his courses in 1867 and continued up to 1875, when for illness reasons he had to return to Italy, where he died.

Ramorino made journeys in the Province of Buenos Aires for geologies and anthropological ends, keeping a great relation with Florentino Ameghino and who mentioned him in his first publications calling him the “illustrated professor” and expressing that Ramorino would have been the first, around the end of 1869, who mentioned the presence of the american fossil man. Ramorino accompanied Ameghino in many of his excursions and they both gathered materials that were then studied by Ameghino.

In the University of Buenos Aires, Ramorino taught Mineralogy and Geology, he worked, acquiring collections, instruments for physics and chemistry, books and editing “Elements of Mineralogy” (Rudimentos de Mineralogía) (1869). In 1868 there were more than 110 students registered in the class of Natural History, but the classroom was very small.

Moreover Ramorino developed an outstanding activity related to the italian community living in Buenos Aires and at that time it was very important: he was part of the directing committee of the Italian Hospital (founded in 1863), he was co-founder of the “Círculo Italiano” and of the Argentine Scientific Society (1872).

Because of his illness, in 1870 he had to leave for 5 months for Geneva, and Dr. Domenico de Bortolazzi, Doctor in Medicine and Surgery of the University of Padova replaced him. Like other scientific italians, as Ramorino, Demarchi, Speluzzi, Rosetti, Bortolazzi, he took part in important activities of the italian community.

Thus, thanks to Drs. Strobel and Ramorino, the University of Buenos Aires was able to start the teaching and the studies of Natural Sciences, which was recognized by the Chancellor, Juan M. Gutiérrez (1877) when



Dr. Egidio Sandro Foroglio  
(1897-1954)



Dr. Joaquín Frenguelli  
(1883-1958)



Dr. Enrique Fossa Mancini  
(1884-1950)



Dr. Galdo Bonarelli  
(1871-1951)

stating: “The Chairs of natural history... which had been given at the beginning to the professors Strobel and Ramorino have introduced many young people to the study of the Nature”. One of them was Eduardo L. Holmberg (1852-1937).

The second half of the XX century registered another important Italian contribution, represented by the expedition of Santiago Bove (1852-1887), Lieutenant of the Italian Navy, and charged by President Roca for the scientific exploration of Tierra del Fuego and seas of the South. To this travel the geologist Domingo Lovisato (1842-1916), zoologist Dr. A. Vinciguerra, the painter and photographer S. Roncagli (Secretary of the Italian Geographic Society) and Dr. Carlos Spegazzini (1858-1926), of the University of Buenos Aires, participated. The trip took place between the 1<sup>st</sup> May and 3<sup>rd</sup> of September 1882 and they were able to make important collections, specially in botanics and geology, in Montevideo, Santa Cruz, Isla de los Estados and Punta Arenas (Chile).

Spegazzini, an excellent Italian botanic that arrived in Argentina in 1879, at the beginning of his university career, he was supported by the Genoese Dr. Domingo Parodi (? -1889), another notable botanic.

Also Dr. Pedro Scalabrini (1848-1916) has to be mentioned. He was educator and paleontologist, which he arrived from Italy when he was 20 years old and lived in Paraná (Province of Entre Ríos), where he taught in the Chair of Philosophy and in Natural Sciences in the Secondary School. Between 1870-1910 he made important paleontological excursions, he was a founder of museums and helped Ameghino in the study of the geology of Entre Ríos.

Another outstanding scientist was Dr. Augusto Cesar Scala (1880-1933), Genoese, arrived in 1883, who in 1904 graduated as Pharmacist in the University of Buenos Aires, but he dedicated his time in Botany, specializing in Histology and Micrography. He occupied other teaching jobs in Buenos Aires and La Plata where he became Provisional President of the University.

Another justified memory should be given to Engineers Emilio Rossetti (1939-1908) and Bernardino Speluzzi (? -1898) who arrived together with Strobel to teach Mathematics in the University of Buenos Aires.

Likewise important at the end of the XIX century, were the evangelizing work of Monseñor José Fagnano (1844-1916), in the Island of Tierra del Fuego and the explorations of Father Alberto M. De Agostini (1883-1960), all extraordinary contributions to the social development and the progress in Geography, Geology and Biology of the South American austral region.

### **The Italian participation during the first half of the XX century**

At the beginning of the XX century Argentina was strengthened both socially and scientifically. The geological explorations were planned by the Division of Mines, Geology and Hydrology which had a prestigious group of European geologists, the majority of which were Germans. In the year 1911 a relevant Italian personality was added, Dr. Guido Bonarelli (1871-1951), who developed a fruitful, 16 years long activity in our country. When he arrived to Buenos Aires, Bonarelli was already a well known scientific and humanist, pioneer in the petroleum investigations, but had also, a great knowledge in Paleontology, Archeology and Anthropology.

A great friend of his, Professor Cayetano Rovereto (1870 -? ), Geology Professor in the University of Genova, which arrived to Buenos Aires in 1909 and was a geologist in the Ministry of Public Works, recommended him to the General Directory of Mines to work in the north of Argentina. Bonarelli was contracted on April 4, 1911 up to 1918 (when he returned to Italy), he made sacrificed campaigns in the north of the country and in Bolivia, all related to the technical and genetic interpretation of the oilfields.

The creation of Yacimientos Petrolíferos Fiscales (YPF), in June 1922, offered another opportunity for Bonarelli to return to Argentina, in the year 1923, when he was working as Director of the Geology Division of said Office; at that time he studied the petroleum basins of different parts of the country. This work which he developed up to the beginning of 1927, when he returned to Italy called by the Government of said country.

Bonarelli's contribution to the stratigraphy, tectonic and paleontology of Argentina were really notable and went from Tierra del Fuego and Southern Chile up to Northwestern Argentina. Between 1925 and 1927 with his friend and fellow countryman Ernesto Longobardi, very well known for his

investigations on the chemistry of the different petroleum, he realized the geoagologic map of the Mesopotamia.

Through the mediation of Bonarelli, YPF contracted Drs. Enrique Fossa Mancini (1884-1950), María Casanova (1899-1958), Ivo Conci (1901-1951), Daniel Ramascioni and Vincenzo Franceschi. Thus, Bonarelli became the founder of the Geology Division of YPF and his studies led him to the discovery of the anticlines of Northern Argentina that then became oilfields.

Bonarelli was followed by Fossa Mancini, another well known personality for his culture and knowledge in stratigraphy, paleontology, petrography, tectonics and gravimetry related to the oilfields, which he had applied in Venezuela. In YPF he headed during 5 years the Geologic Committee of the San Jorge Gulf; he then took part in the creation of the Exploration Department and in the organization of a scholarships system for new geologists. In 1939 he resigned to dedicate his time to the university teaching in the National University of La Plata, where he taught Mineralogy and Petrography and he took the Chairmanship of the Department of Geology until his death. Under his direction many prominent Argentine geologists obtained the master degree.

In 1925, Fossa Mancini suggested that YPF contract Dr. Egidio Feruglio (1897-1954) and they both worked together between 1927 and 1931 in the San Jorge Gulf. Feruglio worked in YPF up to 1941, at which moment he joined the Petroleum Institute of the National University of Cuyo, returning to Italy in 1948.

Feruglio had a deep knowledge of the Patagonian geology, on which subject he published very important papers related to his stratigraphy and paleontology of Paleozoic, Mesozoic and Cenozoic. Important were also his contributions on the Patagonian terraces and chains of the South Patagonia. His work called "Geological description of the Patagonia" (1939-1940) in three volumes still is a source of geological information of this region which has not been yet surpassed. In "Palaeontographia Patagonica" (1936-37), he discussed the geology and biostratigraphy of the region of the Lago Argentino.

Ivo Conci and María Casanova worked on petrography, mineralogy and sedimentology of strata of different geological ages.

One of the personalities of major importance of this time, was Dr. Joaquín Frenguelli (1883-1958) who arrived from Italy in 1911 and worked as a Medical Doctor, up to 1929, in the city of Santa Fé. He began to take an interest in the study of the Pampeano of Córdoba, then extended to the Buenos Aires Atlantic coasts as well as the ravines of the Paraná city. Since 1926 and during twenty years he investigated the Patagonian stratigraphy; between 1923 and 1955 his studies of diatoms, flagellates, etc., both fossils and living, converted him into an international authority. From 1941 he started a series of important paleobotanic contributions on the Gondwanic flora.

He was professor in the National University of the Litoral (Paraná) and, from 1934, in the National University of La Plata, getting to be Director of the Museum and Professor of Invertebrate Paleontology and Paleobotany. He published more than 274 papers on a large variety of themes, which are a proof of his great knowledge (Teruggi, 1980).

The papers of Bonarelli, Fossa Mancini, Feruglio and Frenguelli constitute one of the most solid pillars of the Argentine geology in the XX century.

Concluding this work on the importance of the Italian scientifics in Argentina we shall mention Engineer Galdino Negri (1866-1929), born in the Elba Island (Italy) who worked in the La Plata Astronomic Observatory between 1906-1921 and then directed the seismic section of Villa Ortuzar (Buenos Aires). He is considered to be the founder of the Argentine Sismology.

## BIBLIOGRAPHY

- Bonarelli, L. 2002. Guido Bonarelli (1871-1951). Vida y obra científica. 136 págs. Milán. Traducción castellana por Juan Carlos Ferrari.
- Camacho, H.H. 1971. Las Ciencias Naturales en la Universidad de Buenos Aires. Estudio histórico. 150 págs. EUDEBA, Temas. Buenos Aires.
- Camacho, H.H. 2001. La Ciencia en la Argentina de entreguerras. Las Ciencias Geológicas en la Argentina, hasta 1939. Saber y Tiempo 12, julio-diciembre: 177-220. Buenos Aires.
- Caraffa, P.I. 1926. Contribución italiana al desarrollo intelectual en la República Argentina. Ensayo histórico-biográfico. 80 págs. La Plata.

- Caraffa, P.I. 1931. Dr. Pablo Mantegazza in occorrenza del primo centenario del suo genetliaco, 1831 ottobre 1931. Monografia Biografica, 24 págs. La Plata.
- Frenguelli, J. 1950. Profesor Doctor Enrique Fossa-Mancini 1884-1950. Revista Asociación Geológica Argentina V, 2: 77-80. Buenos Aires.
- Gualco, J. N. 1997. La epopeya de los italianos en la Argentina. 157 págs. Editorial Plus Ultra. Buenos Aires.
- Petriella, D. 1979. Los italianos en la historia de la cultura argentina. págs. 63-94. Asociación Dante Alighieri. Buenos Aires.
- Riccardi, A.C. 1999. Homenaje de fin de siglo a los pioneros de la geología argentina del siglo XX. XIV Congreso Geológico Argentino, Relatorio: 173-187. Salta.
- Teruggi, M.E. 1981. Joaquín Frenguelli. Vida y obra de un naturalista completo. 69 págs. Asociación Dante Alighieri. Buenos Aires.
- Università di Parma. 1998. Pellegrino Strobel (1821-1895). Omaggio nel centenario della morte. Alma Mater-Aula Magna, Parma 28 ottobre 1995. Pubbl. Museo di Storia Naturale 9: 1-600. Parma.

## DEEP-SEISMIC IMAGING ACROSS LOS CHIHUIDOS ARCH, NEUQUEN BASIN, ARGENTINA (38° SL)

1-03

Alberto H. Comínguez<sup>1</sup>, Juan R. Franzese<sup>2</sup>

<sup>1</sup> CONICET - Facultad de Ciencias Astronómicas y Geofísicas, Universidad Nacional de La Plata, Paseo del Bosque S/N, La Plata, Buenos Aires, Argentina. Email: ahcominguez@yahoo.com

<sup>2</sup> Centro de Investigaciones Geológicas, Universidad Nacional de La Plata - CONICET, Calle 1 No. 644, La Plata, Buenos Aires, Argentina. Email: franzese@cig.museo.unlp.edu.ar

### Abstract

A mathematical reprocessing of old seismic lines let to know the crustal structure down to 30 km depth. Deep seismic discontinuities were interpreted as the top of the lower Crust and the ancestral master-shear which controlled the rift basin geometry during the late Cretaceous – early Jurassic. In addition, important inversion events were recognized by seismic stratigraphic analysis of the basin, and dated as Pliensbachian – Torcian and Bathonian – Callovian.

### Introduction

About 220 million years ago, part of the Proto-Pacific margin of Gondwana suffered a strong process of continental extension (Mpodozis and Ramos, 1989, Franzese & Spalletti, 2001). This tectonic event was induced by the thermal-mechanical collapse of a Late Paleozoic orogenic belt, giving place to a marginal active basin (Neuquén basin) during the whole Mesozoic, between the current 30° - 40° SL. The Neuquén Basin is an ensialic extensional basin modified by subsequent growth of the Andean magmatic arc. Its complex post-rift stage comprises multiple episodes of Mesozoic and Cenozoic inversion, and the development of the Andean fold and thrust belt and Late Tertiary foreland basin (Vergani et al, 1995).

Syn-extensional processes led to the creation and evolution of several isolated troughs with NNW-SSE and ENE-WSW orientations (Vergani et al. 1995, Legarreta y Uliana 1996a, Franzese & Spalletti, 2001). The syn-rift infill (Pre-Cuyo Group) consists of coarse-grained continental sediments, volcanics, and volcanoclastic materials. The transition to an initial post-rift stage (Cuyo Group) is marked by the widespread development of marine paleoenvironments during the Lower Jurassic (Vergani et al.,1995). However, the distribution and thickness of the early sequences of the Cuyo Group locally match up with the Pre-Cuyo depocentres, signifying that extensional faulting was an important control of sedimentation during the Early Jurassic at least in some areas of the basin (Vergani et al.,1995).

During the post-rift, the existence of localized tectonic-inversion episodes controlled the evolution of the basin (Vergani et al.,1995). Re-structuration events are very evident in the Huincul dorsal area (Fig. 1), where they contributed to the generation of significant hydrocarbon fields. Early interpretations sustained that the Huincul arch would have been the product of post-Jurassic strike-slip movements along a transcurrent fault system (Ploszkiewicz et al.,1984), although more recent



interpretations argue that they were generated through inversion of the initial halfgrabens in a NNW-SSE compressive stress field during the Middle Jurassic (Vergani et al., 1995; Veiga et al., 1997). Evidence of older local inversions involving some areas of the Huincul Arch during the early Jurassic was addressed by Pángaro et al. 2002, and specifically during the Toarcian by Vergani (2003). Other events of tectonic re-structuration were observed by Pángaro and Bruveris (1999), who described normal fault systems produced by transtensive deformation, controlling the contemporaneous sedimentation in central-sectors of the basin during the late Jurassic-early Cretaceous.

The inversion produced by the Andean tectonic shortening is very complex. Evidence of backarc tectonics such as thrust belts and foreland basins could have been as old as Late Cretaceous (Diraison et al., 2000). During the Tertiary (and overall in the Pliocene) compressive tectonics gave place to a fold and thrust belt that reconfigured the whole occidental sector of the basin (Fig. 1). Even during this tectonic phase, the influence of old structural alignments of the initial basin is present in the deformation style (Zapata et al., 1999).

While the geometry and evolution of tectonic inversion is considerably known in the oil productive areas of the Huincul arch, studies along Los Chihuidos Arch (the other inverted arch of the basin) are less abundant. This structure is a N-S structure (Fig. 1), described as a Tertiary large wavelength fold superimposed over a pre-Cretaceous structural high (Ramos, 1978). Deep-seismic mathematical reprocessing across Los Chihuidos Arch allowed us to describe evidence of the main deep structure of the Neuquén basin for the first time as well as to give much insights on the inversion structures that controlled the basic stratigraphic pattern of this huge depocenter.

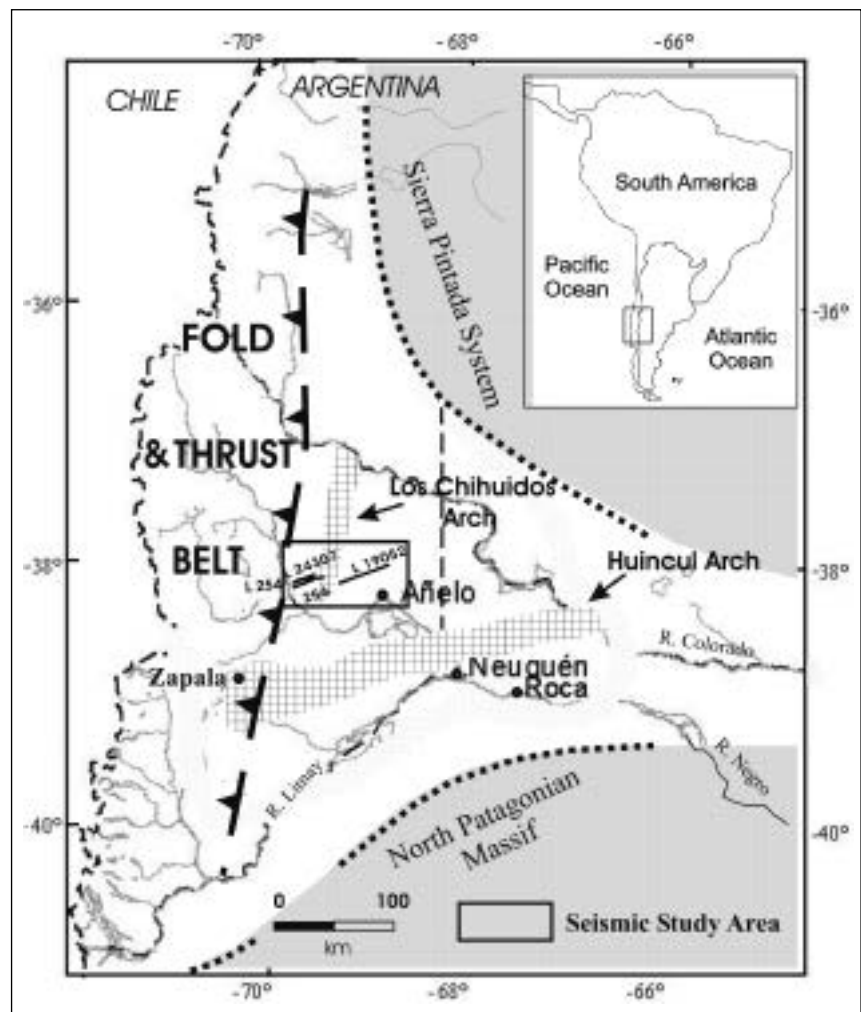
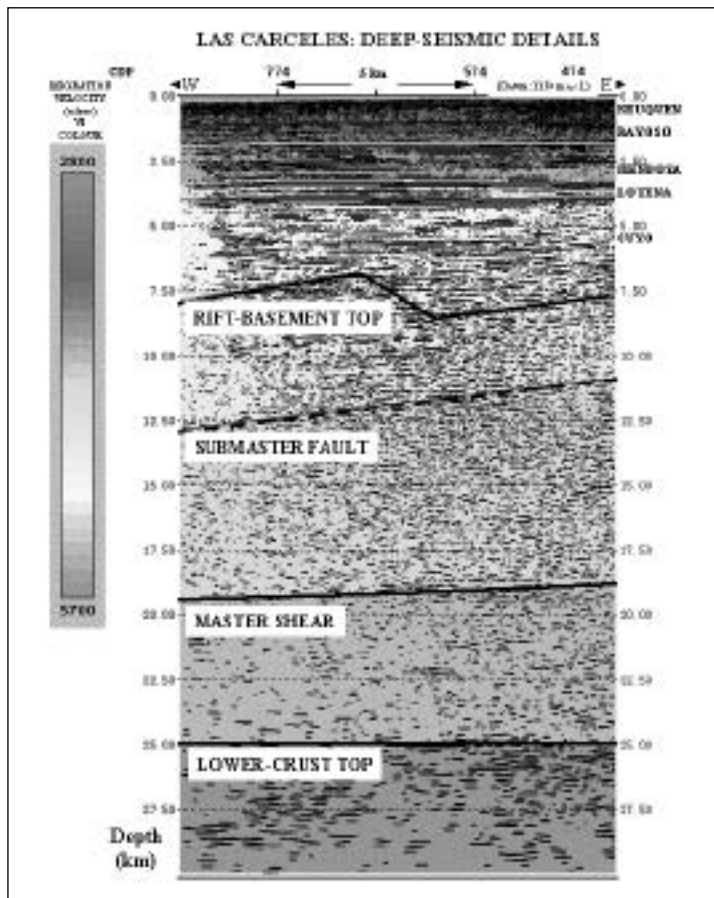


Fig. 1 - Tectonic sketch of the Neuquén Basin. Seismic lines are enclosed by a rectangle which identifies the study area located in the central part of the Basin.

## Seismic Processing and Results

Deep seismic sections were obtained by mathematical reprocessing of conventional Vibroseis data recorded in the central sector of the Neuquen Basin. The lines involved linear upsweeps with frequency band of 12-65 Hz and time-length of 8 sec. The field records were characterized by time-lengths of 13 sec and a sampling period of 4 msec. The Self-Truncating Extended Correlation algorithm (Okaya and Jarchow, 1989) was used to compute cross-correlation between the sweep and the records. The original frequency-band of 12-65 Hz was preserved for the first 5 sec of trace. However, this band was affected by an upper-frequency decreasing from 5 sec on, at a predicted linear-rate of 6.625 Hz/sec. Hence, correlated deep-records with a time-length of 11 sec and a final trace-band of 12-25 Hz were calculated. Depth-migration was implemented on the extended traces. Consequently, progressive models of crust velocity were iteratively matched with the resulting migrated section. The iterative process was considered concluded when it was observed acceptable coincidence between the model and its consequent depth-migrated profile. The basin stratigraphy in the area consists of a continental sequence of initial sinrift (Precuyano) deposited on halfgrabens, followed by strong cycles of marine and continental postrift units (Cuyo, Lotena, and Mendoza groups). In addition, continental sediments are present covering the older sequences (Rayoso and Neuquén groups). The initial structuration is considered to be of Superior Triassic-Liasic in age. Whereas, the postrift phase would have extended until Early Cretaceous. The analysis in the area of Las Cárcelas (Fig. 2) reveals the following: (1) The lower-crust top is placed at about 23-24 km; (2) An oblique reflector horizon located between 16 and 18 km depth, is considered as a master shear that controlled the extensional system; (3) A submaster fault, between 8.5 and 12 km depth, is partially recognized in seismic sections; (4) The top of the rift basement is characterized by irregular depths that, from W to E, ranges from 9 to 5 km; (5) Evident features of tectonic inversion, including synrift as well as part of postrift sequences (i.e. Cuyo and maybe Lotena groups) are observed to the W of Los Chihuidos arch (this inversion episode was possibly initiated in the Bathonian-Callovian). In



Bajada de Añelo (Line 19052 in Fig. 1), the study demonstrated that: (1) The top of the pre-liasic basement is located at about 5 km depth, showing a smooth topographic relief; (2) In the central-western sector are detected features of bipolar inversion (this inversion episode dated Pliensbachian-Torcion is previous to the Bathonian-Callovian inversion, and is not reported in previous papers); (3) The middle level of the Cuyo group is characterized by oblique reflections related with a strong sedimentary progradation toward the west.

Fig. 2 - Depth-migrated window of seismic Line 254, evidencing seismic-stratigraphic sequences of the Basin and local details of the Crust.

## Conclusions

Seismic profiles acquired in both the eastern and western sectors of Sierra de los Chihuidos, showed the deep structure of the Neuquén basin. Deep reprocessing of historical industrial seismic-lines supplied interpretive information down to approx. 30 km. Thus, seismic data reprocessed with “self-truncating extended correlation” (Okaya and Jarchow, 1989) confirmed an economic way of acquiring deep-seismic information where Vibroseis records are available. In addition, the FMED algorithm (Sacchi et al., 1996) was an appreciated mathematical tool for recognizing the different synrift and sag sequences. The first results reveal that: (1) An acoustic contrast at about 24 km depth, must be the top of the lower crust; (2) An oblique reflector between 16 and 18 km depth, must be assumed as the local image of the master shear that controlled the extension system during the Late Triassic-Early Jurassic period; (3) A sub-master fault dipping about 8° W, surely have been controlled the evolution of ‘Las Cárceles’ area; (4) An important inversion event initiated during the Bathonian-Callovian, sensibly affected the western sector of the ‘dorso de los Chihuidos’; (6) Pliensbachian-Toarcian inversion developed during the transition to the Cuyo Group (related with attractive small-traps in a marine environment), has not been evidenced in the area by other studies, although Pángaro et al. (2002) and Vergani (2003) reported it in the Huincul Arch region; (7) In the western sector, a middle Jurassic postrift episode is characterized by a deltaic high energy depositional system, prograding to the west.

## REFERENCES

- Franzese, J.R., and Spalletti, L.A., 2001. Late Triassic – early Jurassic continental extension in southwestern Gondwana: tectonic segmentation and pre-break-up rifting. *Journal of South American Earth Sciences*, 14, 257-270.
- Legarreta, L., Uliana, M.A., 1996. The Jurassic succession in west-central Argentina: stratal pattern, sequences and paleogeographic evolution. *Palaeogeography, palaeoclimatology & palaeoecology*, 120, 303-330.
- Mpodozis, C. & V. A. Ramos, 1989, The Andes of Chile and Argentina, in G. E. Ericksen, M. T. Cañas Pinochet & J. A. Reinemund (eds.), *Geology of the Andes and its relation to hydrocarbon and mineral resources: Circum-Pacific Council for Energy and Mineral Resources Earth Science Series*, 11, 59-90.
- Okaya, D. A., and Jarchow, C. M., 1989, Extraction of deep crustal reflections from shallow Vibroseis data using extended correlation: *Geophysics*, 54, 552562.
- Pángaro F., and P. Bruveris, 1999. Reactivación tectónica multipisódica de sistemas extensionales, Cuenca Neuquina, Argentina. XIV Congreso Geológico Argentino, Salta. Actas I: 231-234.
- Pángaro, F., R. Corbera, O. Carbone y G. Hinterwimer, 2002. Reservorios Precuyanos, V Congreso de Exploración de Hidrocarburos, Mar del Plata Argentina, October 29th - November 2th, 2002, CD Proceedings.
- Ploszkiewicz, J.V., I.A. Orchueta, J.C. Vaillard, and R.F. Viñes, 1984, Compresión y desplazamiento lateral en la zona de falla de Huincul, estructuras asociadas, provincia del Neuquen: Noveno Congreso Geológico Argentino, San Carlos de Bariloche, 2, 163-169.
- Ramos, V.A., 1978. Estructura. In: VII Congreso Geológico Argentino, Relatorio, Geología y recursos naturales del Neuquen, 99-118. Buenos Aires, Argentina.
- Sacchi, M. D., Velis, D. R., and Comínguez, A. H., 1996, Minimum entropy deconvolution with frequency-domain constraints. In E.A. Robinson and O.M. Osman (eds.), *Deconvolution II*, Society of Exploration Geophysicists, 278-285.
- Vergani, G., A.J. Tankard, H.J. Belotti & H.J. Welsink, 1995, Tectonic evolution and paleogeography of the Neuquén Basin, Argentina, in A.J. Tankard, R. Suárez, S., and H.J. Welsink, *Petroleum basins of South America: AAPG Memoir* 62, 383-402.
- Vergani, G.D., 2003, Control estructural de la sedimentación jurásica (Grupo Cuyo) en la Dorsal de Huincul, Cuenca Neuquina, Argentina. Modelado de falla listrica, invertida, Unpublished Repsol-YPF paper.
- Zapata, T., Brissón, I., and Dzedalija F., 1999, The structures of the Andean fold and thrust belt in relation to basement control in the Neuquén Basin, *Boletín de Informaciones Petroleras (BIP)*, Año XVI, no. 60, 112-121.

## REFLECTIONS ON THE SCOTIA ARC AT ITS CENTENNIAL

1-04

Ian W.D. Dalziel

*Institute for Geophysics and Department of Geological Sciences*

*John A. and Katherine G. Jackson School of Geosciences; University of Texas at Austin*

One hundred years ago the Steam Yacht *Scotia* of the Scottish National Antarctic Expedition charted the narrow, eastward-closing, and largely submarine ridge joining the Andean Cordillera to the Antarctic Peninsula that we know today as the Scotia Arc. The base of the expedition led by Dr. W.S. Bruce, Omond House on Laurie Island in the South Orkney Islands group, was handed over to

Argentina as a meteorological station in February 1904. Thanks to the ongoing support of the Argentine Government, *Base Orcadas* is the oldest continually manned station in Antarctica. It thus seems fitting at GeoSur 2004 to offer some reflections on a century of research on the origin and development of the Scotia arc, with emphasis on current thinking, outstanding problems, and the continuing potential of this fascinating and exciting region for understanding how the Earth works.

The origin of the Scotia arc may be traceable back to a pronounced late Precambrian embayment in the Gondwana supercontinent in the vicinity of southern Africa caused by the separation of another continent (possibly Laurentia) during the opening of the Iapetus Ocean basin. Following a complex history of Paleozoic subduction along its proto-Andean margin, the entire Gondwana supercontinent was in an extensional tectonic regime during the Middle to Late Jurassic and Early Cretaceous. Southern Patagonia, Tierra del Fuego, and the Antarctic Peninsula were located along the Pacific margin when fragmentation began in Late Jurassic times, probably with the tip of the peninsula located 'outboard' of southernmost South America as the Weddell Sea and Rocas Verdes basin began to open. In the mid-Cretaceous, however, the Andean margin experienced the first compression related to the uplift of the present Cordillera, as South America moved rapidly west in a mantle (i.e. Atlantic hot spot) reference frame, impinging on the downgoing Pacific ocean lithospheric floor and inverting the Rocas Verdes basin and other back-arc basins north along the margin. Sinistral motion of southern South America relative to Antarctica was probably initiated at that time as the Peninsula separated and rotated clockwise. Also initiated in the basin inversion of the mid-Cretaceous was the westward underthrusting in the region, if perhaps not actual subduction, that presaged the present day east-facing South Sandwich arc.

The eastward closing Scotia and Caribbean arcs are among the most striking tectonic features on present-day Earth. The Caribbean arc is widely believed to have originated with the Mesozoic-Cenozoic emplacement of a microplate of Pacific provenance between the North and South American continents. The Scotia arc, however, resulted from northwest-southeast directed seafloor spreading during Cenozoic renewal of left-lateral transtensional motion that generated the Scotia plate beneath Drake Passage and the central Scotia Sea between the South America and Antarctica during the time interval ~30-6 Ma. Analysis of global plate motions demonstrates present-day left-lateral latitudinal motion of ~22mm/yr between these two continents across the Scotia arc. Teleseismic data indicate left-lateral motion for earthquakes occurring in a narrow zone along the Strait of Magellan-Seno Almirantazgo-Lago Fagnano-North Scotia Ridge transform plate boundary. Measurements on GPS monuments in Tierra del Fuego clearly show ~6.5mm/yr of left-lateral motion along the segment of the South America-Scotia plate boundary across Tierra del Fuego. Hence approximately 16mm/yr must be taken up along the South Scotia Ridge and Shackleton Fracture Zone transforms. As the volcanically South Sandwich Islands are retreating into the South Atlantic Ocean basin at ~60mm/yr relative to South America, most of this motion must reflect the back arc spreading in the eastern Scotia Sea to which Atlantic mantle appears to be contributing.

The Caribbean and Scotia arcs have been suggested, however, to be the foci of asthenospheric return flow from the closing Pacific Ocean basin into the opening Atlantic Ocean basin. The Patagonian orocline where the north-south trending Andean Cordillera swings sharply eastward through 90° into the North Scotia Ridge has also been proposed as the location of 'corner flow' where north-south directed asthenospheric flow beneath the Nazca and Antarctic plates as they are subducted beneath the South American plate, inferred from shear wave splitting, is deflected easterly into the Scotia arc. Geochemical data do indicate that Pacific mantle is flowing into the Caribbean arc and did flow into the Scotia arc during the formation of the Scotia plate. Results of another shear wave splitting study, however, indicate that such flow may be weak at present. One of the outstanding tectonic problems of the Scotia arc region is the tectonic mechanism by which the South Georgia microcontinent was translated eastward relative to South America from its well established original position immediately east of Cape Horn. It is interesting to speculate whether this motion could have been related to asthenospheric flow.

In addition to its important tectonic setting, the Scotia arc is located in a highly critical position with respect to global climatic systems. Opening of Drake Passage and the Scotia Sea during the Cenozoic permitted formation of a completely globe-encircling circumpolar current. The westerly wind system that drives this current reaches its maximum velocity at the latitude of Tierra del Fuego and the North

Scotia Ridge. The opening of the oceanic gateway between the South American and Antarctic continents is often cited as a critical factor in the initiation of Earth's most recent glaciation. Suggestions have been made that the opening of oceanic pathways like that of the Scotia arc may have played a critical role in the onset of pre-Cenozoic glaciations on the planet. Conversely, the Shackleton Fracture Zone appears to have the potential to become a future subduction zone that could create a volcanic isthmus across Drake Passage, thus closing the gateway once again. Studies of the relationship of climate and tectonics in the turbulent region between the southernmost Andes and the Antarctic Peninsula clearly continue to have major potential for making critical contributions to understanding of Earth System processes.

## **AEROGEOPHYSICAL IMAGING REVEALS A COMPOSITE TERRANE OVER PALMER LAND (ANTARCTIC PENINSULA)**

1-05

F. Ferraccioli, P. Jones, A.P.M. Vaughan, A. Dean, P.T. Leat

*British Antarctic Survey, High Cross, Madingley Road, Cambridge CB3 0ET, UK*

### **Summary**

The Antarctic Peninsula has typically been regarded as a complete Andean-type arc-trench system. Several suspect terranes have more recently been proposed over the Antarctic Peninsula. Accretionary complex rocks of the Western Domain and microcontinental(?) arc rocks of the Central Domain may have collided against the para-autochthonous Eastern Domain at about 100 Ma. Aeromagnetic and aerogravity data were simultaneously collected as part of the 2002-03 Antarctic campaign to test a terrane hypothesis for the region from a new geophysical perspective. The resulting aerogeophysical images show that, beneath the ice, contrasting aeromagnetic and aerogravity signatures delineate two distinct zones within the Central Domain. Preliminary geochemical data suggests that the eastern zone of the Central Domain includes a segment of intra-oceanic arc crust. This crustal fragment is currently located in an inboard position. However, it likely originally formed outboard of the former Gondwana margin and may have been shuffled to its current position along major faults imaged in the new aerogeophysical data.

### **Introduction**

The Antarctic Peninsula has traditionally been considered as a complete Andean-type arc-trench system (Storey & Garrett, 1985). Recent geological evidence suggests that the Palmer Land segment of the Antarctic Peninsula crust is more complex than previously proposed (Vaughan & Storey, 2000) and includes three fault-bounded tectono-stratigraphic terranes (Fig. 1). Accretionary complex rocks of the Western Domain and microcontinental arc rocks of the Central Domain (CD) may have docked against the para-autochthonous Eastern Domain during the late Early-Cretaceous Palmer Land event (Vaughan et al., 2002). This recent terrane model predicts that the Eastern Palmer Shear zone represents a suture between the CD and the Eastern Domain (Vaughan & Storey, 2000; Vaughan et al., 2002).

During the 2002/03 Antarctic campaign a combined aeromagnetic and aerogravity survey was performed by the British Antarctic Survey over Palmer Land as part of the multi-disciplinary SPARC (Superterrane in the Pacific Margin Arc) project. The utility of aeromagnetic investigations in studying accretionary tectonics along a convergent continental margin is well recognised for example over the North American Cordillera (e.g. Saltus et al., 1999). In the Antarctic context, key crustal elements over Early Paleozoic East Antarctic terranes have also been delineated using aeromagnetic data (Finn et al., 1999; Ferraccioli et al., 2002). Over 20,000 km of line data were acquired from a Dash-7 aircraft flying from Rothera as part of the new SPARC survey. Line spacing was 5 km for most of the survey area, with some regions at 10 km. Nominal flight altitude was 2,800 m. Occasional departures from the survey altitude to 3600 m were imposed by topography and weather conditions.

This new aerogeophysical survey links previous BAS aeromagnetic campaigns performed in the 90' over Graham Land (Johnson, 1999) with Russian surveys flown over southern Palmer Land (Golynski et al., 1999). It also provides the first aerogravity dataset crossing the entire width of Palmer Land. Previous aerogravity data were restricted to individual lines flown along-strike of the Antarctic Peninsula (Jones and Johnson, 1995).

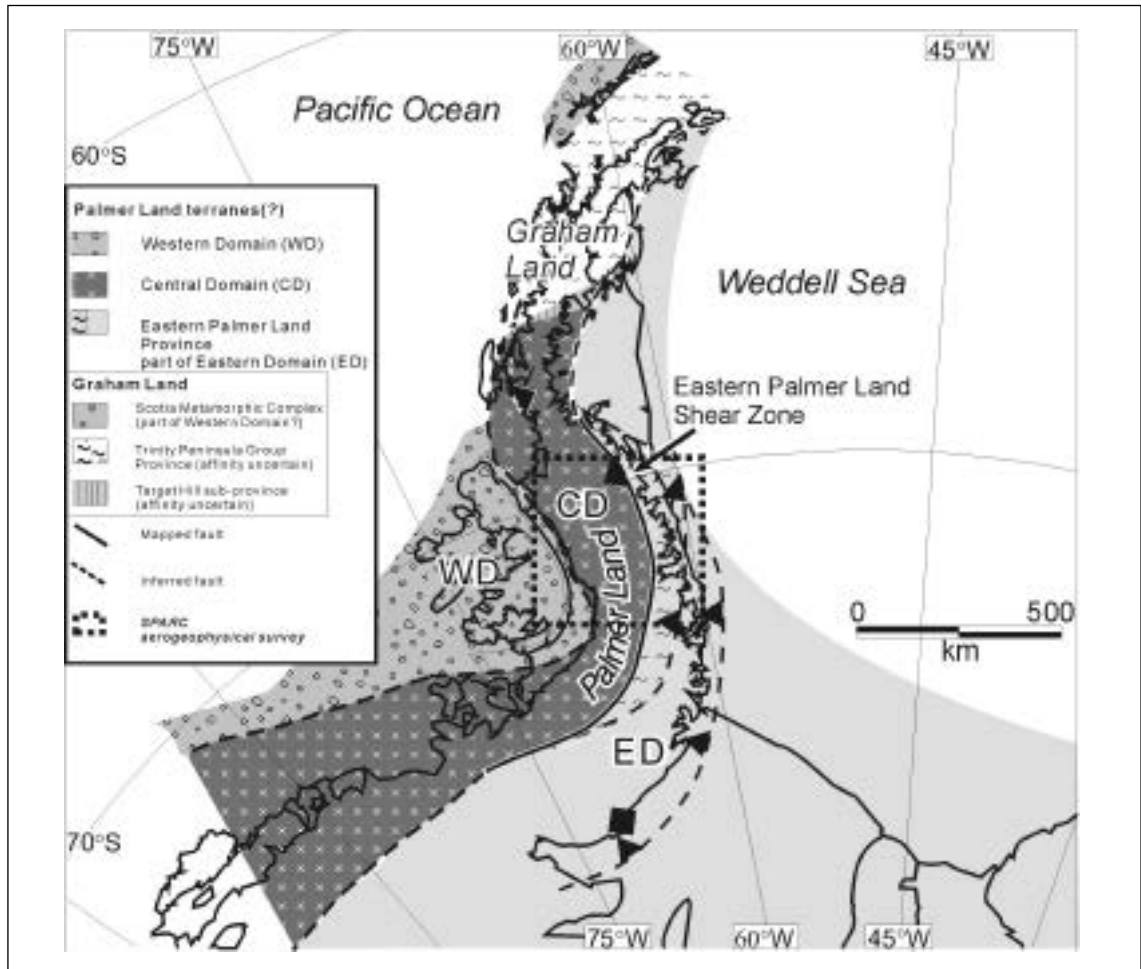


Fig. 1 - Fault-bounded tecto-stratigraphic terranes over the Antarctic Peninsula (from Vaughan & Storey, 2000). Note the location of the SPARC aerogeophysical survey.

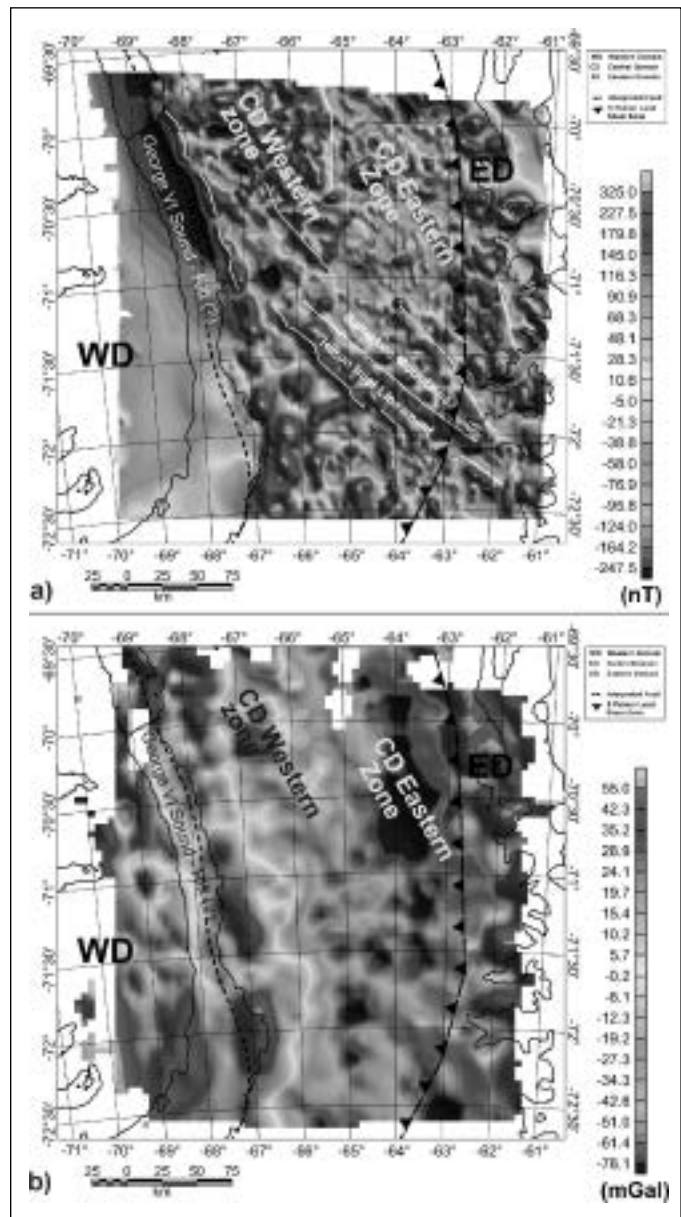
### Data processing

Aeromagnetic processing included magnetic compensation, IGRF removal, diurnal correction, levelling and microlevelling in frequency domain (Ferraccioli et al., 1998). Aeromagnetic data were gridded with a 1 km cell size to produce the total field map. A reduced grey-scale aeromagnetic anomaly map is displayed in Figure 2a. Standard processing steps were taken to convert the raw gravity data to free air anomalies. Differential, carrier phase, kinematic, GPS methods were used to calculate all the navigational information used in these corrections. The vertical acceleration of the aircraft was calculated by double differencing GPS height measurements. An additional correction was made for gravimeter reading errors caused by the platform tilting, when it was subjected to horizontal accelerations. The data were low pass filtered for wavelengths less than 8 km and the complete Bouguer anomaly correction was calculated (Fig. 2b).

Fig 2a-b - New Aeromagnetic and Bouguer Gravity anomaly maps for Palmer Land. White lines show major interpreted aeromagnetic lineaments.

### Interpretation

The CD appears from the resulting aeromagnetic and gravity images to comprise of two distinct zones. The western zone includes highly magnetic and dense rocks and is separated from less magnetic, less dense rocks of the eastern zone by a sharp aeromagnetic lineament. The newly observed magnetic anomalies over the western CD are part of a high-amplitude pattern characteristic of the western side of the Antarctic Peninsula, and known as the Pacific Margin Anomaly (Garrett, 1990; Maslanyi et al., 1991; Johnson, 1999). The crust we assign to the western CD has been previously interpreted as newly generated arc crust formed during Early Cretaceous extension (Vaughan et al., 1998). The broad similarity in magnetic patterns observed over magmatic arc terranes in California and Japan (Finn et al., 1999) supports magmatic arc sources for the newly detected anomalies over the western zone of the CD. The more-weakly magnetic crust we assign to the eastern CD has been interpreted to the north of our survey area as reflecting a back-arc (Johnson, 1999). However, mafic dykes collected as part of SPARC, now define two discrete dyke populations within the eastern zone of the CD. The first previously unidentified group of dykes are tholeiitic in character. The second seemingly more abundant dykes are calc-alkaline in composition. Initial petrogenetic interpretation of the dykes suggests an island arc origin for part of the eastern zone of the CD, with generation of tonalitic/granodioritic plutonic rocks at mid crustal levels and intrusion of tholeiitic basaltic dykes. This was then followed by accretion onto the continental margin and amalgamation of this terrane with the continentally derived Eastern Domain. Calc-alkaline mafic dykes were subsequently intruded. Island arc crust of the eastern zone of the CD must have originally formed in the Pacific Ocean outboard of the Gondwana margin and was then shuffled to its present position adjacent to the former continental margin along major fault zones. Several of these inferred fault zones are delineated as prominent aeromagnetic and gravity lineaments.



now define two discrete dyke populations within the eastern zone of the CD. The first previously unidentified group of dykes are tholeiitic in character. The second seemingly more abundant dykes are calc-alkaline in composition. Initial petrogenetic interpretation of the dykes suggests an island arc origin for part of the eastern zone of the CD, with generation of tonalitic/granodioritic plutonic rocks at mid crustal levels and intrusion of tholeiitic basaltic dykes. This was then followed by accretion onto the continental margin and amalgamation of this terrane with the continentally derived Eastern Domain. Calc-alkaline mafic dykes were subsequently intruded. Island arc crust of the eastern zone of the CD must have originally formed in the Pacific Ocean outboard of the Gondwana margin and was then shuffled to its present position adjacent to the former continental margin along major fault zones. Several of these inferred fault zones are delineated as prominent aeromagnetic and gravity lineaments.

### REFERENCES

- Finn C., Moore D., Damaske D. & Mackey T (1999), *Geology*, 27, 1087-1090.
- Ferraccioli F., M Gambetta, & E. Bozzo (1998), *Geophys. Prospecting*, 46, 177-196.
- Ferraccioli, F., E. Bozzo, & Capponi G (2002), *Geophys. Res. Lett.* 29(10), doi 10.1029/2001GL014138.
- Garrett, S.W. (1990), *JGR*, 95, 6759-6777.

- Golynsky A.V., Masolov V.N. (1999), *Annali di Geofisica*, 42(2), 333-351.
- Jones, P.C., Johnson A.C. (1995), *IUGG XXI, Spec. Rep.*, 117-123.
- Johnson, A.C. (1999). *JGR* 104 B3: 5031-5046.
- Maslanyj, M.P., Garrett, S.W., Johnson, A.C., Renner, R.G.B., Smith, A.M. (1991), *BAS GEOMAP Ser. Sheet 2*, BAS, Cambridge, U.K., 37 pp.
- Saltus R.W., Hudson T.L., Connard G.G. (1999), *GSA Today*, 9(3), 1-6.
- Storey, B.C. & Garrett, S.W. (1985), *Geol. Mag.*, 122, 5-14.
- Vaughan, A.P.M., Warenham, C.D., Johnson, A.C., Kelley, S.P. (1998), *EPSL* 158, 143-155.
- Vaughan, A.P.M. & Storey, B.C. (2000), *J. Geol. Soc.*, 157, 1243-1256.
- Vaughan, A.P.M. Kelley S.M., Storey B.C. (2002), *Geol. Mag.*, 139, 465-471.

## **THE CARIBBEAN PLATE CURRENT PROBLEMS: AN EXAMPLE FOR EVOLUTION OF SMALL PLATES**

1-06

G. Giunta

*Dipartimento Geologia, Università di Palermo (Italy); giuntape@unipa.it*

The Caribbean Plate consists of a nearly undeformed central portion (Colombia and Venezuela Basins) bounded by active margins involving the interaction with the neighbouring Nazca, Cocos, North and South America, from the Mesozoic to Present. The northern (Guatemala and Greater Antilles) and southern (northern Venezuela) Plate margins mainly consist of collisional belts (shear zones), while the western (Central America isthmus) and eastern (Lesser Antilles) margins are represented by convergent systems and related magmatic arcs.

The Caribbean Plate evolutionary history from the Jurassic-Early Cretaceous until the Present time, was realized through plume, accretionary and collisional tectonics.

The timeline of major Caribbean events is characterised by these tectonic regimes (plume and spreading, accretionary, collisional), from the Jurassic early proto-Caribbean stage of oceanization, through two Middle-Late Cretaceous eo-Caribbean accretionary stages of oceanic subductions, up to the collisional event leading to the present Caribbean Plate. The differences among the well known reconstructions of Pindell and Barrett (1990), Pindell (1994), Meschede and Frisch (1998), Giunta (1993), Giunta et al. (2002 a,b,c, 2003) consist on the role of some important constraints recognized during the last years.

The spatial-temporal definition of the Caribbean Plate evolutionary stages is based on tentative paleogeographic identifications of the following elements: (1) continental margins of North and South America, and of minor blocks (Maya, Chortis, Guaniguanico, Venezuelan Cordillera de la Costa), (2) rifted continental margins, closely related to the main continental plates (Escambray in Cuba, Caucagua-El Tinaco and Tinaquillo in Venezuela), (3) oceanic realm, with MORB and MORB to OIB affinities, related to an oceanic thin crust, thickened with a plateau character, coming from east to west, (4) a first intra-oceanic convergence producing subduction complexes and related volcanic arcs, with IAT and CA affinities, (5) sub-continental subductions and melanges with rock blocks of MORB affinity, and (6) a second intra-oceanic subduction zones producing Tonalitic Arc magmatism.

The puzzle-like arrangement of the present Caribbean deformed margins seems to be related to: (1) the Caribbean Plateau insertion between the two Americas; (2) the extension and reciprocal interference of both North America and Andes Cordilleras on the Caribbean area; (3) the original geometry of the geotectonic elements, from which the peri-Caribbean Terranes derive. The palinspastic restoration of the oldest geotectonic elements suggests a Middle Jurassic-Early Cretaceous location of their original paleo-domains in a westernmost, "near mid-America" position, almost at the western corners of the American plates.

### **Proto-Caribbean event**

The proto-Caribbean oceanic crust was generated since the Late Jurassic by multiple spreading centres in an intra-America setting with an Atlantic affinity at an equatorial latitude. It was thickened at its western end by plume related magmatism in an easternmost Pacific setting during the



Cretaceous, obtaining an irregular oceanic plateau character. Several evidences strongly suggest a spatial continuity of this oceanic domain with the Bahamas, Maya and Chortis continental margins to the north, and the Guayana shield to the south, through rifted continental margins with WPT magmatism. How many ophiolitic units can be referred to the unthickened oceanic proto Caribbean crust is difficult to establish because several data suggest that some units should better fit with an intra- or back-arc supra-subduction (SSZ) origin.

## Accretionary event

### 1° eo-Caribbean stage

Starting from the Early Cretaceous, the South Atlantic opening and related westward and north-westward motion of the American plates led to ocean-ocean and ocean-continent plate convergences (“eo-Caribbean” 1<sup>st</sup> phase of Giunta, 1993), producing several SSZ and magmatic arcs. Evidences of the proto-Caribbean oceanic lithosphere subduction are also provided by the HP/LT metamorphosed units (metamorphic climax has been obtained at  $96.3 \pm 0.4$  Ma.) outcropping in the Caribbean margins. They are related to an ocean-ocean subduction or subordinately to an ocean-continent subduction. Moreover, portions of the previously rifted continental margins were also involved in the subduction zones, reaching in places the eclogite facies. This oldest intra-oceanic convergence is supposed to have affected the eastern sector of the proto-Caribbean domain, where subduction of the thinner portions of the oceanic lithosphere was favoured. At the same time the western sector was undergoing progressive crustal thickening, ultimately (Late Cretaceous) leading to a well defined oceanic plateau structure (Fig. 1).

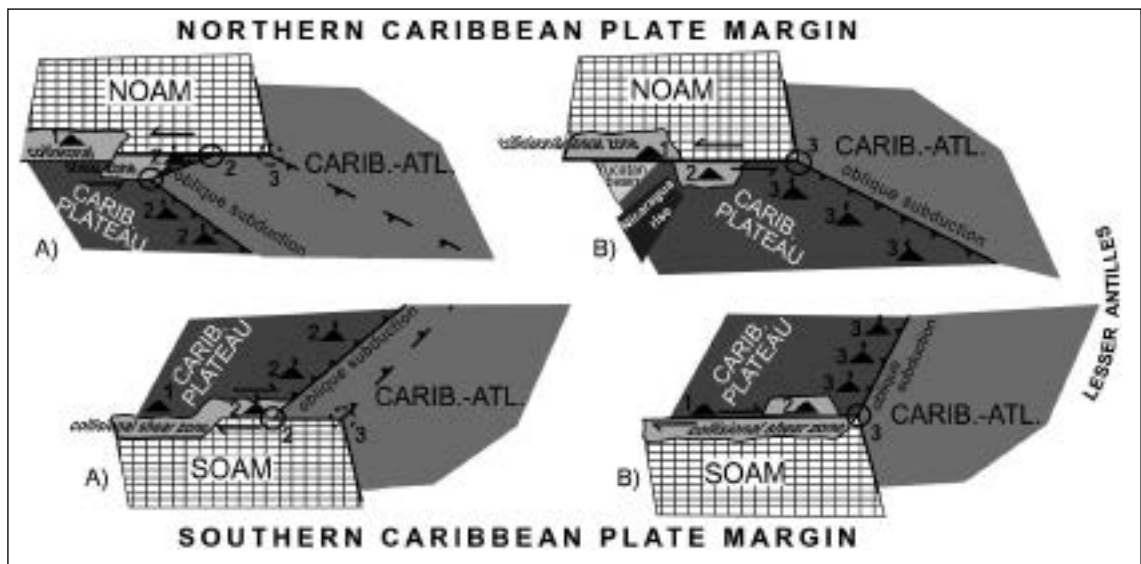


Fig. 1 - Cartoon model of the accretionary (with volcanic arcs) to collisional shear zones evolution related to the opposite triple-junction (circles) shifting eastward, from Late Cretaceous to Eocene (1- to -3). NOAM: North American continental plate; SOAM: South American continental plate.

This view is significantly different from the model proposed by Pindell and Barrett (1990) and Pindell (1994) where in Barremian-Albian times the subduction was located in a Pacific area corresponding to the present Central American Isthmus. Still some important questions need to be resolved:

(1) the mid-Cretaceous location and the subduction directions of either ocean-ocean or ocean-continent convergences, and subordinately, (2) the ocean floor or back-arc pertinence of the MOR-type ophiolitic units, (3) both the volcanic arc complexes and thinned continental crusts involvement in subduction zones.

In a tentative to fit as best all the recognized constraints, at least three models can be proposed, on the basis of the location of strike-slip faults. They almost represented free boundaries among different

geodynamic environments in the proto-Caribbean area, taking into account that the Caribbean evolution, since mid-Cretaceous, has been dominated by a strongly-oblique tectonic regime. It would have characterized subduction, exhumation, emplacement and dismembering processes (see also Giunta et al., 2002 b).

The whole geological data confirm that the first eo-Caribbean accretionary stage ends in the Late Cretaceous, when the unthickened oceanic realm was involved in subduction below the thicker oceanic plateau, with a likely westward sinking of the lithospheric slab. This implies a flip of the intraoceanic subduction direction or a continuous westward subduction, depending on the subduction direction proposed by different models.

### 2° eo-Caribbean stage

Since the Late Cretaceous, the kinematics of the Caribbean plate is closely related to the eastward drifting of the proto-Caribbean oceanic plateau (Colombia and Venezuela Basins) that produced: 1) a diachronous tonalitic magmatism (from 86 Ma) associated with a westward dipping oblique subduction of the proto-Caribbean-Atlantic ocean floor below the plateau; an opposite dismembering of subduction complexes of different ages along an E-W trend (north and south Caribbean margins). This seems to be the consequence of the eastward shifting of both the northern and southern triple junctions (Fig. 2), allowing to the progressive bending of the Aves- Lesser Antilles arc. Moreover, the Caribbean oceanic plateau was trapped by different rotation rates of the Chortis, Chorotega and Choco blocks during the construction of the western plate margin (Central American Isthmus).

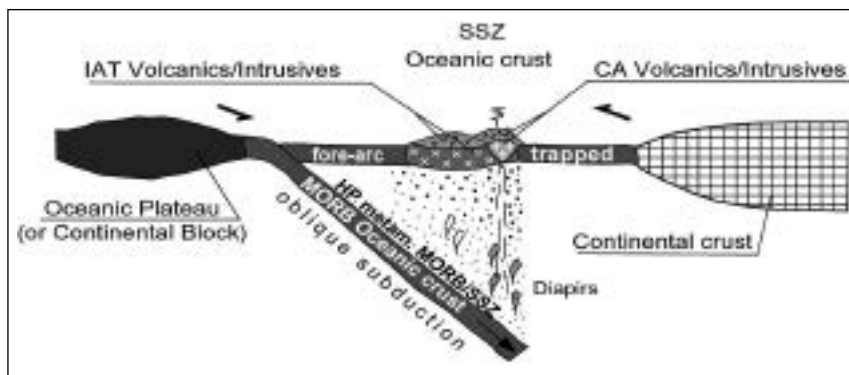


Fig.2 – Cross-section representing the mid-Cretaceous 1<sup>st</sup> eo-Caribbean accretionary stage. (SSZ Cordilleran-like Ophiolites).

During this second eo-Caribbean phase, westward-dipping oblique subduction of the oceanic lithosphere took place beneath both the oceanic plateau and the previous magmatic arcs (Fig. 3), giving rise to (1) the widespread tonalitic arc magmatism of the northern and southern Caribbean plate margins (in Guatemala, Cuba, Hispaniola, Puerto Rico, and Venezuela and Dutch Antilles), (2) the HP/LT and amphibolitic metamorphic effects in both the ophiolitic units and continental margins (Cuba, Hispaniola, Puerto Rico and Venezuela), as well as (3) the onset of the Aves/Lesser Antilles magmatic arc system.

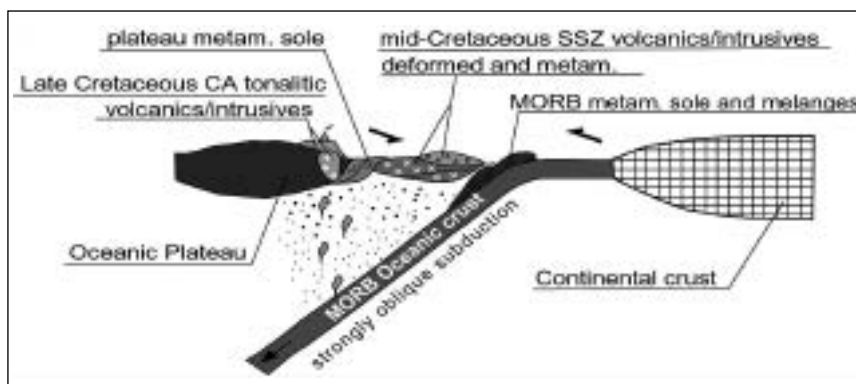


Fig. 3 – Cross-section representing the Late Cretaceous 2<sup>nd</sup> eo-Caribbean accretionary stage. (SSZ Cordilleran-like Ophiolites and Tethyan-like Ophiolites subordinately).

Transpressional tectonics along the northern and southern margins of the Caribbean plate caused the progressive lateral dispersion and opposite rotation (sinistral vs. dextral, respectively) of the older structural elements. This resulted in significant differences between the two margins: along the northern margin the younger (tonalitic) magmatic arc generally rested on the deformed belt, which includes both the older arc systems and the eastward migrating front of the new accretionary wedges. Along the southern margin however the tonalitic magmatism was decoupled from the older arc, being intruded in both undeformed and deformed oceanic plateau and in part in the rifted continental margin units.

### Collisional event

Actually, taking into account that the Late Cretaceous to Present geodynamics of the Caribbean plate has been mainly driven by the eastward drift of the Caribbean plateau with respect to the North and South America plates, the present plate is mainly represented by the Cretaceous plateau crust. It is trapped in the Colombia and Venezuela basins by the intervening Atlantic and Pacific subductions and related volcanic arcs. The former produces the Aves-Lesser Antilles arc, while the latter builds the Central American isthmus, as a mosaic of different blocks reciprocally juxtaposed and facing the Middle American Trench. As a result, both the northern and southern boundaries of the Caribbean correspond, since the Late Cretaceous, to two wide shear zones, where, during Late Cretaceous-Tertiary, large-scale tear faulting, still extensively active (e.g., Motagua fault in Guatemala, El Pilar fault in Venezuela), favoured eastward dispersion and uplifting of the previous subduction-accretion systems (Fig. 4).

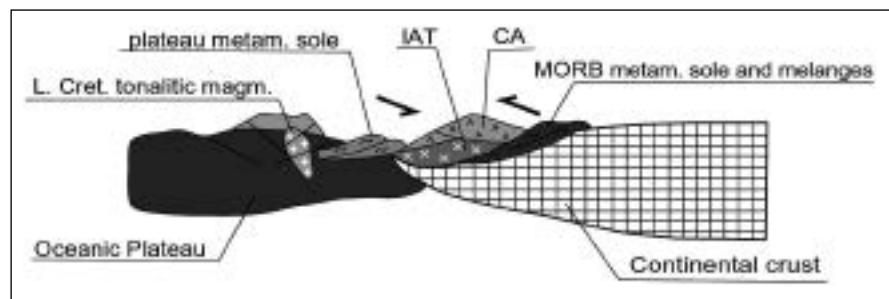


Fig. 4 – Cross-section representing the Late Cretaceous-Tertiary Collisional event.

During the collisional events the main structural elements of the present Caribbean were essentially established in the Paleocene onwards. Fore- or back-arc and piggy-back basins, on the deforming plate borders, were filled by clastic and volcanoclastics sediments. On the northern and southern continental margins, thrust belt-foredeep systems began to develop, involving previously deformed belts along north- or south-verging fronts (Sepur Basin in Mexico-Guatemala; Foreland Basin in Cuba; Piemontine Basin in Venezuela).

The evolution of the Caribbean plate margin has been the subject of many scientific debates during the last two decades: the proposed kinematic models seem in part to be speculative, because they are based much more on unresolved problems than on recognized facts. In particular, the major causes of debate currently are: (1) the original location of the proto-Caribbean oceanic realm; (2) the Early Cretaceous paleogeography and morphology of the margins of the North and South American continents and minor blocks; (3) the polarity of the Cretaceous subduction zones; (4) the locations of and relationships between simultaneous intraoceanic and sub-continental subduction zones, as well as (5) the progressive insertion through tectonic erosion of both the rifted continental portions and supra-subduction complexes in the subduction systems; (6) the possibility of a subduction polarity reversal; (7) the number of magmatic arcs.

Most of the peculiarity of the Caribbean Plate is represented by the above mentioned still unresolved questions; new geological constraints should be recognized, in the aim to improve alternative tectonic models.

### REFERENCES

- Giunta G. (1993) Los margenes mesozoicos de la Placa Caribe: Problematicas sobre nucleacion y evolucion. 6° Congreso Colombiano de Geologia Mem., III, 729-747.
- Giunta G., Beccaluva L., Coltorti M., Siena F. (2002 a) Tectono-Magmatic Significance of the Peri-Caribbean Ophiolitic Units and

- Geodynamic Implications. In *Caribbean Geology into the Third Millennium* (T. Jackson Ed.), Univ. West Indies, ch. 2, 15-34.
- Giunta G., Beccaluva L., Coltorti M., Siena F., Vaccaro C. (2002 b) The southern margin of the Caribbean Plate in Venezuela: tectono-magmatic setting of the ophiolitic units and kinematic evolution. *Lithos*, 63, 19-40.
  - Giunta G., Beccaluva L., Coltorti M., Siena F., Mortellaro D., Cutrupia D. (2002 c) The Peri-Caribbean Ophiolites: structure, tectono-magmatic significance and geodynamic implications. *Caribbean Journal of Earth Science*, 36, 1-20.
  - Giunta G., Marroni M., Padoa E., Pandolfi L. (2003) Geological constraints for the Geodynamic evolution of the southern margin of the Caribbean Plate. AAPG, Sp.Vol.
  - Meschede M., Frisch W. (1998) - A plate tectonic model for the Mesozoic and Early Cenozoic history of the Caribbean plate. *Tectonophysics*, 296, 269-291.
  - Pindell J.L. (1994) - Evolution of the Gulf of Mexico and the Caribbean. In Donovan, S.K., Jackson, T.A. (Eds.), *Caribbean Geology: An Introduction*, U.W.I. Publ. Ass. Kingston, 13-39.
  - Pindell J.L., Barrett S.F. (1990) Geological evolution of the Caribbean region: a plate-tectonic perspective, in G. Dengo and J.E. Case, eds., *The Caribbean Region: Boulder, Colorado*, Geological Society of America, *The Geology of North America*, H, 339-374.

## THE WEST-DIRECTED SUBDUCTION ZONES OUTSIDE OF THE PACIFIC: SCOTIA, CARIBBEAN, TYRRHENIAN AND CARPATHIANS DOMAIN

1-07

M. Guidarelli(\*), O. Gonzalez(\*\*, \*\*\*), R. Raykova(\*\*\*\*), T. Pinat(\*), G.F. Panza(\*, \*\*\*)

(\*) *Department of Earth Sciences – University of Trieste, Via E.Weiss 4 – 34127 TRIESTE – Italy*

(\*\*) *Centro Nacional de Investigaciones Sismológicas, Ministerio de Ciencia, Tecnología y Medio Ambiente, Calle 17, 61, Rpto. Vista Alegre – SANTIAGO DE CUBA Cuba*

(\*\*\*) *The Abdus Salam International Centre for Theoretical Physics, SAND Group, Strada Costiera, 11 – 34100 MIRAMARE TS Italy*

(\*\*\*\*) *Geophysical Institute – Bulgarian Academy of Sciences, Acad.G.Bonchev str. bl.3 – 1113 SOFIA Bulgaria*

### Summary

West-directed subduction zones constitute a very interesting tectonic feature, which present strong differences with respect to classic subduction zones. Only few of these zones are located outside the Pacific Ocean area and among these there are the Scotia Sea region, the Caribbean region, the Tyrrhenian region and the Carpathians region. It is generally recognised that similar geodynamic constraints favoured the development of Barbados, Sandwich, Apennines and Carpathians, so a better understanding of lithospheric characteristics and tectonic structures in each of these regions may provide a better insight into similar features within other regions. In the last few years tomographic studies have been performed in these areas: Scotia Region (Vuan et al., 2000); Tyrrhenian Region (Ponte vivo and Panza, 2002); Caribbean Region (Gonzales et al., 2000, 2004). The presence of such tomographic studies suggests a comparative study of the four domains using all available information, in order to understand to what extent these areas are comparable, and how a better understanding of the lithospheric features in one region may provide a better insight into the similar peculiar features in the other regions.

### Abstract text

According to Doglioni et al. (1999) west-directed subduction zones constitute a very interesting tectonic feature and they present strong differences with respect to classic subduction zones as for example Alpine or Andean ones. West-directed subduction zones form very fast and have very short life; they are characterized by an age usually less than 50 Ma. West-directed subduction zones are generated both in case of high convergence rate among plates (e.g. in West Pacific Area) and no or very low convergence (e.g. Carpathians). They show an arcuate shape with an average length of 1500-3000 Km and they always present both a frontal accretionary wedge and a back-arc basin fast propagating together toward the East direction; so the subducted lithosphere is replaced by new asthenospheric material in the back-arc. In this feature we can recognise that their peculiar shape is due to their internal kinematical behaviour, characterized by the westward drift of the lithosphere with

respect to the asthenosphere. Moreover the West-directed subduction zones present very pronounced foredeeps and trenches, and they also show the highest subsidence rates of any basin on Earth. All these observations result valid both in case of subduction of oceanic lithosphere and of thin continental lithosphere. As pointed out by Doglioni et al. (1999), it appears that the West-directed subduction zones, which are worldwide Tertiary and Quaternary features, possibly form only in the presence of particular geodynamic constraints: along the back-thrust belt of earlier East-directed subduction zones and in the presence of oceanic or thinned continental lithosphere in the foreland of the related back-thrust belt.

Only few west-directed subduction zones are located outside the Pacific Ocean area, among these there are the Apennines, the Carpathians, the Barbados, the Sandwich.

Lliboutry (2000) also proposed a similar evolution for the Caribbean and Scotia domains. The West Indies Arc and the Scotia Arc has drifted in a similar way, eastward relative to North and South America respectively. Strike-slip movements occur along the northern and southern boundaries of both Caribbean and Scotia plates.

As similar geodynamic constraints favoured the development of the Barbados, the Sandwich, the Apennines and the Carpathians, a better understanding of lithospheric characteristics and tectonic structures in each of these regions may provide a better insight into the similar features within the other regions.

We propose here new tomographic maps recently obtained at the University of Trieste for the Mediterranean and the Carpathians regions (Fig. 3 and Fig. 4). The presence of tomographic studies with comparable resolution, suggests a comparative study of the four domains using the information available, in order to understand to what extent these areas are comparable, and how a better understanding of the lithospheric features in one region may provide a better insight into the similar peculiar features in the other regions.

The tomographic study of Vuan et al. (2000) shows low velocity anomalies following the plate boundary between the South America and the Scotia plates, the South Sandwich Island arc, the South Scotia Ridge, and the Bransfield Strait. The Scotia Sea is characterized instead by a high velocity anomaly (see Fig.1).

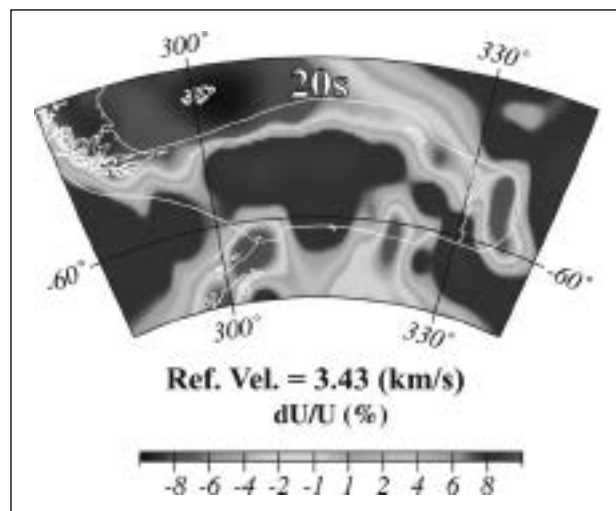


Fig. 1 - Rayleigh wave group velocity maps for the Scotia Sea region presented as percent deviation from an average reference velocity (modified from Vuan et al., 2000).

At the Caribbean Sea, the group velocity tomography map highlights low velocity anomalies in the western part of the domain for all the periods analysed, while the anomaly along the northern boundary of the Caribbean plate is present for periods above 20 s. High velocity anomalies characterize the western half of the Caribbean Sea, but they decrease in amplitude for the higher periods (see Fig.2).

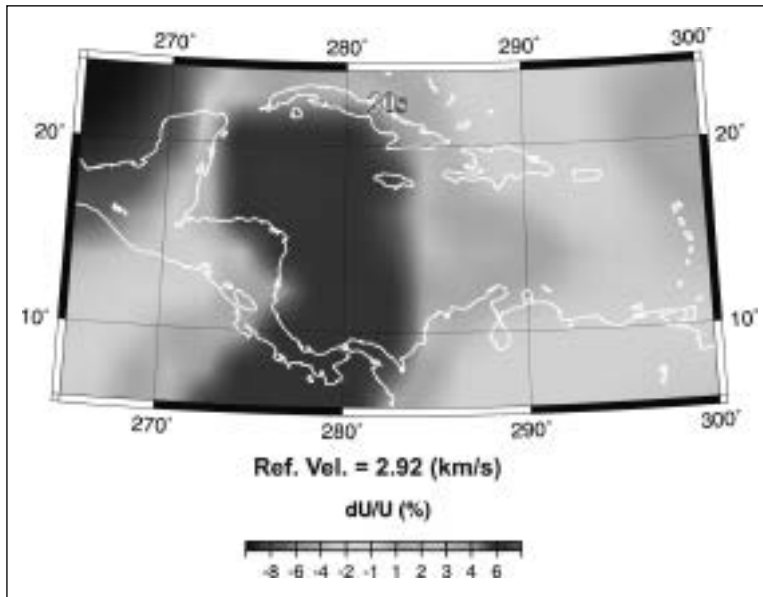


Fig. 2 - Rayleigh wave group velocity maps for the Caribbean Sea region presented as percent deviation from an average reference velocity (modified from González et al., 2004).

In the Mediterranean low velocity anomalies are found at the shortest periods along the Apennines and in the Ionian Sea. The high velocity anomaly in the Central Mediterranean is well pronounced at periods between 15-35 seconds (see Fig. 3).

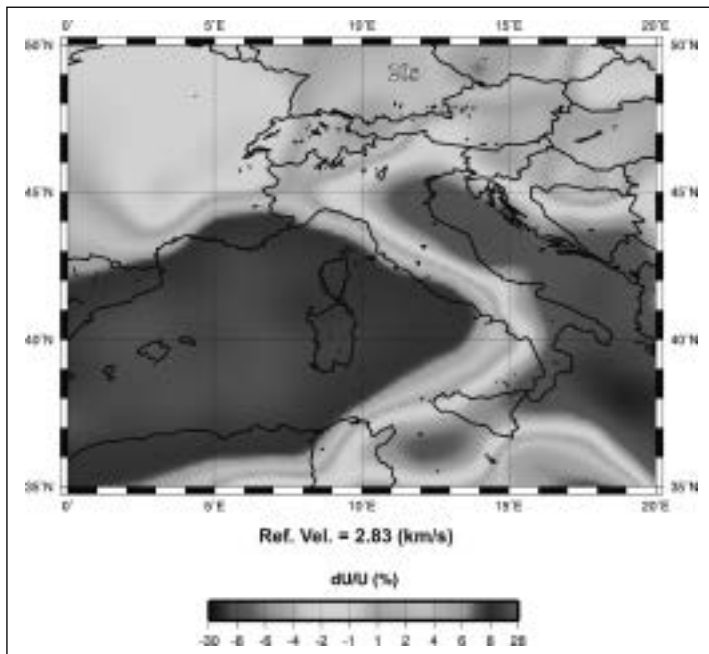


Fig. 3 - Rayleigh wave group velocity maps for the Mediterranean Sea region presented as percent deviation from an average reference velocity.

Unlike the other three domains, the Carpathians region is not characterized by the presence of a sea basin. The main feature is a low velocity anomaly in correspondence with the Carpathians Mountains, while higher velocities are found in the area west to the chain.

We present here the tomographic map for the four regions at the period of 20 s. The maps at that period reflect the properties of the boundary between the crust and the upper mantle. Some similar features can be highlighted comparing the three tomographic maps. The maps at 20 s, especially those for the Central Mediterranean and the Scotia Sea, show low velocity anomalies for group velocities in

correspondence to the possible subduction zones, while the basin west to the subduction is characterized by a high velocity anomaly. The high velocity anomaly is less pronounced in the map for the Carpathian area. The tomographic maps for the Caribbean Sea don't cover, at present, the Barbados subduction zone, but they exhibit a similar high velocity anomaly in the central part of the analysed domain. At higher periods the velocity anomalies are less pronounced than those at shorter periods in all the four regions.

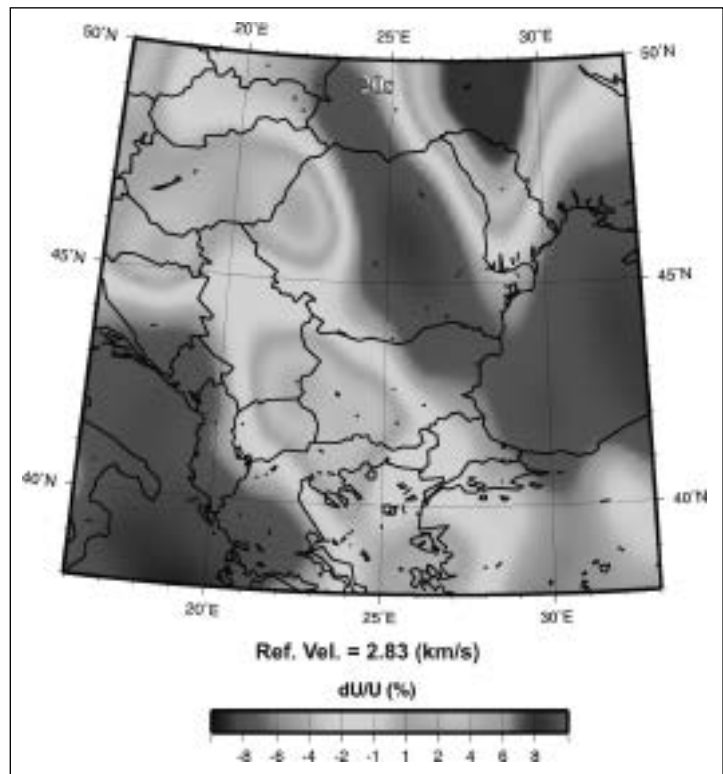


Fig. 4 - Rayleigh wave group velocity maps for the Carpathians region presented as percent deviation from an average reference velocity.

## REFERENCES

- Doglioni, C., Gueguen, E., Harabaglia, P. and Mongelli, F., (1999), On the origin of west-directed subduction zones and applications to the western Mediterranean, in: Durand, B., Jolivet, L., Horváth, F., and Séranne, M. (eds), *The Mediterranean Basins: Tertiary Extension within the Alpine Orogen*, Geological Society, London, Special Publications, 156, 541-561.
- González, O., Alvarez, L., Panza, G.F., and Chimera, G., (2000), Modelos de corteza de la región del Caribe a partir de la dispersión de ondas superficiales, in: *Sismicidad de Cuba y estructura de la corteza en el Caribe*, Editorial Academia, La Habana, Cuba, 45-56.
- González, O., Alvarez, L., Chimera, G., and Panza, G.F., Crust and upper mantle structure in the Caribbean Region by group velocity tomography and regionalization, submitted.
- Lliboutry, L., (2000), *Quantitative Geophysics and Geology*, Springer-Praxis Series in Geophysics.
- Ponteviso, A., and Panza, G.F., (2002), Group velocity tomography and regionalization in Italy and bordering areas, *Physics of the Earth and Planetary Interiors*, 134, 1-15.
- Vuan, A., Russi, M., and Panza, G.F., (2000), Group velocity tomography in the subantarctic Scotia Sea region, *Pure and Applied Geophysics*, 157, 1337-1357.

## NORTHERN ANTARCTIC PENINSULA – SOUTHERN PATAGONIA: A PRELIMINARY STRATIGRAPHIC FRAMEWORK FOR COMPARISON OF PALEOGENE EVENTS

1-08

S.A. Marensi

*Instituto Antártico Argentino, Cerrito 1248, Buenos Aires (1010), Argentina  
and CONICET and Universidad de Buenos Aires*

### Summary

Paleogene time witnessed dramatic changes in oceanic circulation, climate and distribution of landmasses, fauna and flora. Southern high latitudes hold one of the most complete records of the climatic optimum of the Cenozoic (Early Eocene) up to the extensive Cenozoic Antarctic glaciation

since Late Eocene-Early Oligocene, including the development of the psicrosphere and the final break-up of Gondwana.

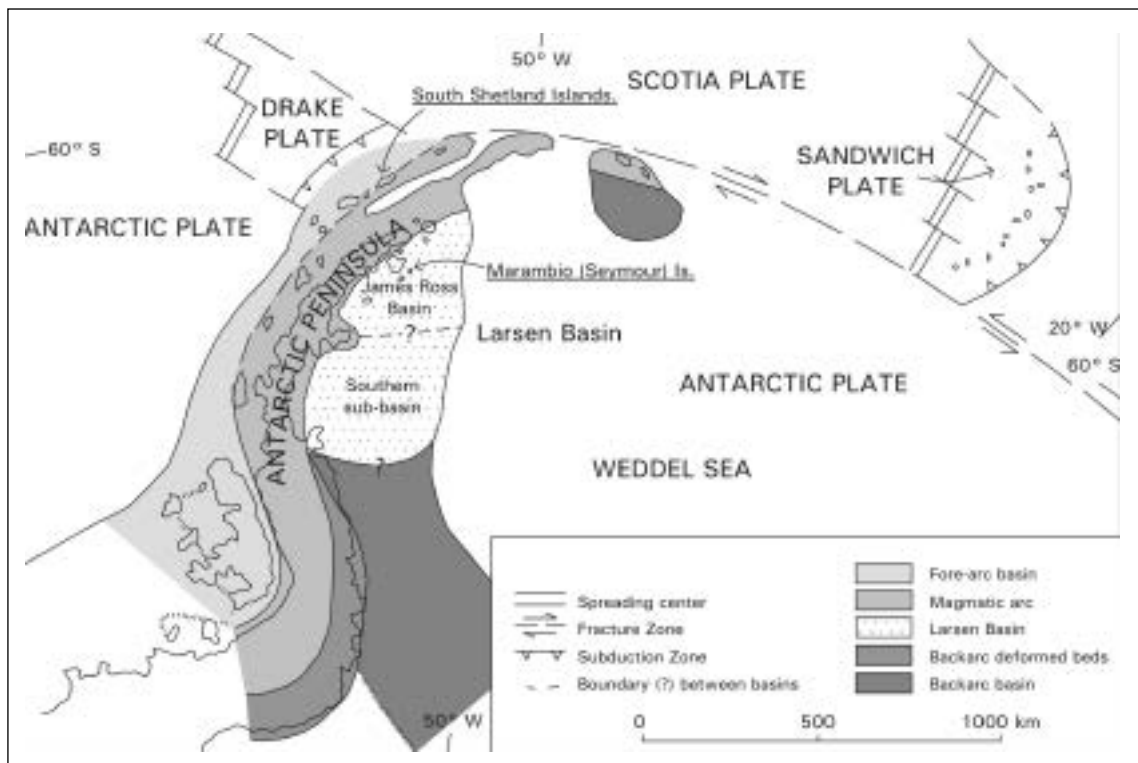
In order to understand how these events succeeded and to compare their consequences at different locations, a solid chronostratigraphic framework must be firstly developed.

This paper is aimed to present a preliminary correlation scheme between northern Antarctic Peninsula and southernmost South America using the Paleogene sedimentary record of the back-arc James Ross Basin, outer or fore-arc King George Island and the foreland Austral Basin in selected locations.

### Abstract text

The climatic evolution of the Southern Ocean was strongly influenced by rearrangements of the Southern Hemisphere land masses, and is related to circulation changes affecting global heat transport (Stott, et al., 1990). The Antarctic Peninsula (AP) located at almost the same paleolatitude (60-65°) since at least the Cretaceous (Lawer et al., 1992), was the Gondwana centrepiece. The separation of South America from Antarctica cleared the way for a free Circum Antarctic Current that produced the thermal and physical isolation of Antarctica. Before this event, the northern tip of the AP and southernmost South America (SSA) were physically connected by means of an isthmus that allowed the dispersal of plants and animals to and from the two continents (Marenssi et al., 1994; Shen, 1995; Reguero et al., 1998). The climatic, biogeographic and geologic history of these two neighbouring areas is recorded in Cretaceous-Paleogene sedimentary rocks of both regions. In order reconstruct the palaeoenvironment a tight stratigraphic framework must be firstly built out. It will then allow to identify related physical, biotic, climatic and oceanographic changes occurring at different places, at the same or different times (i.e. faunal heterochroneity).

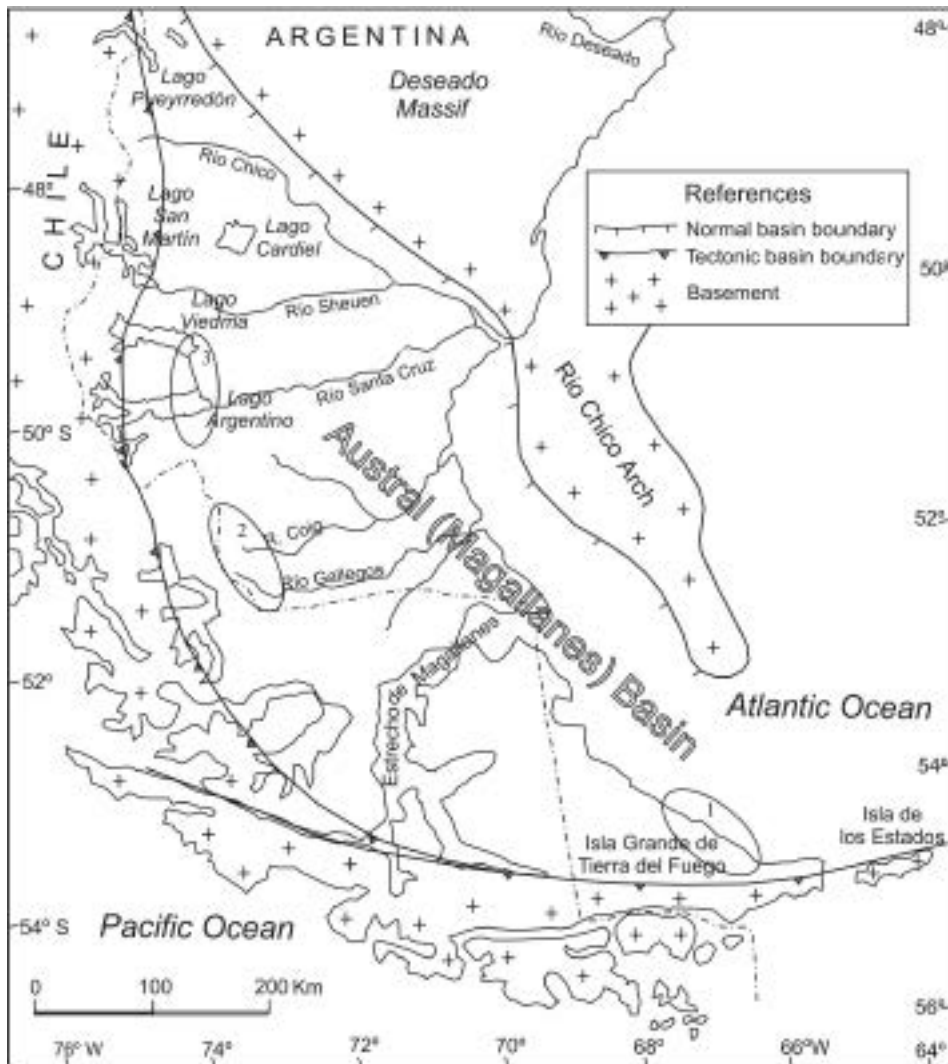
Antarctic Paleogene sedimentary rocks are only exposed around the northern part of the AP, on the South Shetland Islands and on the James Ross Island Group (Fig. 1). They were deposited in very different tectonic settings and environments. The South Shetland sequence represents an outer-arc (Birkenmajer, 1995) or fore-arc (Elliot, 1988) succession composed mainly by terrestrial volcanic and sedimentary deposits. By far, the most complete and well understood James Ross sequence is made up of marine clastic rocks deposited within a back-arc basin (Elliot, 1988; Hathway, 2000).





Tertiary deposits in SSA accumulated during the foreland stage of the Austral or Magallanes Basin (Fig. 2). Nowadays, these strata crop out in southernmost Argentina (Santa Cruz and Tierra del Fuego provinces) and Chile and are also present in the subsurface to the East. During Tertiary times, uplift and shortening occurred along the western and southern edges of the basin related to the development of the Patagonian Andes fold and thrust belt.

The aim of this contribution is therefore to review and summarize the available information about Paleogene rocks cropping out on the AP and southernmost Argentina (SSA), and to set up a correlation scheme between these regions in order to facilitate future comparative research.



Two separated Antarctic areas will be treated here: the King George Island (South Shetland Islands) and the Seymour Island (James Ross Archipelago) areas (Fig.1).

King George and the neighbour Nelson Island consist of several tectonic blocks bounded by two systems of strike-slip faults of Tertiary (54-21 Ma) age (Birkenmajer, 1989). Paleogene rocks of the Fildes Peninsula area were grouped into the Fildes Peninsula Group (Hawkes, 1961; Barton, 1965) composed of Campanian to uppermost Oligocene or earliest Miocene subalkaline volcanic rocks and plant bearing volcanoclastics. Based on lithologic, biotic and volcanic characteristics Shen (1995), subdivided this Group into five formational units named Half Three Point (Late Cretaceous), Jasper (Paleocene), Agate Beach (Paleocene), Fossil Hill (Eocene), Block Hill (Eocene) Formations and Suffield Point Volcanics (Miocene). The Kraków block comprises olivine-basalt and andesite lava

flows of the Maastrichtian-Eocene (74-42 Ma) Mazurek Point Formation (Birkenmajer, 1980 a,b); Dingle et al., (1997) and Dingle & Lavelle (1998) revised the chronology of Late Cretaceous-Cenozoic cryogenic strata from northern Antarctic Peninsula. These authors proposed that the King George Island Paleogene sequence represent a pre-glacial period followed by a glacial ("Polonez" c.a. 29.3 Ma) event separated by one interglacial ("Wawel") from the early Neogene "Melville" glaciation. The Warszawa block contains the most complete Paleogene sequence represented by the upper part of the King George Island Supergroup (Birkenmajer, 1980 a, b) ranging from Maastrichtian to uppermost Oligocene or earliest Miocene. A particularly complete, nearly continuous section of Early Cenozoic stratiform volcanic-sedimentary complex (Ezcurra Inlet and Point Hennequin groups, sensu Barton, 1965) is exposed between the Bransfield strait and the Ezcurra-Martel inlets. The Ezcurra Inlet Group (Barton, 1965; Birkenmajer, 1980 a, b) consists of two formations. The oldest one, the Paleocene-Eocene Arctowski Formation of Shen (1995) is made up of basalt and andesite lava flows, flow breccias, tuffs and fine to coarse-grained clastic sedimentary rocks with plant remains and coal seams. The youngest unit, the Late Eocene Point Thomas Formation of Shen (1995) consists of basaltic-andesitic lava and pyroclastic complex with explosion breccias. The Oligocene Point Hennequin Group (Barton, 1965; Shen, 1995) is made up of andesite and trachyandesite lava flows with two plant-bearing volcanoclastic intervals.

In the James Ross Basin (del Valle et al., 1992) the Paleogene record is represented by the uppermost 25 to 90 meters of the 1000 meters thick Maastrichtian- Danian López de Bertodano Formation (Sadler, 1988; Marenssi & Santillana, 1999). It is covered by the 255 meters thick, unconformity-bounded, Danian Sobral Formation (Santillana et al., 1999). The Upper Paleocene Cross Valley Formation (Elliot & Trautman, 1982) is another unconformity-bounded sedimentary unit 160 m thick. It fills up a narrow and deep scour or canyon cut down into the Marambio Group beds. Finally, the Early Eocene to latest Late Eocene La Meseta Formation (Elliot & Trautman, 1982) is another unconformity-bounded unit (La Meseta Alloformation of Marenssi et al., 1998a).

The southeastern Atlantic margin of Tierra del Fuego (Fig.2.1) exposes excellent outcrops of Late Cretaceous-Paleogene foreland deposits. The approximately 50 m thick Rio Bueno Formation rests on an angular unconformity upon Campanian strata. This unit was dated as late Paleocene based on their nanoflora and benthic foraminifers (Olivero & Malumian, 1999). The Eocene La Despedida Group (Olivero & Malumian, 1999) comprises 1600 meters of mudstones and sandstones. This group was subdivided into the middle Early Eocene Punta Torcida, Middle Eocene Leticia and latest Middle Eocene to Late Eocene Cerro Colorado formations (Olivero & Malumian, 1999). The Cerro Colorado Formation may be correlative with part of the Rio Turbio and Man Aike formations in the Santa Cruz Province (Olivero & Malumian, 1999). Subhorizontal mudstones and sandstones of the Cabo Peñarío Leona formations (Olivero & Malumian, 1999) unconformably cover the La Despedida Group. These units represent a marine to non-marine complex of latest Eocene-Oligocene age (Malumian & Nañez, 1989).

In the Río Turbio area (Fig.2.2), the 550 m thick Cerro Dorotea Formation (sensu Hunicken, 1955) contains foraminifers and nannoplankton that suggest a Danian age for the lower part (NP3 Zone) and an early Late Paleocene age for the upper interval of this unit (Malumian & Carames, 1997; Carrizo et al., 1990). The 600 m thick, coal bearing, Rio Turbio Formation (Hunicken, 1955; Archangelski, 1968) has been dated in different ways. Based on invertebrates, palynomorphs and microplankton this unit ranges from latest Early to early Late Eocene (Malumian & Carames, 1997; Camacho et al., 1998). Griffin (1991) describes the presence of *Venericor sp.* a worldwide Eocene guide fossil also present in the Middle Eocene Man Aike Formation (Camacho et al., 1998). Accordingly, the calcareous nannoplankton also suggests a Middle Eocene Age (Carrizo et al., 1990). According to Biddle et al. (1986) and Malumian & Carames (1997) the Rio Turbio Formation rests on top of a regional mid-Thanetian unconformity. The overlying 400 m thick Rio Guillermo Formation rests disconformably on the Rio Turbio Formation. Palynological studies suggest an Eocene age (Arguijo & Romero, 1981). According to its stratigraphic reconstruction Malumian & Caramés (1997) considered a Late Eocene age for this unit. Strata assigned to the 450 m thick Arroyo Oro Formation (Danderfer, 1982) comprise two lower intervals of continental origin (Rio Leona Formation of Malumian & Carames, 1997) and an upper marine member (Centinela Formation of Malumian & Carames, 1997). Its age has been discussed according to their correlation, stratigraphic position and

fossiliferous assemblages, ranging from Middle Eocene (Camacho et al., 1998) to latest Oligocene-Early Miocene (Malumian & Carames, 1997). Based on our observations in the Lago Argentino area we favor the second possibility.

In the Lago Argentino (Fig. 2.3) area the Middle Eocene Man Aike Formation unconformably rests on greenish sandstones of the latest Maastrichtian Calafate Formation (Marensi et al., 2002b). Subsurface samples of this unit also yielded microfossils of Middle Eocene age (Malumian, 1990; Concheyro, 1991). The 180 m thick Rio Leona Formation unconformably covers the Man Aike Formation at the southern margin of Lago Argentino (Marensi et al., 2000) and at the Cerro Fortaleza locality (Camacho et al., 1998). The age of this unit is not well constrained but similar beds at the Rio Turbio area were considered latest Eocene to Early Oligocene by Malumian (1990) and Nañez (1989). Marensi & Casadío (2002) indicated that the Rio Leona and Centinela Formations constitute a depositional sequence of Oligocene-early Miocene age.

Finally, the 160 m thick Centinela Formation is composed of mudstones, sandstones, coquinas and tuffs and contains a unique decapod fauna. Recent and unpublished  $^{87}\text{Sr}/^{86}\text{Sr}$  age determinations from oysters have shed minimum ages of 21.5 to 22 Ma (Early Miocene) and micropaleontological studies support an Oligocene-Miocene age for this unit (Casadío et al., 2000; Casadío et al., 2001).

In summary, at the present time there are only few key time intervals that may allow a detailed comparison of events from northern AP and southern SA:

The Paleocene upper López de Bertodano, Sobral and Cross Valley formations in the James Ross Basin and the Dorotea Formation in the Austral Basin.

The Eocene La Meseta Formation in Antarctica and the La Despedida Group, Río Turbio and Man Aike formations in southernmost South America.

Our future research tasks is therefore addressed to: 1) analyze these key units in order to get as much information as possible for comparison between the two studied areas; 2) try to fill the “blanks” in the chronostratigraphic chart.

## REFERENCES

- Archangelski (1968), *Ameghiniana* 5 (10): 406-416.
- Arguijo & Romero (1981), VIII Congreso geológico Argentino, *Actas* 4, 691-717.
- Barton (1965), *Scientific Reports, British Antarctic Survey*, 44: 1-33.
- Biddle et al. (1986), *International Association of Sedimentology, Special Publication* 8, 41-61.
- Birkenmajer (1980 a), *Bulletin de L'Académie Polonaise des Sciences, Serie des Sciences de la Terre*, 27 (1-2): 49-57.
- Birkenmajer (1980 b), *Studia Geologica Polonica*, 64: 7-65.
- Birkenmajer (1989), *Polish Polar Research*, 10: 555-579.
- Birkenmajer (1995), In: Srivastava, R.K. & R. Chandra (eds.), *Magmatism in relation to diverse tectonic settings*. Oxford & IBH Publishing Co. PVT. LTD. New Delhi. pp: 329-344.
- Camacho et al. (1998), *Revista de la Asociación Geológica Argentina*, 53: 273-281.
- Carrizo et al. (1990), *Segundo Simposio sobre el Terciario de Chile, Actas I*: 29-50.
- Casadío et al. (2000), *Reunión Anual de Comunicaciones. Asociación Paleontológica Argentina, Resúmenes* 9.
- Casadío et al. (2001), *Reunión Anual de Comunicaciones de la Asociación Paleontológica Argentina. Ameghiniana, Suplemento* 38 (4): 30R.
- Concheyro (1991), *Ameghiniana* 22(3-4): 385-399. Buenos Aires.
- Danderfer (1982), *Yacimientos Carboníferos Fiscales*, unpublished report N° 1168, 11p. SEGEMAR.
- Del Valle et al. (1992), *Antarctic Science*, 4: 477-478.
- Dingle & Lavelle (1998a), *Palaeogeography, Palaeoclimatology, Palaeoecology* 107: 79-101.
- Dingle et al. (1998b), *Journal Geological Society of London* 155: 433-437.
- Elliot & Trautman (1982), In C. Craddock (ed.), *Antarctic Geoscience*. Madison: University of Wisconsin Press: 287-298.
- Elliot (1988), In: R.M. Feldmann and M.O. Woodburne (Eds.), *Geology and Paleontology of Seymour Island, Antarctic Peninsula*. Geological Society of America, *Memoir* 169: 541-555.
- Griffin (1991), *Journal of Paleontology* 64 (3): 377-382.
- Hathway (2000), *Journal of the Geological Society* 157: 417-432.
- Hawkes (1961), *Scientific Reports of the Falkland Islands Dependencies Survey*: 26: 1-28.
- Hunicken (1955), *Revista del Instituto Nacional de Investigaciones en Ciencias Naturales, Ciencias Geológicas* 4: 1-161.
- Lawer et al. (1992), In: Kennet, J. & D. Warnke (eds.), *The Antarctic paleoenvironments: A perspective on Global Change*. American Geophysical Union, *Antarctic Research Series*, 56: 7-30.
- Malumian & Carames (1997), *Journal of the South American Earth Sciences* 10(2): 189-201.
- Malumian & Nañez (1989), *Revista de la Asociación Geológica Argentina* 43 (2): 257-264.
- Malumian (1990), *Revista de la Asociación Geológica Argentina* 45 (3-4): 364-385.

- Marensi & Casadío (2002), IX Reunión Argentina de Sedimentología, Córdoba, 2002. Resúmenes: 55.
- Marensi & Santillana (1999), IV Jornadas sobre Investigaciones Antárticas, Buenos Aires 1 al 5 de septiembre de 1997. II: 251-256.
- Marensi et al. (1994), Antarctic Science 6 (1): 3-15.
- Marensi et al. (1998), In S. Casadío (ed.): Paleógeno de América del Sur y de la Península Antártica. Asociación Paleontológica Argentina, Publicación Especial 5: 137-146.
- Marensi et al. (2000), II Congreso Latinoamericano de Sedimentología y VIII Reunión Argentina de Sedimentología. Mar del Plata, Marzo 2000. Resúmenes: 109-110.
- Marensi et al. (2002), Revista de la Asociación Geológica Argentina, 57 (3): 341-344.
- Olivero & Malumian (1999), AAPG Bulletin 83 (2): 295-313.
- Reguero et al. (1998), In: S. Casadío (Ed.), Paleógeno de América del Sur y de la Península Antártica. Revista de la Asociación Paleontológica Argentina, (Ameghiniana) Publicación Especial 5: 185-198.
- Sadler (1988), In R.M. Feldman y M.O. Woodburne (eds.), Geological Society of America, Memoir 169, 303:320.
- Santillana et al. (1999), IV Jornadas sobre Investigaciones Antárticas, Buenos Aires 1 al 5 de septiembre de 1997. II: 262-266.
- Shen (1995), In: Shen, Y. (ed.), Stratigraphy and palaeontology of Fildes Peninsula, King George Island, Antarctica. State Antarctic Committee, Monograph 3: 1-36. Science Press, Beijing.
- Stott, et al. (1990), In: P.F. Barker, J.P. Kennett, et al. (eds.), Proceedings of the Ocean Drilling Program, Scientific Results, Vol. 113: 849-863.

## **GEOMETRIES, DEFORMATION STYLES AND KINEMATICS OF THE FUEGINAN ANDES AND MAGALLANES FOLD-AND-THRUST BELT (TIERRA DEL FUEGO ISLAND)**

**1-09**

Marco Menichetti, Marco Cenni, Dario Gattini, Alberto Gaudio, Michele Mattioli

*Università di Urbino, URBINO - Italy*

Geological field surveys conducted in Tierra del Fuego Island in the Fueginan orogen and in the Magallanes fold-and-thrust belt carried out during the last years in the frame of the PNRA, give new insight of the geometries of the geological structures and the kinematic evolution of the region. The geological surveys were conducted at different structural levels, from the basement rocks to the sedimentary cover, from the hinterland to the foreland of the whole chain. The availability of remote-sensing data, aerial images, as well as new topographic maps, have helped the geological and structural surveys in the field.

Despite at least a century of geological studies in the Tierra del Fuego Island, the stratigraphy and relationship between the basement and the cover rocks are not well constrained in terms of lithology, thickness and age. The remoteness of the area and the absence of roads have limited the collection of geological information in the past. Data derived from isolate outcrops were often extrapolated to all the chain. Furthermore, the Argentina/Chile boundary, that vertically cuts the Island, has produced a different stratigraphic nomenclature.

The Fueginan orogen is the southernmost part of the 3800-km-long, N-S-trending Andean Cordillera. The geodynamic history of the Fueginan Andes from Late Cretaceous began with the shortening of back-arc basins by horizontal contraction and crustal thickening, with huge and widespread emplacement of magmatic bodies. The contraction involved and inverted the Upper Jurassic rocks and the extensional structures of the Rocas Verdes marginal basin. The collisional phase started in the Albian, and was probably related to major changes of plate drifts. The uplift of the Cordillera, the emplacement of plutonic rocks and the intracontinental polyphase deformation result from thick-skinned tectonics. In the Fueginan Orogen, a high grade metamorphic rock of the Upper Paleozoic to Lower Tertiary of the Cordillera Darwin and the Ophiolitic Complexes of the Rocas Verdes basin form the major stacks of the internal thrusts.

The Tierra del Fuego region, from a structural point of view, can be roughly subdivided, from south to north, in several WNW-ESE-trending physiographic provinces. The most internal province includes the Beagle Channel area, comprising partially the southern archipelago and its northern shore, with

the metamorphic core complex of the Cordillera Darwin. Here the oldest units, formally the metamorphic basement of the chain, comprise polydeformed medium to high-grade metasediment and metavolcanic rocks with garnet and amphibolites facies.

A second physiographic province comprises the Sierra Sorondo, the Valle Carbajal and the Sierra Alvear, that constitute the Fuegian Cordillera, characterized by NE-verging thrust complexes. The basement rocks – the schist and phyllites and the deformed mafic rocks outcropping here – are in prehnite-pumpellyite to greenschist metamorphic facies. The more external province is located north of Lago Fagnano, where the sediments of the SW part of the Magallanes foreland basin are involved in the deformation.

The geometry of the structures derived from at least three tectonic phases that affected the region since the Jurassic. The rates and style of the evolution of the mountain chain, with folding and thrusting at different structural levels, are the result of horizontal shortening and the resulting structures could be geometrically and kinematically linked. The grade of the deformation varies in intensity from ductile to brittle from internal zone to external foreland as well as from the lower to upper crustal levels.

The first tectonic phase, occurred in Late Jurassic to Early Cretaceous, is connected to the Rocas Verde marginal basin formation. This event produced large extensional structures, with NW-SE trending normal faults, with a throw of hundreds of meters and with the development of half graben basins few km wide. These structures are well displayed in the seismic reflection profiles both on-shore and in the Atlantic off-shore, while in the field they are represented by mafic dike swarms in the basement rocks and in the Yagan and Tobifera Fm.

The second and main tectonic phase, known as Andean phase, was mostly contractional and developed from the Middle-Late Cretaceous. It was responsible of the Cordillera formation with a thick-skinned tectonic style. Several basement wedges are thrust through the north in complex slices. This phase can be subdivided in two events: the first (Middle-Upper Cretaceous) produced folds and slate cleavage; the following, with folds and crenulation cleavage development, was associated with the formation and emplacement of NE-verging fold-and-thrust systems. These contractional events migrated from south-west to north-east and progressively involved in the deformation the Magallanes foreland basin.

The widest volcanic bodies are located in the core of the largest anticlinal structures and constitute the footwall of the major stacks of the thrust systems.

Penetrative structural fabrics are localized in the shear zones associated with main faults with presence, in some cases, of mylonitic deformation. At microstructural scale, the ductile kinematic indicators present a fabric with S-C mylonites, fractured and displaced feldspar grains, rotated porphyroclasts and mica fish. In the whole Meso-Cenozoic sedimentary succession, the orogenic shortening is produced by folds with different wavelengths. South of the Carbajal valley, recumbent synform structures are very common in the Sierra Sorondo as well as in the Sierra Alvear. The folds are tighter in the southern part and becoming wider through the north, with a WNW-ESE axes trend plunging few degrees to either quadrant. The axial planes dip to S and SW with different angles varying from few degrees in the overthrust folds to the subvertical in the disharmonic folds. Also the slaty cleavage is well developed in the southern part of the Island and affect also the sediments of the Magallanes basin north of the Lago Fagnano.

The later tectonic phase is related to E-W sinistral wrench tectonics especially in the southern part of the Island. This wrenching is the result of a vector component of the transform system between South America and the Antarctic Peninsula plates and could be related, from the Late-Oligocene, to the development of the oceanic floor in the western Scotia Sea. The main strike-slip fault in the region is the Magallanes-Fagnano system, which is constituted by several splays that are superimposed on the Andean structures. Other wrench faults allocated along E-W lineaments which present a significant morphological expression like narrow valleys and elongated fjords. Positive and negative flower structures are well displayed in many outcrops. The main structures are transtensional, with development of asymmetric and restricted pull-apart basins. They are constituted by several en-echelon segments with a ESE-WNW trend, connected with releasing side-step structures. The transtensional fault system includes sub-vertical structures with a cumulative offset of hundreds of meters. Deformation is mainly brittle, while the kinematic analysis indicates a prevalent left-lateral

transtensional component. These structures are superposed onto the older lineaments and suggest that they may have reactivated pre-existing weak zones, formed by Cretaceous-Tertiary shortening. In the western part of the Island, low-angle transtensional normal faults could be related to the general uplift of the region. The left-lateral strike-slip and normal faults in a Quaternary fluvio-glacial deposit along the main E-W lineament let us to consider the wrench tectonism still active.

## **TECTONICS OF THE SOUTHERNMOST ANDES: A COMPARISON BETWEEN THE PATAGONIAN AND THE FUEGIAN CORDILLERAS**

1-10

Victor A. Ramos

*Laboratorio de Tectónica Andina – F.C.E. y N - Universidad de Buenos Aires  
Ciudad Universitaria – Pabellón 2 – (1428) Buenos Aires – Argentina*

### **Abstract**

The southern Patagonian Andes share with the Fuegian Andes a similar metamorphic basement, but their Mesozoic and Cenozoic histories are quite different. The first important difference is the timing and orientation of rifting.

The early stage of rifting preserved in the Chon Aike magmatic province, well exposed in the Deseado massif, was mainly developed along west-northwest trends. The eruption of the Bajo Pobre flood basalts marked a period of extension and rapid fault-driven subsidence, rapid rift propagation into continental areas accompanied by major doming of rift flanks, and extrusion of flood basalts and intrusion of dikes and sills. During this Lower Jurassic flood basalt event there was a new kinematic regime established in the Deseado massif, with WNW fault-driven subsidence creating new depocenters almost perpendicular to older Permo-Triassic graben trends. This Early Jurassic extension did not occur through reactivation of the Triassic and old basement fabrics. New half graben structures thus formed persisted and received volcanic and clastic input during most of the Jurassic, and show the thickest accumulations on the southern side. The sporadic flood basalts represented an event of relatively short duration prior to 166-160 Ma. The Middle Jurassic Chon Aike Formation with thickness from 600 to 1,200 m, crops out across the entire Deseado massif and is composed of rhyolitic ash-flow tuffs (ignimbrites) with lesser agglomerates and pyroclastic breccias, scarce fine tuffs, and lavas associated with isolated rhyolite domes. This volcanic rocks filled half-graben systems with WNW-trending faults and occurred from about 166 Ma to 150 Ma. The volcanic activity widened westward to the Patagonian Cordillera more than 500 km across the region.

The age and the structural trend of these events point out to a northeast to southwest extension, which coincided with the opening of the Weddell sea, based on the study of recent magnetic and gravity data. It is important to remark that this time span and orientation is seen mainly in the southernmost Patagonian Cordillera, and the Fuegian Andes, as well as in the Malvinas plateau. North of the Malvinas escarpment, the age and trend of the rifting change to a north-northeast trend and is several millions years younger.

The second important difference is the magnitude of the Paleogene compression. The southernmost Patagonian Andes have important synorogenic deposits of Late Eocene age, fission track evidence of uplift in the Cordillera Darwin, and excellent growth strata of that age in the Fuegian Cordillera. This evidence is coherent with seismic data of the Malvinas basin where the inception of the first foreland basin developed during the Late Eocene.

On the other hand, the northern part of the Patagonian Cordillera lacks evidence of a conspicuous Paleogene deformation. This is closely correlated with the collision of the Aluk-Farallon oceanic ridge along the trench, south of 43°30'S.

A similar relationship is noticeable south of 46°30'S along the Patagonian Cordillera, where important tectonic uplift, orogenic shortening, and plateau basalts are indicating an important episode of ridge collision corresponding to the northward shifting of the Antarctic-Nazca ridge. The

southernmost Fuegian Andes does not record this episode as in the last 30 m.y. the continental margin at these latitudes was controlled by strike-slip deformation related to the east displacement of the Scotia plate.

As a result of all this ridge-collision heating, the southernmost Patagonian Andes record an outstanding uplift related to deglaciation rebound.

## SEISMIC IMAGING OF THE MAGALLANES-FAGNANO FAULT SYSTEM (TIERRA DEL FUEGO REGION)

1-11

Yagupsky D.<sup>1</sup>, Tassone A.<sup>1</sup>, Lodolo E.<sup>2</sup>, Menichetti M.<sup>3</sup>, Vilas J.F.<sup>1</sup>

1 *Instituto de Geofísica "Daniel A. Valencio", Universidad de Buenos Aires (Argentina)*

2 *Istituto Nazionale di Oceanografia e di Geofisica Sperimentale (OGS), Trieste (Italy)*

3 *Istituto di Geodinamica e Sedimentologia, Università di Urbino (Italy)*

The Magallanes Fagnano Fault System (MFS) is one of the principal tectonic lineament of the modern sinistral transform boundary between the South America and Scotia plates (Fuenzalida, 1972; Dalziel, 1989). This 3000 km-long boundary runs from the Antarctica-South America-Scotia triple junction in the vicinity of the Taitao Peninsula to the Tierra del Fuego Atlantic offshore, crossing the southernmost tip of South America along the Magallanes Strait, the Seno Almirantazgo (Winslow, 1982) and the northern margin of lago Fagnano (Klepeis, 1994; Lodolo *et al.*, 2002 a and b). It continues under the lineal depression of the Turbio and Irigoyen rivers (Lodolo *et al.*, 2002b), reaching the Atlantic shoreline in coincidence with the estuary of the Irigoyen river (Ghiglione, *et al.* 2002; Lodolo *et al.*, 2003). In the continental platform the MFS strikes E-NE (Lodolo *et al.*, 2002a and b; this work) and parallels the northern slope of both the North Scotia Ridge and the Burdwood Bank. It was proposed (Klepeis, 1994) that the present MFS might have undergone strike-slip movements before the Oligocene development of the transform boundary between the Scotia and South American plates along the North Scotia Ridge. Since Middle Cretaceous, the inner parts of Fueguinian Andes would have undergone transcurrent tectonics in the Beagle Channel region (Cunningham, 1993 and 1995), and other strike-slip lineaments, paralleling the MFS, are found in the Tierra del Fuego region. Herein we present new geophysical data which allow us to characterize the behavior of different segments of the MFS in the offshore areas within the Argentine platform. This new information is analyzed in combination with the available geological and geophysical data from the eastern (Burdwood Bank) and western regions (onland Tierra del Fuego). Four seismic profiles which traverse the strike of the MFS are shown in Fig. 1. Two principal pull-apart basins (Western and Eastern Basins, Fig. 1), associated with the MFS, were recognized: Both basins are strongly asymmetric and are bounded by a sub-vertical discontinuity which reaches the ocean floor. The sedimentary architecture of the two basins is similar, indicating a common tectonic evolution. Similar asymmetric basins are typically found along transform plate boundaries and displaying increasing sedimentary thickness towards the fault and normal-strike extension (Ben-Avraham, 1992).

The **Western Basin** is 6-km-wide; the MFS main fault is the northern boundary of the basin, and extends from the ocean floor to around 1.8 s twt and tilts the basal Paleogene unit. The upper Oligocene?-Miocene filling shows syn-extensional progressive unconformities (Fig. 1) resulting from the transtensional activity of the MFS in the area.

The **Eastern Basin** is about 80 km to the east of the Western Basin, and was crossed by two parallel seismic profiles. As revealed by the GSI-22 seismic line (Fig. 1), the Eastern Basin is around 9-km-wide with a sedimentary fill which reaches 3 s twt. The northern boundary is defined by a south-dipping, high-angle discontinuity which reaches the ocean floor, and interpreted as the main fault of the MFS. A set of subsidiary normal faults is also found, the deepest of which reaches 3.5 s twt under the central depocenter, and displaces the basal basin filling with an upper tip at 1.5 twt against an

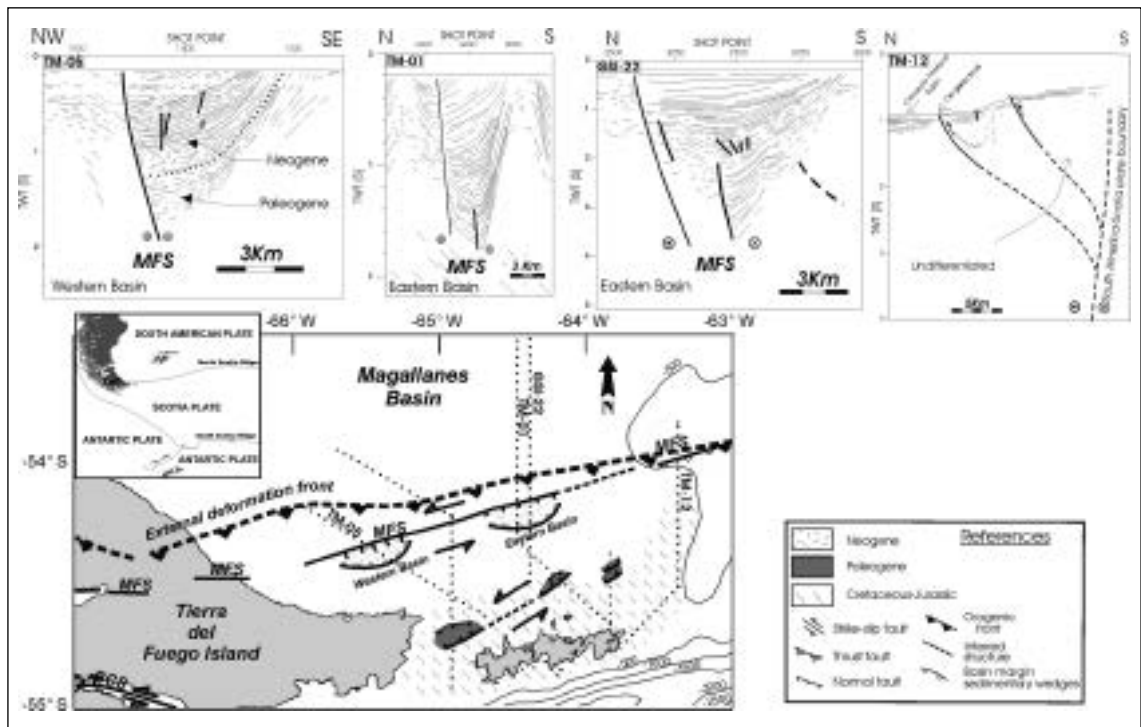


Fig. 1 - Simplified structural map of the studied area including bathymetry contours every 500 m. Dotted segments represent the grid of seismic tracks in the Atlantic Ocean. Submarine outcrops of interest are shown. Line-drawing of lines TM-05 (Western Basin) and TM-01 and GSI-22 (Eastern Basin) present transtensive structural arrays associated with the Magallanes-Fagnano fault system (MFS), whilst in profile TM-12 a transpressive array associated with this segment of the Scotia-South America plate boundary is seen.

T = Tertiary; BCS = Beagle channel system; TdF = Tierra del Fuego island.

unconformity. This unconformity separates a compressional phase (associated synclinal) from a syn-extensional sedimentation phase linked to the transtensional activity of the MFS. Therefore, the displacement locus changed during the basin evolution from the above described deepest direct fault to the main fault of the MFS. The TM-01 cross section (Fig. 1) exhibits features similar to the GSI-22, but in this case the vertical scale was exaggerated to accentuate some characteristics. Evidence of transtensional activity was also reported onland in Tierra del Fuego (Klepeis, 1994). The extensional features recognized along the MFS result from extensional overlaps among the MFS segments which reactivate discontinuities developed during the Upper Cretaceous-Tertiary compressive stage. The easternmost seismic profile (TM-12, Fig. 1) shows some striking differences in relation to MFS dynamics. Two high-angle emergent reverse faults produce a topographic high of about 0.5 s twt. This elevated area is interpreted as the result of a regional convergent curvature in the MFS which produced a transpressive deformation zone (Fig. 1). The northern slope of the Burdwood Bank, located 100 km to the east of profile TM-12, is also characterized by a set of Cenozoic thrusts branching from the plate boundary and defining the orogenic front (Ramos, 1996). Both blind and emergent Cenozoic north-verging thrusts were described in the northern slope whereas in the top of the Burdwood Bank a shallow piggy-back basin allowed the transport of the Tertiary-Quaternary sediments over the thrust slices. This tectonism would have evolved during the Late Oligocene to Miocene (Ludwig and Rabinowitz, 1982) due to the mainly transpressive transforming activity associated with the beginning of sea floor spreading in the Scotia plate (Ramos, 1996).

Therefore, we conclude that the interpreted structural pattern of profile TM-12 indicates a change in the plate boundary dynamics, which is transtensional to the west of  $63^{\circ} 30' W$  and transpressional eastwards (Fig. 1).

To the south of the MFS, some elongated extensional basin were recognized (Fig. 1), bounded by



high-angle normal faults. These faults reach 0.7 s twt, and involve Cretaceous units of the inner fold-and-thrust belt and bound isolated depocenters 5-10 km wide filled with Tertiary units (Paleogene?) affected in term by normal faults. These basins are inferred to be related to transtensional movements likely linked to extensional overlaps among fault segments. This interpretation is supported by the existence of similar structures located onland in Tierra del Fuego at the same latitude, i.e. in the Carabajal valley (Caminos *et al.*, 1981), and along the northern shoreline of the Beagle Channel (Cunningham, 1993, Caminos *et al.*, 1981), where evidence of sinistral strike-slip have been reported. The two offshore transtensional structure, likely diachronous, evolved in continuity with the Beagle Channel fault system and the MFS, in line with Cunningham's proposals (1993, 1995). This author suggested that the Beagle Channel sinistral fault system relates with the movements produced by the Antarctic Peninsula-South America separation during the Upper Cretaceous-Tertiary, whereas the MFS would have evolved later in relation with the western Scotia Sea Middle Tertiary evolution.

## REFERENCES

- Ben-Avraham, Z., 1992. Development of asymmetric basins along continental transform faults. *Tectonophysics*, 215: 209-220.
- Caminos, R., Haller, M., Lapido, J., Lizuain, O., Page, A. y Ramos, V., 1981. Reconocimiento geológico de los Andes Fueguinos. Territorio Nacional de Tierra del Fuego: VIII Congreso Geológico Argentino, (San Luis, Argentina), Actas 3: 759-786.
- Cunningham, W.D., 1993. Strike-slip faults in the southernmost Andes and the development of the Patagonian orocline. *Tectonics*, 12(1): 169-186.
- Cunningham, W.D., 1995. Orogenesis at the southern tip of the Americas: The structural evolution of the Cordillera Darwin metamorphic complex, southernmost Chile. *Tectonophysics* 244: 197-229.
- Dalziel, I.W.D., 1989. *Tectonics of the Scotia Arc, Antarctica, Field trip Guide, Vol. T180, 206pp.* AGU, Washington DC.
- Fuenzalida, R.H., 1972. Geological correlation between the Patagonian Andes and the Antarctic Peninsula and some tectonic implications. Master Thesis, 75 pp., Stanford Univ., Ca.
- Ghiglione, M.C., Ramos, V.A. y Cristallini, E.O., 2002. Estructura y estratos de crecimiento en la faja plegada y corrida de los Andes Fueguinos. *Revista Geológica de Chile*, 29 (1): 3-27.
- Klepeis, K.A., 1994. The Magallanes and Deseado fault zones: major segments of the South American-Scotia transform plate boundary in southernmost South America, Tierra del Fuego: *Journal of Geophysical Research* 99: 22001-22014.
- Lodolo, E., Menichetti, M., Tassone, A., Geletti, R., Sterzai, P., Lippai, H. and Hormaechea, J.-L., 2002a. Researchers target a continental transform fault in Tierra del Fuego. *EOS Transactions AGU*, 83 (1): 1-6.
- Lodolo, E., Menichetti, M., Tassone, A. and Sterzai, P., 2002b. Morphostructure of the central-eastern Tierra del Fuego Island from geological data and remote-sensing images. *European Geophysical Society, Stephan Mueller Special Publication Series*, 2: 1-16.
- Lodolo, E., Menichetti, M., Bartole, R., Ben-Avraham, Z., Tassone, A. and Lippai, H., 2003. Magallanes-Fagnano continental transform fault (Tierra del Fuego, Southernmost South America). *Tectonics*, 22(6): 1076: 15-1 to 15-26.
- Ludwig W.J. and Rabinowitz, P.D., 1982. The collision complex of the North Scotia Ridge. *Journal of Geophysical Research*, 87 (35): 3731-3740.
- Ramos, V.A. 1996. Evolución Tectónica de la Plataforma Continental. En: Ramos, V. A y M. A. Turic (Eds.). *Geología y recursos naturales de la plataforma continental argentina. Relatorio del 13 Congreso Geológico Argentino y 3 Congreso de Exploración de Hidrocarburos.* Buenos Aires. Asociación Geológica Argentina e Instituto Argentino del Petróleo, 385-404.
- Winslow, M.A., 1982. The structural evolution of the Magallanes Basin and neotectonics in the southernmost Andes. In: Craddock, C. (Ed.), *Antarctic Geoscience.* University of Wisconsin, Madison: 143-154.



## **Session 2**

---

**GEODYNAMIC AND  
TECTONICS**



**DEVELOPMENT OF ASYMMETRIC BASINS ALONG  
THE MAGALLANES-FAGNANO FAULT  
AND OTHER CONTINENTAL TRANSFORM FAULTS****2-01**

Zvi Ben-Avraham\*, Emanuele Lodolo\*\*

\* *Department of Geophysics and Planetary Sciences, University of Tel Aviv, Israel*\*\* *Istituto Nazionale di Oceanografia e di Geofisica Sperimentale (OGS), Trieste, Italy*

Many basins associated with wrench or transform faults are asymmetrical, both longitudinally and laterally; the sense of basin asymmetry changes along the strike of transform faults. Geophysical data from the Dead Sea fault, the Magallanes-Fagnano fault (Tierra del Fuego region), the Polochic fault (Guatemala) and other transforms, indicate that wrench-induced asymmetric basins are bounded on only one side by a transform fault. This implies that, during the evolution of such basins, maximum compression was parallel to the transform. The direction of extension can change during the geologic evolution of a basin.

A possible explanation of this observation takes the strength of the fault into consideration. In the case of a weak fault in a strong crust, the horizontal principal stresses would probably rotate to orientations parallel and perpendicular to the fault, thus minimizing the shear stress on the main fault.

The asymmetry in large transform basins may result from simultaneous strike-slip motion and fault-normal extension. Periods of oblique extension can alternate with periods of orthogonal extension. The asymmetry formed during periods of oblique extension is often preserved in the stratigraphic record.

The Magallanes-Fagnano continental transform system represents a major segment of the South America-Scotia plate boundary in the Tierra del Fuego region. It runs from the Atlantic offshore to the westernmost arm of the Magallanes Strait, and traverses broadly E-W the entire Isla Grande, the main island of Tierra del Fuego. A significant part of the fault trace is hidden by the Lago Fagnano, a 105-km-long, mostly asymmetric pull-apart basin developed within the principal displacement zone of the fault system. Geological and geophysical data acquired in the last four years along most of the length of the fault have imaged with unprecedented detail the surface and sub-surface structure of the transform system and its associated basins. The Magallanes-Fagnano fault system is composed of distinct tectonic lineaments arranged in an *en-echelon* geometry and is represented by mostly near-vertical faults. In the Atlantic sector, the fault system seems to be composed by a single master fault, along which a highly asymmetric basin has formed. At around 63°W, the fault terminates by splaying into secondary normal faults that dissipate the horizontal displacement along the system. In the central-eastern part of Isla Grande, the fault segments have been principally identified from analyses of remote-sensing images where their morphological expression is very well discernible. These segments are located within river valleys and are generally associated with localized gravity minima. Restraining bends and overlapping step-over geometry characterize the central part of the Magallanes Strait. In the Pacific entrance of the Magallanes Strait, asymmetric sedimentary basins have also developed.

Surprising morphological, structural and tectonic analogies have been found in other continental transform systems, and in particular in eastern Guatemala, where the seismically active Polochic and Motagua faults mark a significant part of the North America-Caribbean plate boundary. These tectonic lineaments, running broadly ENE-WSW, are located along wide river valleys bordered by elongated and steep mountain chains. Structural data analyses and geophysical evidence have shown that the tectonic nature of the Polochic fault is mainly transtensional in its eastern part, whereas is mostly transpressional to the west. This regime is responsible for the development of the rhomboidal pull-apart basins, like the Lago de Izabal, and wide depressions, like the Motagua valley in eastern Guatemala. Contractual structures (push-ups) characterize these transform systems in central Guatemala. Locally, restraining- and/or releasing-bend configuration determines the presence of related geological features like pressure ridges and rhombo-shaped basins.

Among the common characteristics of both transform systems (Magallanes-Fagnano and Polochic-Motagua), their gently curved trend, the presence of a subduction trench in their westernmost

termination, the formation of large and elongated lakes within the principal displacement zone of the faults, the highly asymmetric configuration of their sedimentary fill. Interesting similarities also exist with the Dead Sea fault. Several asymmetric basins exist along this fault. They are usually divided into distinct segments similar to the situation with the Magallanes-Fagnano. The sense of the asymmetry changes along the fault, a common feature to other continental transforms. The sedimentary architecture in basins along all these continental transforms, in which the thick end of the depositional wedge abuts the transform segment, suggest simultaneous strike-slip motion and transform-normal extension.

## PLATE KINEMATICS OF THE ANTARCTIC PENINSULA

2-02

R. Dietrich, A. Rülke

*Technische Universität Dresden, Institut für Planetare Geodäsie, D-01062 Dresden, Germany  
contact: dietrich@IPG.geo.tu-dresden.de*

### Abstract

Since 1995 up to present time GPS Campaigns were carried out every austral summer in the frame of the Standing Scientific Group on Geoscience of the Scientific Committee on Antarctic Research (SCAR).

Data acquired during 1995 to 1999 were analysed with the Bernese Software 4.2 and the results have been used to contribute a regional densification solution to the International Terrestrial Reference Frame (ITRF). For this purpose the resulting SINEX files were submitted to the IERS in Paris as a regional densification solution for the ITRF2000 (Altamimi et al., 2002). Thus the ITRF2000 solution provides an excellent information on Antarctic neotectonics (Fig. 2).



Fig. 1 - GPS observations during the SCAR1998 Epoch GPS Campaign at the Argentine base San Martin. The white GPS antenna can be seen in the picture, while the GPS receiver is outside of the display window.

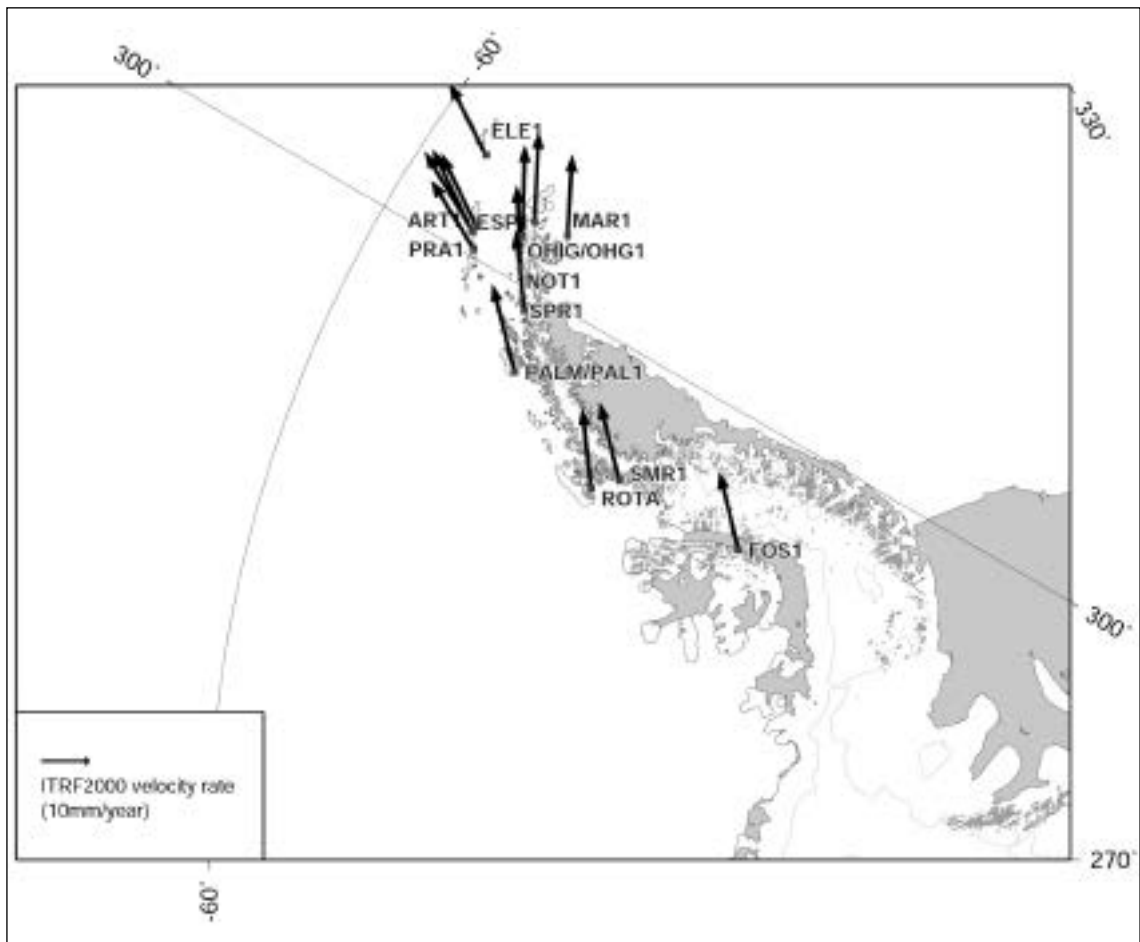


Fig. 2 - Horizontal velocity rates of the ITRF2000 solution at the Antarctic Peninsula

Since 1999 the SCAR GPS Campaigns have been continued up to present time. We will present new computations which include this additional data up to 2004. The new analyses was performed with the Bernese Software, Version 5.0.

We will compare the new results with the ITRF2000 solution. The obtained station velocities shall be used to set a special focus on the neotectonics of the Antarctic Peninsula and its neighbouring plates. The results demonstrate the potential of these campaigns based on GPS measurements over a 10 year time span.

## REFERENCES

- Altamimi, Z., P. Sillard and C. Boucher: A new release of the International Terrestrial Reference Frame for earth science applications. *J. Geophys. Res.* 107 (B10), 2214, doi:10.1029/2001JB000561, 2002.
- Dietrich, R., R. Dach, G. Engelhardt, J. Ihde, W. Korth, H.-J. Kutterer, K. Lindner, M. Mayer, F. Menge, H. Miller, C. Müller, W. Niemeier, J. Perl, M. Pohl, H. Salbach, H.-W. Schenke, T. Schöne, G. Seeber, A. Veit and C. Völksen: ITRF coordinates and plate velocities from repeated GPS campaigns in Antarctica - an analysis based on different individual solutions. *Journal of Geodesy* 74 (11/12), pp. 756-766, 2001.
- Dietrich, R. and A. Rülke. Plate Kinematics and Deformation Status of the Antarctic Peninsula based on GPS. *Global and Planetary Change*. In Press.

**BREAKUP OF GONDWANA AND OPENING OF THE SOUTH ATLANTIC:  
REASSESSMENT BASED ON MAGNETIC ANOMALIES****2-03**Marta E. Ghidella<sup>1</sup>, Lawrence A. Lawver<sup>2</sup>, Lisa M. Gahagan<sup>2</sup><sup>1</sup> *Instituto Antártico Argentino, Cerrito 1248, 1010 Buenos Aires, Argentina.**Fax: +54 11 4813 7807 Email: mghidella@dna.gov.ar*<sup>2</sup> *Institute for Geophysics, University of Texas at Austin, 4412 Spicewood Springs Road #600  
Austin, Texas 78759-8500 U.S.A. Fax: +1-512-471-0433 Email: lawver@ig.utexas.edu*

The opening history of the Weddell sea is critical to understanding the breakup of Gondwana and the evolution of Antarctica since Early Jurassic times. The dispersal of the Gondwanide fragments is important to understanding the development of past ocean circulation. Unfortunately the tectonics of the Weddell Sea region is difficult to resolve because of the paucity of data coverage and the region's inherent complexity. Although considerable progress has been achieved in the past 15 years with new marine aeromagnetic data and satellite derived gravity anomaly maps, there are still several models which differ in crustal ages and schemes of opening.

Seafloor spreading magnetic anomalies are not uniquely identified in the Weddell Sea for the time between breakup and Chron 34 (83.5 Ma; Gradstein et al., 1994). The discrepancy is particularly bad for anomalies older than M0 (120.4 Ma; the older end of the Cretaceous Normal Super Chron) with even the identification of M0 not well known in many areas. Thus there are big uncertainties from breakup until after the time when the South Atlantic began to open. If seafloor spreading in the Weddell Sea started at about the same time as between Africa and Antarctica, as recorded in the conjugate sets of M-series marine magnetic anomalies off Dronning Maud Land (Bergh, 1987) and in the Mozambique Basin, then the earliest flowline trends in the Weddell Sea should presumably have the same poles of rotation as those further east, if a simple two-plate breakup took place.

The present day Southern Ocean is shown in Figure 1 from the Weddell Sea in the southwest to the Mozambique Basin in the northeast. South of Africa there are two prominent fracture zone [FZ] trends, the Du Toit FZ and the Andrew Bain FZ, which appear to be "small circle aligned" with trends in the Weddell Sea: both the C34 isochron and the gravity anomaly T. However, these Southwest Indian Ridge FZs were created after the South Atlantic opened. South of these FZs, on older crust, the separation between Antarctica and West Gondwana began and the alignment should be found. This is a difficult area with little correlateable magnetics data. Should the flowlines in this area follow the Du Toit and Andrew Bain (and also Astrid Ridge, in the Riisen Larsen Sea) fracture zones trend or was there a third plate in the initial breakup of Gondwana?

Ghidella and Lawver (1999) worked on a model based on the rotation poles of the PLATES program (<http://www.ig.utexas.edu/research/projects/plates/plates.html>) and the reconstruction of Gondwana is provided by Lawver et al. (1999). A study of the flowlines generated by the movement of the major plates, South America (SAM), Africa (AFR) and Antarctica (ANT) with poles resulted in a two phase opening for the Weddell Sea that was first suggested by Lawver et al. (1985). The first phase was an opening in a NE-SW direction with respect to the present position of Africa and is compatible with the passive, non volcanic morphology of the eastern margin of the Antarctic Peninsula, and with the seafloor spreading character of observed NNE-SSW striking lineations in the Weddell Sea (Kovacs et al., 2002). For the second phase, an average N-S directed movement results between 132 Ma and C34 and later, coeval with initial opening in the South Atlantic.

Jokat et al. (2003) presented a new model based on aeromagnetic data collected along the East Antarctic coast during five seasons. These data cover important gaps in critical areas: the Lazarev Sea and the Dronning Maud margin, as well as part of the Riiser-Larsen Sea. The new data and a revised interpretation of the magnetic anomalies in the Riiser-Larsen Basin off Dronning Maud Land report the oldest identified magnetic anomaly as M24An (153.08 Ma) in the Riiser-Larsen Sea, confirming the models proposed by Bergh (1987) and Roeser et al. (1996) although differing in detail. The results indicate that the earliest spreading direction in the area was not as oblique as previously suggested until 150 Ma. In the Lazarev Sea zone they find magnetic anomalies aligned to the margin, that they interpret to mean there has been no east-west spreading in the region offshore Dronning Maud Land. With these new data and other informations we present a scenario for two plate Gondwanide rifting



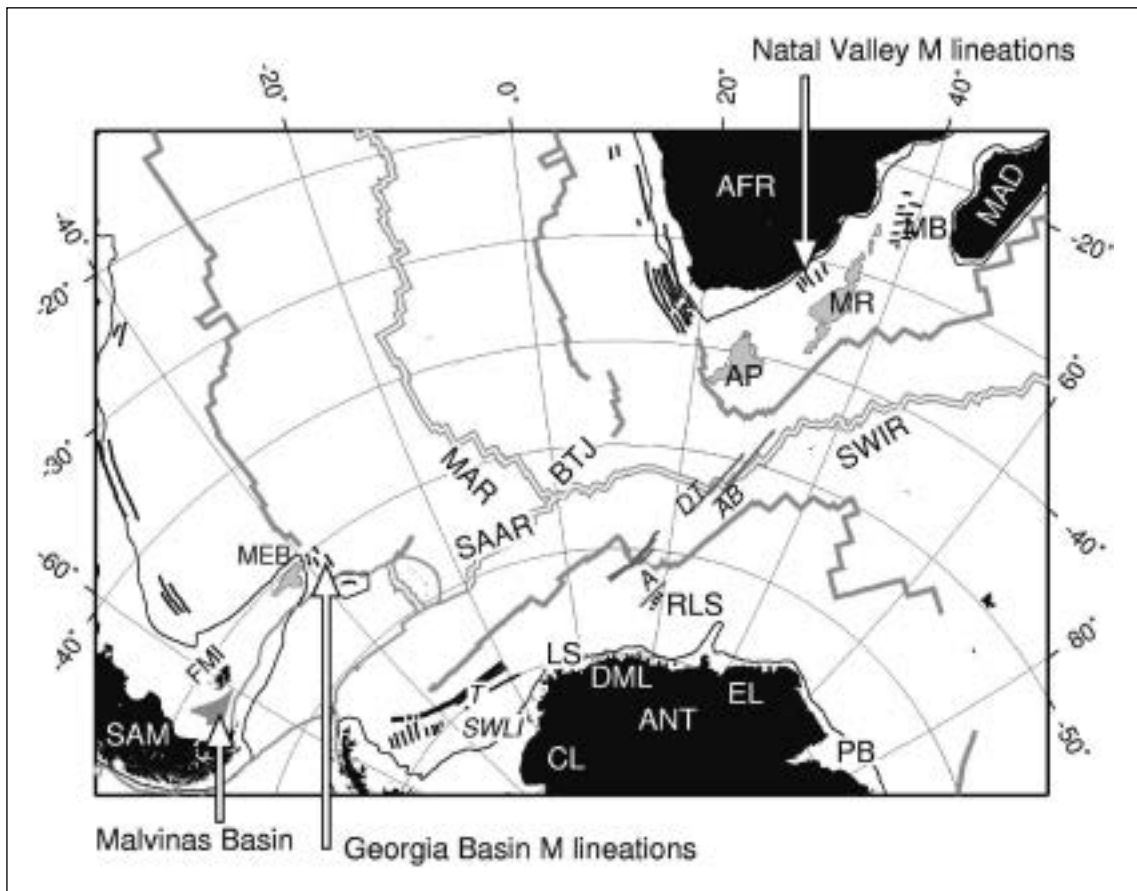


Fig. 1 - Present day main features of the Antarctica, South America and Africa spreading systems. Some detail is included in the Weddell Sea, as the gravity anomaly T and the magnetic south west striking lineations (SWLI). The Mesozoic lineations from Cande et al. (1989) are plotted as bold black lines. Also shown are some particular fracture zones: Du Toit (DT), Andrew Bain (AB) and Astrid (A). Note that these fz's appear to be small circle aligned with anomaly T. The thick gray lines correspond to the 83.5 Ma isochron from AGEGRID (Müller et al., 1997). The present day spreading centers are represented by a double gray line. Conjugate M anomalies in the Natal Valley and Georgia Basin are pointed at by arrows, as well as the Malvinas Basin, a possible site for a Jurassic aborted rift. AFR: Africa; ANT: Antarctica; AP: Agulhas plateau; BTJ: Bouvet Triple Junction; CL: Coats Land; DML: Dronning Maud Land; EL: Enderby Land; FMI: Falkland/Malvinas Islands; LS: Lazarew Sea; MAD: Madagascar. MAR: Mid Atlantic Ridge; MB: Mozambique Basin; MEB: Maurice Ewing Bank; MR: Mozambique Ridge; PB: Pridtz Bay; RLS: Riisen-Larsen Sea; SAAR: South American - Antarctic Ridge; SAM: South America; SWIR: Southwest Indian Ridge.

in Jurassic time that started in the southern/south-western Weddell Sea as well as off Dronning Maud Land and in the Mozambique Basin.

Particularly appealing from the work in Jokat et al. (2002) are the magnetic anomalies along a corridor that goes from about 18.5°W, 63.5°S to near the Dronning Maud coastline at about 8°W, as part of it traverses oceanic crust created from relative SAM-ANT motion. The oldest identified magnetic anomaly found along this corridor is M13n, which is 137.10 Ma in the Kent and Gradstein (1985) Geomagnetic Polarity Time Scale (GPTS) or M14n, 135.84 Ma in the Gradstein et al. (1994) GPTS, although M16n, M17n and M19n are indicated on Jokat et al. (2003)'s Figure 3. The implicated motion of SAM-ANT is very different from the ANT-AFR motion immediately to the east and hence a triple junction must have developed as coeval SAM-AFR movement was needed for closure. If these identifications are correct this would mean that the South Atlantic was already open or was beginning to open. The oldest magnetic anomaly identified in the Southern South Atlantic is M10n off the Falkland/Malvinas Plateau so any East-West anomaly in the southern Weddell Sea would imply the

establishment of a triple junction prior to 131.64 Ma. This time is coincident with eruption of the Parana/Etendeka flood basalts also taken by some as the initiator of opening of the South Atlantic. The initial breakup of Gondwana most probably resulted from the impact of a major plume at the junction of the African and Antarctic cratons. The ancestral Bouvet hotspot created a large region of thickened oceanic crust now represented by the Falkland/Malvinas Plateau, the Mozambique Plateau and the Weddell Sea Embayment, as well as the flood basalts in the region of the Karoo Basin. Together with the formation of the long linear dykes seen as the Ferrar dolerites, it may have been the key factor that broke apart the Gondwanide cratons, resulting in the separation of West Gondwana (Africa / South America) from East Gondwana (Antarctica / India / Madagascar / Australia). The track of a nearly fixed Karoo hotspot connects to Bouvet Island and comes very close to the southern Natal Valley, close in time to the opening age of ~M12 determined by Goodlad et al. (1982). While Goodlad et al. (1982) used the Larson and Hilde (1975) timescale their block model does not correspond to the Larson and Hilde model after M4 so their M12 identification will be reexamined.

In the period leading up to continental separation at 132 Ma, the South Atlantic region was affected by widespread rifting and the impact of a second mantle plume (Paraná –Etendeka) centered on Brazil and Namibia. Oblique extension on the margins of the future South Atlantic started about 135 Ma, just before impact of the Paraná -Etendeka plume at 132 Ma. One effect of early rifting is the formation of a number of basins on the Argentine shelf at high angle to the eventual continental margin. When the South Atlantic rift reached the northern edge of the Falkland/Malvinas Plateau, it shifted substantially eastward, where a nearly fixed Karoo hotspot would have been at ~135 Ma. Watkeys et al. (2002) report post-Karoo volcanism along the Lembobo monocline from 146 Ma until 133 Ma for the Bumbeni complex, at about 28°S, 32°E. It is located north of the South Tugela Ridge (Ben-Avraham et al., 1997) in the Natal Valley, and may support the idea that the Parana/Etendeka and Karoo mantle plumes influenced the rifting and spreading that left the Falkland/Malvinas Plateau as part of South America.

If there were east-west trending magnetic anomalies in the southern Weddell Sea as proposed by Jokat et al. (2003) (also LaBrecque and Ghidella, 1997, and older papers) prior to documented opening in the South Atlantic, then a different third arm of a triple junction must be proposed. One possibility for an early third arm of the triple junction (assumed RRR) is a failed arm. A possible location for a failed rift is the Malvinas Basin, which began to rift in late Jurassic (Galeazzi, 1996). While it does not seem to have had major or rapid subsidence at the very beginning, the three plate situation may not have started until later, ie. M19n (~143 Ma) or even M13n (135 Ma) if Jokat et al. (2003) speculations are correct.

## REFERENCES

- Ben-Avraham, Z., C.J.H. Hartnady, A.P. le Roex, 1995: Neotectonic activity on continental fragments in the South West Indian Ocean: Agulhas Plateau and Mozambique Ridge. *J. Geophys. Res.* 100, pp. 6199-6211.
- Bergh, H.W., 1987: Underlying fracture zone nature of Astrid Ridge off Antarctica's Dronning maud Land, *J. Geophys. Res.* 92, 475-484.
- Cande, S.C., J.L. LaBrecque, R.L. Larson, W.C. Pitman, X. Golovchenko, and W.F. Haxby, 1989: Magnetic lineations of the world's ocean basins, AAPG, Tulsa, OK, USA.
- Galeazzi, J. S., 1996: Cuenca de Malvinas. In V. A. Ramos, & M. A. Turic (Eds.), *Geología y recursos naturales de la plataforma continental Argentina* (pp. 273–309). XIII Congreso Geológico Argentino y III Congreso de Exploración de Hidrocarburos (Buenos Aires).
- Ghidella, M.E., L.A. Lawver, L.M. Gahagan, 1999: Insights into the Central Weddell Sea Herringbone Pattern from Gravity and Magnetism data. Poster presented at the VIII International Symposium on Antarctic Earth Sciences (Wellington, New Zealand), Abstracts Volume, p. 118.
- Goodlad, S.W., A.K. Martin and C.J.H. Hartnady, 1982: Mesozoic magnetic anomalies in the southern Natal Valley. *Nature* 295, 686-688.
- Gradstein, F.M., F.P. Agterberg, J.P. Ogg, J. Hardenbol, P. van Veen, J. Thierry, Z. Huang, 1994: A Mesozoic time scale. *J. Geophys. Res.* 99 B12, pp. 24051–24074.
- Jokat, W., T. Boebel, M. König, and U. Meyer, 2003: Timing and geometry of early Gondwana breakup, *J. Geophys. Res.*, 108(B9), 2428, doi:10.1029/2002JB001802.
- Kent, D.V., and F.M. Gradstein, 1985: A Cretaceous and Jurassic geochronology, *Geological Soc. Am. Bull.* 96, 1419-1427.
- Kovacs, L.C., P. Morris, J. Brozina, and A.A. Tikku, 2002: Seafloor spreading in the Weddell Sea from magnetic and gravity data, *Tectonophysics* 347, 43-64.
- LaBrecque, J.L., and M.E. Ghidella, 1997: Bathymetry, depth to magnetic basement, and sediment thickness estimates from aerogeophysical data over the western Weddell Basin, *J. Geophys. Res.*, 102, p.p. 7929-7945.
- Larson, R.L. and T.W.C. Hilde, 1975: A revised time scale of magnetic reversals for the Early Cretaceous and late Jurassic. *J. Geophys. Res.* 80, p.p. 2586-2594.

- Lawver, L.A., Sclater, J.G., and Meinke, L., 1985: Mesozoic and Cenozoic reconstructions of the South Atlantic. *Tectonophysics*, 114, pp. 233-254.
- Lawver, L.A., Gahagan, L.M. and Dalziel, I.W.D., 1999: Antarctica, Keystone of Gondwana, [www.ig.utexas.edu/research/projects/plates/movies/akog.ppt](http://www.ig.utexas.edu/research/projects/plates/movies/akog.ppt)
- Müller, R.D.; Roest, W.R.; Royer, J.-Y.; Gahagan, L.M.; Sclater, J.G., 1997: Digital isochrons of the world's ocean floor. *J. of Geoph. Res.* 102, (B2), pp. 3211-3214.
- Roeser, H.A., J. Fritsch, and K. Hinz, 1996: The development of the crust off Dronning Maud Land, East Antarctica. In: *Weddell Sea Tectonics and Gondwana Breakup*. Storey, B.C., King, E.C., Livermore, R.A. (eds.), Special Pub. No 108, Geol. Soc. of London, pp. 243-264.
- Watkeys, M.K., 2002: Development of the Lebombo rifted volcanic margin of Southeast Africa, in: *Volcanic Rift Margins*, (eds.) Menzies, M.A., Klempner, S.L., Ebinger, C.J., and Baker, J., Geological Society of America Special Paper 362, 27-46.

## **CRONOLOGY OF OROGENIC FRONT PROPAGATION IN THE FUEGUIAN FOLD-THRUST BELT**

**2-04**

Matías C. Ghiglione (\*, \*\*), Victor A. Ramos (\*\*), Eduardo B. Olivero (\*)

(\*) *Centro Austral de Investigaciones Científicas (CADIC – CONICET), Ushuaia, Tierra del Fuego.*

(\*\*) *Laboratorio de Tectónica Andina, FCEyN, UBA, Ciudad Universitaria C1428EHA, Buenos Aires, Argentina*

### **Summary**

The sequence of orogenic front migration in the Fueguian fold-thrust belt since the Late Cretaceous is established from a synthesis of structures, unconformities and distribution of synorogenic-units. The development of the Fueguian Andes is the result of three major episodes of thrusting: (1) Late Cretaceous, (2) Early Paleocene and (3) Lower to Middle Eocene. Other evidences in the southernmost Andes can be linked to these three deformation events to broadly characterize the behavior of the Fuegian orogenic wedge in terms of the critical taper models.

### **Introduction**

It is generally accepted that the Fueguian Andes propagated since the Late Cretaceous to the Neogene. However, the precise timing of the different structural phases and the relation between the uplift of the inner domain and the propagation of the deformational front remains uncertain.

New structural and sedimentological data were collected in the Fueguian fold-thrust belt by studying low tidal and cliff exposures along the Atlantic coast (Fig. 1). The data on structures, unconformities and distribution of synorogenic-unit in the external or thin skinned Fuegian fold-thrust belt were used to establish the chronology of orogenic front migration. To explain the development of the orogenic wedge, we adopted the symptomatic approach (DeCelles and Mitra, 1995) and the concept of migration of deformational fronts with the assumption that critical wedge theory (e.g. Davies et al., 1983) governs the overall behavior of the orogene. Likewise, data on time-space distribution of thrust faulting, erosion and sediment accumulation were used in combination with previously published data from the hinterland to qualitatively infer the state of the wedge (subcritical, critical or supercritical; DeCelles and Mitra, 1995) through time.

The studied cross section includes the Fueguian foreland fold-thrust belt, the Magallanes-Fagnano fault zone, the orogenic front and the Lower Miocene foredeep (Fig. 1). The stratigraphic units mentioned here include eight Formations (Fig. 2) (see Olivero and Malumián, 1999; Olivero et al., 2003 and references therein): 1) Bahía Thetis Formation (upper-Campanian – Maastrichtian); 2) Policarpo; 3) Tres Amigos Formation 4) Cerro Ruperto Formation (early Eocene); 5) Río Bueno Formation (lower-middle Eocene); 6) Punta Torcida Formation (early Eocene); Leticia Formation (Middle Eocene); 7) Cerro Colorado Formation (upper Middle Eocene-Oligocene); 8) Desdémona Beds (Lower Miocene).

## Unconformities

In the frontal limb of the San Vicente anticline the Tres Amigos Formation (late-Paleocene) rests in angular unconformity dipping 35°NW over the Policarpo Formation (Maastrichtian-Danian), which dips 60°NNW. This unconformity (“a” in Figs. 1 and 2) reflects the fact that the San Vicente anticline began its development immediately after the Danian; and reveals that over a short period of time between the Danian and the Late Paleocene, the Policarpo Formation was folded, eroded and covered by the Tres Amigos Formation.

In the Río Bueno sector, the gently deformed large amplitude folds of the Río Bueno Formation (lower-middle Eocene) lay upon previously folded and faulted Upper Cretaceous to lower Eocene rocks. In Ancla Point the Río Bueno Formation covers the Cerro Ruperto Formation through an angular unconformity (“b” in Figs. 1 and 2) that represents a maximum gap of about 2 Ma. The angular unconformity between the Río Bueno Formation and the Cerro Ruperto Formation reflects an orogenic front migration that took place around the Early to Middle Eocene boundary. The final deformation took place after the lower Middle Eocene deposition of the Río Bueno Formation.

The northern flanks of the Campo del Medio and Irigoyen anticlines are composed of unconformably bounded syntectonic sequences that show a decreasing dip up-section (Ghiglione *et al.*, 2002). These unconformities include: angular unconformities (“c” in Figs. 1 and 2) between the Punta Gruesa Formation (Lower Eocene) and the Leticia Formation (Middle Eocene); and progressive and syntectonic intraformational unconformities (“d” in Figs. 1 and 2) within the Leticia Formation.

In Punta Isleta crop-out a syntectonic intraformational unconformity (“e” in Figs. 1 and 2) within Late Eocene deposit of the Cerro Colorado Formation.

The younger syntectonic intraformational unconformity (“f” in Figs. 1 and 2) is located north of Punta Gruesa, within the Lower Miocene foredeep deposits.

In summary, we found the following unconformities in the geological cross-section along the Atlantic coast (Figs. 1 and 2): a) Late Maastrichtian–Danian/Paleocene: syntectonic angular unconformity in Tres Amigos Bay; b) Lower middle Eocene/ lower Eocene (maximum gap of about 2 Myr): syntectonic angular unconformity in Ancla Point. c) Lower Eocene/Middle Eocene: angular unconformities in Campo del Medio and Irigoyen anticlines. d) Middle Eocene: progressive unconformities and syntectonic intraformational unconformity in Campo del Medio and Irigoyen anticlines. e) Late Eocene: syntectonic intraformational unconformity in Punta Isleta. f) Mid Lower Miocene: syntectonic intraformational unconformity north of Punta Gruesa.

## Chronology of deformational front migration and state of the orogenic wedge

The evolution of the Fuegian Andes cycled between subcritical, critical and supercritical stages. The earliest orogenic stage in the late Cretaceous involved prograde metamorphism, uplift and development of topography within the rear of the orogenic wedge. The first episode of rapid exhumation and cooling of Cordillera Darwin took place between 90 and 70 Ma (Nelson, 1982; Kohn *et al.*, 1995) following the uplift of the Rocas Verdes Block located to the south (Nelson, 1982). During its initial uplift, Cordillera Darwin was transported northward by thrusting located at lower structural levels (Kohn *et al.*, 1995). However, there is not evidence showing thrust-propagation within the sedimentary cover during the Late Cretaceous. Apparently, the wedge began this first cycle in a critical stage and imbricate forward from the Rocas Verdes Block to the northern boundary of Cordillera Darwin. Afterward, the wedge became supercritical sliding northward along a basal decollement located in the lower structural levels of Cordillera Darwin. The first uplift and shortening of the rear of the wedge produced subsidence and aggradation in the foredeep; the wedge was subjected to regional erosion (marked by regional unconformities, see Biddle *et al.*, 1986) that ultimately caught up with tectonic thickening and caused the wedge to become subcritical and stall. After a second stage of uplift started in the hinterland at ~65 Ma (Kohn *et al.*, 1995), the basal decollement ramped upward and northward into weak Cretaceous and Paleocene shale. The first thrust-propagation that affected the foredeep deposits took place at ~60 Ma as shown by the angular unconformity within Early Paleocene units in Tres Amigos Bay. This fact reveals that the wedge became critical ~5 Myr after the initiation of the second cycle of basement thickening at 65 Ma, and

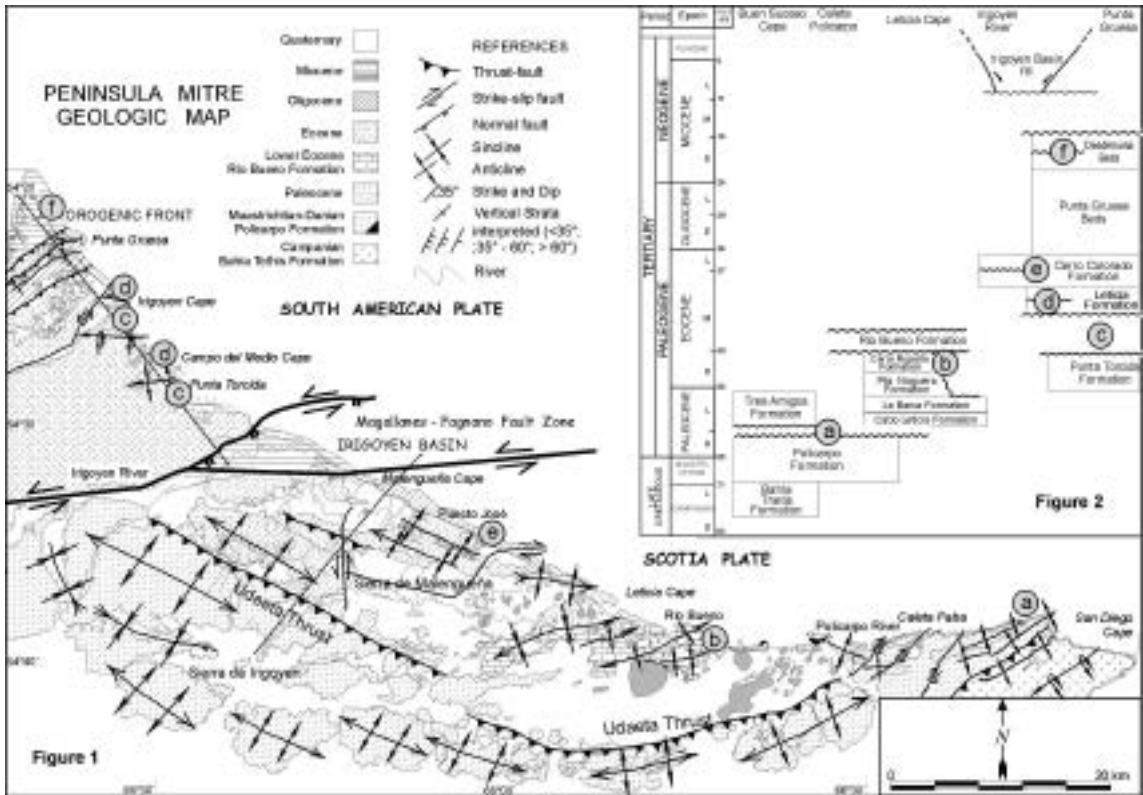


Fig. 1 - Structural map of the Peninsula Mitre based on field observation and photo-interpretation; after Ghiglione (2003).

Fig. 2 - Late-Cretaceous to Cenozoic stratigraphic columns for the Fuegoian Fold-Thrust Belt in Peninsula Mitre after Olivero and Malumián (1999); Olivero et al. (2003) and references therein.

propagated forward until Tres Amigos Bay. Through the early Eocene, the wedge remained subcritical and deformation became confined to the interior of the wedge.

The major orogenic front migration from Tres Amigos Bay to Irigoyen Cape took place in the Lower to Middle Eocene boundary as shown by multiple unconformities (b, c and d in Figs. 1 and 2). During this cycle of major thrust displacement (critical wedge), erosion ultimately caught up to the rate of uplift, and regional unconformities developed on top of the wedge. The wedge then stalled because its upper slope was no longer steep enough for critical taper, and a cover of sediment (lower Eocene to Oligocene deposits) was deposited atop the wedge as taper was rebuilt by the continuous shortening and uplift of the rear of the wedge.

Although the post-Eocene deformation is evidenced by the presence of Late Eocene and mid Lower Miocene syntectonic intraformational unconformities (e and f respectively in Figs. 1 and 2), out-of-sequence thrusts, and the post Middle Eocene tightening of the folds; there is not evidence showing a significant migration of the deformational front during the same period. Furthermore, the tectonic uplift of the inner sector stopped at ~38-40 Ma (Nelson, 1982; Kohn et al., 1995), marking the end of the Fuegoian Andes as a compressive orogenic wedge.

**REFERENCES**

- Biddle, K.T., et al., 1986, Int. Ass. of Sedim., Spec. Pub. 8, Blackwell Scientific Pub., pp. 41-61, London. 1986.
- Davis, D., Suppe, J., Dahlen, F.A., 1983, Journal of Geophysical Research 88, 1153-1172.
- DeCelles, P.G.; Mitra, G., 1995, Geological Society of America, Bulletin, 107: 454-462.

- Ghiglione, M.C., Estructura y Tectónica de la Costa Atlántica de Tierra del Fuego PhD Thesis, UBA 150 pp.
- Ghiglione, M.C., V.A. Ramos, E.O. Cristallini, 2002, Revista Geológica de Chile, 29, 17-41.
- Kohn, M.J., F.S. Spear, T.M. Harrison, I.W.D. Dalziel, 1995, Journal of Metamorphic Geol., 13, 251–270, 1995.
- Nelson, E.P., 1982, Journal of the Geological Society, 139, 755761.
- Olivero, E.B and N. Malumián, 1999, American Association of Petroleum Geologists Bull., 83, 295–313.
- Olivero, E.B., N. Malumián, S. Palamarczuk, 2003, Revista Geológica de Chile. Vol. 30, No. 2, p. 245-263.

## **TECTONIC AND GEODYNAMIC EVOLUTION OF THE SOUTH SANDWICH ARC AND EAST SCOTIA SEA**

**2-05**

Robert D. Larter

*British Antarctic Survey, High Cross, Madingley Road, Cambridge CB3 0ET, UK; r.larter@bas.ac.uk*

### **Introduction**

The South Sandwich arc and its associated back-arc basin in the East Scotia Sea are presently the most tectonically and seismically active parts of the Scotia Sea region. They have developed entirely during Neogene and Quaternary times and represent the latest stage in the ongoing eastward expansion of the Scotia Sea.

The South Sandwich arc is situated on the small, 'D'-shaped Sandwich Plate, which is overriding the southernmost part of the South American Plate at the South Sandwich Trench (Fig. 1). The convergence direction is ENE–WSW and the convergence rate at the trench increases from 67 mm/yr in the north to 81 mm/yr in the south (Thomas et al., 2003). To the west of the arc, the Sandwich Plate is separating from the larger Scotia Plate at the East Scotia Ridge (ESR) back-arc spreading centre, where the modern full spreading rate increases slightly from 63 mm/yr in the north to 69 mm/yr in the south (Livermore, 2003). Spreading has occurred at the modern rate for less than 2 Myr, having increased in a series of steps since the Middle Miocene (Larter et al., 2003). The relative simplicity of the tectonic setting and history of the South Sandwich subduction system make it an ideal natural laboratory in which to study tectonic and magmatic processes associated with subduction. Results from studies of this system may thus help in unravelling the tectonic evolution of subduction systems that have had a more complex history, like those in southern South America and the Antarctic Peninsula.

### **Previous Studies**

Until 1995 most of what was known about the South Sandwich arc and East Scotia Sea was based on fieldwork and research cruises carried out more than 20 years earlier. Geochemical studies of the island arc were mainly based on samples collected during an expedition in 1964 (Baker, 1978). Barker (1970) recognized that marine magnetic profiles collected during the 1960s provided evidence for E–W back-arc spreading in the East Scotia Sea since at least 8 Ma. Additional profiles collected during the 1970s revealed more of the extent of the back-arc basin and provided the basis for an analysis of spreading rate changes since 8 Ma (Barker & Hill, 1981). Geochemical studies of the ESR were, until recently, entirely based on just four dredge hauls collected from close to the spreading axis in 1974 (Saunders & Tarney, 1979).

### **Results of Recent Studies**

In 1995 the British Antarctic Survey started a new research project that focussed on the South Sandwich subduction system, the Sandwich Lithospheric and Crustal Experiment (SLICE). The aim was to carry out a range of investigations that would exploit the relative simplicity of the South Sandwich system to improve understanding of tectonic and magmatic processes associated with intra-oceanic subduction.

During the first phase of the project the HAWAII-MR1 towed sonar system was used to collect swath bathymetry and sidescan sonar data covering the entire ESR and a sector of the forearc and trench.

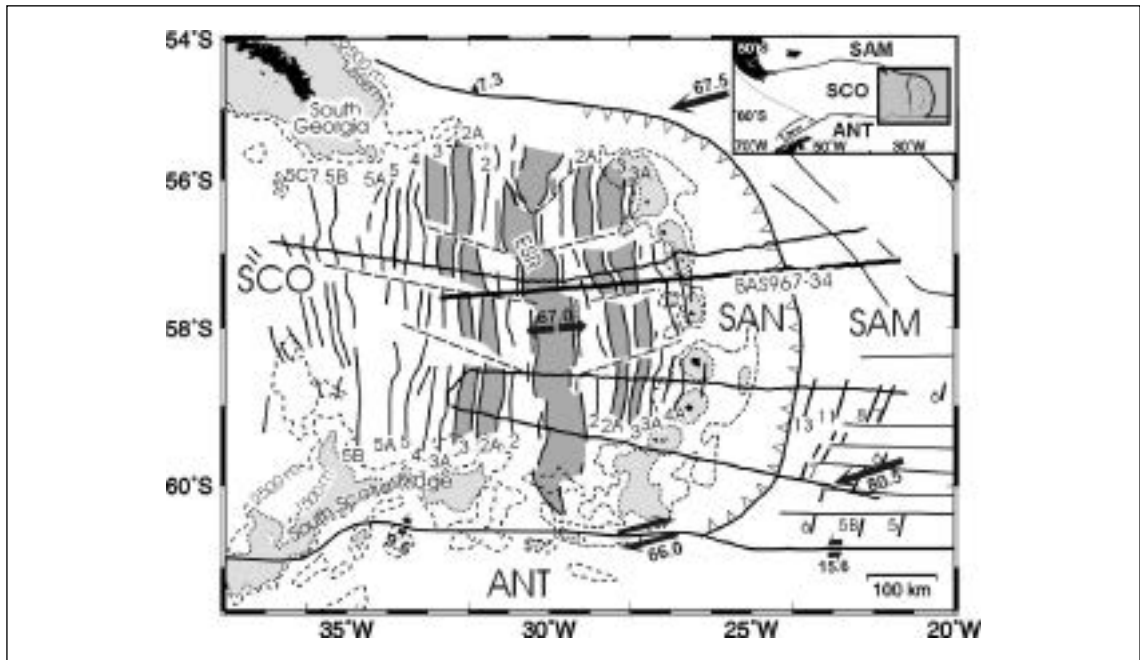


Fig. 1 - Location map showing the tectonic setting of the South Sandwich arc and East Scotia Sea, after Larter et al. (2003). Grey-filled box on inset shows location of main map. Magnetic lineations in East Scotia Sea and on South American Plate are labelled with chron number. BAS multichannel seismic lines are shown as solid lines, with line BAS967-34 (Fig. 2) marked by a thicker line. Arrows indicate vectors of relative plate motion, lengths being proportional to rates (annotated in mm/yr).

The data from the ESR revealed that it consists of nine segments separated by non-transform offsets, and showed systematic along-axis changes in ridge morphology that have been interpreted as being related to variations in magma supply caused by shallow mantle flow around the ends of the subducting slab (Livermore et al., 1997; Bruguier & Livermore, 2001). Subsequently, the sonar data were used to guide a sampling programme that provided supporting evidence for the inferred mantle flow pattern and also revealed along-axis variations in magma composition caused by addition of subduction components to the back-arc mantle (Leat et al., 2000; Fretzdorff et al., 2002, 2003; Livermore 2003).

New marine magnetic profiles collected during the course of the project, together with the discovery that the ESR contains no transform offsets, provided the basis for a re-evaluation of the back-arc spreading history. It is now clear that there has been organized sea-floor spreading in the East Scotia Sea since at least 15 Ma, making it the world's longest-lived extant back-arc basin (Larter et al., 2003). As organized spreading was probably preceded by a period of arc rifting, it now seems likely that the trigger for the start of East Scotia Sea extension may have been a change in the direction of South American–Antarctic relative motion at about 20 Ma.

Although marine magnetic profiles on the western flank of the ESR indicate a continuous record of back-arc spreading since 15 Ma, most of the South Sandwich island arc lies on crust formed on the eastern flank at about 10 Ma (Fig. 1). If back-arc extension was symmetrical following a transition from arc rifting to organized spreading at about 15 Ma, crust originally formed at the ESR extends 70–80 km east of the present arc (Vanneste & Larter, 2002; Larter et al., 2003). Back-arc spreading is usually initiated close to the line of a pre-existing arc, so the arc has probably migrated or jumped westward relative to the Sandwich Plate during the growth of the East Scotia Sea. Analyses of peridotites dredged from the trench-slope break 75–85 km ENE of the northernmost arc island suggest that there was an older arc to the east of the modern one (Pearce et al., 2000). The present arc–trench gap of 140–160 km is one of the narrowest among modern subduction systems, so if an earlier arc was situated to the east of the present arc it seems likely that a substantial part of the earlier

forearc has been removed by subduction erosion. If the arc has retreated by 80 km and the original arc–trench gap was the same as the modern one, the average rate of forearc slope retreat since 15 Ma has been 5.3 km/Myr (Larter et al., 2003).

Multichannel seismic profiles and earthquake catalogue data provide evidence of a mid-forearc zone of trench-normal extension. This has been interpreted as a consequence of large-scale gravitational collapse of the forearc slope related to ongoing subduction erosion (Vanneste et al., 2002). Earthquake catalogues also show that the magnitudes of the largest forearc earthquakes are low compared to most other subduction zones, suggesting that relatively low inter-plate stress may be factor contributing to gravitational collapse and subduction erosion.

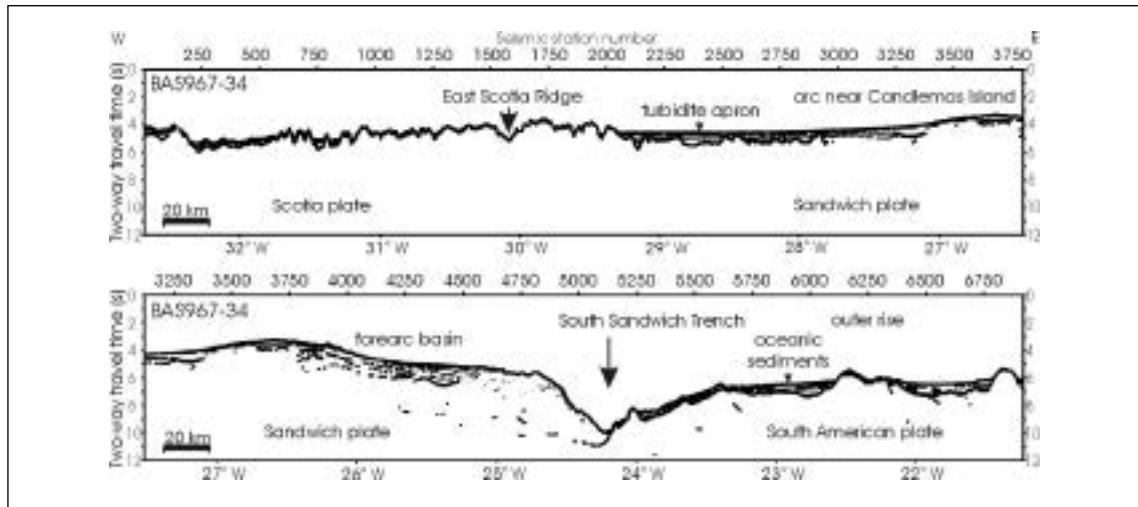


Fig. 2 - Interpreted line drawing of multichannel seismic reflection profile BAS967-34. Note that the two panels overlap by about 70 km. Vertical exaggeration at the sea floor is 8:1.

Seismic reflection, wide-angle seismic and gravity data collected during the SLICE project constrain the forearc frontal prism to be small (Fig. 2; Vanneste & Larter, 2002; Larter et al., 2003). Assuming the present trench sediment thickness is representative of the time-averaged thickness since 15 Ma, Vanneste & Larter (2002) calculated >95% of the sediment that has entered the northern part of the trench since 15 Ma must have been subducted.

Seismic and gravity data constrain the South Sandwich arc crust to be less than 20 km thick (Larter et al. 2003). The fact that the arc has been built on relatively young back-arc crust provides a basis for calculation of the crustal growth rate, which has been estimated to be 72 km/Myr for each km along the arc (Larter et al. 2003). This value is within the range of growth rates estimated for the Aleutian and Izu-Bonin arcs, which have been built over a much longer interval (Holbrook et al., 1999). Wide-angle seismic data indicate the presence of a mid-crustal layer with a seismic *P*-wave velocity of 6.0–6.5 km/s that is at least 2 km thick beneath the southern part of the arc. The velocity range of this layer suggests that it consists of plutonic rocks of intermediate–silicic composition. Volumetric and geochemical arguments indicate that the rocks in this layer were not produced by fractional crystallization, but are melts of amphibolitic arc crust (Leat et al., 2003).

## REFERENCES

- Baker, P.E., 1978. *The South Sandwich Islands: III. Petrology of the volcanic rocks*. British Antarctic Survey Scientific Reports, **93**, 34 pp.
- Barker, P.F., 1970. Plate tectonics of the Scotia Sea region. *Nature*, **228**, 1293–1296.
- Barker, P.F. & Hill, I.A., 1981. Back-arc extension in the Scotia Sea. *Philosophical Transactions of the Royal Society of London*, **A 300**, 249–262.



- Bruguier, N.J. & Livermore, R.A., 2001. Enhanced magma supply at the southern East Scotia Ridge: evidence for mantle flow around the subducting slab? *Earth and Planetary Science Letters*, **191**, 129–144.
- Holbrook, W.S., Lizarralde, D., McGeary, S., Bangs, N. & Diebold, J., 1999. Structure and composition of the Aleutian island arc and implications for continental crustal growth. *Geology*, **27**, 31–34.
- Fretzdorff, S., Livermore, R.A., Devey, C.W., Leat, P.T. & Stoffers, P., 2002. Petrogenesis of the back-arc East Scotia Ridge, Southern Atlantic Ocean. *Journal of Petrology*, **43**, 1435–1467.
- Fretzdorff, S., Haase, K.M., Leat, P.T., Livermore, R.A., Garbe-Schönberg, C.-D., Fietzke, J. & Stoffers, P., 2003.  $^{230}\text{Th}$ – $^{238}\text{U}$  disequilibrium in East Scotia backarc basalts: implications for slab contributions. *Geology*, **31**, 693–696.
- Larter, R.D., Vanneste, L.E., Morris, P. & Smythe, D.K., 2003. Structure and tectonic evolution of the South Sandwich arc. In: Larter, R.D. & Leat, P.T. (eds), *Intra-Oceanic Subduction Systems: Tectonic and Magmatic Processes*. Geological Society, London, Special Publications, **219**, 255–284.
- Leat, P.T., Livermore, R.A., Millar, I.L. & Pearce, J.A., 2000. Magma supply in back-arc spreading centre segment E2, East Scotia Ridge. *Journal of Petrology*, **41**, 845–866.
- Leat, P.T., Smellie, J.L., Millar, I.L. & Larter, R.D., 2003. Magmatism in the South Sandwich arc. In: Larter, R.D. & Leat, P.T. (eds), *Intra-Oceanic Subduction Systems: Tectonic and Magmatic Processes*. Geological Society, London, Special Publications, **219**, 285–313.
- Livermore, R., 2003. Back-arc spreading and mantle flow in the East Scotia Sea. In: Larter, R.D. & Leat, P.T. (eds), *Intra-Oceanic Subduction Systems: Tectonic and Magmatic Processes*. Geological Society, London, Special Publications, **219**, 315–331.
- Livermore, R., Cunningham, A., Vanneste, L. & Larter, R., 1997. Subduction influence on magma supply at the East Scotia Ridge. *Earth and Planetary Science Letters*, **150**, 261–275.
- Pearce, J.A., Barker, P.F., Edwards, S.J., Parkinson, I.J. & Leat, P.T., 2000. Geochemistry and tectonic significance of peridotites from the South Sandwich arc–basin system, South Atlantic. *Contributions to Mineralogy and Petrology*, **139**, 36–53.
- Saunders, A.D. & Tarney, J., 1979. The geochemistry of basalts from a back-arc spreading centre in the East Scotia Sea. *Geochimica et Cosmochimica Acta*, **43**, 555–572.
- Thomas, C., Livermore, R. & Pollitz, F., 2003. Motion of the Scotia Sea plates. *Geophysical Journal International*, **155**, 789–804.
- Vanneste, L.E. & Larter, R.D., 2002. Sediment subduction, subduction erosion and strain regime in the northern South Sandwich forearc. *Journal of Geophysical Research*, **107**(B7), 2149, 10.1029/2001JB000396.
- Vanneste, L.E., Larter, R.D. & Smythe, D.K., 2002. A slice of intraoceanic arc: insights from the first multichannel seismic reflection profile across the South Sandwich island arc. *Geology*, **30**, 819–822.

## AGULHAS PLATEAU, MAUD RISE AND NE GEORGIA RISE, PRODUCTS OF A TRIPLE JUNCTION?

2-06

Lawrence A. Lawver, Lisa M. Gahagan

*Institute for Geophysics, University of Texas at Austin, 4412 Spicewood Springs Road #600  
Austin, Texas 78759-8500, U.S.A. – Fax: +1-512-471-0433 – E-mail: lawver@ig.utexas.edu*

A new model for the opening of the South Atlantic combined with extrapolation of motion between Antarctica and Africa during the time of the Cretaceous Normal superchron (120.4 Ma to 83.5 Ma) leads to an interesting juxtaposition of three oceanic plateaux; Agulhas Plateau, Maud Rise and NE Georgia Rise. Gohl and Uenzelmann-Neben (2001) proved the oceanic origin of the Agulhas Plateau and related its formation to the Maud Rise and possibly to the Mozambique Ridge. They suggested the Bouvet hotspot as the cause of the excess volcanism. Kristoffersen and LaBrecque (1991) related the Agulhas Plateau to both the Northeast Georgia Rise and to Maud Rise. They suggested that at least part of the Northeast Georgia Rise was formed by excess volcanism at a spreading center. It appears that the three plateaux formed at or near a triple junction. Satellite gravity data from Sandwell and Smith (1997) have been digitized to give an approximation to the extent of the abnormal crust related to each of these plateau and plate velocities have been extrapolated for South America to Africa motion and for Africa to Antarctica motion to determine their locations in an absolute plate motion framework. The three plateaux are clearly overlapped prior to 102 Ma. The excess magmatism which formed them may have begun as early as 101 Ma and lasted until 96.5 Ma (Fig. 1) when the three plateaux are no longer coincident. Isolated volcanism may have continued on the southern tail of Agulhas Plateau until 90 Ma. During this period the Karoo/Bouvet hotspot track is significantly north of all of the plateaux. It is probable that excess volcanism at a transient Ridge-Ridge-Ridge triple junction produced the three plateaux that were then separated. Since there is no apparent hotspot track either leading to the plateaux or away from them other than a short tail on Agulhas Plateau, it is difficult to relate them to a long-lived hotspot or mantle plume.

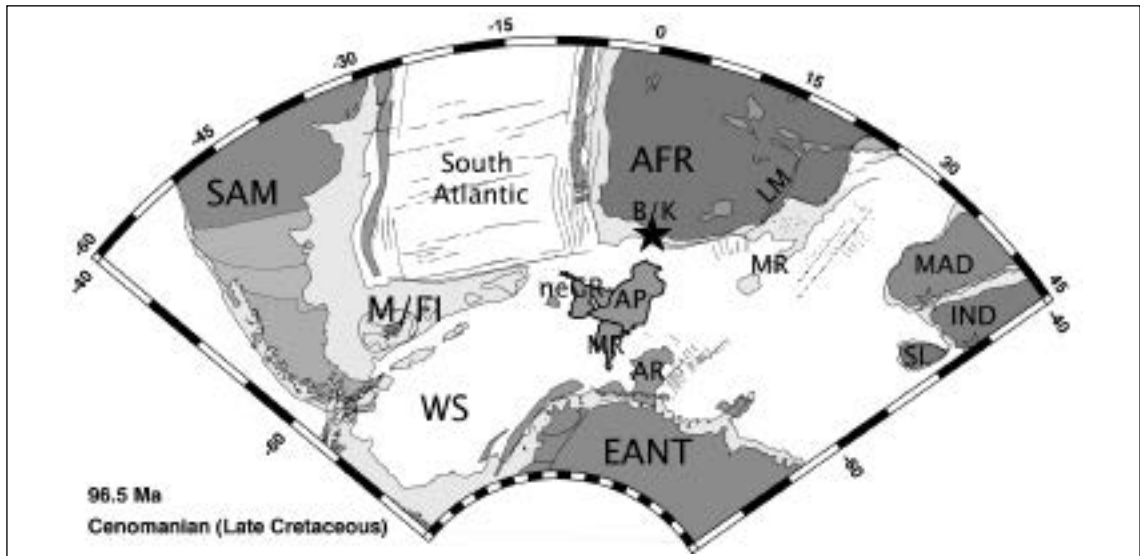


Fig. 1 - Reconstruction of the South Atlantic region at 96.5 Ma showing the adjacency of the Agulhas Plateau (AP), Maud Rise (MR) and the Northeast Georgia Rise (neGR). The black star is the location of a fixed Bouvet hotspot (B/K) at 96.5 Ma and closely correlates to the location of a fixed Karoo mantle plume. AFR = Africa, AR = Astrid Ridge, EANT = East Antarctica, IND = India, LM = Lebombo Monocline, MAD = Madagascar, M/FI = Malvinas/Falkland Islands, MR = Mozambique Ridge, SAM = South America, SL = Sri Lanka, WS = Weddell Sea. Continental material is darker grey color as are oceanic plateaux and seaward dipping reflectors. Satellite gravity lineations are coast orthogonal lines while coast parallel lines are marine magnetic anomalies.

## REFERENCES

- Gohl, K. and Uenzelmann-neben, G., 2001. The crustal role of the Agulhas Palteau, southwest Indian Ocean: evidence from seismic profiling. *Geophys. J. Int.* 144, 632-646.
- Kristoffersen, Y. and LaBrecque, J., 1991. 2. On the tectonic history and origin of the Northeast Georgia Rise. In: Ciesielski, P.F., Kristoffersen, Y. (eds.), *Proc. Of the Ocean Drilling Program, Scientific Results*, vol. 114, 23-38.

## SOUTH AMERICA - ANTARCTICA PLATE MOTION AND TECTONICS OF THE SOUTHERNMOST ANDES, SCOTIA SEA AND ANTARCTIC PENINSULA

2-07

Roy Livermore<sup>1</sup>, Graeme Eagles<sup>2</sup>, Peter Morris<sup>1</sup>, Adrian Nankivell<sup>1,3</sup>

1 *British Antarctic Survey, High Cross, Madingley Road, Cambridge, CB3 0ET, UK*

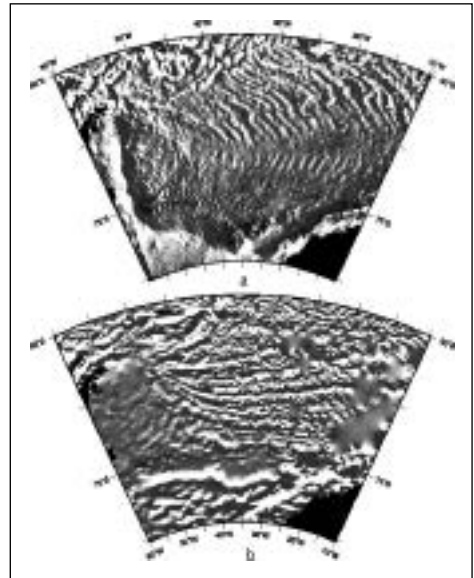
2 *Alfred Wegener Institute for Polar Research, Bremerhaven, Germany*

3 *Department of Earth Sciences, Oxford University, Parks Road, Oxford, UK*

Satellite-derived free-air gravity anomaly maps of the Weddell Sea reveal a remarkable pattern of curved, parallel lineations that has come to be known as the ‘herringbone pattern’ (Fig. 1a). These lineations record a history of motion between the South American (SAM) and Antarctic (ANT) plates since the Early Cretaceous, involving abrupt changes of direction and rate. Magnetic anomaly maps show a similarly striking pattern (Fig. 1b), and permit the dating of the events recorded by the gravity ‘flow lines’. However, the use of these data to calculate finite rotations for the SAM-ANT plate pair is handicapped by the loss of most of the northern flank of the spreading system by subduction beneath the Scotia Sea.

We applied new methods for extracting flow lines of relative plate motion from satellite free-air gravity anomalies, and combining these with magnetic anomaly picks from one or both sides of a spreading centre in a joint inversion for the best-fitting set of reconstruction poles and rotation angles. We used a compilation of available data from the Weddell Sea and South American – Antarctic Ridge

Fig. 1 - Weddell Sea free-air gravity (a) and magnetic (b) anomalies



to constrain SAM-ANT motion since chron C34 (83 Ma). Earlier motion is estimated by addition of published rotations in the circuit through the African plate (AFR).

Using our new rotations, we produced reconstructions of SAM relative to a fixed ANT at 10 Ma intervals from 160 Ma to the present (Fig. 2). In these maps, the continental edge of SAM is represented by the 3000 m isobath, which includes the Falkland Plateau, while the extent of the Antarctic Peninsula (ANP) is shown by the 2000 m contour. We have not attempted to apply corrections for deformation and shortening in the southernmost Andes. The western and central domains of ANP have exact analogues in the fore-arc and magmatic arc of the southern Andes. We thus suggest that the ANP was actually part of the SAM plate until the Middle Cretaceous, and fix ANP to SAM prior to 120 Ma.

### Break-up to 123 Ma:

During the first phase of spreading (c.160 – 123 Ma), West Gondwana (SAM and AFR) moved northeastward relative to East Antarctica, creating M-series anomalies in the southern Weddell Sea, Mozambique Basin and the Somali Basin. This motion caused the ANP, rigidly attached to SAM, to converge obliquely with East Antarctica, finally docking at 130 – 100 Ma, and resulting in the creation of the Palmer Land shear zone, a major tectonic boundary within ANP, that separates arc-related rocks from marine sedimentary and crystalline basement rocks of Gondwana. Continued motion of AFR towards the northeast (relative to ANT) led to the propagation of a rift into West Gondwana, defining the SAM and AFR plates, and initiating the southern Mid-Atlantic Ridge. The driving forces exerted by the Andean subduction zone, now pulled SAM towards the Pacific, as today, causing a cusp to form at the weakest point, which subsequently became the SAM-ANP plate boundary.

### 123 – 90 Ma:

As SAM rotated about the new cusp, a broad curve formed in the SAM-ANT flow line trends as they changed from NNE to WNW. This bend occurs within the Cretaceous magnetic quiet zone, so that precise dating is difficult but probably occurred within the interval 110 – 90 Ma. The c.90° change in direction of SAM motion led to increased rates of convergence at the southern Andean subduction zone, a major pulse of magmatism in the Andean batholith, closure of the Rocas Verdes basin, and a widespread deformational event south of Beagle Channel. At this time, rotation of the Patagonian orocline began, as the zone adjacent to the cusp became dominated by sinistral, strike-slip faulting. The change in SAM plate motion entailed major changes in the SAM-ANT-AFR circuit, resulting in the opening of the equatorial Atlantic, extension in the AFR-ANT basin, and generation of a major magmatic pulse, that formed a large igneous province at the proto-Bouvet triple junction. This province was subsequently divided by the formation of fracture zones into the Northeast Georgia Rise, Agulhas Plateau and Maud Rise.

### 90 – 48 Ma:

Spreading between SAM and ANT continued, at a slow rate in a WNW-ESE direction (c. 15 km/Ma), until about chron C30 (65 Ma), when an abrupt change to N-S motion, accompanied by ultraslow spreading (c. 5 km/Ma), occurred. We attribute this ultraslow phase to the presence of a tectonic obstruction between SAM and ANT within the region of the cusp, which persisted until C21 (48 Ma).

### 48 – 23 Ma:

At C21 (48 Ma), the obstruction was overcome, and slow spreading resumed. This released SAM and allowed Drake Passage opening to commence. This created a shallow (< 1000 m) seaway, which isolated terrestrial organisms in the ANP from South America. Rifting and spreading in Powell Basin commenced at this time. Spreading commenced at the West Scotia Ridge at some time close to the Eocene – Oligocene boundary, leading to the creation of a deep-water connection which completed the circumpolar deep pathway.

### 23 - 15 Ma:

A major change in SAM-ANT motion near chron C6 (23 – 20 Ma) resulted in profound changes in spreading geometry. The South American – Antarctic Ridge underwent a change from WNW-ESE spreading with many small-offsets, to W-E spreading with long-offset transforms. Spreading at the WSR became decoupled from that of the surrounding SAM and ANT plates, and relative motion commenced on the North Scotia Ridge and South Scotia Ridge. Subduction at the Jane-Discovery trench ceased, as did opening in the back-arc Jane Basin. Spreading also ceased in Powell Basin. A new subduction zone was formed at the proto-South Sandwich trench, and spreading in the east Scotia Sea was under way by 15 Ma.

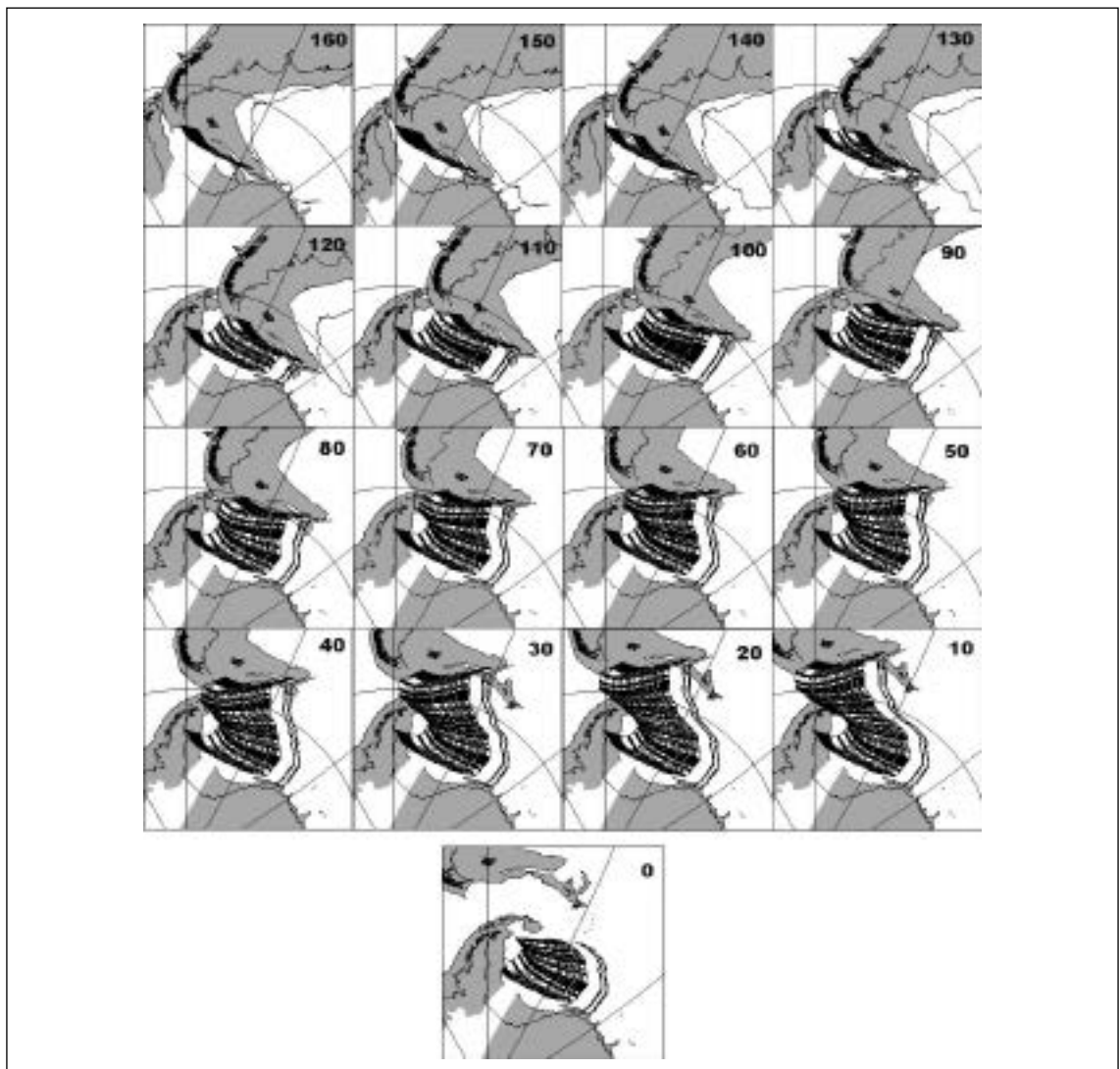


Fig. 2 - Reconstructions of SAM-ANP-ANT-AFR at 10 Ma intervals

**SPREADING REGIME AND TECTONICS IN THE WESTERNMOST SCOTIA SEA****2-08**

E. Lodolo\*, A.A. Schreider\*\*

\* *Istituto Nazionale di Oceanografia e di Geofisica Sperimentale (OGS), Trieste - Italy*\*\* *P.P. Shirshov Institute of Oceanology, Russian Academy of Science, Moscow - Russia*

A new map of magnetic Chron distribution for the westernmost Scotia Sea is compiled, on the basis of new acquired magnetic profiles and all available data for the region (Fig. 1). Spreading processes along two identified corridors initiated nearly simultaneously just prior Chron C10n(y) at 28.365 Ma. Sea-floor accretion at the westernmost ridge axis of the Scotia Sea (1<sup>st</sup> corridor) stopped sometimes at Chron 3An.1n (5.912-6.157 Ma), whereas spreading in the 2<sup>nd</sup> corridor ended earlier, within Chron 4r (8.302-8.335 Ma). In the eastern part of the western Scotia Sea ridge system, between Quest and Endurance FZ's, spreading stopped at Chron C4An (8.697-9.140). This pattern shows progressive termination of accretion vs. time from N-E to S-W.

The present-day tectonic stress in the western region of the Scotia Sea, originated by the relative motion between the South America and Antarctic plates, is mostly accommodated along the Shackleton Fracture Zone (SFZ) relief, which borders to the west the Scotia plate, along the western segment of the Magallanes-Fagnano transform fault (i.e., a major segment of the South America-Scotia plate boundary), and along the westernmost South Scotia Ridge - Elephant Island platform.

**Regional tectonics and data analysis**

The tectonic development of the Scotia Sea was mostly reconstructed from the identification of the linear marine magnetic anomalies (Barker and Burrell, 1977; Tectonic Map of the Scotia Arc, 1985; Livermore et al., 1994; Maldonado et al., 2000).

The onset of spreading in the Drake Passage, which led to the final separation between South America and Antarctic land masses, was not precisely determined because the lack of magnetic profiles across the two conjugate margins of the western Scotia Sea. The evolution of most of central and eastern parts of the Scotia Sea remains largely speculative (Barker et al., 1991). The western border of the present-day Scotia plate is the NW-SE-trending, left-lateral SFZ, which juxtaposes the oceanic lithospheres of the former Phoenix plate to the W with the western Scotia plate to the E. It extends for over 800 km from the southernmost South America to the northern tip of the Antarctic Peninsula. The SFZ forms part of the sinistral fracture system that accommodates the relative motion between the South America and Antarctic plates around the Scotia plate (Livermore et al., 1994). The tectonic development of the SFZ is commonly associated with the Drake Passage opening. From Oligocene time, at about 29 Ma, when spreading processes in the Drake Passage started, the SFZ became a structural boundary between the new-forming oceanic lithosphere of the western Scotia Sea and the Pacific oceanic plate to the W, and since then the fault acted as a left-lateral transform plate boundary. Recent studies of focal mechanisms show that the present-day relative motion along the SFZ is mainly transpressive, indicating an oblique convergence between the Antarctic and Scotia plates (Pelayo and Wiens, 1989).

The structural framework of the southern part of the SFZ has been investigated through the analysis of a 130-km-long multichannel seismic reflection profile acquired orthogonally to the fracture zone near the 60° parallel S (line IT-42, see location in Fig. 1). A strong and mostly continuous reflector found at about 8.0 s two-way traveltime is very clear across the entire section and is interpreted as the Moho discontinuity. A peculiar aspect of this reflector is its upward bend just to the W of the SFZ relief, which is shallower of about 1 s two-way traveltime with respect to the depth of the Moho on the E of the SFZ. Data show a complex system of troughs developed along the eastern flank of the crustal ridge, containing tilted and rotated block, and a presence of a prominent listric fault developed within the oceanic crust. This system represents a mostly extensional feature associated with the transform system. Present-day tectonic activity is found mostly in correspondence of the Shackleton relief, whereas fault-induced deformation is negligible within the entire trough system. This indicates that the E-W-directed stress regime present in the Drake Passage region is mainly dissipated along a narrow zone within the Shackleton ridge axis.

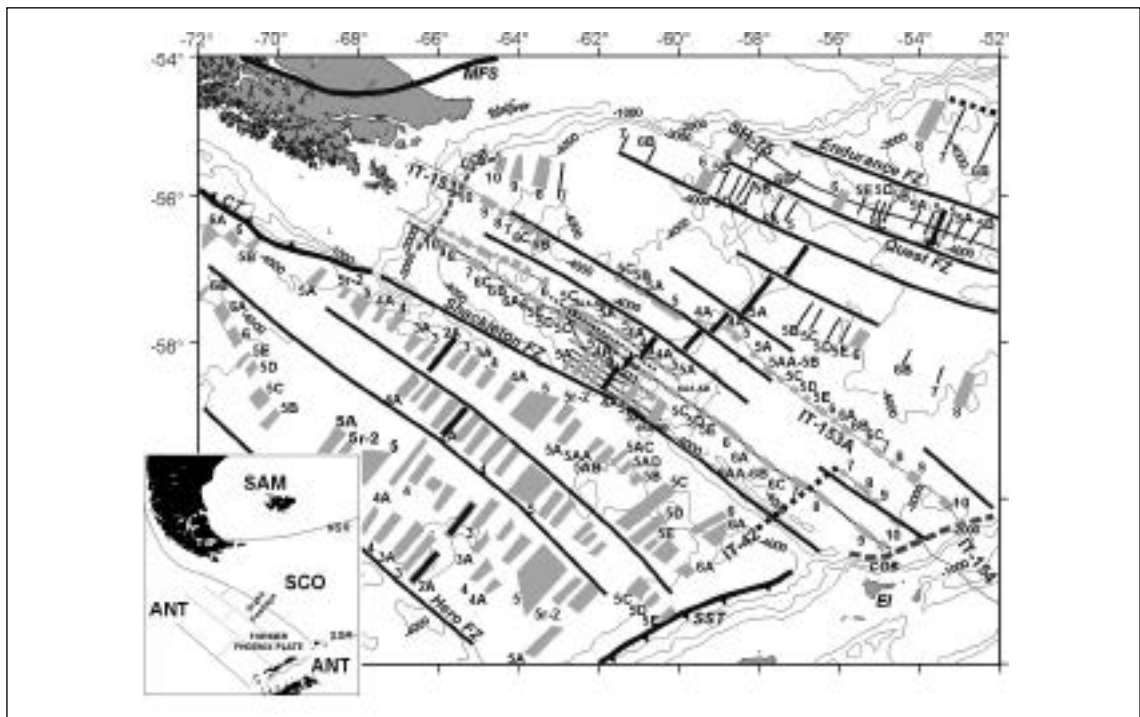


Fig. 1 - Magnetic Chron distribution for the western Scotia Sea and south-western Pacific Ocean, obtained from all identified magnetic anomalies in the region (Barker and Burrell, 1977; Tectonic Map of the Scotia Arc, 1985; Livermore et al., 1994; Lodolo et al., 1997; Maldonado et al., 2000; Schreider et al., 2003), re-interpreted magnetic anomalies along published profiles (thin segments in the Figure), and from original profiles IT-153, IT-153A, and IT-154. Simplified bathymetry from satellite-derived data (Sandwell and Smith, 1997). Box in the left-bottom corner shows a simplified plate tectonic sketch for the region. SAM = South America plate; ANT = Antarctic plate; SCO = Scotia plate; NSR = North Scotia Ridge; SSR = South Scotia Ridge; CT = Chile Trench; SST = South Shetland Trench; EI = Elephant Island; MFS = Magallanes-Fagnano transform system (Lodolo et al., 2003); TdF = Tierra del Fuego Island; COB = Continent-ocean boundary.

The tectonic evolution of the SFZ from Chron C10r (28.909-29.663 Ma) up to the present time, can be quite confidently reconstructed, on the basis of the identified magnetic anomalies in the western sector of the Scotia Sea and in the south-western Pacific Ocean.

1. Between Chron C10r (28.909-29.663 Ma) and Chron C3An.1n (5.912-6.157 Ma), the SFZ separated two spreading systems: the Phoenix ridge system to the W and the western Scotia ridge system to the E. The Phoenix ridge system acted at that time as a boundary between the lithospheric plates of Antarctica and Phoenix, and the western Scotia ridge system acted as a boundary between the North Scotia plate and South Scotia plates. During this time span, E-W left-lateral and N-S divergent interplate motion between South America and Antarctica was accommodated by the now extinct spreading centres of the western Scotia Sea. A tectonic event occurred during that period was the progressive eastward migration and successive subduction of the Phoenix-Antarctic-Nazca triple junction beneath the southern Chile Trench (Larter and Barker, 1991).
2. Between Chron C3An.1n (5.912-6.157 Ma) and Chron C2A (2.613-3.599 Ma), the SFZ separated the still active Phoenix ridge system (separating the Phoenix and Antarctic plates) and the just died western Scotia ridge system. At about 6 Ma, the North Scotia plate and the South Scotia plate became a single plate (Scotia plate). The Phoenix and Antarctic lithospheric plates continued to grow at the Phoenix spreading ridge system till Chron C2A. During the time span 6-3 Ma, motion between South America and Antarctica was mainly E-W (most of the region to the E of the SFZ was already formed and was locked because spreading stopped at the western Scotia ridge), and the SFZ accommodated left-lateral shear between these two major plates. The change in the tectonic regime - from mainly extensional to transpressional - occurred sometimes at 6 Ma.

3. Between Chron C2A (2.613-3.599 Ma) to the present time, SFZ separated the Antarctic plate from the Scotia plate. When spreading at the Phoenix ridge system stopped at Chron C2A, the Phoenix and Antarctic plates became a single plate (Antarctic plate). The convergence between the Scotia plate and the Antarctic plate is accommodated through diffuse compressional deformation and strike-slip faulting along the main relief of the SFZ.

## Discussion

The analysis of seismic data, and tectonic considerations, suggest that the main relief of the southern SFZ was formed by oceanic crustal uplift in response to the regional stress field having a mostly E-W trend, as pointed out by Pelayo and Wiens (1989) on the basis of focal mechanisms. Present-day plate motions in the Scotia Sea region, determined at the southern Chile trench and at the South America-Antarctic ridge system, is partitioned into sinistral strike-slip along both the North and South Scotia Ridge (Pelayo and Wiens, 1989). These authors reported earthquakes with a component of compression in the Drake Passage, and concluded that convergence between the Scotia plate and the Antarctic plate in this region is accommodated through diffuse compressional deformation and strike-slip faulting along the SFZ. Seismic data show that much of the present-day deformation is concentrated in a very narrow zone in correspondence of the SFZ relief, where sub-vertical faults dissecting the flanks of the ridge may accommodate the motion between the two major plates. The set of low-angle faults that bound the sub-basins of the Shackleton trough system to the E of the relief appear inactive because do not affect the upper sedimentary strata. The trough system may have formed during the first phase of the SFZ development, when the stress field regime was predominantly extensional, and was responsible for crustal block rotation and the development of half-graben structures. The orientation of the SFZ, at an approximate angle of 45° to the direction of the stress vector, is well justified: it accommodates the stress with left-lateral strike slip faulting mostly along the axis of the relief.

The timing of the changing regime from mainly transtensional to transpressional may be determined taking into account the main tectonic events that occurred in the western Scotia Sea and Phoenix plate, where spreading processes stopped at about 6 and 3 Ma, respectively. The tectonic regime during the Drake Passage opening phase was mostly transtensional, when the southern South America and the Antarctic Peninsula were progressively pulled away, and the new-forming SFZ acted as a railway road along which one land mass slip with respect to the other. After cessation of spreading in both the spreading system to the E and W of the SFZ, the relative motion between the two major South America and Antarctic plates was not longer dissipated within the Scotia plate, because the plate became rigid, and the predominant E-W motion was mostly distributed along the SFZ, that became the site for absorbing and accommodating the tectonic stress field of the region between the two plates.

## REFERENCES

- Barker, P.F. and Burrell, J., 1977. The opening of Drake Passage. *Marine Geology*, 25, 15-34.
- Barker, P.F., Dalziel, I.W.D. and Storey, B.C., 1991. Tectonic development of the Scotia Arc region. In: *The Geology of Antarctica* (R.J. Tingley, Ed.), Oxford Science Publications, 215-248.
- Livermore, R., McAdoo, D. and Marks, K., 1994. Scotia Sea tectonics from high-resolution satellite gravity. *Earth and Planet. Sci. Letters*, 123, 255-268.
- Larter, R.D. and Barker, P.F., 1991. Effects of ridge crest-trench interaction on Antarctic-Phoenix spreading: Forces on a young subducting plate. *Journ. Geophys. Res.*, 96, 19,586-19,607.
- Lodolo, E., Coren, F., Schreider, A.A. and Ceccone, G., 1997. Geophysical evidence of a relict oceanic crust in the South-western Scotia Sea. *Mar. Geophys. Res.*, 19/5, 439-450.
- Lodolo, E., M. Menichetti, R. Bartole, Z. Ben-Avraham, A. Tassone, and H. Lippai, 2003. Magallanes-Fagnano continental transform fault (Tierra del Fuego, southernmost South America), *Tectonics*, 22(6), 1076, doi:10.1029/2003TC001500.
- Maldonado, A., Balanya, J. C., Barnolas, A., Galindo-Zaldivar, J., Hernandez, J., Jabaloy, A., Livermore, R., Martinez-Martinez, J. M., Rodriguez-Fernandez, J., de Galdeano, C. S., Somoza, L., Surinach, E. and Viseras, C., 2000. Tectonic of an extinct ridge-transform intersection, Drake Passage (Antarctica). *Marine Geophys. Res.*, 21, 43-68.
- Pelayo, A.M. and Wiens, D.A., 1989. Seismotectonics and relative motions in the Scotia Sea region. *Journ. Geophys. Res.*, 94, 7293-7320.
- Sandwell, D.T. and Smith, W.H.F., 1997. Marine gravity anomaly from Geosat and ERS-1 satellite altimetry. *Journ. Geophys. Res.*, 102, 10,039-10,054.
- Schreider, A.A., Bulychev, A.A., Galindo-Zaldivar, J., Maldonado, A., Gilod, D.A., 2003. The Phoenix ridge geo-chronology in the South Pacific. *Okeanologia*, 43, 2, 279-285 (in Russian).
- Tectonic Map of the Scotia Arc, 1985. BAS Misc (3), Cambridge, British Antarctic Survey.

**GEOLOGICAL CROSS-SECTION ACROSS THE FUEGINAN ANDES  
IN THE TIERRA DEL FUEGO ISLAND****2-09**

Marco Menichetti

*Istituto di Geodinamica e Sedimentologia, Università di Urbino– Italy – menichetti@uniurb.it*

The geometric and kinematic plate reconstructions for the southern margin of the Gondwanaland are not well enough constrained because of the complexity of the tectonic events, related to the Upper Jurassic extensional phases and the Middle-late Cretaceous shortening of the Andean chain. In the Fueginan Andes the structures are superposed by significant counterclockwise rotations, related to wrench tectonism. Retrodeformable geological cross-sections through the orogenic belt are constructed to reach a satisfactory palinspastic restoration of this Andean region. The sections are constructed combining field geological data with available reflection seismic profiles, acquired both on-shore and off-shore the Tierra del Fuego, and with magnetic and gravimetric measurements. This methodology can be applied in the extensional Mesozoic basin as well as in the Meso-Cenozoic contractional orogen and partially in the wrench structures.

Back-arc crustal stretching and widespread silicic volcanism associated with break-up of Gondwanaland affected, from Middle to Late Jurassic, the whole Andean region. In the Patagonian and Fueginan Andes, a metamorphic basement, possibly Paleozoic in age, was affected in the Late Jurassic and Early Cretaceous by extensional tectonics, associated with a mafic volcanism and with the development of the Rocas Verdes back-arc basin. This latter was floored with oceanic crust (ophiolitic complex), which now outcrops for more than 800 km from Cape Horn to the North of Sarmiento Cordillera. A system of asymmetric and tilted fault blocks with a NW-SE general trend, was deformed by a listric normal fault dipping through SE. The geometrical pattern of the extensional structures is characterized by alternating and partially overlapping half graben with grow basin, bounded by a secondary fault plane. These structures are arranged in a right stepped geometry with transfer zones oriented WNW-ESE, that possibly locally constitute depressions where the extensional crustal thinning is renewed by magmatic accretion. In the half graben filled with volcanoclastic series of the Tobifera Fm. It is possible to recognize two sedimentary sequences, separated by unconformities. They probably represent the rift sequences of the Upper Jurassic related to the mechanical and thermal subsidence of the basin. The geometry of the normal fault system, which include sub-vertical structures with cumulative offsets from many hundreds to one thousand of meters, suggest an extension of at least the 15 % in several sectors of the Rocas Verdes marginal basin. The stretching in the crust increases towards west and southwest, where the thinning allowed the local formation of oceanic floor.

In the Middle Cretaceous, variations of plate drifts, linked to the opening of the Southern Oceans, change the tectonic regime from extensional to contractional. The Andean Cordillera developed along a collisional margin by horizontal shortening and crustal thickening of the basement rocks.

In the Late Cretaceous and Cenozoic time, a general counterclockwise rotation of the structures of the southernmost Andean Cordillera occurred. This was a response of the relative motion between South America and the Antarctic Peninsula, when the oceanic floor in the western Scotia Sea developed (Late Oligocene).

In the Fueginan Orogen, high grade metamorphic rocks of the Upper Palaeozoic to the Lower Tertiary of the Cordillera Darwin and the Ophiolitic Complexes of the Rocas Verdes basin form the major stacks of the internal thick-skinned basement-involved thrusting. The main structures are represented by SW-dipping, NW-SE-trending thrust sheets, and by strike-slip faults, related to a left lateral wrench component.

The contractional faults propagated in the Meso-Cenozoic sedimentary cover in a thin-skinned tectonic mode, forming NE-verging fold-and-thrust belt. These contractional structures present at least two main detachment levels: the lower is located in the Tobifera Fm., while the shallower is located in the Cenozoic clastic sediments. The different thrust sheets evolved in different stages and their emplacement towards the continent, in- or out-of-sequence, produced a shortening of the basement rocks of few thousand meters thick volcanoclastic filling of the Rocas Verdes basin and of the 7000 m-thick siliciclastic sedimentary cover in the Magellan foredeep basin.



The Meso-Cenozoic uplift of the Cordillera Darwin, with a rapid exhumation of the basement rocks, emplacement of plutons and intracontinental polyphase deformation, could be related to restraining bend structures with a step-over geometry of the different strike slip fault segments. The transtensional nature of the wrench structures is evident along the main tectonic lineaments of the Tierra del Fuego Island, from the arms of the Beagle Channel to the Magallanes-Fagnano fault system. Several asymmetric and restricted pull-apart basins developed in the different segments in an en-echelon arrangement with a ESE-WNW trend, connected with releasing side-step structures. These transtensional features are superposed onto the older lineaments and suggest that they may have reactivated pre-existing weak zones, formed during the Cretaceous-Tertiary shortening. Nevertheless the activation of the Mesozoic half graben structures is uncertain, while locally several basement seated reverse faults affect the whole sedimentary cover.

The orogenic shortening of the Fuegian Andes including the Magallanes fold-and-thrust belt reaches many hundreds of kilometers with a significant left-lateral wrenching component.

## BIBLIOGRAPHY

- Alvarez-Marrón, J., McClay, K.R., Harambour, S., Rojas, L., Skarmeta, J., 1993, Geometry and evolution of the frontal part of the Magallanes Foreland Thrust and Fold Belt (Vicuna area), Tierra del Fuego, southern Chile. *Am. Assoc. Petrol. Geol. Bull.* 77 1904-1921.
- Bhrun R.L., 1979, Rock structures during back-arc basin deformation in the Andes of Tierra del Fuego *Geol.Soc.Am.Bull.*, vol.90, 998-1012
- Caminos, R., 1980, Cordillera Fueguina: geología regional Argentina. Segundo Simposio Academia Nacional de Ciencias Lie. V. II. p. 1463-1501.
- Lodolo, E., M. Menichetti, A. Tassone and P. Sterzai, Morphostructure of the central-eastern Tierra del Fuego Island from geological data and remote-sensing images. *EGS Stephan Mueller Special Pub. Series*, vol. 2, 1-16, 2002b.
- Lodolo E., Menichetti M., Bartole R., Ben Avram Z., Tassone A., Lippai H., 2003 - Magallanes-Fagnano continental transform fault (Tierra del Fuego, southernmost South America). *Tectonics* 22, 6, 1076, doi:1029/2003TC0901500,2003
- Kreamer, P.E., 2003, Orogenic shortening and the origin of the Patagonian orocline (56°lat). *Journal of South Am. Earth Sci.* 15, pp. 731-748

## DIFFERENT STYLES OF CONTINENTAL GROWTH AT THE CONVERGENCE ZONE OF SOUTHERN CHILE

2-10

Polonia A.<sup>1</sup>, Loreto M.-F.<sup>2</sup>, Torelli L.<sup>2</sup>, Vera E.<sup>3</sup>

1 *ISMAR, Sezione Istituto Geologia Marina, CNR, Via Gobetti 101, 40129 Bologna, Italy*  
[Fax: 39-51-6398940, Tel: 39-51-6398888, [alina.polonia@ismar.cnr.it](mailto:alina.polonia@ismar.cnr.it)]

2 *Dip. Scienze della Terra, Università di Parma, Viale delle Scienze 78, 43100 Parma, Italy*

3 *Dip. Geofisica, Universidad de Chile, Plaza Ercilla 803, Santiago, Chile*

The southern tip of South America off Chile has suffered a long phase of ocean-continent convergence which has shaped the continental margin through different phases of accretion and tectonic erosion. The present accretionary wedge is a discontinuous geological record of plate convergence and records only the late Miocene accretionary processes resumed after Chile ridge consumption, occurred 14 Ma (Cande and Leslie, 1986). The subduction of the mid oceanic ridge should have strongly affected the configuration of the continental margin and much of the pre-collisional accretionary wedge was eroded during subduction of the Chile ridge. The volume of accreted sediments in the accretionary complex, in fact, is consistent with an accretionary history no older than 10-14 Ma (Polonia et al., 1999; Rubio et al., 2000).

The present tectonic setting is driven by relative movements between Antarctic, Scotia and South America plates (Fig. 1) which meet at about 50°S-52°S at the Fuegian triple junction (Polonia et al., 2001). The slip vector is roughly orthogonal to the margin at about 51°S (DeMets et al., 1990), while it becomes progressively more oblique south of 53°S. The obliquity of subduction is mainly related to the sharp bend of the continental margin at these latitudes. This 90° bend, is interpreted on the basis

of structural and paleo-magnetic data as a product of tectonic rotation (Dalziel et al., 1973, Burns et al., 1980, Cunningham, 1991, Diraison et al., 2000).

Previous works (Herron et al., 1977, Winslow et al. 1982, Polonia et al., 1997, Polonia et al., 1999; Rubio et al., 2000; Polonia et al., 2001) have progressively improved the knowledge of the crustal structure of the margin. The subduction complex is formed by a narrow and well defined accretionary wedge developed at the toe of the backstop. The continental basement is constituted partly by the Paleozoic accretionary wedge and partly by the Jurassic Patagonian Batholith. A well developed forearc basin grows in some areas above the contact between these two domains and a sedimentary section, about 2 Km thick in the depocenter, rests on the basement and appears largely undeformed. Despite the lack of seismic activity, data collected reveals how large folds and thrust faults characterise the structure of the margin from 51°S to 57°S (Polonia et al., 1997, Polonia et al., 1999) and this was interpreted also by Rubio et al. (2000) as an indication that subduction is still active or is only recently ceased.

Variations in structural style and in the geometry of the forearc region setting off Southernmost Chile, have been interpreted as related to the existence of different structural domains: the nature of their boundaries is still unclear mainly because of the lack of high resolution bathymetric data. They have been tentatively related to tectonic lineaments belonging to the Magellan Fault system and/or to the character and morphology of the subducting lower plate (lateral heterogeneities, sea-mounts and fracture zones) which produces a segmentation of the margin (Polonia et al., 2001).

We analyse multichannel seismic data in conjunction with the available altimetry data to address the regional architecture, accretionary rates and mode of continental growth of the continental margin from 51°S to 56°S. Some profiles have been processed at the Marine Geodynamic Dpt. of the Geomar (Kiel) in the frame of the EC-IHP project to obtain full pre-stack depth migrated seismic sections through the application of the SIRIUS/GXT (Migpack) software package. The software combines the pre-stack depth migration process with the technique called “depth-focusing error analysis” and allows to construct a very accurate velocity model that contemplate both lateral and vertical velocity variations.

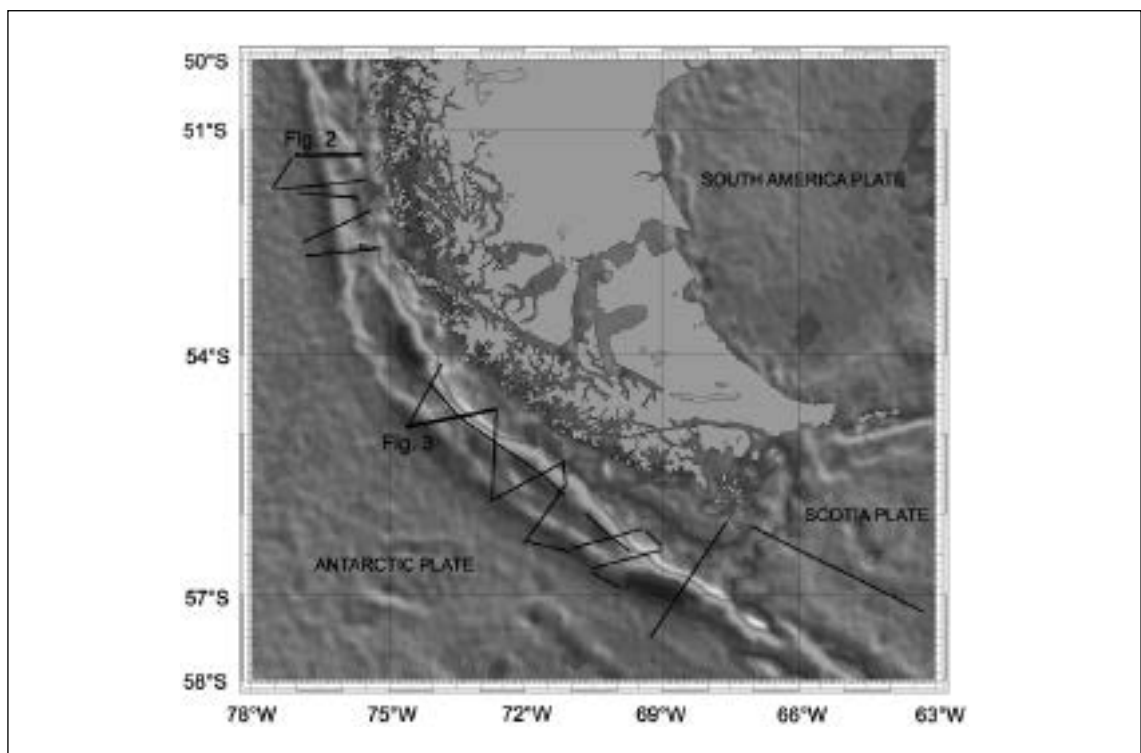


Fig. 1 - Seismic lines position map.

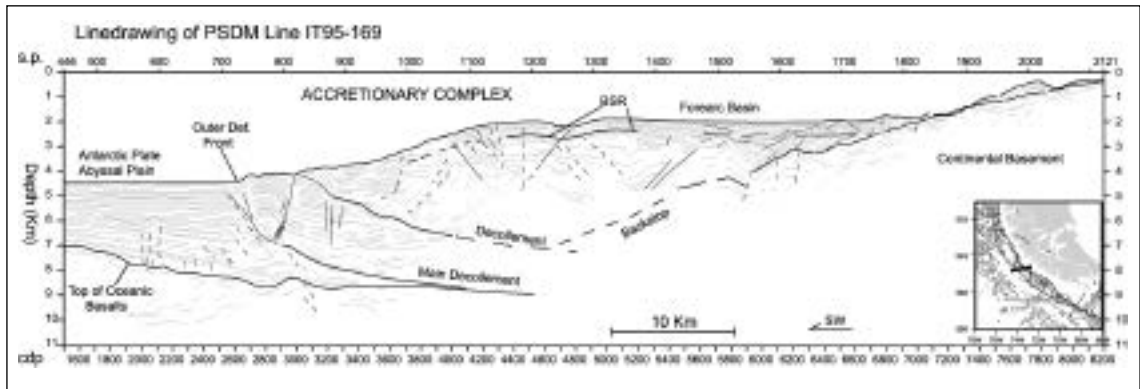


Fig. 2 - Line-drawing of seismic profile IT95-169.

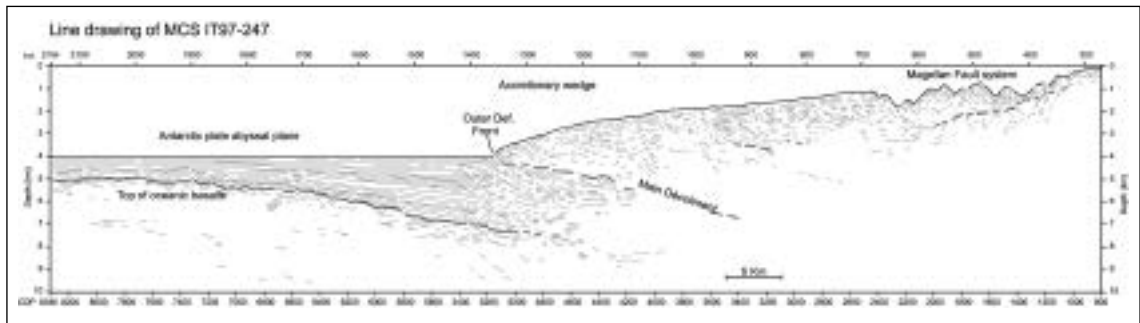


Fig. 3 - Line-drawing of seismic profile IT97-247.

Pre-stack depth migrated seismic sections image a widely varying frontal wedge morphology, different rates of accretion and underthrusting and a high degree of structural diversity within the accretionary wedge. These observations suggest that different modes of accretion together with tectonic erosion may be active concurrently along the trench at different locations.

The seismic profiles collected in areas of subduction-driven accretionary processes clearly show how the continental margin is a terraced forearc, where a well developed mid slope terrace is present between the trench/outer high and the upper continental slope. The accretionary wedge is wide and a variable volume of deformed sediments is present between the toe of the backstop and the trench. The topographic slope ranges from  $4^\circ$  to  $6^\circ$  while taper angle is about  $8^\circ$ . In some regions the décollement is deep and soles out on the top of oceanic basalts implying that most of trench sediments are involved in accretionary processes and sediments are uplifted and piled up in the form of imbricate thrust sheets. Elsewhere, pre-stack depth sections provide clear evidence that at least one, 3 Km thick and relatively undeformed sheet is being emplaced beneath the wedge through underthrusting (Fig. 2). In this area, in the rear part of the frontal fold, seaward dipping reflectors and a concave shape of the wedge suggest that the wedge has undergone tectonic erosion steepening the surface slope with the consequent collapse of the margin and a lowering of the taper angle. In this reconstruction underthrusting reactivated to increase surface slope through frontal uplift and erosion.

In areas where the wedge is non-accretionary, the continental margin shows steeper continental slopes and these are usually associated with a narrow accretionary wedge, more intense sediment disruption and very shallow décollement levels (Fig. 3). These features are peculiar of the northern region that faces the strait of Magellan, but are present also to the south where they alternate with the structural pattern of typical accretionary margins. In some areas the toe of the backstop is close to the trench implying that the volume of accreted sediments is very limited. Beneath the middle slope, the backstop shows large landward rotated fault blocks, whose existence is confirmed also by seismic migration velocity distribution. Faults bounding tilted blocks extend into the basement where they end at a slightly seaward dipping reflective zone located at about 2 Km below the seafloor. These sub-

horizontal reflective horizons probably form a detachment area beneath the sequence of rotated blocks. Uppermost sediments are chaotic suggesting the occurrence of sediment slumping and gravitational sliding. In this tectonic setting the décollement is generally very shallow and sediments below it in the trench may be divided in two units. The upper one is disrupted and deformed through underplating: shortening is responsible of short wavelength folds, while tilting of sediment strata produces unconformable relationship with the main décollement. The lower unit is constituted by concordant sediment layers and appears to move within the subduction channel without being strongly deformed.

Typical accretionary wedges are generally characterised by low tapers with smooth surface slope and subducting plate, low convergence rates and thick trench sediment, while non-accretionary wedges display large tapers with irregular surface slopes and rough subducting plate, high convergence rates and almost no trench fill (von Huene and Scholl, 1991; Lallemand et al., 1994). The constructive versus destructive character of the margin tectonics depends critically on the physiography of the subducting plate but is also strictly related to sediment thickness in the trench, climate conditions (glacial-interglacial fluctuations) and lithology of the incoming sedimentary section. The wedge in southern Chile is marked by a large quantity of sediments (2-3 Km thick) and was classed as a typical accretionary wedge by von Huene and Sholl (1991). Despite the rather uniform and thick sedimentary section in the trench, seismic data show that taper angle, width of the accretionary wedge, accretion and underthrusting rates and structural vergence widely vary along the margin and the transition from tectonic erosion to accretion and different modes of continental growth occur very rapidly. The acquisition of multibeam data and further analysis of structural style in the accretionary wedge, progression of structures along strike, relations between outboard subduction and inboard strike-slip systems may contribute to address processes governing plate subduction along this remote oblique convergent continental margin.

## REFERENCES

- Burns K. L., Rickard M. J., Belbin L., Chamalaun F., 1980. Further paleomagnetic confirmation of the Magallanes orocline. *Tectonophysics*, 63, 75-90.
- Cande S.C. and Leslie R.B. (1986) Late Cenozoic Tectonics of the Southern Chile Trench. *Journal of Geophysical Research* 91, 471-496.
- Cunningham D.W., Klepeis K.A., Gose W.A., and Dalziel I.W.D., 1991. The Patagonian Orocline: New paleomagnetic data from the Andean Magmatic Arc in Tierra del Fuego, Chile. *Journ. of Geophys. Res.*, v. 96, n. B10, 16061-16067.
- Dalziel I.W.D., Kligfield R., Lowrie W. and Opdyke N.D., 1973. Paleomagnetic data from the southernmost Andes and the Antarctic, in: *Implications of Continental Drift to the Earth Sciences*, vol. 1, ed. by D.H. Tarling and S. K. Runcom, pp. 87-101, Academic, San Diego, Calif.
- DeMets C., Gordon R.G., Argus D.F. and Stein F. (1990) Current plate motions. *Geophysics Journal International* 101, 425-478.
- Diraison M, Cobbold PR, Gapais D, Rossello EA, Le Corre C., 2000. Cenozoic crustal thickening, wrenching and rifting in the foothills of the southernmost Andes, *Tectonophysics*, 316 (1-2): 91-119 JAN 15 2000
- Herron E.M., Bruhn R., Winslow M. and Chuaqui L. (1977) Post Miocene tectonics of the margin of Southern Chile. In: *Island Arcs, Deep Sea Trenches and Back Arc Basins* (Talwani M. and Pitman W.C. III eds.) pp. 273-284. AGU, Washington, D.C.
- Lallemand S., Schnurle P, Malavieille J., 1994. Coulomb Theory Applied to Accretionary and Non accretionary Wedges - Possible Causes for Tectonic Erosion and or Frontal Accretion. *Journal of Geophysical Research-Solid Earth*, 99 (B6): 12033-12055.
- Polonia A., Brancolini G., Loreto M.-F., Torelli L., 2001 The accretionary complex of Southernmost Chile from the Strait of Magellan to the Drake Passage. *Terra Antartica*, 8(2), p. 87-98.
- Polonia A., Brancolini G., Torelli L., Vera E., 1999. Structural variability at the active continental margin off Southernmost Chile. *Journal of Geodynamics* 27, 289-307.
- Polonia A., Brancolini G., Torelli L., Vera E., Busetti M. and Zanolla C. (1997). The Southernmost Chilean margin: preliminary results of a geophysical survey. In: *The Antarctic Region: Geological Evolution and Processes* (Carlo Ricci ed.), pp. 653-660, Terra Antartica Publication, Siena.
- Rubio E., Torne' M., Vera E. and Diaz A., 2000. Crustal structure of the southernmost Chilean margin from seismic and gravity data. *Tectonophysics*, 323, 39-60.
- von Huene R. and Sholl D.W., 1991. Observations at convergent margins concerning sediment subduction, subduction erosion, and the growth of continental crust. *Reviews of Geophysics*, v. 29, p. 279-316.
- Winslow, M.A. 1982, The structural evolution of the Magallanes basin and neotectonics in the southernmost Andes. In: *Antarctic Geoscience* (C. Craddock ed.), pp. 143-154, University of Wisconsin Press, Madison.

## NORTHWARD MOTION OF SOUTH AMERICA, SCOTIA SEA DEVELOPMENT, AND CARIBBEAN CONVERGENCE

2-11

R. Somoza

INGEODAV - CONICET (Argentina) [somoza@gl.fcen.uba.ar](mailto:somoza@gl.fcen.uba.ar)

The paleomagnetic data from South America indicate that during the Late Cretaceous the continent was located at higher than present latitudes, about  $5^{\circ}/6^{\circ}$  farther south for sites in the Andean belt. Then, sometime during the Cenozoic the plate moved northward up to their present latitudes. A problem to estimate the timing of this drift is the yet poorly known apparent polar wander curve of South America for the Cenozoic. The only available pole from Lower Tertiary rocks arises from ca 50 Ma basalts in Patagonia (Butler et al., 1991), but this paleopole has been rejected as a reliable record of the time-averaged paleofield by those authors. However, paleolatitudes derived from Paleocene to Eocene volcanic and plutonic rocks in northern Chile agree with those predicted by this patagonian basalts pole (Fig. 1) suggesting it constitutes a suitable Eocene pole position. This Eocene paleopole is indistinguishable from the Late Cretaceous pole, suggesting little South American apparent polar wander between Late Cretaceous and Eocene. Thus, the Cenozoic drift of South America towards higher latitudes occurred between the Oligocene to Recent time span. It is hypothesized that this northward motion began during late Oligocene to early Miocene times, be roughly coeval with major kinematics changes in the Andean subduction zone (e.g. Somoza, 1998). Below it is shown that this hypothesis may be reconciled with the tectonic evolution in both the southern and northern margins of the continent.

During Early Cenozoic, the southern margin of the continent worked as a sinistral strike slip zone, accommodating the westward motion of South America respect to West Antarctica (e.g. Dickson Cunningham et al., 1995). Southernmost South America and the Antarctica Peninsula, although parts of different plates, remained in physical contact till the early Oligocene (~30 Ma), when they began to move apart. These extensional conditions gave place to generation of oceanic crust in the intervening zone, culminating with the opening of the Drake Passage (Barker and Burrell, 1977). Today, the southernmost area in South America and the northern tip of the Antarctica Peninsula are separated about 500 km in a N-S direction, with the Scotia microplate occupying the intervening space (Fig. 1)

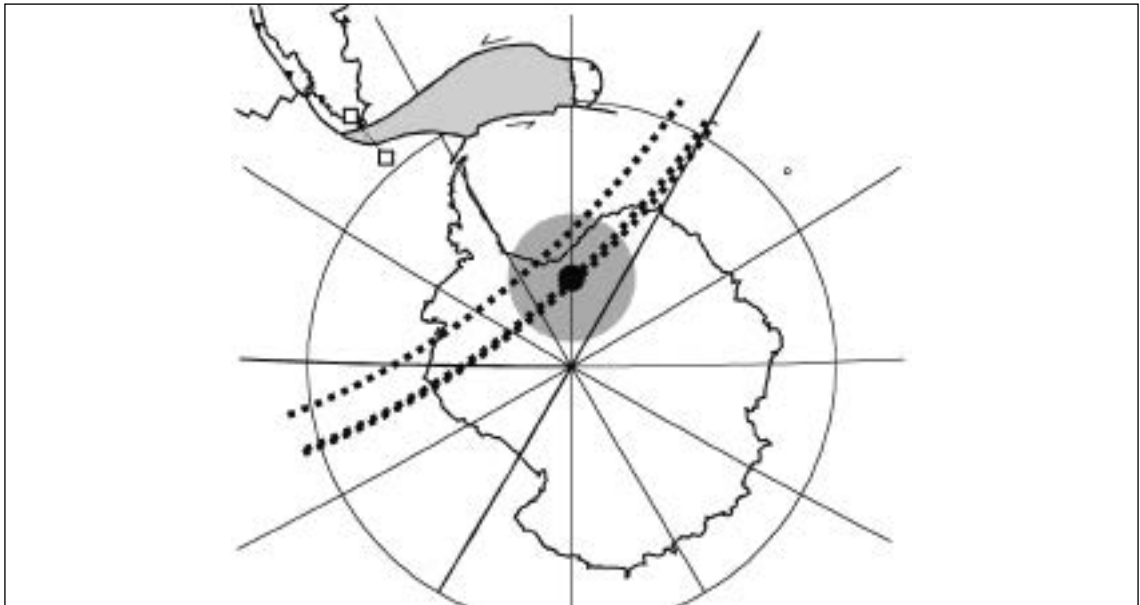


Fig. 1 - Black dot depicts the 50 Ma South American paleomagnetic pole and its 95% confidence level (gray circle). Shaded curves after Paleocene to Eocene paleolatitudes derived from paleomagnetic data in northern Chile support the paleolatitude indicated by the 50 Ma pole position. White squares indicate the current latitude and the suggested Eocene latitude for a locality in the Austral basin, southern South America.

The Early Cenozoic tectonics in northern South America was dominated by westward motion of the continent respect to the Caribbean plate (Pindell et al., 1988), although in NW Colombia this kinematic regime is superposed with Andean deformation. The sedimentary record of Venezuela indicates passive margin conditions for most of the Paleogene (Erikson and Pindell, 1993). A major change in tectonic conditions occurred in the Oligocene to early Miocene, when establishment of an overall transpressive regime lead to development of north and south vergent thrust belts, and the beginning of subduction in the Southern Caribbean Deformed Belt (e.g. Erikson and Pindell, 1993; Algar and Pindell, 1993; Colletta et al., 1997). It is suggested that this N-S component of contraction during Oligocene - Miocene times is related to increased South America - Caribbean convergence related to northward motion of South America. The N-S shortening in the northern margin of South America is of lower magnitude than the N-S extension in the Scotia Sea. This difference is mainly explained by coeval northward motion (but at lower rate) of the Caribbean plate (Acton et al., 2000), although some distributed internal deformation in South America may have occurred.

## REFERENCES

- Acton et al. (2000), Proceedings of the Ocean Drilling Program, Scientific Results, 165, 149-173.
- Algar and Pindell (1993), Tectonics, 12, 814-829.
- Barker and Burrell (1977), Marine Geology, 25, 15-34.
- Butler et al. (1991), Journal of Geophysical Research, 96, 6023-6034.
- Colletta et al. (1997), Tectonics, v. 16, p. 777-794.
- Dickson Cunningham et al. (1995), Journal of Geophysical Research, 100, 8257-8266.
- Erikson and Pindell (1993), Geology, 21, 945-948.
- Pindell et al. (1988), Tectonophysics, 155, 121-138.
- Somoza (1988), Journal of South American Earth Sciences, 11, 211-215.

## **PALEOMAGNETISM FROM UPPER TRIASSIC-LOWER JURASSIC ROCKS IN THE DESEADO MASSIF: NEW INSIGHTS ON THE BEHAVIOR OF PATAGONIA DURING THE BREAKUP OF GONDWANA**

**2-12**

H. Vizán<sup>1</sup>, R. Somoza<sup>1</sup>, G. Taylor<sup>2</sup>

*1 CONICET - Departamento de Ciencias Geológicas, FCEyN, Universidad de Buenos Aires, Argentina*

*2 Department of Geological Sciences, University of Plymouth, UK*

Patagonia, the Malvinas/Falkland plateau, and West Antarctica underwent widespread extensional tectonics during the early stages of Gondwana breakup. Paleomagnetic studies have shown that clockwise vertical-axis rotations in crustal blocks of different sizes constitute an important component of the Mesozoic deformation in these regions (e.g. Taylor and Shaw, 1989; DiVenere et al., 1995; Geuna et al., 2000). In particular, the large rotation detected on dolerite dykes in the West Falkland Island (Taylor and Shaw, 1989) greatly influenced the pre-breakup reconstructions of Western Gondwana (e.g. Ben-Avraham et al., 1993; Macdonald et al., 2003). The regional extent of this large rotation is, however, still unknown. This led us to investigate the pre-Jurassic paleomagnetic record of the Deseado Massif (Fig. 1), the closest continental region to the Malvinas/Falkland Islands, to determine whether it records a Jurassic-Cretaceous rotation history. We sampled fine-grained sandstones, siltstones, and mudstones from two sections in the Upper Triassic El Tranquilo Formation as well as the Bajo La Leona and La Calandria plutons which have yielded Rb-Sr ages of 202 and 203 Ma (Pankhurst et al., 1993).

All of the remanences isolated in samples from the plutonic rocks have reverse polarity. Five sites from La Calandria show very high inclinations and high between-site dispersion. Probably undetected tilt affected our sampling here, and accordingly these results are not considered further. Results from five sites in the La Leona locality gave a paleopole located at 39° S, 238° E, A95=11°. The paleolatitude predicted by this pole for the sampling area is similar to that predicted by coeval reference poles (Fig. 1). The La Leona pole position with respect to the coeval reference poles implies

a clockwise tectonic rotation of the sampling locality without important tilting (Fig. 1), although some incomplete sampling of paleosecular variation may contribute to the pole discordance. It must be considered however that we have no information to estimate the paleohorizontal in this plutonic complex.

Most samples from the El Tranquilo Formation showed a high temperature, high coercivity magnetic component of normal polarity. The gentle tilt shown by two sampled sections precludes applying a relevant tilt-test. Results from eight in-situ site directions yield a paleopole located at  $52^\circ$  S,  $246^\circ$  E,  $A95=12^\circ$  (ET-is in Fig. 1), whereas the paleopole for the tilt corrected site directions (ET-tc in Fig. 1) is located at  $58^\circ$  S,  $225^\circ$  E,  $A95=12^\circ$ . Paleomagnetic behavior and rock magnetism suggest that the observed remanence is carried by magnetite. Petrographic observations reveal that large particles of magnetite occur as disseminated grains within slightly undulating stylolithes, indicating a secondary origin for these large oxide grains. The common occurrence of iron-less biotite suggests magnetite grew after iron remobilization from these silicates. We therefore interpret the isolated remanence in the El Tranquilo Formation to be a remagnetization. Since this process would have involved considerable time, it is likely that the time-averaged paleomagnetic vector from the El Tranquilo Formation averages out the paleosecular variation of the geomagnetic field. In this context, comparison with expected paleolatitudes allows to estimate the remagnetization-age. Figure 1 allows us to consider two end-member ages: i) a Late Triassic-earliest Jurassic, post-tilt remagnetization (ET-is pole) or ii) a latest Jurassic-Neocomian, pre-tilt remagnetization (ET-tc pole). Geology in the sampling area does not constrain the timing of tilting. In the post-tectonic remagnetization case, tilting could have occurred during the development of the Triassic-Jurassic unconformity reported for the El Deseado Massif by Homocv and Constantini (2001). Alternatively, if the remagnetization is pre-tectonic, the age of tilt would have occurred during the latest Jurassic - Neocomian time span, its upper bound being constrained by the widespread presence of flat-lying Aptian strata in the region. Nevertheless, Fig. 1 shows that, whichever is the case, both the paleopoles ET-is and ET-tc are deviated clockwise from their corresponding reference poles.

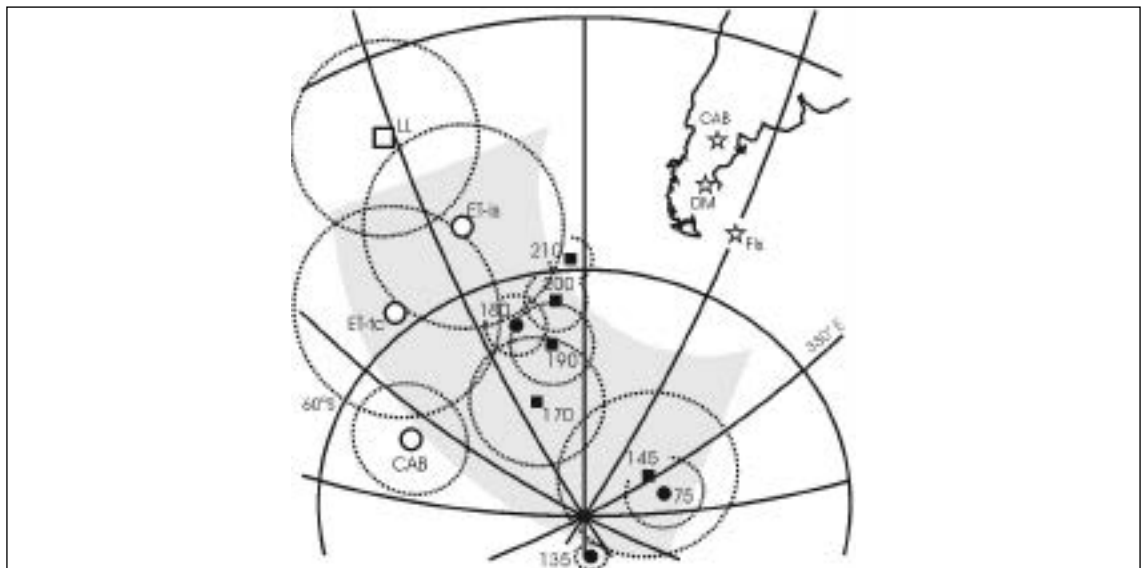


Fig. 1 - Stars depict sampling localities in the Deseado Massif (DM), Cañadon Asfalto Basin (CAB), and Malvinas/Falkland Islands (FIs). Open symbols show paleomagnetic pole positions from units in Patagonia: El Tranquilo Formation (ET-is and ET-tc indicating poles derived from in-situ and tilt-corrected magnetizations, respectively), La Leona plutonic complex (LL), and Cañadon Asfalto basin (CAB). Solid symbols represent reference poles for South America, where squares denote poles transferred from North America and Europe (database from Torsvik et al., 2001), and circles showing autochthonous reference poles from South America. Grey circular sector denotes an area enclosing the expected position for paleopoles yielding paleolatitudes between  $45^\circ$  and  $70^\circ$  for the sampling zone in the Deseado Massif. Note that, despite the rather large confidence interval of the paleopoles from the Deseado Massif, i) they do not overlap any younger reference pole, ii) they predict paleolatitude in agreement with the apparent polar wander curve of South America, and iii) all of them are deviated clockwise from their corresponding reference poles.

Our results suggest the occurrence of clockwise vertical-axis rotations in Mesozoic localities from the Deseado Massif. Uncertainties about the age of rotation preclude a correlation with clockwise rotations detected in other areas of southwestern Gondwana. Nevertheless, the amount of rotation found in these units is comparable with that observed farther north in Upper Jurassic-Neocomian rocks from the southern border of the North Patagonian Massif (CAB in Fig. 1), and strongly differ from the large rotation detected in the Malvinas/Falkland Islands (FIs in Fig. 1). This latter contrast suggests that the intervening region between the Deseado Massif and the islands, in the present Argentine shelf, has been a zone of major structural discontinuity, or at least of decreasing rotational deformation for the case that the observed rotations in both these areas were roughly coeval.

## REFERENCES

- Ben Avraham et al. (1993), *Earth Planetary Science Letters*, v. 117, p. 43-58.
- DiVenere et al. (1995), *Journal of Geophysical Research*, v.100, p. 8133-8151.
- Geuna et al. (2000), *Earth Planetary Science Letters*, v. 181, p. 145-160
- Homocv and Constantini (2001), *AAPG Bulletin* v. 85 (10) p. 1795-1816
- Macdonald et al. (2003), *Marine and Petroleum Geology*, v. 20, p. 287-308
- Pankhurst et al. (1993), *XII Congreso Geológico Argentino, Actas, Tomo IV*, pp.134-141
- Taylor and Shaw (1989), *AGU Geophysics Monographs Series*, vol. 50, pp. 59-72
- Torsvik et al. (2001), *Earth and Planetary Science Letters*, vol. 187, p. 55-69



# **Session 3**

---

**EARTHQUAKE  
SEISMOLOGY**



## EARTHQUAKE EPICENTRES IN TIERRA DEL FUEGO FROM MAY 1999 TO MARCH 2004

3-01

G. Connon<sup>1</sup>, L. Barbero<sup>1</sup>, C. Ferrer<sup>1</sup>, J.L. Hormaechea<sup>1</sup>, N. Sabbione<sup>2</sup>, R. Pinciroli<sup>2</sup>,  
C. Rastelli<sup>2</sup>, M.P. Plasencia Linares<sup>2</sup>

<sup>1</sup> Estación Astronómica Río Grande, Tierra del Fuego, Argentina (CONICET & UNLP)

<sup>2</sup> Facultad de Ciencias Astronómicas y Geofísicas, Universidad Nacional de La Plata, Argentina (UNLP)

Contact: gerardo@earg.gov.

### Abstract

Digital seismograms recorded by stations Despedida (DSPA), Río Grande (EARG), Puerto Parry (IDEA) and Termas del Río Valdés (TRVA) located in Tierra del Fuego and Isla de los Estados have been processed and analyzed to get new information about the seismic activity characterizing the region.

A Güralp CMG-3T Broad Band seismometer installed at DSPA station and a temporary operating Lennartz LE-3D Lite 1 Hz sensor at EARG, IDEA and TRVA provided the observational data.

Tierra del Fuego shows a complex tectonic setting. The island is crossed by a transform margin characterized by left lateral movement which extends from the North Scotia Ridge on the east to the Chilean Trench on the west. This fault system constitutes a major segment of the South American-Scotia plate boundary (Dalziel I, 1984, Lodolo et al., 2002).

Magallanes Fagnano Fault System (MFFS) splits the Tierra del Fuego into two continental blocks (Lodolo et al., 2002). The main fault of this system, trending E-W, is parallel to the Fagnano Lake major axis.

Earlier studies revealed a significant level of low to medium magnitude seismicity with epicentres in the continental part of the region and the surrounding oceanic areas (Plasencia et al., 2002; Febrer, 2002).

All the available digital recordings have been processed using the SEISAN software developed by Bergen University, Norway. Epicentral locations, determined using a Single Station Location (SSL) method as described by Plasencia et al. (2002) will be presented. The latitudinal distribution of epicentres shows that a relevant number of events is related with the MFFS (epicentral latitudes between 54° and 55° south) while another group of events appears to be related with an active graben located in northern Tierra del Fuego (Diraison et al., 1997; Bujalesky, personal communication, 2004).

### REFERENCES

- Dalziel I., The Scotia Arc: An international geological laboratory. *Episodes*, Vol. 7, n 3, 1984.
- Diraison, M. P. Cobbold, D. Gapais, E. Rosello. Magellan Strait: Part of Neogene rift system, *Geology*, 25, 703-706, 1997.
- Febrer, J.M. I. La Red ASAIN de Observación Sismológica en Antártida. II. Sismicidad en Tierra Del Fuego. XXI Reunión Científica de la AAGG. Rosario, Santa Fe, 23-27 sept. 2002.
- Klepeis K., The Magallanes and Deseado fault zones. Major segments of the south transform plate boundary in the southernmost South America, Tierra del Fuego. *J. Geophys. Res.*, 99, B11, 22001-22014., 1994.
- Lodolo E., M. Menichetti, A. Tassone, R. Geletti, P. Sterazi, H. Lippai and J.L. Hormaechea, Researchers Target a Continental Transform Fault in Tierra del Fuego. *Eos Trans. AGU*, 83, 1, 2002.
- Plasencia M., Connon G., Hormaechea J. L., Sabbione N. Determinación Preliminar De Epicentros Registrados en la Estación Sismológica DSPA (Ea. Despedida), Provincia De Tierra Del Fuego. XXI Reunión Científica de la AAGG. Rosario, Santa Fe, 23-27 sept. 2002.

## LITHOSPHERIC STRUCTURES AND REGIONAL SEISMICITY IN THE SCOTIA SEA AREA: A REVIEW

3-02

M. Guidarelli(\*), M.P. Plasencia Linares(\*\*, \*\*\*, \*), M. Russi(\*\*\*), G.F. Panza(\*, \*\*\*)

(\*) *Department of Earth Sciences – University of Trieste, Via E.Weiss 4 – 34127 TRIESTE – Italy*

(\*\*) *Depto de Sismología e Inf. Meteorológica, Fac. Cs. Astronómicas y Geofísicas, Univ. Nacional de La Plata, Paseo del Bosque s/n, 1900 La Plata – Argentina*

(\*\*\*) *Istituto Nazionale di Oceanografia e di Geofisica Sperimentale – OGS, Borgo Grotta Gigante 42c- 34010 SGONICO TS Italy*

(\*\*\*\*) *The Abdus Salam International Centre for Theoretical Physics, SAND Group, Strada Costiera, 11 – 34100 MIRAMARE TS Italy*

### Summary

The Scotia Sea region is a complex tectonic area characterized by many active tectonic processes and rapid changes in plate motion and configuration. Many features of the Scotia Sea are well understood; nevertheless, some details of the tectonic interactions, plate boundaries and relative plate motions are still uncertain. In this perspective, the determination of lithosphere characteristics and the identification of relevant discontinuities, together with the determination of focal mechanisms are very important to study the present day tectonics and to understand the geodynamical evolution of the Scotia Sea region.

In this study we sum up the results obtained in the last few years from the analysis of events recorded in the Scotia Sea with different seismological methodologies, and we present some new results for the determination of focal mechanisms and structural parameters for the region under study.

### Abstract text

The Scotia Sea region, located between the Antarctic Peninsula and the South Sandwich Islands, is a place of active tectonic processes, which had a complex tectonic evolution over the past 40Ma. The Scotia Sea is the result of the Tertiary disruption of a continuous Antarctic-Andean margin (Barker & Burrell, 1977), which began between 60 Ma and 34 Ma ago (Lawver et al., 1985). The Scotia Sea and the surrounding Scotia Arc have evolved by extension behind an east-migrating subduction zone, at the boundary between the South American and Antarctic plates (Barker, 2001).

The Scotia Sea region crust is mainly of oceanic structure and origin; the region is bounded on three sides by the Scotia Arc, islands and submarine ridges of the North and South Scotia Ridge and South Sandwich island arc that are a mixture of old continental fragments, arc volcanoes, remnant arc and accretionary prism. Two small plates can be identified between the major South American and Antarctic plates, the Scotia plate and the Sandwich plate. Most of the boundaries of those plates lie within the Scotia Arc, and almost all plate motion is east-west (Barker, 2001).

The identification of relevant discontinuities and the determination of focal mechanisms are very important to determine the present-day tectonics and to understand the geodynamical evolution of the Scotia Sea.

In the last decade there had been an instrumentation deployment in the islands and continental regions surrounding the Scotia plate in particular by OGS-IAA (Osservatorio Geofisico Sperimentale - now Istituto Nazionale di Oceanografia e Geofisica Sperimentale – and Istituto Antartico Argentino). The availability of regional earthquakes records by broadband digital seismometers allowed us the application of seismological methodologies to the analysis of earthquakes in the Scotia Sea region. We proceed here to a short review of the results obtained in the last few years from the study of waveforms recorded in the Scotia Sea region using different seismological methodologies, from surface wave tomography to waveform inversion.

Vuan et al. (1999) proposed preliminary S-wave velocity models along selected paths in the Scotia Sea region; but in a more comprehensive study, Vuan et al. (2000), presented tomographic maps of the region, obtained from group velocity tomography (Ditmar and Yanovskaya, 1987; Yanovskaya and Ditmar, 1990). Low velocity anomalies follow the plate boundary between the South America and the Scotia plates, the South Sandwich Island arc, the South Scotia Ridge, and the Bransfield Strait. The Scotia Sea is characterized instead by a high velocity anomaly. The dispersion measurements obtained

from tomography have been regionalized and then inverted, using a non-linear inversion scheme (Valyus et al., 1969; Knopoff, 1972; Valyus, 1972; Biswas and Knopoff, 1974; Panza, 1981), to obtain shear wave velocity models for the main geological and tectonic features. Vuan et al. (2000) have found a continental type crust beneath the tip of the Antarctic Peninsula and the South America, under the Bransfield Strait and part of the South Scotia Ridge. They have shown S-waves velocities between 4.45 km/s and 4.65 km/s beneath the oceanic type crust, but larger variations beneath the continental type crust areas.

The availability of average structural parameters for the lithosphere of the Scotia Sea region allows us the waveform inversion of regional earthquakes to retrieve focal mechanisms and source time functions. The INPAR method (e.g. Šílený et al., 1992) is particularly suitable in regions such as the Scotia Sea, where the high level of seismic noise, typical of oceanic environments, and the small number of stations, makes it difficult to determine the fault plane solutions using standard techniques, such as the first arrivals technique. Particularly important is the capability of this method to give reliable results, even when only a few seismograms from a limited number of stations are available (e.g. Kravanja et al., 1999). Vuan et al. (2001) determined seismic moment tensors with the INPAR inversion method and obtained results reproducing the CMT catalogue parameters, even using a limited number of signals.

As the results of the study by Vuan et al. (2001) justify a systematic use of the methodology in the Scotia Sea region, we have analysed a set of earthquakes recorded in the Scotia Sea and surrounding areas. 16 events have been inverted to obtain their source parameters; the waveforms used were recorded by the OGS-IAA and IRIS broadband instruments, and, for the events in the Bransfield Strait, by the instruments of the Antarctic SEPA project. The results are generally in agreement with the source parameters of the CMT catalogue. The source mechanisms obtained are plotted in Fig. 1, together with the two mechanisms obtained by Vuan et al. (2001).

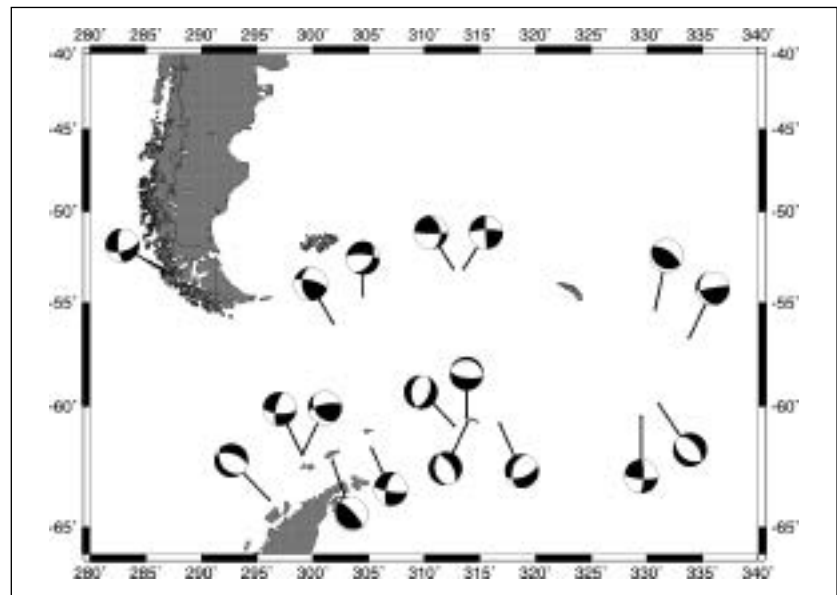


Fig. 1 - Focal mechanism solutions determined from moment tensor inversion using the INPAR method.

Waveform inversion methodologies can be used to retrieve structural parameters. Inversions that make use of the full waveform of the seismic signal, including both body waves and surface wave modes, should in principle be superior to methods based on more narrowly selected discrete data, such as arrival times or phase velocities. Waveform inversion also allows us to make use of the information contained in the higher mode signal without having to stack seismograms and identify modes.

An inversion scheme has been developed by Du & Panza (1999), using modal summation as an efficient means of forward modelling, to invert the properties of a laterally homogeneous Earth. They used the analytical method for computing differential seismograms with respect to structural model parameters proposed by Du et al. (1998). Guidarelli et al. (2003) extended the analytic technique for the calculation of differential seismograms with respect to the medium parameters in order to deal

with liquid layers. In this way they were able to apply the inversion scheme of Du & Panza (1999) to the earthquakes of the Scotia Sea, and show the feasibility of the application of waveform inversion to retrieve structural models in the Scotia Sea region. We have used the same inversion method to refine the structural models of the area obtained with surface wave tomographic techniques (Vuan et al., 2000). We have obtained so far the structural models shown in Fig. 2, corresponding to different paths crossing the Scotia Sea region. The analysis of more source-receiver paths will lead to determination of 3D models for the entire Scotia Sea area.

The study of Scotia Sea earthquakes with different seismological methodologies has allowed to obtain information of different type: information about seismic sources and about lithospheric structure. All that information can be used to study the tectonics and the geodynamical evolution of the Scotia Sea.

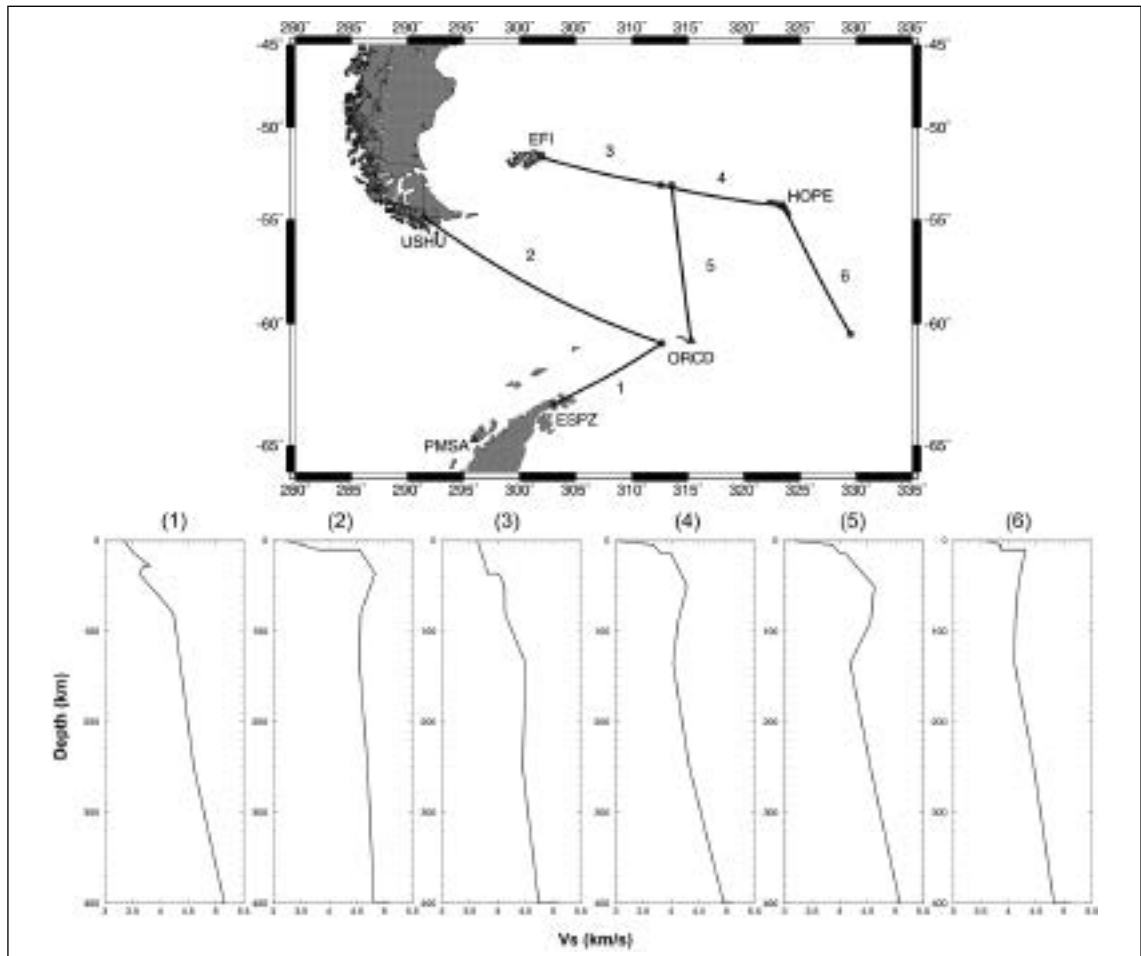


Fig. 2 - Upper 400 km S-velocity models obtained after waveform inversion of seismograms in the Scotia Sea region. The number above each structural model corresponds to the source-receiver path in the map.

## REFERENCES

- Barker, P.F., and Burrell, J., (1997), The opening of the Drake Passage, *Marine Geology*, 25, 15-34.
- Barker, P.F., (2001), Scotia Sea regional tectonic evolution: implications for mantle flow and palaeocirculation, *Earth Science Review*, 55, 1-39.
- Biswas, N.N., and Knopoff, L., (1974), The structure of the upper mantle under the U.S. from the dispersion of Rayleigh waves, *Geophysical Journal of the Royal Astronomical Society*, 36, 515-539.
- Ditmar, P.G., and Yanovskaya, T.B., (1987), A generalization of the Backus-Gilbert method for estimation of lateral variations of surface wave velocity, *Izv. Akad. Nauk SSSR, Fiz. Zemli*, 6, 30-60.
- Du, Z.J., Michelini, A., Panza, G.F., and Urban, L., (1998), P-SV multimode summation differential seismograms for layered structures, *Geophysical Journal International*, 134, 747-756.

- Du, Z.J, and Panza, G.F., (1999), Amplitude and phase differentiation of synthetic seismograms: a must for waveform inversion at regional scale, *Geophysical Journal International*, 136, 83-98.
- Guidarelli, M., Russi, M., Plasencia Linares, M.P., and Panza G.F., (2003), The Antarctic Seismographic Argentinean Italian Network and the progress in the study of structural properties and stress conditions in the Scotia Sea region, *Terra Antartica Reports*, 9, 25-34.
- Knopoff, L., (1972), Observations and inversion of surface wave dispersion, *Tectonophysics*, 13, 497-519.
- Kravanja, S., Panza, G.F., and Šílený, J., (1999), Robust retrieval of seismic point source time function, *Geophysical Journal International*, 136, 385-394.
- Lawver, L.A., Keller, R.A., Fisk, M.R., and Strelin, J.A., (1995), Bransfield Strait Antarctic Peninsula: active extension behind a dead arc, in Taylor, B., Ed. *Back arc basins: tectonic and magmatism*, New York: Plenum Press, 315-342.
- Panza, G.F., (1981), The resolving power of seismic surface waves with respect to the crust and upper mantle structural models. In: Cassinis R. Ed., *The solution of the inverse problem in geophysical interpretation*, Plenum Publishing Corporation, 39-77.
- Pelayo, A.M., and Wiens, D.A., (1989), Seismotectonics and relative plate motions in the Scotia Sea Region, *Journal of Geophysical Research*, Vol. 94, No. B6, 7293-7320.
- Šílený, J., Panza, G.F., and Campus, P., (1992), Waveform inversion for point source moment tensor retrieval with optimization of hypocentral depth and structural model, *Geophysical Journal International*, 108, 259-274.
- Valyus, V.P., Keilis-Borok, V.I., and Levshin, A.L., (1969), Determination of velocity profile of the European upper mantle, *Doklady of the Acad. Sci. USSR, Earth Sciences Section, English Translation by Amer. Geol. Inst.*, 185, 1-6, 4-7.
- Valyus, V.P., (1972), Determining seismic profiles from a set of observations. In *Computational Seismology* (ed. Keilis-Borok, V.I.), Consult. Bureau, New York.
- Vuan, A., Cazzaro, R., Costa, G., Russi, M., and Panza, G.F., (1999), S-wave velocity models in the Scotia Sea region, Antarctica, from nonlinear inversion of Rayleigh waves dispersion, *Pure and Applied Geophysics*, 154, 121-139.
- Vuan, A., Russi, M., and Panza, G.F., (2000), Group velocity tomography in the subantarctic Scotia Sea region, *Pure and Applied Geophysics*, 157, 1337-1357.
- Vuan A., Russi, M., Costa, G., and Panza, G.F., (2001), Moment tensor waveform inversion in the sub-Antarctic Scotia Sea region: feasibility tests and preliminary results, *Terra Antartica*, 8(2), 55-62.
- Yanovskaya, T.B., and Ditmar, P.G., (1990), Smoothness criteria in surface wave tomography, *Geophysical Journal International*, 102, 63-72.

## THE 4 AUGUST 2003 EARTHQUAKE RECORDED BY ASAIN NETWORK IN ANTARCTICA AND TIERRA DEL FUEGO.

3-03

M.P. Plasencia Linares<sup>1,2,3</sup>, B.G. Bukchin<sup>5</sup>, M.Guidarelli<sup>2</sup>, M. Russi<sup>3</sup>, G.F. Panza<sup>2,4</sup>

1 *Depto. de Sismología e Inf. Meteorológica, Fac. Cs. Astronómicas y Geofísicas, Univ. Nacional de La Plata, Paseo del Bosque s/n, 1900 La Plata - Argentina*

2 *Department Of Earth Sciences – University of Trieste, Via E. Weiss 4 – 34127 Trieste - Italy*

3 *Istituto Nazionale di Oceanografia e Geofisica Sperimentale - OGS, Borgo Grotta Gigante 42/c, 34010 Sgonico (Trieste) – Italy*

4 *The Abdus Salam International Center for Theoretical Physics ICTP, Trieste – Italy*

5 *International Institute of Earthquake Prediction Theory and Mathematical Geophysics, Moscow, Russia*

### Abstract

To improve the knowledge of the earth structure and to investigate earthquake mechanisms a seismograph network uniformly covering the study area is a necessary prerequisite. The Antarctic Seismographic Argentinean Italian Network (ASAIN) is the answer to this need as far as it concerns the Scotia Sea region. Orcadas station is operated as an ASAIN station since 1997, and it constitutes a contribution to the regional Scotia Sea network and to the global network in an area of the southern hemisphere that was previously completely uncovered. Orcadas station is, in effect, the ASAIN station that shows the best percentage of functioning time and during 2003 it worked for the whole year without any interruption as it is doing this year. Together with other ASAIN stations it provided digital recordings of the 4<sup>th</sup> August 2003, 7.5 magnitude earthquake, and its major aftershocks. But, being in the immediate proximity of the source area it is also the only station recording the whole sequence of events which begun on August 4<sup>th</sup>, 2003 “Orcadas Centenary Earthquake” so providing a detailed information on the evolution of the seismic phenomenon. The main shock and principal aftershocks seismograms have been extracted from the database in order to apply inversion techniques to refine

the existing structural models of the main tectonic features. Waveforms are used for the moment tensor inversion with the synthetic Green's functions calculated from the structural models obtained by surface wave group velocity tomography. Whenever possible we compare our results with other studies, i.e. Harvard Centroid Moment Tensor (CMT).

## Introduction

On August 4<sup>th</sup>, 2003 04:37:19 GMT a major earthquake shook the south eastern Scotia Sea along the South Scotia Ridge. Its magnitude has been evaluated as 7.5 and its epicentre located at Lat. 60.55S, Lon. 43.49W (IRIS Seismic Monitor earthquake list) about 70 km East from the Argentinean Base Orcadas (Laurie Is., South Orkney Is.) where ASAIN station ORCD is operated (Russi and Febrer, 2001). The reported depth (10 km) is an imposed value for the corresponding parameter in the location program. A significant number of stations were used to locate the earthquake, but ASAIN station data weren't used due to the unavailability of real-time or almost real time connections with the ASAIN sites (Guidarelli et al., 2003).

In the following days the data from DSPA (Estancia Despedida, Tierra del Fuego) and JUBA (Base Jubany, South Shetland Is.) were recovered but only at the end of March 2004, when the Italian and Argentinean researchers, responsible for the maintenance and upgrading of the instrumentation at ORCD station, came back from the field the complete data set became available for processing.

The three stations were recording on August 4<sup>th</sup> and provided uninterrupted recording until today. All the relevant aftershocks show clear seismograms and phases on the three stations while Base Orcadas station, which is within the quake source area, is recording also the hundredths of microseisms accompanying the seismic sequence.

## The August 4<sup>th</sup>, 2003 "Orcadas Base Centenary Earthquake"

The South Orkney Microcontinent (SOM), a remnant of the original continuous ridge linking the tip of South America with the Antarctic Peninsula, represents the biggest (250 × 350 km) continental element of the South Scotia Ridge between the Antarctic and the Scotia Plates (Dalziel & Elliot, 1973; de Wit, 1977; Dalziel, 1984).

A complex geodynamic setting characterizes the northern side of the SOM where the main tectonic feature is represented by the sinistral transform fault running through it, where the Antarctic - Scotia plate border is also located (Forsyth, 1975). The southeast and southwest borders of the SOM are passive margins connecting the SOM to the Powell Basin on the west and to the Jane Basin on the East sides. A detailed description of the geological structure and tectonics of the SOM can be found in Busetti et al. (2001).

Fig. 1 shows the epicentral distribution of the aftershocks, with magnitudes up to 5.6, which followed the main shock deduced from the listings published in the international seismic catalogues. The majority of the epicentres lie very close to the sinistral transform fault representing the Antarctic-Scotia plate border.

The 7.5 magnitude earthquake that shook the South Orkney Is. on August 4<sup>th</sup>, 2003 represents the strongest known event in SOM region. It has been nicknamed the "Orcadas Centenary Earthquake" because exactly one hundred year ago the Orcadas Base was founded and has been continuously open since then. All ASAIN broadband digital seismographs recorded on scale waveforms on the three components exception made for ORCD, 70 km from the epicenter, where the P onset is properly recorded while the S group is saturated. The three component seismogram recorded at JUBA is shown in fig. 2.

Immediately following the "Centenary Earthquake" a notable aftershock sequence started. Within three hours from the main shock about twenty events exceeding magnitude 4.0 occurred. 24 hours later the number of events between magnitude 3.6 and 5.6 exceeded 50. As obvious ORCD station also recorded several hundredths microseisms. Vertical component seismograms of some relevant aftershocks occurred within a 15 minute time window a few hours after the main shock are shown in fig. 3.

The geographical distribution of the aftershocks greater than magnitude 3.6 occurred from August 2003 – to April 15<sup>th</sup>, 2004 covers an ellipsoidal area with the major axis extended for more than 150



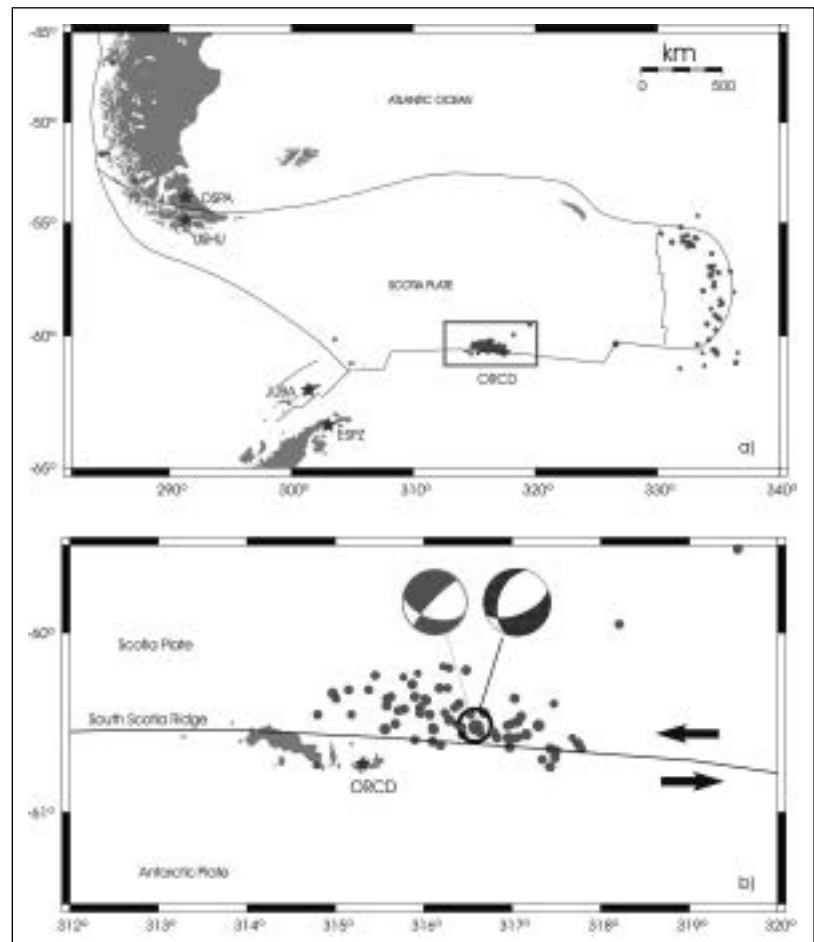


Fig. 1 - a) Map of Scotia sea region seismicity for the period August 4<sup>th</sup> 2003 – April 15, 2004. Blue stars: ASAIN stations. b) Magnification of the area in the green rectangle in fig a) showing the epicentres of the Centenary Earthquake and of the aftershocks with magnitude > 3.6 occurred before april 15, 2004. The main shock focal mechanism retrieved in this study (black symbol) and the solution from Harvard CMT (green symbol) are also shown.

km in the east-west direction along the main trend of the border between the Antarctic and the Scotia plates (fig. 1).

The availability of average structural parameters for the lithosphere of the Scotia sea region allows us performing the waveform inversion of regional earthquakes to retrieve focal mechanics and source time functions. The INPAR methods (e.g. Šílený et al., 1992) is particularly suitable in regions such as the Scotia Sea, where the high level of seismic noise, typical of oceanic environments, and the small number of stations, makes it difficult to determine the fault plane solutions using standard methods, such as the first arrivals technique. Particularly important is the capability of this method to give reliable results even when only a few seismograms from a limited number station are available (e.g. Kravanja et al., 1999).

We apply INPAR to investigate the focal mechanisms of the “Centenary Earthquake” and of its more relevant aftershocks using all the available seismograms from ASAIN and those recorded by the IRIS/USGS stations installed in the region. Fig. 1 shows the solution of a preliminary analysis obtained for the main shock and its comparison with the results proposed by Harvard CMT.

## Conclusion

The analysis of the data recorded by ASAIN stations JUBA, DSPA and ORCD since August 4<sup>th</sup>, 2003 shows that the seismic period initiated with the Orcadas Centenary Earthquake is still continuing. It is a matter of fact that, after 8 months from the start of the seismic period the seismicity level recorded by the ORCD station is still very high. The “Centenary earthquake” has given us the opportunity to record the complete seismic sequence caused by the greatest earthquake ever recorded in the South Orkney Island region. The information which will be obtained applying the quantitative seismology

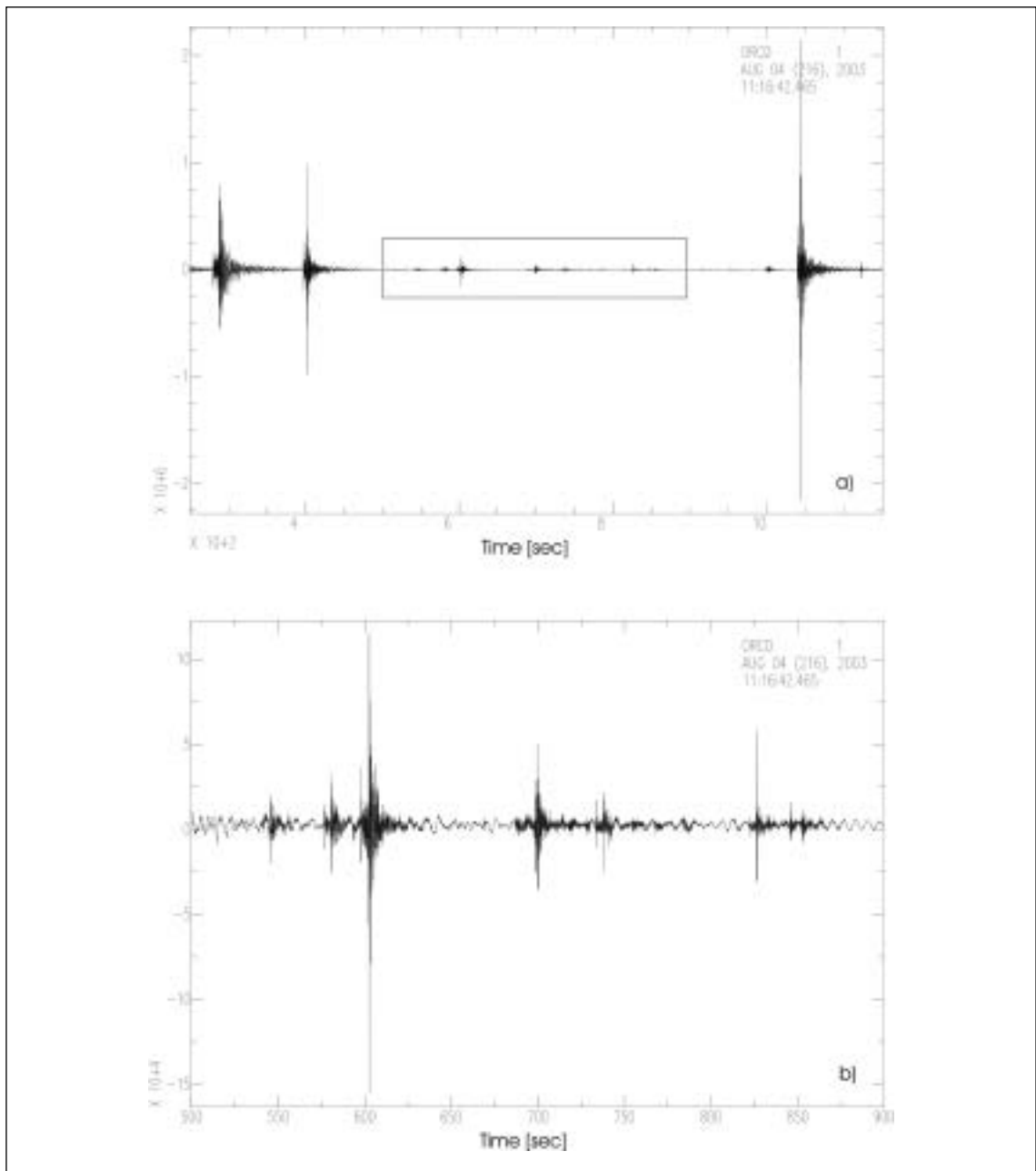


Fig. 2 - August 4<sup>th</sup>, 2003, 04:37:19 earthquake seismograms recorded at JUBA station.

methods to investigate the seismic sources will result in a better understanding of the complicated dynamics of this segment of the South Scotia Ridge and its interaction with the surrounding areas.

### Acknowledgements

The project “Broad-band seismology in the Scotia Sea Region” is financially supported by the Italian Programma Nazionale di Ricerche in Antartide in the framework of the PNRA research area “Geodesia e Osservatori”. Thanks are due to the Argentinian Institutions cooperating to the ASAIN: Dirección Nacional del Antártico - Instituto Antártico Argentino, Centro Austral de Investigaciones Científicas of Ushuaia and Universidad Nacional de La Plata. We are also extremely grateful to the military and civilian personnel operating in the Argentinian Bases Esperanza, Jubany, Orcadas and

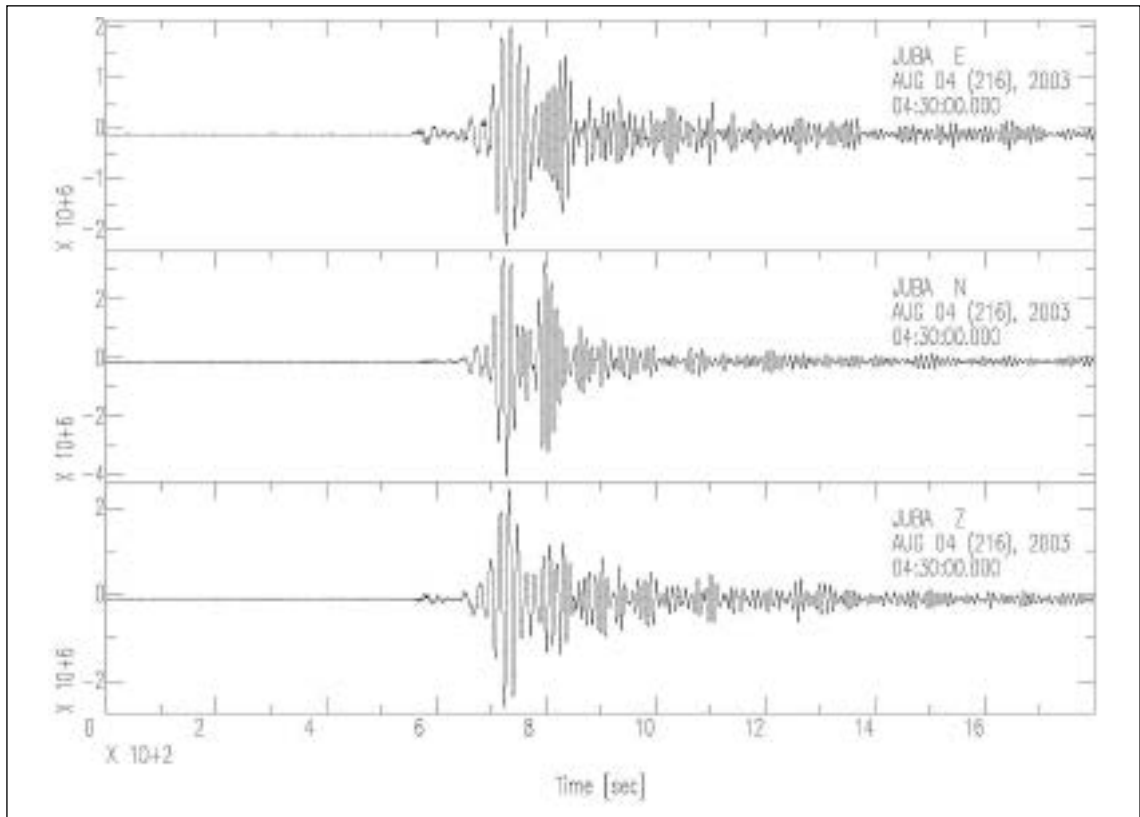


Fig 3 - a) ORCD station vertical component seismogram showing aftershocks recorded in a fifteen minute window seven hours after the main shock. b) Zoom of the rectangle in fig. a) showing only 400 sec of record.

Marambio for their help in maintaining the field installations and in the seismographic stations operation. We also thank the Abdus Salam International Centre for Theoretical Physics (ICTP) and the OGS for financing my TRIL fellowship. Software GMT by Wessel & Smith has been used to produce the maps of fig. 1.

## REFERENCES

- Bukchin B. G., 1989. Estimation of earthquake source parameters In: V. I. Keilis-Borok (Editor), *Seismic surface waves in a laterally inhomogeneous earth*. Kluwer Academic Publishers Dordrecht, 229-245.
- Bukchin B. G., 1990. Determination of source parameters from surface waves recordings allowing for uncertainties in the properties of the medium. *Izv. Akad. Nauk. SSSR, Fizika Zemli*, 25, 723-728.
- Busetti M., Zanolla C. & Marchetti A., 2000. Geological structure of the South Orkney Microcontinent. *Terra Antartica*, 8(2), 71-78.
- Dalziel I.W.D., 1984. Tectonic evolution of a forearc terrane, southern Scotia Ridge, Antarctica. Geological Society of America, Special paper 200, 32 p.
- Dalziel I.W.D. & Elliot D. H., 1973. The Scotia Arc and Antarctic margin. In: Stehli F. G. and Nairn A.E.M. (eds.), *The ocean basins and continental Margins*, vol. I, The South Atlantic. Plenum Press, New York, 171-246.
- De Wit M.J., 1977. The evolution of the Scotia Arc a key to the reconstruction of the southwestern Gondwanaland. *Tectonophysics*, 37, 53-81.
- Forsyth D.W., 1975. Fault plane solutions and tectonics of the South Atlantic and Scotia Sea. *Journal of Geophysical Research.*, 80, 1439-1443.
- Guidarelli, M., Russi, M., Plasencia Linares, M.P., Panza, G.F., 2003. The Antarctic Seismographic Argentinean-Italian Network and the Progress in the Study of Structural Properties and Stress Conditions in the Scotia Sea Region. *Terra Antartica Reports*, 9.
- Kravanja, S., Panza, G.F., & Šílený, J., 1999. Robust retrieval of seismic point source time function. *Geophysical Journal International*, 136, 385-394.
- Russi M. & Febrer J.M., 2001. Broad-band seismology in the Scotia Sea region, Antarctica. Italian and Argentinean contributions to the Scotia Sea Broad-band Network. *Terra Antartica*, 8(2), 29-34.
- Šílený J., Panza G. F. & Campus P., 1992. Waveform inversion for point source moment tensor retrieval with optimization of hypocentral depth and structural model. *Geophysical Journal International*, 108, 259-274.

## FURTHER DEVELOPMENTS OF THE ASAIN NETWORK IN ANTARCTICA AND TIERRA DEL FUEGO

3-04

M. Russi<sup>1</sup>, M.P. Plasencia Linares<sup>2,1,3</sup>, M. Guidarelli<sup>3</sup>

1 *Istituto Nazionale di Oceanografia e Geofisica Sperimentale – OGS  
Borgo Grotta Gigante 42/c, 34010 Sgonico (Trieste) – Italia*

2 *Depto de Sismología e Inf. Meteorológica, Fac. Cs. Astronómicas y Geofísicas,  
Univ. Nacional de La Plata, Paseo del Bosque s/n, 1900 La Plata – Argentina*

3 *Dipartimento di Scienze della Terra, Università di Trieste, via Weiss 48, 3412700 Trieste - Italia*

4 *The Abdus Salam International Centre for Theoretical Physics - ICTP  
Strada Costiera 11, 34100 Trieste - Italia*

### Introduction

An optimal global coverage of the Southern Hemisphere with broad-band seismographic stations is still an objective far from being reached. It has been remarked by many authors that this is especially true in the southern hemisphere, where relevant information on medium and low level seismicity is lost due to the lack of an appropriate density of stations in the oceanic regions and in the inhospitable Antarctic areas. Such a situation existed, at least until about a decade ago, in the wide region formed by the continental areas of southernmost South America (Patagonia and Tierra del Fuego), the Antarctic Peninsula and the oceanic region limited by the islands and ridges of the Scotia Arc. No permanent broad-band land station was operating there before 1992 and until today only a few temporary deployments of sea bottom seismographs on the oceanic floor of the Scotia Sea have been performed.

Since then a relevant effort has been conducted by some national antarctic programs to install a broad-band regional network capable of providing the seismological data base necessary to allow seismologists to afford the study of those areas using the powerful mathematical tools provided by digital seismology. Seven land stations have been put into operation up to now. Four of them constitute the Antarctic Seismographic Argentinean Italian Network (ASAIN), while three broad band stations are operated at Palmer station (PMSA), on the Falkland/Malvinas Is. (EFI) and on South Georgia Is. (HOPE) by the Incorporated Research Institutions for Seismology (IRIS) consortium.

In the following sections which follow we will present in detail the history and the state of the art of the ASAIN, also providing also some information about the planned expansion of the network with new land installations in Tierra del Fuego and in the Antarctic Peninsula.

### The ASAIN: History

Several permanent broad-band seismographic stations operating today in the Scotia Sea area (fig. 1a). Four of them constitute the ASAIN (fig. 1b). The ASAIN project started on February 1992 when a temporary station based on a three component broad-band Teledyne Geotech BB-13 seismograph and PDAS-100 recorder was installed at the Argentinian Base Esperanza (ESPZ) by the Osservatorio Geofisico Sperimentale di Trieste (today Istituto Nazionale di Oceanografia e di Geofisica Sperimentale - OGS) and the Instituto Antártico Argentino (IAA) (Russi et al., 1996). During two years the station provided continuous monitoring of the Scotia Sea regional seismicity and its recordings were used to obtain significant new information on the large-scale structure of the lithosphere in the Scotia Sea area (Russi et al., 1994).

Based on the analysis of these results, a preliminary plan for the development of a Scotia Sea region seismographic network was prepared jointly by the OGS and the IAA. The network layout included five stations located as shown in fig. 1c. Contacts were made with the British Antarctic Survey (BAS) and the United States Geological Services (USGS) to check their opinion and to establish reciprocal cooperation.

Working ASAIN stations, after 12 years from the beginning of operation of ESPZ station, are shown in fig. 1b. Two stations have been installed at sites along the South Scotia Ridge at the Argentinian Antarctic bases Jubany (JUBA, 2002, South Shetland Is.) and Orcadas (ORCD, 1997, Laurie Is., South Orkney Is.), while one is installed at Parque Nacional Lapataia in Tierra del Fuego, about 20 km about to the west of Ushuaia city (USHU, 1995), and a fourth station is located at Estancia

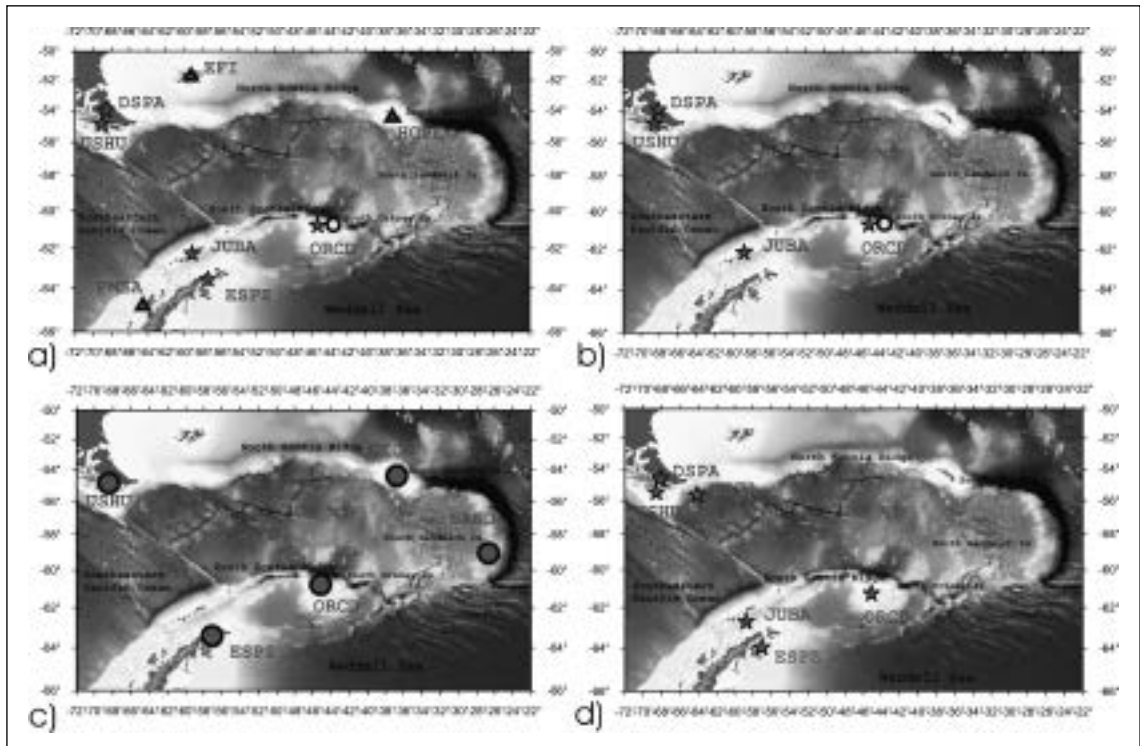


Fig. 1 - a) permanent broad-band stations located in the Scotia-Sea area. Stars: ASAIN; red circles: IRIS consortium; b) ASAIN: station location map (November 2003); c) ASAIN: the initial project (1992); d) ASAIN: network configuration after opening of new stations at Base Esperanza and Isla de Los Estados (2005-2006). The yellow circles in a) and b) mark the epicentre of the August 4th, 2003 earthquake.

Despedida (DSPA, 2002), about 40 km about to the west of Rio Grande city (Tierra del Fuego). ESPZ station, which has been the first broad-band station installed in the Scotia Sea region, has been temporarily closed at the beginning of 2002.

As it can be easily understood from the stations installation chronology, the technology and capabilities of the seismological equipment available on the market suffered a kind of revolution along the last decade. Technological progress allowed us to pass from 3.5", 1.44 Mb diskettes as recording media, allowing only three day storage autonomy, to three months local recording autonomy using Reftek 72A-08 systems, when ESPZ station was transformed into a permanent observatory (February 1995). The same kind of instruments was employed later when USHU and ORCD observatories started operation. Today all ASAIN stations are equipped with Guralp broad-band seismographs CMG-3T using GPS timing and great capacity storage media, allowing continuous recording of more than 18 months of three component seismic channels at 40, 20 and 1 sample/sec.

### The ASAIN: Research

The continued operation of ASAIN stations provides researchers the necessary broad-band seismograms needed to apply the seismological techniques to the analysis of regional seismicity and to investigate the structural properties and the geodynamics of the Scotia Sea region (Guidarelli et al., 2003). The results from research are then used to outline the evolution of the ASAIN and the improvements in the network geometry.

Surface waves group velocity tomography has been applied to the recordings of events located in the Scotia Sea region to obtain fundamental mode group velocity maps for Rayleigh and Love waves in the period range from 15 to 50 sec; significant lateral variations in the velocity values reflect the complexity of the tectonic and geological features. Regional shear velocity vs. depth models have been computed inverting averaged dispersion data (Vuan et al., 2000) by means of a "Hedgehog" non-linear procedure (e.g. Valys, 1969; Panza, 1981).

The moment tensor waveform inversion schemes developed by Sileny et al. (1992) and Sileny (1998) have then been applied to some selected regional events - employing the basic piece of information represented by the velocity models and regional earthquake data recorded by ASAIN and nearby IRIS stations - to investigate their focal mechanisms and source characteristics (Vuan et al., 2001). Work is in progress to apply the above method also to the ASAIN waveform data collected on the occurrence of the August 4, 2003, 7.5 magnitude South Orkney Is. earthquake and during the long aftershock sequence which followed the main event (fig. 2).

### The ASAIN: On going developments

The seismic sequence initiated by the “Centenary Earthquake”, the 7.5 magnitude event which shook the Orkney Is. On August 4<sup>th</sup>, 2003 when Orcadas base was preparing to celebrate its 100 years of continued operation, clearly put into evidence the guidelines to be followed in the short and medium term ASAIN development plans (fig. 2).

Orcadas base is only accessed during summer by the Argentinean Icebreaker A.R.A. Almirante Irizar, so serious instrumental faults may cause heavy data losses up to one year and more. Remote accessibility to the seismograph appears then to be an indispensable tool both to check its state of health and for to recover the data recovery. Almost the same is true for all Antarctic ASAIN sites.

According to the above, maximum priority has been given to a plan for the upgrade of all ASAIN stations with remote access facilities. The unavailability of a remote link facility is the only missing brick we need to add to allow easy data recovery and quick distribution of the data to international data centres like NEIC and ORFEUS.

On February 2005, Esperanza station will be reinstalled and a remote access link will be enabled. INMARSAT terminals are already operating at DSPA and ORCD. Nevertheless the communication costs are very heavy high and technical solutions allowing lower costs and higher data transfer rates are being sought to allow remote access and real-time monitoring of the seismicity at each ASAIN station site.

Work is also in progress to upgrade a temporary station (ESTD) installed by Estación Astronómica de Río Grande (EARG) researchers on the Isla de Los Estados (east of Tierra del Fuego) to broadband recording (fig. 1d).

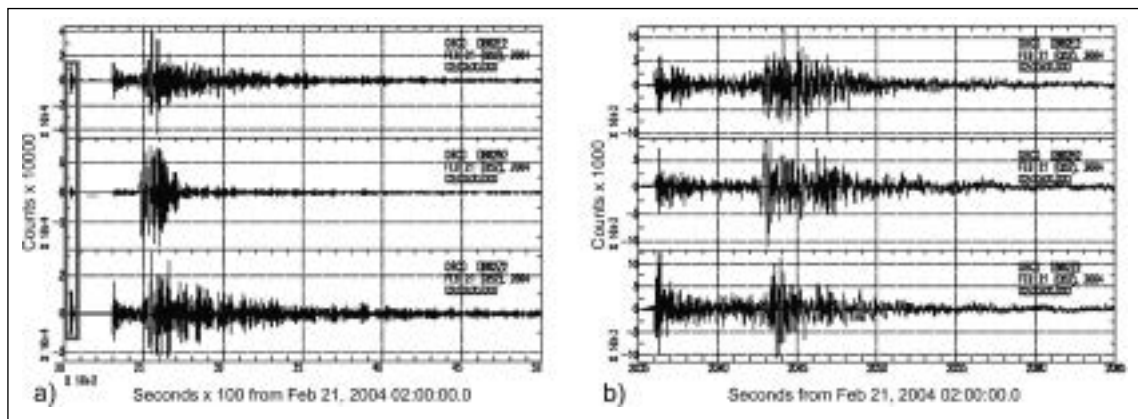


Fig. 2 - a) ORCD three component broad band recording of the South Atlantic ocean February 21, 2004, 6.5 magnitude earthquake. The red rectangle evidentiates a local microearthquake seismogram; b) zoomed display of fig 2a microearthquake signal.

### Conclusions

Since its beginning in 1992 the ASAIN network has proved an extremely effective tool in providing high quality data to researchers and in enhancing coordinated international cooperation among the Antarctic programs of the countries involved in the seismological investigation of the Scotia Sea area. Strong international cooperation is a prerequisite if we want to expand the station coverage to the

eastern part of the Scotia Sea in the South Sandwich area (as hypothesized in the 1992 version of the ASAIN project) and focus our work on selected areas of special interest as Tierra del Fuego, South Orkney Is. region, South Shetlands Is. and Bransfield Strait. The same is true if we want to perform long-duration broadband OBS deployments on the Scotia sea ocean floor to enhance the network detection power according to the requests of the international scientific community (Trieste International Workshop, 1999).

## Acknowledgments

The project “Broad-band seismology in the Scotia Sea Region” is financially supported by the Italian Programma Nazionale di Ricerche in Antartide in the framework of the PNRA research area “Geodesia e Osservatori”. Thanks are due to the Argentinian Institutions cooperating to the ASAIN: Dirección-Nacional del Antártico- Instituto Antártico Argentino, Universidad Nacional de La Plata - UNLP, Centro Austral de Investigaciones Científicas of Ushuaia. We are also extremely grateful to the military and civilian personnel operating in the Argentinian Bases Esperanza, Jubany, Orcadas and Marambio for their help in maintaining the field installations and in the seismographic stations operation. We also thank the Abdus Salam International Centre for Theoretical Physics (ICTP) and the OGS for financing Dr. Plasencia’s TRIL fellowship.

## REFERENCES

- Broadband Seismic Observations and the Geodynamics of the Scotia Sea Region, Antarctica. International Workshop, Trieste, 25-26 October 1999. *Terra Antartica* Vol. 8 (2), 28.
- Guidarelli, M., M. Russi, M.P. Plasencia Linares & G.F. Panza, 2003. The Antarctic Seismographic Argentinean-Italian Network and the progress in the study of structural properties and stress conditions in the Scotia Sea region, *Terra Antartica Reports*, 9, 25-34.
- Panza, G.F., 1981. The resolving power of seismic surface waves with respect to crust and upper mantle structural models. In *The Solution of the Inverse Problem in Geophysical Interpretation* (ed. Cassinis, R.) (Plenum Publishing Corporation).
- Russi, M., Febrer, J., Costa, G., Nieto, D.Y., and Panza, G.F., 1994. Analysis of digital waveforms recorded at the seismographic station Esperanza, *Terra Antartica*, 1(1), 162-166.
- Russi, M., G. Costa, & J.M., Febrer, 1996. Broad band seismology in the Scotia region. The Base Esperanza seismological observatory. In *Programma nazionale di Ricerche in Antartide, Italian Geophysical Observatories in Antarctica*. Antonio Meloni and Andrea Morelli editors, 51-65.
- Russi, M. & J.M., Febrer, 2001. Broad-band seismology in the Scotia Sea region, Antarctica. Italian and Argentinean contributions to the Scotia Sea Broad-band Network. *Terra Antartica*, vol. 8 (2), 29-34.
- Sileny, J., 1998. Earthquake source parameters and their confidence regions by a genetic algorithm with a “memory”. *Geophysical Journal International*, 134, 228-242.
- Sileny, J., P. Campus & G.F. Panza, 1992. Waveform inversion for point source moment tensor retrieval with variable hypocentral depth and structural model. *Geophysical Journal International*, 109, 259-274.
- Russi, M., J. Febrer, G. Costa, D.Y. Nieto & G.F. Panza, 1994. Analysis of digital waveforms recorded at the Seismographic Station Esperanza. *Terra Antartica*, vol 1, n° 1, 162-166.
- Valys V.P., 1972. Determining seismic profiles from a set of observations. In: VI. Keilis-Borok (ed.) *Computational Seismology*, Consult. Bureau, New York.
- Vuan A., M. Russi, & G.F. Panza, 2000. Group velocity tomography in the Subantarctic Scotia Sea region, *Pure and Applied Geophysics*, 157, 1337-1357.
- Vuan A., M. Russi, G. Costa & G.F. Panza, 2001. Moment tensor waveform inversion in the Sub-Antarctic Scotia Sea region: feasibility tests and preliminary results, *Terra Antartica*, 8(2), 55-62.





# Session 4

---

## **MAGMATIC PROCESSES**



## DISCOVERY OF ALKALI-BASALTS IN TIERRA DEL FUEGO

4-01

Rogelio Daniel Acevedo

*Centro Austral de Investigaciones Científicas (CADIC-Conicet)**Bernardo Houssay n° 200. V9410BFD, Ushuaia. rogelio.acevedo@cadicush.org.ar*

Alkali basaltic rocks with ultramafic inclusions have been discovered at the southernmost part of Argentina (Acevedo and Quartino, 2003). These outcrops represent the first documented appearances of alkaline volcanism in Tierra del Fuego.

Best expositions are found 500 m East to Beatriz mine, at 54°51'15"S/68°27'W, next to Beagle Channel, over the south slope of Monte Susana (E sample). They consist of an amygdaloidal aphyric black basalt hosted in slates (N75°E/50/60°SE) deposited during the Mesozoic. Another area, near Autódromo Municipal, shows basalts (A samples) without visible contact relations but many macrocrystals of amphibol (A2 sample), feldspar (A3 sample), olivine and xenoliths can be seen. Other smaller portions were taken among erratic boulders along Península Ushuaia coasts (P samples).

The petrography, texture and composition of numerous samples of basalts and xenoliths were investigated by petrographic observations and electron microprobe analysis. Xenocrysts of amphibol (kaersutite), K-Na feldspar, and minor olivine (Fo<sub>81-91</sub>), orthopyroxene (En<sub>87-92</sub>), clinopyroxene (En<sub>53</sub>Fs<sub>11</sub>Wo<sub>36</sub>), spinel, flogopite, Fe-Ti minerals and a diversity of xenoliths, mainly lherzolitic, pyroxenite and wehrlitic, are contained in the basalt groundmass. This is composed by laths of plagioclase (Ab<sub>79-86</sub>An<sub>2-6</sub>Or<sub>12-15</sub>), olivine (Fo<sub>82-87</sub>), pyroxene, opaque minerals, apatite and glass, with intersertal, hyalopilitic and pilotaxitic textures, without visible signals of deformation. Former amygdules are filled by analcite, zeolites, sodalite and calcite.

The normative IUGS classification, based on nepheline content, shows that this rock is an alkali basalt, except for the E sample that is a subalkali basalt (Table 1). The chemical classification, considering immobile elements such as Zr/TiO<sub>2</sub> versus Nb/Y indicates also an alkali basalt. Plots of total alkali versus silica over the TAS diagram fall in the foidite (Na-rich or nephelinite) and basanite fields.

Table 1

sample	SiO <sub>2</sub>	Al <sub>2</sub> O <sub>3</sub>	Fe <sub>2</sub> O <sub>3</sub>	MgO	CaO	Na <sub>2</sub> O	K <sub>2</sub> O	TiO <sub>2</sub>	P <sub>2</sub> O <sub>5</sub>	MnO
E1	43,63	13,53	13,04	4,83	8,27	3,32	1,05	2,80	1,36	0,24
A1	40,25	12,91	12,91	7,42	10,09	2,86	1,94	2,70	1,35	0,23
A4	41	12,21	12,93	11,05	9,89	4,32	2,26	2,77	1,51	0,23
P1	37,15	11,52	13,07	9,02	12,02	2,84	2,05	2,39	2,53	0,29
P2	38,95	11,75	12,76	9,79	11,51	3,21	1,42	2,51	2,01	0,25
P3	43,90	13,19	12,46	6,27	8,96	4,03	2,27	2,61	1,36	0,23

sample	Ba	Ni	Zr	Sc	C/Tot	S/Tot	SUM	LOI	SUM	#Mg
E1	723	75	233	12	0,07	0,04	92,41	7,4	99,81	0,24
A1	571	110	214	12	0,05	0,08	92,98	7	99,98	0,33
A4	648	208	179	16	0,07	0,08	98,52	1,4	99,92	0,42
P1	1087	139	219	11	0,07	0,02	93,36	6,6	99,96	0,37
P2	600	181	183	13	0,12	0,08	94,54	5,4	99,94	0,40
P3	703	66	215	13	0,06	0,17	95,63	3,8	99,43	0,30

sample	Q	ab	an	or	ne	di	en	ol
E1	2	28	19	6	0	4	10	0
A1	0	20	17	11	2	13	0	9
A4	0	11	7	13	14	19	0	13
P1	0	7	11	12	11	20	0	9
P2	0	14	13	8	7	18	0	11
P3	0	27	11	13	4	13	0	7

Primitive mantle-normalized REE, with strong LREE enrichment and HREE depletion, exhibit similar patterns through all the sampling. The REE patterns are fractionated with La/Yb~30 (Table 2).

Table 2

sample	Y	La	Ce	Pr	Nd	Sm	Eu	Gd	Tb	Dy	Ho
E	42,3	73	149	19,2	60	14,2	4,39	14,4	2,21	10,6	1,33
A1	35,3	70	133	17,9	56	13,2	4,15	12,7	1,96	9,28	1,12
A4	36,3	77	143	19,1	59	13,3	4,17	12,5	1,96	9,34	1,14
P1	49,8	120	222	29,1	86	19,8	6,15	16,6	2,74	12,4	1,61
P2	40,9	88	169	22	66	15,4	4,8	14,5	2,25	10,3	1,28
P3	37,3	67	129	17,2	54	13	4,11	11,3	1,93	9,06	1,17

sample	Er	Tm	Yb	Lu	Hf	Rb	Sr	Ta	Th	U	Nb
E	4,58	0,41	3,12	0,33	7,1	46,6	1643	7,4	7,5	2,6	89,4
A1	3,87	0,35	2,57	0,28	6	48,2	1547	6,6	7,4	2,4	87,8
A4	3,96	0,36	2,62	0,29	5,5	33,2	1484	6,4	7,2	2,2	83,8
P1	5,16	0,48	3,4	0,39	6	33,3	2157	8,2	10,8	3,1	98,6
P2	4,31	0,39	2,92	0,31	5,3	29,2	1831	6,9	8,5	2,6	83,5
P3	3,94	0,37	2,71	0,31	6,3	43,1	1755	7,5	7,7	2,6	87,3

K-Ar isotopic technique on individual macrocrysts were made at the Instituto de Geocronología y Geología Isotópica (InGeIs). Ages of  $146 \pm 5$  Ma (A2 amphibol) and  $127 \pm 4$  Ma (A3 alkali feldspar) have been obtained. One K-Ar basalt whole rock data reported  $8.3 \pm 0.3$  Ma. Nevertheless, these fertile samples show geochemical features typical of deep derived material. Based on the present-day tectonic setting, those data suggest that the basalt is older than its isotopic age.

The nature of the inclusion indicate a deep origin, possibly originated from the low crust and/or upper mantle.

## REFERENCES

- Acevedo, R.D. and Quartino, B.J. 2003. Basalto alcalino portador de xenolitos ultramáficos en Tierra del Fuego. *Revista Asociación Geológica Argentina*. Submitted.

## LITHOLOGIC TYPES OF THE JEU-JEPEN DIORITE ISLA GRANDE DE TIERRA DEL FUEGO

4-02

Acevedo Rogelio Daniel<sup>1</sup>, Roig Claudio<sup>2</sup>, Valín-Alberdi María Luz<sup>3</sup>

1 Centro Austral de Investigaciones Científicas (CADIC-Conicet)  
Bernardo Houssay n° 200. V9410BFD, Ushuaia. rogelio.acevedo@cadicush.org.ar

2 Universidad Nacional de la Patagonia SJB (Sede Ushuaia)  
Darwin y Canga, Ushuaia. australis@infovia.com.ar

3 Universidad de Oviedo. Departamento de Geología  
Arias de Velasco S/N°. 33005 Oviedo, Spain. mlvalin@geol.uniovi.es

## Geological background

The Jeu-Jepen Diorite (JJD) is a igneous body located at  $54^{\circ}35'S/67^{\circ}15'W$  in front of the southeasternmost end of Fagnano lake. It was consolidated  $93 \pm 4$  Ma (Acevedo *et al.*, 2000) and hosted in a sedimentary unit with a low grade of regional metamorphism (Beauvoir= Yahgan Formation, Early Cretaceous). An aureole of contact metamorphism that produced a biotite-bearing hornfels was found.

On the western slope of the Mt. Jeu-Jepen, a quarry was used for the removal of blocks to build the

Rio Grande Harbour. Extractive activity permits to recognize that the intrusive complex consists of a stock composed by many lithologic types:

- 1) a grained diorite (-gabbro), with a porphyroid local border, containing nodules of coarse-grained hornblendite;
- 2) a central syenite with radiated veins crossing through diorite;
- 3) a bulked irregular monzonite, in contact with the syenite mass and around the diorite;
- 4) a system of plutonite-associated melanocratic dikes.

## Petrography

**Diorite:** is a fine to medium-grained grey rock of dioritic to gabbro-dioritic composition. Microscopic texture consists of hypidiomorphic arrangement of no uniformly-sized clinopyroxene and plagioclase that form the greater part of this rock, with biotite and magnetite filling the interstices. Quartz is not present. Optical and chemical microanalysis indicate that clinopyroxene is augite-diopside and plagioclase is andesite-labradorite, which locally allow to discriminate between diorite and gabbro. Intense deformation delineates rocky lenses that become cataclastic until mylonitic.

In the outer parts of the body, there is a porphyroid diorite with subhedral phenocrysts of twinned plagioclase (andesite with secondary albite rim) 4/5 mm of shape and a groundmass constituted by alkali feldspar (albite and perthite) and clinopyroxene (diopside), biotite and magnetite.

In the lower part of the stock, there are a lot of ultramafic nodules, dark green in colour, with rounded borders, included within the diorite. The texture is coarse-grained and the composition is from gabbroic to piroxenitic-hornblenditic. The more conspicuous mineral is hornblende with subordinate clinopyroxene. Idiomorphous laths of plagioclase (oligoclase-andesite) are also present. As accessory minerals there are sphene, apatite, magnetite, pyrite and chalcopyrite. Looking at the thin section, the replacement-texture is frequent where clinopyroxene is altered into hornblende and hornblende is altered into biotite.

Aggregates of leucocratic pockets garnet-bearing, with perthites, plagioclase, quartz, apatite and biotite, placed in the diorite, is also locally observed.

**Syenite:** a mass of coarse-grained plutonic rock, composed essentially by potassic feldspar, is positioned at the core complex. It is constituted by microperthitic orthose (with undulated extinction) and clinopyroxene, biotite, sphene, zircon and opaque minerals.

**Monzonite:** is a medium-grained rock, pinky-grey in colour, folded and fractured. In the thin section, the texture is hypidiomorphic to allotriomorphic granular. Composition is represented by plagioclase (oligoclase-andesine) and K-feldspar (microperthitic orthose) in variate amounts and clinopyroxene (diopside). Also sparse biotite and amphibole as minor constituents are present. Magnetite (and goethite), sphene and apatite as accessory minerals.

**Melanocratic dikes:** many black dikes cut the plutonic complex. At naked eyes texture is aphanitic with micas and mafic minerals fluidally disposed. Petrographic observations reveal a combination of clinopyroxene (diopside), plagioclase (andesine) and magnetite, with hornblende, K-feldspar and apatite, forming a groundmass of intergranular texture. Based on dike-like condition and Fe-Mg phenocrysts, this rock can be considered as a calc-alkaline lamprophyre.

## Analytical techniques

Minerals were analysed with a Camebax S50 Cameca model electron microprobe analyser at the Servicios Científico-Técnicos of the Oviedo University (Spain).

Whole rock ICP analysis were made by Acme Labs (Canada) and are given in the following Table 1:

Major	SiO <sub>2</sub>	TiO <sub>2</sub>	Al <sub>2</sub> O <sub>3</sub>	Fe <sub>2</sub> O <sub>3</sub>	MnO	MgO	CaO	Na <sub>2</sub> O	K <sub>2</sub> O	P <sub>2</sub> O <sub>5</sub>	Cr <sub>2</sub> O <sub>3</sub>	LOI	Total
hornblendite	37,23	1,62	15,04	20,08	0,28	6,87	12,62	2,14	1,35	1,42	0,002	0,9	99,74
px-hornbl	41,04	1,58	11,04	16,71	0,19	9,86	14,14	1,71	1,39	0,41		1,4	99,69
diorite	48,2	0,92	17,22	10,93	0,25	5,06	10,44	3,15	2,6	0,55	0,01	0,5	100
monzonite	58,5	0,39	19,88	4,31	0,11	1,23	4,99	4,91	4,74	0,14		0,3	99,98
syenite	62,7	0,26	19,19	2,38	0,08	0,32	1,67	5,86	6,5		0,014	0,3	99,43
lamprophyre	47,2	0,98	15,61	10,69	0,27	6,27	11,42	3,01	0,84	0,47	0,02	2,9	99,86

Trace	Ba	Rb	Sr	Ta	Nb	Hf	Zr	Y	Th	U	Ni	Sc	Zn	Cu
hornblende	322	50,3	1208	0,5	2,3	1,9	35	17,1	3,5	1,4		35		
px-hornbl	391		540				43	13				138	76	280
diorite	519	84	1193	0,5	4,5	2,6	52	21	6,2	1,4	20	24		
monzonite	1597		1430		11		73	16						
sienite	608	132,3	475	1	10,7	4,8	155	14,4	18,6	4,3				
lamprophyre	250		1171				34	17			26	31		

REE	La	Ce	Pr	Nd	Sm	Eu	Gd	Tb	Dy	Ho	Er	Tm	Yb	Lu
hornblende	21	38	6,19	24	6,47	1,87	4,97	0,83	4,28	0,54	1,89	0,18	1,34	0,14
px-hornbl														
diorite	33	68	9,94	33	7,82	2,12	6,26	1,02	5,15	0,69	2,53	0,25	1,92	0,21
monzonite		64												
sienite	30	63	7,12	20	3,5	0,96	3,77	0,51	2,69	0,37	1,54	0,19	1,46	0,18
lamprophyre														

Norms	zircon	ortose	albite	anort	nefelin	diops	enstat	forster	cromit	ilmenit	hematit	sphen	perovs	apatite
hornblende		7,98	8,52	27,44	5,19	16,91		6,5		0,6	20,08		2,22	3,36
px-hornbl	0,01	8,21	5,84	18,34	4,67	34,73		5,92		0,41	16,71		2,32	0,97
diorite	0,01	15,36	23,19	25,17	1,87	16,51		3,47	0,01	0,53	10,93		1,09	1,3
monzonite	0,01	28,01	41,54	18,21		4,27	1,08			0,24	4,31	0,65		0,33
sienite	0,03	38,41	49,58	6,86		0,84	0,16	0,17	0,02	0,16	2,38	0,43		
lamprophyre	0,01	4,96	25,47	26,6		19,43	5,73	0,61	0,03	0,56	10,69	1,68	1,11	

## Discussion and conclusions

DJJ belongs to *Andean Diorites* (Nordenskjöld, 1905) as lateral part (*Monzonitic Series* by Kranck, 1932) of the Andean Batholith plutonic axis.

According to field observations, petrologic evolution is explained from a magmatic chamber where undersaturated silica melts are dominated mainly by the crystallization of the diorite (l.s.). They were trailed through a common elutriation phenomenon with ultramafic accumulation collapsed by gravity differentiation. A second, authopenetrative consanguineous episode, rich in potassium, which produced syenite and the consequently authometasomatism and monzonite generation over dioritic bulk, then occurred finally, residual parental liquids introduced lamprophyres. Petrographic and compositional relations among the varieties of JJD are interpreted as the result of fractional crystallization that represents the major magmatic mechanism.

Geochemistry of JJD is calc-alkaline. Geochemical alkaline affinities are due to the later enrichment in potassium. Feldspathoids are absent. The JJD actual geographic position respect to the Magallanes-Fagnano fault is merely casual.

## REFERENCES

- Acevedo, R.D.; Roig, C.E.; Linares, E.; Osters, H.A.; Valín-Alberdi, M.L.; Queiroga-Mafra, J.M. 2000. La intrusión plutónica del Cerro Jeu-Jepén. Isla Grande de Tierra del Fuego, República Argentina. *Cadernos do Laboratorio Xeolóxico de Laxe*. Vol.25: 357-359. A Coruña. Spain.
- Kranck, E.H. 1932. Geological investigations in the Cordillera of Tierra del Fuego. *Acta Geographica* 4(2). 231 p. Helsinki.
- Nordenskjöld, O. 1905. Die Krystallinischen Gesteine der Magellansländer. *Svenska Expeditionen till Magellansländerna*. 1(6): 175-240.

## IRON SULFIDES RELATED TO FUMAROLIC VENTS IN DECEPTION ISLAND, ANTARCTICA

4-03

Alberto T. Caselli, Selvia M. Tourn, Cintia Bengoa

*Dpto. Ciencias Geológicas, Facultad de Ciencias Exactas y Naturales. UBA, Ciudad Universitaria, Pab.2, C.P. C1428EHA Buenos Aires, Argentina. acaselli@gl.fcen.uba.ar, selvia@gl.fcen.uba.ar, cintiabengoa@hotmail.com*

### Introduction

Deception Island (62°57' SL, 60°38' WL) is one of the three emerged volcanoes that are part of a volcanic complex developed on the rift axis of the Strait of Bransfield (González-Ferrán et al. 1971). This late Neogene basin was developed on the Mesozoic-Cenozoic continental arc exposed in the Antarctica Peninsula and the South Shetland Islands. At the time of formation the area was under the influence of the movement of the Pacific, Antarctic and Scotia plates (Galindo-Zaldívar et al., 1996) in connection with a slow subduction rate in the South Shetland trench (Larter 1991; Lawver et al 1995). The Bransfield is not a normal back-arc basin since it is not currently linked with an active volcanic arc; for that reason it is better described as a marginal marine basin (Barker and Austin 1994, González-Casado et al., 2000).

Deception Island has a submerged basal diameter of 30 km and a height of 1500 m from the marine bottom. It is part of a continuous low axial volcanic ridge and several axial and off-axis seamounts and islands (Gracia et al., 1996). It is mainly composed of volcanics and pyroclastics of basaltic andesite composition with dacitic flows subordinated. It constitutes at present the most active volcanic focus in the area with a recent eruptive history in the years 1840, 1967, 1969 and 1970. Several geothermically anomalous surficial areas (Fig.1) of different temperatures and gaseous emanations of varied chemical composition have been found in the island (Martini and Giannini 1988; Villegas and Caselli 1993; Villegas et al., 1997a and b; Caselli et al., 1994; Caselli et al., 2002; 2004). The gaseous vents located in Fumaroles Bay constitute one of the major vent fields in the island, with CO<sub>2</sub> and H<sub>2</sub>S-rich emissions. Subsequent to an important seismic crisis in the summer of 1999 related to the intrusion of dikes to subsurficial layers (dos Santos Afonso and Caselli 2002, Caselli et al., 2004),

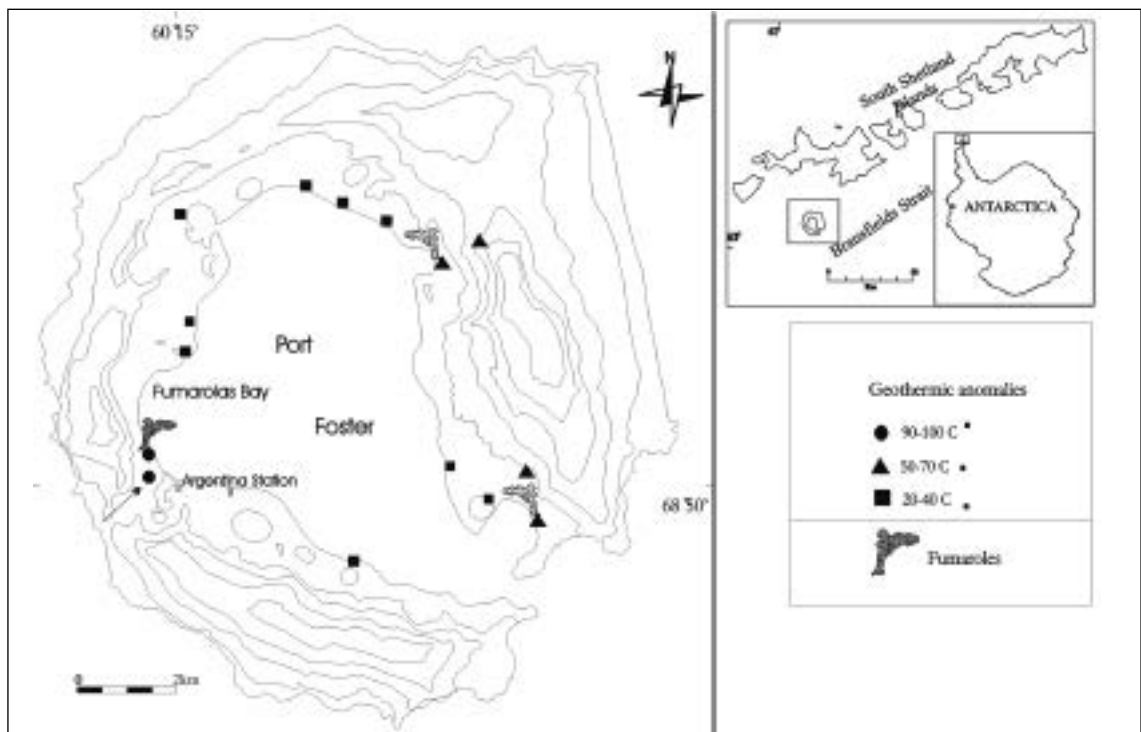


Fig. 1 - Location map and distribution of geothermal anomalies.

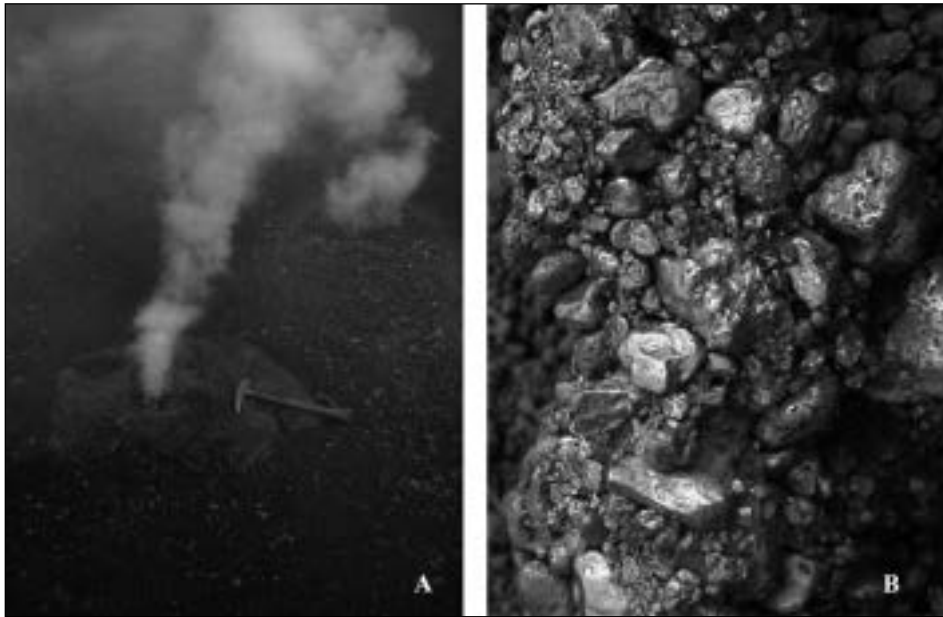


Fig. 2 - A) View of the fumaroles; B) pyroclastics coated and cemented by pyrite.

pyrite deposits were found covering the pyroclastics around the fumarole holes. Earlier, the existence of anomalies of Fe, Mn, Zn, As and Ba in sedimentites of the caldera bottom (Port Foster) had been reported by Rey et al. (1995) linking them with hydrothermal processes.

The back-arc basins have a great metallogenic potential in connection with hydrothermal mineralization of massive sulfides. Consequently, Deception Island constitutes a unique opportunity to study the evolution of an active volcano linked with ore formation processes in a back-arc basin environment. In this sense, a synthesis of the main elements known up to now in the area and a preliminary discussion of the metallogenic perspectives for basins of this nature are given in this paper.

### Description of the fumarolic system and geochemistry

The system is mainly represented by three fumaroles located at the beach of Fumaroles Bay and several subaqueous emissions near the coast (Fig 2A). Temperatures of 98°-100°C were registered at the hole mouths with a strong attenuation when moving away from them. The chemical composition of the emanations is mainly represented by steam (water vapor), followed by CO<sub>2</sub> as other important constituent; minor amounts of H<sub>2</sub>S, SO<sub>2</sub>, N<sub>2</sub>, H<sub>2</sub>, O<sub>2</sub>, Ar and CH<sub>4</sub> are present; also rather significant quantities of ethane (C<sub>2</sub>H<sub>6</sub>) were registered in some of the samples analyzed. It is remarkable that since 1999 the proportion of SO<sub>2</sub> registered in the fumaroles was considerably increased (Caselli et al. 2004, Agosto et al. 2004). As a consequence, from that year until the present time deposits of native sulfur, and iron sulfide in thin layers were observed coating or cementing the pyroclastics on the beach (Fig. 2B). It was also determined experimentally that an iron sulfide patina was formed on iron objects buried in the fumaroles in less than an hour of exposure. Studies with electronic microscopy and spectroscopy of X rays (EDAX) on the formed sulfides indicated a chemical composition of iron sulfide with framboid morphology. By diffraction of X-rays it was determined that the only iron sulfide deposited was pyrite. They form microscopic aggregates of pyrite grains of about 0.2-micrometer average in size often in spheroid clusters resembling raspberry seeds.

### Discussion and final considerations

The fumaroles of Deception Island have a strong hydrothermal character in the sense that they are low-pressure systems which major emission is water vapor. The magma injection in subsurficial layers occurred in 1999 gave origin to changes in the pressure and temperature conditions of the fusion which resulted in a higher exsolution of volatile components. Progressive pressure decrease allows the



expansion of the already existent bubbles due to pure decompression and diffusion of the volatile through the liquid toward them. The cooling of a magma reservoir or of dykes located in relatively shallow positions contributes to increase this process. As this gas has very low viscosity it can escape from the reservoir through cracks generating a slow but continuous gas loss noticed in the earth surface (Greenland et al., 1985; Gerlach and Graeber 1985). As the gas is ascending through flaws to the surface, equilibrium conditions with the wall rock are not reached emerging as SO<sub>2</sub>-rich emissions (dos Santos Afonso and Caselli 2002, Caselli et al., 2004). Linked with these emissions, deposits of native sulfur and iron sulfides with framboid morphology are formed on the earth surface.

Active hydrothermal vent systems and polymetallic sulfide deposits are known from many places on the global ocean ridge system and from back-arc basins like the well studied Lau Basin in the Southwestern Pacific (Hawkins Jr., 1995). Evidence of hydrothermal circulation in the Lau Basin was obtained in the form of stained pillow surfaces in a part of the spreading center. Occurrences of hydrothermally formed nontronite and manganese oxide crusts (birnessite) and metallic sulfides (pyrite and chalcopyrite) impregnating volcanic rocks were dredged from one of the ridges (Von Stackelberg et al., 1985). The sulfides occur mainly with basaltic andesite and rhyodacite (Fouquet et al., 1991; Hawkins Jr., 1995). In the vent fields studied different types of deposits were recognized. They consist of low-temperature hydrothermal Fe-oxides and Mn-oxide crusts that cover higher-temperature sulfides, the crusts being related to hydrothermal discharges (40°C) through permeable andesitic rocks. Also, barite chimneys and masses of barite mixed with sulfides that were formed by medium- to high-temperature discharges were found in an inactive vent field. The highest temperature deposits found were black (320-400°C) and white (250-320°C) smokers.

The recent superficial deposits of native S and S<sub>2</sub>Fe (pyrite) and the anomalies of Fe, Mn, Zn, As and Ba detected in sediments of the caldera bottom of Deception island are no doubt similar to the minerals and elements produced by hydrothermal activity in back-arc basin settings. The still scarce hydrothermal mineralogy identified in Deception Island possibly belongs to an early stage in the evolution of these hydrothermal-magmatic systems.

## REFERENCES

- Agosto M.R., Caselli A.T. y dos Santos Afonso M., 2004. Depósitos de piritas framboidales en fumarolas de Isla Decepción (Shetland Del Sur, Antártida): Implicancias metalogénicas. *Revista de la Asociación Geológica Argentina* 59 (1): 152-157.
- Barker D.H.N. y Austin J.A. 1998. Crustal diapirism in Bransfield Strait, West Antarctic: evidence for distributed extension in marginal-basin formation. *Geology* 22, 657-660
- Caselli, A., Cohen, M. y Villegas, M.T., 1994. Geoquímica de gases fumarólicos de la isla Decepción. Su evolución e implicancias volcanológicas. Terceras Jornadas de Comunicaciones sobre Investigaciones Científicas Antárticas. Buenos Aires. Acta, 171-174.
- Caselli, A., dos Santos Afonso, M., Rizzo, C., García, A. y Ortiz, R., 2002. Caracterización geoquímica de los gases volcánicos de isla Decepción (Shetland del Sur, Antártida). *Revista de la Asociación Geológica Argentina*. 57 (1): 69-79.
- Caselli A.T., dos Santos Afonso M. y Agosto M.R., 2004. Gases Fumarólicos de Isla Decepción (Shetland Del Sur, Antártida): Variaciones químicas y depósitos vinculados a la crisis sísmica de 1999. *Revista de la Asociación Geológica Argentina* 59 (2): en prensa.
- dos Santos Afonso, M. y Caselli, A.T., 2002. Variaciones en la geoquímica de gases fumarólicos de Isla Decepción (Antártida) vinculadas a intrusiones ígneas someras. XV Congreso Geológico Argentino, El Calafate, Santa Cruz, Argentina, 2002. *Actas Tomo I*: 450-455.
- Fouquet, Y., von Stackelberg, U., Charlou, J.L., Donval, J.P., Foucher, J.P., Erzinger, J., Herzig, P., Muhe, R., Soakai, S., Weidlicke, M., and Whitechurch, H., 1991. Hydrothermal activity in the Lau back-arc basin: Sulfides and water chemistry. *Geology* 19:303-306.
- Galindo-Zaldívar J., Jabaloy A., Maldonado A. and C. Sanz de Galdeano, C. 1996. Continental fragmentation along the South Scotia Ridge transcurrent plate boundary (NE Antarctic Peninsula). *Tectonophysics* 259: 275-301.
- Gerlach T.M. y Graeber E., 1985. Volatile budget of Kilalhuea. *Nature*, 313: 273-277
- González-Casado J.M., Giner-Robles J.L. and L. López-Marín J. 2000. Bransfield Basin, Antarctic Peninsula: not a normal backarc basin. *Geology* 28: 1043-1046.
- González-Ferrán, O., Munizaga, F. y Moreno, H., 1971. Síntesis de la evolución volcánica de isla Decepción y la erupción de 1970. Instituto Antártico Chileno. Serie Científica, 2, 1-14.
- Gracia, E., Canals, M. Y 15 autores más, 1996. Morphostructure and evolution of the central and eastern Bransfield Basins (NW Antarctic Peninsula). *Marine Geophysical Researches* 18: 429-448.
- Greenland, L.P., Rose, W.I. and Stokes, J.B., 1985. An estimate of magmatic gas content and gas emissions from Kilauea volcano, Hawaii. *Geochimica et Cosmochimica Acta* 49 (1): 125-129.
- Hawkins Jr., J.W., 1995. The geology of the Lau Basin. In *Backarc Basins Tectonics and Magmatism*. Ed. Brian Taylor, Plenum Press, New York. 63-138.
- Larter 1991. Debate: preliminary result of seismic reflection investigations and associated geophysical studies in the area of the Antarctic Peninsula. *Antartic Science* 3: 217-222.
- Lawver L.A., Keller R.A., Fisk M.R. and Strelin J.A., 1995. Bransfield Strait, Antarctic Peninsula: active extension behind a dead arc. (In Tylor B., ed. *Back-arc basins: tectonics and magmatism*. New York

- Martini, M. and Giannini, L., 1988. Deception Island (South Shetland): an area of active volcanism in Antarctica. *Memoria de la Sociedad Geológica Italiana*, 43, 117-122.
- Rey, J., Somoza, L. y Martínez-Frías, J., 1995. Tectonic, volcanic, and hydrothermal event sequence on Deception Island (Antarctica). *Geo-Marine Letters* 15: 1-8
- Villegas, M.T. y A.T. Caselli, 1993. Fumarolas de Decepción: evolución a lo largo del verano austral. Modelo de despresurización del acuífero. *V∞ Simposio de Estudios Antárticos*, Barcelona, España. Actas p.1-15.
- Villegas, M.T., Caselli, A.T. y García, A., 1997a. Nuevas aportaciones en el estudio de las variaciones estacionales de los gases volcánicos de la Isla Decepción (Islas Shetland del Sur, Antártida). *Boletín de la Real Sociedad Española de Historia Natural*. Madrid, España. Tomo 93, N° 1-4: 145-153.
- Villegas, M.T., R.Ortiz, A.Caselli and M.Cohen, 1997b. Chemical variations of fumarolic gases in Deception Island, South Shetland I., Antarctica. In *The Antarctic Region: Geological Evolution and Processes*. C.A. Ricci (Ed.) Terra Antarctica Publication pp.1077-1082, Italy.
- Von Stackelberg, U., and Shipboard Party, 1985. Hydrothermal sulfide deposits in back-arc spreading centers in the southwest Pacific. *Bundes. Geowiss. Rohstoffe Circ.* 2:2-14.

## EMPLACEMENT FABRICS OF THE CONCÓN DYKE SWARM, CENTRAL CHILE 4-04

C. Creixell<sup>1</sup>; M.A. Parada<sup>2</sup>; P. Roperch<sup>3</sup>; C. Arriagada<sup>2</sup>; D. Morata<sup>2</sup>

1. MECESUP-, Depto. Geología, Universidad de Chile (ccreixel@ing.uchile.cl)

2. Departamento de Geología, Universidad de Chile

3. Institute de Recherche pour le Development (IRD); Santiago, Chile

### Introduction

The occurrence of dyke swarms is mainly associated to intraplate extensional settings, in some cases clearly related to plume processes and continental fragmentation. In more restricted cases, the development of dyke swarms is related to active continental margins, such as the Middle Jurassic in Western North America (Glazner et al., 1999). In the Andean arc of central Chile, mafic dyke swarms were developed between Middle Jurassic and Early Cretaceous (Irwin et al., 1987; 1989), and reveals a more complex magmatic and tectonic history. In this study, we present field, structural, petrographic and paleomagnetic data about the emplacement of the Concón Dyke Swarm (CDS).

### Geological Setting

The Concón Mafic Dike Swarm is exposed along ca 10 km along the shore line between Concón and Reñaca, in the Coastal batholith of central Chile (33°30' S, Fig. 1). At this latitude, the batholith is composed by granitoid rocks of Upper Palaeozoic to Lower Cretaceous age (Parada et al., 1999). In the study area (Reñaca beach), a Rb-Sr whole rock isochron of 299±31 Ma has been obtained in granitoids hosting the CDS (Hervé et al., 1988). Ar-Ar ages of 169.6±3.6 and 165±2.6 Ma were obtained in mafic dyke and microdiorite respectively at Punta Curaumilla (ca. 20 km south of study area). These ages are broadly similar to U-Pb (163-160 Ma) and Rb-Sr (156.3±1.2 Ma) ages obtained in syntectonic intrusions at the same locality (Godoy & Loske, 1988).

### Geology and fabrics of the Concón Mafic Dyke Swarm

The CDS comprise gabbroic intrusions 0.5 to 15 metres thick. Geological features allows us to recognise two groups of dykes:

a) Group 1: includes 3-15 meters thick diabase dykes (N32°-76°W/53°-90°SW). The dykes show chilled margins and highly penetrative shear deformation parallel to dyke walls. Petrographically they are characterised by porphyritic texture due to abundant plagioclase and minor Mg-hornblende phenocrysts. The fine grained mass is composed by calcic amphibole, biotite, magnetite, minor quartz and secondary sphene. Opaque grains are present in 1 to 4%. This groundmass shows solid-state recrystallisation around phenocrysts. Plagioclase phenocrysts also show these effects as albitic overgrowth rims (An<sub>24-18</sub>) over primary calcic cores (An<sub>58-44</sub>). Some dykes are mylonitised (site RN03). Equilibrium temperatures of hornblende and plagioclase crystallisation (Holland & Blundy, 1994) fall between 621 and 680° C.

b) Group 2: intrusions of this group are thinner (<1.5 meters) than those of group 1 and in most

outcrops they cut them. These dykes have variable orientation N40-86°W/50-90°SW. As in Group 1, margins are chilled and sheared. Texturally they are characterised by the presence of Mg-hornblende phenocrysts in a fine grained matrix composed of calcic amphibole, plagioclase ( $An_{56-45}$ ), minor magnetite (1 to 3.5%) and secondary sphene. Solid state textures are absent, in agreement with crystallisation temperatures of amphibole and plagioclase (~700° C).

### Field Relations

Planar foliations N0°-45°NW/72-90°SW in the country rock are the older tectonic features in the area. Intrusion of mafic dykes was developed in already deformed country rocks. Discrete sinistral shear fractures (S-C structures) in the country rocks are associated to Group 1 intrusions. Locally we can observe that mafic magma (branches) was emplaced in spaces generated by these shear planes. Xenoliths in these thick dykes have sinistral-sigmoid shape whereas others are only sinistrally rotated. Mineral lineation at the margins are parallel to walls, but 40-20° clockwise oblique in central portions of the dykes, generating an asymmetrical fabric pattern. This oblique lineation is approximately parallel to the shear fractures observed in the country rocks. Local branches pointing to NW are considered as evidence of SE to NW magma flow (fig. 2). Group 2 dykes cut all these previous structures, including shear zones and Group 1 dykes, but they are locally cutted by discrete NNE-trending dextral shear zones. Mineral lineations show the similar asymmetrical pattern observed in Group 1 intrusions.

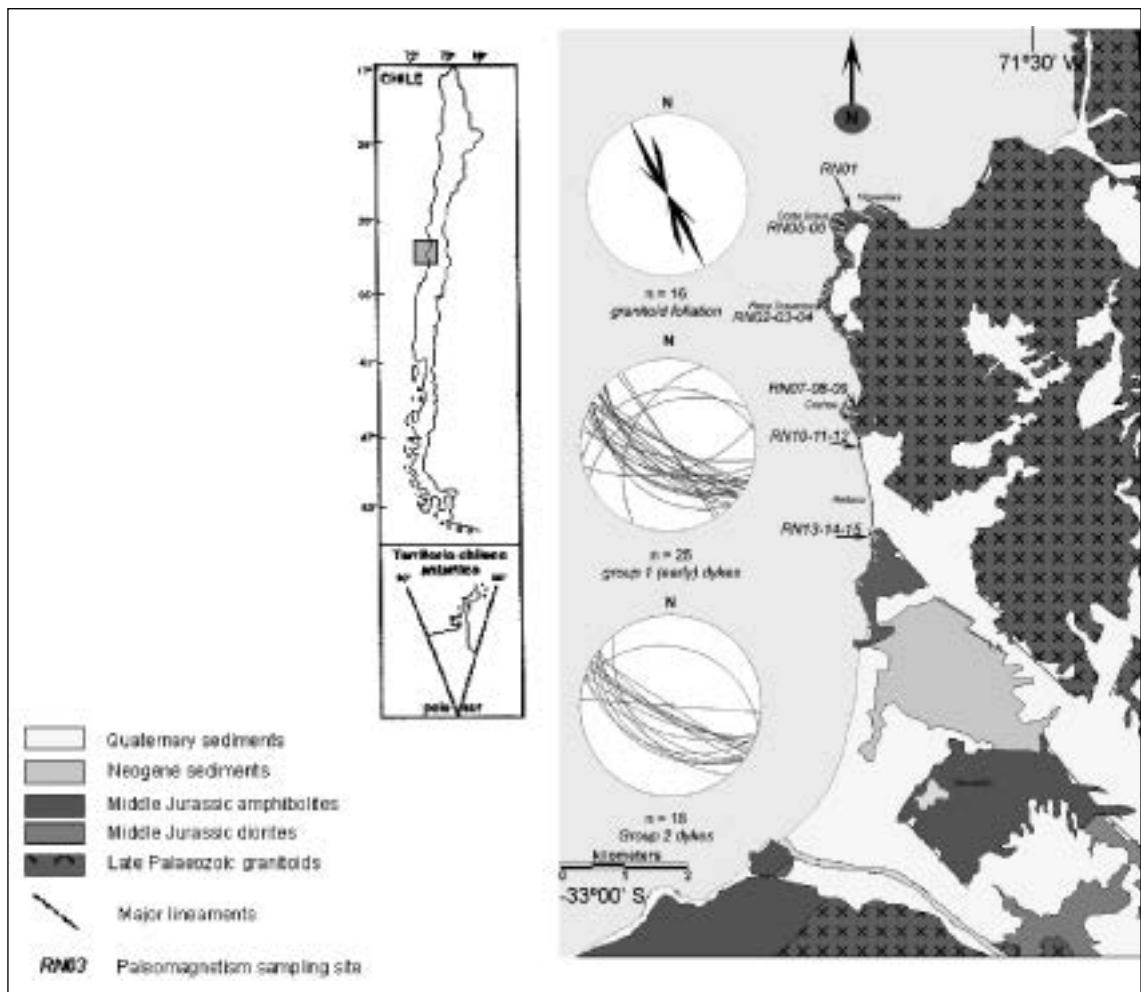


Fig. 1 - Simplified geological map of the study area. Stereograms show orientations of country rock foliation and orientation of mafic dykes. Location of paleomagnetism sampling sites are also showed. White lines indicate location of main dyke outcrops.

## Anisotropy of Magnetic Susceptibility (AMS)

Magnetic properties of mafic dykes and country rocks were measured in several sites (fig.1). A variable number of cores were collected in each site (generally between five and ten). AMS was measured with the KLY3-S Kappabridge at the Paleomagnetism Laboratory of Departamento de Geología, Universidad de Chile.

For Group 1 dykes (six sites), as is typical for basaltic dykes, AMS values don't exceed 8%, with the exception of sites RN03 and RN09 (mean 26.2% and 20.3% respectively). These dykes are characterised by the strongest mylonitic fabrics. Curie experiments indicate that magnetite is the main carrier of the magnetisation. In most cases, shape parameter T indicates that ellipsoids are mainly oblate. In all ellipsoids K1 and K2 poles define a plane perpendicular to K3 poles. In most cases, magnetic fabrics are similar to field fabrics, foliation planes and lineation are oblique to dyke trends in central portions of the body and parallel to walls at margins (fig. 2). Magnetic lineations plunge to SE in most cases, with low plunge angles at margins (between 7 and 21°). Foliation planes are predominantly horizontal, probably reflecting also the effects of horizontal stresses. Magnetic fabrics in associated country rocks are strongly consistent with fabrics measured in the field.

Dykes of group 2 have AMS values that do not exceed 5%, with exception of near-margin data on site RN12 (15 to 25%). In these rocks, Curie experiments indicate that magnetite is the main carrier of the magnetisation. Ellipsoids are oblate and characterised by K1 and K2 defining a magnetic plane, perpendicular to K3 poles. As in dykes of Group 1, magnetic fabrics are constantly oblique to dyke trends in central portions of the intrusions. Magnetic lineations are highly variable in sense and plunge, probably reflecting greater effects of tectonic stresses or particle interactions than in Group 1 dykes.

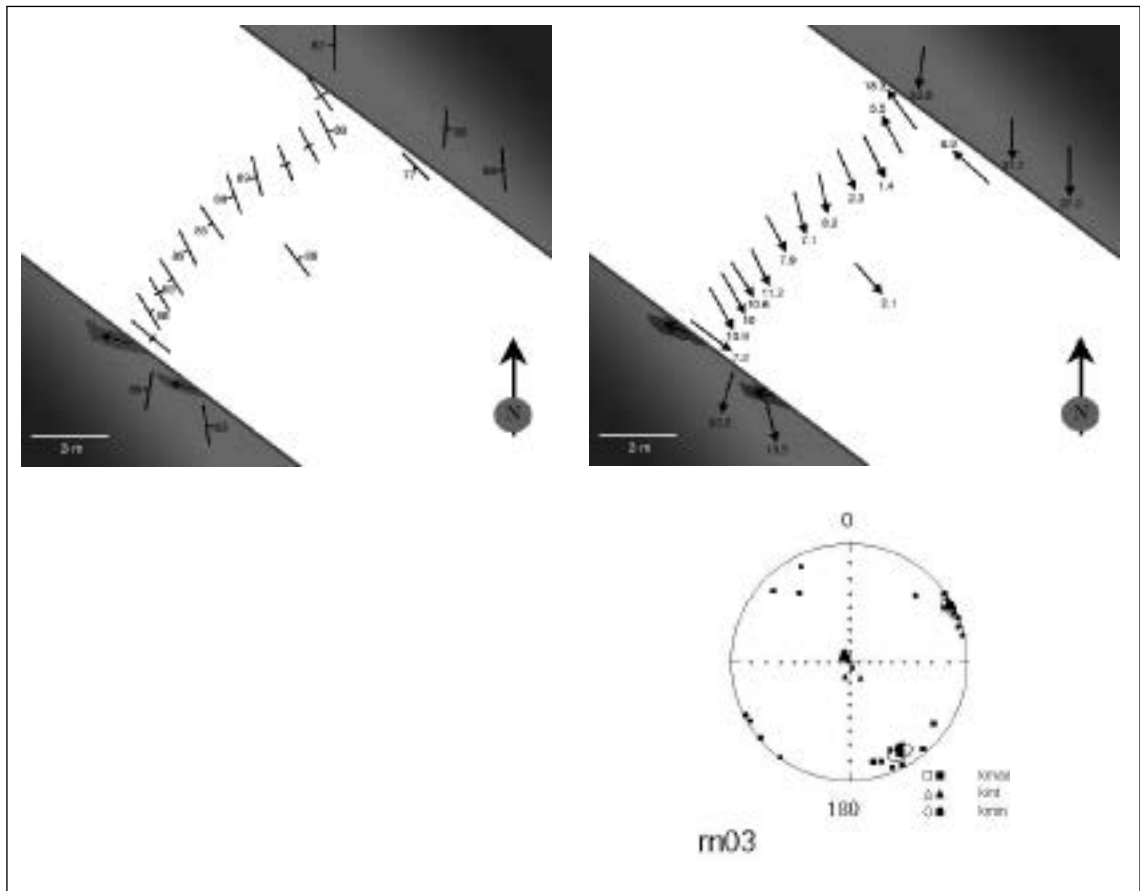


Fig. 2 - Schematic representation of magnetic fabrics and field features of a mafic dyke (site RN03). a) foliation, b) lineation, c) stereographic projection of K1, K2 and K3 axis.

## Interpretation and conclusions

A consistent feature of the CDS is the presence of asymmetrical fabrics with respect to dyke walls. These features are observed in all sub-fabrics: plagioclase and amphibole mineral lineations and magnetic sub-fabrics. That type of fabric resemble a “sinistral fabric” in tectonised rocks and cannot be expected in a situation of pure magma flow in a fracture channel, where a symmetrically imbricated or wall-parallel fabric is developed (i.e. Knight & Walker, 1988). Previous workers show the importance of the presence of sheet-like magmatic bodies with oblique fabrics (i.e. Hutton, 1992; Correa-Gomes et al, 2001; Féménias et al, in press). In these cases, the occurrence of asymmetrical fabrics are explained by variable degree of wall-rock displacement along the magma-filled fracture at the time of intrusion. It means that the magma was emplaced along shear zones. Correa-Gomes et al. (2001), based on theoretical models, indicate that this kind of asymmetrical fabrics can be formed by the combination of magma flux stresses and dominant sinistral shear stresses. Following these interpretations, the data available for the CDS indicates that both group of dykes were emplaced along shear fractures with sinistral movements. The tectonic stresses associated with these shear movements were active during magma emplacement, and in the case of dykes of Group 1, these forces were active also shortly after consolidation of the magmatic bodies, as suggested by solid state fabrics. In dykes of Group 2, absence of solid state fabrics and minor development of shear fractures in the associated country rocks indicates that tectonic stresses were more restricted in time and probably in magnitude.

Magmatic flow directions interpreted from field indicators and magnetic lineations indicates that magma flow come from SE to NW in the case of Group 1 intrusions. These magma flow vectors were near horizontal. For the case of Group 2, the information is still ambiguous and we expect that future additional data allows us to recognise the flow pattern of these dykes.

The present results indicate that the basaltic magmas of the Concón dyke swarm were emplaced along NW-shear fractures, associated with sinistral shearing. This kind of syn-tectonic emplacement probably was a characteristic feature of the Jurassic Andean arc at this latitude, where other syn-tectonic mafic intrusions has been recognised (Godoy & Loske, 1988) and opens a new perspective on the tectonic study of the Mesozoic arcs of the central Andes.

## Acknowledgments

This research was financed by Fondecyt Project N° 1031000 (D.M.). Natalia Astudillo is also acknowledged by helping in laboratory technics and data processing.

## REFERENCES

- Correa-Gomes, L.C.; Souza Filho, C.R.; Martins, C.J. & Oliveira, E.P. 2001. *Journal of Structural Geology* (23): 1415-1428.
- Féménias, O.; Diot, H.; Berza, T.; Gauffriau, A. & Demaiffe, D. in press. *Journal of Structural Geology*
- Gana, P.; Wall, R. & Gutierrez, A. 1996. *Sernageomín*.
- Glazner, A.; Bartley, J.M. & Carl, B. 1999. *Journal of Structural Geology* (21): 1275-1283.
- Godoy, E. & Loske, W. 1988. *Revista Geológica de Chile* (15), N°2: 119-127.
- Hervé, F.; Godoy, E.; Parada, M.A.; Ramos, V.; Rapela, C.; Mpodozis, C. & Davidson, J. 1987. *American Geophysical Union, Geodynamics Series* 18. 97-114.
- Hervé, F.; Munizaga, F.; Parada, M.A.; Brook, M.; Pankhurst, R.; Snelling, N.J. & Drake, R. 1988. *Journal of South American Earth Sciences* (1): 185-194.
- Holland, T. & Blundy, J. 1994. *Contributions to Mineralogy and Petrology*, 116: 433-447.
- Hutton, D. 1992. *Transactions of the Royal Society of Edinburgh: Earth Sciences* (83): 377-382.
- Irwin, J.; Sharp, J.; Spangler, R. & Drake, R. 1987. *Journal of Geophysical Research* (92): 3603-3614.
- Irwin, J. 1989. *Journal of South American Earth Sciences* (2): 305-309.
- Knight, M.D. & Walker, G.P.L. 1988. *Journal of Geophysical Research* (93): 4301-4319.
- Parada, M.A.; Nystrom, J. & Levi, B. 1999. *Lithos* (46): 505-521.

## METAMORPHIC P-T CONDITIONS OF RHYOLITES IN THE MAGALLANES FOLD AND THRUST BELT, PATAGONIAN ANDES

4-05

F. Hervé(\*), H.-J. Massonne(\*\*), T. Theye(\*\*), M. Calderón(\*)

(\*) *Departamento de Geología, Universidad de Chile, Casilla 13518, Correo 21, Santiago, Chile*

(\*\*) *Institut für Mineralogie und Kristalchemie, Universität Stuttgart, Azenbergstr.18, D-70174 Stuttgart, Germany*

### Summary

Foliated metarhyolites of the Late Jurassic Tobífera Formation form two thrust sheets in the Patagonian Andes fold and thrust belt. The metamorphic mineralogy indicates a metamorphic evolution between about 3 kbar (~ 250°C) and close to 7 kbar and 350°C, and their synkinematic nature suggests that they formed during the Mid Cretaceous tectonic event in the area.

### Introduction

The Tobífera Formation is a Late Jurassic unit of the Magallanes basin in southern South America. It is mainly composed of siliceous volcanic rocks, including rhyolites, tuffs, and ignimbrites, with minor intercalated basalts and clastic sedimentary rocks. The igneous rocks are interpreted to be the product of crustal anatexis (Pankhurst & Rapela, 1995) which took place during widespread extensional events preceding the dismembering of the Gondwana supercontinent and, thus, the opening of the Atlantic Ocean. The Tobífera Formation also crops out in the thrust and fold belt of the Patagonian Andes which limits the Magallanes basin to the west. Here it is mainly composed of foliated metarhyolites and metatuffs.

No previous study about the metamorphic conditions attained by the metarhyolites has been done yet. In this paper we report the mineral associations developed during the metamorphic and deformational event which foliated and almost completely reequilibrated the mineralogy of the Tobífera rocks. From there we deduce the P-T conditions of their metamorphism.

### Field geology

As shown in Fig. 1, metarhyolitic rocks of the Tobífera Formation form two elongated bodies which correspond to thrust sheets of the Patagonian fold and thrust belt. They are thrust over Early Cretaceous sediments to the east, and are in turn thrust over by granitic and Paleozoic rocks from the west. The Sarmiento ophiolite seems to form a thrust slice between them.

SHRIMP U-Pb dating of zircons in the metarhyolites have yielded an age of 151.7 Ma (Hervé, unpublished) in the northern part of Fiordo Peel, and ages of ca. 150 Ma in areas further south in both thrust sheets (Calderón, unpublished data). A leucocratic foliated granite with mirolitic cavities at the intersection of Fjords Peel and Calvo showed a 150 Ma U-Pb zircon age (Hervé, unpublished). Other granite bodies gave U-Pb zircon ages of ca. 19 Ma (Fanning et al., 2001).

The strong foliation in the metarhyolites is NS with dips of 45 to 70° W. Highly plunging lineations are discernible. The foliation in the rhyolites is parallel to the axial plane cleavage in folds in the Early Cretaceous pelites of the Zapata formation at Canal Quirque, as well as to the thrust plane. Considering these observations, the metamorphism of the rhyolites and the development of the foliation probably took place during the thrusting of the Tobífera Formation to the east during a Mid Cretaceous (ca. 100 Ma) event (Dalziel, 1986).

### Petrography

The metarhyolites display a strong penetrative mylonitic foliation at the outcrop scale, which is not homogeneously developed throughout the whole unit. The presence of abundant quartz porphyroclasts up to 1 cm in diameter is conspicuous as well as the frequent occurrence of quartz veins often parallel to the foliation. Well developed strain shadows are observed in the porphyroclasts indicating top to the east displacement. The matrix is very fine grained. In some outcrops breccia and fiamme structures are preserved pointing to the presence of pyroclastic rocks in the succession.

Two samples of metarhyolitic rocks were studied in detail. Sample FO0016 from Fiordo Peel is composed of mm-sized subautomorphic quartz porphyroclasts, sericitized plagioclase, and spindle

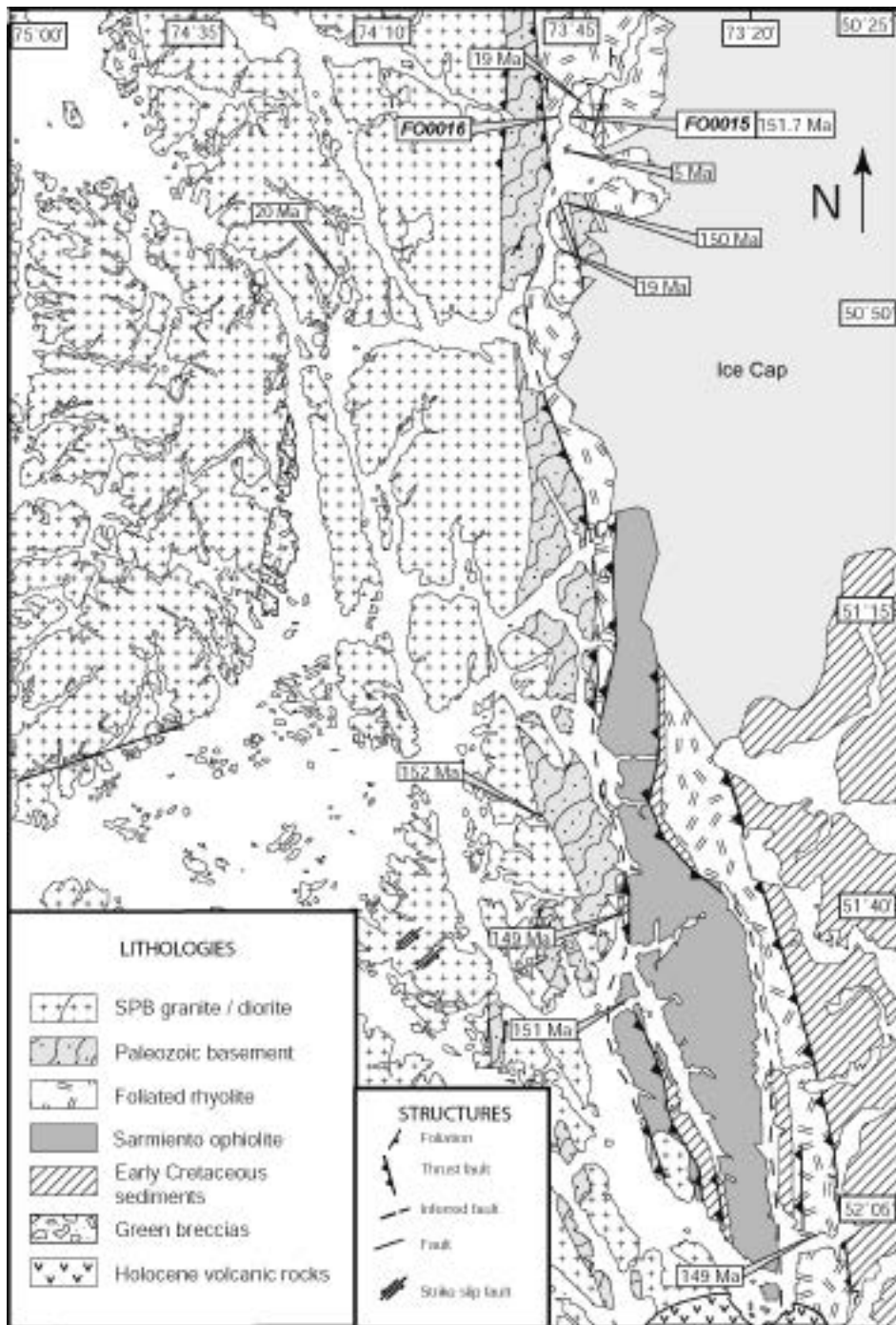


Fig. 1 - Geological map of the studied area.

shaped bodies of fine grained aggregates of phyllosilicates, probably representing flattened pumice fragments, embedded in a fine-grained matrix. These rock features can be attributed to an ignimbrite structure. The rock is penetratively foliated with the foliation mainly defined by white mica and elongated trails of epidote. The strain shadows around the quartz porphyroclasts are composed of calcite, K-feldspar, white mica and quartz elongated parallel to the foliation. The minerals of the matrix are less than 30 microns in size and consist of a rather isotropic intergrowth of K-feldspar, albite, quartz, white mica, chlorite, epidote, allanite, calcite, with accessory stilpnomelane, biotite, pyrrhotite/pyrite, sphalerite, apatite, zircon, and ilmenite decomposed to titanite and rutile. Except

allanite, ilmenite and pyrrhotite which are probably of igneous origin, this mineral assemblage seems to have reequilibrated during the metamorphic episode.

Sample FO0015, also from Fiordo Peel, is probably of subvolcanic origin. The foliation is mainly defined by white mica, and by K-feldspar, calcite and quartz fibers in the strain shadows of the quartz porphyroclasts. In addition to white mica, the matrix consists of K-feldspar, albite, and quartz with less opaque minerals than in FO0016.

### Mineral chemistry

The above samples were studied first under the polarizing microscope and subsequently with a CAMECA SX100 electron microprobe with 5 wavelength-dispersive spectrometers. The minerals in the pressure shadows are similar in composition to the minerals in the matrix indicating that the whole mineral assemblage was equilibrated during metamorphism.

The structural formulae (double formula unit = d.f.u.) of potassic white micas in sample FO0015 scatter around 6.47 Si/d.f.u. Na and Ti contents are generally low as typical for low-temperature metamorphic white micas. In sample FO0016 white micas show a stronger compositional variation. In addition to a cluster again around 6.47 Si/d.f.u., others are clearly richer (~6.9/d.f.u.) and poorer in Si (6.2/d.f.u.). Chlorite is a common mineral in FO0016, where it shows a slight compositional variability: Si contents and  $X_{Mg}$  vary between 5.4 to 5.8/d.f.u. and 0.41 to 0.44, respectively.

Plagioclase in both samples is almost pure albite as typical for low-temperature metamorphic rocks. K-feldspar is widespread in the matrix of both rocks. Titanite, ilmenite, and rutile form large aggregates (leucoxene) demonstrating that these aggregates are alteration products of former magmatic minerals probably ilmenite. Stilpnomelane in FO0016 typically forms intergrown aggregates.  $X_{Mg}$  of stilpnomelane is around 0.23. Biotite is significantly richer in Mg ( $X_{Mg} \sim 0.45$ ) as typical for biotite + stilpnomelane - bearing assemblages.

### Conditions of metamorphism

Qualitatively, we can estimate a P-T range from the observed mineral assemblage. K-feldspar + chlorite is only stable at low metamorphic temperatures. For instance, Massonne (1995) estimated maximum T around 330°C (P ~2 to 6 kbar) for the stability of this assemblage. This is widely confirmed by thermodynamic calculations of phase relations, for instance, in the system  $K_2O$ -FeO- $Al_2O_3$ - $SiO_2$ - $H_2O$  by Massonne & Szpurka (1997). However the corresponding P-T curve (2 kbar, 350°C; 4 kbar, 310°C) of the reaction chlorite + K-feldspar = muscovite/phengite + biotite + quartz +  $H_2O$  is significantly curved. As small biotite crystals had already formed in sample FO0016, metamorphic temperatures around 330°C or somewhat higher might have been reached. Referring to this temperature, metamorphic pressures could have been elevated due to the assemblage phengite + stilpnomelane. Calculation results by Massonne & Szpurka (1997) point to minimum pressures of 4 kbar (T>300°C). However, as no jadeite was observed, maximum pressures of 10 kbar (~300°C) should be taken into account (Popp & Gilbert, 1972).

The calculated P-T positions of equilibria using the thermodynamic data set by Vidal et al. (2001) showed a strong scatter considering the various mineral compositions of FO0016. Thermobarometry with phengite (see, e.g., Massonne, 1995) shows an increase of P from almost 4 kbar to 7 kbar with rising Si content of the mica at 300°C. If we would additionally consider that Si-rich phengites formed at the highest T (~350°C), and that the Si poorest micas were stable at the lowest T (~250°C = earliest stage) of the formation of the metarhyolites, the detectable P-T path would start at about 3 kbar (~250°C) and end close to 7 kbar and 350°C.

### Discussion and conclusions

The uncertainties of the P-T data are related to the variability of mineral compositions within the studied rocks and to the lack of control of thermodynamic parameters, such as water activity, effective during the metamorphic processes. However, a general trend toward rather high metamorphic pressures at low temperatures of metamorphism is clearly shown by the observed mineral associations. The P-T path derived by phengite thermobarometry (3 kbar, 250°C - 7 kbar, 350°C) using thermodynamic calculation methods is at least compatible with the mineral assemblages found.



Thus, we take it here as the most probable metamorphic conditions in which the metamorphism of the metarhyolites evolved.

Although as yet there is no dating of the phases formed during this metamorphism, the syntectonic nature of the minerals suggests that the metamorphism took place during the thrusting of the rocks during the Middle Cretaceous. This implies that the rhyolites were buried to 10 km and then to somewhat more than 20 km depth sometimes between 150 and 100 Ma contemporaneously to the construction of a large portion of the South Patagonian batholith and of the Sarmiento ophiolite. Massonne et al. (this volume) indicate that muscovite-garnet-bearing granites, probably also 150 Ma in age, were emplaced at a depth corresponding to 5.5 kbar, the same range indicated by the metamorphic minerals in the studied rhyolites. The emplacement of the Early Miocene plutons appears to be unrelated to the observed metamorphism.

### Acknowledgments

Field work was supported by Fondecyt Project 1010412 to FH. Laboratory work was undertaken at Universität Stuttgart under a BMBF – CONICYT agreement to HM and FH. Captain Conrado Alvarez and his crew took us in the yacht Penguin to these remote areas.

### REFERENCES

- Dalziel (1986), in: Coward & Ries, eds.: Geol. Soc. London Spec. Publ. 19, 389-404
- Fanning et al. (2001), Exp. Abstr. Vol., III Southam. Symp. Isotope Geology, 30-33
- Massonne (1995), in: Dallmeyer, Franke & Weber, eds.: Pre-Permian geology of central and eastern Europe. Berlin: Springer Verlag, 132-137
- Massonne & Szpurka (1997), Lithos 41, 229-250
- Pankhurst & Rapela (1995), Earth Planet. Sci. Lett. 134, 23-36
- Popp & Gilbert (1972), Am. Mineralogist 57, 1210-1231
- Vidal et al. (2001), Am. J. Sci. 301, 557-592

## MONITORING MAGMATISM OF THE PATAGONIAN BATHOLITH THROUGH THE U-PB SHRIMP DATING OF DETRITAL ZIRCONS IN SEDIMENTARY UNITS OF THE MAGALLANES BASIN

4-06

Francisco Hervé<sup>1</sup>, Estanislao Godoy<sup>2</sup>, Constantino Mpodozis<sup>3</sup>, Mark Fanning<sup>4</sup>

1 *Departamento de Geología, Universidad de Chile, Casilla 13518, Correo 21, Santiago.*  
fherve@cec.uchile.cl

2 *Servicio Nacional de Geología y Minería, Avda. Santa María 0104, Santiago.*  
egodoy@sernageomin.cl

3 *SIPETROL, Avda. Vitacura 2736, Santiago, cmpodozis@sipetrol.cl*

4 *Research School of Earth Sciences, The Australian National University, Canberra ACT 0200, Australia. markfanning@anu.edu.au*

### Introduction

The Late Cretaceous to Tertiary Magallanes Foreland Basin (MFB) located at the southern tip of South America lies east and north of the Patagonian-Fuegian-Andes, largely dominated by the Mesozoic to Cenozoic granitoids of the Patagonian Batholith. The MFB was formed as a consequence of the tectonic closure of the quasi-oceanic Rocas Verdes Basin (RVB), interpreted either as a back-arc basin or as a failed arm of the Proto Weddell Sea, which propagated northwards along the edge of western Patagonia during the Late Jurassic. Extension and lithospheric stretching, which created the RVB, occurred in conjunction with widespread silicic volcanism associated to the Middle to Late Jurassic Chon Aike Large Igneous Province (“Tobífera” Formation in Magallanes). Thermal subsidence after Late Jurassic rifting is recorded by a transgressive sequence of quartziferous sandstones (Springhill Formation), and extensive Upper Jurassic-Lower Cretaceous anoxic to suboxic black shales (i.e. Erezcano, Zapata, Río Mayer, Estratos con Favrella formations). During the Early to Middle Late Cretaceous the quasi-oceanic floor of the RVB seems to have been consumed by oblique,

west-directed, subduction, which terminated with the closure of the oceanic RVB space in the Turonian (Fildani et al 2003). Collision against the South American margin of the small continental micro plate, which partially detached from Patagonia during RVB opening, was accompanied by thrusting and tectonic loading of the passive South American margin of the former RVB, which led to the formation of the MFB in the Late Cretaceous. The MFB is a flexural, peripheral foreland basin, filled by more than 8 km of Cretaceous and Cenozoic marine sedimentary successions. It records two stages of foreland basin development during the Turonian-Maastrichtian and the Palaeocene-Oligocene. The entire evolution of the MFB can be linked to changes in the tectonic conditions, leading to the uplift of the Patagonian-Fueguian Andes, the opening of the Drake Passage and the formation of the Scotia Sea Plate during the Neogene.

In this contribution, we present 8 new SHRIMP U-Pb ages on detrital zircon populations in Cretaceous to Neogene sedimentary rocks of both the Late Jurassic-Early Cretaceous pre foreland as well as the Late Cretaceous-Tertiary foreland and post foreland basin stages (Fig. 1, Table 1). These are compared with U-Pb crystallization ages of the Patagonian Batholith, which allows the monitoring of the magmatic history of the Patagonian Batholith, as sediments derived from it form an important component of the MFB infill. The new detrital zircon ages also allow to better constrain the maximum accumulation ages for some of the sedimentary units, until now only dated considering their fossiliferous content.

### SHRIMP U-Pb detrital zircon ages in the Magallanes Basin

The ages of detrital zircon grains were determined in each of the samples shown in Table 1. The followed methodology was the same as in Hervé et al (2003). The maximum possible age of sedimentation of the analysed rock is the age of the youngest detrital zircon. Sample location appears in Figure 1, with the exception of sample Cañadón 20, which comes from the bottom of an oil well near the eastern entrance of the Straits of Magellan, and of sample FF9905, collected at Fiordo Falcon, north of the area shown in the figure 1.

We also compare the different zircon population for each sample with a data set of over 50 zircon U-Pb crystallization ages of the South Patagonian Batholith (Bruce et al, 1991; Martin et al, 2000), which includes more than 40 new SHRIMP U-Pb zircon ages (Hervé, unpublished). This new database indicates that the batholith was formed by the amalgamation of plutons spanning from 152 Ma to 18 Ma. Older foliated leucogranites constitute isolated satellite bodies, both east (Bahía Pia, 164 Ma; Mukassa and Dalziel, 1996) and west (Diego de Almagro, 157 Ma, Hervé & Fanning, 2003) of the Patagonian Batholith, which are probably related to the extensional phase that generated the silicic Chon-Aike LIP. In the Cordillera Sarmiento area, granitic rocks, the Tobífera rhyolitic rocks and associated garnet bearing leucogranitic dykes have been dated 150 Ma (see Calderón et al, this volume), with an exception of 172 Ma (Pankhurst et al, 2000). Other peaks of activity on the Batholith seem to occur at 140-130, 120-110, 90-70 and 20-10 Ma.

Sample number	Formation	Biostratigraphic age	Youngest detrital zircon age (Ma $\pm$ 2S)	Maximum age after U-Pb detrital zircon
Cañadón 20	Springhill	Valanginian?	153.4 $\pm$ 2.1	Oxfordian
FF9905	Zapata ?	Tithonian-Aptian	178	Toarcian
FO0212a	Zapata ?	Tithonian-Aptian	131.4 $\pm$ 1.3 (Ave of 29)	Berriasian
FO0313	Punta Barrosa	Albian-Cenomanian	92.0 $\pm$ 1.3	Turonian
FO0323	Rocallosa	Late Campanian - Maastrichtian	78 $\pm$ 2.5	Campanian
FO0319	Cerro Dorotea	Early Paleocene (Danian)	67.4 $\pm$ 1.5 (Ave of 5)	Maastrichtian
FO0323	Rocallosa	Late Campanian - Maastrichtian	78 $\pm$ 2.5	Campanian
FO0325	Chorrillo Chico	Paleocene?	58 $\pm$ 2.2	Selandian
FO0322	El Salto	Miocene	21.8 $\pm$ 1.5 (Ave of 36)	Aquitian

Table 1 - Stratigraphic units where SHRIMP U-Pb detrital zircon age determinations have been done in this work, with indications of the previously assigned biostratigraphic age, and the age of the younger individual zircon crystal or grouping of crystals. Stage names are from IUGS-UNESCO (2000) International Stratigraphic Chart.

## Discussion

Sample Cañadón 20 corresponds to a quartz rich sandstone from the Springhill Formation, collected from the previously mentioned core, and deposited directly over the Tobífera Formation (not precisely dated there) during the Neocomian. The detrital zircon age pattern reveals a small population of 540 Ma zircons, a great predominance of 170 Ma zircons and a youngest age of 153 Ma. The age of the oldest zircons is similar to the conventional U/Pb age reported by Sollner et al (2000) and Pankhurst et al (2003) for a sample of ortogneisses collected from the Gaviota 6 well in northern Tierra del Fuego, which indicates a contribution from the local, pre-Jurassic basement. The 170 Ma age matches well with those of the Marifil (Chon Aike) Formation rhyolites which crop out further north, in the Deseado Massif (Pankhurst et al, 2000) and may well extend in the subsurface to the south along the eastern Magallanes region. The 153 Ma age fits with the age of the Tobífera volcanic rocks, which crop out to the west, on the foothills of the Andean Cordillera, and is the youngest component of the Chon-Aike LIP (Féraud et al, 1999; Pankhurst et al, 2000). Stratigraphically unconstrained samples from rocks assigned to the “Zapata” Formation (Katz, 1963) collected at Canal Gajardo (FO0212a) and Fiordo Falcón (FF9905) yield minimum detrital zircon ages of 178 Ma (Fiordo Falcón) and 131 Ma (Canal Gajardo) respectively. At Fiordo Falcón populations of 300 Ma and 550 Ma, as well as several Proterozoic and Archean grains, were observed. At Canal Gajardo only some grains with 200

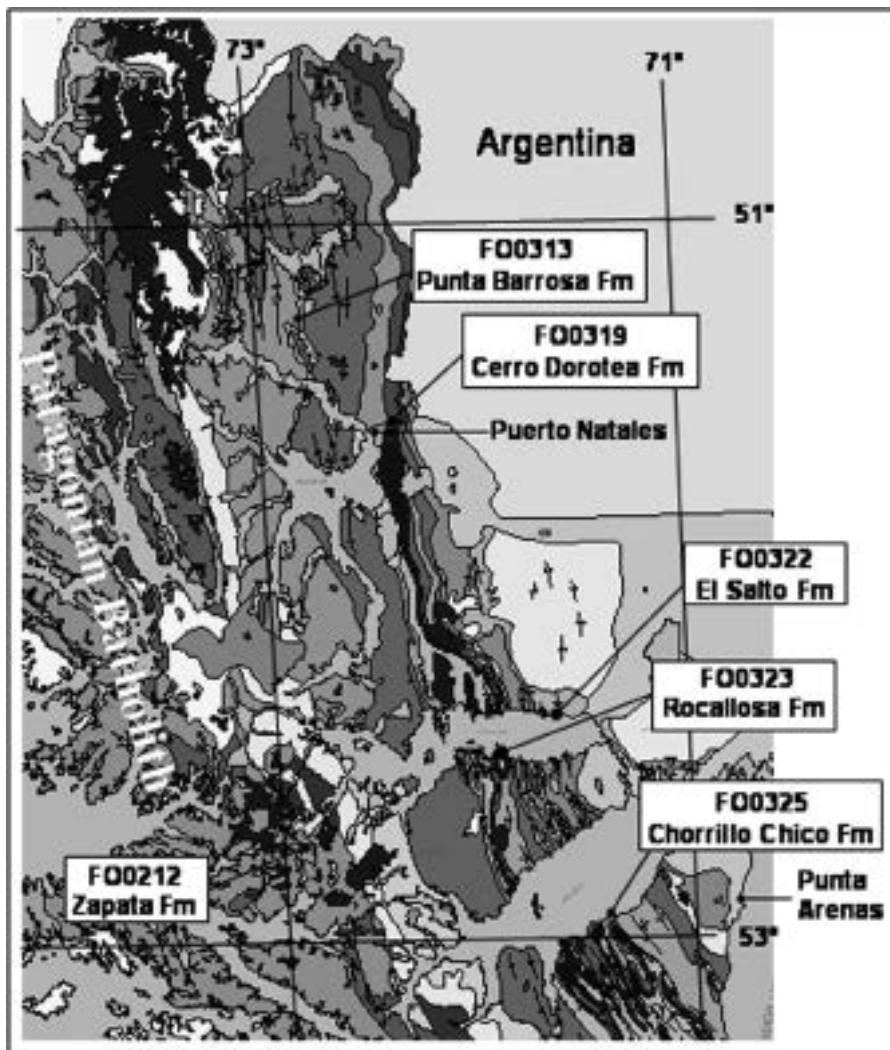


Fig. 1 - Sample location with indication of stratigraphic units.

Ma to 750 Ma ages are present beside the Cretaceous peak. No 178 Ma component has been found to date in the Patagonian Batholith, but 140 to 130 Ma ages are common along its western edge. Zircons so old are however difficult to interpret, as no evidences for the erosional unroofing of Patagonian Batholith during the deposition of the Zapata formation have been presented so far.

Sample FO0313 is from the Punta Barrosa Formation, a more than 1000 m thick, sandy-shale unit deposited by turbidite lobes moving from north to south (Scott, 1966; Wilson 1991) during the inception of the MFB (“starved or underfilled” Cretaceous foreland basin stage); Mella (2001). It shows a large population of 120 Ma zircons, also present in the samples analysed by Fildani et al (2003), which possibly denote the erosion of mid-Cretaceous plutons belonging to the Patagonian Batholith. A few zircons of 150 Ma attest to the erosion of Tobífera volcanics and/or coeval intrusives. Finally, a peak at 200 Ma may well indicate the erosion of granitoids associated to the Early Jurassic Subcordilleran Batholith (Rapela et al., 2003) which crops out to the north of the MFB, in good agreement with the northern provenance of the Punta Barrosa sediments. Katz (1963) and Cortés (1964) suggested an Albian-Cenomanian age for the Punta Barrosa, based on its very sparse ammonite assemblage. However, the occurrence of zircons as younger as 92 Ma in sample FO0313, which confirms a similar detrital zircon age reported by Fildani et al (2003) for the basal sandstone layer of the formation, is in contradiction with this “paleontological” age as they doubtlessly point out that the formation cannot be older than the latest Turonian (see below).

Ages of detrital zircons from Sample FO0323 (Rocallosa Formation at Punta Rocallosa, Isla Riesco, Fig. 1) are, in contrast, totally consistent with their stratigraphic position and the age based on paleontological evidence (Late Campanian-Maastrichtian; Castelli et al., 1992) This sample shows zircons populations at 90 Ma, 130 Ma and 150-160 Ma, quite similar to those of sample FO313 and, additionally, much older zircons at 550-600 Ma and 1200 Ma which may well represent the reworking of the Eastern Andes Metamorphic Complex (Hervé et al, 2003). The Rocallosa Formation is the youngest unit deposited during the final “overfilled” stage of the Cretaceous foreland Basin (Mella, 2001).

FO0319 is a sandstone sample collected east of Puerto Natales (Fig. 1) placed at the southern extension of outcrops, which Malumián et al (2000) include, in Argentina, on their Paleocene (Danian) Cerro Dorotea Formation. The sample shows, as in the Punta Barrosa and Rocallosa samples, a small peak at 150 Ma and a larger population of 110 Ma zircons, but also younger zircons dated 67 Ma (Late Maastrichtian). This younger zircon age is only slightly older than the biostratigraphic age for the Cerro Dorotea Formation. Provenance of this zircon is difficult to assess, as intrusive or volcanic rocks of that age are not widely known for the Patagonian Batholith.

Sample FO0325 is a fine-grained sandstone from the Chorrillo Chico Formation collected near the base of the unit, on the northern shore of Seno Otway (Fig. 1) where it overlies the Rocallosa Formation. This sample shows a few Permian zircons and main peaks of 140-160, 110 and 80-90 Ma, not very different to those on the older Cretaceous samples. The Chorrillo Chico Formation has been generally attributed to a “Paleocene” age (Natland et al, 1974; Mella, 2001) considering its foraminiferal content. However as their younger zircon (58 Ma) shows, its age cannot be older than the Selandian (middle Paleocene). This leaves the possibility open for a late Maastrichtian to (at least) middle Paleocene hiatus between the Rocallosa and Chorrillo Chico Formations, which merit to be further investigated.

The youngest analysed sample corresponds to FO0322, a tuffaceous epiclastic sandstone from the post foreland basin El Salto Formation at the north shore of Seno Skyring (Fig. 1). It shows a very prominent peak at 22 Ma, which includes 36 of the 38 analysed grains, besides a 150 Ma old grain and one of Permian age. The El Salto Formation of Miocene age (Mella, 2001) correspond to the basal unit of the thick blanket of continental sediments, which covered large tracts of southern Patagonia after the end of the Cenozoic subsidence in the MFB.

## Conclusions

The use of detrital zircon SHRIMP ages revealed itself as a powerful tool in tracing the provenance of sediments in the MFB and indirectly dating the main periods of magmatism in southern Patagonia. Detrital zircon content in the MFB sedimentary rocks show that magmatism, although punctuated by

region-wide pulses of intense activity, seems to have been almost continuous in the Patagonian Batholith from the Late Jurassic to the Paleogene. As detrital zircons were continuously incorporated in MFB sediments from the Late Cretaceous, zircon ages can be used to constrain their maximum deposition age. Our new data confirm previous zircon ages reported by Fildani et al (2003) which indicate that the Magallanes Foreland Basin did not form prior to 92 Ma and allow to reassign the age of the Punta Barrosa Formation which, until now, has been attributed to the Aptian-Cenomanian, due to its dubious ammonite content (Katz, 1963; Wilson, 1991; Harambour and Soffia, 1988). Data for the Chorillo Chico Formation preliminarily suggest a possible early to middle Paleocene hiatus, and a break in sedimentation between the Late Cretaceous and Tertiary MFB stages. During the Miocene the basin was flooded with detritus of a contemporary active magmatic source, also well documented in the Patagonian Batholith, which appears to be one of the main sources of detritus at that time.

## Acknowledgements

This work was funded by Fondecyt project 1010412 to FH & EG. S. Elgueta from ENAP provided the sample from Cañadón 20 core. V. Faúndez helped with the figure.

## REFERENCES

- Bruce, R. M., Nelson, E. P., Weaver, S. G., Lux, D. R., 1991, Temporal and spatial variations in the southern Patagonian Batholith : constraints on magmatic arc development. In Harmon, R.S. and Rapela C.W. (eds): Andean magmatism and its tectonic setting. Geological Society of America, Special Paper 265, p. 1-12.
- Calderón, M., Hervé, F. and Fanning, C. M. (This volume). Late Jurassic birth of the Rocas Verdes Basin at the Sarmiento ophiolitic complex: Evidence from zircon U-Pb SHRIMP geochronology.
- Castellí, J.C., Rojas, L., Robertson, R., 1992, Evaluación geológica y petrolera bloques Última Esperanza sur e Isla Riesco: ENAP (unpublished report), 196 p, Santiago.
- Cortés, R., 1964., Estratigrafía y un estudio de paleocorrientes del flysch cretáceo del Departamento de Ultima Esperanza: Tesis de grado. Universidad Técnica del Estado, 117 p., Santiago.
- Féraud, G., Alric, V., Fornari, M., Bertrand, H., Haller, M., 1999, <sup>39</sup>Ar/<sup>40</sup>Ar dating of the Jurassic volcanic province of Patagonia: migrating magmatism related to Gondwana break-up and subduction: Earth and Planetary Science Letters, v. 172, p. 83-96.
- Fildani, A., Cope, T.D., Graham, S. A., Wooden, J. L., 2003, Initiation of the Magallanes foreland basin: Timing of the southernmost Patagonian Andes orogeny revised by detrital zircon provenance analysis: Geology, v. 31(12), p. 1081-1084.
- Harambour, S., Soffia, J. M., 1988, Evaluación Geológica y Petrolera del extremo Norte de Ultima Esperanza: ENAP (unpublished report), 180 p., Santiago.
- Hervé, F., Fanning, C. M., 2003, Early Cretaceous subduction of continental crust at the Diego de Almagro archipelago, southern Chile: Episodes v.26 (4), p. 285-289.
- Hervé, F., Fanning, C. M., Pankhurst, R., 2003, Detrital zircon age patterns and provenance of the metamorphic complexes of southern Chile: Journal of South American Earth Sciences, v. 16, p. 107-123.
- Malumián, N., Panza, J. L., Parisi, C., Nañez, C., Caramés, A., Torre, E., 2001, Hoja Geológica 5172-III, Yacimiento Río Turbio (1:250.000): Servicio Geológico Minero Argentino, Boletín N° 247, p. 1-108, Buenos Aires.
- Katz, H. R., 1963, Revision of Cretaceous Stratigraphy in the Patagonian Cordillera of Ultima Esperanza, Magallanes Province, Chile: American Association of Petroleum Geologists Bulletin, v. 47(3), p. 506-524
- Martin, M., Pankhurst, R.J., Fanning, C.M., Thomson, S.N., Calderón, M., Hervé, F., 2001, Age and distribution of plutons across the Southern Patagonian Batholith: New U-Pb data on zircons: South American Symposium on Isotope Geology, Extended Abstracts (CD), p. 585-588, Sociedad. Geológica de Chile, Santiago.
- Mella, P., 2001, Control tectónico en la evolución de la cuenca de antepaís de Magallanes, XII Región, Chile: Universidad de Concepción, Departamento de Ciencias de la Tierra, Memoria para optar al Título de Geólogo, 149 p., Concepción.
- Mukasa S., Dalziel, I.W.D., 1996, Southernmost Andes and South Georgia Island, North Scotia Ridge: zircon U-Pb and muscovite Ar - Ar age constraints on tectonic evolution of southwestern Gondwanaland: Journal of South American Earth Sciences 9: 349-365.
- Natland, M. L., González, E., Cañon, A., Ernst, M., 1974, A system of stages for correlation of Magallanes Basin sediments: Geological Society of America, Memoir 139, p. 1-126.
- Pankhurst, R. J., Riley, T. R., Fanning, C. M., Kelley, S. P., 2000, Episodic silicic volcanism in Patagonia and the Antarctic Peninsula: chronology of magmatism associated with the breakup of Gondwana: Journal of Petrology, v. 41, 605-625.
- Pankhurst, R. J., Rapela, C. W., Loske, W. P., Marquez, M., Fanning, C.M., 2003, Chronological study of the pre-Permian basement rocks of southern Patagonia: Journal of South American Earth Sciences v. 16, p. 27-44.
- Rapela, C. W., Pankhurst, R. J., Fanning, M. J., 2003, The Early Jurassic Subcordilleran Plutonic Belt of Patagonia (42°-44°S): Proto Pacific subduction coeval with the Karroo mantle plume. Proceedings, X Chilean Geological Congress (CD ROM), Concepción.
- Scott, K. M., 1966, Sedimentology and dispersal patterns of a Cretaceous flysch sequence, Patagonian Andes, southern Chile: American Association of Petroleum Geologists Bulletin, v. 50, p. 72-107.
- Söllner, F., Miller, H., Hervé, M., 2000, An Early Cambrian granodiorite age from the pre-Andean basement of Tierra del Fuego (Chile): the missing link between South America and Antarctica? : Journal of South American Earth Sciences, v. 13, p. 163-177.
- Wilson, T. J., 1991, Transition from back-arc to foreland basin development in the southernmost Andes: Stratigraphic record from Ultima Esperanza District, Chile: Geological Society of America Bulletin, v. 103, p. 98-111.

## THE PALEOCENE–EOCENE SEJONG FORMATION, BARTON PENINSULA, KING GEORGE ISLAND, ANTARCTICA: ERUPTIVE AND DEPOSITIONAL PROCESSES AND ENVIRONMENTS

4-07

Seung Bum Kim<sup>1</sup>, Young Kwan Sohn<sup>2</sup>, Moon Young Choe<sup>1</sup>, Jong Ik Lee<sup>1</sup>, Soon Do Hur<sup>1</sup>

<sup>1</sup> Korea Polar Research Institute, KORDI, Ansan P.O. Box 29, Seoul 425-600, Korea

<sup>2</sup> Department of Earth & Environmental Sciences, Gyeongsang National University, Jinju 660-701, Korea

### 1. Introduction

The King George Island (KGI), South Shetland Islands, Antarctic Peninsula, is a remnant of Mesozoic island arc and consists of a stratiform complex of basaltic to andesitic rocks. The lowest part of the complex (Late Paleocene to Eocene) crops out in the Barton Peninsula, southwest KGI, and comprises a lower volcanoclast-rich succession (Sejong Formation, 100–200 m thick) and an upper succession (ca. 200–300 m thick) of basaltic andesite lavas interlayered with subordinate tuffs. This study attempts to unravel the eruptive and depositional processes and environments of the Sejong Formation based on detailed facies analysis and field mapping.

### 2. Lithofacies and Facies Associations

Based on composition, texture (coherent vs clastic) and grain size, nine lithofacies are identified in the Sejong Formation: basaltic lava (lithofacies BL), basaltic agglutinate (BA), basaltic tuff breccia (BTB), basaltic lapilli tuff (BLT), andesitic lava (AL), andesitic tuff breccia (ATB), andesitic lapilli tuff (ALT), reworked conglomerate (C), and sandstone/siltstone couplets (S/Z). These rocks can be grouped into three facies associations indicating distinctive eruptive and depositional environments: (1) spatter/cinder cones (Facies Association (FA) I), (2) volcanoclastic apron (FA II), and (3) distal apron to floodplain (FA III).

#### 2.1. Facies Association I

FA I comprises basaltic rocks that form semi-circular patches in map view. It consists of central massive/vertically jointed lava (lithofacies BL) and the fringing agglutinates and tuff breccias (lithofacies BA & BTB) through a zone of outward dipping compound lava flows (lithofacies BL). The central coherent basalt is most fresh and hardened, forming a distinctive edifice and shows vertical to subhorizontal joints arrayed in a fan-shaped fashion. This suggests emplacement of the basalt as vent-filling lava pond or plug. The adjacent piles of lava flows consist of thin (>1 m thick) units superimposed with indistinct boundaries, lacking intervening clinkery breccias. Each flow unit is generally non-vesicular. Part of them comprises slabby, flow foliated clasts reminiscent of overlapping toes at the front of pahoehoe flows. The outermost agglutinates are characterized by flattened and stretched basaltic spatters, either non- to incipiently vesicular or highly vesicular in the central part with chilled glassy margins. Aerodynamically shaped, moderately to highly vesicular (or amygdaloidal) bombs are also associated with subordinate amounts of dense lapilli. The agglutinates are interlayered with lava flows or overlain by bomb-rich basaltic tuff breccia. These features indicate that FA I has resulted from Hawaiian, fire-fountaining to Strombolian eruptions from discrete spatter/cinder cones in a subaerial setting.

#### 2.2. Facies Association II

FA II comprises the bulk of the Sejong Formation. It is unconformably or conformably underlain by FA I and is interlayered with the deposits of FA III. It consists dominantly of very thick (up to 12 m thick), tabular beds of andesitic to basaltic, either welded or non-welded, lapilli tuffs and tuff breccias (lithofacies BTB, BLT, ATB & ALT), and rare intervening andesitic lava flows (lithofacies AL). Each volcanoclastic unit is rather irregularly bedded and is characterized by ungraded and disorganized fabric. They consist mainly of accidental lithic fragments that are angular blocky shaped with angular corners. Essential fragments with elliptical to circular shaped with irregular margins are present in much lesser amounts. Clasts show a various degree of vesicularity (0-80%) and a wide range of phenocryst content (0-50%). Clast size is also widely variable, ranging from pebble to boulder grade (max. 90 cm in diameter) but small pebble size clasts are apparently deficient in tuff breccias. Matrix

materials consist predominantly of vitric fine ash with subordinate amount of crystal fragments. Andesitic lava flow shows an abrupt lobate termination

The common welded features, together with the dominance of vitric materials in the matrix, suggest a primary pyroclastic origin of the FA II deposit. The coexistence of rounded clasts and angular blocky clasts and the large grain size (common boulder-grade clasts) suggest specifically explosive magmatic (Vulcanian) eruptions and consequent generation of block-and-ash flows. The thick-bedded nature, the lack of stratification and channel incision, and the ungraded and disorganized fabric collectively indicate dense, laminar pyroclastic flows. On the other hand, the presence of stubby lava flows and the lack of ash fall deposits suggest an accumulation in a near-vent setting. FA II deposit is therefore interpreted as volcanoclastic aprons extending from a collapsed flank of a dome volcano.

### 2.3. Facies Association III

FA III occurs in fault contact with FA I or intercalated with FA II deposits. It consists mainly of sandstone/siltstone couplets (lithofacies S/Z) locally with resedimented conglomerates (lithofacies C). The sandstone/siltstone couplets are characteristically diffusely bedded and are upward graded from sandstone-dominant base to siltstone-dominant top. Siltstone layers are mostly homogeneous, red to brown in color and locally bioturbated (vertical burrows). Abundant plant fossils are recovered in some horizons. Sandstone layers are generally sharply based with occasional scours and are commonly normally graded with an upward increase in silt content. Cross-stratification is relatively rare. The couplets are frequently deformed and distorted with flame structures. Resedimented conglomerates are typically irregularly bedded with common protruding clasts. Each unit is inversely graded with large amounts of boulder-size clasts near the top. Elongate clasts are mostly oriented parallel to the bedding surface. Matrix comprises extremely poorly sorted, red-brown muddy sandstone.

The color, texture, structure and bedding features of the sandstone/siltstone couplets collectively suggest suspension sedimentation from rapidly waning floods. Ephemeral shallow channels are indicated by the scours. The common flame structures suggest rapid aggradations likely due to high flood frequency. The resedimented conglomerates are interpreted as debris flows based on the prominent inverse grading, irregular bedding and the presence of protruding clasts. Intimate association of debris flow deposits is indicative of relative proximity to the source area. FA III is therefore interpreted as floodplains developed on the volcanoclastic aprons during inter-eruptive periods. Hydrologic remobilization processes were probably active during and in the immediate aftermath of the eruptions.

## 3. Conclusions

Based on detailed facies analysis and field mapping, volcano-sedimentary evolution of the Sejong Formation is reconstructed. Initial stage is marked by the basalt/agglutinate complexes of FA I. They are interpreted as spatter/cinder cones built by Hawaiian, fire-fountaining to Strombolian eruptions. Second stage is represented by repetitive emplacement of block-and-ash flows and attendant lava flows (FA II), which suggests onset of explosive (Vulcanian) and effusive eruptions of more evolved (intermediate) volcanic centers. They may have formed aprons or lobes on the collapsed sector of a dome volcano. Hydrologic remobilizations were active during and in the immediate aftermath of the eruptions, resulting in the interlayered fluvial deposits of FA III. The changes in eruption styles and volcano types may have resulted from compositional differentiation of parental magma.

## IMPLICANCES OF THE ACTIVITY OF FLUOR-RICH FLUIDS ON BASALTS AFFECTED BY VERY LOW GRADE METAMORPHISM IN CHAPELCO HILLS, NEUQUÉN, ARGENTINA

4-08

C.I. Martínez Dopico(\*), E. Gallegos(\*\*), M.E. Vattuone(\*\*\*)

(\*) *Departamento de Ciencias Geológicas, Facultad de Ciencias Exactas y Naturales, Universidad de Buenos Aires, Argentina. carmen@gl.fcen.uba.ar*

(\*\*) *Departamento de Ciencias Geológicas, Facultad de Ciencias Exactas y Naturales, Universidad de Buenos Aires, Argentina. ernestog@gl.fcen.uba.ar*

(\*\*\*) *Departamento de Ciencias Geológicas, Facultad de Ciencias Exactas y Naturales, Universidad de Buenos Aires, Argentina. Instituto de Geología Isotópica (CONICET), Ciudad Universitaria, 1428, Buenos Aires, Argentina. elena@gl.fcen.uba.ar*

### Summary

Fluorite, infilling fractures of volcanic rocks affected by very low grade metamorphism (VLGM) under zeolite and prehnite-pumpellyite facies located at Chapelco Hills, in assemblages with fluorapophyllite, sericite and copper oxides, have been found. It indicates that circulating fluids were rich in F<sup>-</sup>. The presence of this element would be due to exhalative processes, related to the emplacement of Miocene granitic magmas in the area.

### Abstract text

Fluorite has been found in very low grade metamorphic associations, outcropping at 10 kilometers south to San Martín de los Andes, in the western boundary of Chapelco Hills. Coordinates of the sampling area are 40° 18' 25.7" S and 71° 23' 11.1" W. The outcrops are mainly lava flows and amygdaloid basaltic dykes of Paleogene age, affected by VLGM in zeolite and prehnite-pumpellyite facies (Vattuone & Latorre, 1996).

The rocks of the area show amygdaloid structures of several sizes, elongated in response to a cataclastic deformation, infilled by white secondary minerals, alternated with green areas corresponding to the metabasalt matrix. This alternation gives them a foliated appearance. Some kilometers south to the outcrop, Jurassic granodioritic rocks with fractures carrying hydrothermal alteration are found (Vattuone & Latorre, 2003).

With the microscope, a cataclastic texture can be seen as evidence of the disposition of secondary minerals, mainly wairakite and laumontite, the latter with cleavages filled by copper minerals. These zeolites are embedded in a "matrix", composed mainly by green mafic phyllosilicates (montmorillonite/nontronite), chlorite/smectites mixed layers and chlorite, together with pumpellyite, epidote, sphene, pectolite and calcite.

Fluorite appears in small crystals of cubic and octahedral habits, occasionally twinned, in a greenish blue color, with a very low refraction index, concentrated along fractures following the apparent foliation.

In these rocks calcic minerals prevail: laumontite, wairakite, pumpellyite, epidote, prehnite, sphene and pectolite, as an indicator of temperatures around 250°C, a high geothermal gradient, high  $fO_2$  and pressures around 1 kb, in zeolite and prehnite-pumpellyite facies (Vattuone & Latorre, 1996).

At low temperatures and high  $fO_2$ , native copper, chabacite and later cuprite, fluorapophyllite and sericite (phengite) could have been formed in the central part of some amygdaloid structures (Vattuone & Tourn, 2002 and Tourn & Vattuone, 2002).

The residual hydrothermal fluids are enriched in alkali but the presence of F<sup>-</sup> as dissolved gaseous phase turns them locally acid (Bateman, 1957). Hot acid solutions, product of the condensation of F<sup>-</sup> gaseous vents, introduced into fractures of the zeolitized rocks and easily attacked the calcic minerals, forming fluorite and also contributing to the formation of fluorapophyllite and phengite.

Fluorite is a mineral with high F<sup>-</sup> percentage and it appears in fractures as a substitute of minerals with Ca<sup>2+</sup>. We believe that its finding, in this case associated with fluorapophyllite and phengite, is an indication of a high degree concentration of fluorine in the final phase of fluids, as a result of the exhalative processes due to the intrusion of granitic magmas, which would have occurred 24 Ma ago



(Latorre & Vattuone, 1998), as a result of the Pehuenche phase, with the introduction of Miocene granites in the area.

## REFERENCES

- Bateman, A.M. (1957). Yacimientos minerales de rendimiento económico. Ed. Omega, Barcelona, 975 p.
- Latorre, C y Vattuone, M.E. (1998). Edad K/Ar de volcánitas afectadas por metamorfismo de muy bajo grado en el C° Chapelco, Neuquén. X Congreso Latinoamericano de Geología, Bs. As., Actas II, 197-200.
- Tourn, S. M. y Vattuone, M.E. (2002). Cobre nativo y cuprita en una paragénesis ceolítica en amígdalas de lavas basálticas, Chapelco, provincia de Neuquén. Mineralogía y Metalogenia 2002, Bs. As., Artículo, 425-432.
- Vattuone, M. E. y Latorre, C. (1996). Metamorfismo de muy bajo grado en rocas volcánicas de la Formación Ventana, San Martín de los Andes, Neuquén, Argentina. Revista Geológica de Chile 23, 187-200.
- Vattuone, M. E. y Latorre, C. (2003). Edad jurásica para los granitoides aflorantes al norte del lago Falkner, Neuquén, Andes patagónicos septentrionales, República Argentina. Décimo Congreso Geológico Chileno 2003, 4 p.
- Vattuone, M.E. y Tourn, S. M. (2002). Polimorfo ortorrómbico de la serie fluorapofilita/hidroxiapofilita asociado a chabacita y laumontita en amígdalas de basaltos, Chapelco, Neuquén. Mineralogía y Metalogenia 2002, Bs. As., Artículo, 441-446.

## MAGMATIC MUSCOVITE AND GARNET IN GRANITES OF THE SOUTHERN PATAGONIAN BATHOLITH

4-09

H.-J. Massonne(\*), M. Calderon(\*\*), F. Hervé(\*\*)

(\*) *Institut für Mineralogie und Kristallchemie, Universität Stuttgart, Azenbergstr.18, D-70174 Stuttgart, Germany*

(\*\*) *Departamento de Geología, Universidad de Chile, Casilla 13518, Correo 21, Santiago, Chile*

### Summary

In the minor granite bodies of the Southern Patagonian Batholith, dykes and small intrusions occur containing garnet and muscovite. On the basis of their texture and composition, these minerals are unequivocally interpreted to be of magmatic nature. We demonstrate this by rare symplectites consisting either mainly of garnet and quartz or muscovite, plagioclase, and quartz. These mineral assemblages formed by cotectic crystallization. Typically, garnets are close to the spessartine-almandine solid solution series as garnets from other granites worldwide as well. Muscovites contain some amounts of celadonite component (10-17 mol%) as typical for potassic white mica in two-mica granites. It is, thus, possible that the melts, crystallizing to small garnet and muscovite-bearing granite bodies in the Southern Patagonian Batholith, were formed from metasediments below instead of representing differentiation products from voluminous granites. We used the celadonite contents in muscovite to determine the depths of crystallization of this phase. The results of 18 to 22 km point to a deep erosion of the Southern Patagonian Batholith mainly during Tertiary times.

### Introduction

The Southern Patagonian Batholith represents an ensemble of plutonic rocks ranging from gabbros to granites (Bruce et al., 1991). These intruded the margin of the South American continent from Late Jurassic to Tertiary times as a result of melting processes triggered by the subducted oceanic lithosphere of the Antarctic plate. Typically, the so formed magmatic arc consists of I-type granitoids. However, in very minor portions of the batholith small granite bodies occur containing garnet and muscovite. These minerals would indicate S-type granitoids, if they would have crystallized from melting. Our study was, thus, focused on the magmatic or metamorphic nature of garnet and muscovite. In addition, we tried to characterize the depth level of the formation of muscovite.

### Sample description

At the southern shore near the end of Seno Iceberg, a large body of homogeneous biotite granite is outcropping. This body is crosscutted by numerous aplitic dykes containing intergrowths of garnet or white mica with felsic minerals discernible with the naked eye (Fig. 1a) Our samples are from these dykes (S48°43.49', W73°59.74', WGS84).

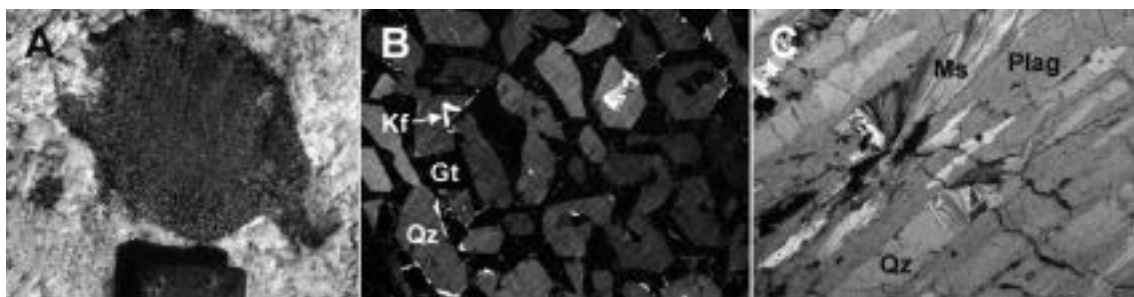


Fig. 1 - Intergrowths (symplectites) of mafic and felsic minerals in dykes in biotite granite near the end of Seno Iceberg. A) Several cm-sized symplectite of garnet and quartz. B) Section of A) seen under the polarizing microscope using crossed nicols (sample CH99-24a). Image width is 5 mm. C) Intergrown lamellae consisting mainly of plagioclase, quartz or muscovite in CH99-24b. Image width is 5 mm. For abbreviations see Table 1.

CH99-24a is a symplectite consisting mainly of garnet and quartz (Fig. 1b). Such rare intergrowths were already reported, for instance, by Zhang et al. (2001) from the Italian Alps and interpreted as the result of cotectic crystallization of both minerals. Minor K-feldspar occasionally occurs between garnet and quartz. Small grains of K-feldspar and plagioclase can be enclosed in quartz. CH99-24b contains intergrowths consisting of up to one mm wide lamellae of muscovite, plagioclase or quartz (Fig. 1c). K-feldspar is a minor constituent of these lamellar portions in the rock.

Sample CH00-27 was collected at the end of a Fjord at Peninsula Staines (S51°32.14', W73°48.20', S.Am.69). At the contact to metapelitic rocks a porphyritic granite occurs which also contains mm-sized spots of red garnet. In thin sections, these garnets show a texture (Fig. 2a) interpreted as skeletal growth. As almost only quartz is found between the garnet branches, this intergrowth is an equivalent to that of sample CH99-24a (Fig. 1a). Further mm-sized phenocrysts are quartz, K-feldspar, and biotite. These minerals also occur in the fine-grained matrix together with plagioclase, muscovite and accessories of apatite and zircon.

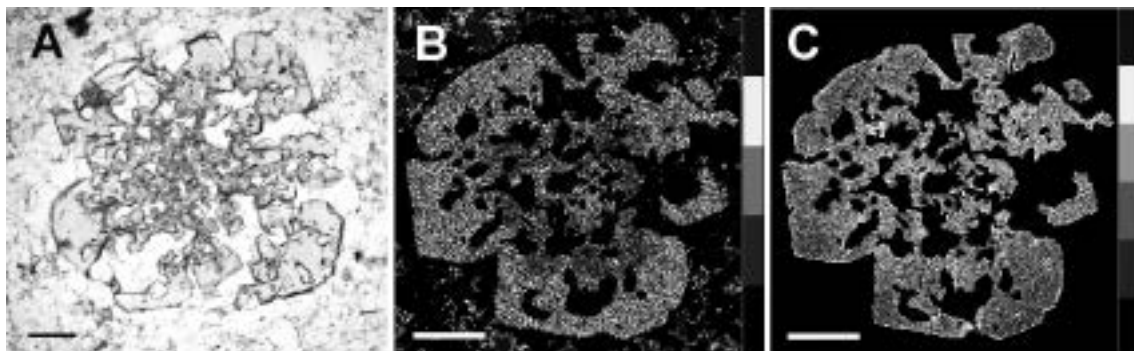


Fig. 2 - Intergrowths of garnet and quartz in porphyritic granite CH00-27. A) Under the polarizing microscope using plain light. B) Concentration map of Ca of a similar object as in A). C) Mn concentration map. Increasing contents are shown by the grey tone scale from the bottom to the top. Scale bars represent 0.2 mm.

### Mineral analytics

The chemical compositions of the minerals were determined with an electron microprobe (EMP) with five wave-length dispersive spectrometers. Standard conditions (15 kV, 15 nA, slightly defocused beam, 20 s counting time on peak and background, synthetic and natural phases as standards) and the PaP correction procedure were applied. Representative analyses, thus determined, are given in Table 1. In addition, specific areas were scanned step-wise (counting times: 100 ms per step) and subsequently processed to obtain element concentration maps. Such maps are presented in Fig. 2.

Garnet in CH00-27 shows an increase of the Fe content from core (Gt3) to rim (Gt4). Mn contents behave opposite (Fig. 3). At the outermost rims the Fe and Mn trends reverse. Ca and Mg contents are more or less constant. The characteristics of the outermost rims was observed for garnet of sample CH99-24a in regard of inner portions (Gt1)

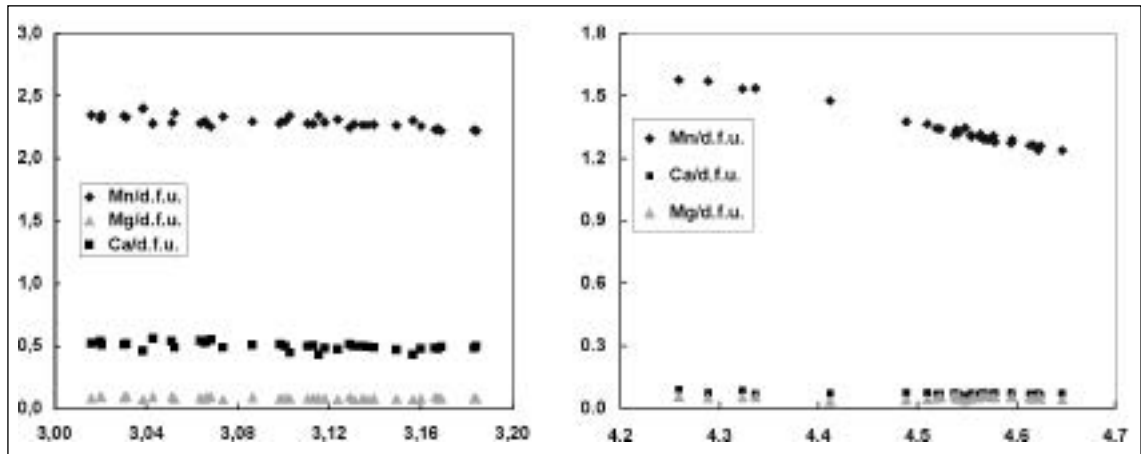


Fig. 3 - Compositional variation of garnet in A) CH99-24a, B) CH00-27. X-axes:  $Fe^{2+}$ /double formula unit (d.f.u.)

Table 1 - Representative analyses of minerals in our studied rocks. Bt = biotite, Gt = garnet, Kf = K-feldspar, Ms = muscovite, Plag = plagioclase, Qz = quartz.

Sample Mineral	CH99-24a				-24b				CH00-27							
	Gt1	Gt2	Kf1	Plag1	Plag2	Ms1	Ms2	Gt3	Gt4	Kf2	Kf3	Plag3	Plag4	Ms3	Ms4	Bt
SiO <sub>2</sub> (wt.%)	36.17	35.98	64.31	67.41	68.58	46.04	46.77	35.51	35.86	64.39	64.82	67.66	65.85	45.78	45.75	32.29
TiO <sub>2</sub>	0.09	0.07	0.03	0.00	0.01	0.02	0.00	0.06	0.00	0.00	0.00	0.01	0.02	0.15	0.10	1.17
Al <sub>2</sub> O <sub>3</sub>	20.15	19.99	18.19	19.74	19.47	33.57	32.72	19.75	20.23	17.93	18.07	19.51	20.62	32.32	34.73	18.99
FeO	24.03	23.27	0.13	0.01	0.00	3.80	3.91	32.37	34.31	0.05	0.06	0.06	0.07	4.17	2.44	31.39
MnO	16.07	17.03	0.05	0.00	0.03	0.01	0.00	11.28	8.92	0.00	0.01	0.01	0.01	0.10	0.04	0.43
MgO	0.35	0.32	0.04	0.01	0.00	0.20	0.41	0.21	0.23	0.00	0.00	0.00	0.00	0.33	0.32	1.07
CaO	2.78	2.81	0.15	0.65	0.10	0.00	0.01	0.44	0.41	0.00	0.00	0.75	2.04	0.00	0.14	0.00
Na <sub>2</sub> O	0.04	0.04	0.59	11.70	11.77	0.24	0.21	0.04	0.03	0.62	1.27	11.48	10.67	0.31	0.46	0.06
K <sub>2</sub> O			15.25	0.09	0.08	10.63	10.34			15.29	14.42	0.14	0.25	10.54	9.62	9.00
BaO			0.02	0.02	0.00	0.15	0.13			0.05	0.02	0.00	0.00	0.02	0.03	0.03
Total	99.68	99.50	98.75	99.63	100.06	94.65	94.51	99.65	100.03	98.32	98.67	99.62	99.52	93.70	93.62	94.43
F						0.03	0.01							0.29	0.26	0.10
Si	5.926	5.899	2.999	2.965	2.995	6.240	6.325	5.845	5.885	3.014	3.013	2.975	2.911	6.285	6.174	2.652
Al <sup>IV</sup>			1.000	1.024	1.002	1.760	1.675			0.989	0.990	1.011	1.074	1.715	1.826	1.348
Al <sup>VI</sup>	3.891	3.862				3.602	3.541	3.832	3.912					3.513	3.699	0.490
Ti	0.010	0.009	0.001	0.000	0.000	0.002	0.000	0.007	0.000	0.000	0.000	0.000	0.000	0.016	0.010	0.072
Fe <sup>3+</sup>	0.109	0.138	0.005	0.000	0.000	0.000	0.000	0.168	0.088	0.002	0.002	0.002	0.003			
Fe <sup>2+</sup>	3.183	3.052				0.431	0.442	4.289	4.622					0.478	0.275	2.156
Mn	2.230	2.365	0.002	0.000	0.001	0.001	0.000	1.572	1.241	0.000	0.001	0.000	0.001	0.011	0.005	0.030
Mg	0.086	0.078	0.003	0.001	0.000	0.041	0.083	0.051	0.057	0.000	0.000	0.000	0.000	0.066	0.065	0.131
sum						4.077	4.067							4.085	4.054	2.879
Ca	0.488	0.493	0.008	0.031	0.005	0.000	0.002	0.077	0.072	0.000	0.000	0.035	0.097	0.000	0.021	0.000
Ba			0.000	0.000	0.000	0.008	0.007			0.001	0.000	0.000	0.000	0.081	0.120	0.009
Na	0.012	0.011	0.054	0.998	0.996	0.062	0.055	0.011	0.009	0.057	0.114	0.978	0.915	0.001	0.002	0.001
K			0.907	0.005	0.005	1.838	1.784			0.913	0.855	0.008	0.014	1.845	1.656	0.943
sum			0.969	1.034	1.006	1.907	1.848			0.970	0.970	1.022	1.025	1.927	1.798	0.954
F						0.026	0.013							0.290	0.261	0.102
OH						1.974	1.987							1.710	1.739	1.898

and margins (Gt2) in contact to quartz. Muscovite in CH99-24b shows a slight decrease of Si/d.f.u. probably from inner portions (Ms2) to the margins (Ms1) of the white mica aggregates (Fig. 4). A similar trend was observed for CH00-27 where cores of white mica in K-feldspar are richer in Si (Ms3) than the rims of these micas and those (Ms4) in the fine-grained matrix. Decreasing in Si contents is accompanied by decreasing in Mg+Fe contents, according to decreasing in celadonite component, although Fe contents alone seem to slightly decrease with rising Si in CH00-27. Biotite

in CH00-27 is slightly zoned which is discernible only by slightly decreasing in Ti contents from core to rim. Plagioclase and K-feldspar in this sample show lower contents of the components anorthite and albite, respectively, in matrix grains (Plag3, Kf2) compared with large phenocrysts (Plag4, Kf3). However, even in small feldspar grains of the matrix a decrease of these components from core to rim is discernible. A slight compositional zoning could also be proven for feldspars in samples CH99-24.

### Geothermobarometry

The compositions of muscovite were used for geothermobarometry as this phase coexists with quartz, K-feldspar, garnet (and biotite). Assuming crystallization temperatures around 650°C only and water activities close to 1.0 at least for the final crystallization of the granitic melts, pressures between 4 and 6.5 kbar result from the method reported in Massonne (1984). In addition, thermodynamic calculations were undertaken with the almandine, annite,

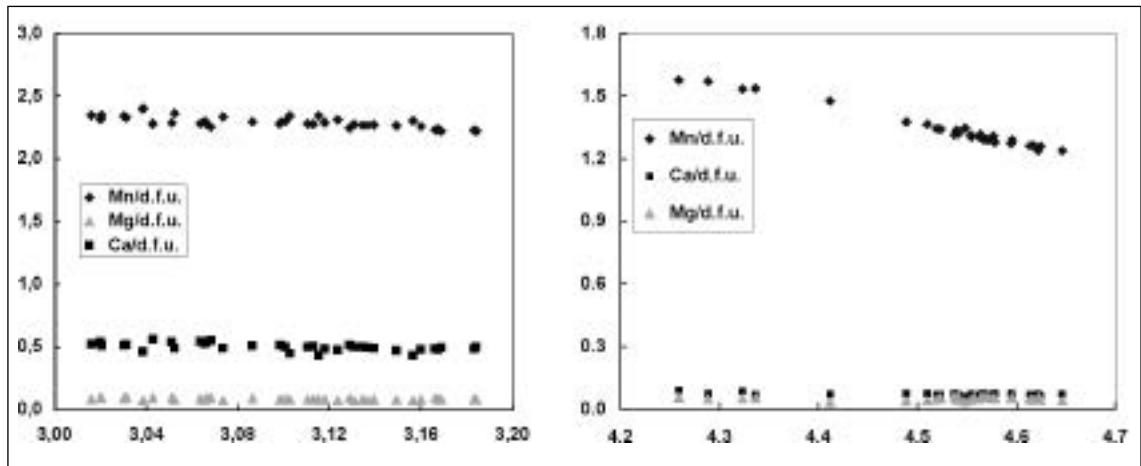


Fig. 4 - Compositional variation of muscovite in A) CH99-24b and B) CH00-27. X-axes = Si/d.f.u.

Table 2 - Geothermobarometric results obtained by thermodynamic calculations.

Sample	Mineral compositions	P (kbar), T (°C)	P (kbar), T (°C)
CH99-24	Gt1, Ms2	7.04, 650	9.08, 700
	Gt2, Ms1	6.20, 650	8.13, 700
CH00-27	Gt3, Ms3	5.53, 650	7.37, 700
	Gt4, Ms4	4.51, 650	6.18, 700
	Bt1, Ms3	5.97, 650	7.26, 700
	Bt1, Ms4	4.66, 650	5.84, 700

and Fe<sup>2+</sup>-Al-celadonite components of the mafic minerals using data and mixing models, for instance, given by Brandelik & Massonne (2004). The activity of K-feldspar was set to 0.95. The P-T positions of equilibria such as 3 Fe<sup>2+</sup>-Al-celadonite + muscovite = 4 H<sub>2</sub>O + 4 K-feldspar + almandine were calculated. The results given in Table 2 confirm the pressures derived by Massonne's (1984) method.

### Conclusions

From the textural observations reported above, we conclude that both mafic minerals, garnet and muscovite, formed in our samples by crystallization of granitic melts. This is confirmed by the observed compositional trends of these minerals and coexisting feldspars because the corresponding zoning patterns can also be found in S-type granitic rocks worldwide. However, such granites are believed to have formed by melting mainly of metasedimentary rocks. Thus, it could be that the garnet and muscovite-bearing granitic rocks originated through melting of metasediments below the granitoids of the magmatic arc, instead of representing differentiation products of the large volumes of these I-type granitoids.

The geothermobarometric evaluation gave pressures around 5.5 kbar. These pressures correspond to Earth's depths of about 20 km. We interpret these as intrusion levels which are cut currently at the surface. As a consequence of this, significant erosion of the western continental margin of southernmost South America, involving the magmatic arc, must have taken place presumably in Late Tertiary times.

### Acknowledgments

Our study was financially supported by a CONICYT - BMBF (CHL O1A 6A and CHL 99/031) agreement and by FONDECYT project 1010412 (to FH). We also thank Captain C. Alvarez and his crew in the yacht Penguin.

### REFERENCES

- Brandelik & Massonne (2004), *Comp. Geosc.*, in press
- Bruce et al. (1991), *Geol. Soc. Am. Spec. Paper*, 265, 1-12
- Massonne (1984), *Fortschr. Miner.*, 62, Beiheft 1, 147-149
- Zhang et al. (2001), *Schweiz. Mineral. Petrogr. Mitt.*, 81, 89-113

## EFFECTS OF METAMORPHISM ON MAGNETIC SUSCEPTIBILITY AND FERROMAGNETIC MINERALS IN THE SARMIENTO OPHIOLITE COMPLEX, SOUTHERN CHILE

4-10

S. Singer<sup>(1)</sup>, A. Rapalini<sup>(1)</sup>, M. Calderón<sup>(2)</sup>, F. Hervé<sup>(2)</sup>

(1) INGEODAV, Depto. Cs. Geológicas, F.C.E.y N., Universidad de Buenos Aires, Argentina

(2) Depto. de Geología, Universidad de Chile, Santiago, Chile

### Introduction

The Sarmiento Ophiolitic Complex (SOC), located in the southern Andes of Chile, represents the mafic portion of the Late Jurassic to Early Cretaceous oceanic floor of an extensional back-arc basin partly closed and uplifted in the Mid Cretaceous (Fig. 1; Stern and De Wit, 2003; Calderón et al., this volume). The SOC is exposed at least in two thrust slices and its igneous pseudo-stratigraphy consists of mainly mafic pillow lavas, dykes, and gabbros. These rocks underwent a non-deformative "ocean floor metamorphism" prior to its uplift and exposure which developed secondary mineral assemblages in a vertical steep metamorphic gradient passing from zeolite to actinolite facies, followed by a transition to fresh gabbros (Stern et al, 1976; Elthon and Stern, 1978). Syntectonic greenschist facies assemblages in mylonitic rocks bordering the thrust slices, represent a different metamorphic event, that probably occurred either during or before the Late Cretaceous (ca. 75 Ma, K-Ar whole rock dating; see Rapalini et al., this volume). In order to have a better understanding of the incidence of the mentioned metamorphic processes on the natural remanent magnetization in the ophiolite, a susceptibility survey and a study of ferromagnetic (*s.l.*) minerals were carried out. As part of a classic paleomagnetic study (see Rapalini et al, this volume), the ophiolite was sampled (drilled) at 11 sites distributed on different stratigraphic levels.

### Magnetic Susceptibility

The bulk magnetic susceptibility ( $K$ ) of any given material defined by  $K = M / H$  where,  $M$  is the induced magnetization in the material by a weak magnetic field of constant strength ( $H$ ), being dimensionless in the *Système International* (SI). In particular, within a rock, each mineral contributes with its own susceptibility and concentration to the total susceptibility of the rock. Thus, the bulk susceptibility represents an addition of susceptibilities of all minerals that are present in a sample,

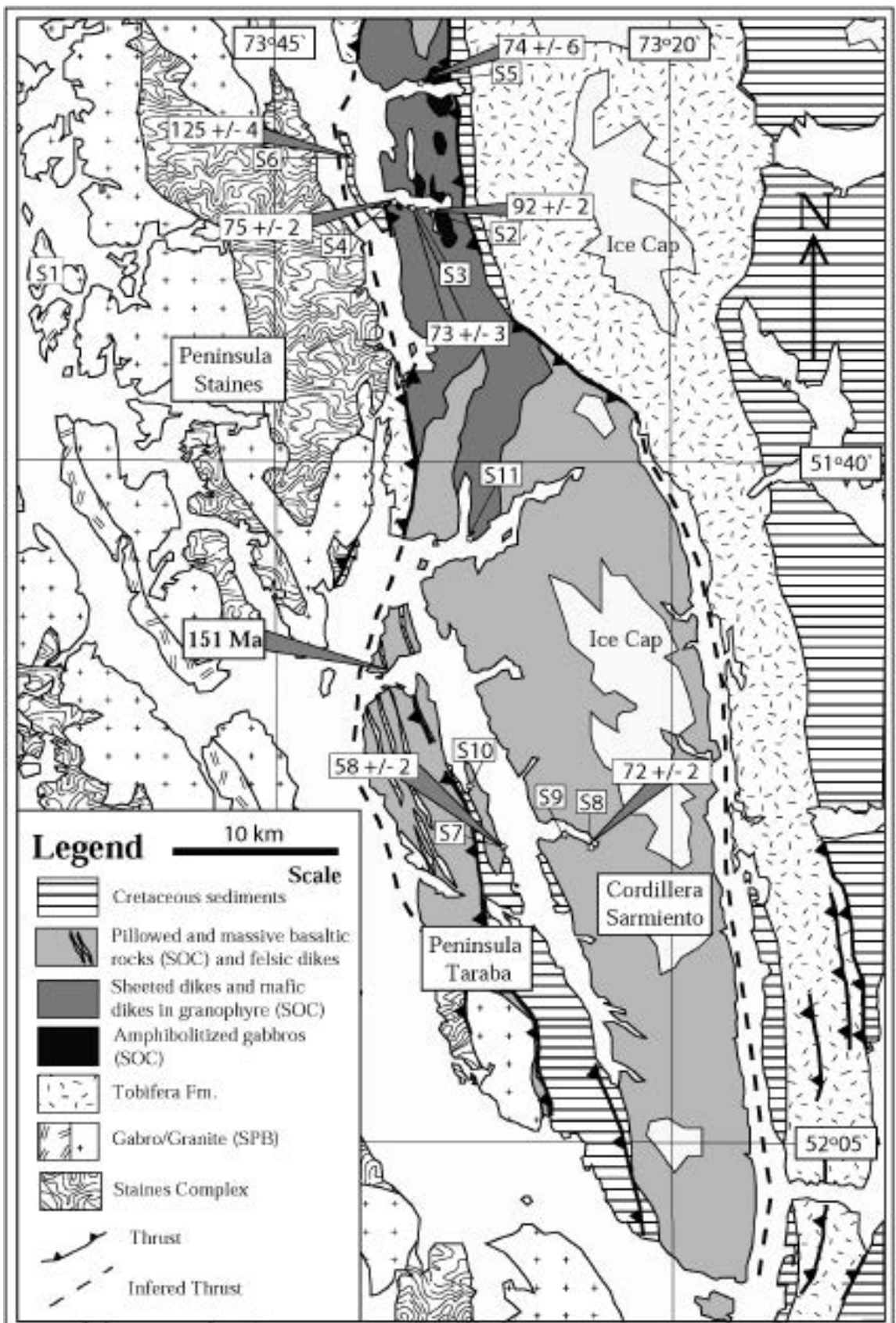


Fig. 1 - Simplified geologic map of the Sarmiento Ophiolite and radiometric ages.

although if magnetite is present, even at low concentrations, it controls this property due to its very high susceptibility. As a consequence, rock susceptibility gives us a first idea of the contribution of magnetite. Taking into account this later concept, informal classification schemes based on the magnetic susceptibility have been established to assign a magnetic behavior to each rock (Tarling and Hrouda, 1993, Clark, 1999). In this work, measurements of susceptibility were performed with a Bartington MS2 susceptibilimeter. Site arithmetic means (*Kmean*) and their standard deviation (SD) are summarized in Table 1 and illustrated in Fig. 2.

Sites	Kmean ( $10^{-5}$ SI)	SD	Magnetic behavior
1 <sup>a</sup>	1190	140	Moderately ferromagnetic
1B	142	22	Weakly ferromagnetic
2 <sup>a</sup>	246	50	Weakly ferromagnetic
2B	84	13	Paramagnetic
3	88	12	Paramagnetic
4	468	175	Moderately ferromagnetic
5	49	14	Paramagnetic
6	63	4	Paramagnetic
7	57	-	Paramagnetic
8	59	11	Paramagnetic
9	66	5	Paramagnetic
10	49	4	Paramagnetic
11	64	2	Paramagnetic

Table 1 - Site mean magnetic susceptibility and magnetic behavior

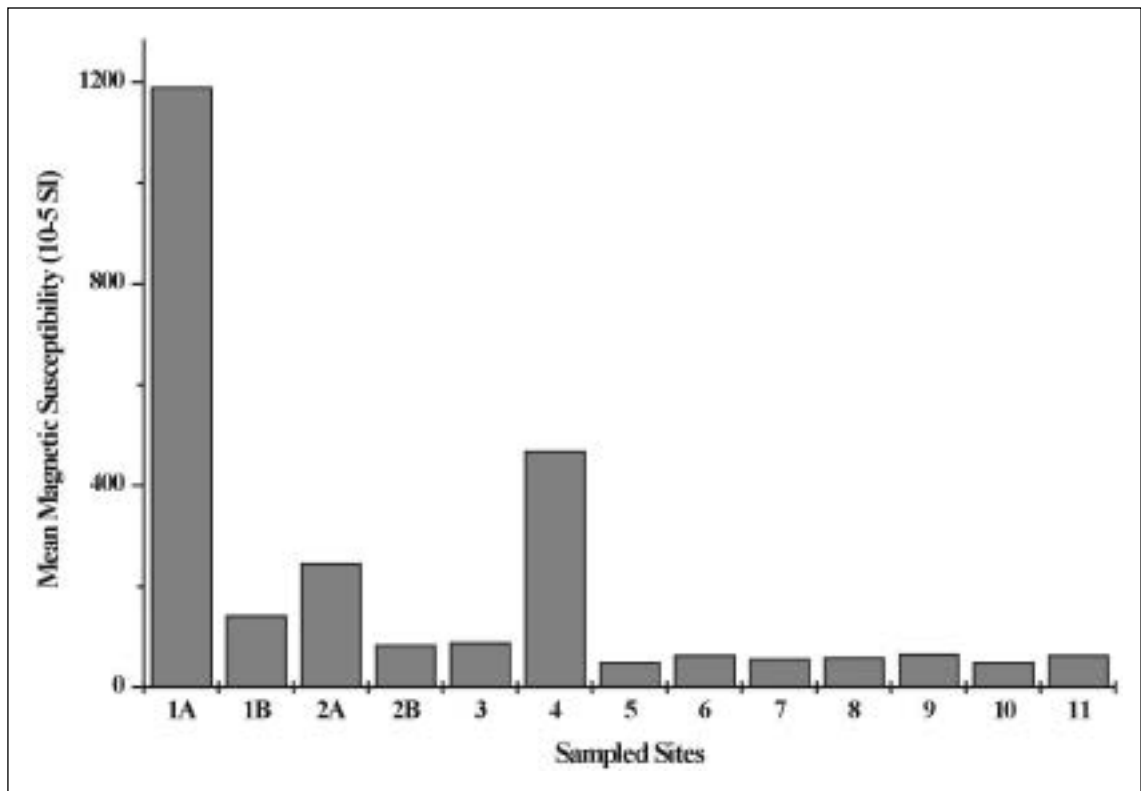


Fig. 2 - Plot of site mean magnetic susceptibility.

## Ferromagnetic (s.l.) Minerals

The studied rocks show metamorphic assemblages consisting of actinolite/tremolite, titanite, epidote, chlorite/smectite, quartz, Na-plagioclase and carbonates in mafic dykes and gabbros of the northern area, and epidote, chlorite/smectite, titanite, actinolite/tremolite, pumpellyite and carbonates in mafic dykes and lavas from the southern area (Fig.1). Magnetic minerals were identified by microscopic observations under reflected (oil-immersion objectives) and transmitted light. The optical observations on each site are the following:

**Site 1A:** polished sections belonging to gabbros formed by olivine, hypersthene and plagioclase, show networks of almost pure secondary magnetite, product of partial serpentinisation of olivines. Neither primary Fe-Ti oxides nor residual minerals, product of breakdown of the former are found. Sulfides (possibly pyrrhotite) are observed.

**Site 1B and 2A** are gabbros not yet studied.

**Site 2B:** dike crosscutting gabbro shows ilmenite crystals rimmed by titanite. These crystals present a distinctive morphology similar to that of titanomagnetites although ilmenite does not seem to have been originally intergrown with magnetite. Thus, we consider that the explanation for this morphology requires further studies.

**Site 3 :** sheeted dike similar to that of site 2B, although the replacement of ilmenite by titanite is greater, including pseudomorphs.

**Site 4:** sheeted dike with titanomagnetite and ilmenite crystals.

**Site 5 :** sheeted dike without Fe-Ti oxides. It presents sulfides and grumous titanite as titanium-bearing mineral.

**Site 6:** lamprophyric dike with abundant sulfides. Fe-Ti oxides are not found.

**Site 7:** pillow lava was not yet studied. Microscopic observations were made on a hydrothermal vein, associated to this pillow lava, which shows an infill of sulfides. They present cubic morphology and anisotropy under crossed nicols. Possibly, these grains may be pyrite with As, Co, or Ni content.

**Sites 8, 9 and 10:** pillow lavas do not show Fe-Ti oxides. They present titanite as titanium-bearing mineral and abundant sulfides.

**Site 11 :** sheeted dike with description similar to site 5.

## Discussion

The analysis of the susceptibility values together with the preliminary optical observations, indicate a very good agreement between the results obtained by both proceedings. Thus, ferromagnetic gabbros show high susceptibility values due to the presence of magnetite, while basic dikes and pillow lavas have susceptibilities controlled by the paramagnetic mineral fraction, which is concordant with the absence of magnetite in them.

From the analysis of this preliminary results the following inferences may be drawn:

In these rocks the metamorphic processes have performed strong effects on ferromagnetic minerals. These metabasites are distinctly poor in titanomagnetites, as indicated by their low magnetic susceptibilities except for the ferromagnetic gabbros that represent the unique example where the metamorphism (serpentinisation) has generated magnetites. By the way, basic dikes show preserved titanomagnetites and/or ilmenites partially to totally replaced by titanite, while in the pillow lavas, the titanomagnetites have been destroyed, leaving titanite as witness of the presence of a primary titanium-bearing mineral.

The evidence suggest that in these rocks (which contain silicates that can accommodate Fe<sup>+3</sup> in their structures), equilibria between Fe oxides and Fe<sup>3+</sup> in silicates has played an important role in determining the occurrence and abundance of titanomagnetites during metamorphism.

## REFERENCES

- Stern, C., De Wit, M. and J. Lawrence, 1976. Igneous and Metamorphic Processes Associated With the Formation of Chilean Ophiolites and Their Implication for Ocean Floor Metamorphism, Seismic Layering, and Magnetism. *Journal of Geophysical Research*, 81, 4370-4380.
- Elthon, D. and C. Stern, 1978. Metamorphic petrology of the Sarmiento ophiolite complex, Chile. *Geology*, 6, 464-468.
- Stern, C. and M. De Wit, 2003. Rocas Verdes ophiolites, southernmost South America: remnants of progressive stages of development of oceanic-type crust in a continental margin back-arc basin, from Dilek, Y. and Robinson, P. T. (eds.) 2003. *Ophiolites in Earth History*, Geological Society, London, Special Publications, 218, 1-19.



- Rapalini, A., Calderón, M., Hervé, F., Cordani, U., and S. Singer, 2004. First Paleomagnetic Results On The Sarmiento Ophiolite, Southern Chile: Implications For The Patagonian Orocline, this volume.
- Tarling, D. and F. Hrouda, 1993. The magnetic Anisotropy of the Rocks. Chapman and Hall, London, 217 pp.
- Clark, D., 1999. Magnetic petrology of igneous intrusions: implications for exploration and magnetic interpretation. Exploration Geophysics, 30, 5-26.
- Calderón, M., Hervé, F., and C. Fanning, 2004. Late Jurassic Birth of the Rocas Verdes Basin at the Sarmiento Ophiolitic Complex: Evidence from Zircon U-Pb Shrimp Geochronology, this volume .

## THE ORIGIN OF PLATINUM IN TIERRA DEL FUEGO: GEOLOGICAL EVIDENCE 4-11

E. Zappettini (\*), L. Villar (\*\*), S. Segal (\*), A. Celeda (\*), A. Romano (\*), D. Acevedo (\*\*\*)

(\*) *Servicio Geológico Minero Argentino –SEGEMAR–*

(\*\*) *CONICET* (\*\*\*) *CONICET-CADIC*

### Introduction

The first description of native platinum from Tierra del Fuego is provided by Kyle (1890) who analyzed heavy minerals from El Páramo. Beder (1930) describes native platinum from Cordoba and mentions the platinum from Tierra del Fuego, suggesting its possible relation with peridotites from the Magellan Strait.

Petersen and Methol (1948) described the heavy minerals of Tierra del Fuego beach sediments, identifying magnetite, hematite, hornblende, tourmaline, olivine, garnet, pink quartz, zircon, pyrite and minor amounts of native gold and native platinum. Finally, Methol and Sister (1949) analyzed a gold nugget from Cañadón Tortugas from northern Tierra del Fuego and established the absence of platinum.

### Geology

The analyzed samples (Fig. 1) belong to “Mina Agustina”, property of Compañía Minera El Páramo S.R.L., located at Cabo Nombre, 185 north of Rio Grande city.

In the area the beach comprises four zones: storm beach, high swash zone, low sandy swash zone and low muddy swash zone (Bujalesky, 1997).

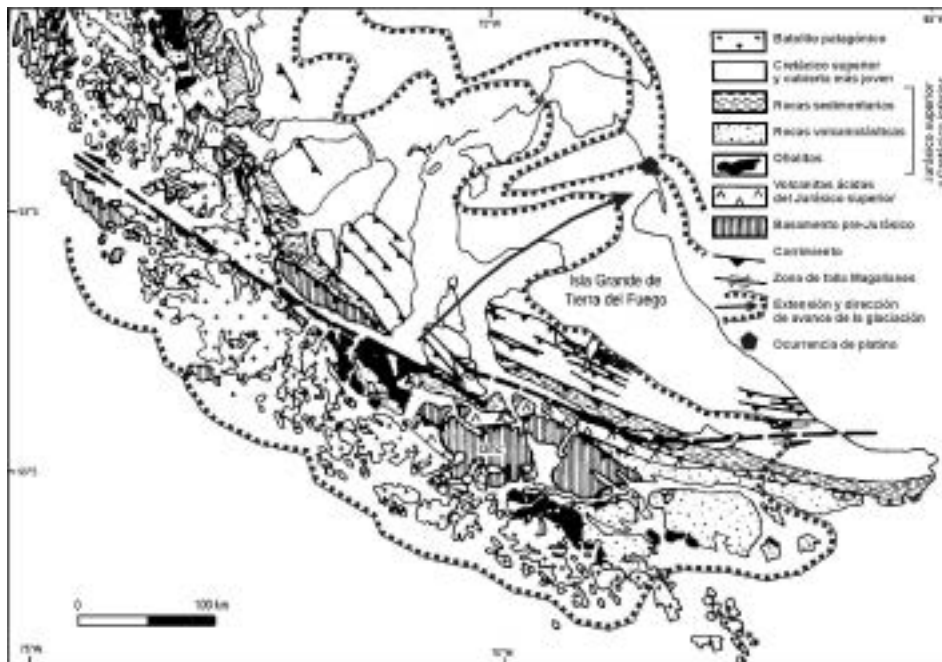


Fig. 1 - Geology of the Fuegan Andes, extension of Quaternary glaciation and location of Pt mineralization (modified from Ramos and Alemann, 2000 and Caldenius, 1932)

The storm beach zone that was sampled, is located above the high tide level and is reached by storm waves. This section consists of gravel and medium and coarse sand. It includes levels, known as *pay streak*, where heavy minerals are concentrated.

### Sample processing

The sample was processed *in situ* with a Knelson KC MD with 7.5" diameter gravimetric concentrator. The obtained concentrate included other than native gold other heavy minerals as well as lithoclasts. The concentrate was classified and granulometric fractions were separated with sieves of ASTM 12, 20, 30, 60 and 120 mesh.

From the retained material of each granulometric fraction (excepted the one retained with mesh 12) ferromagnetic minerals were separated with a permanent magnet. The remnant material was processed with a Carpco electromagnetic separator, with an intensity of current of 2.5-2.7 A, 5mm opening, obtaining magnetic and no magnetic products. From the non-magnetic material, heavy minerals were separated with bromoform ( $d = 2.89 \text{ g/cm}^3$ ), in order to facilitate the recognition of platinum. The percentage of each separated product, referred to the total original concentrate is indicated in Table 1.

Granulometric fraction	Weight % of the granulometric fraction	Weight % of ferromagnetic minerals	Weight % of magnetic minerals 2.5-2.7 A	Weight % of non magnetic minerals	
				Light	Heavy
>12	24.0	24.0			
12 – 20	11.5	0.7	3.7	7.1	
20 – 30	20.0	1.2	8.0	10.7	0.1
30 – 60	30.1	5.3	8.0	16.3	0.5
60 – 120	13.7	7.4		0.6	5.7
< 120	0.7	0.3	0.4		
Total	100.0	100.0			

Table 1. Distribution of granulometric and magnetic mineral fractions from Mina Agustina concentrate

### Mineralogy and petrography

The fraction +20 (3) is constituted by almost 100% of lithic grains. These are: gabbros (Fig. 2) plagioclase rich gabbros (plagioclase > pyroxene), pyroxenites with minor plagioclase, plagioclasites, granodiorites, diorites with zoned plagioclase, cataclastic acid plutonic rocks, pyroxenitic andesites, amphibolites, basalts, porphyric basalts with clinopyroxene phenocrysts, porphyric basalts with green phenocrysts (amphibol or pyroxene), partially serpentinized ultramafic rocks (figure 3), sedimentary and metamorphic rocks. Also euhedral to anhedral garnet grains can be observed. Oxidized iron minerals (limonites) can be found surrounding the silicates. Orthopyroxene in basal sections is a common constituent of this fraction.

The fraction +30 (3) is also predominantly constituted by lithic grains which are: amphibolites, diabases, basaltic lava, medium to fine grain basalts, several types of basaltic rocks, orthoamphibolites, sedimentary and metamorphic rocks. Mineral grains are: euhedral to anhedral garnet with inclusions of elongated bodies of opaque minerals (these can be isorientated); twined plagioclase, orthopyroxene, cataclastic quartz, zoned plagioclase derived from mesosilicic plutonic rocks, and scarce grains of euhedral serpentinized olivine. The oriented opaque mineral inclusions in garnet consist of small flakes of magnetite or ilmenite. In these grains small and disseminate pyrite chips can be observed. These chips are between 7 and 15 microns in size.

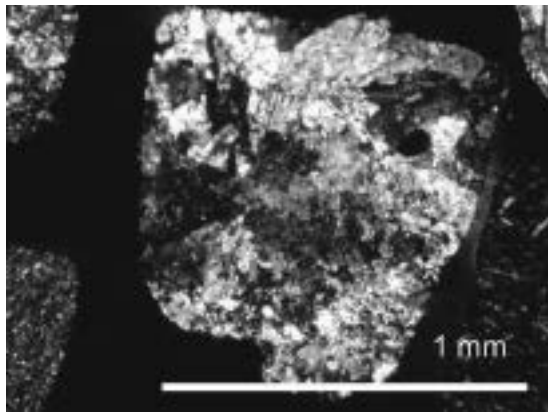


Fig. 2 - Serpentinized ultramafic rock.  
Crossed nichols

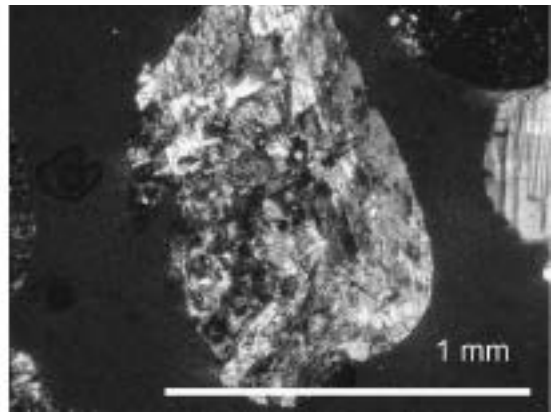


Fig. 3 - Gabbro or cumulate with plagioclase, pyroxene and probable olivine. Crossed nichols

The +50 (5) fraction is made by 90% of lithic grains. These are: magmatic mesosilicic rocks, sedimentary rocks, plagioclase and scarce quartz crystals.

The fraction +60 (3) shows a great variety of Fe, Ti and Mg oxides; the most conspicuous being titanomagnetite, magnetite, ilmenite, as well as some idiomorphic grains of hematite containing relicts of ilmenite. Scarce small anhedral grains of chromite, with sizes between 18 and 28 microns, have been observed.

The fraction +120 (1) contains: small grains of ilmenite, titanomagnetite, leucoxene, small slabs of ilmenite associated with rutile, grains of magnetite-hematite completely martitized and euhedral to subhedral grains of hematite with magnetite relicts. In one of the titanomagnetite grains isoferroplatinum was identified with reflected light and electron beam microscope (figure 4). The rounded grain is white to moderate gray in colour and has moderate reflectivity.

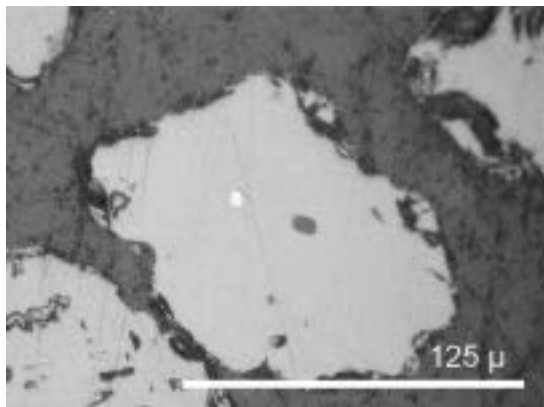


Fig. 4 - Isoferroplatinum included in titanomagnetite

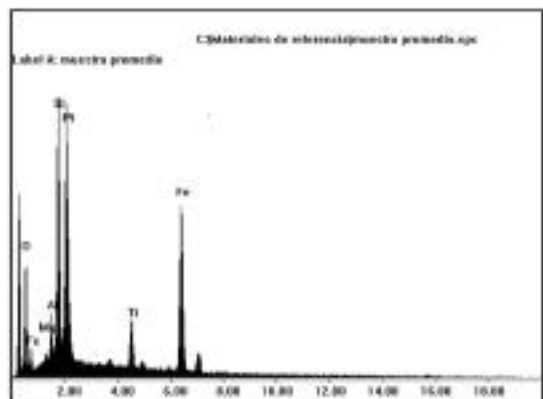


Fig. 5 - EDAX spectra of platinum included in titanomagnetite

The fraction +120 (6) consists of 80 to 90% opaque grains. Ilmenite is the most conspicuous mineral. Some grains are homogeneous and others are made by ilmenite intergrown with hematite lamellae. Some have inclusions of rutile. Titanomagnetite is the second mineral in order of abundance. This is the only fraction that shows native gold and Platinum Group Minerals (PGM). Isoferroplatinum has been observed as inclusions in titanomagnetite and in garnet. The PGM inclusions, detected by the scanning electron microscope are 12 to 23 microns in size. Silicates from this fraction consist of subhedral to anhedral light pink partially anisotropic garnet, orthopyroxene.

## Analysis with wavelength dispersive spectrometer

Grains from different granulometric fractions were analyzed with a Philips (XL 30 ESEM) scanning electron microscope. Also polished sections were analyzed using a wavelength dispersive spectrometer (EDAX). Various spectra and semi quantitative analyses were thus obtained. The presence of isoferroplatinum was confirmed. The associated minerals and the morphologies were also studied. Figure 5 shows the spectrum obtained from an isoferroplatinum inclusion in titanomagnetite identified in one grain from fraction +120(6). The atomic weight composition is as follows: O: 30,02%, Mg: 0,72%, Al: 2,91%, Si: 9,04%, Pt: 29,92%, Ti: 5,57%, Fe: 21,81%. The results indicate the close association of platinum with Fe-Ti minerals.

## Discussion

Gomez Peral et al. (1997) proposed that heavy minerals to the south of San Sebastian Bay were concentrated from alluvial materials, located in old river mouths prior to the post-glacial transgression. There are evidences that alluvial native gold in the Fuegan Andes is related to granitic rocks (Caldenius, 1932). Otherwise, the analysis of heavy minerals and lithoclasts from beach material sampled to the north of San Sebastian Bay has confirmed the presence of PGE minerals, associated with lithoclasts and minerals that can be related to ophiolitic associations. In the Fuegan Andes, during the Jurassic-lower Cretaceous the “Cuenca Marginal Rocas Verdes” basin was formed, with development of oceanic crust in its axis (Sarmiento and Tortuga Complex ophiolites, Ramos and Alemann, 2000). We propose that PGE minerals identified have an independent origin from native gold, and can be related with the ophiolites identified in the Chilean sector of Tierra del Fuego. These rocks were partially eroded by the glacial activity with subsequent drift deposits formation, exposed in the northern part of Tierra del Fuego (Caldenius, 1932) (Fig. 1). This unit carries ilmenite, titanomagnetite, garnet and PGE minerals that were reconcentrated by fluvial and marine action.

## REFERENCES

- Beder, R. 1930. Sobre la existencia de platino nativo en una serpentinita de Alta Gracia, provincia de Córdoba. *Revista Minera* II: 97-101. Buenos Aires.
- Bujalesky, G. 1997. Patrón espacial y dinámica de canales de sobrelavado de la costa de Tierra del Fuego. *Revista de la Asociación Geológica Argentina*, 52 (3): 257-274.
- Caldenius, C. 1932. Las glaciaciones cuaternarias en el Patagonia y Tierra del Fuego. Publicación 95. Dirección General de Minas y Geología, Buenos Aires. 152 páginas y 42 láminas
- Gómez Peral, M.A. y Martínez, D. E. 1997. Distribución de minerales pesados en playas del litoral atlántico de la Tierra del Fuego, entre cabo San Sebastián y cabo Domingo. *Revista de la Asociación Geológica Argentina*, 52(4): 504-514.
- Kyle, J.J. 1890. El platino nativo de la Tierra del Fuego. *Anales de la Sociedad Científica Argentina*. 29: 51.
- Methol, E.J. y Sister, R.G. 1949. Informe sobre los aluviones auríferos del Depto. de San Sebastián entre Río Gamma y Cabo Espíritu Santo, Tierra del Fuego. Dirección General de Industria Minera. 42p. 20figs. Inédito.
- Petersen, C. y Methol, E.J. 1948. Nota preliminar sobre rasgos geológicos generales de la porción septentrional de Tierra del Fuego. *Revista de la Asociación Geológica Argentina*, 3: 279-292.
- Ramos, V. y A. Alemann 2000. Tectonic Evolution of the Andes. In *Tectonic Evolution of South America* (ed. Cordani, U., E. Milani, A. Thomaz Filho y D. Campos) 31st. International Geological Congress, Rio de Janeiro. 635-685.

# **Session 5**

---

**GEOMORPHOLOGY  
AND GEODESY**



## REGIONAL GEOID DETERMINATION IN TIERRA DEL FUEGO INCLUDING GPS LEVELLING

5-01

D. Del Cogliano<sup>1</sup>, R. Dietrich<sup>3</sup>, A. Richter<sup>3</sup>, R. Perdomo<sup>1</sup>, J.L. Hormaechea<sup>2</sup>, G. Liebsch<sup>33</sup>, M. Fritsche<sup>3</sup>

<sup>1</sup> Universidad Nacional de La Plata, Facultad de Astronomicas y Geofisicas, Argentina

<sup>2</sup> Estacion Astronomica Rio Grande, Tierra del Fuego, Argentina

<sup>3</sup> Technische Universität Dresden, Institut für Planetare Geodäsie, Germany

<sup>33</sup> now: Bundesamt für Kartographie und Geodäsie, Außenstelle Leipzig, Germany

contact: catans@infovia.com.ar

### Abstract

In recent years, the accuracy of global geoid models has improved remarkably. A number of observation techniques have become applicable for refining regional geoid determinations. However, in many remote areas our knowledge about the geoid does not reach the increasing demands related with the use of GPS for all geodetic purposes, yet.

For the Argentinean part of Tierra del Fuego, gravimetric field observations, precise leveling measurements as well as GPS positioning on leveling lines along main roads carried out in 1998 and 1999, have been used to determine a regional geoid model. The resulting regional model has been compared with the global geoid model EGM96.

Another approach consists in the use of a natural water surface as a local indicator for an equipotential surface. In the case of Tierra del Fuego, the Fagnano lake level, with an East-West extension over 100 Km, might be appropriated for the detection of the local geoid shape and gradients. The main interference can be expected from hydrodynamical effects producing a deviation of the lake surface from the undisturbed equilibrium state, which would reflect pure gravitational forces.

In 2003 and 2004, measurements with a GPS buoy have been carried out at some 50 locations on Lago Fagnano. The kinematic processing of the GPS observations allowed the determination of ellipsoidal lake-level heights. Tide gauge measurements are available in order to correct the observed instantaneous lake-surface topography for disturbing external effects.

In the present contribution, the analysis and combination of these observations is shown. The consistency of the obtained results with measurements by different methods and the feasibility of the proposed approach are discussed.

### Description

In 2001, a geoid model in Tierra del Fuego (Argentina) was obtained (fig. 1) from altimetric points and GPS measurements along 300 Km of the main roads of the region (Del Cogliano et al., 2001). The comparison of this model with the global EGM96 model showed an important gradient in the East-West direction in the Fagnano lake area, suggesting that further investigations were necessary (fig. 2).

In the frame of the German-Argentine (SEPCYT-BMBF) cooperation agreement, the Institut für Planetare Geodäsie (IPG) - Technische Universität Dresden (Germany) and the Facultad de Ciencias Astronómicas y Geofísicas de la Universidad Nacional de La Plata (Argentina), conducted several research activities in the Fagnano lake area during the 2003 and 2004 summers in order to determine its surface behavior.

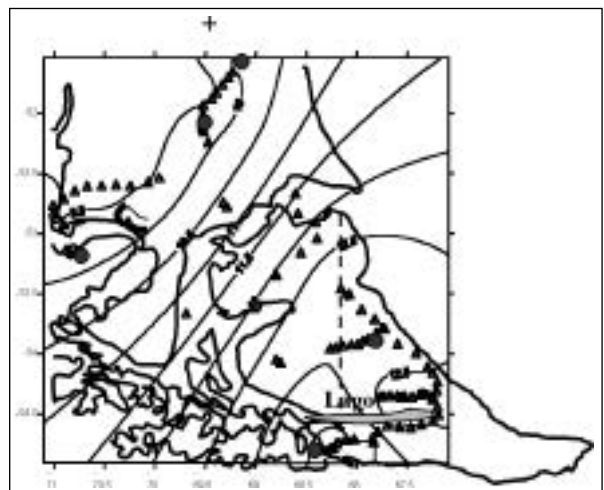


Fig. 1 - Observed geoid undulation (Nobs). The triangles show the leveling points with GPS observations. Isolines each 50 cm.

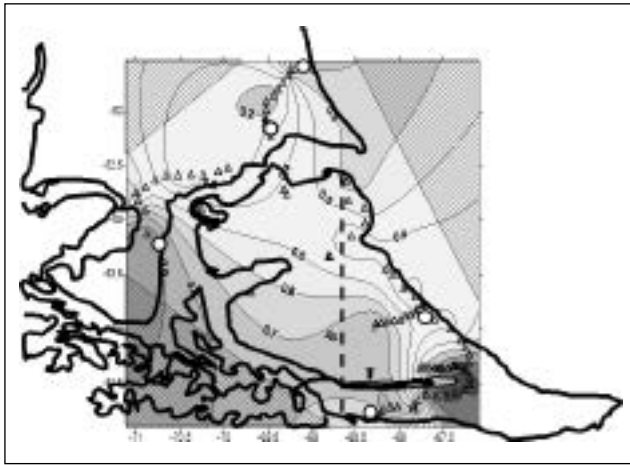


Fig. 2 - Nobs - N(EGM96). Isolines each 10 cm.

These activities included the establishment of new GPS reference points on the lake sides related to the existing GPS network, the installation of three pressure tide gauges along the lake, and the measurement of several profiles on the surface using a GPS buoy.

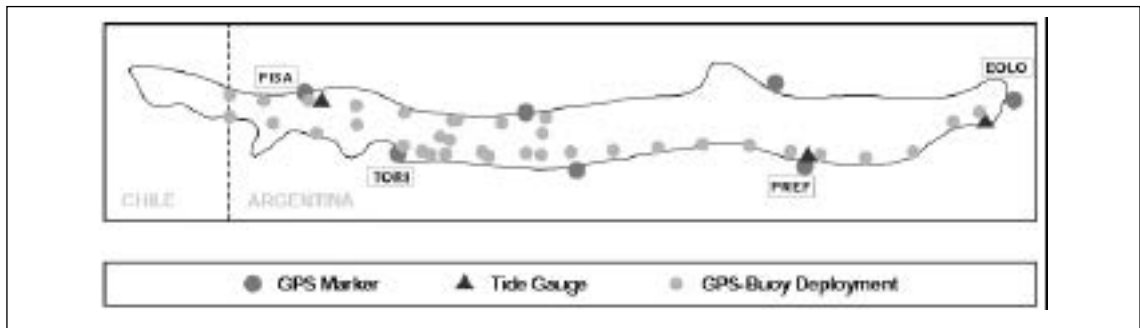


Fig. 3 - Distribution of the observation points.

The tide gauges records are related to the reference ellipsoid operating the GPS buoy over the tide gauges. This can be done simply obtaining the buoy ellipsoidal height by GPS and subtracting the water column height measured with the tide gauge. With this information, all the tide gauges measurements of the lake surface heights can be transformed into ellipsoidal heights.

The GPS buoy is operated in kinematic mode from a boat, simultaneously with two reference stations located near the lake. As shown in fig.4 the buoy antenna is protected with a plastic radom. This radom introduces systematic effects that can be eliminated by using the same radoms in the antennas of the reference stations.



Fig. 4 - GPS Buoy with radom.

Consequently, the reference stations were used with radoms to support the kinematic survey on the lake surface or without radoms with geodynamic purposes.

In this way the continuous records of the three tide gauges describe the lake level variations with time. During the complete year, the tide gauges sample rate was 60 minutes, while during the intensive summer campaigns, 5 and/or 2 minutes were used. On the other hand, GPS buoy measurements were obtained with a 1 sec. sample rate thus a mathematical filter was applied to reduce the results to common points.



This work shows the results of a complete year of tide gauges records and two summer intensive campaigns including 50 profiles of the lake surface obtained with the GPS buoy.

The GPS profiles of the lake surface can be referred to a common mean lake level by using the simultaneous tide gauges measurements.

The relation between the lake level and the geoid surface was made using geometric leveling from the altimetric lines to the GPS reference points located in the lake coast (EOLo y PRE2).

The analysis of this information allowed the determination of a mean lake level and its appartments from an equipotential surface. The possibility of integrating this new data to the previous geoid model is discussed.

## REFERENCES

- D. Del Cogliano, J.L. Hormaechea, R. Perdomo, F. Galban, E. Lauría, G.Ramos. 2001. Geoid Study in Tierra del Fuego. IAG Symposia. Volume 124. Vertical Reference Systems. Springer.

## HORIZONTAL DISPLACEMENTS IN THE MAGALLANES-FAGNANO FAULT ZONE DETERMINED BY REPEATED GPS OBSERVATIONS

5-02

J.L. Hormaechea<sup>1</sup>, D. Del Cogliano<sup>2</sup>, R. Perdomo<sup>2</sup>, R. Dietrich<sup>3</sup>, G. Liebsch<sup>33</sup>, A. Richter<sup>3</sup>, M. Fritsche<sup>3</sup>

<sup>1</sup> Estacion Astronomica Rio Grande, Tierra del Fuego, Argentina

<sup>2</sup> Universidad Nacional de La Plata, Facultad de Astronomicas y Geofisicas, Argentina

<sup>3</sup> Technische Universität Dresden, Institut für Planetare Geodäsie, Germany

<sup>33</sup> now: Bundesamt für Kartographie und Geodäsie, Außenstelle Leipzig, Germany

contact: jlhor@earg.gov.ar

In 1993, the first geodetic GPS network in Tierra del Fuego was established and measured by the Universidad Nacional de La Plata and the Estacion Astronomica Rio Grande. It consisted of 23 points well distributed in the Argentinean part of Isla Grande, with the exception of Península Mitre area (Fig. 1). The network expands from Cabo Espíritu Santo (52° 50' S) to Beagle Channel (55°00'S). The Magallanes-Fagnano Fault System main trace (54°30'S) divides the network asymmetrically.

The Magallanes-Fagnano Fault System (MFFS) runs from the western arm of the Magallanes Strait to the Atlantic offshore (Lodolo et al., 2003) splitting Isla Grande into two continental blocks. A significant part of the MFFS is hidden by Fagnano Lake, an elongated, 105 km-long depression.

From 1993 to 2002, the original geodetic network was measured repeatedly to study its stability and to reveal the existence of present-day tectonic displacements.

An attempt to detect horizontal displacement was performed after 1999 field work and revealed a relative left lateral motion of SAM and SCO plates of about 5 mm/yr (Del Cogliano et al., 2000).

In that study, the E-W components of relative position vectors for interplate baselines showed a significant change over the 1993-1999 interval.

After 2000 and 2002 surveys, additional data and longer observational time intervals allowed a better determination (Perdomo et al., 2002).

Three sets of adjusted coordinates corresponding to 1993, 2000 and 2003 surveys were used. The displacement of each mark over the interval was calculated as the difference  $\Delta \mathbf{x}$  between adjusted coordinates. This difference was modelled as follows:

$$\Delta \mathbf{x} = \Delta \mathbf{x}_0 + \mathbf{v} \Delta t,$$

where  $\mathbf{v}$  is site horizontal velocity vector and  $\Delta t$  is the time interval between two epochs of observation.

The basic assumption was that the only reason for displacements in the area covered by the network is the relative motion of SAM and SCO plates. Each side of the fault is treated as a rigid body.

The north side of the master transform fault (SAM plate) is used as the reference side and the south side (SCO plate) is regarded as the moving side.

Results are shown in the following table. ( $V_{\text{north}}$  and  $V_{\text{east}}$  are vector  $v$  components):

Surveys	Interval Years	$V_{\text{north}}$ Mm/yr	$\sigma(V_n)$ Mm/yr	$V_{\text{east}}$ mm/yr	$\sigma(V_e)$ Mm/yr
2002-1993	8.25	+ 0.9	$\pm 0.9$	+ 6.4	$\pm 0.9$
2000-1993	6.18	- 0.8	$\pm 0.7$	+ 6.5	$\pm 0.7$
Weighted averaged		+ 0.0	$\pm 0.8$	+ 6.5	$\pm 0.8$
Combined Solution		+ 0.7	$\pm 0.6$	+ 6.7	$\pm 0.6$

An independent study performed by Smalley et. al. (2003), which considers a thick lithospheric model, determined a relative motion of 6.6 mm/yr with observational data from 1994 to 2002.

In 2003 the network was densified in the Magallanes-Fagnano Fault System zone with the aim of detecting detailed movements in the fault region. Eight new GPS stations were established along the northern and southern shores of Lago Fagnano. The monumentations consist of concrete pillars or bedrock markers. The central and south points of this enhanced network were observed in February 2003, and re-observed in February 2004. In both campaigns, all points were continuously occupied for at least 24 hours, the new points along the lake 48 hours or more.

In this presentation, the configuration, realisation and processing of the network observations are described. The results of the analysis of relative horizontal point motions is presented, with an emphasis on the two recent campaigns. Particularly, the impact of an earthquake of magnitude 3.7 on April 26, 2003 on the displacement of the GPS points close to the epicentre is of special interest.

The achieved accuracies are discussed and compared with the expected relative horizontal displacements due to transform crustal motions along the tectonic plate boundary between Scotia and South America plates.

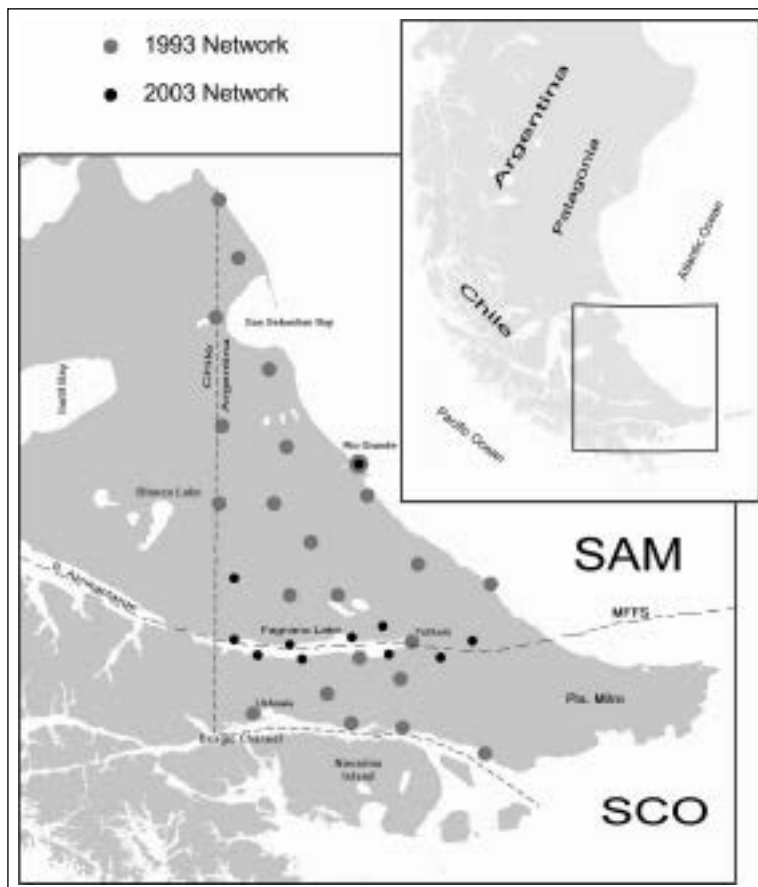


Fig. 1 - Geodetic Network in the Argentinean part of Isla Grande of Tierra del Fuego and the Magallanes-Fagnano Fault System.

## REFERENCES

- Del Cogliano R., Perdomo, R., Hormaechea J.L., Martinioni D., Olivero E., Strelin J. GPS detection of movements between SCO and SAM plates in the Argentinean part of Tierra del Fuego Island. 31st International Geological Congress, Rio de Janeiro, Brasil, 6-17 aug. 2000.
- Del Cogliano R., Perdomo, R., Hormaechea J.L. Desplazamiento entre placas tectónicas en Tierra del Fuego. Actas de la XX Reunión Científica de la Asociación Argentina de Geodestas y Geofísicos. Mendoza, Argentina, oct. 2000.
- Lodolo E., Menichetti M., Tassone A., Geletti R., Sterzai P., Lippai H., Hormaechea J.L. Researchers Target a Continental Transform Fault in Tierra del Fuego. EOS Transactions, Vol.83, N°1, January 2002.
- Perdomo R., Hormaechea J.L., Del Cogliano D. Tectonic Studies with GPS in Tierra del Fuego. Simposio International Association of Geodesy: "Deformación reciente de la corteza terrestre en Sudamérica y regiones adyacentes". Santiago de Chile, Chile, 21-25 oct. 2002.
- Smalley R., Kendrick E., Bevis M., Dalziel I., Taylor F., Lauría E., Barriga R., Casassa G., Olivero E., Piana E.

## GEOID UNDULATION ON THE ANDEAN CORDILLERA

5-03

Antonio Introcaso<sup>(1)</sup>, Luis Eduardo Lenzano<sup>(2)</sup>, Ana María Robin<sup>(2)</sup>, María Virginia Mackern<sup>(2)</sup>

(1) Grupo de Geofísica – IFIR (UNR, CONICET)

(2) Unidad de Aplicaciones Geodésicas y Gravimétricas – IANIGLIA. CONICET. CRICYT

Gravity field distortion can be developed: a) from gravity anomalies (traditional method); b) from geoid undulations (modern method); c) from both a) and b).

In this work we build a geoid undulation profile on an Andean section at 33° South latitude from an equivalent sources technique. We compare it with an EGM96 model and we test it in the Argentine Andes with ( $h-H$ ) measured values.

Isostatic undulation in Airy model, compared with residual undulation in Andean wavelengths, points out a reasonable balance, agreeing with previous seismic and gravimetric studies.

Because of this, we consider geoid undulations as another instrument – that can be independent or complementary to the traditional ones – to carry on tectonic studies of geologic structures.

### Introduction

The aim of this work is to emphasize the possibility of using geoid undulation analysis for tectonic studies. To this purpose, we have considered an Andean section located at 33° South latitude, extending from the Andean axis 600 km to the Pacific Ocean and 930 km to the east.

We have calculated a geoid undulation profile, based on an equivalent sources technique (Guspí et al., 2004) that uses Free Air anomalies as input values. The result exhibits high resolution. The corresponding EGM96 model undulation has less resolution. It has been filtered from continental wavelengths (more than 1600 km) and then compared with the equivalent sources result.

From the Andean axis to the east, an accurate GPS levelling was carried out on about 300 km. The values of ( $h-H$ ) so obtained validate both our values of  $N$  and the global EGM96 model values (Fig. 1). On the Andean axis the residual undulation is about 15 m (from EGM96 model and equivalent sources technique) and about 18 m (from GPS measurements).

In order to compare this residual undulations with the corresponding isostatically compensated model (Introcaso et al., 1992) we have considered the mathematical expressions for a simplified dipolar model (Haxby and Turcotte, 1978).

The obtained Andean undulation of 18 m points out: 1) reasonable isostatic compensation in Airy model, and 2) efficiency in using geoid undulations for tectonic analysis, particularly on the Andean Cordillera.

### Geoid construction

Information on EGM96 geopotential model was obtained from the Crustal Dynamics Data Information System (<http://cddisa.gsfc.nasa.gov/926/egm96/gendesc.html>). This model is composed by: (1) a combined solution of degree and order 70; (2) a diagonal block (DB) solution from degree

71 to 359, and (3) a numerical quadrature (NQ) solution for degree 360 (Lemoine et al., 1998).

The geoid undulation profile we have built was obtained by: a) equivalent sources technique, along the whole continental section; and b) ( $h-H$ ) method, along 300 km from the Andean axis to the east. The equivalent sources technique, very usual in geophysical applications (Dampney, 1969; Hansen & Miyazaki, 1984; Guspí, 1991) has been also used in Geodesy to calculate geoid anomalies (Lehmann, 1993; Antunes & Catalao, 2000). We have considered a method presented by Cordell (1992), who proposed an equivalent sources model to grid and reduce to a reference level a potential field whose values are given on an irregular distribution at different elevations. The source is built in such a way that the gravity potential calculated from the point masses numerically fits the measured values (Guspí et al., 2004).

Two sets of stations are considered: a sparser one with geoid values ( $h-H$ ), and a denser one with Free Air anomalies values. The source depth of each arrangement is set as proportional to the nearest station in the same group. Therefore, in general, sources beneath geoid stations are deeper than the ones beneath gravity stations. Even the proportionality coefficients can be taken as different values to enlarge differences. Gravity effects of the whole set must fit measured gravity values. Then potential  $V$  and undulation values  $N$  are computed from this well defined arrangement, as:

$$V_p = G \sum \frac{m_i}{l_i} \quad \text{and} \quad N_p = \frac{V_p}{\gamma}$$

where  $\gamma$ . gravity.

Geoid undulations, as gravity anomalies, are measured with standard errors and variances, representing the most probable distribution of their “real” values. The model – as we have just said – must fit measured values within their variances, and so there will be infinite solutions. Instead of assuming measuring variances as given, Bayesian criterion (for example Zeyen & Pous, 1991; Ulrych et al., 2001) assigns an a-priori probability distribution to the model parameters and looks for a maximum a-posteriori probability distribution, i.e. a joint probability of having the most probable model with the most probable fitting to the data. The a-priori model parameters distribution enhances some selected features. In the present work, we only impose a smoothness restriction to the model parameters, to avoid great oscillations (Xia & Sprowl, 1991), and this is achieved assuming a Gaussian distribution (Sacchi & Ulrych, 1996). Under this hypothesis, the problem can be solved with a single linear system of equations (Guspí et al., 2004).

Values of ( $h-H$ ) are the differences between ellipsoidic altitudes (obtained by GPS measurements using POSGAR98 frame, and referring to WGS84 ellipsoid, see Lenzano et al. (2002) for further details) and orthometric altitudes (measured by IGM, Argentina).

Fig. 1 shows geoid profiles obtained by different methods, showing reasonable agreement among them.

## Discussion

A geoid undulation profile on an Andean section located at 33° South latitude revealed reasonable isostatic compensation with a root dimension that doubles the “normal” crust thickness. These results agree with earlier studies of the zone using a seismic-gravimetric model (Introcaso et al., 1992), showing the efficiency of the geoid undulation analysis for tectonic studies.

Residual undulations obtained by subtracting continental undulation (wavelength of approximately 1600 km) from the whole undulation, reaches maximum values of 15 to 18 m, agreeing with the Andean building.

As a comparison model for evaluating the isostatic behaviour, a compensated model in Airy hypothesis is considered (Haxby & Turcotte, 1978).

The maximum undulation found (about 18 m) corresponds to residual undulations obtained (EGM96 and equivalent sources) revealing isostatic equilibrium.

The importance of analyzing geoid undulations for tectonic studies is shown.

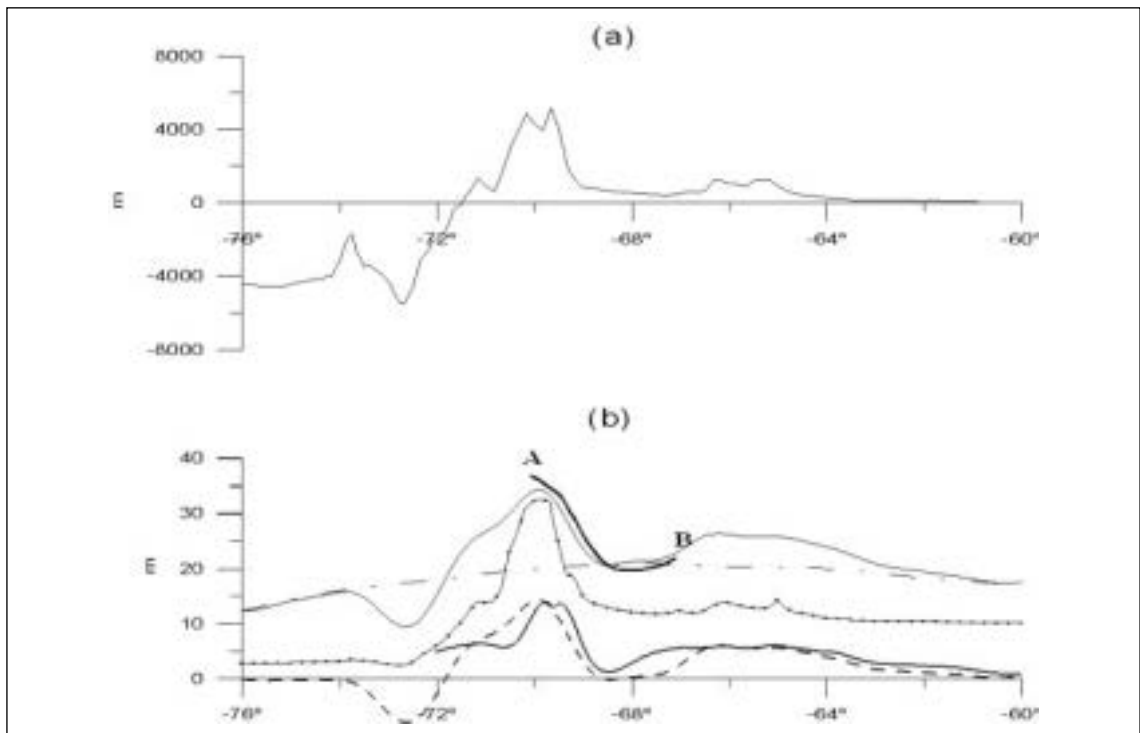


Fig.1. (a) Oceanic depth and topographic altitudes along EW South American section located at 33° S latitude. (b)

- AB** ..... Geoid undulation obtained from  $(h - H)$  values  
 ——— geoid undulation corresponding to EGM96 model with 360 terms  
 - - - - intermediate wavelength inspired on EGM96 model with  $n = m = 50$   
 - - - - residual undulation (short wavelength)  
 ..... undulation corresponding to compensated model (Haxby & Turcotte, 1978)  
 ——— equivalent sources effect (Guspi et al., 2004)

## REFERENCES

- Antunes, C. Catalao, J., 2000. On the comparison between point mass and collocation methods for geoid determination, April EGS/AGU meeting.
- Cordell, L., 1992. A scattered equivalent-source method for interpolation and gridding of potential-field data in three dimensions, *Geophysics*, 57, 629-636.
- Dampney, C.N.G., 1969. The equivalent source technique, *Geophysics*, 34, 39-53.
- Guspi, F., 1991. Rapid modeling and inversion of axisymmetric potential fields using equivalent sources, *Revista de Geofísica*, 47, 19-26.
- Guspi F., Introcaso, A., Introcaso, B. 2004. Gravity-enhanced representation of measured geoid undulations using equivalent sources. *Geophysical Journal International*. In press.
- Hansen, R.O., Miyazaki, Y., 1984. Continuation of potential fields between arbitrary surfaces, *Geophysics*, 47, 787-795.
- Haxby, W.F., Turcotte, D.L. 1978. On isostatic geoid anomalies. *Journal of Geophysical Research*, 94(B4), 3576-3890.
- Introcaso, A., Pacino, M.C., Fraga, H. 1992. Gravity, isostasy and andean crustal shortening between latitudes 30°S and 35°S. *Tectonophysics*, 205, 31-48.
- Lehmann, R., 1993. The method of free-positioned point masses - geoid studies on the Gulf of Bothnia, *Bull. Géodésique*, 67, 31-40.
- Lemoine, F., Kenyon, S., Factor, J., Trimmer, R., Pavlis, N., Chiuw, D., Cox, C., Klosko, S., Luthcke, S., Torrence, M., Wang, Y., Williamson, R., Pavlis, H., Rapp, R. & Olson, T., 1998. The development of the joint NASA, CSFC and NIMA geopotential model EGM96, NASA/TP - 1998 - 206861, Goddard Space Flight Center.
- Lenzano, L.E., Robin, A.M., Mackern Oberti, M.V. Marco Geodésico de la provincia de Mendoza. Su integración a POSGAR. XXI Reunión Científica AAGG (Rosario, Argentina, September 2002), 139-144.
- Sacchi, M.D., Ulrych, T.J., 1996. Estimation of the discrete Fourier transform, a linear inversion approach, *Geophysics*, 61, 1128-1136.
- Ulrych, T.J., Sacchi, M.D., Woodbury, A., 2001. A Bayes tour of inversion: A tutorial, *Geophysics*, 66, 55-69.
- Xia, J., Sprowl D.R., 1991. Correction of topographic distortions in gravity data, *Geophysics*, 56, 537-541.
- Zeyen, H., Pous, J., 1991. A new 3-D inversion algorithm for magnetic total field anomalies, *Geophys. J. Int.*, 104, 583-591.

**MORPHO-STRUCTURE OF LAGO FAGNANO (TIERRA DEL FUEGO)  
AND ADJACENT AREAS****5-04**Lippai H<sup>1</sup>, Lodolo E<sup>2</sup>, Tassone A<sup>1</sup>, Hormaechea J-L<sup>3</sup>, Menichetti M<sup>4</sup>, Vilas J.F<sup>1</sup>, TESAC Party1 *Instituto de Geofísica "Daniel A. Valencio", Universidad de Buenos Aires (Argentina)*2 *Istituto Nazionale di Oceanografia e di Geofisica Sperimentale (OGS), Trieste (Italy)*3 *Estación Astronómica Río Grande, Tierra del Fuego (Argentina)*4 *Istituto de Geodinamica e Sedimentologia, Università di Urbino (Italy)*

Lago Fagnano occupies an important part of the Magallanes-Fagnano continental transform system (MFS), which represents a major segment of the South America-Scotia plate boundary across the Isla Grande de Tierra del Fuego (Lodolo et al., 2003). The lake, trending broadly E-W, is about 110-km-long, with average width of about 7 km. Only its westernmost tip (about 15 km) is located in Chilean territory. In order to analyze the morphological expression of the submerged segment of the MFS, a bathymetric map of the entire Lago Fagnano was derived from data collected during four separate field campaigns (2000, 2001, 2002 and 2003) along D-GPS-fixed transversal profiles and longitudinal tie-lines. A total of forty-three profiles were acquired, in spite of the often prohibitive meteorological conditions, with a 200 kHz echo-sounder and an ECHOTRAC-DF-3200 MK II installed on a Zodiac boat of the *Prefectura Naval – Dpto. Lago Fagnano*. The bathymetric map has been integrated with the available topography of the surrounding region provided by the *Planification Subsecretary of the Tierra del Fuego Govern* (Fig. 1).

The acquired bathymetric profiles have delineated the main morphological features of the Lago Fagnano. The floor is divided into distinct parts, which suggests that the basin is composed of different sub-basins. In most areas, the basin floor is highly asymmetric in shape, with flat depocentral areas. The most pronounced asymmetry of the basin is seen in the eastern end of the lake, where there is also the deepest depression (maximum water depth of 206 m). The steeper slope of the basin, along the northern shore of the Lago Fagnano, also coincides with the most pronounced regional topographic gradient. The total throw along the northeastern shore of the Lago Fagnano, considering also the submerged part of the lake, is of the order of 600 m. The drainage system in this area shows a peculiar pattern: a very short surface stream system flowing toward the lake, with the separation boundary paralleling the shoreline and running along the ridge summit. This anomalous stream network configuration was possibly generated by the action of the fault strand in this sector of the Lago Fagnano, with rapid uplift of the hanging wall of the ridge as a consequence of isostatic rebound (see Fig. 2). A prominent secondary fault (the Rio Claro fault), forming an angle of about 130° with the master segment of the eastern Lago Fagnano, laterally offsets the principal fault. This splay fault aligns with the eastern flank of a wedge-shaped, graben-like depression occupied by the Rio Claro river, and it is very clear in the remote-sensing maps. Strands of the transform on both sides probably border the central, symmetrical part of the lake floor. The eastern-half of the lake presents a maximum water depth of 165 m. This part of the basin is broadly symmetric in shape and, like the eastern part of the lake, presents a relatively flat depocentral area. Along the westernmost part of the Lago Fagnano, two major, sub-parallel tectonic lineaments control the shape of the floor. Onshore, those lineaments define large graben structures, and bound on both sides a tilted sliver of crust (Monte Hope). An elevated area (about 35 m below the lake level) is found in the central part of the Lago Fagnano, morphologically separating the western and eastern part of the lake. This structure may represent a pressure ridge formed within the principal displacement zone of the MFS.

The peculiar morphology of Lago Fagnano, and its location within the principal displacement zone of the MFS, contrast in part with the postulated glacial origin for the lake as proposed by some authors (see discussion in Bujalesky et al., 1997). However, the glacial activity, in combination with the tectonic activity, has played an important role in shaping the morphology of the Lago Fagnano basin. The general morphology of Lago Fagnano is clearly controlled by the tectonic activity along the MFS and its geometry most probably reflects its sub-bottom structure. It represents the surface expression of at least two large pull-apart basins, formed by strands of the MFS.

The most widely accepted models to explain the tectonic development of pull-apart basins suggest that such basins are formed at places where bends or step-overs occur along the trace of strike-slip

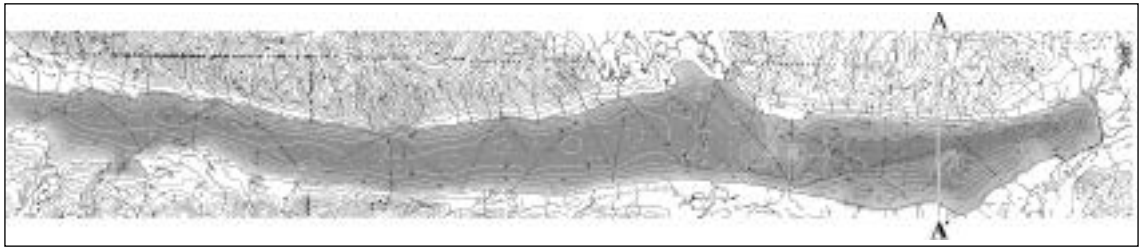
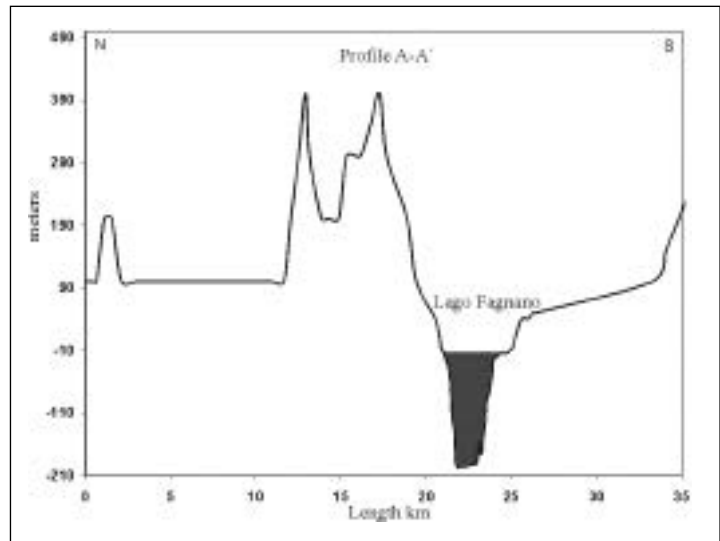


Fig. 1 - Bathymetric map of the Lago Fagnano (Argentinean sector) constructed on the basis of the corresponding D-GPS-fixed tracks (thin black lines), and topographic contours of the surrounding areas. The stream network surrounding the lake is also drawn. Profile A-A' is presented in Fig. 2.

Fig. 2 - A-A' profile (location in Fig. 1). The most pronounced asymmetry of the basin and the deepest depression is seen in this sector. The steeper slope of the basin, along the northern shore of the Lago Fagnano, also coincides with the most pronounced regional topographic gradient.



faults, leading to *en-echelon* segmentation of the faults. In this case, the two longitudinal sides of such basins would be bounded by strike-slip faults, while the transverse faults, which trend diagonally to the strike-slip faults, are predominantly normal faults (Aydin and Nur, 1985). These transverse faults may be considered secondary features forming the complementary sides of a bend or step-over across which the basin was extended. In real cases of strike-slip environments, such as the Dead Sea rift system and the Gulf of Elat (Aqaba) (Ben-Avraham et al., 1979), bathymetric and seismic records have shown that the asymmetry is generated when only one side of the basin is bounded by the transform segment (master fault), and the asymmetry is towards the transform fault. Comparable features have been imaged by seismic profiles in the Lago Izabal, a pull-apart basin developed within the continental Polochic transform system of eastern Guatemala (Menichetti et al., 2004, submitted paper to GSA Bull.).

Other important structural features in strike-slip environments are represented by the obliquely-oriented cross faults (transverse faults) which bound different pull-apart basins. Well known examples have been reported in the Gulf of Elat (Ben-Avraham et al., 1979) and eastern Sinai (Eyal et al., 1986). Field observations suggest that these transverse faults are not second-order features that evolved in response to increasing strain across the respective basin, but are more fundamental features that form an integral part of the transform fault system. Sometimes, transverse faults tend to extend beyond the basins into the adjacent areas, and in most cases it seems that they predate the development of the respective basins. The fault-related Rio Claro wedge-shaped depression, forming an angle of  $130^\circ$  with the eastern Lago Fagnano master fault, may be considered an example of transverse fault, which separates the highly asymmetric basin of the eastern Lago Fagnano from the central, symmetrical part of the lake.

The observation that the basin asymmetry is toward the transform fault, suggests that subsidence was mostly governed by extension in a direction normal to the regional strike of the transform, at the same time that strike-slip motion is taking place (Ben-Avraham, 1992; Ben-Avraham and Zoback, 1992).

## REFERENCES

- Aydin, A., and A. Nur, The types and role of stepovers in strike-slip tectonics, in: Strike-Slip Deformation, Basin Formation and Sedimentation, edited by K. T. Biddle and N. Christie-Blick, Spec. Publ. Soc. Econ. Paleontol. Mineral., 37, 35 – 44, 1985.
- Ben-Avraham, Z., G. Almagor and Z. Garfunkel, Sediments and structure of the Gulf of Elat (Aqaba) – Northern Red Sea, *Sedimentary Geology*, 23, 239-267, 1979.
- Ben-Avraham, Z. and M.D. Zoback, Transform-normal extension and asymmetric basins: an alternative to pull-apart models, *Geology*, 20, 423-426, 1992.
- Ben-Avraham, Z., Development of asymmetric basins along continental transform faults, *Tectonophysics*, 215, 209-220, 1992.
- Bujalesky, G.G., Heusse, C., Coronato, A.M., Roig, C.E. and J.O. Rabassa, Pleistocene glaciolacustrine sedimentation at Lago Fagnano, Andes of Tierra del Fuego, Southernmost South America, *Quaternary Science Reviews*, 16, 767-778, 1997.
- Eyal, Y., M. Eyal, Y. Bartov, G. Steinitz, and Y. Folkman, The origin of the Bir Zreir rhomb-shaped graben, eastern Sinai, *Tectonics*, 5, 267-277, 1986.
- Lodolo, E., M. Menichetti, R. Bartole, Z. Ben-Avraham, A. Tassone, and H. Lippai, Magallanes-Fagnano continental transform fault (Tierra del Fuego, southernmost South America), *Tectonics*, 22(6), 1076, doi:10.1029/2003TC001500, 2003.

## GEODETIC DETERMINATION OF RELATIVE PLATE MOTIONS AND CRUSTAL DEFORMATIONS DUE TO SOUTH AMERICA, SCOTIA AND ANTARCTIC PLATE INTERACTIONS

5-05

R. Smalley, Jr.<sup>1</sup>, E. Kendrick<sup>2</sup>, M.G. Bevis<sup>2</sup>, I.W.D. Dalziel<sup>3</sup>, F. Taylor<sup>3</sup>, E. Lauría<sup>4</sup>, R. Barriga<sup>5</sup>, G. Casassa<sup>6</sup>, E. Olivero<sup>7</sup>, E. Piana<sup>7</sup>, A. Zakrajsek<sup>8</sup>

<sup>1</sup> Center for Earthquake Research and Information, University of Memphis

<sup>2</sup> University of Ohio

<sup>3</sup> Inst. of Geophysics, Jackson School of Geosciences, University of Texas at Austin

<sup>4</sup> Instituto Geográfico Militar de Argentina

<sup>5</sup> Instituto Geográfico Militar de Chile

<sup>6</sup> Centro de Estudios Científicos, Valdivia, Chile

<sup>7</sup> Centro Austral de Investigaciones Científicas

<sup>8</sup> Instituto Antártico Argentino

### Summary

Global Positioning System (GPS) measurements provide the first direct measurement of plate motions and crustal deformation due to South America, Scotia and Antarctic plate interactions. As is found farther north in the Andes, deformation along the north-south striking western margin of South America, where Antarctica subducts beneath it, is not uniform across the orogen, but seems to be concentrated along its eastern limit. Along the southern east-west striking plate boundary of South America, between it and the Scotia plate, left-lateral strike-slip motion with a relative velocity of  $6.6 \pm 1.3$  mm/year is observed across the Magallanes-Fagnano Fault system. Site velocities on the Scotia Plate side are faster with respect to stable South America than the relative velocity across the deformation zone associated with the strike-slip fault by an additional 1-2 mm/yr. This suggests there may be a wider region of diffuse left-lateral deformation in the “corner” of the South America plate in southern Patagonia. The north-south components of the GPS velocities do not support existence of active, large-scale transpression or transtension between the South America and Scotia plates along this section of the plate boundary. Sites on the Antarctic Peninsula and the South Shetland Islands show opening occurring across the Bransfield Strait, while a site on the South Orkney Islands indicates that the islands are in a region of significant plate margin deformation. In addition to tectonics related to the various plate boundaries, a vertical glacial isostatic adjustment signal is also found in the region of the Patagonian ice fields.

Abstract: We are using GPS geodesy to study the geodynamics of the interactions between the South America, Antarctic and Scotia plates plus other sources of crustal deformation. The South America and Antarctic plates interact in two places, one along the east-west oriented southern margin of South America, and the other along the north-south oriented western margin of South America. The southern margin is divided into two parts. On the eastern part the two plates interact across a divergent plate



boundary, while along the western part the Scotia Arc is found between them. The Scotia Arc is composed of the Scotia and South Sandwich Plates, which are small, young, principally oceanic plates that formed in response to changes in the relative plate motions of South America and Antarctica during the past 30 Myr. Unfortunately most of the Scotia plate boundary is submarine and the few places where it is subaerial and GPS measurements can be made (Tierra del Fuego, South Georgia Island, South Orkney Islands, South Sandwich Islands) are plate boundary zones with attendant plate boundary deformation or volcanoes. Even where the plate boundary cuts across the southern part of Tierra del Fuego, rift structures north of the boundary and the GPS data in southern Patagonia are consistent with additional regional scale tectonic deformation due to drag around the southwest corner of South America, suggesting a continuing development of the Patagonian orocline. There is a very low level of seismicity observed along the South America – Scotia boundary, which is generally thought to be due to the slow rate of movement between the two plates across a locked fault. GPS measurements can directly address the questions of plate movement and its partitioning among candidate faults, overcoming some of the geologic problems related to the complex geologic history of the region. GPS determined velocities are shown in Figs. 1a and 1b.

In the austral summer of 1993-94 a sparse GPS network was installed and measured in Chilean southern Patagonia and Tierra del Fuego. Between 1995 and 1997 a network of continuous GPS stations was installed throughout Argentina and Chile. In 1998, in Argentina, the network was densified in Tierra del Fuego and expanded in southern Patagonia. All sites, except the continuous stations in Punta Arenas and Puerto Williams, were installed in rock outcrop to minimize problems due to monument stability. The velocity field defined by the GPS measurements in Tierra del Fuego (Fig. 1b) clearly shows an increase in velocity from the north to the south with respect to stable South America. The velocity gradient is concentrated in the region of the Magallanes-Fagnano fault and is

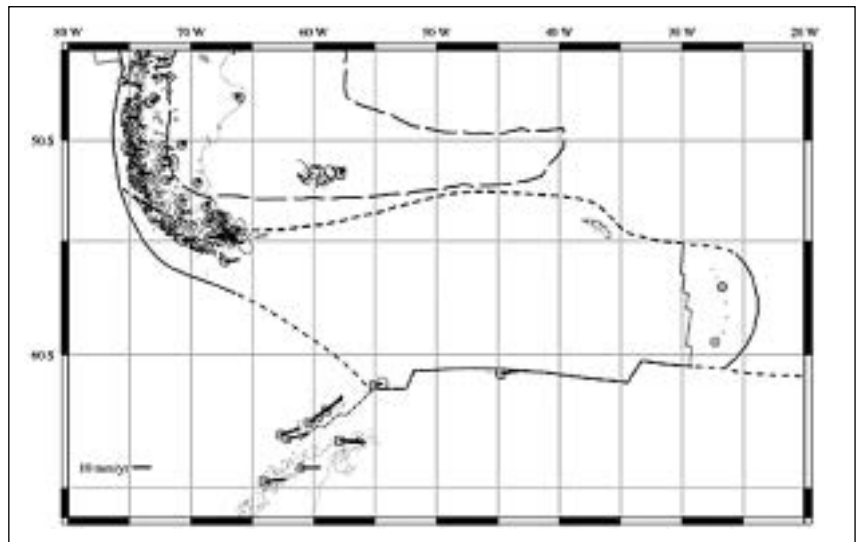
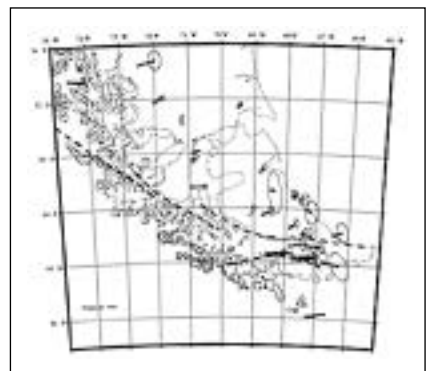


Fig. 1a - Map showing sites and velocities for the Scotia Arc GPS Network. Boxes indicate continuous GPS stations. Circles indicate sites with episodic GPS measurements. Plate boundaries shown by solid lines for subduction margins, dotted lines for mid ocean ridges and small dashes for strike-slip margins. The long dashed line shows the limit of stable continental South America.

Fig. 1b - Map showing sites and velocities for denser subset across the section of the plate boundary in Tierra del Fuego. Major faults, including the strike slip plate boundary between South America and Scotia plates shown by dashed lines.



associated with the plate boundary. As expected, movement of the sites on the Scotia Plate side is almost directly east, which is left-lateral with respect to stable South America. A grid search inversion for the fault parameters with the locking depth held at 15 km determined the position of the down-dip end of the model fault to be coincident with the surface trace of the Magallanes-Fagnano fault (latitude  $-54.54^\circ \pm 0.11^\circ$ ) at the eastern end of Lago Fagnano, defining a vertical fault. The relative velocity across this segment of the plate boundary was found to be  $6.6 \pm 1.3$  mm/yr. A test which included inverting for locking depth in addition to the relative velocity and velocity offset, was made and produced a result that is close to and statistically indistinguishable from the result of the inversion in which the depth was fixed at 15 km, while reducing the RMS by half. Even though the sampling is sparse on the southern side of the Magallanes-Fagnano fault, the GPS velocities suggest that the major mapped faults there, principally an inferred fault in the Beagle Channel, are not currently active.

The model used to describe the deformation pattern is two-dimensional. The GPS network is concentrated in a north-south transect across Lago Fagnano, through which the fault is inferred to pass, but the exact trace of the fault in the lake is unknown. The mapped fault is not straight, containing several en echelon offsets. Between Lago Fagnano and the Atlantic coast, east of most of the GPS network, the fault is relatively straight and strikes slightly south of east. It also includes a small lake that may be a small pull-apart structure in a releasing en echelon offset. To remain in Lago Fagnano, the fault has to bend, or contain en echelon offsets at a scale smaller than the lake. To the west, in the Seno Almirantazgo, the strike of the fault bends approximately  $30^\circ$  to strike WNW-ESE and the fault continues to the triple junction in a relatively rectilinear manner with several restraining en echelon offsets. In the area of the bend, there is also a sub-parallel fault, the Deseado Fault, on the north side of the Magallanes-Fagnano Fault. The average strike of Lago Fagnano is east-west, the direction chosen for the strike of the model fault. If the model fault is coincident with the trace of the Magallanes-Fagnano Fault to the east of Lago Fagnano, it does not coincide with the fault in Lago Fagnano or in Seno Almirantazgo to the west of the lake without bends or en echelon offsets. Because the geometry of the GPS network is limited in both cross and along-strike sampling, it does not allow the GPS velocity field to resolve second-order deformations that may be caused by deviations of the fault from being straight, multiple fault strands, active transtension or transpression across en echelon offsets and small amplitude releasing or restraining bends. While geologically reasonable, it is not justifiable to use a more complicated fault model to fit the GPS data. All the velocities are stated with respect to stable South America, so points distant from the plate boundary on the South American side should have zero, or due to uncertainty in the reference frame definition, small velocities. Inverting for a velocity offset parameter allows the reference side of the fault to have a non-zero asymptotic velocity. This allows the consideration of the small motion of sites used to define the fixed South America plate and/or allow possible regional deformations, such as that related to drag tectonics around the corner geometry of the triple junction to occur across a wider plate boundary. This suggests consideration of a model similar to the western US where the relative plate motion is partitioned between the plate boundary and a region of distributed deformation in the continental plate. Considering the additional  $1.4 \pm 0.8$  mm/yr of velocity offset between the strike-slip deformation pattern and stable South America, which is defined at the 1 mm/yr level, the GPS results suggest a velocity of  $8.0 \pm 2.1$  mm/yr for the relative plate movements. This estimate is in agreement with the magnitudes of the velocities along the Beagle Channel and at Cape Horn. The Euler pole of Pelayo and Weins (1989) predicts 5.3 mm/yr left-lateral transtensional motion with respect to stable South America. The position of the pole was determined using slip vectors and transform azimuths, while the magnitude was determined by closure. The GPS vectors show a faster relative plate movement with a statistically insignificant transpressional component.

Figure 1a shows the velocities for sites on the Antarctic Peninsula and the South Shetland Islands. The GPS confirms opening across the Bransfield Straits at about 1 cm/yr. A single continuous GPS site on the South Scotia Ridge in the South Orkney Islands indicates that the South Orkney islands, while positioned well to the Antarctic side (south) of the mapped strike-slip plate boundary are moving significantly with respect to the Antarctic plate, suggesting the plate boundary in this area includes a very wide area of deformation or that a separate South Orkney block or micro plate exists and has some movement with respect to the Antarctic plate.

## **Session 6**

---

**MARINE GEOLOGY  
AND GEOPHYSICS**



## MORPHOLOGY AND SEDIMENTARY PROCESSES ON THE TERRACED ACCRETIONARY PRISM OF SOUTHERNMOST SOUTH AMERICA

6-01

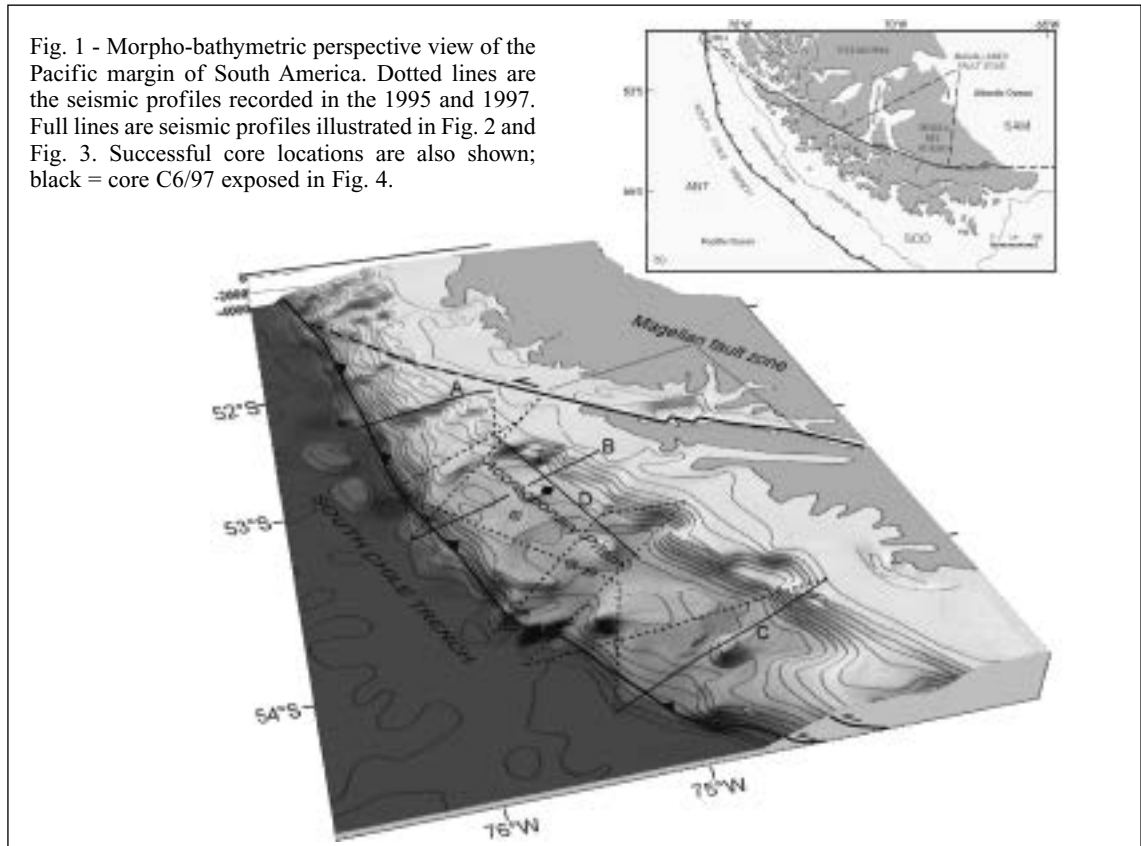
R. Bartole, D. Morelli, A. Cuppari

*Dipartimento di Scienze Geologiche, Ambientali e Marine – DISGAM  
Via Weiss 2 – 34127 TRIESTE Italy*

At the southernmost end of South America convergence processes between the Antarctic and Scotia plates are at the origin of the terraced accretionary prism that characterize the South Chile margin (Cande and Leslie 1986). In order to investigate the morphotectonic and sedimentary characters of this margin, two geoscience cruises were carried out in 1995 and 1997 within the frame of the PNRA (Programma Nazionale di Ricerche in Antartide). The cruises were planned with the following aims:

1. to improve the morpho-structural framework of the continental margin, with emphasis on the terraced fore-arc basin, in order to identify how the morphology exerted its influence on the sedimentation;
2. to identify the seismostratigraphic characters of the depositional and erosional features in order to reconstruct the main sedimentary processes;
3. to recognize the environmental changes linked to the recentmost climatic variations.

The examined segment is located west and south of the Strait of Magellan between the latitudes 52°30' and 54°30' S (Fig. 1). Both multichannel and monochannel seismic records were acquired using two synchronous G.I. Guns of 3.44 l each. They provided intermediate and high resolution profiles. As a whole the two surveys consist of 10 profiles nearly orthogonal and 3 subparallel to the margin, for a total length of 1129 km (610 n.m.). Four successful gravity cores were also recovered from the forearc basin in water depths ranging from c.a. 1900 to 2600 m. An exhaustive description of data, analyses and results concerning these surveys has been reported in Bartole et al. (2001). In this paper we summarize the main results obtained from seismostratigraphic analyses and we outline the objectives of the next cruise in this area.



## Morphology and sedimentary features

The South Chile continental margin is composed of five morpho-structural elements, namely the trench, the accretionary prism, the forearc basin, the upper slope and the continental shelf, which are herein briefly described. These elements are well distinguished south of 53° S, about at the Magellan Strait mouth, where the terraced accretionary prism enlarges considerably. At around 54° Lat S the width of the margin reaches its maximum, being about 100 km from the shelf-break down to the toe of the prism. On the contrary, north of 52°30' S the bathymetric expression of the accretionary basin is absent and the margin is shaped as an only steep slope.

### *Trench*

The latitudinal segment we consider in this study represents the southernmost part of the 5000 km long Peru-Chile trench. At these latitudes the sediment input rate is high and comparable to the Aleutian and Oregon-Washington trenches (Schweller & Kulm, 1978). As a consequence the trench lacks of bathymetric expression being completely filled by a well layered sequence that rests over the oceanic crust. The time-thickness of the trench infilling reaches about 2.0 seconds t.w.t. in the northern profiles off the Magellan Strait, decreasing to about 1.6 s t.w.t. in the southern profiles (Fig. 2a and 2c). Analysis of seismic characters highlighted the occurrence in the lowermost levels of a pelagic-hemipelagic sequence, which gradually passes upward to the typical seismic facies of a trench turbiditic wedge. Local resedimentation processes, interpreted as representing to coarse-grained proximal turbidites, seem to be active at the base of one of the rare canyons, which cut the lower slope at the front of the accretionary prism.

### *Accretionary prism*

The forearc region is formed by an accretionary prism with a wide forearc basin. The top of the prism shows a discontinuous outer-arc high, that is a topographic relief (Fig. 2b and 2c). It separates the highly deformed frontal zone of the prism from the almost undeformed sedimentary sequence of the basin. The position of this outer high, its morphologic and topographic expressions change frequently along the forearc region, thus reflecting the inner structural complexity of the prism (Polonia et al. 2001).

### *Forearc basin*

Bounded oceanward by the discontinuous outer-arc high of the accretionary prism, it forms a wide bathymetric terrace (the "Fuegian Terrace" of Herron et al., 1977) with water depths ranging from -1250 m near 53° S to -2900 m at about 54°30' S. Also the width of the basin changes considerably along the examined latitudinal transect: from less than 20 km at 52°30' where the terrace is absent and a unique trench inner slope develops (Fig. 2a), up to a maximum width of about 40 km near 54° S (Fig. 2c). North of 53° S, off the Magellan Strait, the outer high of the prism is missing and the forearc basin shrinks losing its bathymetric expression (Fig. 1b and 2a).

The basin infilling is characterised by undisturbed or slightly disturbed sediments, up to 1 s t.w.t. thick, lying over the accreted units of the prism (Fig. 2c). High resolution profiles reveal that both depositional and erosional features are present at the surface of the basin. The former are small lens-shaped depositional bodies, well imaged at the base of the upper slope (Fig. 3). The latter are weak surficial incisions, which allow bypassing of the sediments to the trench through the topographic depressions of the outer-arc high (Fig. 2 and 3a).

### *Upper slope*

The upper slope shows an average width of 10 km with steepness between 6° to 8° (about 10% to 14%). Higher values recognizable on seismic sections are apparent steepnesses due to the occurrence of small canyons and gullies that drain the sediments from the continental shelf down to the forearc basin. There are also bodies with both stratified and chaotic internal configuration interpreted as gravity driven deposits, such as slides, slumps and/or debris flows (Fig. 2b and 2c). Below a thin sheet of slope sediments, most sections image a strong oceanward dipping reflector identified as the continental backstop (Fig. 2c).

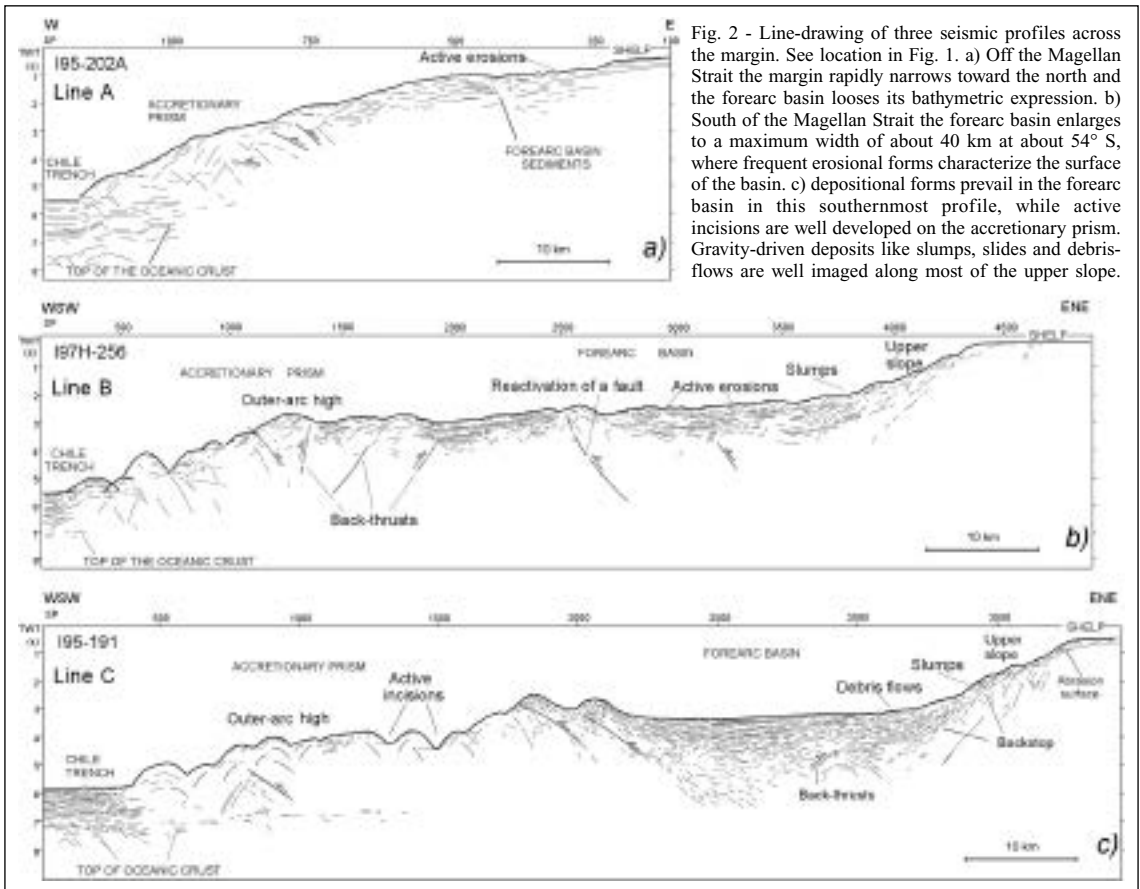


Fig. 2 - Line-drawing of three seismic profiles across the margin. See location in Fig. 1. a) Off the Magellan Strait the margin rapidly narrows toward the north and the forearc basin loses its bathymetric expression. b) South of the Magellan Strait the forearc basin enlarges to a maximum width of about 40 km at about 54° S, where frequent erosional forms characterize the surface of the basin. c) depositional forms prevail in the forearc basin in this southernmost profile, while active incisions are well developed on the accretionary prism. Gravity-driven deposits like slumps, slides and debris-flows are well imaged along most of the upper slope.

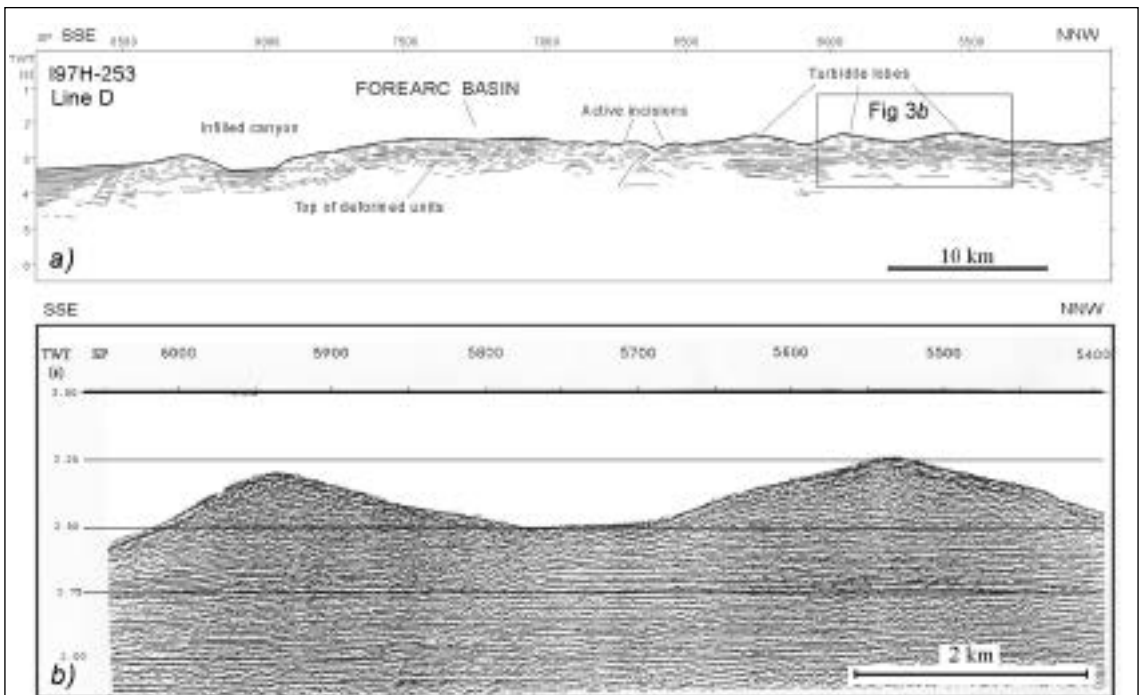


Fig. 3 - a) Line-drawing of a profile acquired in the forearc basin near the base of the upper slope. Depositional and erosional processes alternate in this proximal area. See the infilled canyon on the left and the depositional lens-shaped bodies on the right. b) Close-up of the depositional bodies interpreted as turbiditic lobes.

### Continental shelf

Little is known about the shelf as the seismic profiles cover only the portion close to the shelf-break. The profiles, however, show a generally thin sedimentary sequence characterized by aggradational geometries, resting on a high amplitude reflector that represents an erosional surface (Fig. 2c). Off the Magellan Strait the sequence is very thick and shows a progradational style, typical of the glaciated margins. This would suggest the persistence of a large ice tongue at the mouth of the Strait during the Late Tertiary and the Plio-Pleistocene glacial advances (Mercer, 1976; Raedeke, 1978; Meglioli et al., 1990; Clapperton et al., 1995).

### Upper pleistocene-holocene sedimentation and climatic variations

Starting from the Miocene, the South Chile margin underwent important climatic variations linked to the glacial events (Mercer, 1976; Meglioli *et al.*, 1990). From the last Quaternary glacial expansion the margin turned from a subpolar climate to a temperate one. Therefore the margin is an ideal region for the reconstruction of environmental changes on the base of stratigraphic and sedimentary records. The sediment cores sampled in the forearc basin have revealed a good potentiality of the area in terms of palaeoenvironmental reconstructions (Presti *et al.*, 2000). Analyses of the cores in fact, allowed the recognition of three sedimentary sequences linked to the depositional processes of the late Pleistocene-Holocene (Fig. 4). The lower unit (3) dates back prior to the LGM (Late Glacial Maximum), before  $20000 \pm 70$  yr BP. It consists of a muddy fine-grained turbidite successions (*sensu* Galloway, 1998) with a coarse dispersed sub-angular sandy and pebble fraction interpreted as an ice rafting deposition. This unit is consistent with the occurrence of a wide ice cap on the continent (Clapperton, 1992) that supplied fine grained siliciclastic material to the seawater mass. The intermediate unit (2), deposited between 20000 and 16950 yr BP (extrapolated dating), is a structureless hemipelagic sequence with sparse gravel-sized angular clasts that indicate a discontinuous ice-rafted debris supply. This would be related to the fluctuations of the glacier fronts during the LGM. The increasing of sandy and biogenic carbonate content in the upper unit (1) indicates the onset of present-time environmental and climatic conditions.

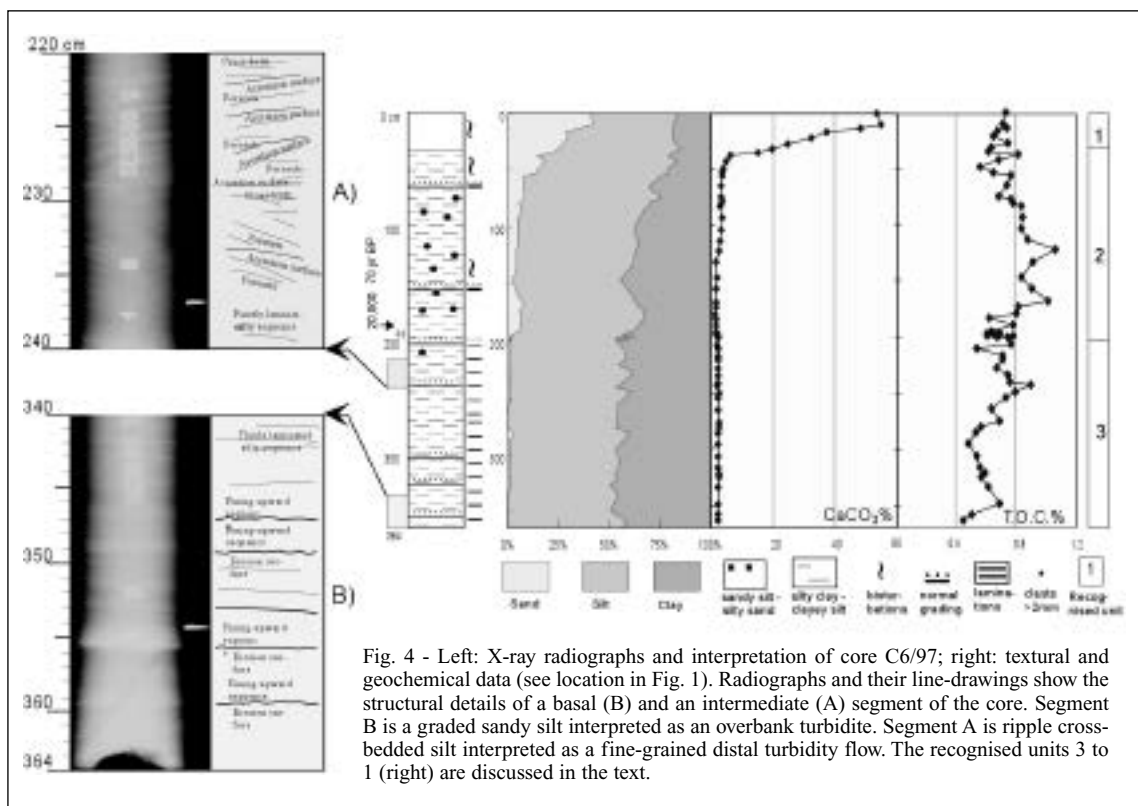


Fig. 4 - Left: X-ray radiographs and interpretation of core C6/97; right: textural and geochemical data (see location in Fig. 1). Radiographs and their line-drawings show the structural details of a basal (B) and an intermediate (A) segment of the core. Segment B is a graded sandy silt interpreted as an overbank turbidite. Segment A is ripple cross-bedded silt interpreted as a fine-grained distal turbidity flow. The recognised units 3 to 1 (right) are discussed in the text.



## Aims of the future research

To better understand the sedimentary processes of this margin sector, the ongoing research is focused to investigate the following areas in order to obtain further informations regarding the depositional and erosional processes: the continental shelf (inner and outer portion) the base of the upper slope (gravity driven deposits), the forearc basin (depositional bodies and erosional channels). Multibeam data and high resolution acoustic profiles are the tools to be used to achieve the reconstruction of detailed morphology, acoustic stratigraphy and facies analyses.

## REFERENCES

- Bartole R. et al. (2001), Morphostructural and Sedimentological Aspects of the South Chile Margin between 52° 30' and 54° 30' Lat. S. *Terra Antarctica*, 8(2), 99-110.
- Cande S.C. & Leslie R.B. (1986). Late Cenozoic tectonics of the southern Chile trench. *J. Geophys. Res.*, 91, 471-496.
- Clapperton C.M. (1992), La Ultima Glaciacion y Deglaciacion en el Estrecho de Magallanes: implicaciones para el poblamiento de Tierra del Fuego. *Anales Inst.Patag.*, 21, 113-128.
- Clapperton C.M. et al. (1995), The last glaciation in the Central Magellan Strait, southernmost Chile. *Quaternary Res.*, 44, 133-148.
- Galloway W.E. (1998), Siliciclastic slope and base-of slope depositional systems: component facies, stratigraphic architecture and classification. *AAPG Bull.*, 82, 4, 569-595.
- Herron E. M. et al. (1977), Post Miocene tectonics of the margin of Southern Chile. In Talwani M. and Pitman W. C. III (Eds.) "Island Arcs, Deep Sea Trenches and Back Arc Basins", AGU, Washington, D.C., 273-284.
- Meglioli A. et al. (1990), Cronologia relativa y absoluta de los depositos glaciarios de Tierra del Fuego, Argentina y Chile. *Actas II Decimo Primer Congreso Geologico Argentino*, San Juan, 457-460.
- Mercer J. H. (1976). Glacial history of southernmost South America. *Quat. Res.*, 6, 125-166.
- Presti M. et al. (2000), Compositional and Sedimentological Features of a Late Quaternary Core from the Southern Chilean Margin. *Terra Antarctica Reports*, 4, 95-100.
- Polonia A. et al. (2001), The Accretionary Complex of Southernmost Chile from the Analysis of Multichannel Seismic Data, *Terra Antarctica Reports* 8 (2), 87-98.
- Raedeke L. D. (1978), Formas del terreno y depositos cuaternarios, Tierra del Fuego Central, Chile. *Revista Geologica de Chile*, 5, 3-31.
- Scheweller J. & Kulm L.D. (1978), Depositional Patterns and Channelized Sedimentation in Active Eastern Pacific Trenches. In D.J. Stanley and G. Kelling Ed. *Sedimentation in submarine canyons, fans and trenches*. Stroudsburg, Pennsylvania, Dowden, Hutchinsons & Ross.

## SEISMOSTRATIGRAPHY AND RECENT SEDIMENTARY EVOLUTION OF AN ASYMMETRIC EXTENSIONAL BASIN AT THE WESTERN ARM OF THE MAGALLANES-FAGNANO TRANSFORM SYSTEM

6-02

R. Bartole, W. Colautti, E. Colizza, C. Salvi, F. Tosoratti

*Dip. Sc. Geologiche, Ambientali e Marine (DISGAM) Università degli Studi di Trieste, Via E. Weiss 2, 34127 Trieste - Italy*

### Introduction

In 1995, in the frame of the PNRA (Progetto Nazionale di Ricerche in Antartide) the Dipartimento di Scienze Geologiche, Ambientali e Marine (DISGAM - University of Trieste) performed a marine geological survey within the Pacific entrance of the Magellan Strait with the aim *a)* to verify the occurrence and effects of the Magellan Fault along the western part of the South America-Scotia plate boundary; and *b)* to investigate the sedimentary architecture of the sequences of this sector of the Strait, with particular interest to those recording the Pleistocene glacial events. The survey consisted of 290 km of intermediate resolution multichannel seismic reflection profiles and three gravity cores. These data were acquired in a marine enlargement of the Magellan Strait north of Isla Desolacion, between Cabo Pilar and Isla Tamar with the *R/V OGS Explora* (Fig. 1).

The analysed data were integrated by a high-resolution seismic line acquired all along the Strait in 1991 and by other three cores collected during different surveys in 1991 and 1995. The present work summarizes the previous report of Bartole et al. (2000) and provides new results obtained by recent analyses of the seismic and sampling data.

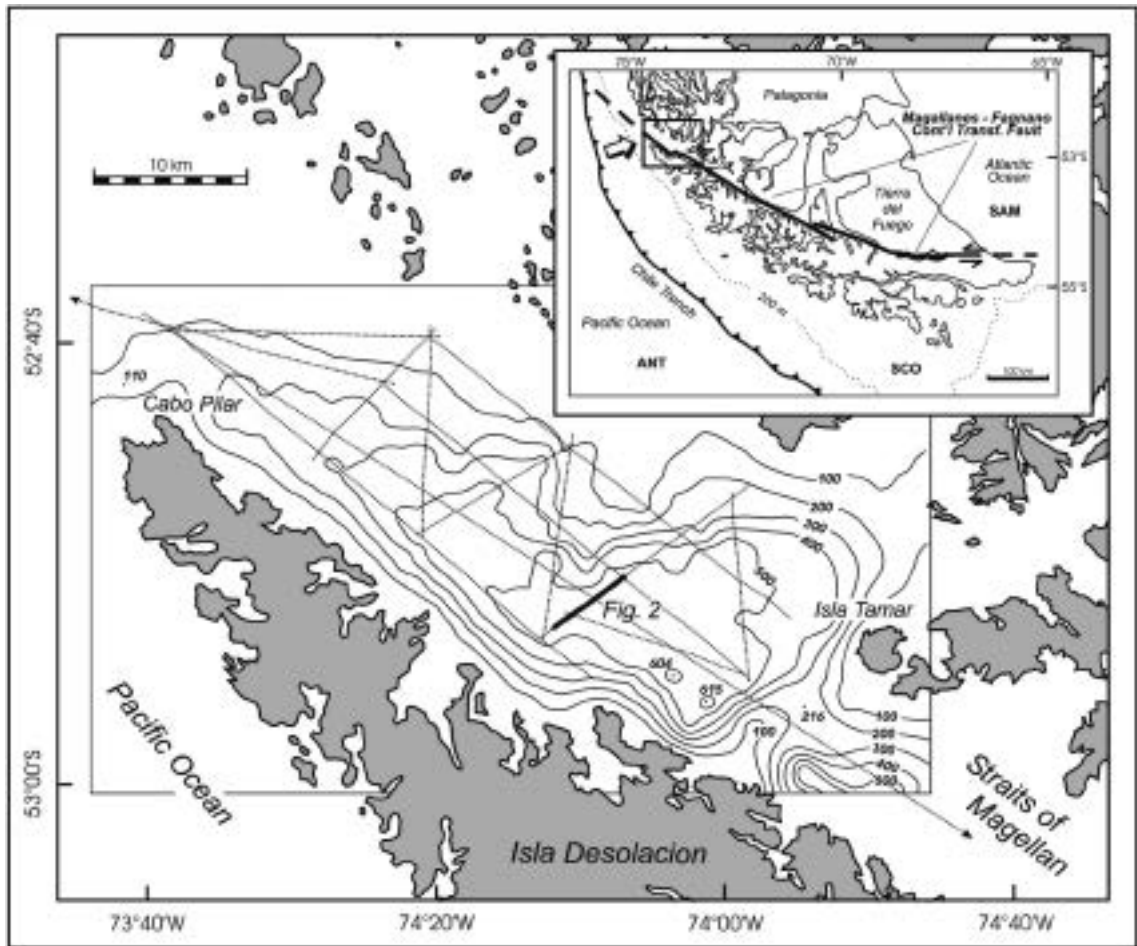


Fig. 1 - Plate interactions in the South American-Scotia Sea region. ANT: Antarctic plate; SAM: South American plate; SCO: Scotia plate. Bathymetry of the basin located at the Pacific mouth of the Magellan Strait and tracks of PNRA seismic profiles.

### Geologic framework

The geodynamic pattern at the southern tip of South America is ruled by the interaction of three plates: the South American (SAM), the Scotia (SCO) and the Antarctic (ANT) plates (Fig. 1 inset). The relative motion between the SAM and SCO plates is accommodated by a 3000 km-long left-lateral transform boundary, represented by the North Scotia Ridge in the South Atlantic oceanic domain (Dalziel, 1974; Forsyth, 1975; Pelayo & Wiens, 1989).

In the continental domain of southernmost South America the SAM-SCO boundary is a left-lateral transform boundary called Magallanes-Fagnano fault system that runs from the Atlantic coast, through the Fagnano Lake up to the Pacific arm of the Magellan Strait with a length of nearly 600 km (Fig. 1 inset).

The rising of interests about this continental plate boundary dates back to the seventies (Fuenzalida, 1972; 1976) although most of the efforts concerning this continental transform boundary (represented by analyses of limited tracts and areas of the fault system) were published in the last decade (Cunningham, 1993; Klepeis, 1994; Klepeis and Austin, 1997; Bartole et al., 2000; Lodolo et al., 2002a; Lodolo et al., 2002b).

The recent work of Lodolo et al. (2003) provides an exhaustive and up-to-date frame on morphology and structural expression about the whole length of this continental transform boundary. Combined analyses of geological surveys, geophysical (seismic reflection, bathymetry and gravity) and remote sensing data image the Magallanes-Fagnano fault system as set of distinct tectonic lineaments,

constituting en-echelon segments of the transform system and are represented by mostly near-vertical faults. The occurrence of several asymmetric depocenters along the principal displacement zone, in which the thickest part of the sedimentary wedge abuts the master segments of the fault system suggests simultaneous strike-slip motion and transform-normal extension. This is a common feature found also in other continental transtensional environments (Ben-Avraham & Zoback, 1992).

### Basin structure

Seismic and bathymetric data figure the basin as an asymmetric, tectonically-controlled depression parallel to Isla Desolacion, with the southwestern side steeper than the northeastern side (Fig. 1). The basin is about 70 km long, with the main axis being elongated NW-SE. Both depth and width increase toward its southeastern side, where maximum depth of -615 m occurs.

The basement structure of the basin fit well with its bathymetric expression: to the SW the depression is sharply bounded by a large-throw sub-vertical normal fault, identifiable as a master segment of the Magallanes-Fagnano fault system. The basin is shaped as a NW-SE trending semigraben, tilted SSW (Fig. 2), toward the master segment of the Magallanes-Fagnano system. Maximum basement depths, in fact, occur on the southern side of the basin near Isla Desolacion, where vertical throws of up to 1 s twt can be measured on seismic profiles. At the Pacific sill seafloor vertical displacements of about 80 m document a recent movement of the Magallanes master fault. On the contrary, inside the basin basement faults have small throw (0.1-0.2 s twt) and rarely propagate into the overlying sediments. The rose-diagram of basement fault population reported in Fig. 2, is consistent with the left-lateral transform movement of this segment of the Magallanes-Fagnano system.

About the age of the transtensional deformation, that led to the initial development stages and then to the consequent beginning of sedimentation, there are two hypothesis: the first, according to Klepeis and Austin (1997), is to refer to the Late Tertiary (younger than 30 Ma) as the beginning of transtensional deformations along the Magallanes-Fagnano plate boundary; the other possibility has been suggested by Lodolo et al. (2003) who proposed a younger age of the deformation i.e. between 9.5 and 7.2 Ma, coeval to the spreading activity final stages in the Western Scotia Sea.

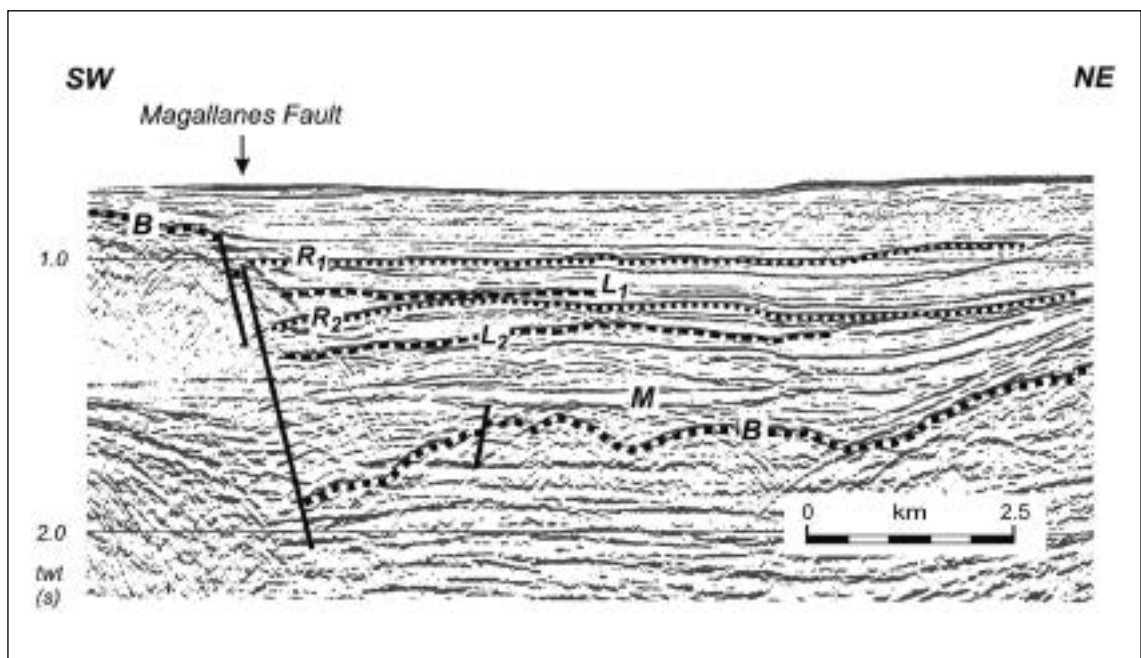


Fig. 2 - Close-up of profile AI95-199 (see position in Fig. 1) showing the seismic image of the Magallanes transform segment (from Bartole et al., 2000). The sedimentary infilling of the basin is characterized by several unconformities. Local unconformities (L1 and L2) are interpreted as erosional surfaces related to glacial expansions. B: seismic basement (mainly Patagonian batholith); M: sea bottom multiple. R1 and R2: regional unconformities.

## Seismic stratigraphy

Parallel and sub-parallel reflectors, onlapping the faulted basement, showing a weak sedimentary growth toward the south, characterize the sedimentary architecture of the basin (Fig. 2). As the basin floor is almost flat, the thickness of the sedimentary infilling is mainly controlled by the basement structure, with the maximum values (up to 1.2 s twt corresponding to 1400-1500 m) occurring near the Magallanes fault.

The sedimentary sequence is represented by medium to high-amplitude, continuous reflectors, alternated with low and very low amplitude events; locally semi-transparent facies have been observed. Several unconformities of both regional and local extension, can be recognized at different stratigraphic levels (Fig. 2). Seismic facies variability and a number of erosional unconformities occur in the SE enlarged and deeper part of the basin. These changes are due to variations in both seismic parameters, such as signal amplitude and continuity, and internal geometry of the seismo-stratigraphic sequences.

Processing of a set of seismic profiles, mainly using DMO (dip moveout) correction and post-stack Kirchhoff migration, brought to a consistent improvement in the recognition of basement structures and geometry of the sedimentary infilling.

## Recent sediment sampling and analysis

Textural and carbonate analyses of the six gravity cores recovered from bottom sediments of the basin are reported in Fig. 3. All the cores are characterized by clayey silt, sand content being generally less than 10% in cores MB91-57R, SS95-9, SS95-10 and at the bottom of core SS95-6. Core MG95-2 and the topmost portion of core SS95-6 present a sand content higher than 20%. In the topmost portion (last 17 cm) of core MB91-47, collected near the outer sill of the basin where the Pacific Ocean waters are drawn into the Strait, the sand fraction equals the silt fraction, on the contrary lower sand percentages characterize the bottom of the core.

As far as the carbonate content, cores MB91-57R, MG95-2 and SS95-9 show high CaCO<sub>3</sub> content along all their length, while in cores SS95-6, SS95-10 and core MB91-47 CaCO<sub>3</sub> is high only in the topmost part, decreasing towards the bottom.

The sediments of all the cores have been deposited in a Holocene marine environment except for core MB91-47 whose older sediments are of late Pleistocene age, i.e. 21680+<sub>-</sub>170 yr B.P. (see Colizza et al. this vol.). The Holocene sedimentation is always characterized by an increase of the carbonate component (>10 %) with values >30% since 6000 yr B.P.

The carbonate sedimentation is related to the Holocene climatic improvement and to an increase of Pacific water circulation inside the Strait. In fact, during the Last Glacial Maximum (24000 - 18000 yr B.P.) according to Clapperton (1992) an extensive ice cap still persisted on the western arm of the Strait, probably occupying the Pacific entrance, and then preventing a free sea water circulation (Bartole et al., 2000; Colizza & Salvi, 2000).

## Conclusion

The newly acquired seismostratigraphic and structural data allow us to say that the Pacific entrance of the Magellan Strait is an extensional basin in a strike-slip context. This implies that the late Tertiary-Quaternary history of the western tract of the Magellan fault has been ruled by transtensional deformation.

Since the basin lies at the mouth of what, during glacial periods, was one of the greatest ice streams system of the region, flowing from the Patagonian/Fuegian Andes towards the Pacific shelf (Clapperton, 1992), it is possible that both glacial abrasion and drift deposition affected the basin. The numerous unconformities and erosional surfaces identified seen on seismic profiles together with the seismic facies variability are emphasized through the specific processing strategy adopted.

All the cores are characterized by prevalent clayey silt sediment with low percentage of sand, constituted by biogenic carbonates. This biogenic fraction is of Holocene age, while the pre-Holocene portion is silico-clastic.

Comparing the cores sampled in this basin with those collected in the Pacific Ocean (Caffau, 1998; Montesanti, 1998; Presti et al., 2000) and the cores collected in another basin inside the Strait (Amore

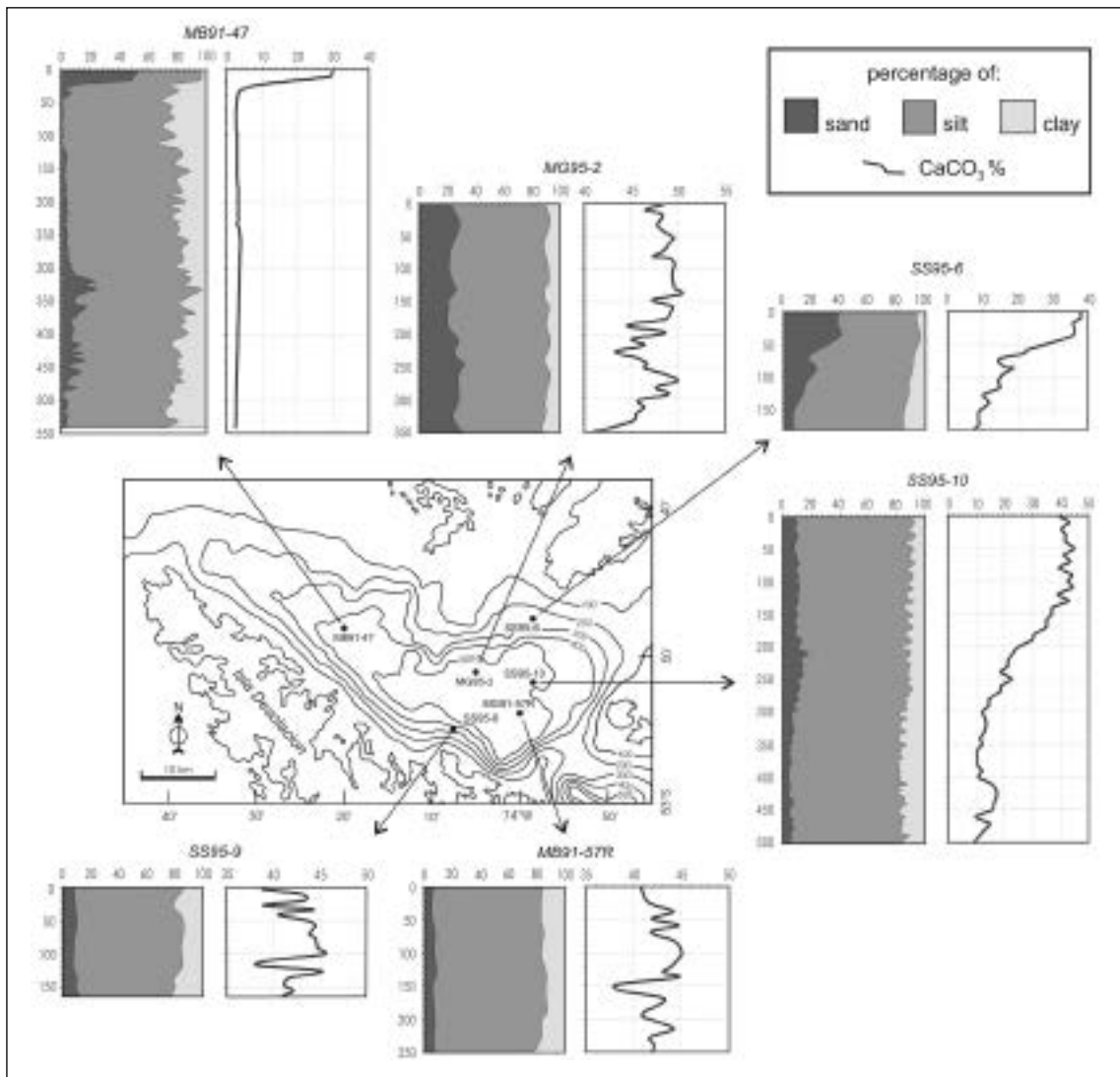


Fig. 3 - Textural and carbonate content of the six cores sampled in the studied area.

et al., 2000; Colizza & Salvi, 2000) a diachronism of the beginning of carbonate sedimentation linked to the climatic improvement in the South Pacific margin has been identified: 14000 yr B.P. in the Pacific Ocean, 10000 yr B.P. in the studied basin and 8-7000 yr B.P. inside the Magellan Strait.

## REFERENCES

- Amore F.O. et al., 2000. Holocene calcareous nanofossils and planktonic foraminifera assemblages in the western Magellan Straits (Chile). *J. of Nannoplankton Res.*, 22, 2, 79-80.
- Bartole et al., 2000. The Pacific entrance of the Magellan Strait: preliminary results of a seismic and sampling survey. *Terra Antarctica Reports*, 4, 81-94.
- Ben-Avraham Z. and Zoback M. D., 1992. Transform-normal extension and asymmetric basins: an alternative to pull-apart models. *Geology*, 20, 423-426.
- Caffau M., 1998. Evoluzione delle paleocomunità planctoniche (nannofossili calcarei e foraminiferi planctonici) in relazione alle variazioni climatiche ed ambientali tardo quaternarie nell'area a Nord-Ovest dello Stretto di Magellano.. PhD Thesis unpublished. Univ. degli Studi di Trieste.
- Clapperton C. M., 1992. La última glaciación y deglaciación en el estrecho de Magallanes: implicaciones para el poblamiento de Tierra del Fuego. *Ans. Ins. Pat., Ser. Cs. Hs., Punta Arenas (Chile)*, 21, 113-128.

- Colizza E. and Salvi G., 2000. Sedimentological analyses of three cores collected in the Pacific sector of the Strait of Magellan. *Terra Antarctica Reports*, 4, 69-74.
- Colizza E. et al., 2004. Holocene carbonate sedimentation in the northwestern section of the Magellan Strait: textural, geochemical and micropaleontological preliminary results. (this volume).
- Cunningham W.D., 1993. Strike-slip faults in the Southernmost Andes and the development of the Patagonian orocline. *Tectonics*, 12, 1, 169-186.
- Dalziel I.W.D., 1974. Evolution of the margins of the Scotia Sea. In: C.A. Burke & C.L. Drake (eds.), *The Geology of Continental Margins*, Springer-Verlag, New York, 567-579.
- Forsyth D.W., 1975. Fault plane solutions and tectonics of South Atlantic and Scotia Sea. *J. Geophys. Res.* 80, 1429-1443.
- Fuenzalida R.H., 1972. Geological correlation between the Patagonian Andes and the Antarctic Peninsula and some tectonic implications. Master thesis, 75 pp; Stanford Univ., Stanford., California.
- Fuenzalida R.H., 1976. The Magellan fault zone. Paper presented at Symposium on Andean and Antarctic Volcanology Problems, Int. Assoc. of Volcanol. and Chem. on the Earth's Inter., Naples, Italy.
- Klepeis K. A., 1994. The Magallanes and Deseado fault zones: Major segments of the South American-Scotia transform plate boundary in southernmost South America, Tierra del Fuego. *J. Geophys. Res.*, 99, B11, 22, 001-22,014.
- Klepeis K. A. and Austin J.A. Jr., 1997. Contrasting styles of superposed deformation in the southernmost Andes. *Tectonics*, 16, 5, 755-776.
- Lodolo E., Menichetti M., Tassone A., Geletti R., Sterzai P., Lippai H. and Hormaechea H.-L. et al., 2002a, Researches target a continental transform fault in Tierra del Fuego. *Eos Trans. AGU*, 83, 5-61.
- Lodolo E., et al., 2002b. Morphostructure of the central-eastern Tierra del Fuego Island from geological data and remote-sensing images. *EGS Stephan Mueller Spec. Publ. Ser.*, 2, 1-16.
- Lodolo E., et al., 2003, Magallanes-Fagnano continental transform fault (Tierra del Fuego, southernmost South America). *Tectonics*, 22, 6, 1076.
- Montesanti A., 1998. Indagini paleoambientali e paleoclimatiche tardo-quadernarie lungo il margine cileno meridionale. PhD Thesis unpublished. Univ. degli Studi di Trieste. 124 pp.
- Pelayo A. M. and Wiens D. A., 1989. Seismotectonics and relative plate motions in the Scotia Sea region. *J. Geophys. Res.*, 94, B6, 7293-7320.
- Presti et al., 2000. Compositional and sedimentological features of a late Quaternary core from the southern Chilean Margin. *Terra Antarctica Reports*, 4, 95-100.

## MARINE GEOLOGY OF THE EREBUS AND TERROR GULF REGION, NW WEDDELL SEA

6-03

Eugene W. Domack, Emily Backman

*Department of Geology, Hamilton College, Clinton New York 13323 USA, edomack@hamilton.edu*

The region of the Erebus and Terror Gulf (ETG) includes adjacent straits of the Prince Gustav Channel, Antarctic Sound, and Admiralty Sound (Fig. 1). The ETG is surrounded by the Trinity/Tabarin Peninsula, the Joinville Island archipelago, and James Ross Island, Vega Island, and Seymour Island. Our data base includes extensive swath (multibeam) mapping, high resolution seismic stratigraphy (using 3.5 kHz CHIRP), jumbo piston cores, bottom video and surface dredging. These data were collected during three cruises of USAP research vessels including: *NB Palmer* 00-03, *NBP-01-07*, and *LM Gould* 04-04. We observe and interpret three distinct seafloor characteristics of the region including: glacially sculpted and streamlined seafloor, the large depositional lobe of the Vega Drift, and an incipient volcanogenic relief restricted to southern Antarctic Sound.

Glacial scour reflects paleo-ice drainage out of each of the coastal reentrants or bays with convergent flow dominating within the central ETG and attests to a much expanded ice sheet across the entire Trinity Peninsula shelf. Ice flow patterns are clearly delineated by large scale crag and tail features, "drumlins", and limited bundle structures or mega scale glacial lineations. Over-deepening of coastal basins such as in Duce Bay, has taken place to an excess of 1200 m. Local deep basins are in filled with post glacial turbidite sediments reaching several tens of meters thick. Of note are a series of coalescing channels that debouch southward into the deep (1000 m) axis of Antarctic Sound, the floor of which reflects glacial erosion in the form of streamlined bedrock sidewalls. Glacial flow patterns are obscured within the ETG by thick sediment drift deposition that post dates widespread glaciation (Fig. 1).

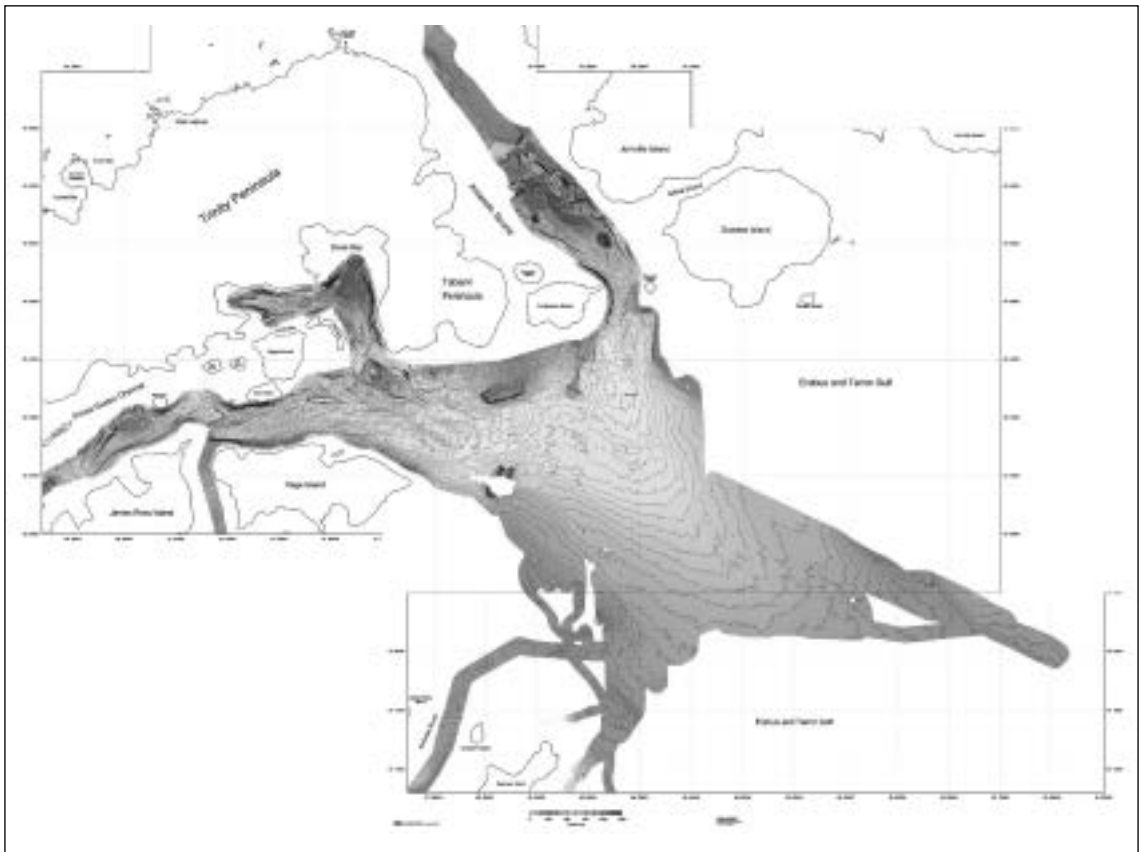


Fig. 1 - Gray scale swath bathymetry map of region of Erebus and Terror Gulf. White dots indicated limits of post-glacial Vega Drift sediment accumulation. Labeled dots are core locations and triangles are bottom video deployments (S6).

The Vega Drift is an extensive (6,140 km<sup>2</sup>) sediment drift deposit that reaches a maximum thickness of 30 m. Detailed isopach maps of sediment thickness reveal a multi-lobed feature with distinct digits that extend toward or from the major channels that open into the ETG (Backman, 2004; Camerlenghi, et al., 2001). High resolution acoustic profiles (CHIRP) reveal a dynamic setting where internal reflectors are undergoing: 1) exposure as rejuvenated bottom currents erode the drift, 2) progressive burial as new deposition accretes over the drift, and 3) pinch-out of reflectors, where long lived currents have prevented drift accumulation. Erosion is also observed in bottom videos that reveal exposure of deep infaunal organisms (tube worms) to depths of several decimeters. Tidal currents play a major role in sediment drift architecture and we speculate that these currents have changed in response to the recent collapse of the Prince Gustav Ice Shelf (Rott et al, 1996). Sediment cores (including three jumbo piston cores) collected from the drift in key localities reveal a record that spans at least the last 10,000 years. Sediments vary from biosiliceous mud to siliciclastic mud that is interbedded at scales of cms (rhythmically laminated) to meters. Biosiliceous mud dominates the uppermost stratigraphy. Of note are the presence of at least two marker ashes (tephras) that correlate across the entire deposit and have geochemical signatures implying derivation from Deception Island, some 210 km distant (Keller et al., 2003). Also present are abundant ikaite crystals that have altered to calcite.

Evidence of active volcanism on the seafloor in and around the Cenozoic Volcanic complex of James Ross Island is vague. Yet we report on the occurrence of three relatively small concentric cones located on the deep seafloor (900 m) of Antarctic Sound. The largest of these is oblong and retains a concentric geometry despite clear glacial scouring of the surrounding seafloor. Data collected in April 2004 indicate that this feature is volcanically active. Bottom videos across the crest of the cone

revealed patches of fresh, black rock with a ropy or bulbous character, as opposed to most surfaces across the cone that have an abundant epifaunal cover. Geothermal anomalies of up to +0.05 °C in ambient water of -1.8 °C were observed over the fresh rock surfaces and a rock dredge brought up abundant rock samples including, glassy textured vesicular specimens, olivine-bearing vesicular basalt, scoria, abundant volcanic sand, and minor ice rafted stones of Peninsula origin. Reports on recent British Admiralty charts of discolored water in the vicinity (reported 1997) led us to conclude that the volcanic cone has been recently been active. The physiographic setting of the active volcanic center and two nearby features are significantly north of the on-shore mapped boundary between dissected arc rocks (Trinity Peninsula Group; ) and the Cenozoic Volcanic rocks of the James Ross Island complex. This suggests a tectonic regime for the area of Antarctic Sound that is more dynamic than previously believed.

### Acknowledgements

We are grateful to US National Science Foundation for support of this work through grants from the Office of Polar Programs (OPP-0338142 and OPP-000306 to Hamilton College). We thank the staff (Raytheon Polar Services) and crew of the *NB Palmer* and *LM Gould* for support of our work and our colleagues, A. Leventer, S. Ishman, R. Gilbert, A. Camerlenghi, and S. Brachfeld for their continued encouragement and intellectual stimulation.

### REFERENCES

- Backman, E. 2004, Depositional Architecture and Seafloor Mapping of the Vega Drift, Erebus and Terror Gulf, Antarctic Peninsula. Hamilton College, BA thesis, Clinton New York, 58 pp.
- British Admiralty Chart, (1998) No. 225.
- Camerlenghi, A., Domack, E., Rebesco, M., Gilbert, R., Ishman, S., Leventer, A., Brachfeld, S., and Drake, A. ('02), 2001. Glacial morphology and post-glacial contourites in northern Prince Gustav Channel (NW Weddell Sea, Antarctica). MARINE GEOPHYSICAL RESEARCHES, v. 22, 417-443.
- Keller R., Domack, E. W., Drake, A., 2003, Potential for the tephrochronology of marine sediment cores from Bransfield Strait and the Northwestern Weddell Sea. INQUAA-XVI Abstracts with program, p. 236-237.
- Rott, H., Rack, W., Nagler, T., and Skvarca, P., 1996. Rapid collapse of the Northern Larsen Ice Shelf, Antarctica, Science, 271, 788-792.

## A GEOPHYSICAL STUDY ALONG THE EASTERN MARGIN OF THE ANTARCTIC PENINSULA

6-04

Wilfried Jokat, Veit Helm, Ralf Krockner

*Alfred Wegener Institute for Polar and Marine Research, D-27568 Bremerhaven, Germany*

The Antarctic Peninsula (AP) reaching up to 62°S is the northernmost part of Antarctica. Its western margin faces the Pacific ocean and has been one of the most important locations to study processes along a glaciated margin with seismic methods. Seismic data have shown that sedimentary structures created by advances and retreats of glaciers/ice streams are highly variable along the margin. Thus, the sedimentation style of the Pacific margin of the AP is not a result of continuous ice shield dynamics, but of more localised sources like ice streams/glaciers. In addition, the deposition of glacial sediments was influenced by subduction processes, which caused several ridge-trench collisions in the different spreading segments approaching the subduction zone along the AP margin. The opposite, eastern margin of the AP, facing the Weddell Sea, has a complete different geological history. It started as a Mesozoic rifted margin during the initial stages of Gondwana break-up. Today it has a more "Antarctic" climate than the Pacific margin. Thus, one of the scientific objectives regarding its younger glacial history is to investigate if similar processes were active during glacial/interglacial periods along the eastern margin and if not, how they differ along both types of margins.

However, performing marine geophysical research along the eastern margin is almost impossible. Previous marine geophysical investigations were confined to the northernmost tip, off James Ross Island, and northward of 66°S on the Larsen Shelf, and only to a minor extent on the slope. Since the



famous drift of Sir Ernest Shackelton, no surface ship was able to enter this area in order to conduct any systematic research programme. In the austral season 2001/02 exceptional ice conditions allowed a Polarstern Expedition to investigate this remote margin from 67°S to almost 69°S (Fig. 1) with a total of six E-W trending multichannel seismic profiles (MCS). Furthermore, a first bathymetric survey indicate a water depth of 3048 m beneath the Endurance sink position (17<sup>th</sup> November 1907) at 68°38'S 52°28'W. One of the surprising scientific results was the discovery of a NE-SW trending mass wastage feature, at best 100 km long, between 67°00'S and 66°00'S. The slide was swath-mapped and crossed by two seismic profiles in the south to investigate its deeper structure. Here, the findings of the entire expedition will be presented.

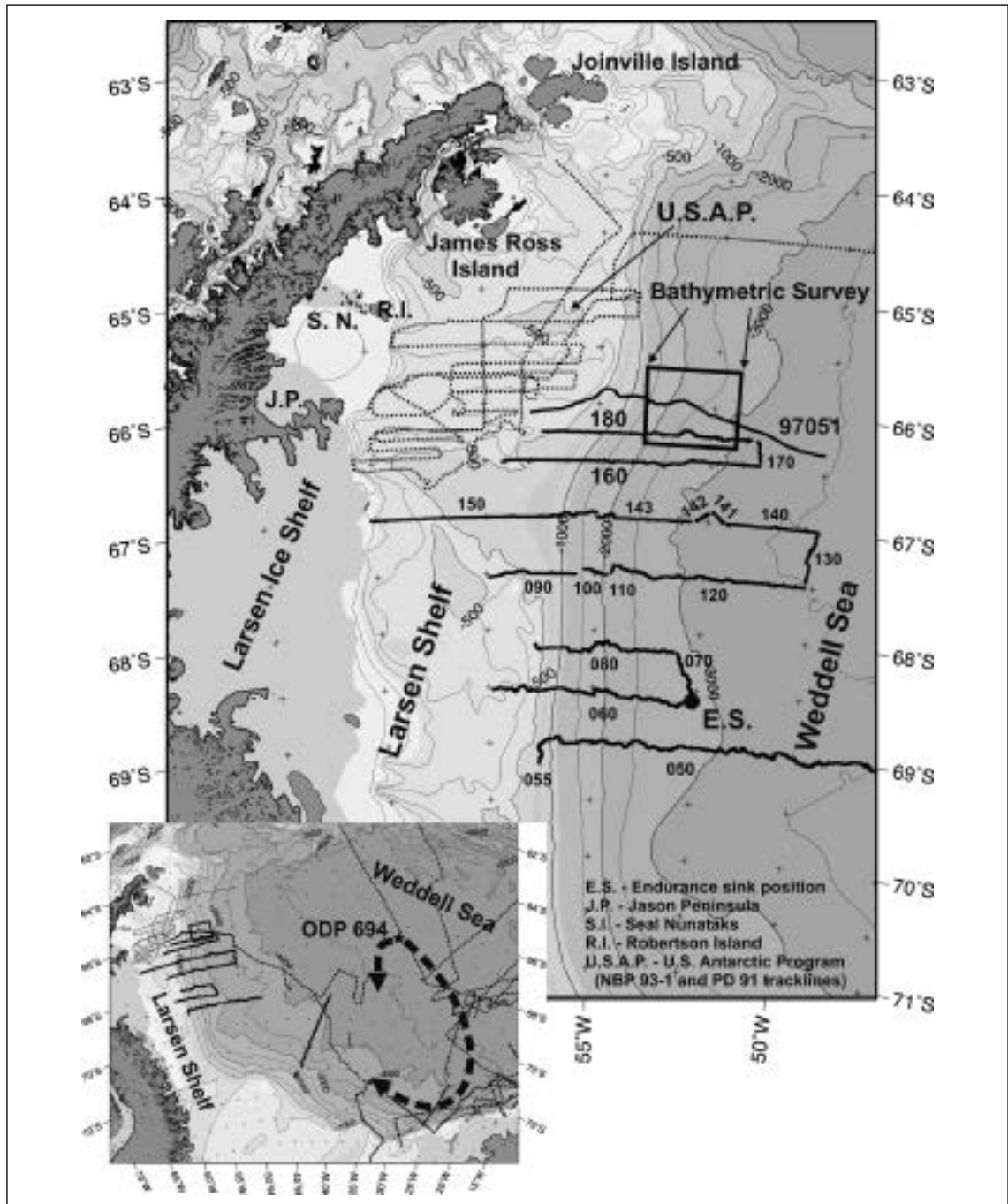


Fig. 1 - Location map of seismic profiles along the eastern continental margin of the Antarctic Peninsula.

**SEISMIC EXPRESSION OF THE WESTERN SCOTIA SEA CONTINENTAL MARGINS**

6-05

C. Sauli\*, E. Lodolo\*, N. Wardell\*, A. Tassone\*\*, A. Polonia\*\*\*

\* *Istituto Nazionale di Oceanografia e di Geofisica Sperimentale (OGS) - Trieste, Italy*\*\* *Instituto de Geofisica "Daniel A. Valencio", Dpto. de Geologia - Universidad de Buenos Aires, Argentina*\*\*\* *Istituto di Geologia Marina (IGM) - Bologna, Italy*

The Western Scotia Sea is part of a rather complex oceanic area bordered by the continental shallow banks of the North Scotia Ridge (NSR), the South Scotia Ridge (SSR), and the Shackleton Fracture Zones (SFZ), a linear topographic high which limits to the west the Scotia plate.

Many authors have indicated the oblique-divergent relative movement between South America and Antarctica, since the Late Cretaceous time, as an important factor that has caused the formation of the Scotia plate (Barker et al., 1991). The similitude between the Paleozoic and Mesozoic rocks of the Andes of the extremity of the South America and the actual Antarctic Peninsula has suggested that the ridges of North and South Scotia represent the fragments of a unique system of Antarctic Peninsula and Andean Cordillera that have been moved eastward by the westward drift of South America. The E-W relative motion of the two major South America and Antarctic plates is partitioned along North and South Scotia Ridge, respectively the left-lateral northern and southern strike-slip boundaries of the Scotia plate.

Magnetic anomalies individuation would have indicated that NW-SE opening of the Drake Passage - the oceanic area that now separates the southernmost South America from the Antarctic Peninsula - has taken place from Oligocene to late Miocene (approximately from 29 to 9 m.y.), followed by the extreme eastern E-W opening of the Eastern Scotia Sea from late Miocene to the present.

This study focuses on the analysis of the two continental margins of the Western Scotia Sea, based on the interpretation of multichannel seismic profiles. The seismic data (TM-11, TM-08A, TM-09, TM-10 and IT-244) acquired along the Tierra del Fuego continental margin, and those (IT-41, I95-154, I95-155, I95-156 and IT-123) acquired along the western termination of the South Scotia Ridge, have been analyzed to see and compare the two margins, expected to represent the conjugate continental margins of the Western Scotia Sea.

The lines were acquired within the Italian PNRA-funded projects *TESAC* (Tectonic Evolution of the South America-Scotia plate boundary during the Cenozoic) in 1999, *SCAPPAM-II* (Southern Chile and Antarctic Peninsula Pacific Margins - phase II) in 1997, *SANSCRITO* (Seismic Analysis and Tectonics of the South Scotia Ridge) in 1995, and during the 1989/90 *OGS Antarctic Campaign* in the circum-antarctic seas. The seismic acquisition parameters comprised generally a 120-channel, 3000-m long streamer (group interval of 25 m), 50 m shot spacing, at 4 msec, obtaining a 30 fold coverage, with the exception of *TESAC* lines which were shot with a 96-channel, 1200 m long streamer (group interval 25 m), 37.5 m shot spacing, at 2 msec, for a coverage of 16.

The data have been processed including predictive deconvolution before the stack, with the aim to increase the vertical resolution and to eliminate reverberations, space-time varying filtering, space-time varying gain, post stack finite-differences time migration and trace mixing.

The seismic sections were interpreted, and for each of them a line-drawing is presented to show principal seismo-stratigraphic characters and tectonic structure of the studied area. The analysis and the interpretation of the presented seismic reflection profiles allow the main tectonic lineaments to be mapped and to evidence the peculiarities, differences and also analogies between the continental margins of the Western Scotia Sea in order to understand its complex geodynamic evolution.

The Tierra del Fuego margin is a more typical passive margin with extensional structures, faulted and tilted blocks, possibly formed during the Drake Passage opening, and in the eastern area, some likely evidences of transtensional tectonic have been found. Along this margin is possible to follow the transition from continental to oceanic crust. The western part of the South Scotia Ridge is bounded by major steep strike-slip faults which coincides with the continental slope and separates the South Scotia Ridge abruptly from the oceanic crust of the South-western Scotia Sea. This margin may be considered as a mega-shear system controlled by strike-slip faulting since the early development of the margin.

## REFERENCE

- Barker P.F., Dalziel I.W.D. and Storey B.C.; Tectonic development of the Scotia Arc region in *Geology of Antarctica*, edited by Tingey R., pp. 215-248, Oxford University Press, New York, 1991.

### 3D CRUSTAL VARIATIONS IN THE PHOENIX-ANTARCTIC RIDGE (P2 SEGMENT)

6-06

E. Suriñach<sup>(1)</sup>, E. L. Flores-Márquez<sup>(2)</sup>, J. Galindo-Zaldivar<sup>(3)</sup>, A. Maldonado<sup>(4)</sup>

1 *Departament de Geodinàmica i Geofísica, Universitat de Barcelona, 08028 Barcelona, España.*  
(emma.surinach@ub.edu)

2 *Instituto de Geofísica, UNAM, Cd. Universitaria, Circuito Exterior, 04510. México, D.F. México.*  
(leticia@tonatiuh.igeofcu.unam.mx)

3 *Departamento de Geodinámica, Universidad de Granada, 18071 Granada, España.*  
(jgalindo@ugr.es)

4 *Instituto Andaluz de Ciencias de la Tierra, CSIC-Univ. de Granada, 18071 Granada, España.*  
(amaldona@ugr.es)

#### Abstract

Gravity and bathymetric data collected by the Spanish R/V Hespérides over the central segment (P2) of the Phoenix-Antarctic Ridge together with data from the Global Gravity Grid and Global Sea Floor Topography (GGSFT) were used to invert the deep 3-D structure of the crust. Water layer contribution to the gravity anomaly was eliminated, taking into account bathymetry. Spectral analysis of the reduced data yielded mean crustal mantle interface depths of 9 km.

#### Introduction

The tectonic evolution of the Southern Atlantic and the connection with the Pacific Ocean along Drake Passage were determined by the interaction between the South America and Antarctic plates, which currently show a main sinistral displacement in the Scotia Arc region (Pelayo and Wiens, 1989) (Fig. 1). Drake Passage, which separates South America from the Antarctic Peninsula, opened between the Oligocene and the Pliocene during the development of the Scotia Arc (Barker et al., 1991). The structure of the Antarctic Plate near the Drake Passage was controlled by the progressive subduction of the former Phoenix-Antarctic spreading centre along the Pacific margin of the Antarctic Peninsula. Several papers have been published on the tectonic evolution of this area, mainly based on interpretation of magnetic reversal anomaly isochrones formed during sea floor spreading (Barker, 1970; Barker, 1982; Larter and Barker, 1991; Livermore et al., 2000). Recently, Eagles (2003) included altimeter-derived free-air gravity data to present a new set of finite reconstruction parameters for Antarctic-Phoenix spreading since chron C5AD.

As a result of the cessation of the activity of the Phoenix-Antarctic spreading center at anomaly C2A (3.3 Ma) (Livermore et al., 2000) a small remnant ( $\sim 9 \times 10^4$  km<sup>2</sup>) of the former Phoenix plate, confined between the Shackleton and Hero Fracture Zones (Fig. 1), has become welded to the Antarctic plate. Three inactive segments can be recognized, P1, P2 and P3 (Larter and Barker, 1991). In the area sediment accumulation has been prevented by the presence of the Antarctic Circumpolar Current. As a consequence, the fossil spreading axis is exposed to bathymetric mapping.

In this paper we determine the 3D deep structure of the P2 segment of the Phoenix-Antarctic Ridge applying geophysical methods including spectral analysis and inversion procedures to the gravity data obtained in the ANTPAC 97/98 cruise with the Spanish R/V Hespérides and the existing Global Gravity Grid database (See <http://topex.ucsd.edu>; Sandwell & Smith, 1997).

#### Geophysical data

During the cruise, the central segment P2 of the Phoenix-Antarctic Ridge between fractures D and E, was surveyed in detail. This is one of the first times that a detailed geophysical survey has been carried

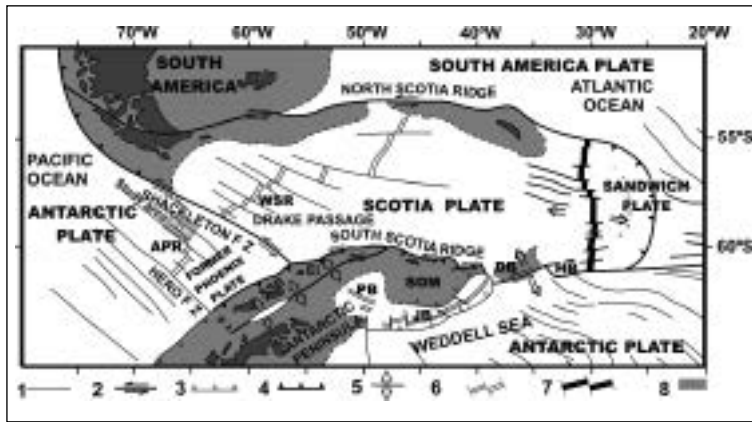


Fig. 1 - Geological setting of the study area in the frame of the Scotia Arc. 1, inactive fracture zone; 2, transform fault; 3, inactive subduction or reverse fault; 4, active subduction; 5, extensional fault; 6, inactive spreading axis; 7, active spreading axis; 8, continent-oceanic crustal boundary. FZ, fracture zone; APR, Phoenix-Antarctic Ridge; WSR, West Scotia Ridge; PB, Powell Basin; SOM, South Orkney Microcontinent; JB, Jane Basin; DB, Discovery Bank; HB, Herdman Bank; SSB, South Shetland Block; EI, Elephant Island.

out in the area. Multichannel seismic (MCS), swath bathymetry, magnetic and gravity profiles were obtained along several transects. More details of the data acquisition and processing of the cruise data were presented in Maldonado et al. (2000) and Galindo-Zaldívar et al. (2000).

Bathymetric and Free Air anomaly data from the Global Gravity Grid and the Global Sea Floor Topography (<http://topex.ucsd.edu>; updated 2001) of the region from 66.9°W 64.6°W and from 59.7°S to 58.2°S were also considered in order to complete the information in the selected area. Hereafter, these data used for the study region will be referred to as the GGSFT database. Figure 2 shows the ANTPAC 97/98 cruise area covered by the swath bathymetry as well as the locations of the actual bathymetric ship measurements embedded in the Global Sea Floor Topography data. The area of our interest is well covered by ship tracks (Fig. 2) with the result that the GGSFT gravity grid has practically no effect on the predicted bathymetry. The process to merge GGSFT database with ANTPAC 97/98 cruise data and processing is described in Flores-Márquez et al. (2003).

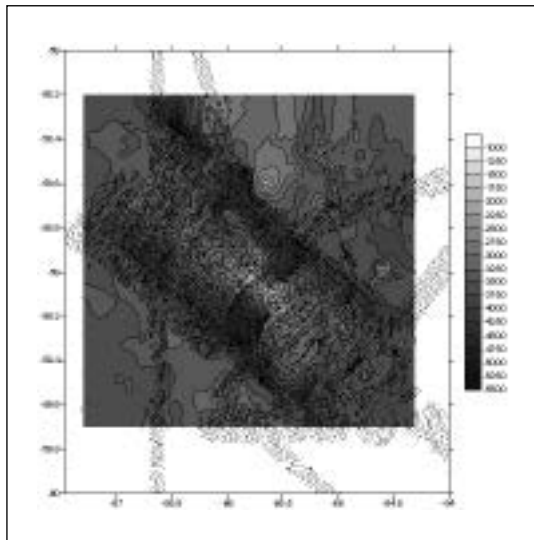
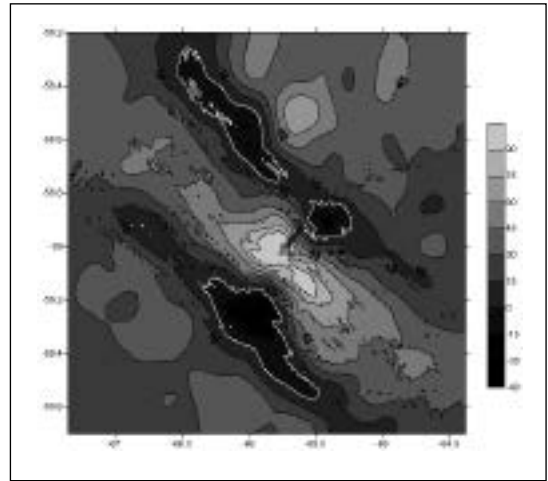


Fig. 2 - Bathymetric map (in m) including data (dots) from the swath bathymetry recovered by SIMRAD EM12 system in the ANTPAC 1997/1998 cruise and from the Global Seafloor (GGSFT) (<http://topex.ucsd.edu>, updated 2001).

### Getting Gravity Anomaly

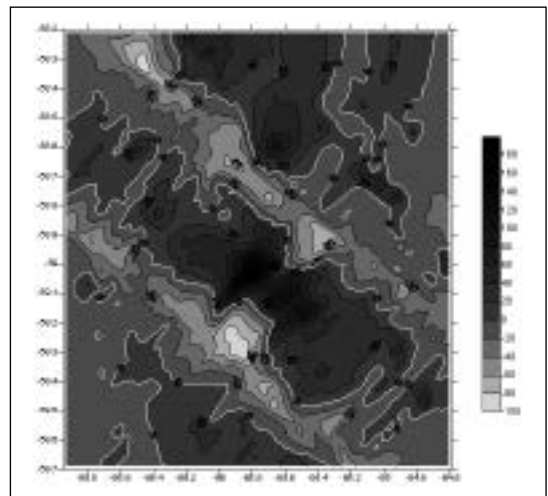
Our aim was to use the Free Air (FA) gravity anomalies (Fig. 3) to obtain the deep crustal structure by employing the inversion method in the same way as with the continental Bouguer anomalies (e.g. Suriñach and Chavez, 1996). It is necessary, however, to eliminate the effect of the sea bottom topography which is superimposed onto the effect of the sub-bottom density changes in the FA anomalies. Water plate correction (WPC) (Flores-Márquez et al., 2003) was applied to reduce the FA anomaly to obtain total global anomaly. The process is slightly different from that used to obtain “the Mantle Bouguer Anomaly” (MBA). Here, we assume that the reduced anomalies are produced by the variations of the crustal-mantle interface (CMI).

Fig. 3 - Free air anomaly map obtained by merging data from the ANTPAC 1997/1998 cruise track lines and the GGSFT data. Isolines every 15 mGal.



The WPC (Fig. 4) was computed by using the difference between the mean density of the crust in the region and the sea water density. The crust density ranges between 2700 and 2900 kg/m<sup>3</sup> and the sea water density is considered as 1030 kg/m<sup>3</sup>. As a result, the density for computing water plate contribution ranges between 1670 and 1870 kg/m<sup>3</sup>. The maximum positive values of the water plate corrections, which reflect the bathymetry, reach 180 mGal, coinciding with the areas reaching minimum depths (app. 1000 m) (Figs. 2 & 4). The negative values (up to -80 mGal) correspond to the deep regions of the zone (app. 5000 m) (Figs. 2 & 4). The reference level of correction (applied in Parker's method, Parker, 1995) is 3600 m, the mean of the ocean depth in the study area, which corresponds to the 0 mGal correction.

Fig. 4 - Gravimetric water plate correction obtained by using Parker's [1995] method considering the merged data of seafloor topography. Isolines every 20 mGal.



The statistical model developed by Spector and Grant (1970) allows us to obtain the average depth of the source of the anomalies (the CMI in our case) from the analysis of their power spectrum. The power spectrum of the total gravity anomaly was analysed as a function of the radial wavenumbers. Figure 5 shows the power spectrum of the total gravity anomaly. The wavenumber of 0.135 km<sup>-1</sup> clearly separates two domains associated with the regional (low wavenumber content) and with the residual (high wavenumber content) anomalies. To isolate the regional contribution, we designed an appropriate Butterworth filter with a cut-off value of 0.135 km<sup>-1</sup>. The depth of the deep sources is approx. 9 km, the maximum of the range in accordance with Spector and Grant (1970). The regional contribution was inverted to obtain the 3D CMI topography using the method applied in Suriñach and Chavez (1996) and Flores-Márquez et al. (2003). This study contributes to the understanding of the tectonic evolution of the Phoenix-Antarctic Ridge.

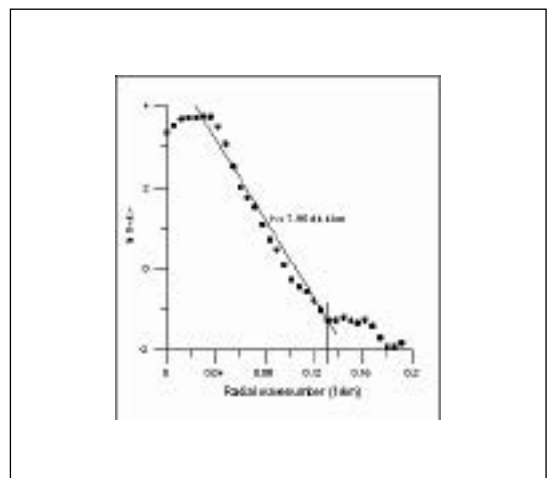


Fig. 5 - Averaged power spectrum of the total gravity anomaly as a function of the radial wave number.

## Acknowledgements

Spain's CICYT supported this research through Project ANT99-0817 and REN2001-2143/ANT and the exchange program between the UB (Spain) and the DGIA-UNAM (México).

## REFERENCES

- Barker, P.F. (1970). Plate tectonics of the Scotia Sea region, *Nature* 228, 1293 -1296.
- Barker, P.F. (1982), The Cenozoic subduction history of the Pacific margin of the Antarctic Peninsula-Ridge crest trench interactions: *Geological Society of London Journal*, v. 139, p. 787–801.
- Barker, P.F., Dalziel, I.W.D and Storey, B.C. (1991). Tectonic development of the Scotia Arc region. In: Tingey, R.J. (Ed.). *Antarctic Geology*. Oxford University Press, Oxford, pp. 215-248.
- Eagle, G. (2003). Tectonic evolution of the Antarctic-Phoenix plate system since 15 Ma *Earth and Plan. Sci. Let.* 217, 97-109.
- Flores-Márquez, E. L., Suriñach, E., Galindo-Zaldivar, J., Maldonado, A. (2003). 3-D Gravity inversion model of the deep crustal structure of the central Drake Passage (Shackleton Fracture Zone and West Scotia Ridge, Antarctica). *Journal of Geophysical Research* 108-B9, 2445-2456.
- Galindo-Zaldivar, J., Jabaloy, A., Martinez, J.M., Maldonado, A., Sanz de Galdeano, C., Somoza, L. and Suriñach, E. (2000). Deep crustal structure of the area of intersection between the Shackleton Fracture Zone and the West Scotia Ridge (Drake Passage, Antarctica). *Tectonophysics*, 320, 123-139.
- Larter, R. D., Barker, P. F. (1991). Effects of ridge crest-trench interaction on Antarctic–Phoenix spreading forces in a young subducting plate. *Journal of Geophysical Research* 96, 19586-19607.
- Livermore, R., Balanya, J.C., Barnolas, A., Galindo-Zaldivar, J., Hernandez-Molina, M., Jabaloy, A., Maldonado, A., Martinez, J.M., Rodriguez-Fernandez, J., Sanz de Galdeano, C., Somoza, L., Suriñach, E., and Viseras, C. (2000). Autopsy on a Dead Spreading Center: The Phoenix Ridge, Drake Passage, Antarctica. *Geology*, 28-7, 607-610.
- Maldonado, A., Balanya, J.C., Barnolas, A., Galindo-Zaldivar, J., Hernandez-Molina, M., Jabaloy, A., Livermore, R., Martinez, J.M., Rodriguez-Fernandez, J., Sanz de Galdeano, C., Somoza, L., Suriñach, E., and Viseras, C. (2000). Tectonics of an extinct ridge-transform intersection, Drake Passage (Antarctica). *Marine Geophys. Res.*, 21, 43-68.
- Parker, R. L. (1995). Improved Fourier terrain correction, Part I: *Geophysics*, 60, 1007-1017.
- Pelayo, A.M. and Wiens, D. A. (1989). Seismotectonics and relative plate motions in the Scotia Sea region. *J. Geophys. Res.* 94, 7293-7320.
- Sandwell, D.T. and Smith, W. H. (1997). Marine Gravity anomaly from Geosat and ERS1 satellite altimetry. *J. Geophys. Res.* 102, 10039-10054.
- Spector, A. and Grant, F. S. (1970) Statistical models for interpreting aeromagnetic data. *Geophysics* 35, 293-302.
- Suriñach, E. and Chávez, R. E. (1996). A 3D crustal model for the northeastern region of the Iberian Peninsula. *Geophysical Research Letters*, 23, 18, 2457-2460.

## 3D MODELLING OF THE SOUTH SCOTIA RIDGE PLATE BOUNDARY (ANTARCTICA)

6-07

S. Susini(\*), M. De Donatis(\*), N. Zitellini(\*\*)

(\*) *LINEE – Laboratory of Information technology for Earth and Environmental Sciences, Università degli Studi di Urbino “Carlo Bo”, Campus Scientifico, 61029-Urbino, Italy – susini@uniurb.it*

(\*\*) *ISMAR - Istituto di Scienze Marine, CNR, Via Gobetti 101, 40129-Bologna, Italy*

3D modelling and visualisation techniques in Earth Sciences represent an advanced synthesis of a process research for analysing different kind of data (geological and geophysical, surface and subsurface data) all together. This is useful to obtain a more realistic geological view and to compute specific evaluation and analysis.

3D modelling is a powerful tool to visualize and understand deep geological structures respect to maps and profiles, which give only a 2-dimension view and don't permit to obtain informations in the boundary areas.

In this paper we present a 3D geologic model of the area between the northern flank of the South Scotia Ridge (SSR) and the Scotia Sea (Fig. 1a), discussing the identified structures and their kinematics.

SSR is a submerged structural high representing the eastern continuation of the Antarctic Peninsula on the sea (Canals et al. 1992, Galindo-Zaldivar et al. 1994) and the site along which one of the major trascurrent plate boundaries on the earth runs (B.A.S. 1985, Klepeis et al. 1989). SSR runs approximately E-W for about 500 km separating the oceanic Scotia Plate from the Antarctic Plate and it is constituted mainly by fragments of continental crust.

Here we use the net of multi-channel seismic (MCS; Fig. 1b) lines acquired by the Italian R/V OGS-Explora during several geophysical surveys (Campaign 1989-90, 1990-91 and 1994-95). The multi-channel seismic reflection lines were performed by the Osservatorio Geofisico Sperimentale (OGS) in the frame of the Italian “Programma Nazionale di Ricerche in Antartide” (PNRA).

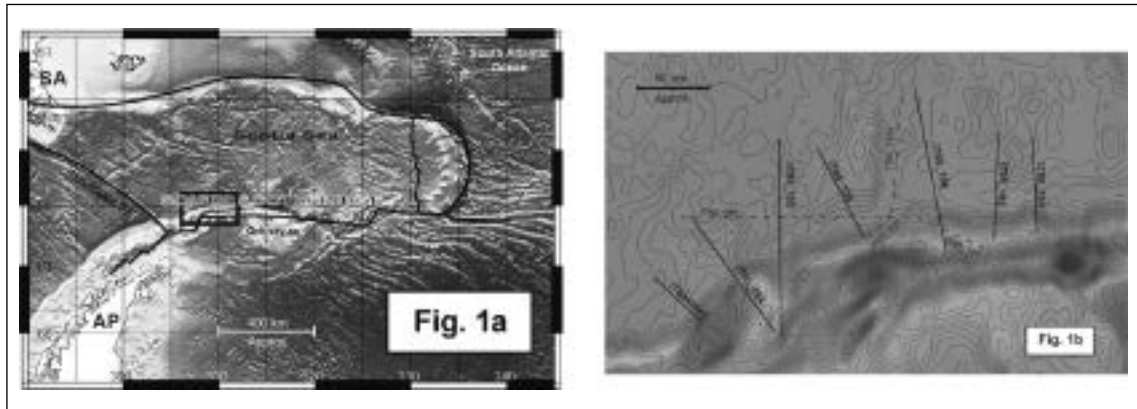


Fig. 1a - Shaded relief map (predicted by satellite-derived gravity data; Sandwell et al. 1995) of the Scotia Plate and adjacent areas. The black box outlines the investigated area of the South Scotia Ridge.  
 Fig. 1b - Bathymetric map (predicted by satellite-derived gravity data; Sandwell et al. 1995). Contour lines interval. 200 m. The position of the multi-channel seismic (MCS) reflection profiles is shown. Black lines represent MCS lines selected in order to perform the 3D model. Dashed lines represent MCS lines used mainly for stratigraphic correlations.

### MCS description

IT89AW4: MCS NW-SE oriented. A high angle, normal fault, NW-dipping represents the plate boundary between the SSR at the footwall and the Scotia Plate at the hangingwall. An ancient accretionary wedge (Lodolo & Zitellini, 1993) is present and buried by an on-lapping sedimentary cover.

IT95\_154: MCS NW-SE oriented. The plate boundary is represented here mainly by high angle normal fault N-dipping. N-dipping normal faults cut the oceanic crust. Post-depositional deformation affects also the uppermost stratigraphic levels and could be still active.

IT95\_155: MCS N-S oriented. The plate boundary is a N-dipping, high angle, normal fault. Continental basement is deformed by high angle NW-dipping normal faults. N-dipping normal faults affect the oceanic basement, whereas the oceanic sedimentary cover seems not to be involved.

IT95\_156: MCS NW-SE oriented. The plate boundary is represented by a sub-vertical/S-dipping fault plane. Approaching to the SSR, the oceanic basement weakly deepens beneath the continental crust and the sedimentary sequence thickens. The oldest sediments, overlying the oceanic basement, are deformed by high angle reverse faults and folds with a pop-up structure-like. The uppermost sedimentary cover is undisturbed.

IT95\_158: MCS NNW-SSE oriented. The plate boundary is represented by a sub-vertical/S-dipping fault plane. Approaching to the SSR, the oceanic basement weakly deepens beneath the continental crust and the oceanic sediment pile thickens. Here oldest oceanic sediments are deformed by folds and thrusts. Uppermost sedimentary cover is undisturbed.

IT95\_162: MCS N-S oriented. Plate boundary is represented by a high angle S-dipping fault plane. Approaching to the continental structure the oceanic basement deepens beneath the SSR and oceanic sedimentary pile thickens.

IT95\_163: MCS N-S oriented. This line crosscuts the SSR where it changes from an almost E-W to a WNW-ESE orientation. Plate boundary is represented by a low angle SSW-dipping fault plane. Approaching the continent a wedge of undeformed sediments is recognizable and it rests upon a southward dipping oceanic basement.

### 3D model

MCS lines have been interpreted underlining the main seismic sequences boundaries and tectonic structures. The seismic lines have been digitised, geo-referenced in the Universal Transverse Mercator (UTM, zone 22, 51° W) system, and therefore converted in geological sections.

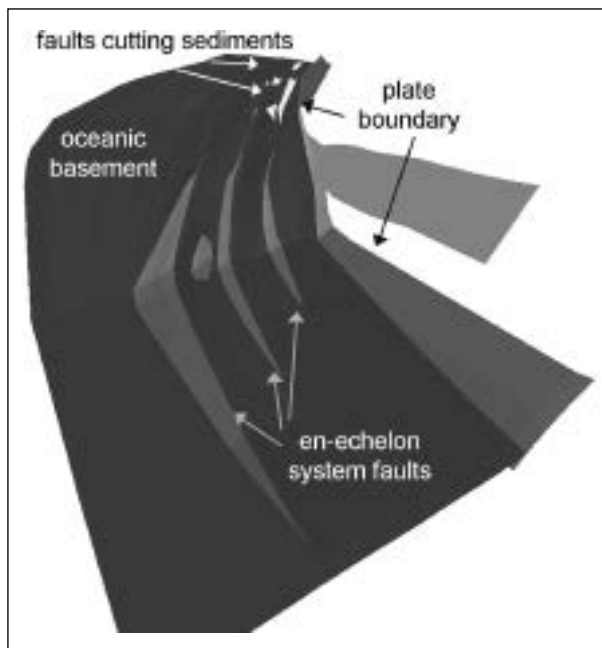
The 3D model has been created by reporting on the surface the geologic elements recognised in the geologic sections which have been derived from seismic lines. To simplify the construction of the 3D model we considered only geologic elements (oceanic and continental basements, and three main sedimentary horizons) recognizable on every geologic section, and the tectonic structures deforming the oceanic environment.

Thanks to this model we can visualize the continental and oceanic crusts, the oceanic sedimentary cover and their deep geological structures. This allow us to analyze the geologic, structural and geomorphic features, their shape and dimension.

In the studied area three main families (Fig. 2) of faults have been classified. The first group is constituted by a strike-slip regime fault zone, representing the plate boundary. This fault zone controls the geometric relations between the SSR and the Scotia Plate. The second family presents an en-echelon geometry and affects the oceanic basement, locally cutting even the oceanic sedimentary pile. This system of faults is located in the western province, where the continental structure changes from a NE-SW to an E-W orientation. The third family of fault deforms only the oceanic sedimentary cover in the central province.

Oceanic basement is deformed only in the western province (Fig. 3), where the en-echelon system fault, cuts and tilt the basement. Here the oceanic basement is at the hangingwall of the high angle normal fault representing the plate boundary. Toward east, fault surfaces dipping changes, the oceanic basement at the footwall start to bend under the continental crust of the SSR and the sedimentary pile thickens approaching to the continental margin.

Three horizons have been identified within the oceanic sedimentary sequence, two of them revealing a widespread extension. Their discontinuity has been detected only where the second family of faults let the oceanic basement crops out. Here, in the offshore sector, deformation occurred after sediments deposition.



Toward east, in the central province, folds and thrusts weakly deform the oceanic sedimentary sequence close to the margin. Ductile and fragile deformation involves mainly the oldest sediments. Deformation in the uppermost levels (sea bottom) is recognisable near the continental margin, whereas in the eastern province, approaching to the plate boundary, the thick oceanic sedimentary sequence seems to be quite undisturbed.

From West to East the sediment thickness slightly increase in approaching to the plate boundary.

Fig. 2 - Oceanic basement and faults, looking East. Vertical Exaggeration = 2.

### Discussion and Conclusion

The tectonic features of this Periantarctic region are strongly controlled by the SSR structure orientation and by the homogeneous deformation regime affecting the entire Scotia plate (Giner-



Robles et al. 2003). The deformational regime is induced by the left lateral movement along its northern and southern boundaries.

New considerations about geology and structures would be provided by subdividing the area in three main provinces (western, central and eastern) revealing different geologic features. These differences concern continental and oceanic basements, oceanic sediments and the relations between inner continental structures of the SSR and the oceanic environment and the different kind of structural styles. Deformation due to the plate boundary, in the western province is sheared between the continental structure and the oceanic crust with mainly transtensional character. Toward east, deformation style changes and the compressional component along the trascurrent margin is well recognizable

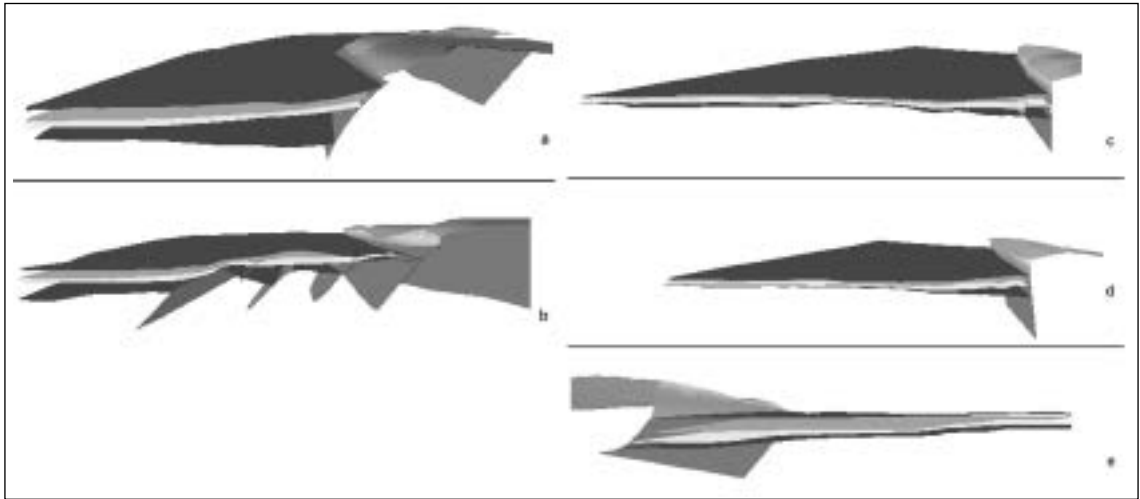


Fig. 3 - 3D model sections, a-d, looking east and moving west to east. e, looking west. V. E. = 2.

## REFERENCES

- British Antarctic Survey (1985), Misc 3. Cambridge; British Antarctic Survey.
- Canals M. et al. (1992), Acta Geologica Hispanica, 27, 89-110.
- Galindo-Zaldivar J. et al. (1994), Terra Antarctica, 1, 303-306.
- Giner-Robles J.L. et al. (2003), Journal of South American Earth Sciences, 16, 179-191.
- Klepeis K.A. et al. (1989), Antarctic Journal, 24, 126-128.
- Lodolo E. and Zitellini N. (1993), Proc. 4<sup>o</sup> Meeting Earth Science in Antarctica.
- Sandwell D.T. et al. (1995), EOS Trans, AGU 76, Spring Meeting. Suppl., S89.

## GAS HYDRATES AND ACTIVE FLUID OUTFLOW NE OF THE SOUTH SHETLAND ISLANDS, ANTARCTIC PENINSULA

6-08

U. Tinivella(\*), F. Accaino(\*), R. Geletti(\*), B. Della Vedova(\*\*)

(\*) *Istituto Nazionale di Oceanografia e di Geofisica Sperimentale – OGS  
Borgo Grotta Gigante 42c – 34010 SGONICO TS Italy*

(\*\*) *University of Trieste, Dipartimento di Ingegneria Civile - DIC  
Via A. Valerio, 10 – 3412700 TRIESTE, Italy*

## Summary

We present the data acquired during the last Antarctic season (February-March 2004) to study the gas hydrate reservoir present NE of the South Shetland Islands. A strong Bottom Simulating Reflector was mapped and integrated with the bathymetric and structural data with the main purpose to reconstruct

the geometry and physical properties of the system and understand the origin, migration and distribution of the gas-phases present on the pacific continental margin of the Antarctic Peninsula. The joint analyses of multidisciplinary data (reflection, refraction and converted seismic data, multibeam and sub bottom bathymetry, CTD and core data) allowed us to determine with good accuracy the physical properties of the hydrated sediments and to discover several important features related to the present activity of the system, such as mud volcanoes, active fluid escapes, collapse features and sliding slopes mainly present nearby the faults bordering the zones where the bottom simulating reflector is strong.

## Introduction

The Bottom Simulating Reflector (BSR) is generated by gas hydrates and free gas trapped below the hydrate stability zone; its regional distribution provides an important clue to their origin and migration, which are related to the geological history and structural setting of the area. In order to improve the understanding of these hydrocarbon gas reservoirs, of their phase change and migration, a question must be asked on which degree of accuracy the spatial distribution of gas in either phase and its volumetric abundance have to be known. Previous studies in the investigated area indicated that a free gas zone is present below the BSR, with variable thickness and with a variable seismic velocity. Moreover, there is a strong correlation between the free gas content in the pore space and the strength of the BSR (Tinivella et al., 2002). Three acquisition cruises during the austral summers 1989-90, 1996-97 and 2003-2004 onboard OGS Explora acquired a multidisciplinary geophysical data set, such as seismic data, multibeam and sub-bottom bathymetry, CTD profiles in the water column and sediment gravity cores, on the Pacific margin of the Antarctic Peninsula, offshore the South Shetland Islands. In this paper, we show the preliminary results obtained this year in the investigated area, in the frame of the Progetto Nazionale di Ricerche in Antartide (PNRA). The most important finding is the complex and active pattern of fluid and mass outflow phenomena from the reservoir, mainly through the faults bordering the field. The main objective of our study is to determine the elastic model of the reservoir, and in particular the spatial distribution and concentration of the gas phases. The integrated analyses of all available data allows to propose a reasonable explanation on the origin, migration and accumulation of the methane present offshore the South Shetland Islands.

## Seismic data

A strong BSR was identified on several multichannel seismic reflection profiles acquired during the Austral summers 1989/1990 and 1996/1997 on the South Shetland Margin (see Tinivella and

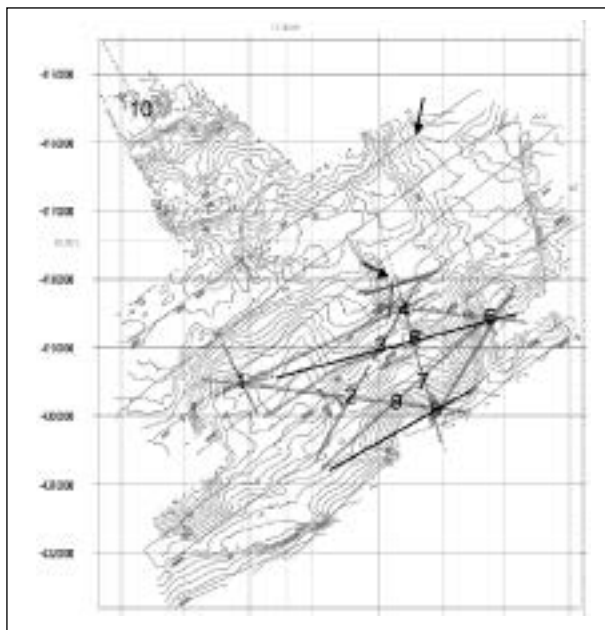


Fig. 1 - Location map of the 2003-04 geophysical survey superimposed on the Reson 8150 Multibeam bathymetric map. The numbers indicate the OBS positions; the arrows the core positions. The long dotted profile, passing on the OBSs 4, 6, 7 and 8 indicate the sleeve guns deep shooting line.

Accaino, 2002 for details on the seismic lines). The air-gun array seismic source in 1989-90 had a total volume of 55 litres, with a shot interval equal to 50 m; the sampling rate was 4 ms. In the 1996-97 cruise, instead, the energy source was made of two 2 GI guns with a total volume of 4 litres, firing every 25 m and the sampling interval was 1 ms. The streamer was in both cases 3000 m long, with a hydrophone group interval of 25 m. One Ocean Bottom Seismometer (OBS), deployed during the 1996-97 cruise, provided energy arrivals from below the BSR and, in particular, the refraction from the base of the free gas zone and the converted waves. The inversion of such events allowed us to reconstruct the compressional and shear wave velocity field in the gas hydrate and free-gas zones (Tinivella and Accaino, 2002).

The good results obtained by the inversion of the OBS data suggested us to propose a new detailed acquisition survey with the purpose to reconstruct the elastic properties of the sediments in the BSR region. In February-March 2004 we acquired new reflection and OBS seismic data in the area where the BSR is particularly strong, deploying nine four-channels OBSs along pre-existing multichannel seismic lines, as indicated in Figure 1. We used a star acquisition scheme to optimise the ray path coverage and the survey time. The seismic source was two GI guns, shot interval of 50 m and the OBS sampling interval of 2 ms. We shot into OBSs following the star arms as indicated in Figure 1. Seismic reflection data were recorded simultaneously with 1 ms sampling rate and 12 s record length. To image the deeper structures, we also fired every 100 m with the 44 litres sleeve guns array along a single profile including the OBSs from position 4 to 8. In this case, the record length was 20 s with a sample rate of 2 ms.

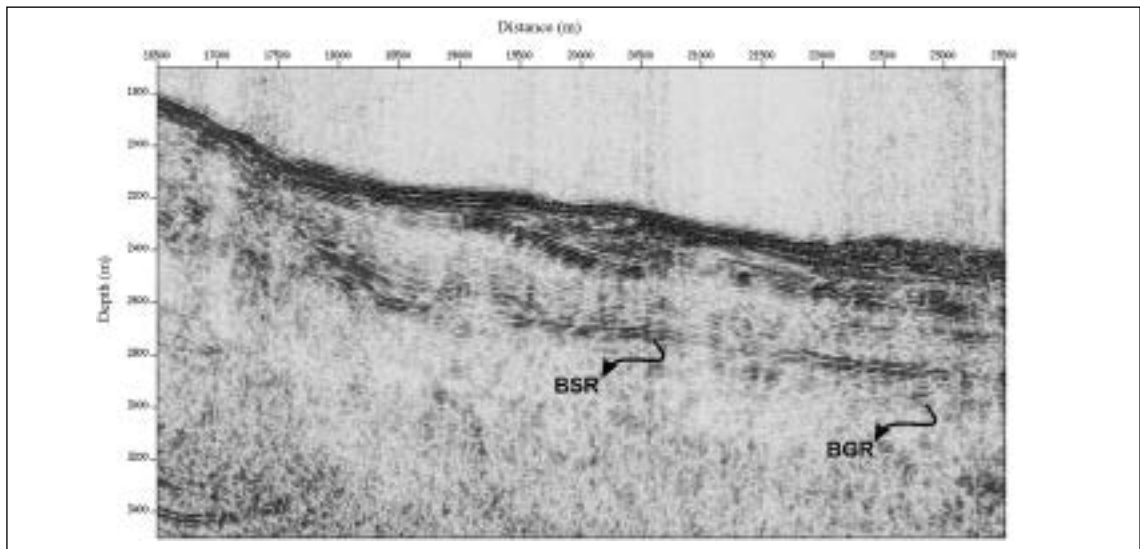


Fig. 2 - Pre-stack depth migration of a selected part of seismic line acquired between OBS 4 and 6.

To compare the BSR seismic results with a BSR blank area, we deployed a single OBS (OBS 10 in Fig. 1) in the trench (5200 m of water depth) and we fired with both systems (GI and sleeve guns) along a seismic line acquired in 1989. In fact, as pointed out in previous studies (i.e., Tinivella et al. 2002), the trench can be considered as a reference zone to calibrate the theoretical models in absence of gas hydrate and free gas.

The reflection seismic data was processed to enhance the BSR and the Base of the free Gas Reflector (BGR). The seismic lines acquired during the first two legs were re-processed to improve the seismic section. In particular, the dip move out correction and the post-stack migration were applied to the data to allow a preliminary interpretation and a preliminary velocity field of the seismic lines. The pre-stack depth migration was then applied iteratively to reconstruct the velocity field with higher accuracy. An example of final pre-stack depth migration is shown in Figure 2, which presents a selected part of the seismic line located between OBS 4 and 6. The profile shows a discontinuous BSR, probably because of localized fluid escapes.

**Other geophysical data**

During the February-March 2004 cruise, we acquired other geophysical data such as: multibeam, CTD profiles in the water column, sub-bottom profiles and two gravity cores. The multibeam data were recorded with a Reson 8150 system over an area of about 5500 km<sup>2</sup>. They allowed us to recognise several important features, such as mud volcanoes and collapse throughs (see an example in Fig. 3) and recent slides from a mud volcano ridge (see an example in Fig. 4).

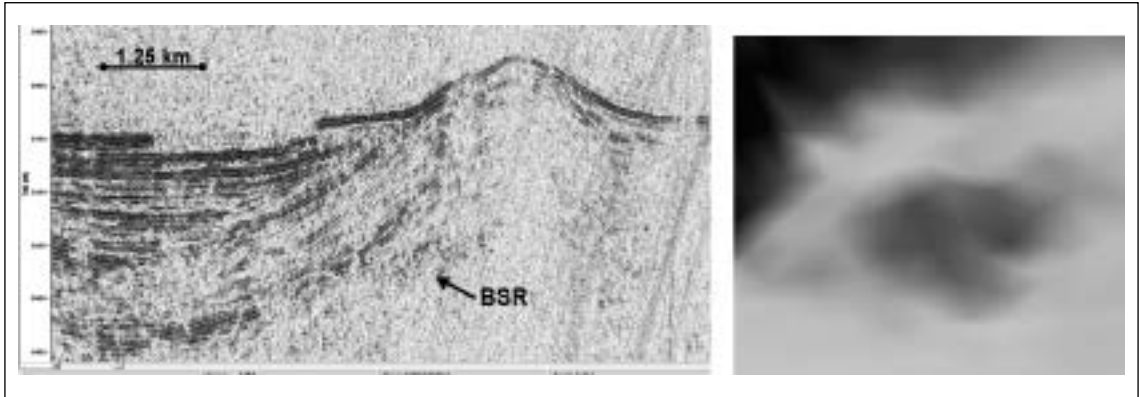


Fig. 3 - Example of mud volcanoes as imaged by MCS data and by multibeam survey. The MCS profile shows also a nice collapse through (50-80 m deep) bordered by faults and possible fluid escapes.

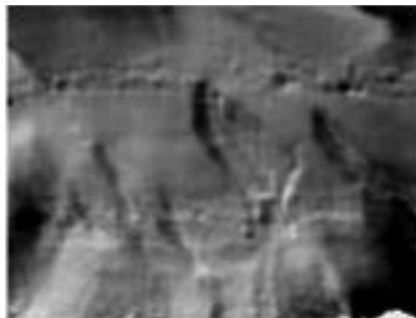


Fig. 4 - Example of aligned slides across the slope of a mud volcano ridge imaged by the multibeam swath. The horizontal length corresponds to about 30 km.

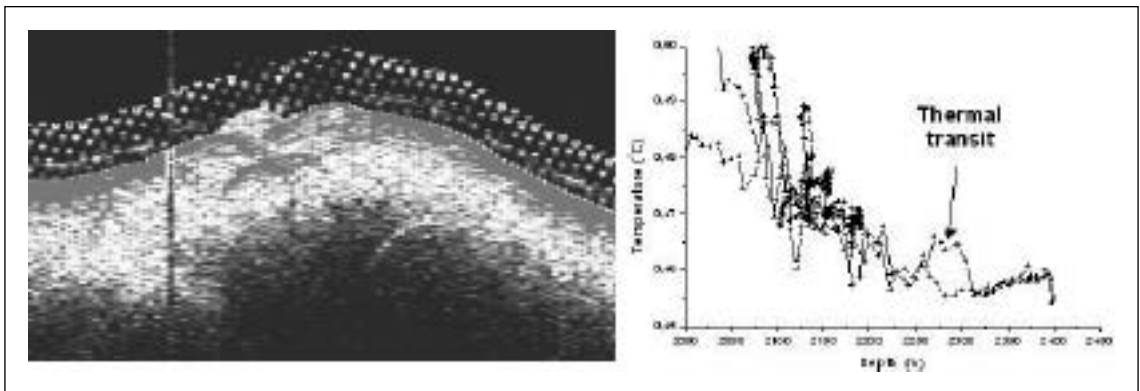


Fig. 5 - Left: Example of fluid expulsion as evidenced by the sub-bottom profile data. Right: Temperature profile nearby a fluid expulsion (from CTD profile).

The multibeam bathymetric imagery was calibrated using the velocity profile in the water column reconstructed from the CTD data. For this purpose, we acquired four CTD profiles; one of them close to a mud volcano indicated a significant positive thermal and salinity anomaly some 60-80 m above the sea floor. Because the anomaly is slight and it was recorded downward only, it is probably correlated with the far field transient of an episodic fluid expulsion event. This evidence is also consistent with the sub-bottom profile acquired across the area, that reveals the presence of several fluid expulsion plumes in the water column at the border of the gas hydrate reservoir. Figure 5 shows an example of this phenomena.

The cores are not yet analysed, but one of them exhibited a strong smell of methane, when recovered onboard.

### Gas hydrate distribution

The seismic data acquired during the last cruise allowed us to better characterize the area where the BSR is present and strong (gas hydrate reservoir), as distinguished from the area where the BSR is subdued or absent. The transition between the two areas is outlined by the presence of normal faults or weakness zones which border the structural high and constitute the escaping channels through which fluids outflow from below the BSR. The distribution of the seismic velocity extracted from the seismic data is used to determine the gas hydrate and the free gas distribution, with the main purpose to estimate the methane volumetric fraction trapped in the marine sediments.

In order to quantify the concentrations of gas hydrate and free gas in the pore space, we used Biot-Geertsma-Smit equations to model the acoustic properties of the different layers associated with the BSR. This approach allows to model two solid phases- grains and clathrates - and two fluid phases – water and free gas - including an explicit dependence on differential pressure and depth, and the effects of cementation by hydration on shear modulus of the sediment matrix. The theory gives both compressional (P) and shear (S) wave velocities assuming adequate physical parameters (Tinivella, 1999). The detailed geological knowledge of the area is essential in order to estimate values and gradients for the physical properties of marine sediments; this information is going to be extracted from the joint analyses of the geophysical data available in the area. In particular, the concentrations of methane in the two phases can be estimated by fitting the theoretical velocity to the experimental P- and eventually S-wave velocities obtained from travel-time inversion. Assuming that positive anomalies are due to the presence of hydrate only, the discrepancies between the inverted velocity profile and the velocity for water-filled normally compacted marine sediments are interpreted as due to the presence of gas hydrate (where positive anomalies are present) and free gas (where negative anomalies are present).

The free gas concentration is difficult to estimate because of the influence of the distribution of the free gas in the pore space and the influence of possible overpressure in the free gas zone. Analysis of AVO curves and Poisson's ratio can help to predict the pore pressure condition (Tinivella, 2000). These analyses integrated with the intermediate and deep crustal sections are useful to better understand the migration of fluids, the physical properties of marine sediments and the consequent origin of the BSR in an area.

The main results derived by joint analyses of P- and S-wave velocities, Poisson's ratio, PP and PS reflection coefficients versus offset allow us to extract information about the physical properties of the sediments in the gas hydrate and free gas zones. A preliminary analysis of the new data shows that the free gas is not always in overpressure condition and that the free gas is uniformly distributed in the pore space. This evidence supports the interpretation that the overpressure and related discharge of mud and fluids are episodic. The thickness of the free gas zone is variable and is related to the BSR strength. The gas hydrate distribution and concentration is quite variable in the area, but is present with continuity in the zone illuminated by the detailed 2004 survey.

### Discussion and conclusions

The analysis of the new geophysical dataset and the accurate processing of the previous multichannel seismic lines allowed us to better reconstruct the 3D geometry and physical properties of the reservoir and to understand the migration and outflow of the mud and fluids from below the gas hydrate zone.

The gas hydrates zone corresponds to the relatively undisturbed portion of the sedimentary cover, whereas the mud and fluid expulsion phenomena are concentrated along the fault systems bordering the reservoir. Outside the field the BSR is very weak or absent. The outflow phenomena, mud volcanoes, collapse troughs and slides are active and likely episodic, indicating that there is a pressure build-up over time, below the BSR. Moreover, the gas hydrate reservoir is located in a structural high, supporting the hypothesis that the free gas is trapped in the sediments because of the hydrate presence. The quite extensive data set available in the BSR area allows us to determine the distribution and concentration of gas phases and to estimate the methane release caused by gas hydrate. The contribution to gas hydrate dissociation, induced by the global change, could also be estimated, evaluating the effects of the past and future changes in temperature and sea level.

## REFERENCES

- Carcione and Tinivella (2000) *Geophysics*, 65, 54-67
- Tinivella (1999), *Bollettino di Geofisica Teorica ed Applicata*, 40, 19-30
- Tinivella (2002), *Journal of Seismic Exploration*, 11, 283-305
- Tinivella and Accaino (2002), *Marine Geology*, 164, 13-27
- Tinivella et al. (2002), *Marine Geophysical Researches*, 23, 109-123

# **Session 7**

---

## **SEDIMENTARY PROCESSES**





**RARE-EARTH ELEMENTS SIGNATURE OF PATAGONIAN MARINE SEDIMENTS PHOSPHATES, ARGENTINA**

7-01

Castro L.N., Fazio A.M.

*Departamento de Geología, Facultad de Ciencias Exactas y Naturales, Universidad de Buenos Aires, Ciudad Universitaria Pab 2. Piso 1. 1428. Buenos Aires, Argentina.  
e-mail: lilianacastro@fibertel.com.ar; amfazio@gl.fcen.uba.ar*

**Summary**

Two groups of phosphatic samples have been analysed for rare earth elements in order to sustain paleoenvironmental interpretation provided by previous sedimentological and paleontological studies. The first group comes from the Late Oligocene-Early Miocene marine Gaiman Formation (Chubut) which deposited in a shallow, storm-marine environment and the second group of samples comes from Maastrichtian-Paleocene Lefipan Formation, both in Chubut province. A significant difference in REE pattern not only reflects their depositional environment, but also the imprint of the diagenesis.

**Abstract text**

Systematic prospecting of Patagonia upper Cretaceous and Tertiary marine levels (UBACYT Ex 081) allow to detect different phosphatic anomalies in several localities. The main are linked to Gaiman Fm (Late Oligocene-Early Miocene), and to Lefipan Fm (Maastrichtian-Paleocene) both located in Chubut province, center Patagonia. Samples have been analysed for rare earth elements (Rees) in order to sustain paleoenvironmental interpretation from former sedimentological and paleontological work. Rees geochemistry of phosphorites provides an interesting tool to understand the depositional environment, but it is necessary to take care if the diagenesis could modify the original pattern. Rees are a geochemically coherent group of elements in which the ionic radii decrease from the lightest element La to the heaviest element Lu. On account of this “lanthanide contraction”, the relative abundance of Rees in different rock types and water display characteristic signatures which are often used in aquatic and solid phase geochemistry. The Rees elements in phosphorites may be derived either directly or indirectly from seawater, due to remobilization from different sources, such as clastic material, ferromanganese oxides or biological debris or the combination of them (Elderfield et al., 1981, and McArthur and Walsh, 1984). In spite of the low Rees seawater contents (less than 100 ppm of total Rees, figs. 1 and 2), the long residence time of the sediments in the oceanic environment promote the active ionic exchange and then their REE enrichment. As a result, and according to the type of deposits and the environmental setting, different Rees patterns are observed. A typical phosphorite is characterized by “seawater pattern” (Jarvis et al, 1994) which is strongly depleted in Ce and enrichment in heavy Rees (HRees), compared to a flat pattern characteristic of shales.

**a) Gaiman Formation**

Gaiman Formation consists of a coarsening upwards succession of mudstones; fine tuffs, tuffs, tuffaceous sandstones and coquinas (Scasso & Castro, 1999). Two types of phosphatic levels have been recognized with reworked and unreworked concretions (Scasso & Castro, 1999). Rees elements analyses from these phosphate concretions exhibit a sigmoid design, meanwhile the host shale has a typical flat pattern. Gaiman phosphatic concretions show 915 ppm Rees and 500 ppm in Y mean content duplicating the average content of worldwide phosphorites (462 ppm and 275 ppm). The Rees pattern in both shows a slight depletion in light Rees (LRees) with weak Ce anomaly (-0.16 to -0.09) and an enrichment in HRees in comparison to the “average shale”, (fig.1). The wavy pattern in the samples could be interpreted that a flat pattern has been slightly modified by local terrigenous influences according to Kidder et al. (2003). On the other hand, the HRees content could represent the primary seawater pattern and not a latter enrichment.

The weak negative cerium depletions in both reworked and unreworked concretions suggest exposure to oxygenated waters, probably during early diagenesis and winnowing. Rees distribution is similar to the nodules in upwelling areas like the Peruvian shelf (Pleistocene-Holocene). Ce/La; Y/La; Th/U and V/Cr ratios also suggest upwelling processes for Gaiman deposits. However, the paleogeographic location of the Gaiman area, far from the shelf edge, is not compatible with an upwelling zone.

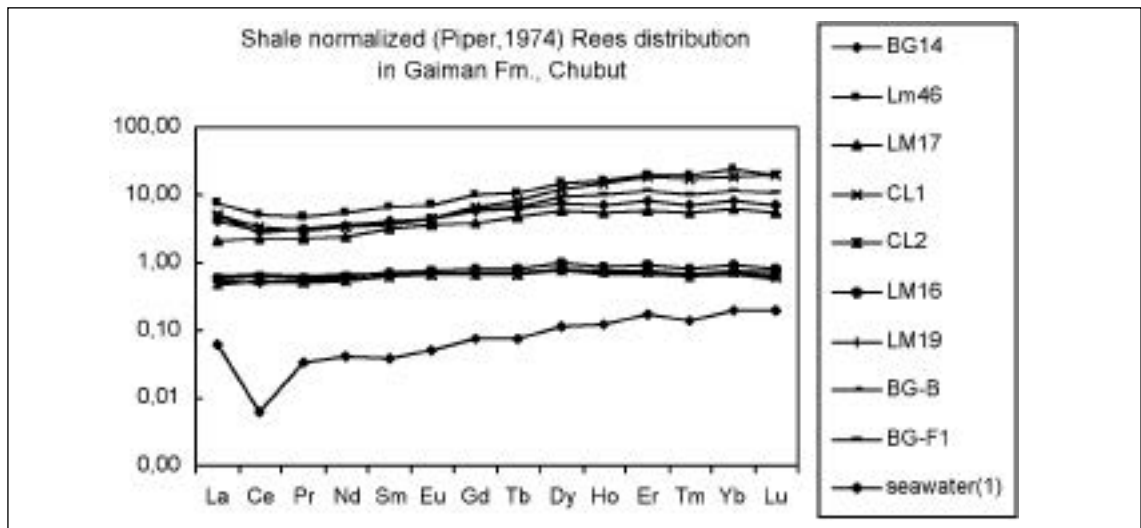


Fig 1 - (') Atlantic seawater data from German et al (1995).

Instead, cold water flooding the continental shelf and mixing with warmer surficial water could account for the high productivity and phosphogenesis. REE distribution pattern could be attributed to shallow marine inner shelf environment which corroborate the hypothesis of shallow, storm-marine environment, suggested by sedimentological and paleontological evidences for Gaiman Fm. (Scasso & Castro, 1999)

## b) Lefipan Formation

The second group of samples come from Lefipan Formation Maastrichian-Paleocene which is constituted by mudstones and siltstones interbedded with cross-bedded sandstones and coquinas. Lefipan concretions show a depletion by up to one order of magnitude in both the LREEs and HREEs compared to the middle REEs (MREEs), producing a concave-down pattern centered in Eu and Dy (Fig. 2). Lefipan phosphatic concretions show 1810 ppm REEs and 650 ppm in Y mean content duplicating the average content of Gaiman phosphates. Most patterns show either MREEs and Ce enrichment, and just one sample has a weak, negative cerium anomaly typical of seawater pattern.

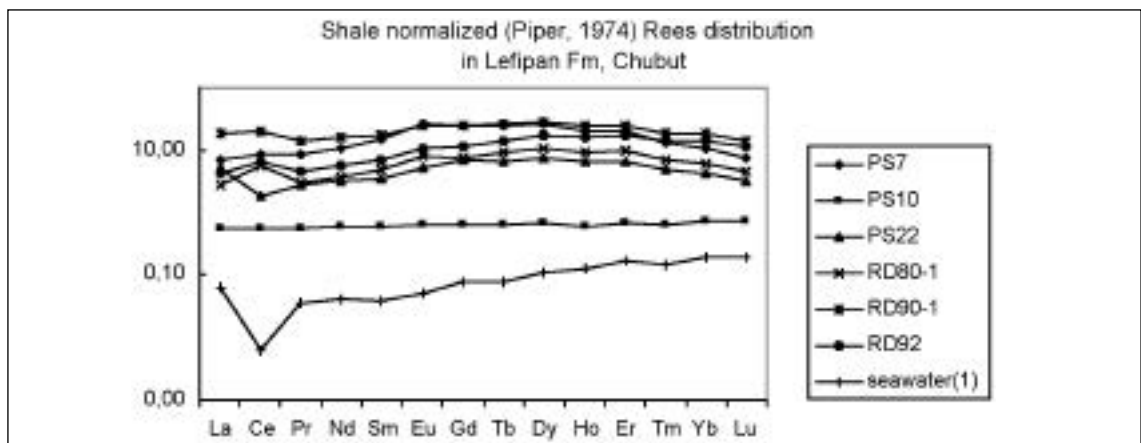


Fig 2 - (') Atlantic seawater data from German et al (1995).

The origin of the MREEs-enriched pattern probably represents differential accumulation of MREEs during phosphate lithification and its host shale. Post-depositional alteration tends to increase REE contents, reverse the Ce depletion and can also concentrate preferentially the MREEs, (Reynard, 1999).

The presence of a distinct negative Ce anomaly reflects an important characteristic feature of seawater. In modern seawater, the progressive Ce anomaly with depth is attributed to the scavenging of Ce due to oxidation to Ce 4+ and its incorporation into Mn and/or Fe oxyhydrides (Shaw & Wasserburg, 1985) or to its enrichment in authigenic minerals. The extent of Ce depletion in seawater does not solely depend on the oxidation potential (German & Elderfield, 1990), but also on microbial activity that catalyses the oxidation of Ce III (Moffett, 1990), as well as the pH (Shield et al., 2001), depth (Piepgras and Jacobsen, 1992), and age of the seawater (German & Elderfield, 1990). In our case, PS22 shows a negative Ce anomaly (-0,44) pointing to a relatively deeper water depositional environment, while other variables (positive Ce anomalies) may broadly reflect local bottom-water redox conditions. The higher Fe oxide contents in Lefipan compared to Gaiman's ones also suggest that an induced flocculation has taken place as a result of water mixing zones. We interpret the Rees behavior in Lefipan concretions as linked to estuarine coastal setting, as also suggested by Olivero and Medina, (1993) who interpreted that depositional environmental range from estuarine barrier island (lower part) to deltaic (upper part). This original pattern was modified by early diagenesis which caused the Rees remobilization and later enrichment given the bell- shape pattern.

Lefipan concretions (Maastrichtian-Paleocene) have higher Rees total contents than Gaiman ones (Late Oligocene-Early Miocene), corroborating the results given by several authors (Jarvis et al. 1994, Mc Arthur and Walsh, 1984) who pointed out that Rees contents increased with the age.

## REFERENCES

- Altschuler Z.S. et al. (1967), US Geological Survey, Professional Paper 575-B, 1,9.
- Castro L. et al. (2000), 31 International Geological Congress. Rio de Janeiro. Simposio Sedimentology 3.5.Ind.231.
- Elderfield H. & Greaves M.J. (1982), Nature, 296, 214-219.
- German C.R. & Elderfield H. (1990), Paleoceanography 5, 823-833.
- German C.R. et al. (1995), Geochimica et Cosmochimica Acta 59(8), 1551-1558
- Jarvis I. et al. (1994), Eclogae Geologicae Helveticae Journal of Swiss Geologicae Society. 87(3), 643-700.
- Kidder D.L. et al. (2003), Chemical Geology, Chemical Geology, 198, 335-353.
- McArthur J.M. & Walsh J.N. (1984), Chemical Geology, 47, 191-220.
- Moffett, (1990), Nature 345, 421-423.
- Olivero E.B. & Medina F. (1993), Asociación Geológica Argentina Revista 48(2), 105-106.
- Piepgras D. J. & Jacobsen, S.B. (1992) Geochimica et Cosmochimica Acta, 56, 1851-1862.
- Piper D.Z. (1974), Chemical Geology, 14, 285-304.
- Scasso, R.A. & Castro, L. N. (1999), Journal of South America Earth Science, 12, 471-487. Elsevier.
- Reynard. B. et al. (1999) Chemical geology 155, 233-241
- Shaw & Wasserburg, (1985) Geochimica et Cosmochimica Acta 49, 503-518.
- Shields G. & Stille P. (2001) Chemical Geology 175, 29-48.

## GEOPHYSICAL RECONSTRUCTION OF THE SEDIMENTARY INFILL OF LAGO ICALMA (39°S, CHILEAN LAKE DISTRICT) SINCE THE LAST DEGLACIATION 7-02

F. Charlet(\*), C. Marchand(\*), S. Bertrand(\*\*), E. Chapron(\*\*\*), M. Pino(\*\*\*\*), R. Urrutia(\*\*\*\*\*), M. De Batist(\*)

(\*) *Renard Centre of Marine Geology, University of Gent, Belgium.*

(\*\*) *URAP, University of Liège, Belgium.*

(\*\*\*) *Geological Institute, ETH, Zuerich, Switzerland.*

(\*\*\*\*) *Universidad Austral de Chile, Valdivia.*

(\*\*\*\*\*) *EULA, Universidad de Concepción, Chile.*

### Summary

The sedimentary infill of Lago Icalma (Southern Chile), encompassing a part of the last glacial and the post-glacial episode, was investigated by high-resolution (sparker) and very high-resolution (3.5 kHz) reflection seismics. A seismostratigraphical approach led to the subdivision of the approx. 115 m-thick sedimentary sequence into four units. The presence of a major erosional unconformity within the infill and a repetition of the sub-glacial to ice-proximal facies (three times) near the outflow of the

*Rio Rucanuco* suggest that the area may have witnessed two glacial readvances during the last deglaciation. The evolution of depocentres of these different units allows us to better understand the related sedimentary processes.

The high-resolution seismic data and physical properties measured on two 8 m-long piston cores show a very important proportion of instantaneous deposits (~23%) within the uppermost units (4c). The strong seismo-tectonic activity is characterised, in the lacustrine infill of the main basin, by mass-wasting deposits located at the foot of basin slopes. A second type of mass-wasting deposit, triggered by heavy rain falls, occurs at the vicinity of incised canyons of the northwestern flank. Thus, major destabilization events and strong volcanic activity are the main forcing factors controlling sedimentation since the last 8000 yr cal. BP.

### Abstract text

Most studies of volcanism, seismicity, deglaciation and climate change in the Chilean Lake District have up to now focused essentially on soils, moraines, peat bogs, ponds, small peri-glacial lakes and oceanic sediments, but their record enclosed in the numerous large lakes that are so characteristic of the area is yet to be explored. Nevertheless, several multidisciplinary investigations of lacustrine records in the world have shown that such records can yield very detailed paleoenvironmental reconstructions: e.g. Lake Annecy (Oldfield et al., 2001), Lake Cardiel (Markgraf et al., 2003), Lake Miscardi (Ariztegui et al., 2001), and Lake Titicaca (d'Agostino et al., 2002). With this work, we want to present the first results of a seismic investigation of *Lago Icalma*, in an attempt to examine the potential of its sedimentary infill to contain a paleoclimatic record, and also to quantify various forcing factors (volcanism, seismicity), which left their imprint on the lacustrine infill.

*Lago Icalma* is located in the North of the Lake District area (*Araucania* region, *Cordillera de los Andes*; 1140 m), in the upper part of the *Bio-Bio* river watershed (Fig. 1). Together, with nearby *Lago Galletue*, it forms the source of the *Bio-Bio River*. *Lago Icalma* is not a piedmont lake like most other lakes of the Lake District. It is formed by two connected flat basins: *Laguna Chica*, on its western part, and *Lago Icalma s.s.* on its eastern part. These are separated by two glacial rock bars (Fig. 2). This relatively small lake can be considered as the infill of an overdeepened glacial valley. The main inflowing rivers are *Rio Huillinco*, entering the lake from the main glacial valley, and *Rio Icalma*, forming the main delta. The lake border at its outlet coincides with a frontal moraine, but the lake is not really moraine-dammed. The successive frontal moraines are cut by the outflowing river, *Rio Rucanuco*.

*Lago Icalma* is surrounded by several active volcanoes (Llaima, Lonquimay, Navidad, calderas Sollipulli) and calderas of Plio-Pleistocene age (Pino Hachado and Meseta del Arco). Its watershed is dominated by a thick (~ 4 to 6 m) soft post-glacial sediment cover, composed of volcanic amorphous material (glass and allophane), interrupted by two important pumice layers (Mardones et al., 1993, Bertrand et al., submitted). The upper pumice layer, dated 3045 yr cal. BP, was also found in the two piston cores (Fig. 4), and can be considered as an excellent spatial isochrone.

*Lago Icalma* is also located in a tectonically active region (Suarez & Emparan, 1997). Active basement faults, recognised along the lake shores, continue into the main lake basin and into the *Laguna Chica* (Fig. 2) and have locally deformed the sedimentary infill. The valley and the lake seem to follow the fault line which has allowed the diffidence of a glacial tongue from the ice flows in the *Icalma* and *Huillinco* valleys, but also from the *Tacura* valley (Mardones and al., 1993). Moreover, *Lago Icalma* is only 20 km from the North-South Aluminé Fault, which more or less coincides with the Chile-Argentina border, and represents an important structure that shapes the morphology of the entire area.

During the austral summer 2001/2002, about 105 km of high-resolution seismic data were recorded using high-resolution (RCMG's "Centipede" comb-type sparker) and very high-resolution seismic sources (3.5 kHz) (Charlet et al., 2003). The sparker signal penetrated the entire sediment fill with a resolution of about 50 cm in the upper layers. The 3.5 kHz source penetrated the upper 15 m with a very-high resolution of about 20 cm.

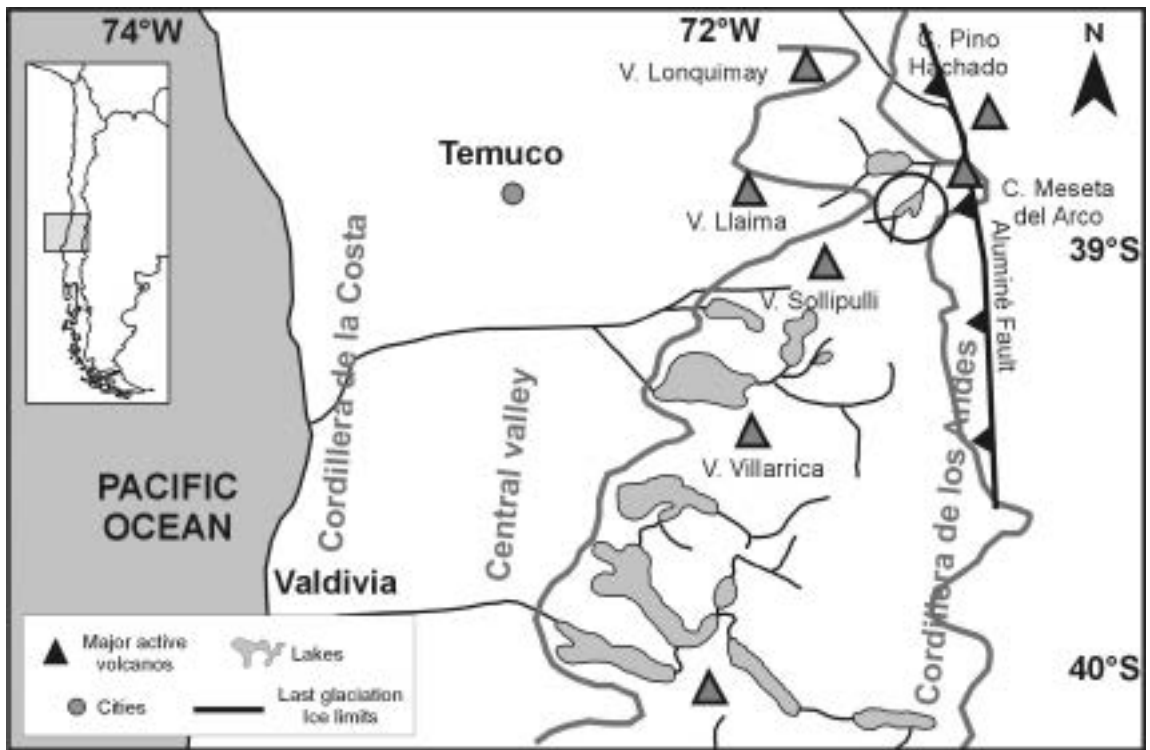


Fig.1 - General location of Lago Icalma in the northern part of the Lake District. The map also shows the maximum extension of the Patagonian Ice cap during the Last Glacial Maximum (LGM) (29-16 ka, Denton et al., 1999).

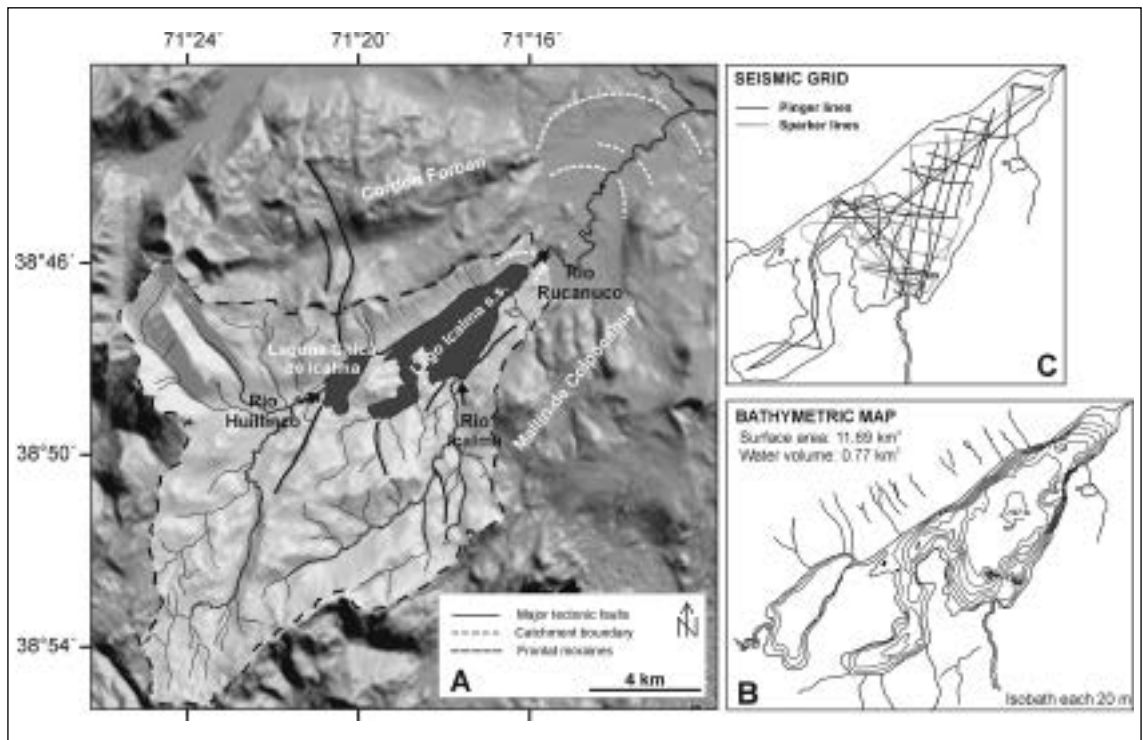


Fig. 2 - A) Detailed setting of Lago Icalma and its surroundings showing the glacial imprint (moraines, glacial-rock bars) on the geomorphology. B) Bathymetric map based on integration of seismic data and published data for *Laguna Chica de Icalma* (Parra et al., 1993). C) Seismic grids (sparker and 3.5 kHz) used for mapping.

The infill of Icalma basin is fully imaged by the sparker data and consists of four main seismic units separated by unconformities (Fig. 3). The succession resembles the typical infill of other glacial lakes (Van Rensbergen et al., 1998). The units are named unit 1 to unit 4 from the bottom to the top:

**Unit 1** is an assemblage of chaotic to irregularly stratified seismic sub-facies occurring at the base of the basin fill (Fig. 3). This unit reaches a maximum thickness of 15 ms TWT. As a whole, Unit 1 is interpreted as glacially derived sediment (glacial moraine), deposited on the onset of the deglaciation of the basin.

This unit has been identified at different levels within the sedimentary fill (Unit 1a, Unit 1b & Unit 1c), which suggest that the basin has experienced glacial conditions during three successive times. The spatial distribution of these units shows depocentres toward the lake outflow (*Rio Rucanuco*).

**Unit 2** is a mostly reflection-free basin fill, characterised by low-amplitude reflectors. It represents the most voluminous unit with a maximum thickness of 65 ms TWT. It can be interpreted as glacio-lacustrine deposits (sub- to pro-glacial). As Unit 1, Unit 2 has been identified at different levels within the sedimentary infill (Units 2a, 2b & 2c).

The unusual distribution and repetition of units 1 & 2 suggests two main pulses of the glacier since the last deglaciation.

**Unit 3c** as a whole is an onlapping basin fill with parallel continuous reflections, interpreted as the result of lacustrine sedimentation dominated by strong sediment-charged underflows originating from the lake tributaries (large floods). It reaches a maximum thickness of 47 ms TWT.

**Unit 4c** is the topmost unit, characterised by parallel, sub-horizontal reflections concordant with the underlying deposits. It reaches a maximum thickness of ~40 ms TWT. Unit 4c is composed of a depocentre in the deepest part of the lake, corresponding to the “underflow” area. Another important depocentre occurs on the north-western elevated platform and possibly represents the “interflow” deposits, which are deflected to the left as a result of the Earth’s rotation (Van Rensbergen et al., 1999).

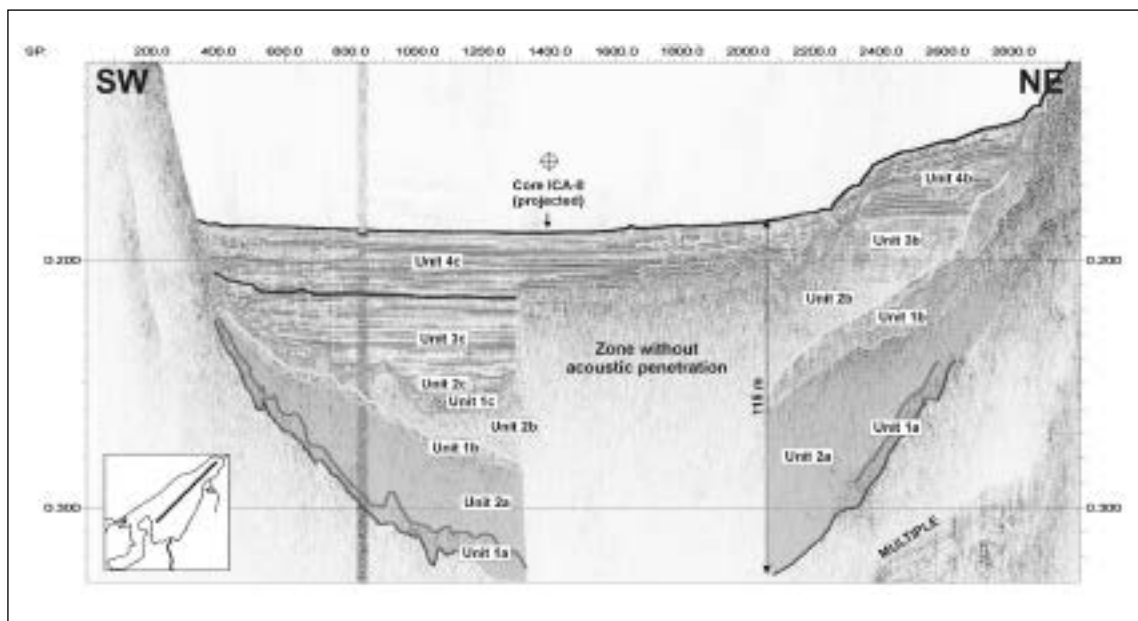


Fig. 3 - Longitudinal sparker profile of Lago Icalma (ical01) showing the 115 m-thick sedimentary infill and the seismic units together with a zone without acoustic penetration (gas).

Based on the very high-resolution seismic data and on the physical property measurements, the upper part of unit 4c can be further subdivided into four main sub-units (SU 4c1, 4c2, 4c3 and 4c4) (Fig. 4). These sub-units are composed of 3 main facies types:

- 1) High amplitude and homogenous chaotic facies: depocentres are located at the vicinity of the canyons, along the steep western slope or at the foothill of the main basin slopes. This facies is interpreted as accumulation of destabilized sediment, triggered by heavy rains falls or seismo-tectonic events.
- 2) High amplitude and irregular stratified facies: depocentres are concentrated in the deepest part of the lake, close to the delta. These deposits are interpreted as flood deposits resulting from underflows coming from the delta, during periods of strong precipitation (Van Rensbergen et al. 1999, Chapron et al., in review).
- 3) Medium to high-amplitude reflectors constituting a stratified facies (forms essentially SU 4c4): depocentres are located on the western part of the lake and on the small high separating the two connected basins. This seismic facies drapes the morphology and can be considered as interflow deposits.

The contemporaneous sedimentation also shows a strong imprint of volcanic activity, identified by very high peaks of magnetic susceptibility (Fig. 4). The many active volcanoes surrounding Lago Icalma hamper the identification of the exact volcanic source for each volcanic deposit identified with the core.

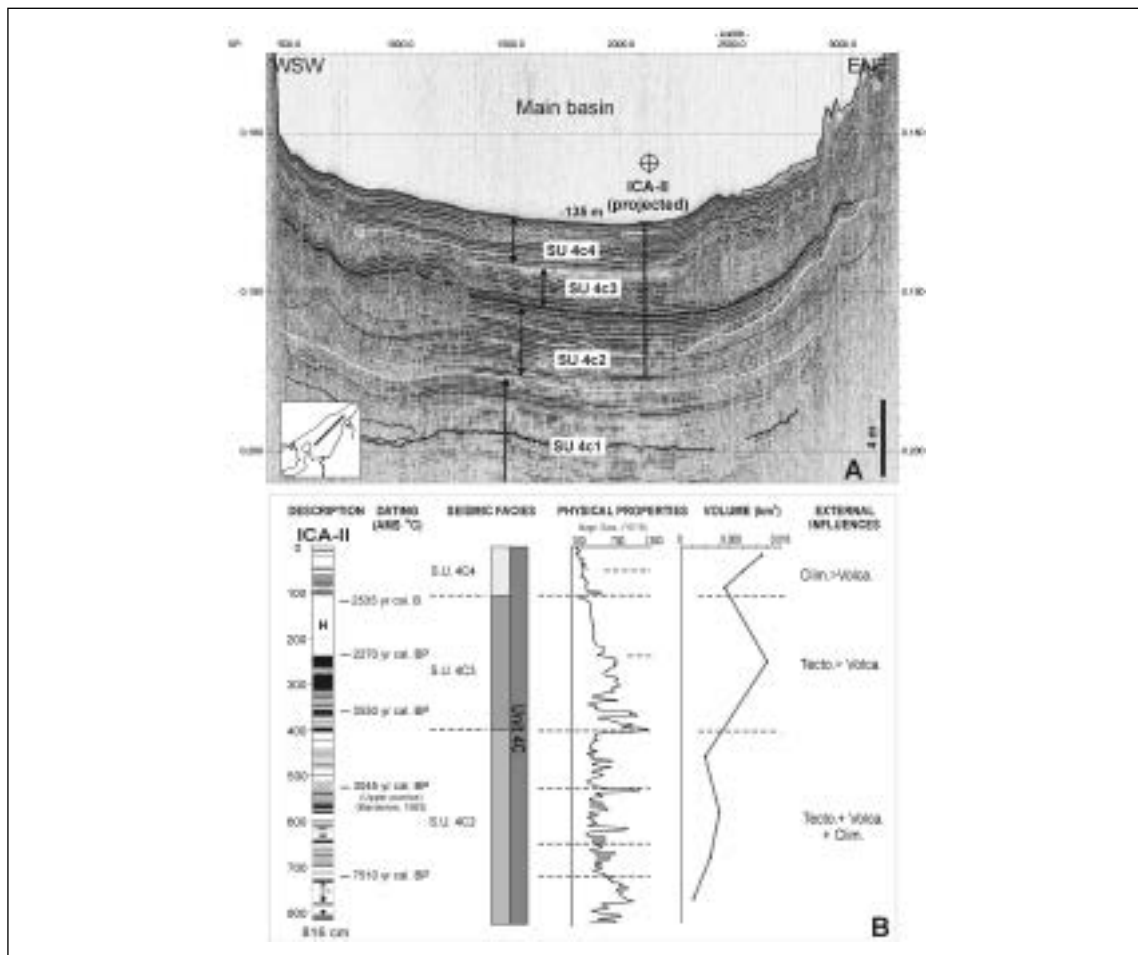


Fig. 4 - A) Very high-resolution pingar profile (ical09) showing the position of piston core ICA-II, the upper unit 4c and its further sub-divisions, as defined respectively from the sparker and pingar data. B) Core description,  $^{14}\text{C}$  AMS dating and magnetic susceptibility measurements allow the subdivision of these units into several sub-units affected by different depositional processes.

Thus, based on sparker seismic data, the successive facies are interpreted as the deglaciation evolution in the drainage basin since the LGM. A further subdivision of the interglacial fill, which could be achieved thanks to the 3.5 kHz seismic data, reveal a strong combined tectonic/volcanic imprint, leaving few indices of paleoclimatic fluctuations. However, the clastic input seems to fluctuate significantly during the middle and upper Holocene.

## REFERENCES

- Ariztegui D. et al. (2001) In "Interhemispheric Climate Linkages", edited by V. Markgraf, chap. 14: 227-240.
- Bertrand S. & Fagel N. (submitted) *Revista Geologica de Chile*.
- Chapron E. et al. (in review). *Terra Nova*.
- Charlet F. et al. (2003) 10° Congreso Geológico 2003. Abstract book. 10 p.
- D'Agostino K. et al. (2002) *Palaeogeography, Palaeoclimatology, Palaeoecology*, 179, 97-111.
- Denton G.H. et al. (1999) *Geographica Annaler*, 81 A, 2 : 107-153.
- Mardones M. et al. (1993) *Monografias científicas EULA ed. Universidad de Concepción, Chile*, 6, 92 p.
- Markgraf V. et al. (2003) *The Holocene*, 13, 4, 581-591.
- Oldfield F. & Berthier F. (2001) *Journal of paleolimnology*, 133-135.
- Parra O. et al. (1993) In « *Monografias científicas EULA ed. Universidad de Concepción, Chile*, 12: 161-188.
- Suárez M. & Emparan C. (1997) *Mapa Geologica de Chile*, 105 p.
- Van Rensbergen P. et al. (1998) *Sedimentary Geology*, 117, 71-96.
- Van Rensbergen P. et al. (1999) *Sedimentary Geology*, 128, 99-129.

## HOLOCENE CARBONATE SEDIMENTATION IN THE NORTH WESTERN SECTOR OF THE MAGELLAN STRAIT: TEXTURAL, GEOCHEMICAL AND MICROPALAEONTOLOGICAL PRELIMINARY RESULTS

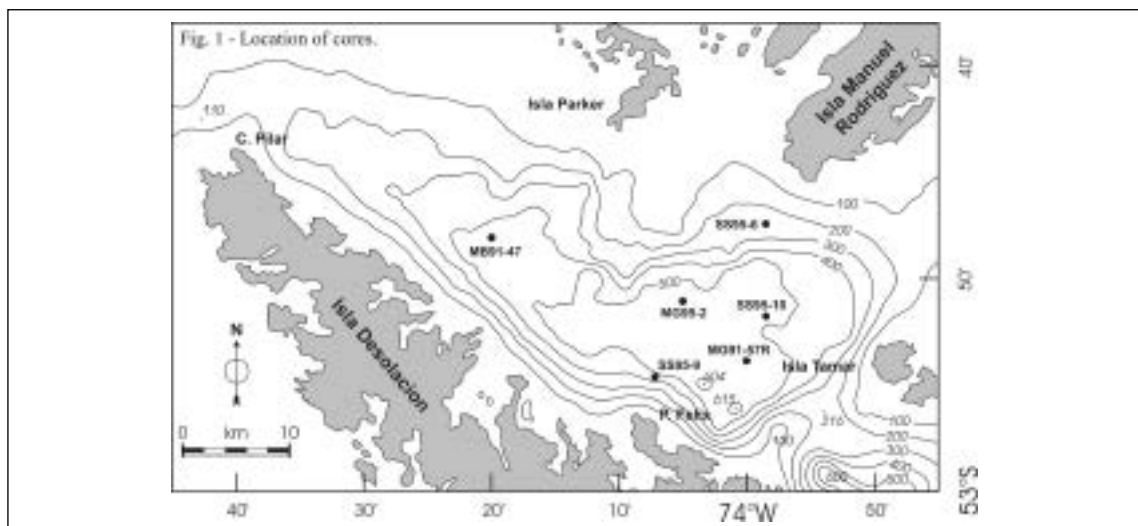
7-03

Ester Colizza<sup>a</sup>, Filomena Ornella Amore<sup>b</sup>, Simona Morabito<sup>b</sup>, Cristinamaria Salvi<sup>a</sup>, Roberto Bartole<sup>a</sup>

*a Dipartimento di Scienze Geologiche, Ambientali e Marine, Università di Trieste, Via E.Weiss 2, 34127 Trieste - Italy*

*b Dipartimento di Studi Geologici ed Ambientali, Università degli Studi del Sannio, Via Port'Arsa 11, 82100 Benevento - Italy*

In this paper we propose textural, geochemical and micropaleontological preliminary results on six gravity cores collected in the North Western basin of the Magellan Strait (Fig. 1) during 3 oceanographic cruises in 1991 (MB91-47; MB91-57R) and 1995 (MG95-2; SS95-6; SS95-9; SS95-10). These cruises were carried out in the framework of the Programma Nazionale di Ricerche in Antartide (P.N.R.A.).





Seismic characteristics of this basin are reported in Bartole et al. (this volume). This sector of the Strait is now characterized by a biogenic carbonate sedimentation (Brambati et al., 1994). Previous studies (Colizza & Salvi 2000; Melis et al. 2000; Amore et al. 2003) have demonstrated that the last deglaciation in the Western sector was not synchronous. The present paper is devoted to focus on palaeoenvironmental and palaeoceanographic evolution of this sector of the Strait during late-Pleistocene and Holocene period and the related changes which occurred in the nannofossils composition.

Core sample	Sample interval (cm)	Uncorrected age (B.P.)
MB91-47	12-14	2360±50
MB91-47	273-276	17360±120
MB91-47	537-539	21680±170
MB91-57R	32-36	2170±50
MB91-57R	140-141	6465±60
MG95-2	187-188	2900±30
SS95-6	28-29	3410±40
SS95-9	109-110	3400±40
SS95-10	0-1	690±30
SS95-10	140-141	5450±50
SS95-10	471	10980±60

Table 1 - Radiocarbon ages for the six studies cores.

Grain-size analyses were obtained by Micromeritics 5000 ET Sedigraph (<62  $\mu\text{m}$  fraction) and wet sieving (>62  $\mu\text{m}$  fraction). Carbonate and Total Organic Carbon (TOC) were determined using a Dietrich-Fruhling calcimeter and the CHN Perkin Elmer Elemental Analyzer respectively. Sediment samples for nannofossils analysis, taken every 2 cm intervals, were analysed using a polarised light microscope with magnification of  $\times 1250$  and Scanning Electron Microscope (SEM). Some levels were radiocarbon dated using an Accelerator Mass Spectrometry (AMS) (Table 1). All the cores are mainly characterised by clayey silt (Fig. 2); the sand content generally is less than 10% in cores MB91-57R, SS95-9 and 10 and at the bottom of core SS95-6. Core MG95-2 and the topmost portion of core SS95-6 present a sand content between 20-34% and 38-40% respectively. Core MB91-47, collected near the sill which draws Pacific Ocean water into the Strait, shows the same content in sand and silt fractions in the topmost part (17 cm), and sand percentage of 2-3%, with moderate and irregular enrichment, toward the bottom. The sand for all the cores is characterised by abundant, well preserved biogenic fraction (mainly planktonic and benthic foraminifers, ostracods, bivalve, bryozoan fragments). The first 17 cm of core MB91-47 are also mainly characterised by a bryozoan fragments, while till the bottom a silico-clastic component prevails.

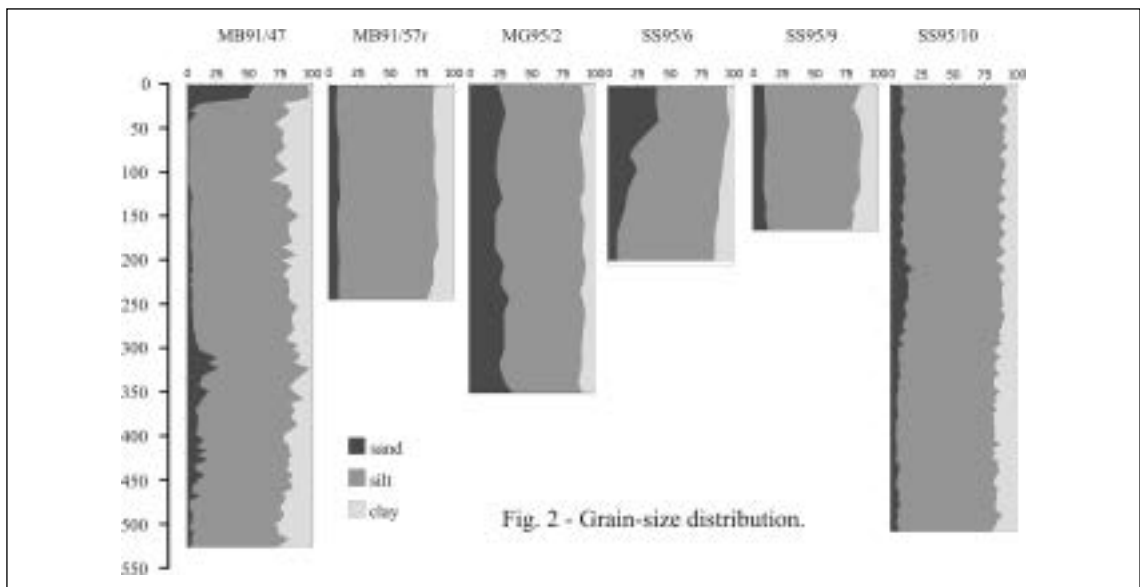
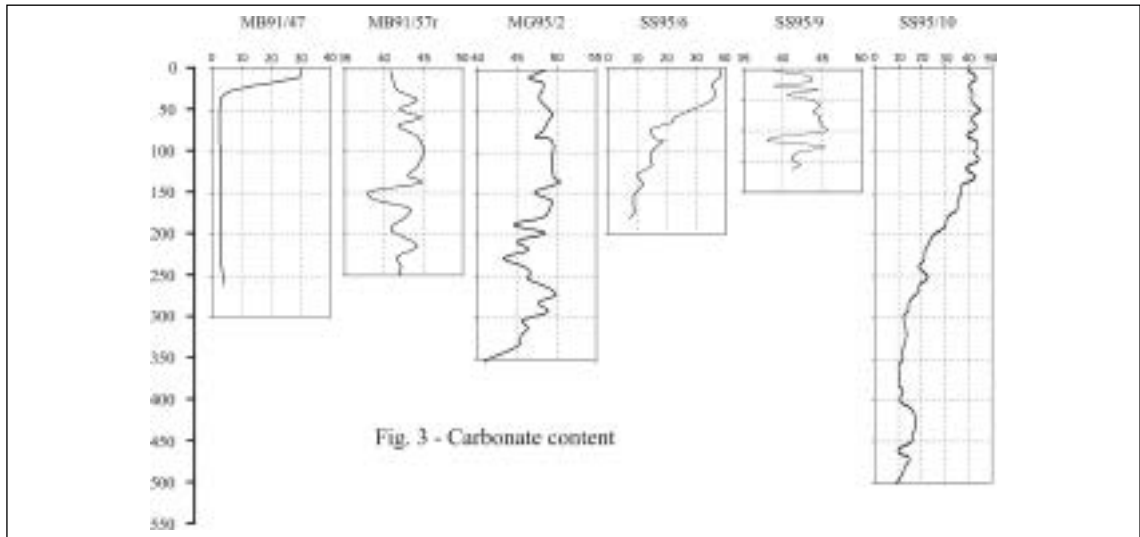


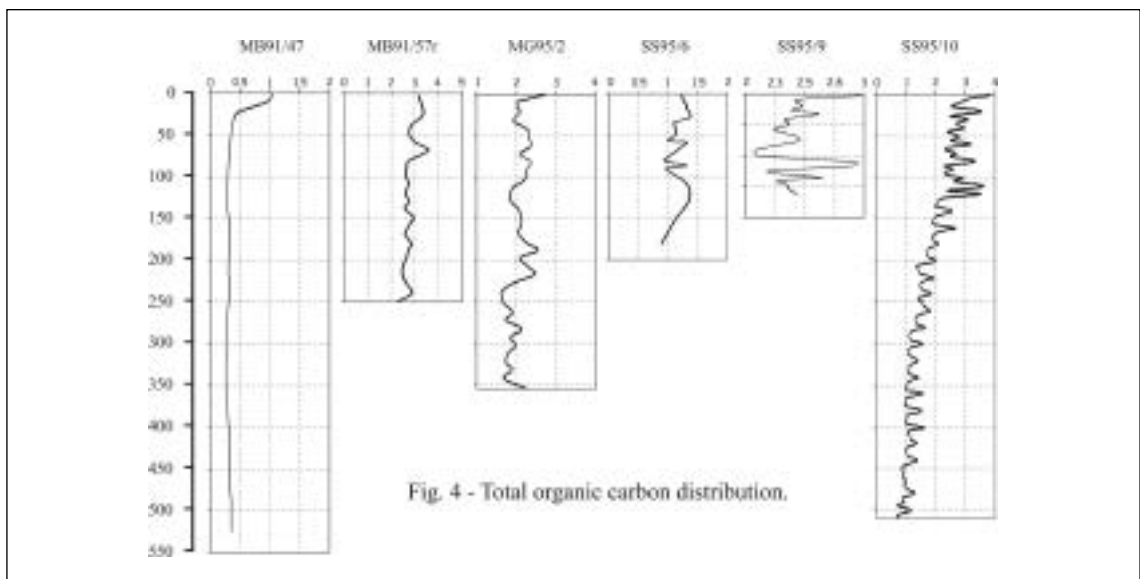
Fig. 2 - Grain-size distribution.

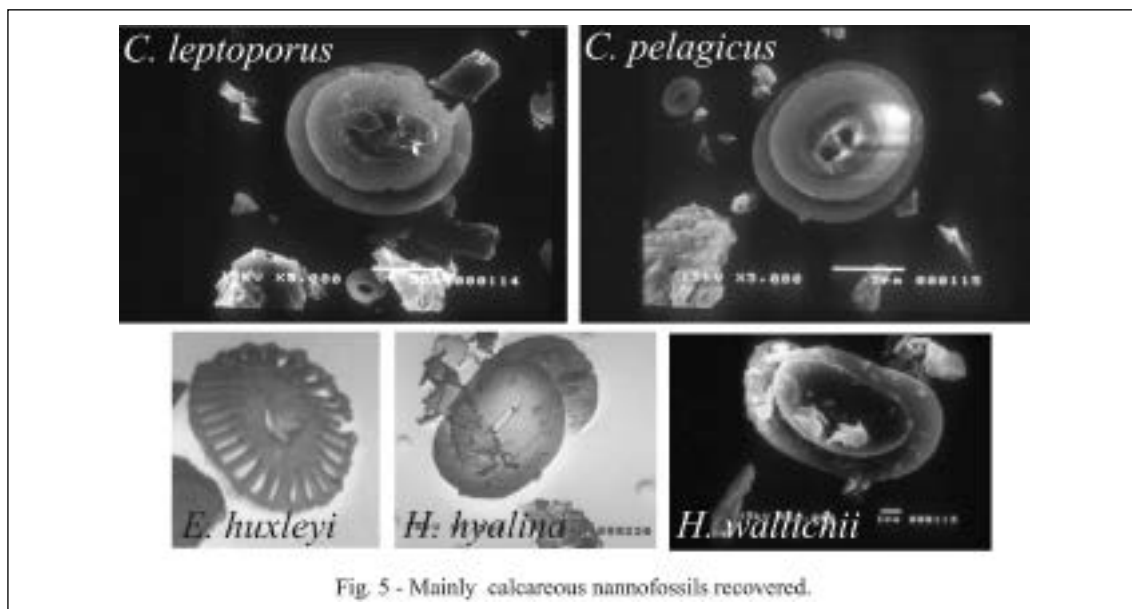
Cores MB91-57R, MG95-2 and SS95-9 show carbonate content (Fig. 3) of 38-49%. The same values are present in cores SS95-6 and 10 between 0-40 cm and 0-160 cm respectively; towards the bottom the  $\text{CaCO}_3$  content decrease (7-9%).  $\text{CaCO}_3$  content in core MB91-47 is quite high in the topmost part of the core (12-29%) and decreases near the bottom (2-4%).



TOC (Fig. 4) presents a similar  $\text{CaCO}_3$  trend: higher values are observed in MB91-57R, MG95-2 SS95-9 sediment cores (mean value 2.82  $\pm$  0.35%; 2.06  $\pm$  0.29%; 9.48  $\pm$  0.27% respectively) and in the topmost part of SS95-10 (mean content 2.93  $\pm$  0.52%). Toward the bottom the carbon content decreases (mean value 1.37  $\pm$  0.35%). TOC mean value is 1.20  $\pm$  0.15% in SS95-6. Core MB91-47 shows high values in the carbonate portion (about 1%), while the TOC content (mean= 0.40  $\pm$  0.23%) decrease in the silico-clastic interval.

A preliminary analysis of calcareous nannofossils assemblages (Fig. 5) in late Quaternary sediments was carried out on cores MB91-57R, SS95-10, SS95-6, SS95-9, and MG95-2. The preservation of nannofossils is always quite good, even if specimens with mechanical breakage, dissolution or calcite overgrowth were observed. The most abundant coccolithophores species were *Gephyrocapsa caribbeanica*, *G. muelleriae* and *Emiliania huxleyi*. The taxa of the genus *Gephyrocapsa* were identified following the taxonomic concept of Matsuoka and Okada (1989) and Findlay and Flores (2000).





*Calcidiscus leptoporus*, *Coccolithus pelagicus*, *Helicosphaera carteri* var. *carteri*, *Helicosphaera carteri* var. *hyalina* and *Helicosphaera carteri* var. *wallichii* are subordinate in the assemblages. Forms of *C. pelagicus* with a large central opening and displaying a bar were observed. *C. pelagicus* is regarded as cold water indicator by McIntyre and Bè (1967). However other authors (Cachão & Moita, 2000; Fenner and Di Stefano 2004) retain that this species is also influenced by nutrient availability. *G. muelleriae* is considered a cold species by Jordan et al. (1996) and increases of this species during the glacial periods are observed by Flores et al. (1999). A preference for temperate/cold water is attributed by Violanti et al. (1991) to *G. caribbeanica*. Most significant peaks of *H. carteri* during the glacial periods are observed by Flores et al. (1999). Roth (1994) consider it a warm water species. A straight relationship between species occurrence and nutrient availability is also suggested by Hiramatsu and De Deckker (1997). Radiocarbon data indicate that the biogenic carbonate fraction is of Holocene period, while silico-clastic sediment is late-Pleistocene. The Holocene sedimentation is characterised by an increase of the carbonate component (>10%) with values >30% from 6000 yr B.P. to Present. The carbonate sedimentation is related to a climatic improvement and to a release of the Pacific water inside the Strait. In fact during the Last Glacial Maximum an extensive ice cap persisted on the western branch of the Strait probably occupying the Pacific entrance and limiting the access to Pacific waters (Bartole et al., 2000; Colizza & Salvi, 2000).

## REFERENCES

- Amore, F.O., Caffau, M., Colizza, E., Salvi, G., Tsakiridau, E., 2003. Holocene calcareous nannofossils and planktonic foraminifera assemblages in the Western Magellan Strait (Chile). Courier Forschungsintitut Senckenberg, Frankfurt.
- Cachao, M., Moita M.T., 2000. *Coccolithus pelagicus*, as a productivity proxy related to moderate fronts off Western Iberia. Mar. Micropaleont., 39, 131-155.
- Bartole R., Colautti W., Colizza E., Salvi C. & Tosoratti F (this volume) – Seismostratigraphy and recent sedimentary evolution of an asymmetric extensional basin of the Western arm of the Magallanes-Fagniano Transform system.
- Bartole R., Colizza E., De Muro S. & Collutti W., 2000 – The Pacific entrance of the Magellan Strait: first result of seismic and sampling survey. Terra Antarctica reports, 4: 81-94.
- Brambati A., Colizza E., Fontolan G., Marinoni L., Setti M., Soggetti F., 1994. From terrigenous to detrital carbonate sedimentation in the Strait of Magellan, Beagle Channel, and adjacent areas, Chile-Argentina (52°-56° lat. Sud). Abstract in International Association of Sedimentology, Ischia, 76-78.
- Colizza, E., Salvi, G., 2000. Sedimentological Analyses of three Cores Collected in the Pacific Sector of the Magellan Strait. Terra Antarctica Reports, 4, 69-74.
- Fenner J., Di Stefano A., 2004. Late Quaternary oceanic fronts along Chatham Rise indicated by phytoplankton assemblages, and refined calcareous nannofossil stratigraphy for the mid-latitude SW Pacific. Marine Geology, 205, 59-86
- Findlay C.S., Flores, J.A., 2000. Subtropical Front fluctuations south of Australia (49°09'S, 146°17'E) for the last 130 ka years based on calcareous nannoplankton. Mar. Micropaleontol. 40, pp. 403-416.
- Flores, J.A., Gersonde, R., Sierro F. J., 1999. Pleistocene fluctuations in the Agulhas Current Retroflexion based on the calcareous plankton record. Mar. Micropaleontol. 37, 1-22.

- Hiramatsu C., DeDecker, P., 1997. The late Quaternary calcareous nannoplankton assemblages from three cores from the Tasman Sea. *Palaeogeogr. Palaeoclimatol. Palaeoecol.*, 131, 391–412.
- Jordan R.W., Zhao, M., Eglinton, G., Weaver, P.P.E., 1996. Coccolith and alkenone stratigraphy at a NW Africa upwelling site (ODP 658C) over the last 130,000 years. In: Mokuilevsky, A., Whatley, R. (Eds.), *Microfossils and Oceanic Environments*. University of Wales Aberystwyth Press, 11–130.
- Matsuoka H., Okada, H., 1989. Quantitative analysis of Quaternary nannoplankton in the subtropical northwestern Pacific Ocean. *Mar. Micropaleontol.*, 14, 97–117.
- McIntire, A., Bé, A.W.H., 1967. Modern Coccolithophoridae of Atlantic Ocean-I. Placoliths and Cyrtoliths. *Deep-Sea Res.* 14, 561–597.
- Melis, R., Pugliese, N., Salvi, G., 2000. Micropaleontology of the cores MB 91/47, 91/40 and 91/54R (Western Magellan Strait). *Terra Antarctica Reports*, 4, 75–80.
- Roth, P. H., 1994. Distribution of coccoliths in oceanic sediments. In: Winter, A., Siesser, W.G. (Eds.), *Coccolithophores*, Cambridge University Press, Cambridge, 199–218.
- Violanti, D., Grecchi, G., Castradori, D., 1991. Paleoenvironmental interpretation of core BAN88-11GC (Eastern Mediterranean, Pleistocene-Holocene) on the grounds of Foraminifera, Thecosomata and Calcareous nannofossils. *Il Quaternario* 4, 13–39.

## MAJOR SEDIMENTARY CHANGES RELATED TO THE BEGINNING OF A GLACIALLY-DOMINATED MARGIN STAGE WEST OF ADELAIDE ISLAND, ON THE ANTARCTIC PENINSULA PACIFIC MARGIN

7-04

F.J. Hernández-Molina<sup>1</sup>; R.D. Larter<sup>2</sup>, A. Maldonado<sup>3</sup>

1 *Dpto. de Geociencias Marinas. Univ. Vigo. 36200 Vigo (Spain), fjhernan@uvigo.es*

2 *British Antarctic Survey (BAS). High Cross, Madingley Road, Cambridge CB3 0ET (UK)*

3 *Instituto Andaluz de Ciencias de la Tierra (IACT), Campus de Fuentenueva, s/n. 18002 Granada (Spain)*

The Pacific continental margin of the Antarctic Peninsula records a complex Cenozoic tectonic and sedimentary history from the Mesozoic to the Present. The margin was an active margin at least from Early Cretaceous time, then became passive when subduction stopped along most of the margin as ridge-crest segments of the Antarctic–Phoenix spreading center migrated into the trench. Such ridge-crest–trench interactions have affected the part of the margin south of the Hero Fracture Zone (HFZ), starting about 50 Ma. As each ridge-crest segment (RCS) arrived at the trench, subduction stopped and the trench was eliminated. These processes were diachronous from SW to NE, and the last RCS which arrived at the margin was the segment directly SW of the HFZ, in latest Miocene and early Pliocene times. Northeast of the HFZ lies the active South Shetland margin (Larter and Barker, 1991; Maldonado *et al.*, 1994). The arrival of each Antarctic–Phoenix RCS at the trench was followed by rapid uplift of the opposing segment of the margin for a period of 1 to 4 Ma, which cut off the supply of terrigenous sediment to the margin. Subsequently, long-term subsidence occurred and favoured the preservation of the Pliocene and Quaternary deposits on the outer shelf and slope (Larter and Barker, 1991; Larter *et al.*, 1997).

Although tectonic processes have been a key factor in the evolution of the margin, environmental changes during the Cenozoic have conditioned the main changes in the depositional style of sedimentation, especially since the Middle Miocene. The margin has changed from being a *non glacially-influenced margin*, to a *glacially-influenced margin*, and finally to a *glacially-dominated margin* (Hernández-Molina *et al.*, 2003). The aim of the present work is to point out the main sedimentary changes related to the beginning of the *glacially-dominated margin stage*, on the part of the Antarctic Peninsula Pacific margin west of Adelaide Island, between 68°–74°W and 65°–67°30'S (Fig. 1). The present study is part of a more extensive integrated regional stratigraphic work (Hernández-Molina *et al.*, in preparation), where seismic units and discontinuities have been correlated from the shelf to the rise through the slope. However, for the present paper, we have focused on the results of the analysis of multichannel seismic (MCS) reflection profiles collected by the *British Antarctic Survey* (BAS), and by Spain Project ANT99-0817 (Fig. 2). Additionally, reflection seismic profiles acquired by the *Istituto Nazionale di Oceanografia e di Geofisica Sperimentale* (OGS), the *Brazilian Antarctic Program*, and the *Rice University of Texas* (USA), have been used to obtain stratigraphic correlations. Results of Ocean Drilling Program Leg 178 (Barker *et al.*, 1999)

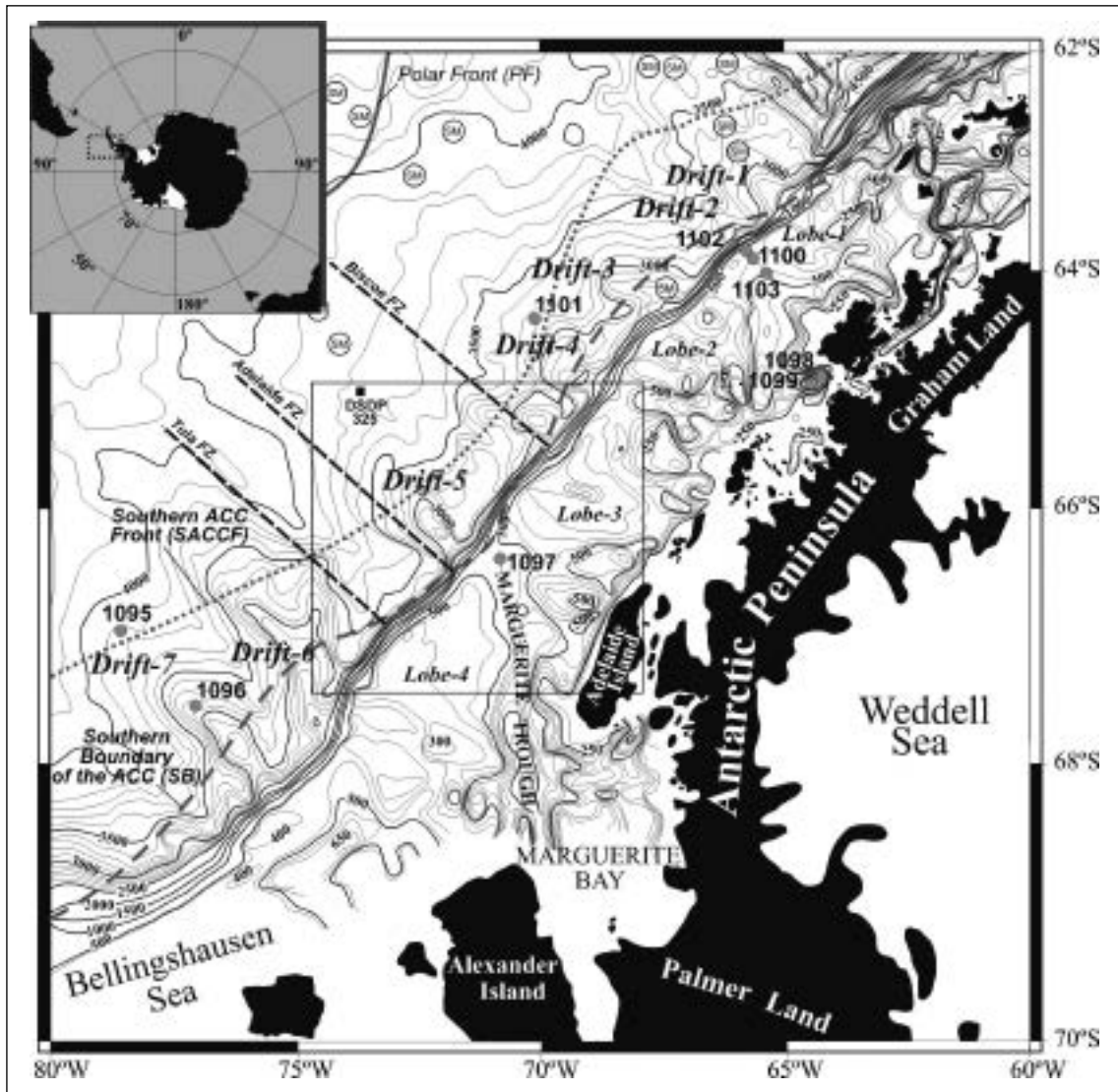


Fig. 1 - Regional setting of the study area.

and DSDP Site 325 (Hollister *et al.*, 1976) were also incorporated in the study, to establish the chronology of the depositional units. The age of the oceanic crust, based on interpretation of marine magnetic anomalies (Larter and Barker, 1991), was used to constrain the age of the oldest sediments on the rise. Magnetic anomaly ages were based on the magnetic reversal timescale of Cande and Kent (1995).

### Main Physiographic features of the margin

The *shelf* is ~140 km wide, with the *Marguerite Glacial Trough* (MGT) located in the central part of the area. The *middle shelf* includes the *Mid Shelf Basin* (MSB), bounded on its NW flank by the *Mid Shelf High* (MSH), both of which having a NE trend. The *outer shelf* is ~52 km wide with a landward slope gradient averaging 0.08° (Fig. 3). The MGT divides Bank-4 to the N from Bank-3 to the S. These banks are the present morphological expression of the sedimentary lobes 4 and 3 defined by Larter *et al.* (1997) The *shelf edge* is identified at an average depth of 488 m. The *continental slope* is steep (10.1° on average) and can be divided into 3 domains (Fig. 2): a) An *upper slope* between 488 and 1135 m of water depth (wd) with an erosional surface dipping 7.6° on average; in this area numerous gullies cut deposits, showing frequent internal erosional surfaces and non-organized seismic facies. b)

A *middle slope* with a convex-up shape and the steepest inclinations ( $16.8^\circ$  on average) between 1135 and  $\sim 2170$  m wd. It is 3.7 km wide and contains a few widely-spaced gullies cutting deposits with a high acoustic response and poor internal organization. c) A *lower slope* dipping  $5.3^\circ$  on average, and 9.3 km wide between 2170 and 3045 m wd. It has a smooth and concave-up external shape cutting deposits with well-organized seismic facies. Locally, high amplitude reflectors related to the occurrence of small channels have been recognized at the base of the slope. The *continental rise* starts at  $\sim 3045$  m wd. It represents a large domain with 2 different types of morphologic features: a) depositional features characterised by 4 *large mounded drifts* (drifts 4A, 4B, 5 & 5A), and b) erosional features characterised by 4 *large turbidite channels*: *Biscoe*; *Lavoisier*; *Adelaide* & *north Tula* following the nomenclature of Rebesco et al. (2002).

### Seismic stratigraphic analysis

Stratigraphic analysis of the Antarctic Peninsula Pacific margin offshore Adelaide Island reveals 3 main evolutionary stages from the Late Miocene to the Recent which clearly represent the growth phases of the margin under glacial influence (Fig. 3). The oldest, *transitional stage* (SU4, *Late Miocene-Early Pliocene*), represents the first progradational unit on the shelf and slope, above the

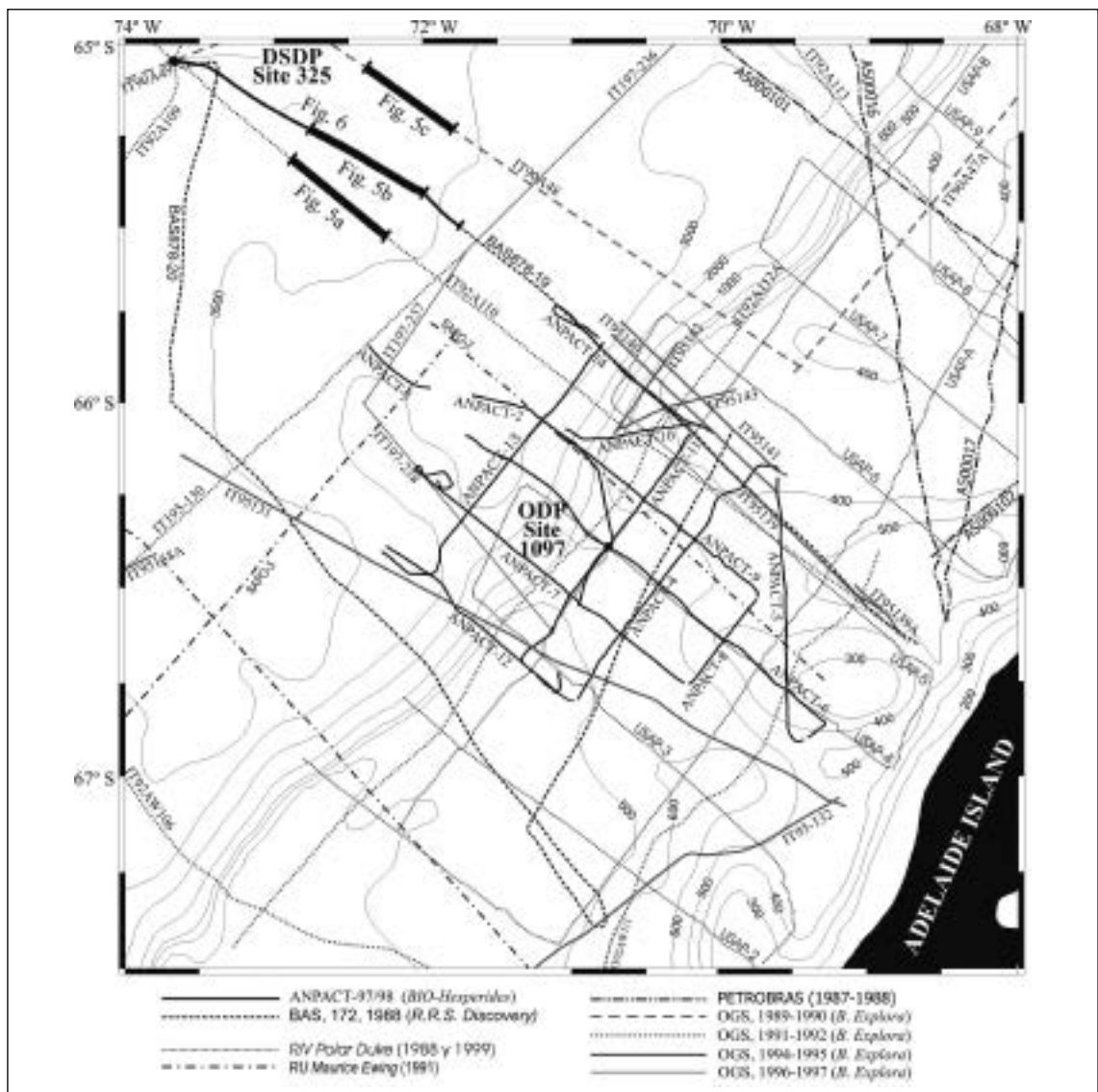


Fig. 2 - Locations of MCS profiles acquired in this area.

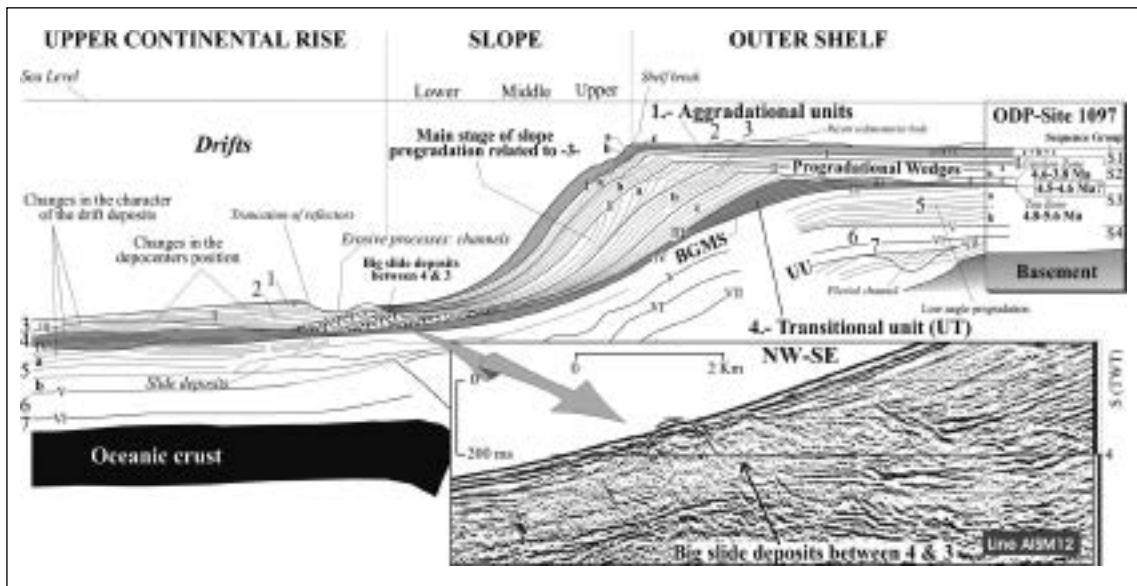


Fig. 3 - Stratigraphic sketch of the continental margin west of Adelaide Island, on the Antarctic Peninsula Pacific margin. A detail of the slide deposits at the top of the SU4 (Transitional Unit) is showed.

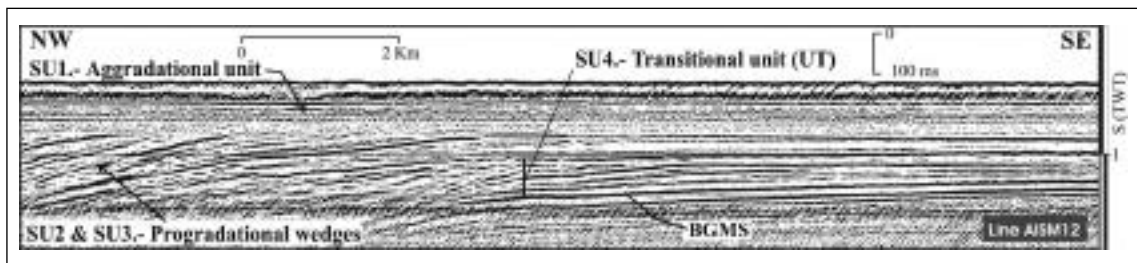


Fig. 4 - SU4 (Transitional unit) on the outer shelf.

*Base of the Glacial Margin Sequences (BGMS).* The SU4 has been defined as the *Transitional Unit (TU)*, which represents an important change in the depositional style of the continental margin (Fig. 3). The middle, *progradational glacially-dominated margin stage* contains two units (SU 3 & 2, *Early to Late Pliocene*). SU3 is composed of 3 progradational wedges (a, b & c) although the youngest one (a) is the thickest and represents the most important progradational stage of the margin. SU2 includes both progradational and aggradational deposits and it recorded a significant change in the margin growth pattern. The youngest *aggradational glacially-dominated margin stage* (SU1, *Quaternary*), recorded the last change in the depositional style of the margin, with a relatively thick upward and outward growth of the sediment wedge.

The *Transitional Unit (TU)* is deposited on the outer shelf, shelf edge and slope, but pinches out landward and is not present in the proximal part of the outer shelf (Fig. 3 & 4). It has massive to transparent facies on the shelf, but in the shelf break and slope it has a wedge shape with a progradational configuration (sigmoid to oblique) with a high acoustic response. On the shelf the upper boundary is an important regional erosional surface, landward dipping. Above this reflector large slide deposits have been identified at the base of the lower slope (Fig. 3). We recognize three domains on the slope within the TU (Fig. 3): a) an *upper slope* with an erosional surface; b) a *middle slope* with a convex-up shape and the steepest inclinations and c) a *lower slope* with a smooth and concave-up shape. Within the TU unit it is possible to identify the morphologic domains which presently characterize the shelf and slope.

On the *upper rise*, the TU contains drift facies on the rise and it records an important change in the depositional style (Fig. 3 & 5). The TU contains a *mega-drift*, composed of mounded elongated and separated deposits with high to moderate acoustic response. Further seaward, sheeted drift facies can

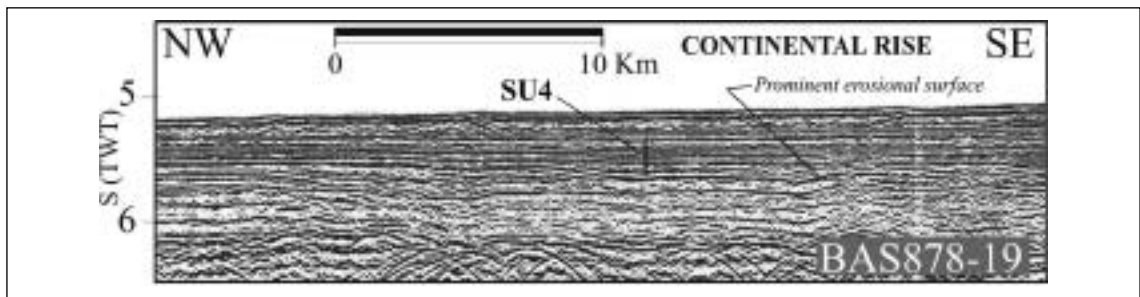


Fig. 5 - SU4 (Transitional unit) on the central continental rise.

be identified in the central rise. Locally, sediment waves and small drifts can be identified in correspondence to some topographic features. The TU is thin, or sometimes absent, in the transition between the upper rise and the lower slope, where a smooth depression (moat) is located. On the rise the bottom of this unit represents one of the most prominent regional erosional surfaces in the sedimentary record (Fig. 5).

TU deposits represent an important change in the stacking pattern of the margin, characterized by the first high-angle progradational unit on the outer shelf. It marks the first change from a *glacially-influenced margin* to a *glacially-dominated margin* where frequent advances of the ice grounding line to the shelf edge occurred. On the rise these deposits represent an important stage in which *along-slope processes* dominated. This could be associated with more widespread changes in thermohaline circulation in the Late Miocene.

This work has been carried out during research fellowships at BAS funded by Spain's Department of Education and Universities (PR2002-0271 & PR2003-0421). This research has been supported through the ANT99-0817 & REN2003-01498 Projects.

## REFERENCES

- Barker, P.F., Camerlenghi, A., et al. Leg 178 Scientific Party, 1999. Proc. ODP, Init. Repts., 178: Ocean Drilling Program, Texas A&M University, College Station, Texas.
- Cande, S. & Kent, D.V., 1995. Revised calibration of the geomagnetic polarity timescale for the Late Cretaceous and Cenozoic. *J. Geophys. Res.* 100, 6093-6095.
- Larter, R. D., & P. F. Barker, 1991. Neogene interaction of tectonic and glacial processes at the Pacific margin of the Antarctic Peninsula. *Spec. Publ. Int. Assoc. Sediment.*, 12, 165-186.
- Larter, R.D., Rebesco, M., Vanneste, L.E., Gambôa, L.A.P., & Barker, P.F., 1997. Cenozoic tectonic sedimentary and glacial history of the continental shelf west of Graham land, Antarctic Peninsula. *Antarc. Res. Series* 71, 1-27.
- Hernández-Molina, F.J.; Larter, R. D.; Maldonado, A., & Rodríguez-Fernández, J., 2003. Pliocene and Quaternary stratigraphic evolution of the Pacific margin offshore of the Antarctic Peninsula offshore from Adelaide Island. 9th International Symposium on Antarctic Earth Science. Postdam (Germany). 8-12, September, Abstracts Volume, 153-154.
- Hollister, C.D., Craddock, C., et al., 1976. Initial Reports of the Deep Sea Drilling Project, 35. U.S. Government Printing Office, Washington, D.C., 930 pp.
- Maldonado, A., Larter, R., & Aldaya, F., 1994. Forearc tectonic evolution of the South Shetland margin, Antarctic Peninsula. *Tectonics* 13, 1345-1370.
- Rebesco, M., Pudsey, C., Canals, M., Camerlenghi, A., Barker, P., Estrada, F., & Giorgetti, A., 2002. Sediment Drift and Deep-Sea Channel Systems, Antarctic Peninsula Pacific Margin. In: Stow, D.A.V., Pudsey, C.J., Howe, J.A., Faugeres, J.C., Viana, A.R. (Eds.). *Deep-Water Contourite Systems: Modern Drifts and Ancient Series, Seismic and Sedimentary Characteristics*. *Geol. Soc., London, Memoirs*, 22, 353-371.

## LATE CRETACEOUS CONGLOMERATES FROM THE CHILEAN MAGALLANES BASIN, AND THEIR RELATION WITH BASIN CLOSURE

7-05

A. Sánchez<sup>1</sup>, F. Hervé<sup>1</sup>, E. Gogoy<sup>2</sup>, M. Solari<sup>1</sup>, J. Fuentealba<sup>1</sup>

<sup>1</sup> Universidad de Chile

<sup>2</sup> Servicio Nacional de Geología y Minería

### Introduction

Three stages are recognised in the evolution of the Magallanes Basin: Structural, Thermal and Foreland Basin stages (Biddle et al., 1986), which may represent the transition from a back-arc to a



foreland basin. The Foreland Basin is characterised by an early upward increment in grain size and ubiquitous coarse polymictic conglomerates that crop out close to mudstones. In the northern half of the basin the conglomerates are included in the Cerro Toro Formation (Cenomanian - Campanian). In Tierra del Fuego, instead, conglomerates that grade laterally to “intraformational conglomerates” crop out in the upper Late Cretaceous – Early Paleocene Cabo Nariz Formation (Rojas et al 1993, ined. ENAP), equivalent to the Chorrillo Chico Formation in Biddle (1986). In the Brunswick peninsula and Riesco island, on the other hand, the conglomerates and sandstones are Maastrichtian in age (Charrier and Lahsen. 1965).

We describe here the petrography and provenance analysis of clasts together with paleocurrent measurements made in flute casts from Cerro Toro Formation, obtained performed at different locations (fig 1). A comparison of the geological setting of the conglomerates between the northern and the southern part of the basin is also discussed, providing a possible interpretation of the results.

## Stratigraphy

A simplified stratigraphic column developed by Wilson (1991) at 51°lat S is here presented:

Pre-Jurassic basement.

- Tobifera Fm., late Jurassic rhyolitic volcanoclastic rocks and black marine mudstones.
- Zapata Fm., early Cretaceous siliceous mudstone, siltstone, black mudstone and fine-grained sandstone.
- Punta Barrosa Fm., Albian? thick sandstone turbidites; shale and thin sandstone turbidites.
- Cerro Toro Fm., late Cretaceous hemipelagic shales and sandstone turbidites that enclose conglomerates.
- Tres Pasos Fm., late Cretaceous shales and sandstones.

At 54° lat S. the stratigraphic column –modified from Alvarez-Marrón (1993)- is mainly:

- Tobifera Fm., volcanoclastic, mainly tuffs.
- Rio Jackson Fm., Cretaceous siltstones and sandstones.
- Vicuña Fm, Cretaceous limestones, dolomites, and green and red marls.
- Cerro Cuchilla Fm., Maastrichtian Siltstones and sandstones; shallow platform facies.
- Cabo Nariz Fm. siltstones, sandstones and conglomerate in turbidite facies

## Results

The clasts of the Cerro Toro Formation samples, after an average obtained from samples collected in 3 different areas (see fig.1), are mainly rhyolites (45%), light coloured granitoids (27%), mudstones (almost 10%); basalts and andesites are less frequent. This is consistent with pebble composition published by Cecioni (1957). It is important to add that there are basalt with quenching texture in sample F00314a; in sample ST0254 there are aprox. 10% limestone concretions clasts and that the rhyolites are not tectonically foliated. (see fig. 1 for locations)

The rhyolites and black mudstones correlate with rocks of the underlying formations, mainly Tobifera and Zapata formations. The granitic clasts have not been dated; they resemble rocks from the Patagonian Batholith. The basalt with quenching texture may come from pillow lava from ophiolitic rocks and the limestone concretions from underlying Zapata Fm.

The paleocurrent directions measured in flute casts from Cerro Toro Formation show the occurrence of South-South East directed paleocurrent that transported the conglomerate clasts. This data obtained at Cerro Benitez (155°) and Cerro Campana (134°) shows that deposition took place parallel to the long axis of the basin. This is coherent with previously performed current measurements in Cerro Toro (Scott, 1966; Sohn et al, 2002). Wilson (1991) also published similar paleocurrent directions in the Punta Barrosa underlying Fm.

At Cabo Nariz, Tierra del Fuego Island, the paleocurrent measurements were not made directly in the conglomerates; instead they were performed in the sandstones that laterally grade into conglomerates. The measurements show a paleocurrent, directed toward northwest (315° azimuth). The petrography -and therefore the provenance analysis- is not yet finished. In the field mainly granitoids and rhyolite could be discriminated. Southeast of Cabo Nariz, near Chile - Argentina

border, in the Argentinean side, a measurement of paleocurrent has been made in imbricated conglomerate clasts, in an Eocene fan-delta deposit, where the current direction trend is  $335^\circ$  (Martinioni et al, 1998).

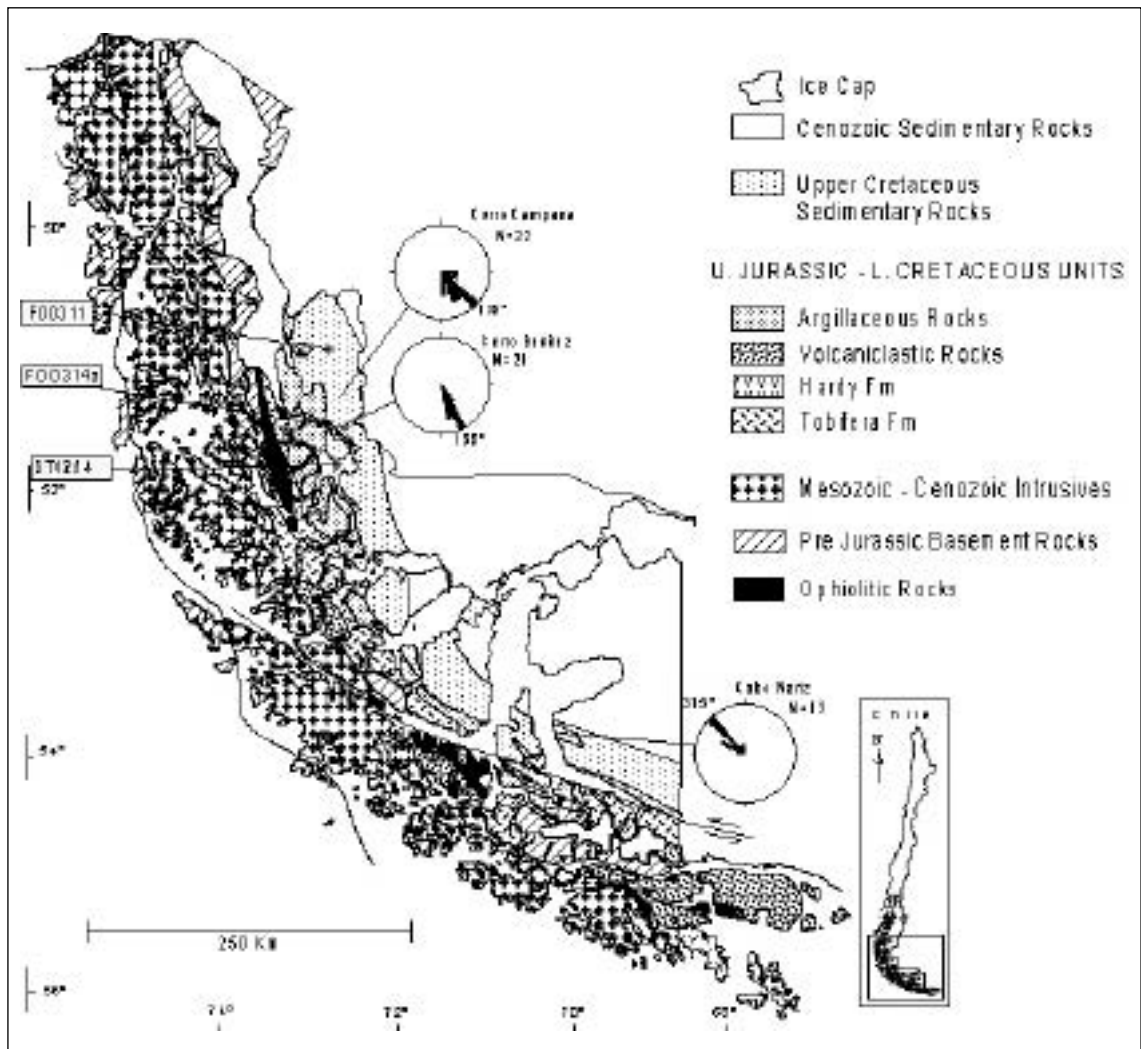


Fig.1 - Simplified geologic map of XII Region, Chile. The boxes show the locations of the studied conglomerate samples from Cerro Toro Fm; F00311 northern Sarmiento lake; F00314a, southern Sofia lake and St0254 Humberto Island. Cerro Campana and Cerro Benitez are the locations of flute cast measurements. Cabo Nariz is the location of flute cast and convolution folds measurement. Note the opposite sense of paleocurrent on the conglomerates of different ages. Geology from Wilson (1991), Thomson and Hervé (2002), Olivero and Martinioni (2001), and Sernageomin (2002).

## Discussion

The two areas here described have similar geologic characteristics. Sample collected in both areas reveal that conglomerates (in Cerro Toro Formation and in Cordillera Nariz) have been interpreted as channel fill facies of submarine fans that prograde parallel to the long axis of the Basin (Scott, 1966; Wilson, 1991; Sohn et al., 2002; Rojas, L., personal communication), but in opposite senses and in different geological times, first in the northern area and later in the southern one. This diachronism from north to south is interpreted to be coeval to southward thickening of the continental crust that enclosed the basin due to a compressional tectonic regime starting at the lower Late Cretaceous. The

erosion of the underlying Zapata and Tobifera formations expressed in the Cerro Toro Formation conglomerates relates to the closure of the Rocas Verdes marginal basin (RVMB) rocks, crustal thickening and development of the Magallanes fold and thrust belt (MFTB).

Regarding the exposure of underlying units in Tierra del Fuego, we still ignore which rocks were eroded to form the Cordillera Nariz conglomerates. Initial field determinations hint to acidic rocks that could derive from Tobifera or crystalline igneous rocks. In the western side of Sierra de Apen, Argentina, the clasts of the exposed conglomerates, are black mudstone and carbonate concretions from Upper Cretaceous mudstone; acidic vulcanites, and quartz from Upper Jurassic – Lower Cretaceous units (Martinioni et al., 1999). The change of facies toward Southeast, from turbidite and submarine fan channel in Cabo Nariz Fm. to fan-delta in Argentina, and estuary facies in Eocene Ballena Fm. (Prieto and Moraga, 1990), together with the paleocurrent direction, show that the continent should be uplifting southward.

Although there is a diachronism from South to North in the beginning and in the cessation of the thrusting and folding in Magallanes region (Biddle et al., 1986), it is important to point out the opposite diachronism in sedimentary processes that fill the basin with coarse grained polymictic conglomerates. Thus the compressional deformation begun first in the southwestern area, but the uplift due to MFTB in the North edge of the Basin was strong at Cenomanian-Campanian, while in the southern edge should be strong in Paleocene. The continental facies first recorded in Argentinean Tierra del Fuego show that the continental margin move northward. A progressive crustal thickening from north to south in the northern part of the basin, and south to north in its southern part, has been also detected.

## Acknowledgments

The study was financed by Proyecto Fondecyt 1010412. Also we like to tanks L. Rojas for share his knowledge about Cabo Nariz area.

## REFERENCES

- Alvarez-Marrón, J., McClay, K. R., Harambour, S., Rojas, L. and Skarmeta, J., 1993. Geometry and evolution of the frontal part of the Magallanes foreland thrust and fold belt (Vucuña area), Tierra del Fuego, southern Chile. *American association of Petroleum Geologists Bulletin*, v. 77 n° 11, p. 1904 – 1921.
- Biddle, K. T., Uliana, M. A., Mitchum, R. M. J. and Fitzgerald, M.G., 1986. The stratigraphic and structural evolution of the central and eastern Magallanes Basin, southern South America. in P. A. Allen and P. Homewood, eds. *Foreland Basins: International Assoc. of Sedimentologists Special publication 8*, p. 41 – 61.
- Cecioni, G., 1957. Cretaceous flysh and molasses in Departamento Ultima Esperanza, Magallanes Province, Chile. *Bulletin of the American Assoc. of Petroleum Geologists.*, v. 41, p. 538 – 564.
- Charrier, R. and Lahsen, A., 1965. El límite Cretáceo - Terciario entre el Seno Skyring y el Estrecho de Magallanes. *Memoria de Título, Universidad de Chile*.
- Martinioni, D. R., Olivero, E. B. and Palamarczuk, S., 1998. Conglomerados del Paleógeno en Tierra del Fuego: evidencias de discordancia entre el Cretácico Superior – (Paleoceno) y el Eoceno de Cuenca Austral. *Paleógeno de América del Sur y de la península Antártica*, Casadio, S. (Ed.). *Asoc. Paleontológica Argentina, Publicación especial v. 5*, p. 129 – 136.
- Martinioni, D. R., Olivero, E. B. and Palamarczuk, S., 1999. Estratigrafía y discordancias del Cretácico Superior – Paleoceno en la region central de Tierra del Fuego. *Simposio “Paleogeno de América del Sur”, Nañoz, C. (Ed.). Servicio Geológico Minero Argentino, Anales v. 33*, p. 7 – 16.
- Olivero, E. and Martinioni, D., 2001. A review of the geology of the Argentinian Fuegian Andes. *Journal of South American Earth Sciences*, v. 14, p. 175 – 188.
- Prieto, X. And Moraga, J., 1990. Ambiente de sedimentación de la Formación Ballena (Eoceno Inferior a Medio), Tierra del Fuego, Magallanes. Segundo simposio sobre el Terciario de Chile, Concepción, p. 267 – 273.
- SERNAGEOMIN, 2002. Mapa Geológico de Chile, Escala 1:1.000.000. *Carta Geológica de Chile, Serie Geología Básica n.75*.
- Scott, K. M., 1966. Sedimentology and dispersal pattern of a Cretaceous flysch sequence, Patagonian Andes, southern Chile. *Bull. A. A. P. G.*, v. 50, p. 72 – 107.
- Sohn, Y. K., Choe, M. Y. and Jo, H. R., 2002. Transition from debris flow to hyperconcentrated flow in a submarine channel (the Cretaceous Cerro Toro Formation, southern Chile). *Terra Nova*, v. 14, p. 405 – 415.
- Thomson, S. and Hervé, F., 2002. New time constraints for the age of metamorphism at the ancestral Pacific Gondwana margin of southern Chile. *Revista geológica de Chile*, v. 29, p. 151 – 165.
- Wilson, T., 1991. Transition from a back-arc to foreland basin development in the southernmost Andes: Stratigraphic record from the Ultima Esperanza District, Chile. *Geol. Soc. of America Bull.*, v. 103, p. 98 – 111.

**SEDIMENTARY CHARACTERISTICS AND FLUVIAL ARCHITECTURE  
OF A GIGANTIC GRAVELLY SUBMARINE CHANNEL:  
THE CRETACEOUS LAGO SOFIA CONGLOMERATE, SOUTHERN CHILE**

7-06

Sohn Y.K.<sup>1</sup>, Choe M.Y.<sup>2</sup>, Y.K. Jin<sup>2</sup>, Lee J.I.<sup>2</sup>, Hur S.D.<sup>2</sup>, Kim Y.<sup>2</sup>, Jo H.R.<sup>3</sup>

<sup>1</sup> Department of Earth and Environmental Sciences, Gyeongsang National University, Chinju 660-701, Korea

<sup>2</sup> Korea Polar Research Institute, Korea Ocean Research and Development Institute, PO Box 29, Ansan 425-600, Korea

<sup>3</sup> Marine Geoenvironments and Resources Research Division, Korean Ocean Research and Development Institute, PO Box 29, Ansan 425-600, Korea

The Lago Sofia Conglomerate encased in the 2 km-thick hemipelagic mudstone of the Cretaceous Cerro Toro Formation (southern Chile), is a deposit of a gigantic submarine channel developed along a foredeep trough (Fig. 1). It is hundreds of meters thick and several kilometers wide. It extends for more than 120 km from north to south, representing one of the largest ancient submarine channels in the world (Fig. 2). The channel deposits consist of four major facies, including thin- and cross-stratified conglomerates (Facies A), massive or crudely stratified conglomerates (Facies B), normally graded conglomerates with intraformational megaclasts (Facies C), and thick-bedded massive sandstones (Facies D). Conglomerates of Facies A and B show laterally inclined stratification, foreset stratification, and hollow-fill structures, indicative of terrestrial fluvial deposits and suggestive of highly competent gravelly turbidity currents. Facies C conglomerates are interpreted to be deposits of composite or multiphase debris flows associated with preceding hyperconcentrated flows. Facies D sandstones indicate rapidly dissipating, sand-rich turbidity currents.

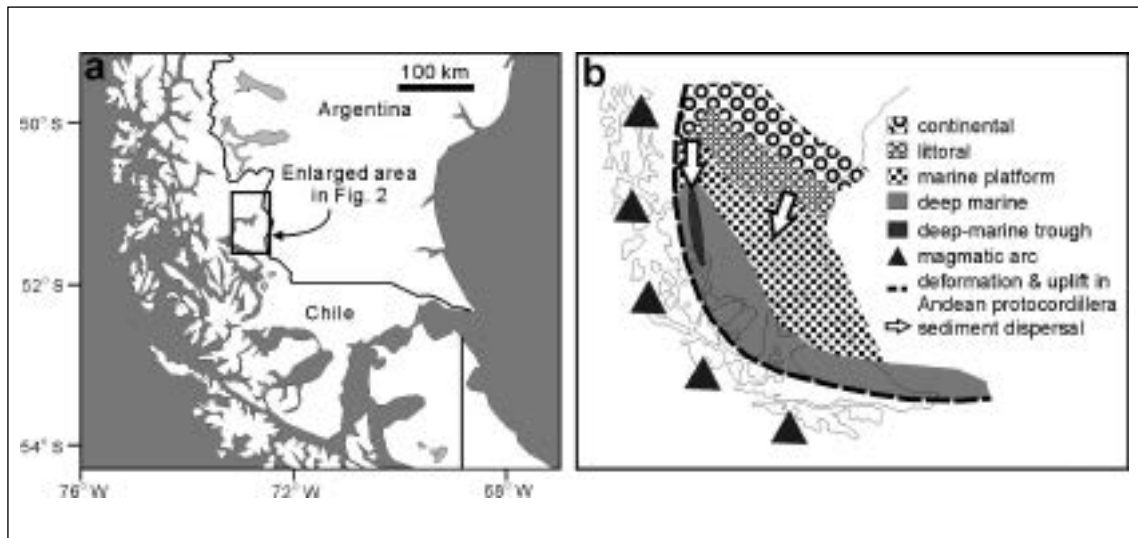
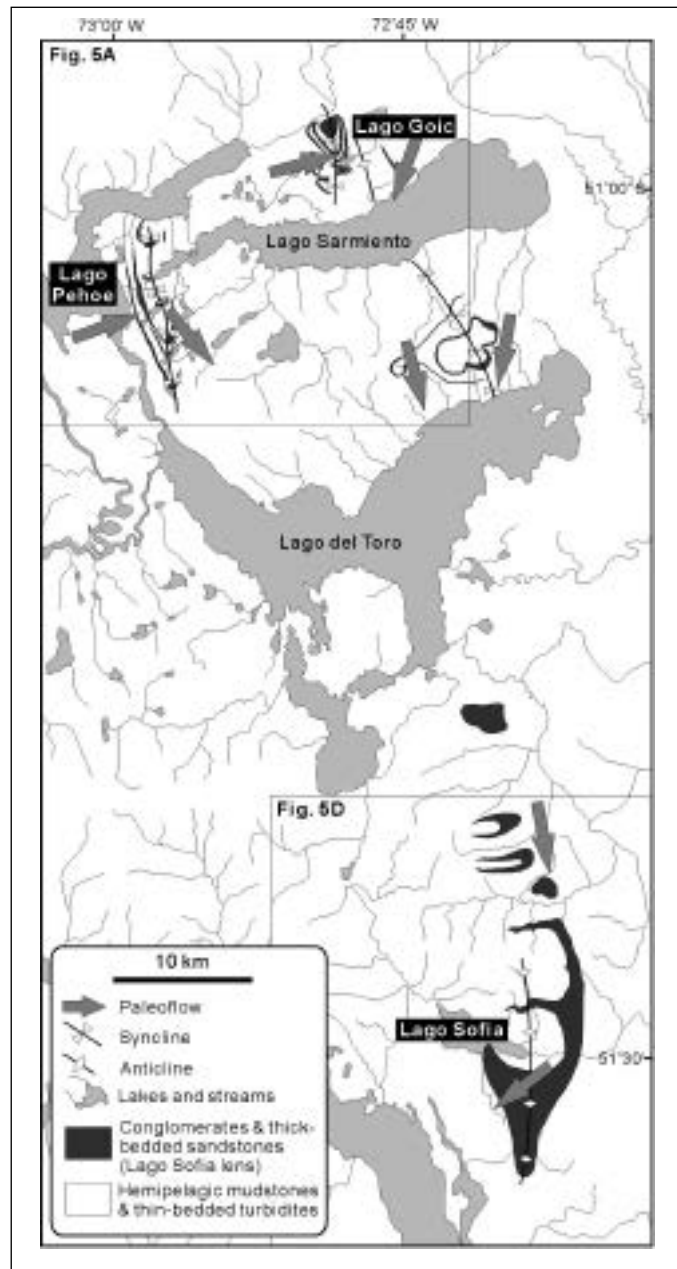


Fig. 1 - (a) Location map of the study area. (b) Depositional setting of the Magallanes Basin during the middle to Late Cretaceous. The basin consisted of a deep, N-S-trending foredeep trough adjacent to the western margin and a gently sloping foreland ramp in its central and eastern parts. Throughout the Late Cretaceous, arc- and cordillera-derived sediment was dispersed axially along the deep-water trough, resulting in a thick (ca. 7 km) Upper Cretaceous sequence of deep-water facies.

The Lago Sofia conglomerate occurs as isolated channel-fill bodies in the northern part, generally less than 100 m thick, composed mainly of Facies C conglomerates and intercalated with much thicker fine-grained facies. Paleocurrent data from these bodies indicate sediment transport to the east and southeast (Fig. 2). They are interpreted to represent tributaries of a larger submarine channel system,

which joined to form a trunk channel in the south. The conglomerate in the southern part is more than 300 m thick, composed of subequal proportions of Facies A, B, and C conglomerates, and overlain by hundreds of m-thick turbiditic sandstones (Facies D) with scarce intervening fine-grained facies. We suggest that the conglomerate here represents vertically stacked and interconnected channel bodies formed by a trunk channel confined along the axis of the foredeep trough.

Fig. 2 - Geologic map of the study area, which largely comprises thick sequences of hemipelagic mudstones and thin-bedded turbidite sandstones (Cerro Toro Formation, Late Cretaceous). The formation contains conglomerate lenses, which extends for more than 120 km from north to south. They are interpreted as the deposit of submarine channels that developed along the axis of foredeep basin. Paleocurrent data indicate that sediment was generally dispersed from north to south with local sediment transport to the east in the northern part.



The conglomerate in the southern part is classified into 5 architectural elements on the basis of large-scale bed geometry and sedimentary facies (Fig. 3): (1) stacked sheets, indicative of bedload deposition by turbidity currents and typical of broad gravel bars in terrestrial gravelly braided rivers, (2) laterally-inclined strata, suggestive of lateral accretion with respect to paleocurrent direction and related to spiral flows in curved channel segments around bars, (3) foreset strata, interpreted as the deposits of large gravel dunes that have migrated downstream under quasi-steady turbidity currents, (4) hollow fills, which are filling thalwegs, minor channels, and scoured hollows, and (5) diamictite or mass-flow deposits of Facies C. The stacked sheets, laterally inclined strata, and hollow fills are laterally transitional to another, reflecting juxtaposed geomorphic units of deep-sea channel systems.

It is noticeable that the channel bodies in the southern part are stacked toward the east, indicating eastward migration of the channel thalwegs (Fig. 4). The laterally inclined strata also dip dominantly to the east. These features suggest that the trunk channel of the Lago Sofia submarine channel system gradually migrated toward east. This eastward channel migration is interpreted to be due to tectonic forcing imposed by the subduction of an oceanic plate beneath the Andean Cordillera just to the west of the Lago Sofia submarine channel.






Elements	Geometry	Description	Interpretation
<p>Stacked sheets (Element S)</p> 	<p>Sheet-like 3-50 m thick Hundreds of meters in lateral extent</p>	<p>Stacked sheet-like beds of clast-supported, pebble-cobble conglomerate Well-rounded, commonly imbricated clasts Medium-grained sandstone matrix Parallel to subparallel bed geometry Individual beds: decimeters thick; massive &amp; graded, bounded by slightly erosional surfaces Thin sandstone interbeds</p>	<p>Stacking of broad gravel sheets and low-relief gravel bars by turbidity currents</p>
<p>Laterally-inclined strata (Element LS)</p> 	<p>Sheet-like or lenticular 7-15 m thick Several tens to 200 m in lateral extent</p>	<p>Low-angle inclined strata of clast-supported, pebble-cobble conglomerate Dip of inclined strata, perpendicular or oblique at high angles to paleocurrent direction Well-rounded, commonly imbricated clasts Medium-grained sandstone matrix Individual beds: decimeters thick; bounded by conformable and slightly erosional surfaces with local scour hollows Thin sandstone interbeds, commonly thinning out updip</p>	<p>Lateral accretion on gravel bars through multiple depositional events (turbidity currents)</p>
<p>Forest strata (Element FS)</p> 	<p>Lenticular 2-4 m thick Several meters in lateral extent</p>	<p>Large-scale, planar &amp; tangential cross stratified, clast-supported, pebble-cobble conglomerate Commonly isolated sets with set thickness of up to 5 m Organized clast fabric</p>	<p>Downstream migration of large gravel dunes</p>
<p>Hollow fills (Element HF)</p> 	<p>Lenticular 2-12 m thick A few meters to 100 m in lateral extent</p>	<p>Lenticular lithosome bounded by concave-up, erosional surfaces Occasionally stepped margin Clast-supported, pebble-boulder conglomerate with occasionally sandstone interbeds</p>	<p>Filling of thalwegs, minor channel forms, and scours</p>
<p>Diamictite (Element D)</p> 	<p>Sheet-like A few meters to 30 m thick Hundreds of meters in lateral extent</p>	<p>Sheet-like lithosome of mud-rich conglomerate resting on concave-up, erosional surfaces and flat, conformable surfaces A single bed or more than one bed of diamictite Two distinct divisions within individual beds: (1) lower division of clast-supported, imbricated, pebble-cobble conglomerate with common basal inverse grading and (2) upper division of matrix-supported, disorganized, pebble conglomerate or pebbly sandstone with interformational clasts High variable paleocurrent directions, commonly perpendicular to those from stratified conglomerates</p>	<p>Sheet-like or tongue-shaped bodies deposited by debris flows with clast-rich frontal parts, originated from the failure of channel banks or slopes flanking the channel system</p>

Fig. 3 - Classification of architectural elements in the Lago Sofia conglomerates.

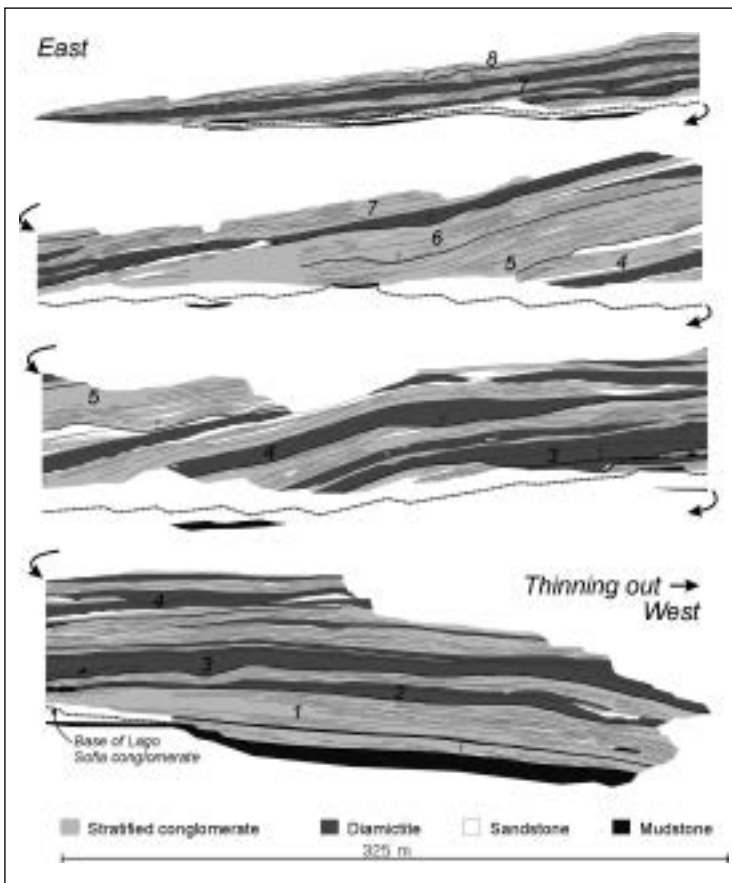


Fig. 4 - Sketch of a large outcrop in the Lago Sofia area, highlighting the architecture of deep-sea channel conglomerate. The outcrop consists of stratified conglomerate, diamictite, and sandstone beds formed in an axial trunk channel. Clast imbrication in stratified conglomerates indicates a sediment dispersal to the southwest, reflecting a southwestward-draining trunk channel. Note the progressive eastward shift of channel complexes (numbered) bounded by major down-cutting surfaces (thick lines), which implies a long-term migration of the axial channel to the east. T=thalweg.

# Session 8

---

**ICE-SHEET  
DYNAMICS**





**THE IMPRINT OF ICE MASSES ON THE CONTINENTAL MARGIN  
DURING GLACIAL MAXIMA: THE SEA FLOOR RECORD WEST  
OF THE NORTHERN ANTARCTIC PENINSULA**

8-01

M. Canals

*University of Barcelona, Spain*

The footprint of large ice streams fed by continental ice masses during glacial expansions is now found on the modern Antarctic continental shelf. This has been investigated mostly west of the Antarctic Peninsula, where multibeam bathymetric mapping and seismic reflection profiles have shown the existence of ancient glacial troughs and subglacial sedimentary systems now flooded after the last sea level rise.

**THE RESPONSE OF THE WARSZAWA ICEFIELD, KING GEORGE ISLAND  
TO RECENT AND PREDICTED FUTURE CLIMATE CHANGE**

8-02

Alun Hubbard<sup>1</sup>, Anne le Brocq<sup>2</sup>*1 Dept of Geography, Drummond Street, University of Edinburgh, UK**2 Centre for Glaciology, Dept of Geography, University of Bristol, UK*

**Abstract**

A time-dependent, first-order ice flow model is applied in three-dimensions to the geometry of the Warszawa ice field at 150 m resolution. The model is coupled to climate through a temperature-index melt model (incorporating a direct radiation algorithm) and a snow-drifting redistribution model which yields the surface mass-balance boundary condition. A set of sensitivity experiments are run in order to validate the model against observables and to further investigate the primary influences on the present day ice surface. These are followed by a series of experiments driven by climate records to replicate last 50 years of observed fluctuations in the ice margin and under IPCC (2000) predictions, the best and worst-case trajectory of the ice field over the next century. The model reveals that the ice field is highly sensitive to climate change, responding quickly to perturbations in the mass balance. Furthermore, the influence of prevailing wind direction and aspect through their effect on mass balance exert a primary control on the present day ice field geometry. The historic simulation reveals that the ice field has been relatively stable until the mid 1950s, after which it steadily retreated. With a continuation of the current warming trend (~4°C per century) observed across the region, the Warszawa ice field will dwindle to a mere 1% of its present volume by the end of the century. More conservative estimates of climate change, offset by increased precipitation still result in significant depreciation in ice volume, but not in total wastage.

**PLIO-PLEISTOCENE ORBITAL PERIODICITIES IN GLACIALLY INFLUENCED  
SEDIMENTS FROM WESTERN PACIFIC MARGIN OF ANTARCTIC PENINSULA**

8-03

M. Iorio(\*), E. Marsella(\*), G. Nardi(\*\*), E. Petruccione(\*\*)

*(\*) Istituto per l'Ambiente Marino Costiero, CNR, Porto di Napoli, Calata Porta di Massa, 80133, Napoli, Italy**(\*\*) Univ. di Napoli, Dip. Scienze della Terra, S. Marcellino 10, 80100 Napoli, Italy*

**Summary**

Spectral analyses of petrophysical and sedimentological data sets from Plio-Pleistocene sediments cored on the Western Antarctic continental rise during Ocean Drilling Program (Leg 178) show non-harmonic wavelength peaks, with probabilities >90%. When the wavelength peaks are normalized, they exhibit an extremely high correlation factor with predicted Earth's orbital variations for the same

time interval. It is also found that both short (~ 95-125 -ky) and long (~400 -ky) eccentricity periodicities clearly emerge from the signal during the whole Pleistocene, without evident switch to obliquity at mid-Pleistocene (~ 0.9 Ma B.P.), as reported in the literature. This suggests that the lithological parameters, proxy of glacial cycles, are controlled, directly or indirectly, by astronomically-forced processes (Milankovitch cycles). Moreover, the constant presence of all orbital periods in the signal since the Lower Pleistocene and the good correlation for the last 2.6 Ma among distant coring sites, based on systematic sedimentological variations at intervals of about 140 and 370 -ky, allow to extend the results at regional scale, confirming the hypothesis of the relative stability of the Antarctic ice sheet, at least since Upper Neogene and suggesting that the ice sheet in the Lower-Upper Pliocene and in the Pleistocene could be sensitive to temperature changes. Finally an age correspondence emerges between the correlated events at 1.07, 2.01 and 2.61 Ma, corresponding to periods of particularly intense ice rafting in the studied area, and relative sea-level highs, suggesting a superimposed eustatic influence.

### Abstract text

The dynamics of the Antarctic ice sheet is a significant component of the global climate system, so the understanding of its driving mechanisms, still uncompletely known, is of great importance in the analysis of the Earth's climatic evolution. New insights in such dynamics came from studies on the glacial-interglacial sedimentation of upper rise sedimentary drifts off the West Pacific margin of the Antarctica Peninsula. In this sector, the irregular relief of the upper rise is due to large hemipelagic sedimentary drifts, that are separated by nine channel systems formed by turbidity fluxes. Drift sediments alternate from rapidly deposited, poorly fossiliferous silt and clays during glacial intervals, to slowly deposited biogenic muds (with only a minor terrigenous component) during interglacial times (Rebesco et al., 1998, Barker et al., 1999; Barker and Camerlenghi, 2002). Here we present the results from spectral analysis and correlation of Plio-Pleistocene sedimentological (Coarse Fraction) and petrophysical (GRAPE bulk density, Magnetic susceptibility, and Chromaticity a\*) data intervals from Sites 1095, 1096 and 1101 ODP Leg 178, drilled respectively from sedimentary drift 7 and 4 (Barker et al., 1999). The spectral analysis program (Horne and Baliunas, 1986; Iorio et al., 1995; Brescia et al., 1995) originally written to deal with unevenly spaced astronomical data sets, is based on a technique which aims to detect the presence and significance of periodicities in unevenly sampled data series. In fact, as it was found in many stratigraphic data sets, the rebinding of the unevenly sampled data to equally spaced bins, and their calculation by means of a conventional periodogram, often alters the perceived frequency and significance of a periodic signal. Among all parameters in the studied intervals, only those with well defined power spectra with more than two wavelengths were considered to record a true cyclic signal (Fig.1). In order to enable comparison from the computed wavelengths expressed in sedimentary thickness (m) and orbital periods expressed in temporal units (ky), the wavelengths of each power spectrum were normalized to their highest well defined frequency, and each orbital calculation for the last 3 Myr computed by Berger and Loutre (1992) was normalized respect to the others (D'Argenio et al., 1998). The two tables of a-dimensional ratios obtained in this way were then cross-correlated, searching for the highest correlation factor. Linear regression analysis of the relative ratios of all wavelengths and orbital periods give correlation factors that are above 0.98, for all power spectra analysed (Fig.1), hence they can be considered strongly linked. Moreover the above data enable a precise computation of the average sediment accumulation rates in the studied intervals (Iorio et al., 2004), which show also a close similarity with both biostratigraphically and palaeomagnetically computed sedimentation rates (Iwai et al., 2002; Acton et al., 2002). Looking at the highest energy peaks (bold marked in Fig. 1), we find out that the short eccentricity (~95 and 123-ky) strongly influences the Lower-Upper Pliocene (Site 1095) and the whole Pleistocene of Sites 1095, 1101 and 1096. The ~400-ky long eccentricity strongly emerges from the Upper Pliocene-Pleistocene sedimentary record of Sites 1095 and 1101. Moreover the ~20ky precession is evident in the Upper Pliocene-Pleistocene of Sites 1096 and 1101. Finally the ~64-ky period characterizes the Lower-Upper Pliocene and Mid Pleistocene of Sites 1095, 1096 and 1101. In order to allow a comparison of the FFT analysis results among all three Sites data sets, all sedimentological and petrophysical data, which were collected at different intervals in each site, were

smoothed with an average window of 140 cm (which is the longest sampling interval). The smoothed data were calibrated in Ma (Fig.2 )

SITE 1095							
0-53 mcd Upper Pliocene to Pleistocene			88-140 mcd Lower to Upper Pliocene				
MS (m)	Astr. (years)		Ms (m)	Grape (m)	Rfa*(m)	+Fr>63 µm (m)	Astr.(years)
			0.98				22394
1.12	39719		1.73			1.50	39719
			2.08	2.13	2.14	2.06	50000
1.60	53864						
			2.36		2.44	2.29	59000
1.99	64000		3.06	<b>2.74</b>	2.82	2.77	<b>64000</b>
						<b>4.01</b>	<b>98715</b>
<b>3.09</b>	<b>111000</b>						
4.15	123818		<b>6.06</b>	<b>6.83</b>	5.36	<b>5.76</b>	<b>123818</b>
<b>8.24</b>	<b>404178</b>				17.87		404178
Corr. 0.993			Corr. 0.996	Corr. 0.999	Corr. 0.998	Corr. 0.993	
A							
SITE 1096							
0-33 mcd Mid to Upper Pleistocene		34-150 mcd Upper Pliocene to Mid Pleistocene					
MS (m)	Astr. (years)		MS (m)		Rfa*(m)		Astr. (years)
1.05	15000						
1.45	18964						
<b>1.79</b>	<b>23708</b>		2.04		2.08		23708
			3.34		3.51		39719
3.39	50000		-		4.39		50000
			-		<b>5.34</b>		<b>64000</b>
<b>6.10</b>	<b>94782</b>		<b>8.06</b>		7.49		<b>94782</b>
			<b>11.50</b>		<b>11.18</b>		<b>123818</b>
			<b>19.58</b>		-		<b>227000</b>
			34.25		-		404178
Corr. 0.995			Corr. 0.999		Corr. 0.998		
B							
SITE 1101							
0-143 mbsf Upper Pliocene to Pleistocene			53-143 mbsf Upper Pliocene to Mid Pleistocene				
MS (m)	Fr>63µm (m)	Astr. (years)	Ms (m)	Grape (m)	Rfa*(m)	Fr>63µm(m)	Astr.(years)
1.0	--	15000	0.91				15000
1.5	--	22394	<b>1.53</b>	1.37	1.53		<b>22394</b>
1.8	--	23708	<b>1.76</b>				<b>23708</b>
2.4	2.35	39719	2.22	2.44	2.27		39719
			2.70			2.68	41090
--	2.8	50000		2.80			50000
--	--	53864		3.15	<b>3.36</b>		<b>53864</b>
						<b>3.89</b>	<b>59000</b>
3.7	3.8	64000	3.99	<b>4.21</b>			<b>64000</b>
	<b>4.8</b>	<b>94782</b>			4.67	<b>4.77</b>	<b>94782</b>
6.8	6.8	98715	6.30				98715
--	8.35	111000				<b>7.19</b>	<b>111000</b>
<b>9.5</b>	10.7	<b>123818</b>	9.45	10.80		10.88	123818
<b>15.4</b>	--	<b>231000</b>					
24.7	<b>26.0</b>	<b>404178</b>		25.21	28.04	21.42	404178
Corr. 0.993	Corr. 0.984		Corr.0.988	Corr. 0.995	Corr. 0.990	Corr. 0.975	
C							

Fig.1.- Depth intervals and data sets parameters used for Fast Fourier Transform analysis and computed wavelengths. A, Site 1095; B, Site 1096; 1 C, Site 1101.

MS, magnetic susceptibility; GRAPE (Gamma Ray Attenuation Porosity Evaluator) density; Rfa\*, chromaticity parameter a\*; Fr>63, percentage of coarse fraction >63 µm in weight %; Astr, computed astronomical periodicities ( Berger and Loutre, 1992), expressed in years. The bold figures indicate the highest energy peaks of the lithological power spectra and the corresponding astronomical periodicities. Corr. is the correlation factor between wavelength data set and astronomical periodicity set. (From Iorio et al., 2004)

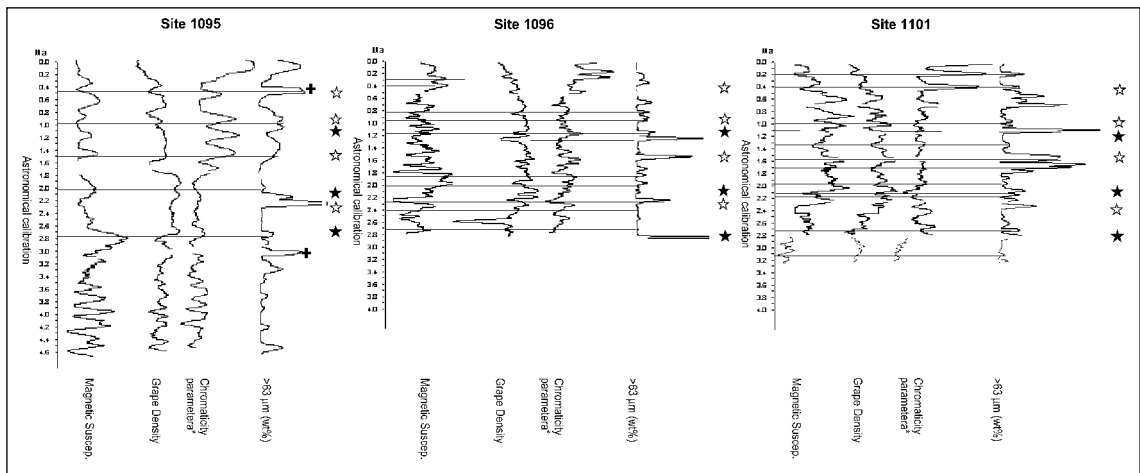


Fig.2.- Smoothed curves of magnetic susceptibility, GRAPE (Gamma Ray Attenuation Porosity Evaluator) density, chromaticity  $a^*$  and coarse fraction ( $>63 \mu\text{m wt}\%$ ). The horizontal black lines refer to four parameters coheval variation for Sites 1095, 1096 and 110 (see text)1. Stars show synchronous changes occurring in all three sites (black stars indicate time of particularly intense ice rafting periods in Site 1101 (Cowan, 2001), the crosses at Site 1095 indicates higher values, omitted for scale clarity). (From Iorio et al., 2004 modified).

using the sedimentation rates astronomically computed (Iorio et al., 2004) as well as biostratigraphically and paleomagnetically constrained (Iwai et al., 2002; Acton et al., 2002) in the intervals excluded from FFT analysis. Subsequently, the variations, of all smoothed and calibrated parameters, synchronously ( $\pm 0.05\text{Ma}$ ) occurring in at least two Sites belonging to two distinct sedimentary drifts (drift 7 and 4), were considered to be an expression of the same event, (horizontal lines in Fig 2) and the averaged age was computed. When the same event was recorded in all three Sites, it was considered an even stronger event, occurring at 0.39, 0.9, 1.07, 1.42, 2.01, 2.13, 2.61 Ma) (stars in Fig.2). The average time interval between two subsequent events during the last 2.6 Ma, was found of  $0.14 \pm 0.04 \text{ Ma}$ , and of  $0.37 \pm 0.17 \text{ Ma}$  for the strongest events recorded in all three Sites. So these time-intervals are close to that computed for the Plio-Pleistocene power spectra of higher energy wavelengths (Fig.1). Finally the constant presence of all the orbital periodicities in the signals since Lower Pleistocene and in part of the Lower-Upper Pliocene of Site 1095, confirms the relative stability of the Antarctic ice sheet since Upper Neogene (Barker and Camerlenghi, 2002;) and implies its sensitivity to the insolation changes during the studied time interval.

## SELECTED REFERENCES

- Acton, D.G., Guyodo, Y., and Brachfeld, S.A., 2002, Magnetostratigraphy of sediment drift on the continental Rise of west Antarctica (ODP Leg 178, Sites 1095, 1096, and 1101), in Barker, P.F., Camerlenghi, A., Acton, G.D., and Ramsay, A.T.S., eds., Proceeding Ocean Drilling Program, Scientific Results 178, [Online].p 1-61.
- Barker, P. F., Camerlenghi, A., Acton, G. D., et al., 1999, Proceeding Ocean Drilling Program, Initial Reports, 178 [CD-ROM]. Available from: Ocean Drilling Program, Texas A&M University, College Station, TX 77845-9547, U.S.A.
- Barker, P.F. and Camerlenghi, A. 2002 Glacial history of the Antarctic Peninsula from Pacific margin sediments. in Barker, P. F., Camerlenghi, A., Acton, G. D., and Ramsay, A.T.S., 2001, Proceedings of the Ocean Drilling Program, Scientific Results, 178, [Online] p.1-40.
- Berger, A. and Loutre, M.F., 1992, Astronomical solutions for paleoclimate studies over the last 3 million years: Earth and Planetary Science Letters, v. 111, p. 369-382.
- Brescia, M., D'Argenio, B., Ferreri, V., Longo, G., Pelosi, N., Rampone, S., and Tagliaferri, R., 1995, Neural net aided detection of astronomical periodicities in geologic records: Earth Planetary Science Letters, v. 139, p.33-45.
- D'Argenio, B., Fischer, A.G., Richter, G.M., Longo, G., Pelosi, N., Molisso, F., and Duarte Morais, M.L., 1998, Orbital cyclicity in the Eocene of Angola: visual and image-time-series analysis compared: Earth and Planetary Science Letters, v. 160, p. 147-161.
- Horne, J.H. and Baliunas, S. L., 1986, A prescription for period analysis of unevenly sampled time series: Astrophysical Journal, v. 302, p. 757-763.
- Iwai, M., Acton G.D., Lazarus D., Osterman L.E., and Williams, T., 2002, Magnetobiochronologic synthesis of ODP Leg 178 rise sediments from the Pacific sector of the Southern Ocean: Sites 1095, 1096, and 1101, in Barker P.F., Camerlenghi A., Acton G.D., and Ramsay A.T.S., eds., Proceeding Ocean Drilling Program, Scientific Results, 178, 1-40.[Online].
- Iorio, M., Tarling, D., D'Argenio, B., Nardi, G., and Hailwood, A.E., 1995, Milankovitch cyclicity of magnetic directions in Cretaceous shallow-water carbonate rocks, southern Italy: Bollettino di Geofisica Teorica ed Applicata, v. 37, p. 109-118.

- Iorio M., Wolf-Welling T., Moerz T. 2004 Antarctic sediment drifts and Plio-Pleistocene orbital periodicities (ODP Sites 1095, 1096, and 1101). SEPM Special Publication N°81, in press.
- Rebesco, M., Camerlenghi, A., and Zanolla, C., 1998, Bathymetry and morphogenesis of the continental margin west of the Antarctic Peninsula: *Terra Antarctica*, v. 5, p. 715-725.

## PERIGLACIAL FEATURES IN NORTHERN TIERRA DEL FUEGO, THE ARGENTINE FUEGIAN ANDES AND NORTHERN JAMES ROSS ISLAND, ANTARCTIC PENINSULA: A COMPARISON

8-04

Jorge Rabassa<sup>1</sup>; Pedro Carrera Gómez<sup>2</sup>; Marcos Valcárcel Díaz<sup>2</sup>; Andrea Coronato<sup>1</sup>  
Augusto Pérez Alberti<sup>2</sup>; Gustavo G. Bujalesky<sup>1</sup>; José María Redondo Vega<sup>3</sup>

1 *Centro Austral de Investigaciones Científicas (CADIC-CONICET). B. Houssay 200 (9410) Ushuaia, Argentina. jrabassa@infovia.com.ar*

2 *Departamento de Xeografía. Universidade de Santiago de Compostela. Plaza da Universidade, 1. 15782-Santiago de Compostela (A Coruña), España.*

3 *Departamento de Geografía, Universidad de León, León, España.*

### Introduction

Several periglacial features have been observed at Cabo Peñas (lat. 53° 50.155' S; long. 67° 35.208' W), close to the sea level, in Northern Tierra del Fuego, and above 1000 m a.s.l. in the surroundings of Monte Alvear (lat. 54° 40' S; long. 68° 04' W), Argentine Fuegian Andes. These features are presently being investigated and they are compared with similar features occurring in a deglaciated area of Northern James Ross Island, Antarctic Peninsula (lat. 63° 45' S, long. 64° 20' W), between present sea level and 200 m a.s.l.

### Northern Tierra del Fuego

In Northern Tierra del Fuego only fossil the periglacial features have been detected. They are represented by ice-wedge casts, vertical stones, cryoturbation and involutions, developed on upraised marine beach deposits. These correspond to the La Sara Formation, a unit formed during Last Interglacial time (Oxygen Isotope Stage 5, ca. 125 ka BP) and covered by Holocene aeolian sandy sediments. The ice-wedge casts were formed under palaeoclimatic conditions of continuous permafrost, with mean annual temperatures as low as -6°C (perhaps even -8°C, due to the highly permeable conditions of bedrock, the beach sand and gravel). In this period the Atlantic coast was located perhaps more than 100 m below present sea level, tens of kilometers farther to the East, climate was much colder and drier than today, and ice-lobe glaciers covered the landscape roughly 100 km southwards along the Lago Fagnano depression and at Bahía Inútil (Chile) ca. 100 km northwestwards.

### The Fuegian Andes

The knowledge of cryogenic (nivation and periglacial) landforms in the Fuegian Andes has been, until recently, very scarce. In this paper, the finding of cryogenic features in the highest portions of a peak nearby Monte Alvear (lat. 54°40'30" S; long. 68°02'30" W; 1077 m a.s.l.) is discussed. The studied area is located at Sierra de Alvear, precisely on the interfluvium of Las Cotorras and Tristán creeks, 25 km NE of Ushuaia. It is a zone of great interest due to its lithological variety (schists, basalts, porphyritic rocks), its topographic features (valley sides with strong slopes and subhorizontal steps, with an extensive, plain summit area), its orientation (N, E and S oriented slopes, with the summit area exposed to all winds) and its climatic characteristics (though no absolute data is still available). This area is herein named as "Monte Alvear", though it is not referred to the Alvear peak itself. The combination of all these factors in a relatively reduced area has generated a series of very well developed landforms linked to cryonival morphodynamics, such as nivation hollows, patterned ground and subnival pavements, and periglacial processes, such as small tors, frost-heaved bedrock features and, again, patterned ground. Below we provide a description of such landforms.

### 1. *Nivation hollows*

These landforms, generated by a set of processes globally included under the term “nivation”, appear where the snow is accumulated during long periods. They are small depressions or steps attached to the slopes, which are progressively deepened by the snow masses accumulated there. Snow creep, summer subnival melting and its associated rill erosion, and gelifluction play a significant role in their genesis. These landforms occur mainly in the E-NE slope of the studied area, between 1000 and 1050 m a.s.l., on a substratum composed of scists and basalts. They form elongated depressions, following contour lines, with a concave cross section, with a marked step in their lower part and occupied by permanent snowbeds. The preferred localization of the nivation hollows along the lee slope may be due basically to the overfeeding of wind-blown snow from the summit surface, that allows the existence of snowbeds thick enough so as to overcome the summer thaw period. Another factor may be the nature of the substratum. The scist outcrops are very soft and they are densely fractured, enabling the erosive action of the different nivation processes.

### 2. *Subnival pavements*

They are preferably located at the SE portion of the summit surface, extending also towards the E slope, always above 1050 m a.s.l. They form sheets of planated clasts, in a silty soil, that cover gentle slopes. Its presence is related to the existence of significant snow thickness, whose weight pushes down the clasts emerging from the silty soil. In areas of gentle slope, the *a*-axes of the clasts clearly tend to be aligned with the slope. This fact is possibly due to snow creep action.

### 3. *Tors*

These are features of small dimensions that are found mostly on the planated surfaces of the NW slope, at around 1020 m a.s.l., though other examples may be observed also at the summit surface. They are small, residual outcrops of upraising volcanic substratum, reaching up to 1.5 m in height. Frost shattering processes are the main force responsible for their genesis. It seems to be a very active process, according to the large number of very recently shattered basaltic fragments observed along the slopes.

### 4. *Frost-heaved bedrock features*

They are produced by the vertical displacement of rocky fragments. They are usually clasts of boulder size, dragged from the substratum by frost shattering, which have been later uplifted above the surface by frost heave generated by water freezing in the joints and other discontinuities. These features are most likely generated in densely fractured rock types. The examples found in the study area are located at the summit surface, in areas of gentle slope, above 1050 m a.s.l. Rocky fragments occur regularly in vertical and subvertical positions, sometimes up to 1.5 m above the surrounding surface, in small, linear outcrops of scists and basalts. Their faces are well defined by discontinuity planes, such as joints and scistosity. At the summit, the isolating effect of the snow cover on the substratum must be negligible, being a highly wind-exposed area. Frost action will be here more energetic and persistent than in the lee-side zones, which undergo a higher snow accumulation, allowing the mobilization of rocky fragments of metric size. These landforms require the existence of permafrost for their genesis and it must be established now whether these forms are still active today in the study area.

### 5. *Patterned ground*

These are the most abundant and varied periglacial landforms in this area. In stepped surfaces and gentle slope valley sides, they are present as clast circles and polygons, gradually passing to coarse material stripes alternating with finer materials as slope increases. Concerning on their morphology, dimensions, clast size and presence/absence of sorting, they are classified through four dominant typologies, following Washburn (1979): sorted stone macrocircles, sorted stone circles, unsorted stone circles and sorted stone stripes. The sorted stone macrocircles are found only at the summit surface, above 1050 m a.s.l., in basalt and scist areas of very gentle slopes or almost flat areas. They are composed by an outer ring formed by coarse clasts of up to 50 cm long *a*-axis, frequently in vertical

position and colonized by lichens. They enclose an inner, bulged core, formed mostly by finer materials (sands and silts), in which larger clasts also appear. In the finer sediment core, small polygons, formed by coarser sands and gravels and sculptured onto the silty matrix, are sometimes observed. These landforms as a whole may reach up to 2 m in diameter. The maximum development of the patterned ground at the summit surface is possibly explained as due to the absence of a snow cover, because of the aeolian transport. It would be thick enough to thermally isolate the soil, which would thus be exposed during a longer time to frost action in depth. The sorted and unsorted stone circles are developed in the subhorizontal steps of NW and N slopes, between 1000 and 1030 m a.s.l., on a basaltic substratum. The former are composed by an outer ring of larger clasts (up to 30 cm long *a*-axis), occasionally vertically arranged, and a core with abundant coarse gravel-size clasts and smaller cobbles, embedded in silts. They reach maximum dimensions ranging from 1 and 1.5 m in diameter. The latter, however, do not present a core with fines. They are formed by heterometric clasts and they frequently present decimetric size boulders along their outer edge. They usually reach up to 1 m in diameter. The striated soils occur preferably along the E slope, above 1000 m a.s.l., where slope range from 8° to 15°, on scists and basalts. They are formed by 5-8 cm wide, 4-6 m long parallel stripes, composed by coarse sands, gravels and small cobbles, aligned following the line of maximum slope and separated each other by 10-15 cm wide, silty-sandy stripes. These landforms seem to have been originated by the action of daily repeated, freeze (nocturnal)-thaw (diurnal) cycles, in the soil upper layers. In this lee-side slope, the accumulation and persistency of snow may be important, as proved by the existence of permanent snowbeds. The striated soil development shall be restricted to the snow free period: from the end of Spring to beginning of the Fall. It is also possible that the snow cover modifies them at each winter, due to the dragging effect of snow creep.

#### *6. Monitoring the air and soil thermal régimes*

To know the thermal régime of the studied mountain sector and to determine its influence on the genesis of the different observed landforms, two automatic recording devices have been installed to measure the air and soil temperatures. Both are based on “Onset” multichannel dataloggers and thermistor sensors. The equipments have been programmed to make and record a measurement every hour, during 338 days. The recovering of the data will be done at the field, by means of connecting the recorders with a laptop. The air temperature measuring instrument was installed in a plain surface at the NW slope, located at 1020 m a.s.l. The sensors are fixed to a pole, at heights of 10, 50, 100 and 200 cm above the ground surface. This instrument will also be used to make an estimation of snow cover thickness. The soil temperature recorder was installed nearby. The sensors were located within the colluvial cover at 1, 5, 10, 15, 20, 25, 50 and 100 cm depths. The obtained readings will allow to know the number of freeze-thaw cycles in the soil, the duration of freezing periods, as well as the velocity of penetration of frost and thaw fronts.

Other periglacial associated features observed in this region include ploughing boulders, protalus ramparts in front of snow patches, cryoplanation terraces and thermokarst depressions.

Most of these landforms seem to be still active today, showing that frozen ground conditions are dominant at these elevations at least during six months, and perhaps all year around, under the present cold-temperate, humid climate conditions.

#### **Northern James Ross Island**

Features identified in Northern James Ross Island comprise the wide distribution of the permafrost, characteristics of ground ice, patterned ground, “rock pingos”, protalus rampart in front of occupied nivation hollows and abandoned glacial cirques, and frosting and up-heaving soil conditions in front of north-facing erratic boulders due to differential exposure to the sun. Outstanding examples of in-situ (e.g., without transportation) rounding of Cretaceous sandstone clasts by frost weathering are presented. Periglacial activity in this area is related to different circumstances, but elevation, ground and bedrock lithology, and age of the deglaciated surface seem to be the most significant. The age of these features ranges from Last Glaciation time (Late Pleistocene) to the Present.

## Discussion

A comparison among the three studied regions shows that permafrost conditions occurring today between sea level and 200 m a.s.l. in Eastern Antarctic Peninsula and seasonal frozen ground above 1000 m a.s.l. in the Fuegian Andes, were also present in Northern Tierra del Fuego during the Last Glaciation, O.I.S. 4 to 2. Being the present mean annual temperature around 5.2°C, the total mean annual thermal depression in Northern Tierra del Fuego would have been more than 10°C (perhaps up to 12°C) in this extra-glaciated landscape during Last Glacial Maximum time.

## REFERENCE

- Washburn, A. L. 1979. *Geocryology. A survey of periglacial processes and environments*. Edward Arnold, London.



# **Session 9**

---

**GEOPHYSICAL  
METHODOLOGIES**



## IMPLEMENTATION OF BIO-TECHNOLOGY FOR EARTHQUAKE PREDICTION

9-01

Sanjay Agarwal, Sandeep Tiwari

*Shri Ramswaroop Memorial College of Engineering and Management, Lucknow, India***Owing to Earthquake variation in the earth's magnetic field takes place**

Physiological processes are accompanied with electrical changes. Heart and brain produce characteristic patterns of voltage variations. There are some typical bio-electric signals can be obtained due to polarization and depolarization of cells in the body namely EEG, ECG & EMG. The classification of EEG pattern is based on the different behaviour of animals in different conditions. Another form of EEG pattern is Evoked Response. Evoked Response is the measurement of the disturbance in the EEG pattern that results from external stimuli. Evoked Response (due to change in neurotransmitter ratio in animal brain) can be received. Animals have great sensitivity towards the variations in Earth's magnetic field (usually as a means of orientation).

Body is composed of cells, blood and water and  $H^+$  ions of the water are distributed randomly in the whole body fluid and if magnetic field is applied these ions are polarized in the direction of magnetic field and give intensified response this response is not obtained generally in the case of natural magnetic field of the Earth. This abnormal response can be received and processed against the normal response and it can be done by using microelectrodes and transducers.

All materials contains nuclei that are either neutrons or protons or a combination of both, possess a nuclear spin and a magnetic moment which has both magnitude and direction. In body tissue or any other specimen, the magnetic moment of the nuclei making up the tissue are randomly aligned and have zero net magnetization ( $M=0$ ).

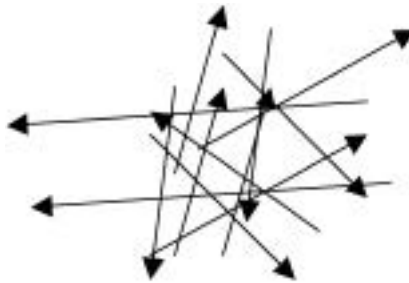


Fig. 1

When a material is placed in a magnetic field  $B_0$ , some of the randomly oriented nuclei experience external magnetic torque, which tends to align individual parallel or anti-parallel magnetic moments to the direction of an applied magnetic field. There is a slight excess of nuclei aligned parallel with the magnetic field and this gives the tissue a net magnetic moment  $M_0$ . It is this differential in this magnetic moment that accounts for the nuclear magnetic resonance signal on which the imaging is based. The magnetic moment being randomly oriented with respect to another, the components in the X-Y plane cancel one another out while the Z components along the direction of the applied magnetic field sum to produce this magnetic moment  $M_0$ .

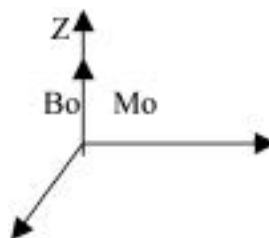


Fig. 2

The application of external magnetic field causes the nuclear magnetic moment to align themselves, producing a net moment in the direction of the applied magnetic field.

According to the electromagnetic theory, any nucleus such as hydrogen proton, which possesses a magnetic moment, attempts to align itself with the magnetic field in which it is placed. This results in a precession or wobbling of the magnetic moment about the applied magnetic field with a resonant angular frequency  $\omega_0$  (Larmour frequency).

Applied external magnetic field creates an energy absorption state from a statistical point of view. When a nucleus with a magnetic moment is placed in a magnetic field, the energy of the nucleus is split into Lower (moment parallel with the field) and higher (anti-parallel with the field). The energy difference is such that a proton with specific frequency (energy) is necessary to excite a nucleus from the lower to higher state.

The excitation energy  $E$  is given by  $E = h \omega_0$ .



Fig. 3

At room temperature, more protons are in low energy state than in a high energy state. The excited protons tend to return or relax to its low energy state with spontaneous decay and re-emission of energy at a later time 't' in the form of radio wave photons. If in a static field, RF waves of the right frequency are passed through the sample of interest, some of the parallel protons will absorb energy and be stimulated or excited to a higher energy in the antiparallel direction, some time later the RF frequency absorbed will be emitted as electromagnetic energy of the same frequency as the RF source. The amount of energy to flip the protons from parallel to anti-parallel orientation is directly related to the magnetic field strength, stronger field require more energy or higher frequency radiation.

Receiving the signals we can classify and process signals pattern using neural network.

Neural network deals with pattern classification, signal processing and control application. Pattern classification task where requirement is to assign an input signal representing a physical object or event to one of several prescribed categories.

This concept of neural network can be used to process signal and to classify these pattern.

## REFERENCES

- R.B. Schall, An Evaluation of the Animal-behavior theory for earthquake Prediction, 1988, California Geology, Vol. 41, No. 2, pp. 41-45.
- M. McNutt and T.H. Heaton, An Evaluation of the seismic-window theory for earthquake prediction, 1981, California Geology, January, 1981, pp. 12-16.
- S.P. Nishenko, Circum-Pacific seismic potential: 1989-99, 1991, Pure and Applied Geophysics, Vol. 135, No. 2, pp. 169-259.
- Earthquake Research at Parkfield, California, for 1993 and Beyond - National Earthquake Prediction Evaluation Council Working Group, 1994, U.S. Geological Survey Circular 1116, 14 p.
- B.A. Bolt, Earthquakes, 1992, W.H. Freeman and Company, 331 p.
- P.L. Ward and R.A. Page, The Loma Prieta Earthquake of October 17, 1989 - What Happened - What is Expected - What can be done, 1990, U.S. Geological Survey
- R.L. Wesson and R.E. Wallace, Predicting the Next Great Earthquake in California, 1985, Scientific American, Vol. 252, No. 2, pp. 35-43.
- D.C. Agnew and L.M. Jones, Prediction Probabilities from Foreshocks, 1991, Journal of Geophysical Research, Vol. 96, No. B7, pp. 11,959-11,971.

## SIMULATION OF SEISMOGRAMS USING THE KELVIN-VOIGT STRESS-STRAIN RELATION

9-02

J.M. Carcione<sup>1</sup>, F. Poletto<sup>1</sup>, D. Gei<sup>1</sup>, M.A.B. Botelho<sup>2</sup>

<sup>1</sup> *Istituto Nazionale di Oceanografia e di Geofisica Sperimentale – OGS  
Borgo Grotta Gigante 42c – 34010 Sgonico, Trieste, Italy*

<sup>2</sup> *Universidade Federal da Bahia, Salvador, Brazil*

### Summary

We design a numerical algorithm for wave simulation in anelastic media in the presence of free surface, which can be used to model seismic waves at the Earth's surface. The modeling simulates 3-D waves by using the Fourier and Chebyshev methods to compute the spatial derivatives along the horizontal and vertical directions, respectively. The stress-strain relation is based on the Kelvin-Voigt mechanical model, which has the advantage of not requiring additional field variables. The model requires two anelastic parameters and twice the spatial derivatives of the lossless case. The high-frequency components of the wave field are more attenuated than the low-frequency components, with the attenuation factors being approximately proportional to the square of the frequency. The methodology is illustrated with two examples. The first one represents a seismic experiment for environmental applications, and the second example shows the simulation of the January 7 (2000) earthquake recorded at Ushuaia seismograph station (Argentina).

### Introduction

Wave modeling is a valuable tool for seismic interpretation and an essential part of inversion algorithms. Problems regarding environmental geophysics, seismic exploration, foundation engineering, earthquake seismology and non-destructive testing (NDT) of materials require the use of full-wave three-dimensional modeling methods. In particular, it is important to model the surface waves (Rayleigh and Love waves) and record the components of the wave field. Moreover, the unconsolidated nature of the shallow layers in many cases, requires an anelastic stress-strain relation to model the dissipation of the wave field. An efficient and highly accurate technique is full-wave modeling by using pseudospectral methods (Carcione, 2001; Carcione et al., 2002). With the pseudospectral approach, free surface can be modeled by the “zero-padding” method. However, this is not optimal, mainly when source and receiver are near the surface (Reshef et al., 1988). To overcome this problem, derivatives along the vertical direction can be computed with the Chebyshev differential operator. Unlike the Fourier method, the Chebyshev method is not periodic and allows for the incorporation of boundary conditions by using characteristic variables, in particular, free surface conditions at the surface and non-reflecting conditions at the bottom of the mesh.

All the modeling algorithms mentioned above solve the wave equation in the space-time domain, where the incorporation of anelasticity requires the use of additional variables, called “memory variables”. Generally, this approach is based on the use of the generalized Zener model or the generalized Maxwell model. Use of memory variables can be expensive in three dimensions, since the Zener model requires six variables for each relaxation mechanism. A model which does not require memory variables is the Kelvin-Voigt mechanical model. We use this model to describe attenuation, because its implementation is simple and only requires the calculation of additional spatial derivatives and the use of two anelastic parameters compared to four parameters when using the Zener model.

The wave equation combines the equation of momentum conservation with the constitutive relations for isotropic and anelastic media based on the Kelvin-Voigt model. The velocity-stress formulation allows the calculation of the particle velocity and stress components simultaneously.

### Equation of motion

The three dimensional Euler-Newton's equations can be expressed as

$$\rho \ddot{u}_i = \frac{\partial \sigma_{ij}}{\partial x_j} + f_i, \quad (1)$$

where  $\rho$  is the density,  $u_i$  are the displacement components,  $\sigma_{ij}$  denote the stress components, and  $f_i$

are the body forces. A dot above a variable denotes time differentiation and the Einstein convention for repeated indices is used. The stress-strain relations for a Kelvin-Voigt solid are a generalization of those for one-dimensional media. They are

$$\sigma_{ij} = (\lambda\theta + \lambda'\dot{\theta})\delta_{ij} + 2\mu\varepsilon_{ij} + 2\mu'\dot{\varepsilon}_{ij}, \tag{2}$$

where  $\lambda$  and  $\mu$  are the Lamé constants,  $\lambda'$  and  $\mu'$  are the corresponding anelastic parameters,

$$\varepsilon_{ij} = \frac{1}{2} \left( \frac{\partial u_i}{\partial x_j} + \frac{\partial u_j}{\partial x_i} \right) \tag{3}$$

are the strain components,

$$\theta = \frac{\partial u_i}{\partial x_i} \tag{4}$$

and  $\delta_{ij}$  is Kronecker's delta.

### Velocity-stress formulation

Introducing the particle-velocity components,  $v_i = \dot{u}_i$  the equations of momentum conservation (1) become

$$\dot{v}_i = \frac{1}{\rho} \left( \frac{\partial \sigma_{ij}}{\partial x_j} + f_i \right). \tag{5}$$

Using equations (3) and (4), the time derivative of the stress-strain relations (2) become

$$\dot{\sigma}_{ij} = \left( \lambda \frac{\partial v_i}{\partial x_i} + \lambda' \frac{\partial \dot{v}_i}{\partial x_i} \right) \delta_{ij} + \mu \left( \frac{\partial v_i}{\partial x_j} + \frac{\partial v_j}{\partial x_i} \right) + \mu' \left( \frac{\partial \dot{v}_i}{\partial x_j} + \frac{\partial \dot{v}_j}{\partial x_i} \right). \tag{6}$$

Substituting (5) into (6) yields

$$\dot{\sigma}_{ij} = \lambda \frac{\partial v_i}{\partial x_i} \delta_{ij} + \lambda' \left[ \frac{\partial}{\partial x_i} \frac{1}{\rho} \left( \frac{\partial \sigma_{ij}}{\partial x_j} + f_i \right) \right] \delta_{ij} + \mu \left( \frac{\partial v_i}{\partial x_j} + \frac{\partial v_j}{\partial x_i} \right) + \mu' \left[ \frac{\partial}{\partial x_j} \frac{1}{\rho} \left( \frac{\partial \sigma_{im}}{\partial x_m} + f_i \right) + \frac{\partial}{\partial x_i} \frac{1}{\rho} \left( \frac{\partial \sigma_{jm}}{\partial x_m} + f_j \right) \right]. \tag{7}$$

Let us express the velocity-stress formulation in explicit form. Define the quantities

$$\begin{aligned} \Pi_x &= \frac{1}{\rho} \left( \frac{\partial \sigma_{xx}}{\partial x} + \frac{\partial \sigma_{xy}}{\partial y} + \frac{\partial \sigma_{xz}}{\partial z} + f_x \right), \\ \Pi_y &= \frac{1}{\rho} \left( \frac{\partial \sigma_{xy}}{\partial x} + \frac{\partial \sigma_{yy}}{\partial y} + \frac{\partial \sigma_{yz}}{\partial z} + f_y \right), \end{aligned} \tag{8}$$

$$\begin{aligned} \Pi_z &= \frac{1}{\rho} \left( \frac{\partial \sigma_{xz}}{\partial x} + \frac{\partial \sigma_{yz}}{\partial y} + \frac{\partial \sigma_{zz}}{\partial z} + f_z \right), \\ \psi &= \frac{\partial \Pi_x}{\partial x} + \frac{\partial \Pi_y}{\partial y} + \frac{\partial \Pi_z}{\partial z} \end{aligned} \tag{9}$$

and

$$\vartheta = \dot{\theta} = \frac{\partial v_x}{\partial x} + \frac{\partial v_y}{\partial y} + \frac{\partial v_z}{\partial z}. \tag{10}$$

Then, equations (5) and (7) can be written in components as

$$\begin{aligned} \dot{v}_x &= \Pi_x, \\ \dot{v}_y &= \Pi_y, \\ \dot{v}_z &= \Pi_z, \\ \dot{\sigma}_{xx} &= \lambda\vartheta + \lambda'\psi + 2\mu \frac{\partial v_x}{\partial x} + 2\mu' \frac{\partial \Pi_x}{\partial x}, \\ \dot{\sigma}_{yy} &= \lambda\vartheta + \lambda'\psi + 2\mu \frac{\partial v_y}{\partial y} + 2\mu' \frac{\partial \Pi_y}{\partial y}, \end{aligned}$$

$$\dot{\sigma}_{zz} = \lambda \dot{\vartheta} + \lambda' \psi + 2\mu \frac{\partial v_z}{\partial z} + 2\mu' \frac{\partial \Pi_z}{\partial z}, \tag{11}$$

$$\dot{\sigma}_{xy} = \mu \left( \frac{\partial v_x}{\partial y} + \frac{\partial v_y}{\partial x} \right) + \mu' \left( \frac{\partial \Pi_x}{\partial y} + \frac{\partial \Pi_y}{\partial x} \right),$$

$$\dot{\sigma}_{xz} = \mu \left( \frac{\partial v_x}{\partial z} + \frac{\partial v_z}{\partial x} \right) + \mu' \left( \frac{\partial \Pi_x}{\partial z} + \frac{\partial \Pi_z}{\partial x} \right),$$

$$\dot{\sigma}_{yz} = \mu \left( \frac{\partial v_y}{\partial z} + \frac{\partial v_z}{\partial y} \right) + \mu' \left( \frac{\partial \Pi_y}{\partial z} + \frac{\partial \Pi_z}{\partial y} \right).$$

Equations (8) and (11) constitute the velocity stress formulation for the Kelvin-Voigt model.

**Examples**

The first example represents a seismic experiment for environmental applications. Figure 1 shows the model properties, source location and the line of receivers. The media are Poisson solids and the mesh has 81 x 81 x 81 grid points. The source (a Ricker-type wavelet) is a vertical force located at 2.5 m depth and has a dominant frequency of 50 Hz.

Fig. 1 - Model, properties, and source and receiver locations to illustrate the propagation of Rayleigh waves. The media are the Poisson solids.

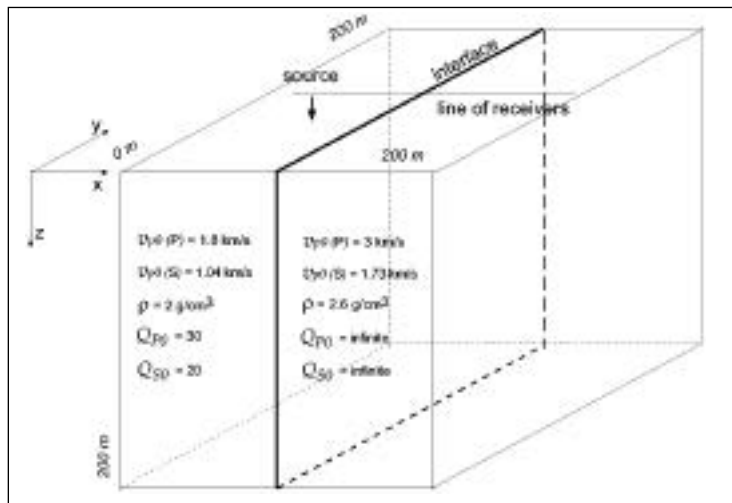


Figure 2 shows the seismograms for the  $v_x$  component, where (a) corresponds to the lossless case and (b) to the lossy case. The incident Rayleigh wave (iR) arrives at the interface at 0.4 s and splits into a reflected Rayleigh wave (iRrR) and a transmitted Rayleigh wave (iRtR).

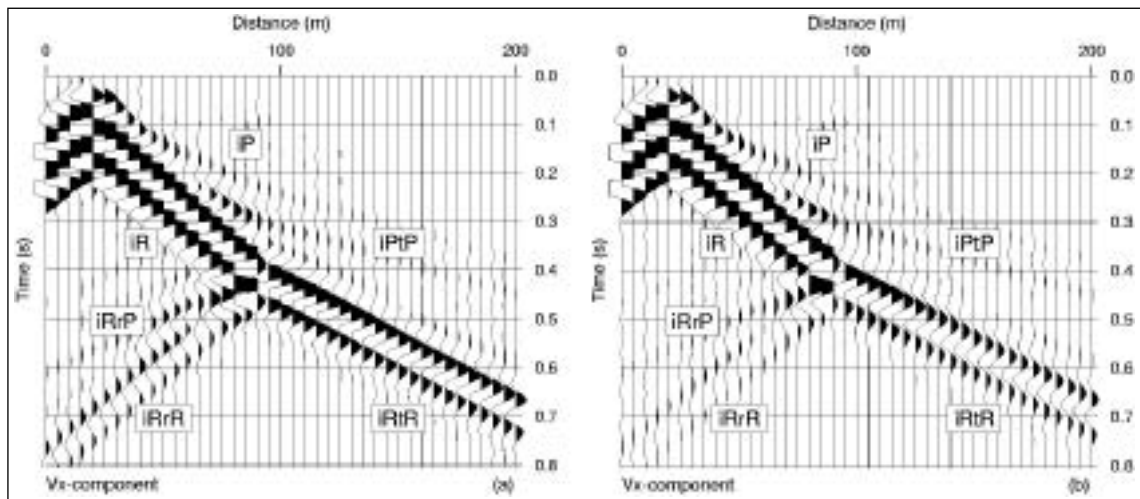


Fig. 2 - Seismograms of the  $v_x$  component (see Fig. 1), where (a) corresponds to the lossless case and (b) to the lossy case. In this case, the incidence medium is viscoelastic. The labels indicate the different waves, with “i”, “r” and “t” denoting incident, reflected and transmitted, and “P” and “R” denoting compressional and Rayleigh, respectively.

The second example represents the simulation of the January 7 (2000) earthquake ( $M_w = 5.5$ ) recorded at Ushuaia (Argentina) seismograph station (USHU) (Fig. 3). The location of the epicenter is indicated by a star, and the source has a depth of 15 km below the sea level (this event is indicated as 010700A in the Harvard CMT Catalog).

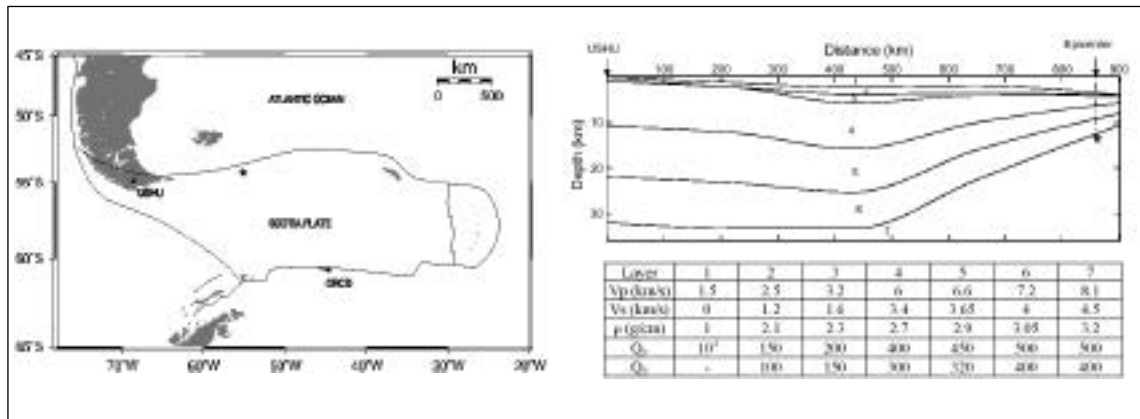


Fig. 3 - Location of the Ushuaia seismograph station (USHU) and the epicenter of the January 7 (2000) earthquake (star) (a), and geological model at the Scotia Plate (b).

In this case, the solution is two dimensional, since a complete 3D has to be built. The mesh has 729 x 101 points with a grid spacing of 1.5 km in the horizontal direction and a vertical size of 106.5 km (the location of the closest grid point to the surface is 174 m). The source is a dip-slip moment tensor with components  $M_{xx} = -M_0 \sin 2\delta$ ,  $M_{zz} = M_0 \sin 2\delta$  and  $M_{xz} = -M_0 \cos 2\delta$ , where  $M_0$  is the moment and  $\delta$  is the dip angle. The rake and strike angles are both equal to  $\pi/2$ . Here, we consider  $M_0 = 1$  and  $\delta = 40^\circ$ . The source time history is a Ricker-type wavelet with 0.2 Hz dominant frequency, and Ushuaia station (the receiver) is located at 870 km from the epicenter. Figure 4 shows the vertical and radial seismograms of the January 7 (2000) earthquake recorded at Ushuaia station (a) and obtained from the simulation (b).

The real and simulated seismograms have a qualitative similarity due to the 2-D nature of the model. Extension of the model to three dimensions is necessary to improve the simulation.

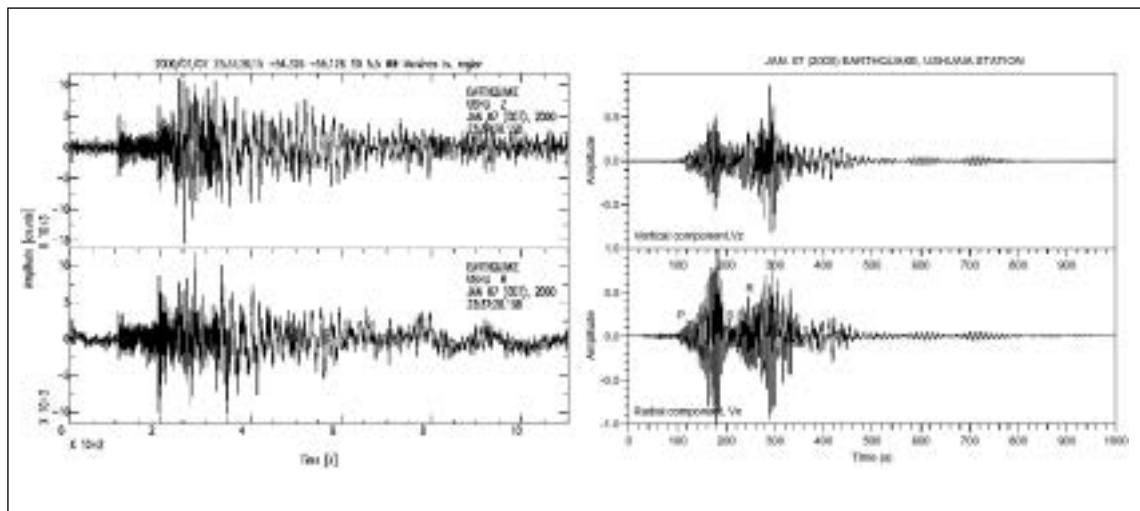


Fig. 4 - Vertical and radial seismograms of the January 7 (2000) earthquake recorded at Ushuaia station (a) and obtained from the simulation (b). The labels P, S and R indicate the compressional, shear and Rayleigh waves.



## REFERENCES

- Carcione, J. M., (1992), Modeling anelastic singular surface waves in the Earth, *Geophysics*, 57, 781-792.
- Carcione, J. M., (2001), *Wave Fields in Real Media. Theory and numerical simulation of wave propagation in anisotropic, anelastic and porous media*, Pergamon Press.
- Carcione, J. M., Herman, G., and ten Kroode, F. P. E., (2002), Seismic modeling, *Geophysics*, 67, 1304-1325.
- Reshet, M., Kosloff, D., and Loewenthal, D., (1984), Elastic wave calculations by the Fourier method, *Bull. Seis. Soc. Am.*, vol. 74, pp. 875-891.

**COMBINED USE OF THE GGSFT DATA BASE AND ON BOARD MARINE COLLECTED DATA TO MODEL THE CRUST-MANTLE INTERFACE BENEATH THE POWELL BASIN, ANTARCTICA**

9-03

René E. Chávez<sup>(1)</sup>, E. Leticia Flores-Marquez<sup>(1)</sup>, Emma Suriñach<sup>(2)</sup>, Jesús Galindo-Zaldivar<sup>(3)</sup>, José Rodríguez-Fernández<sup>(4)</sup>, Andrés Maldonado<sup>(4)</sup>

(1) *Instituto de Geofísica, UNAM, Cd. Universitaria, Circuito Exterior, 04510. México, D.F.*

(2) *Departament de Geodinàmica i Geofísica, Universitat de Barcelona, 08028 Barcelona, España*

(3) *Departamento de Geodinámica, Universidad de Granada, 18071 Granada, España*

(4) *Instituto Andaluz de Ciencias de la Tierra, CSIC-Univ. de Granada, 18071 Granada, España*

### Summary

The Powell Basin is a small oceanic basin located at the NE end of the Antarctic Peninsula developed during the Early Miocene. Data from the Global Gravity Grid, the Global Sea Floor Topography (GGSFT) and on board collected gravity and bathymetric observations from the SCAN 97 cruise were used to determine the 3D crust-mantle interface (CMI) by numerical inversion. This smooth computed model shows an increase in the thickness of the crust towards the continental margins and a NW-SE oriented axis of asymmetry coinciding with the position of an older oceanic spreading ridge. This interface shows a moderate uplift towards the western part, and depicts two main uplifts to the northern and eastern sectors of the basin.

### Introduction

The Powell Basin is a small ocean basin (approximately  $5 \times 10^4$  km<sup>2</sup>), located within the Antarctic Plate, to the NE of the Antarctic Peninsula, close to the limit of the Scotia Plate to the north (Fig. 1). This is a small oceanic basin that is slightly elongated in a NE-SW direction. The basin floor is practically horizontal reaching an average depth of 3200 m, and slightly deepens to the SE. The platforms surrounding the basin present an average depth of 500 m.

The northern margins are very steep, whereas the eastern and western margins have gentle slopes. An inactive spreading ridge located to the center of the basin with a NW-SE direction has been identified. Evidence of this, together with the approximate boundary between oceanic and continental crusts was found from seismic studies carried out in this place (King et al., 1997; Rodríguez-Fernández et al., 1997) and from magnetic studies (Suriñach et al., 1997). Different authors (Larter and Barker, 1991; Livermore and Woollett, 1993; Lawver et al., 1994; Barker, 1995) have discussed in closed detail the chronology of the major events in the evolution of this basin. However, the layouts of the continental margins, the location of the principal tectonic features, the characteristics of the depositional sequences, and the paleoceanographic evolution have not been previously analyzed in detail.

The aim of this study is to determine the 3D structure of the crust-mantle interface (CMI) in the oceanic crust of the Powell Basin, applying a numerical inversion to the gravity data. The Global Gravity Data and the Global Sea Floor Topography databases (GGSFT) (Sandwell and Smith, 1997, <http://topex.ucsd.edu>) were employed in combination with the gravity data collected from the ship transects carried out during the SCAN 97 cruise to compute the geophysical model.

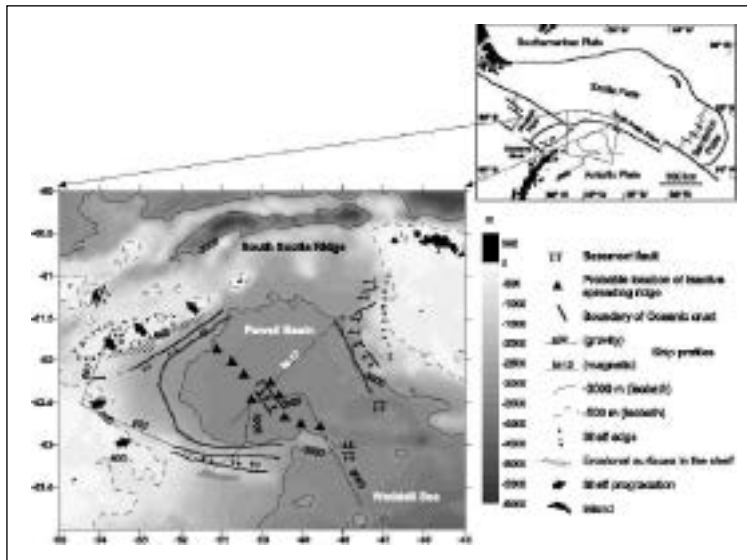


Fig. 1 - Simplified geological chart of the Powell Basin (top right) and main tectonic features within the area (after Rodriguez et al., 1997). The bathymetry map in m obtained from the GGSFT database (Sandwell and Smith, 1997) and the SCAN 97 cruise data are displayed in a gray tone scale (bottom left).

## Geology

Magnetic anomalies obtained from marine transects have been associated to anomalous bodies in the continental basement (Suriñach et al., 1997). These bodies may represent basic igneous rocks, probably gabbros of Cretaceous age, located along the Pacific margin in the Antarctic Peninsula (Garrett, 1990; Maslanyj et al., 1991). Most authors consider this anomaly to be caused by a linear batholithic complex following the arcuate shape of the Antarctic Peninsula. This batholithic body was probably intruded during crustal extensional episodes of the arc in the active margin (Garrett, 1990). There are no high-amplitude magnetic anomalies in the rest of the profiles obtained, which is evidence of the heterogeneous nature of the continental crust around the Powell Basin. However, very low amplitude oceanic sea floor magnetic anomalies have been identified in the central part of the Powell Basin confirming its oceanic nature and suggesting a spreading age ranging between 29.7 Ma and 21.8 Ma (Eagles and Livermore, 2002).

## Gravity and Topographic Data Analysis

A region of 10° Long and 4° Lat covering the Powell basin was selected. This area is approximately square (45° to 55° W and 60° to 64° S) for this latitude (Fig. 1). Gravity and bathymetry data were obtained from the GGSFT version V9.2 from <http://topex.ucsd.edu> (Sandwell and Smith, 1997), for the reference year of 2001. Data collected from ship transects corresponding to 5 profiles carried out by the Spanish R/V Hespérides, during the SCAN 97 cruise, were also included (Fig. 1). The GGSFT database (Sandwell and Smith, 1997) is based on the declassified GEOSAT altimeter data (in June 1995) and the ERS 1 mapping phase, as well as on the widely spaced tracks of the Topex/Poseidon altimeter data. Sandwell and Smith (1997) converted the collected altimeter profiles to grids of vertical gravity gradient and gravity anomaly. We have used the measured depths embedded in the GGSFT database and the bathymetric data collected by the SCAN 97 profiles to establish a whole image of the sea bottom pattern (Fig. 1, gray tone scale map). The areas not covered by these data were filled with the predicted bathymetry of the GGSFT database. Such database was compared with 5 profiles collected from the SCAN 97 fieldwork (g01, g02, gb01, gb02, gb03; in Fig. 1). Free-Air gravity anomalies were compared point to point (Fig. 2). This analysis shows a good agreement between the marine and GGSFT database, although the GGSFT gravity data represent a smooth version of the observations at sea. However, the gravity interpretation was done with a combination of the GGSFT database and the SCAN 97 data, giving double weight to this database in the interpolation process. The Free-Air gravity anomaly (FA) was then interpolated in a regular grid with a  $\Delta x = 4$  km and  $\Delta y = 3.8$  km space interval (Fig. 3). The evidence of an asymmetry along an axis crossing in the NW-SE direction on this central portion (Rodríguez-Fernández et al., 1997) can be observed (black triangles in Fig. 3).

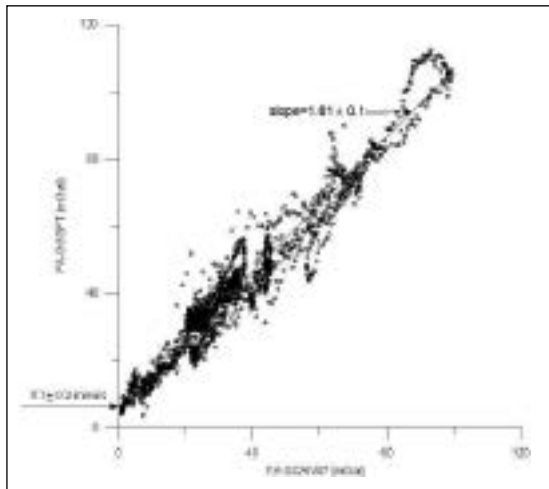


Fig. 2 - Correlation between FA data (GGSFT database) and the SCAN 97 project observations.

The FA anomaly data was corrected for the water-sediment topography ( $g_{w-s}$ ) and for the sediment-crust interface effects ( $g_{s-c}$ ), which are superimposed onto the effect of the sub-bottom density changes reflected in the FA anomaly (Fig. 3). Each correction is obtained by computing the gravity contribution produced by a source of infinite lateral extension bounded by a flat surface ( $z=0$ ) at the top, and a buried topography at the bottom (Parker, 1995). This process is similar to the topographic correction performed on continental surveyed data (Flores-Márquez et al., 2003). Therefore, a total gravity anomaly map can be constructed from:

$$\mathbf{gT} = \text{F.A.} - (g_{w-s} + g_{s-c}) \quad (1)$$

The estimated  $\mathbf{gT}$  anomaly (Fig. 4) depicts a conspicuous NW-SE alignment of low gravity values, which coincides with the location of the inferred inactive spreading ridge (black triangles, Fig. 4). Moreover, a gravity high located to the NE of this feature and not to the SW is observed, indicating an asymmetry in the basin. This map suggests a thin oceanic crust, with steep slopes to the NW and a gentle inclination towards the SE. Negative gravity values (dark grey tones) show a good correlation with the continental crust and positive gravity values (light gray tones) with the oceanic crust.

### Spectral Analysis

A regional-residual separation process is applied to the  $\mathbf{gT}$  anomaly. We attributed that most of the regional field is due to the crust-mantle interface (CMI). We have applied the Spectral Factorization Method (SFM) (Spector and Grant, 1970) to estimate the average depth and the cut-off wavenumbers of the different gravity sources composing the  $\mathbf{gT}$  anomaly (Suriñach and Chavez, 1996). The regional field is estimated by focusing on the long wavelength sources, which are associated to the CMI. The residual field was not of our interest at this point.

The logarithm of the power spectrum of the total gravity anomaly  $\mathbf{gT}$  shown in Fig. 5, was analyzed as a function of the radial wavenumbers (Naidu and Mishra, 1972). We inferred that the wavenumber

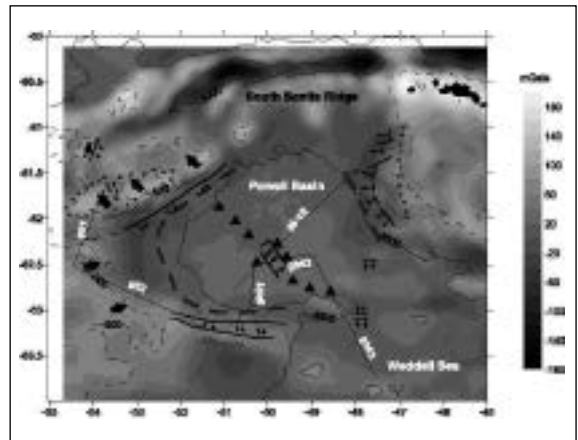


Fig. 3 - FA anomaly from combined GGSFT and SCAN 97 databases. The main tectonic features are overlapped (Fig. 1).

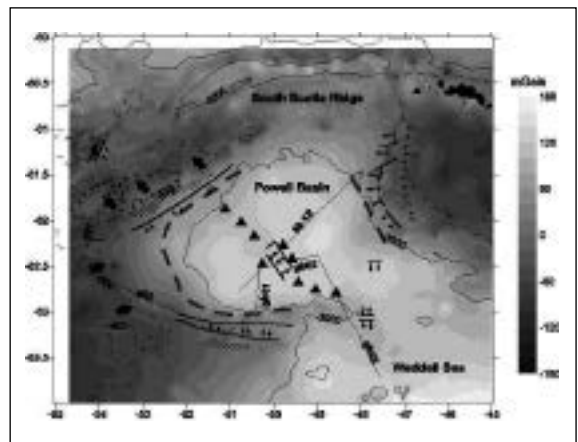


Fig. 4 - Total gravity ( $\mathbf{gT}$ ) anomaly obtained after applying expression (1).

$K_c = 0.075 \text{ km}^{-1}$  separates two domains associated with the regional (low wavenumber content) and the residual and noisy effects (high wavenumber content; Spector and Grant, 1970). A linear regression was applied to the data in that portion of the spectrum to estimate the average depth of the gravity sources (Spector and Grant, 1970). An average depth of  $14.5 \pm 1.1 \text{ km}$  was computed, which can be compared with the depth of  $11.3 \pm 2.3 \text{ km}$  obtained from a refraction study done in a northern location of the Powell Basin (King et al., 1997).

The “Regional” field was calculated by applying a low-pass filter (Butterworth filter). The Powell Basin shows a higher anomaly field suggesting a crustal thinning in relation to the surrounding areas (Fig. 6). The inactive spreading ridge is represented as a slight gravity low running in the NW-SE direction (compare with the location of the black triangles).

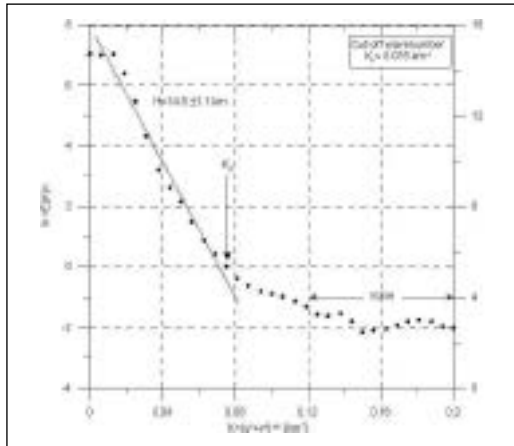


Fig. 5 - Averaged power spectrum of gT anomaly as a function of the radial wave numbers  $K$ . Cut-off wavenumber ( $K_c$ ) indicates a discontinuity in the spectrum. Estimated mean depth of regional sources is also shown.

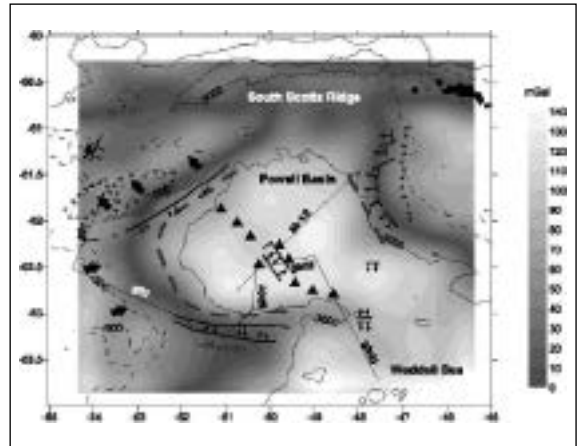


Fig. 6 - Regional anomaly field. A low-pass filter was applied obtained by using the cut-off wavenumber range indicated in Fig. 5.

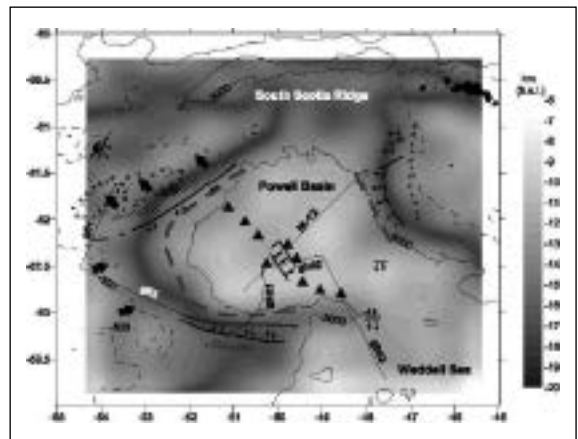


Fig. 7 - 3D geometry of the CMI. Model is obtained by inversion of the regional anomaly (Fig. 8).

### Gravity Inversion

The inversion method used assumes a model consisting of a single layer over a medium (Pilkington and Crossley, 1986). The boundaries of this layer are a horizontal plane  $z=0$  (*upper boundary*), and a surface  $z=h(r)$  (*lower boundary*) defining the interface topography (the CMI). This geometry is obtained by inversion over a reference depth  $z=z_0$ . The irregularities in the interface are considered to be the source of the anomalies. This reference depth is estimated from the corresponding SPF method (Spector and Grant, 1970) and the final buried topography  $h(r)$  is obtained by an iterative approach.

We assumed for the crust and mantle densities of  $2700 \text{ kg/m}^3$  and  $3300 \text{ kg/m}^3$  respectively, according

to the refraction study reported by King et al. (1997); and the seismic velocity-density relationship (Grant and West, 1965, p200). These values yield a density contrast of 600 kg/m<sup>3</sup>. The computed solution (CMI, Fig.7) obtained after four iterations, minimized the root mean square (rms=0.45 mGal). The inverted CMI depicts a conspicuous axis, with deeper CMI values NW-SE oriented, which coincide with the inactive spreading ridge determined by the MCS profiles (black triangles, King et al., 1997; Rodríguez-Fernández et al., 1997). The crust thins up in the Powell Basin, as expected for an oceanic crust. The South Scotia Ridge is characterized by sudden changes in depths.

## Conclusions

Bathymetry and gravity data from the combined database (GGSFT and SCAN 97) were used to obtain the CMI. The geometry obtained does not reveal short-wave anomalies, since GGSFT database perceives a smooth version of the shipborne anomalies. In the absence of a large marine data, the GGSFT database can be used to complement the areas of interest. Nevertheless, the reliability of GGSFT data must be correlated and completed with ship observations in the specific study area. An important contribution of our analysis is the combination of GGSFT data with marine observations on the Powell Basin area. The 3D model computed for the CMI yields evidence of a NW-SE oriented asymmetric axis, which is coincident with the inferred inactive spreading ridge (King et al., 1997). The northeastern part of the basin shows shallower values of the CMI than to the western part of the basin. This may be a consequence of the asymmetric origin of the basin, whose rifting is probably related to a low-angle normal fault dipping towards the NE, and active during spreading.

## Acknowledgements

This study has been partially financed by projects: REN2001-2143/ANT and the interchange program between the Universidad de Barcelona (Spain)-DGIA-UNAM (México).

## REFERENCES.

- Barker, P. F., 1995. Tectonic framework of the Scotia Sea. In Taylor, B., Ed. Backarc Basins, Tectonics and Magmatism. Plenum Press, 281-314.
- Eagles, G., Livermore, R.A., 2002. Opening history of Powell Basin, Antarctic Peninsula. *Marine Geology* 185, 195-205.
- Flores-Márquez, E. L., Suriñach, E., Galindo-Zaldivar, J., Maldonado, A., 2003. 3-D Gravity inversion model of the deep crustal structure of the central Drake Passage (Shackleton Fracture Zone and West Scotia Ridge, Antarctica). *Journal of Geophysical Research* 108-B9, 2445-2456.
- Garret, S. W., 1990. Interpretation of reconnaissance gravity and aeromagnetic surveys of the Antarctic Peninsula. *Journal of Geophysical Research* 95/B5, 6759-6777.
- Grant, F. S., West, G. F., 1965. *Interpretation Theory in Applied Geophysics*. McGraw-Hill, 584p.
- King, E. C., Leitchenkov, G., Galindo-Zaldivar, J., Maldonado, A., y Lodolo, E., 1997. Crustal structure and sedimentation in Powell Basin. In: *Geology and Seismic Stratigraphy of the Antarctic Margin, Part 2, Antarctic Research Series*, Eds. American geophysical Union, 71, 75-93.
- Larter, R. D., Barker, P. F., 1991. Effects of ridge crest-trench interaction on Antarctic-Phoenix spreading forces in a young subducting plate. *Journal of Geophysical Research* 96, 19586-19607.
- Lawver, L. A., Williams, T., Sloan, B., 1994. Seismic stratigraphy and heat flow of Powell Basin. *Terra Antarctica* 1/2, 309-310.
- Livermore, R.A., Woollett, R.W., 1993. Seafloor spreading in the Weddell Sea and Southwest Atlantic since the Late Cretaceous. *Earth and Planetary Science Letters* 117, 475-495.
- Maslanyj, M. P., Garret, S.W., Johnson, A. C., Renner, R. G., Smith, A. M., 1991. Aeromagnetic anomaly map of western Antarctica (Weddell sea sector), Scale 1:2 500 000, B. A. S.
- Naidu, P. S., Mishra, D. C., 1972. Radial and angular spectrum in geophysical map analysis: In: Lainiotis, D. G., and Tannes, N. S., Eds. *Applications and Information of Control Systems*, Reidel Publishing, 447-454.
- Parker, R. L., 1995. Improved Fourier terrain correction, Part I. *Geophysics*, 60, 1007-1017.
- Pilkington, M. y Crossley, D. J., 1986. Determination of crustal interface topography from potential fields. *Geophysics*, 51, 1277-1284.
- Rodríguez-Fernández, J., Balanya, J. C., Galindo-Zaldivar, J., y Maldonado, A., 1997. Tectonic evolution of a restricted ocean basin: the Powell Basin (Northeastern Antarctic Peninsula). *Geodinámica Acta*, 10 (4), 159-174.
- Spector, A. y Grant, F. S., 1970. Statistical models for interpreting aeromagnetic data. *Geophysics*, 35, 293-302.
- Sandwell, D. T. y W. H. F. Smith, 1997. Marine gravity anomaly from Geosat and ERS 1 satellite altimetry, *Journal of Geophysical Research*, 102 (B5), 10039-10054.
- Suriñach E. y Chávez R. E., 1996. A 3D crustal model for the northeastern region of the Iberian Peninsula. *Geophysical Research Letters*, 23 (18), 2457-2460.

## DEPTH-MIGRATED SEISMIC IMAGING NORTH OF 'ISLA DE LOS ESTADOS', ARGENTINA (54° 25' S)

9-04

Alberto H. Comínguez<sup>1</sup>, Alejandro Tassone<sup>2</sup>, Emanuele Lodolo<sup>3</sup>

*1 CONICET-Dpto. Geof. Aplicada, FCAYG, Univ. Nacional de La Plata, Paseo del Bosque s/n, La Plata 1900, Prov. de Bs. As., Argentina; ahcominguez@yahoo.com*

*2 CONICET-Dpto. Geol., FCEyN, Univ. de Buenos Aires, Ciudad Universitaria 1428 Bs. As., Argentina; atassone@gl.fcen.uba.ar*

*3 Istituto Nazionale di Oceanografia e di Geofisica Sperimentale (OGS), Borgo Grotta Gigante 42/C, 34016 Trieste, Italy; elodolo@ogs.trieste.it*

### Abstract

A depth-migrated modeling and interpretation of a seismic reflection profile is presented. The study shows the presence of superposed extensional, compressional and transtensional tectonics, in an area located to the north of Isla de los Estados. The profile, which crosses the offshore part of the Magallanes fold-and-thrust belt, images the deep structural framework of part of this tectonic province. Four main seismic units have been recognized. The major structure identified is a structural high and a down-faulted area with related folds of kilometeric size (3-4 km). Steeply dipping (mainly to the south) reverse faults cut through the folds. Some of these faults represent old extensional faults of the Middle-Mesozoic Rocas Verdes marginal basin rifting, which have been subsequently inverted by compressional stress fields. A noticeable fault system is recognized in the seismic profile, which involves both the sedimentary cover and the acoustic basement. This fault is interpreted as the result of shear stresses produced along the transcurrent South America-Scotia plate boundary.

The Isla de los Estados, located about 60 km off the eastern tip of the Tierra del Fuego Island, may be regarded as the eastern onshore expression of the Fuegian Chain, where volcanoclastics and sedimentary sequences related to the Jurassic-Cretaceous Rocas Verdes basin outcrop (Dalziel et al., 1974b; Caminos, 1980).

### Depth Seismic-Migration Modeling

Depth-migration processing was implemented on an early stack-section (see fig. 2). In particular, we used the  $\Omega$ -X in-depth algorithm (Yilmaz, 2001), obtaining intelligible information down to 4 km depth, depending on noise circumstances. In addition, progressive models of Upper Crust velocity were iteratively matched with its corresponding migrated section. The iterative process was considered concluded when it was observed good coincidence between the model and the main seismic horizons of the depth-migrated section: this methodology guaranteed the consistency of the interpreted model. The main seismic reflectors were identified following the guidelines described in Brown and Fisher (1980). Subsequently, four main discontinuities were identified which allowed to recognize three main units overlying the acoustic basement.

### Description of the Seismic Units

**Unit 1:** This unit corresponds to the acoustic basement (Fig. 3). The top of this unit is defined by a continuous reflector of high amplitude, which only occasionally is affected by faults. High amplitude packages overlying an area of chaotic reflections dipping to the NW were identified in the SE tip of the section (between 0.5 and 0.7 km at shot point 943, Fig. 2). This package is intersected to the SE of shot point 993 by acoustic noise (multiple events). In the NW sector of the seismic profile, the high amplitude reflectors are found at around 2.0 km depth (Fig. 2, shot point 1443).

**Unit 2:** It overlies the Unit 1 and displays a tabular geometry (its thickness varies from 0.25 km in the SE to 0.8 km in the NW sector). The top of this unit is defined by a high amplitude reflector which displays good lateral continuity. This reflector is located at 1.2 km in the northern part of the seismic profile and at around 0.5 km in the southern sector. Some reflector packages of high amplitude (higher than those of unit 1) are recognized in some sectors within this unit: 1.2 km at shot point 1493, 1.2 km at shot point 1443, 1.1 km at shot points 1393 and 1293 (Fig. 2).

**Units 3a and 3b:** They display an irregular shape. They reach up to 1.0 km in thickness (the greatest

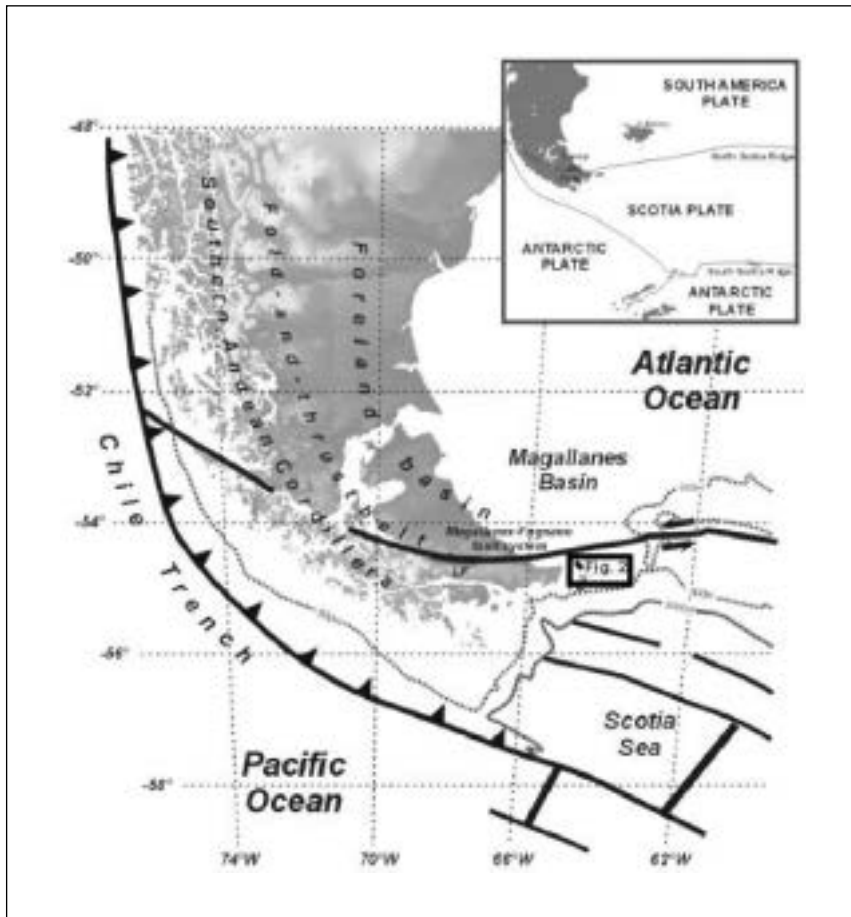


Fig. 1 - Simplified tectonic sketch of the southern tip of South America. Stippled segment (surrounded by rectangle) refers to the seismic profile in Fig. 2. LF = Lago Fagnano; IE= Isla de los Estados.

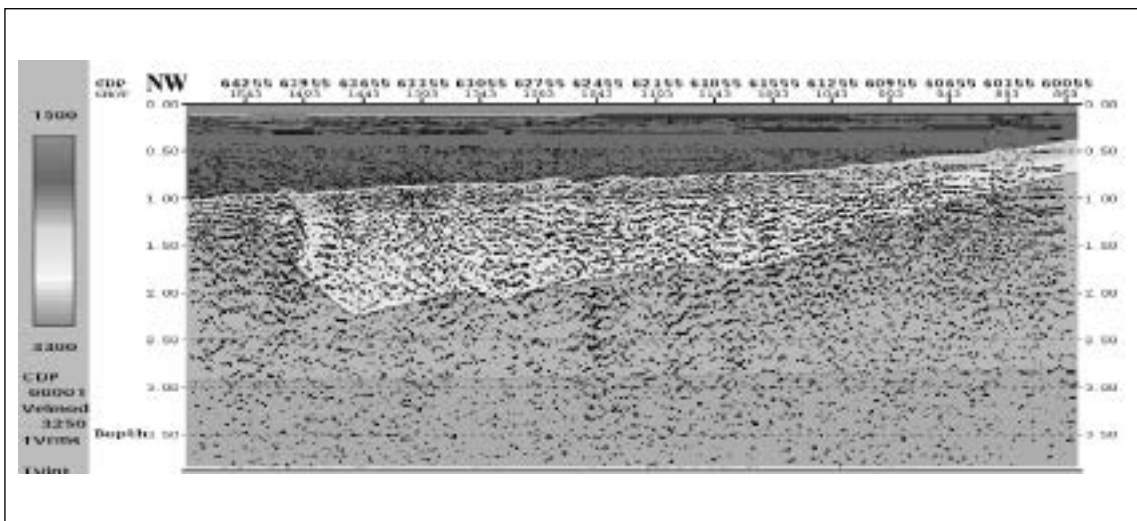


Fig. 2 - Depth seismic-migration modeling. Left column denotes the equivalence between colours and seismic velocities (limit values are indicated at the extremes in m/s).

of the three identified units). The top is defined by a high amplitude reflector which displays a good lateral continuity (Fig. 2). It is located at around 0.25-0.2 km. The internal reflector configurations show moderate amplitude and continuity with low- to moderate frequency.

**Unit 4:** It is the uppermost unit located between the ocean floor and the 0.25 km. It displays a fairly uniform thickness. It is clearly distinguished from the underlying unit 3b by the low frequency of reflectors with low to moderate amplitude and continuity.

## Structure

The southeastern portion of the seismic profile is characterized by a structural high which involves the units 1, 2 and 3. The central and northwestern sectors of the seismic profile presents a major structure dominated by folds of kilometric size (3-4 Km), mostly displayed by units 3 and 4 (Figs. 2 and 3).

A set of steeply dipping (mainly to the S) listric reverse faults cut through the folds. These faults involve both the acoustic basement (unit 1) as the whole sedimentary cover (units 2, 3 and 4). Some of these structures are extensional faults probably related to the rifting phase of the Rocas Verdes basin. In the uppermost section, some of the faults display the characteristics of extensional faults likely resulting from sedimentary compaction.

There is a good correspondence between the interpreted overall structure of the seismic profile and the modeled iso-velocity curves. Between the ocean floor and around 0.25 km, there is a zone of high-angle reverse faults (dipping mainly to the SE) which affect upper unit 3b and unit 4.

Within the seismic profile, some flower structures are defined by intersecting reverse faults (old extensional faults could have been involved in the flower structure also).

## Conclusive Remarks

The above described seismic profile partially cuts across the southern part of the fold and thrust belt of the Fueguian Orogene. (Fig. 1). Taking into account the limitations in correlating offshore seismic units with the known surface units, a preliminary scheme is presented here in order to correlate the offshore units with the reported onshore geology of the Fueguian Orogene (Olivero et al., 1999; Diraison et al., 2000).

The top of unit 1 is characterized by a zone of discontinuous parallel reflections overlying a zone of chaotic reflectors like the one reported for the upper boundary of the acoustic basement of the western Malvinas Basin (Galeazzi, 1998). The internal reflection configurations above described for unit 2 have been interpreted elsewhere (Galeazzi, 1998) as representing the volcanic and volcanoclastic sequences of Tobifera/Lemaire Fms.

Taking into account the stratigraphic correlations, the unit 3 could be related to the deposits which filled the Rocas Verdes basin (Dalziel et al., 1974; Bruhn, 1979), later involved in the compressive Andine tectonics. Onshore, this unit, which has been called either Yahgan Fm. or Beauvoir Fm., reaches the maximum recorded thickness (Caminos, 1980; Olivero et al., 1999).

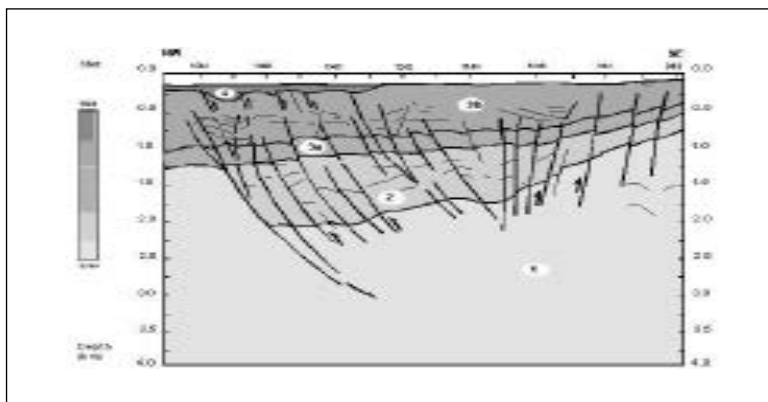


Fig. 3 - Line-drawing showing the structure and seismic units.



Unit 4 may be correlated with the Tertiary sediments of the Magallanes Foreland Basin which were involved in the fold and thrust belt. Along the Atlantic coast of Tierra del Fuego open folding affecting the Tertiary sediments have been reported (Olivero et al., 1999; Tassone et al., 1999). The effects of the Andine tectonics were also recognized along the northern shoreline of Lago Fagnano.

The lateral and vertical relationships observed among the units 2, 3 and 4 have been also reported onshore for the related units (Caminos, 1980; Olivero et al., 1999).

The structural high of the SE portion of the seismic profile could fit well within the overall progressive southward up stepping of the Lemaire/Tobífera and Yahgan/Beauvoir Fms which outcrop to the south in Isla de los Estados (Caminos, 1980) with a subvertical attitude (Dalziel et al., 1974b). The flower fault system recognized in the seismic profile would be related to a transcurrent tectonics.

## REFERENCES

- Brown, L., and W. Fisher, 1980. Seismic stratigraphy interpretation and petroleum exploration. AAPG Cont. Ed. Course Note Ser. 16: 125pp.
- Bruhn, Ronald L., 1979. Rock structures formed during back-arc basin deformation in the Andes of Tierra del Fuego: Geological Society of America Bulletin, Part I, Vol. 90: 998-1012.
- Caminos, R., 1980. Cordillera Fueguina. Geología Regional Argentina. Vol. 2, 1463-1501.
- Dalziel, I.W.D., M.J. de Wit, and K.F. Palmer, 1974a. Fossil marginal basin in the Southern Andes, Nature, 250: 291-294.
- Dalziel, I.W.D., R. Caminos., K.F. Palmer., F. Nullo and R. Casanova, 1974b. South extremity of Andes: Geology of Isla de los Estados, Argentine, Tierra del Fuego. Am. Assoc. Petrol. Geol. Bull., Tulsa. 58: 2502-2512.
- Diraison, M., Cobbold, P.R., Gapais, D., Rossello, E.A. and Le Corre, C., 2000. Cenozoic crustal thickening, wrenching and rifting in the foothills of the southernmost Andes. Tectonophysics, 316: 91-119.
- Galeazzi, J. S., 1998. Structural and Stratigraphic Evolution of the Western alvinas Basin, Argentina. AAPG, Bulletin, V.82, Nro. 4: 596-636.
- Olivero, E.B., Martinioni, D.R., Malumian, N. and Palamarczuck, S., 1999. Bosquejo geológico de la Isla Grande de Tierra del Fuego, Argentina. Actas XIV Cong. Geol. Arg.: 291-294.
- Tassone A.A., Lodolo E. and TESAC Group (Lippai H., Zanolla C., Hormaechea J.L., Coren F., Vidmar R., Rinaldi C.), 1999. Indicadores geofísicos sobre la localización del límite entre las placas Sud America-Scotia en Tierra del Fuego (Argentina). XIV Congreso Geológico Argentino. Salta, Argentina. Actas I: 326-329.
- Winslow, M.A., 1982. The structural evolution of the Magallanes Basin and neotectonics in the southernmost Andes. In: Antarctic Geoscience (C. Craddock, ed.). Madison, University of Wisconsin Press: 143-154.
- Yilmaz, Ö., 2001, Seismic Data Analysis: Processing, Inversion, and Interpretation of Seismic Data, Volume I and II, Stephen M. Doherty Editor, Series; Investigations in Geophysics, Michael R. Cooper, Series Editor, Society of Exploration Geophysicists, Tulsa, OK, USA.

## CRUSTAL STRUCTURE OF THE CHILEAN FOREARC BETWEEN 36° AND 40°S FROM COMBINED OFFSHORE AND ONSHORE SEISMIC WIDE-ANGLE MEASUREMENTS - SPOC 2001

9-05

Stefan Lüth, Peter Wigger<sup>1</sup>, James Mechie, Manfred Stiller, Charlotte Krawczyk<sup>2</sup>, Klaus Bataille<sup>3</sup>, Christian Reichert<sup>4</sup>, Ernst Flüh<sup>5</sup>, SPOC Research Group

1 Freie Universität Berlin, Germany

2 GeoForschungsZentrum Potsdam

3 UdeC, Concepción, Chile

4 BGR Hannover

5 GEOMAR Kiel

Contact: Stefan Lüth, Freie Universität Berlin, Fachrichtung Geophysik, Malteserstr. 74-100, 12249 Berlin, Germany, Phone: +49 30 838 70443, Email: stefan@geophysik.fu-berlin.de

## Introduction

The RV SONNE cruise SO161 took place from October 2001 through January 2002 at the Chile Margin. The goal of the cruise was to investigate the effects of subducting aseismic ridges and fracture zones on seismicity and structure of the Chile Margin (Flüh et al., 2002). The cruise concentrated on two areas, 31°-34°S and 36°-41°S. In the southern area, which is characterized by the subduction of Mocha and Valdivia Fracture Zones (Fig. 1), the offshore operations were extended by onshore

activities in order to illuminate the subsurface of the offshore-onshore transition zone and the onshore forearc of the Chile Margin (Krawczyk et al., 2003).

The mainly land-based operations consist of three approximately 200 km long seismic wide-angle profiles between the Pacific coast and the Main Cordillera, a passive seismic array in the Coastal Cordillera, and a Near-Vertical-Reflection profile in the Coastal Cordillera. The receivers of the three wide-angle profiles (SPOC-North, -Middle and -South) recorded chemical explosions at both ends of the profiles and the airgun shots of RV SONNE cruising along the respective offshore profiles. Additionally, GEOMAR deployed an OBS/OBH profile along airgun-line SO161-038 which is extended onshore by the profile SPOC-South. The recordings of this profile were integrated into the mainly land-based observations in order to achieve a reliable velocity model for the offshore forearc.

### Results of the wide-angle experiment

The onshore profile SPOC-South with its offshore extension along SONNE profile SO161-038/42 is characterized by the most comprehensive coverage compared to the other transects. Shots and receiver locations along this profile allow us to derive a velocity model for a 400 km long transect from the Nazca Plate to the Main Cordillera. Figure 2 shows the resulting velocity model along the transect as it was derived from modelling of phases identified in the shot- and receiver-gathers. From west to east, the model can be divided into three parts. The westernmost part is the oceanic crust and upper mantle of the Nazca Plate. The crustal thickness is 6-7 km. Between the trench and the coastline is the central part of the model, the offshore forearc of the Chile Margin. The westernmost part of it shows very low P-wave velocities (<3.5 km/s). These may be due to the presence of unconsolidated and strongly heterogeneous sediments building up a recent accretionary wedge.

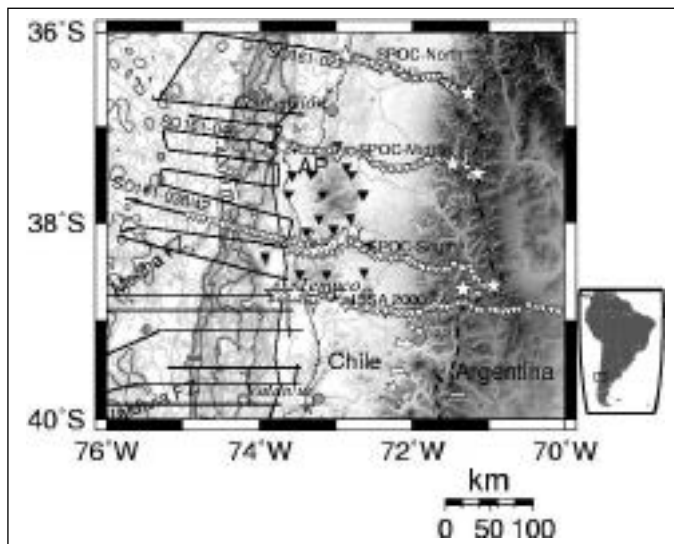


Fig. 1 - Map of the combined offshore and onshore seismic experiment. Three offshore seismic reflection profiles (thin black lines) were extended onshore by additional wide-angle seismic profiles (white stars: shots; white inverted triangles: receivers) and a seismic network in the Coastal Cordillera (black inverted triangles: receivers). Along 39°S the ISSA2000 profile completes the seismic data from the area (Bohm et al., 2002; Lüth et al., 2003). AP: Arauco peninsula.

East of the coast, the onshore forearc of the Chile Margin is located. We observe basically three layers within the crust of the onshore forearc. The uppermost layer is approximately 10 km thick and is characterized by P-wave-velocities typical for upper continental crust. Below this layer, P-wave-velocities increase within two layers to 7.0 km/s, typical for lower continental crust. A clear continental Moho could not be observed. This may be explained by hydration of the continental mantle wedge and/or the presence of subducted meta-sediments between the oceanic slab and the upper plate.

The offshore part of the velocity model of transect SPOC-South was extrapolated to the other two transects SPOC-Middle and SPOC-North as for these profiles no wide-angle information was available. The onshore profiles of these transects however did allow us to derive the geometry of the oceanic Moho from the Trench to the Coastal Cordillera. The three transects are compared with each other in Figure 3. Topography and Moho geometry were plotted with the easternmost end of the Trench

as common reference point. Topography profiles nearly perfectly match for all transects, only the parts east of the Trench differ from each other. The oceanic Moho has a dip angle of approximately 12° below the coastal cordillera along the middle transect (SO161-046) which is about 7° less than the dip angle along the other two transects.

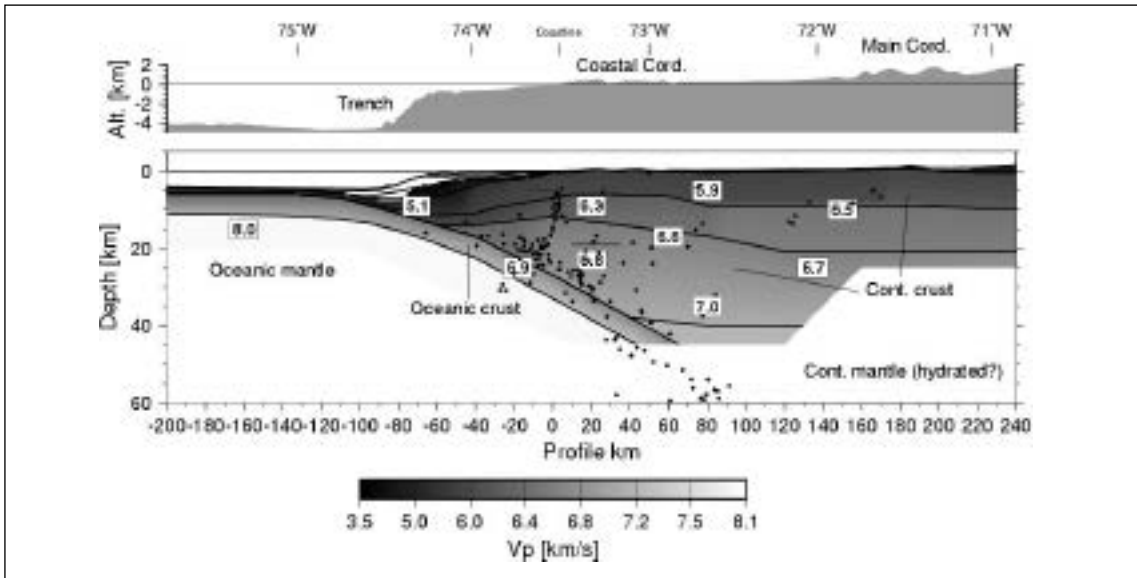


Fig. 2 - Velocity model along the transect of profile SPOC-South. The distribution of P-wave velocities is indicated by the gray-scaled image and numbers in white boxes. Black dots show earthquake hypocenters of seismicity recorded by the ISSA2000 local network (Bohm et al., 2002).

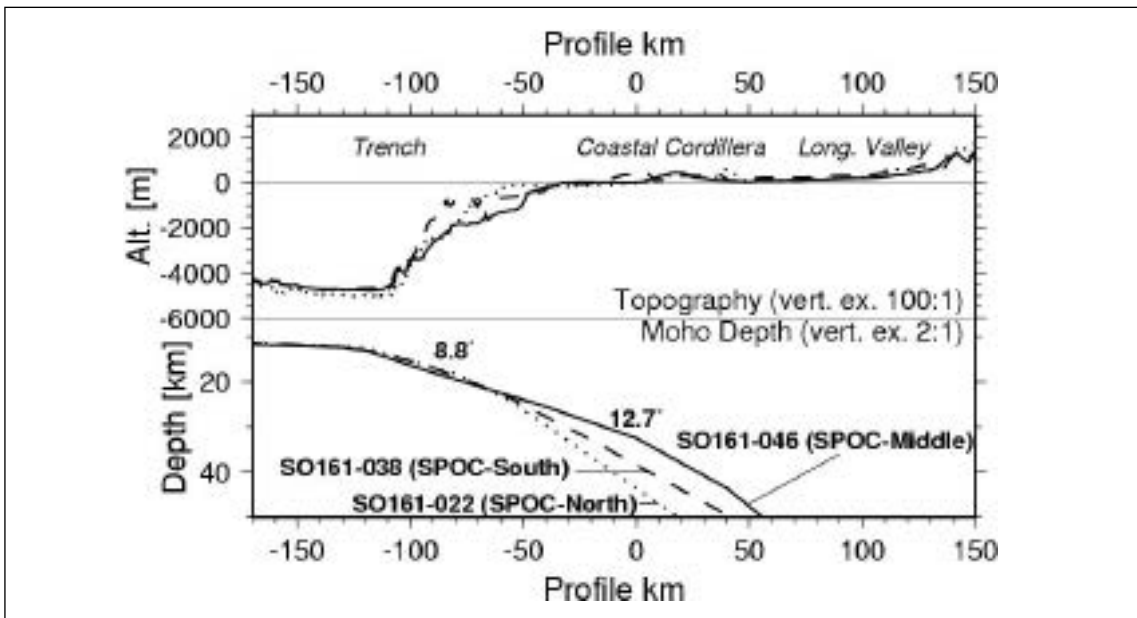


Fig. 3 - Comparison of the geometries of the oceanic Mohos along the profiles SPOC-North, Middle and South.

**Conclusions**

Land-based seismic wide-angle measurements extended the subsurface coverage of SONNE Cruise 161 to the onshore forearc of the Chile Margin. Modelling of the correlated PmP and Pn phases observed on receiver gathers from onshore stations recording SONNE airgun signals and chemical

explosions reveals from North to South varying geometry of the subducting oceanic plate. The dip-angle below the coastal cordillera is smallest along the middle transect, which is located along 37°S and which crosses the Arauco peninsula. The location of the shallow dip-angle of the oceanic slab beneath the coastal cordillera along the profile SPOC-Middle coincides with the landward extrapolation of the Mocha Fracture Zone and the location of the Arauco peninsula (Fig. 1). This peninsula is also characterized by relatively high uplift rates as compared to the surrounding coast region (Bohm et al., 2002). This uplift was suggested to be caused by basal accretion and antiformal stacking of subducted sediments. Another factor contributing to the observed uplift may also be the increased buoyancy of the oceanic crust along the Mocha Fracture Zone as the relatively shallow dip angle of the oceanic Moho along the profile SPOC-Middle suggests that here the slab resists subduction more strongly than along the other transects which are not influenced by the subduction of a fracture zone.

### Acknowledgements

The SPOC-Land operations were funded by GFZ Potsdam, FU Berlin, DFG (SFB 267) and the German Ministry of Research (BMBF, grant 03G0161A). Seismic instruments were provided by GEOMAR, the Geophysical Instrument Pool Potsdam and the FU Berlin. We thank GEOMAR Kiel for providing the OBS/OBH data from the southern transect. We thank all participants in the field operations from Chile, Venezuela and Germany for their committed work.

### REFERENCES

- Bohm, M., S. Lüth, H. Echtler, G. Asch, K. Bataille, C. Bruhn, A. Rietbrock and P. Wigger, 2002. The Southern Andes between 36° and 40°S latitude: seismicity and average seismic velocities. *Tectonophysics* 356: 275-289.
- Flüh, E., H. Kopp and B. Schreckenberger (editors), 2002. RV SONNE Cruise Report SO161-1&4. GEOMAR Report 102, Kiel.
- Krawczyk, C. and the SPOC Team, 2003. Amphibious Seismic Survey Images Plate Interface at 1960 Chile Earthquake. *EOS, Transactions, American Geophysical Union*, Vol. 84, No. 32:301,304-305.
- Lüth, S., P. Wigger and ISSA Research Group, 2003. A crustal model along 39°S from a seismic refraction profile – ISSA 2000. *Revista Geologica de Chile*, Vol. 30, No. 1:83-102.

## INNOVATION IN SEISMIC SURVEY ON SUBGLACIAL LAKES

9-06

D. Nieto Yabar, A. Bratus, E. Del Negro, R. Geletti

*Istituto Nazionale di Oceanografia e di Geofisica Sperimentale – OGS,  
Borgo Grotta Gigante 42c – 34010 SGONICO - TS (Italy)*

### Abstract

The first phase of ELSA (Exploration of Subglacial Antarctic Lakes) project, carried out in December 2003, aimed to test the applicability of the reflection seismic method for the definition of subglacial structures in the Antarctic icecap. The purposes of the survey were to verify: the correct operation of the recording system, the acquisition parameters based on the theoretical models and the quality of the obtainable data, by using different types of sources and acquisition geometries.

### Introduction

The subglacial lakes are water bodies lying between the base of the glacial column and the bedrock. Their existence has been discovered, accidentally, by a series of geophysical surveys started in the 60' years.

Until 90' years the lake presence, under the icecap, was considered nearly a simple curiosity. Subsequently, the radar data supplied from remote sensing measures ERS-1 concurred to obtain

with decimetric accuracy the topography of the icecap surface; some anomalous, flat and relatively narrow areas were localized. Among these, the area close to the Vostok Station, had borders that coincided with the positions of the subglacial lake characterized in the profiles radar of 70' years. The Antarctic ice has a medium thickness of 2200 meters and in some cases, it grew in extremely long times, up to million years. The ice core analysis gives a very precise idea of the temperature to which the ice has been formed. Moreover, the small air bubbles captured in the ice, allowed to study also the composition of the atmosphere in relation to the medium temperature of that period.

The icecap of Antarctica covers numerous lakes (more than 70) that have been, in this way, preserved for million years. The main of these lakes is the Vostok Lake, a large lake located under approximately 4 km of ice in East Antarctica; of great interest, even if with smaller dimensions, is the Concordia Lake, 120 km far from the Italian-French base of Dome-C.

### Data acquisition

In this context, various Italian research centers participate to international programs, in particular to the “ ELSA” (Exploration of the Subglacial Lakes on the Antarctic East Cap). In the frame of this project, the National Institute of Oceanography and Experimental Geophysics - OGS, provides the geophysical searches using reflection seismic survey. The use of seismic method allows, at least in theoretical way, to exceed the limits inborn in the radars prospecting that do not allow to obtain information on structural elements presents under the water level. A recent study carried out by the OGS has modeled the seismic signal in one ideal series of firn, ice, lake water, lake sediments and bedrock (Carcione and Gei, submitted).

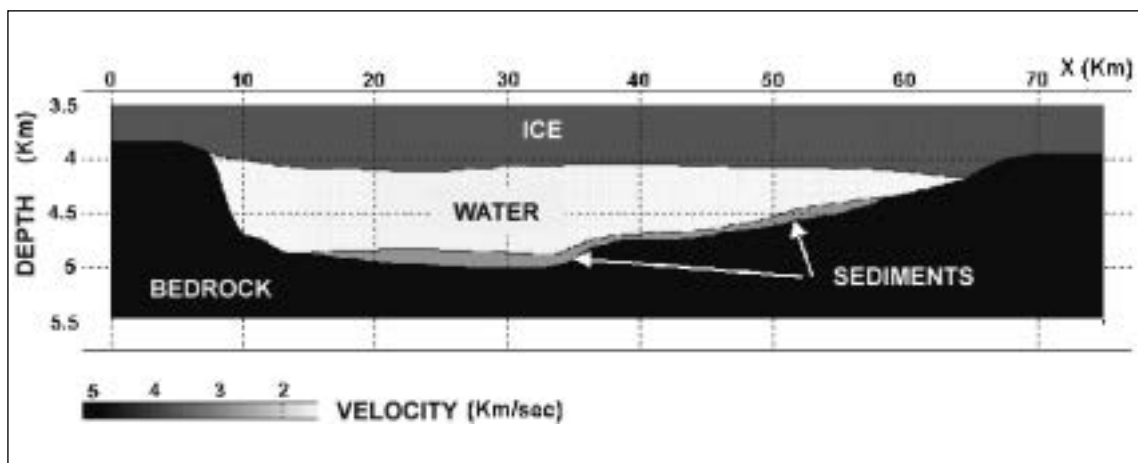


Fig. 1 - Velocity model for a subglacial lake (model of S. Picotti)

This study reveals that the greater reflections are produced by the interfaces ice-water, water-sediments, and sediment-base. The analysis of the polarity of the reflectors and the AVO analysis (Amplitude Versus Offset) can contribute to discriminate the reflectors also for relatively thin lacustrine sediment horizons.

The good result is assured (from the geometric point of view) by the use of long offsets between source and receivers (some kilometers).

In this context OGS has planned, experimented and carried out a multichannel seismic survey planned specifically in order to reconstruct the structure of the subglacial lakes in Antarctica. This isn't properly an innovative technique, but it was necessary to solve many big problems, both technical and operational.

A feasibility study and the consequent instrumental test was carried out in December 2003 in Antarctica.

The test has been lead with the logistic support of ENEA staff.

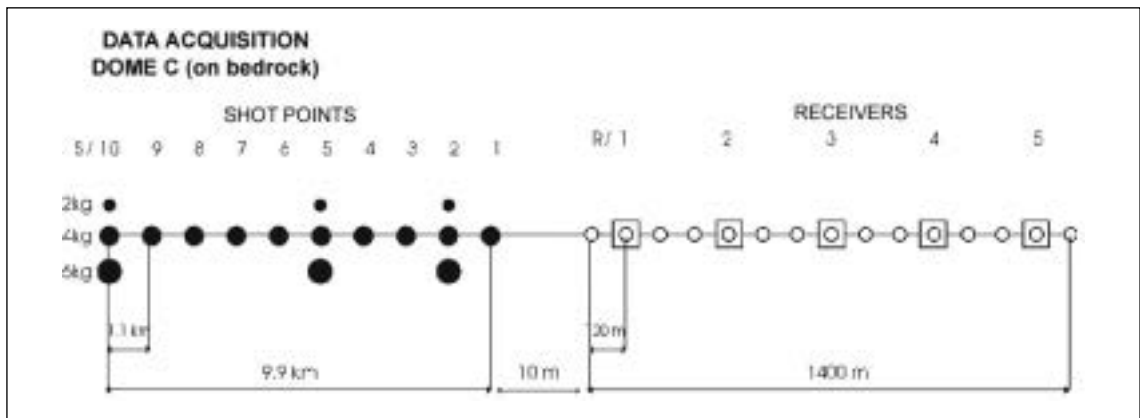


Fig. 2 - Data acquisition scheme

During the design of the instruments it was necessary to consider that temperature of  $\pm -50^{\circ}\text{C}$  are normal in that area. There were many logistic difficulties such as transportation of instruments and staff, problem with the weight of the instruments and more. Because of this the best choice for the seismic data acquisition was the use of remote stations, instead of operating with the conventional methods commonly used in seismic survey.

### The problem of the geophones

The not availability of commercial geophones working under  $-20^{\circ}$  and the low budget of the project, forced to adapt to polar environment the geophones commonly used for conventional seismic survey. So, the behaviour of these geophones at temperature below  $-50^{\circ}$  was studied. To such purpose, various solutions and combinations of geophones have been experienced; they have to satisfy the followings:

Operating temperature  $-60^{\circ}$

Elevated acquisition dynamic (good ratio signal-noise)

Low weight and dimensions

Several combinations of geophones, such as number and electrical connection, have been tested. The best combination is to use 8 geophones, divided in 2 series of 4 geophones, connected in parallel. The geophones case consists of two coaxial container, the inner one contains the 8 geophones.



Fig 3 - The geophones case, a resistor for worming the geophones will be placed in the center of the case.

## Conclusion

All the instruments sets were tested during a survey in Antarctica in December 2003, near the Dome C Antarctic base. All the instruments worked correctly. The data obtained are still under processing. The success of this test survey is a good start for a series of seismic surveys in subglacial lakes using this methods for the seismic data acquisition.

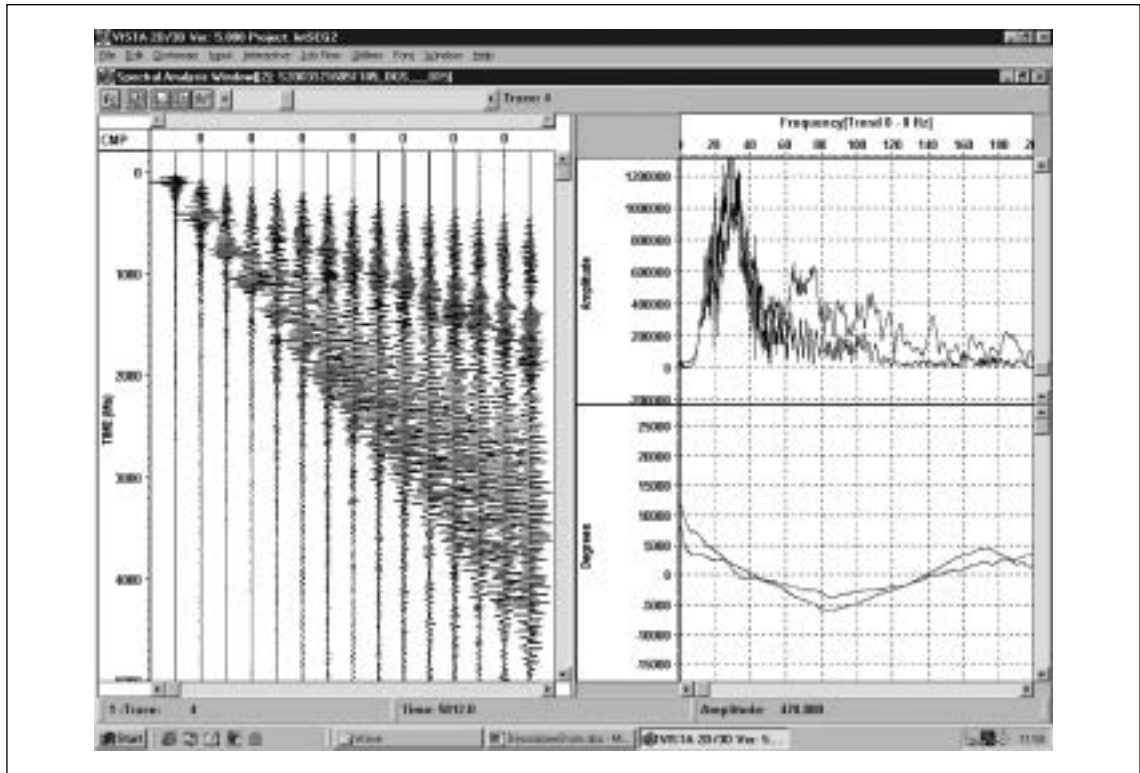


Fig. 4 - Data pattern acquired in Antarctica in December 2003

## REFERENCES

- Carcione J.M., and Gei D., 2003. Seismic modelling study of a subglacial lake. *Geophysical Prospecting*, 51, 501-515;
- Dowdeswell, JA & Siegert, MJ. (1999) The dimensions and topographic setting of Antarctic Subglacial lakes and implications for large-scale water storage beneath continental ice sheets. *Geological Society of America Bulletin* 111(2) 254-263.
- Gorman, MR & Siegert, MJ. (1999) Penetration of Antarctic subglacial lakes by VHF electromagnetic pulses: Information on the depth and electrical conductivity of basal water bodies. *Journal of Geophysical Research – Solid Earth*. 104 (B12) 29311-29320.
- Kapitsa, AP, Ridley, JK, Robin, GQ, Siegert, MJ & Zotikov, IA. (1996) A large deep freshwater lake beneath the ice of central East Antarctica. *Nature*, 381, 684-686.
- Krohn, C. E. and Chen, S. T., 1992, Comparisons of downhole geophones and hydrophones: *Geophysics, Soc. of Expl. Geophys.*, 57, 841-847.
- Jouzel, J, Petit, JR, Souchez, R, Barkov, NI, Lipenkov, VY, Raynaud, D, Stievenard, M, Vassiliev, NI, Verbeke, V & Vimeux, F. (1999) More than 200 meters of lake ice above subglacial lake Vostok, Antarctica. *Science*, 286(5447) 2138-2141.
- Masolov V.N., Kudryavtzev G.A., Sheremetiev A.N., Popkov A.M., Popov S.V., Lukin V.V., Griukurov G.E. and Leitchenkov G.L. 1999. Earth science studies in the Lake Vostok region: existing data and proposals for future research. SCAR International Workshop on Subglacial Lake Exploration, Cambridge, England
- Siegert, MJ & Hodgkins, R. (2000) A stratigraphic link across 1100 km of the Antarctic Ice Sheet between the Vostok ice-core site and Titan Dome (near South Pole). *Geophysical Research Letters* 27(14) 2133-2136.
- Siegert, MJ & Ridley, JK. (1998) An analysis of the ice-sheet surface and subsurface topography above the Vostok Station subglacial lake, central East Antarctica. *Journal of Geophysical Research-Solid Earth*, 103, 10195-10207.
- Siegert, MJ & Ridley, JK. (1998) Determining basal ice-sheet conditions in the Dome C region of East Antarctica using satellite radar altimetry and airborne radio-echo sounding. *Journal of Glaciology*, 44(146), 1-8.
- Siegert, MJ, Hodgkins, R & Dowdeswell, JA. (1998) A chronology for the Dome C deep ice-core site through radio-echo layer correlation with the Vostok ice core, Antarctica. *Geophysical Research Letters*, 25(7), 1019-1022.
- Siegert, MJ, Hodgkins, R & Dowdeswell, JA. (1998) Internal radio-echo layering at Vostok station, Antarctica, as an independent stratigraphic control on the ice-core record. *Annals of Glaciology*, 27, 360-364.
- Zotikov, IA & Duxbury, NS. (2000) Genesis of Lake Vostok (Antarctica). *Doklady Earth Sciences*, 375(8) 1294-1296.





# **Session 10**

---

**PALEOMAGNETISM  
PALEOENVIRONMENTS  
AND PALEOCLIMATIC  
RECONSTRUCTIONS**



## COASTAL MAPPING OF THE QUATERNARY MARINE DEPOSITS IN THE STRAIT OF MAGELLAN (CHILE)

10-01

DeMuro S., Brambati A.

*Dipartimento di Scienze della Terra – Università di Cagliari*

*Dipartimento di Scienze Geologiche, Ambientali e Marine – Università Trieste*

During the last glacial cycle, glaciers drained north-eastward into the Strait of Magellan. The timing of the last advances has been ambiguous but the older dates of 16,590-15,800 up to 10,050 yr for deglaciation have been reported.

This paper focuses on the Strait of Magellan where, after the last glacial cycle, the marine ingression is well defined.

Along the coasts of the eastern Atlantic side of the Straits, it is possible to observe at least four orders of terraces, prevalently marine lying on a meso-Tertiary sedimentary basement or on glacial and glaciofluvial deposits, linked to the last Quaternary main glacial stages.

The four main orders of terraced sequences have been mapped, described and dated using <sup>14</sup>C. Their stratigraphic position and their radiocarbon dating, refer to the Lower Holocene. This time period connects them to the isostasy rebound.

The First and oldest Order, were found regularly between altitudes of 18 and 25 metres. The Second Order is distributed between 6 and 11 metres, and is mainly represented by fossiliferous gravel deposits; sands and silts are also present. It regularly covers most of the coastal stretch and extends in the backland.

The age of formation of the marine deposits, by C14 dating, is comprised on average between 6,000 and 7,000 years B.P.

The Third Order is following the present-day beach, between altitudes of 3 and 5 metres, at the foot of the Second Order terrace. It is made up of gravels and sands and refers preferably to a marine environment. At a slightly lower elevation, lies the Fourth Order marine terrace, distributed between 1.5 and 3 metres.

All terraces present well-preserved characteristics of paleobeach environments (berms, spits and ridges).

The First Order terrace belongs to the palaeogeography, which was evolved during the first phase of the last deglaciation. The other orders are connected with subsequent stages of the last deglaciation, but the influences of the tectonics in their evolution cannot be excluded.

## HOLOCENE DIFFERENTIAL TECTONIC MOVEMENTS ALONG THE ARGENTINE SECTOR OF THE BEAGLE CHANNEL (TIERRA DEL FUEGO) INFERRED FROM MARINE PALAEOENVIRONMENTS

10-02

Gustavo Bujalesky<sup>1</sup>, Andrea Coronato<sup>1</sup>, Claudio Roig<sup>2</sup>, Rabassa Jorge<sup>1</sup>

<sup>1</sup> *Centro Austral de Investigaciones Científicas (CADIC-CONICET), Bernardo Houssay 200 (9410) Ushuaia, Argentina. bujas@infovia.com.ar*

<sup>2</sup> *Universidad Nacional de la Patagonia-San Juan Bosco, Sede Ushuaia*

### Introduction

Numerous outcrops of raised marine deposits have been described along the northern coast of the Beagle Channel (Lapataia, 54°55'S, 68°35'W; Punta Moat, 54°57'S, 66°40'W), Isla Grande de Tierra del Fuego, Argentina (Auer, 1959; Urien, 1968; Rabassa et al, 1986, 2000; Mörner, 1991; Gordillo et al., 1992, 1993; Bujalesky, 1998; Coronato et al., 1999; Grill et al., 2002). These deposits are

Holocene in age and correspond to raised beaches; in some specific cases they are subtidal environments.

The objective of this paper is to analyze the spatial and altitudinal distribution of the studied deposits and to relate them with the regional geological structure and the possible relationships with seismotectonic events that have affected this area during the Holocene.

### Distribution of littoral deposits and landforms

Faulting along the southern coast of Tierra del Fuego defines, at least, three large, major blocks: a) Bahía Lapataia-Ensenada; b) Bahía Golondrina-Bahía Brown and c) Estancia Harberton-Bahía Sloggett (Fig. 1). In these three sectors, at least 26 localities have been dated and studied from the geomorphological, sedimentological, palaeoenvironmental and palaeoecological points of view.

In the Bahía Lapataia-Ensenada area, the subtidal and/or low-energy deposits of early Holocene age (8.2-7.2  $^{14}\text{C}$  ka B.P.; Note: all radiocarbon ages herein presented are the original dates, uncalibrated and uncorrected for reservoir effect) are located between 0.50 and 3 m above present sea level (a.p.s.l.). The beach deposits of middle Holocene age (5.9-3.8  $^{14}\text{C}$  ka B.P.), some of them with mollusk shells in life position, are distributed between 1 and 8 m a.p.s.l.; the most recent ones (2.1-1.4  $^{14}\text{C}$  ka B.P.) are beach deposits located between 2 and 3 m a.p.s.l. This area has been interpreted as a palaeofjord during the Holocene marine transgression (Gordillo et al., 1993). The oldest radiocarbon ages for the Beagle Channel marine deposits have been obtained in this area.

The section comprised between Bahía Golondrina and Bahía Brown presents a wider record of non-functional marine landforms and deposits, corresponding to high-energy environments. The oldest beach levels (5.4 to 5.1  $^{14}\text{C}$  ka B.P.) are located between 10 and 8 m a.p.s.l. in the city of Ushuaia and surroundings (Ushuaia Peninsula and Bahía Golondrina); in this region, the maximum (until today) relative elevation of the Holocene marine deposits has been recorded. Eastwards, in the locality of Playa Larga, a clear sequence of very recent marine deposits ( $405 \pm 55$   $^{14}\text{C}$  yr B.P.), at 1 m above their present counterparts, and others of Middle Holocene age (4.1  $^{14}\text{C}$  ka B.P.) has been described by Gordillo et al. (1992). The easternmost (for this section) localities of Punta Paraná and Bahía Brown present marine levels may be correlated to those of Playa Larga (4.3  $^{14}\text{C}$  ka B.P. at 5.5 m a.p.s.l. and 2.9  $^{14}\text{C}$  ka B.P. at 2.8 m a.p.s.l.) considering both their in age and altitude .

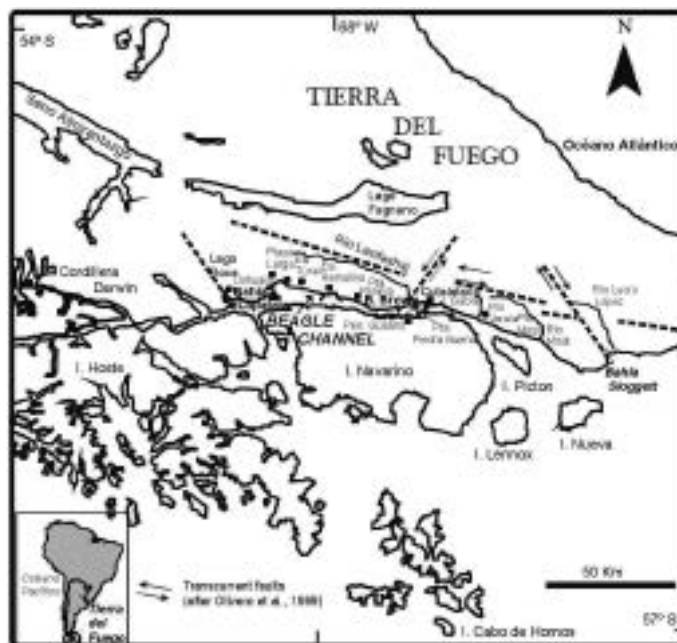


Fig. 1. Location of Holocene marine deposits along the Beagle Channel and major fault distribution.

The section Estancia Harberton-Bahía Sloggett is the most extensive area, in which very little evidence of morphological and/or sedimentary Holocene marine records has been found. The marine beach at Cutralataca, Estancia Harberton, dated at  $2770 \pm 50$   $^{14}\text{C}$  yr B.P., is located at only 1 m a.p.s.l., at least 2 m below its nearest equivalent counterpart at Bahía Brown. The marine beach at Isla Gable ( $4.7$   $^{14}\text{C}$  ka B.P.) is located at 5 m a.p.s.l., at a similar elevation of those westernmost beaches with an age of ca.  $4.1$   $^{14}\text{C}$  ka B.P. and at 3 m below the age-equivalent beaches at Ushuaia. This fact is even more exposed at the Punta Gusano locality, at the southern coast of the Beagle Channel, where the beach with an age of ca.  $4.6$   $^{14}\text{C}$  ka B.P. is located at 3 m a.p.s.l., in an equivalent position to the raised beaches with an age of ca.  $2.9$ – $3.0$   $^{14}\text{C}$  ka B.P. at Bahía Brown and Playa Larga. The Punta Piedra Buena beach (ca.  $1.4$   $^{14}\text{C}$  ka B.P.), in the same portion of Isla Navarino (Chile; Porter et al., 1984), is located at 2 m below its equivalent at Punta Pingüinos (Ushuaia Peninsula). The oldest deposits for this sector appear at the Río Varela locality, and they correspond to a low-energy environment that occupied the region during the Middle Holocene (ca.  $6.2$   $^{14}\text{C}$  ka B.P.), transformed into a coastal lagoon, with transition to fluvial environments. The present position is 1.26 m below the local high-tide level. Similar estuarine environments, though somewhat older ( $7.2$  to  $7.5$   $^{14}\text{C}$  ka B.P.), have been observed in the Bahía Lapataia sector above present sea level, between 0.5 and 3.5 m a.p.s.l. Other marine deposits, datable by  $^{14}\text{C}$  techniques and which may provide evidence for Holocene relative sea level position, have not been observed until now eastwards from Río Varela. The lowest portions of the landscape, in which semi-closed marine environments could have been developed, are covered by peatlands.

Another element of analysis is the absence of littoral anthropogenic shell-middens of Middle Holocene age or younger, whereas the occurrence of these archaeological sites, undoubtedly related to the marine shore, frequently accompanies the Holocene beaches along the Beagle Channel between Bahía Lapataia and Estancia Remolino, along both the A and B sectors.

In the easternmost end of the Beagle Channel, between the foreshore and the storm berm at Bahía Sloggett, remnants of a *Nothofagus* forest, with tree stumps in life position have been described and dated (Rabassa et al., 2003). The stumps are firmly rooted in sandy silts and marsh deposits and have been dated at  $3150 \pm 80$   $^{14}\text{C}$  yr B.P. The relicts of this palaeoforest are located today at the intertidal zone (2–3 m maximum tide amplitude), or even below it, and they are being eroded by wave and tide action.

### Final comments

The full recession of the Beagle Channel Glacier since the Last Glacial maximum (LGM) started at least 12,000  $^{14}\text{C}$  years ago near Ushuaia and was probably completed ca.  $10.1$   $^{14}\text{C}$  ka B.P. (Rabassa et al. 2000). The marine transgression into the Beagle Channel glacial trough took place at least before 8000 years ago, according to the oldest  $^{14}\text{C}$  date available at Bahía Lapataia for Holocene marine shells above present sea level ( $8200$   $^{14}\text{C}$  yr B.P.; Gordillo et al., 1992). A possible reservoir effect of 500 years may be expected for this section of the Beagle Channel (Rabassa et al., 2000).

The transcurrent fault systems with NW-SE and NE-SW orientations bound sectors in which the marine deposits and landforms do not present a clear chronological-altitudinal correlation. Therefore, the incidence of a differential tectonic component in the present emplacement of these marine features should be considered as an important element for analysis in the reconstruction of most recent environmental changes. The raised marine beaches of the Beagle Channel indicate the differential seismotectonic uprising in this region during the last 5000 years (Mörner 1991, Bujalesky 1998, Gordillo et al., 1992). Note that eustatic sea level 5000 years ago was probably only 0.5–1.0 m a.p.s.l. Besides, either the transcurrent faults with NW-SE orientation or the W-E oriented faults of the eastern end of the Beagle Channel would have caused the downwarping of the Bahía Sloggett block. At this locality, the recent drowning of subaerial, near-shore environments is shown by the occurrence of a submerged sub-fossil forest, of late Middle Holocene age. The absolute magnitude of this local movement is estimated in at least 2–3 m, considering that the present *Nothofagus* forest ecosystems are presently located at, as a minimum, at that elevation above present high-tide level in this area.

Thus, it is herein proposed that the seismotectonic movements since the Middle Holocene would have forced the ascent of the western portion of the Argentine sector of the Beagle Channel and the

lowering of its eastern section, at variable mean rates of between 1 and 2 mm/yr in both senses, which has generated a total differential movement of at least, and perhaps more than 12 m since the maximum of the Middle Holocene transgression.

## REFERENCES

- Auer, V. 1959. The Pleistocene of Fuego-Patagonia: Part III: Shorelines displacements. *Annales Academiae Scie. Fennicae. Series A III. Geolog-Geogr.*
- Bujalesky, G. 1998. Holocene coastal evolution of Tierra del Fuego, Argentina. *Quaternary of South America & Antarctic Peninsula*, 11: 247-282, Balkema Publishers, Rotterdam.
- Coronato, A.; Rabassa, J.; Borromei, A.; Quattrocchio, M.; Bujalesky, G. 1999. Nuevos datos sobre el nivel relativo del mar durante el Holoceno en el Canal Beagle, Tierra del Fuego, Argentina. *I Congreso Argentino de Geomorfología y Cuaternario*, Actas I, p: 27-28. Santa Rosa, La Pampa, Mayo 1999.
- Gordillo, S.; Bujalesky, G.; Pirazzoli, P.; Rabassa, J.; Saliège, J. 1992. Holocene raised beaches along the northern coast of the Beagle Channel, Tierra del Fuego, Argentina. *Palaeogeography, Palaeoclimatology, Palaeoecology*, 99: 41-54.
- Gordillo, S.; Coronato, A.; Rabassa, J. 1993. Late Quaternary evolution of a subantarctic paleofjord, Tierra del Fuego. *Quaternary Science Reviews*, 12 (10): 889-897.
- Grill, S.; Borromei, A.; Quattrocchio, M.; Coronato, A.; Bujalesky, G.; Rabassa, J. 2002. Palynological and sedimentological analysis of recent sediments from Río Varela, Beagle Channel, Tierra del Fuego, Argentina. *Revista Española de Micropaleontología*, 34 (2): 145-161.
- Möerner, N. 1991. Holocene sea level changes in the Tierra del Fuego region. *Bol. IG-USP, Special Publication*, 8: 133-151.
- Olivero, E.; Martinioni, D.; Malumián, N.; Palamarzuck, S. 1999. Bosquejo geológico de la Isla Grande de Tierra del Fuego, Argentina. *XIV Congreso Geológico Argentino*, Actas I: 291-294.
- Porter, S.C.; Stuiver, M.; Heusser, C.J. 1984. Holocene sea-level changes along the Strait of Magellan and Beagle Channel, southernmost South America. *Quaternary Research*, 22: 59-67.
- Rabassa, J.; Heusser, C.; Stuckenrath, R. 1986. New Data on Holocene Sea Transgression in the Beagle Channel: Tierra del Fuego, Argentina. *Quaternary of South America and Antarctic Peninsula*, 4: 291-309. Balkema Publishers, Rotterdam.
- Rabassa, J.; Coronato, A.; Bujalesky, G.; Roig, C.; Salemme, M.; Meglioli, A.; Heusser, C.; Gordillo, S.; Borromei, A.; Quattrocchio, M. 2000. Quaternary of Tierra del Fuego, Southernmost South America: an updated review. *Quaternary International*, 68-71: 217-240.
- Rabassa, J.; Coronato, A.; Roig, C.; Martínez, O.; Serrat, D. 2003. Un bosque sumergido en Bahía Sloggett, Tierra del Fuego, Argentina: evidencia de actividad geotectónica en el Holoceno tardío. *II Reunión de Geomorfología Litoral, Resúmenes*, Santiago de Compostela, 19-22 Junio 2003. In press at "Revista Xeografica", Universidad de Santiago de Compostela.
- Urien, C. 1968. Edad de algunas playas elevadas en la Península Ushuaia y su relación con el ascenso costero. *III Jornadas Geológicas Argentinas*, Actas, 2: 35-42.

## SEDIMENTARY PROCESSES IN LAKE PUYEHUE OVER THE LAST 500 YEARS: IMPLICATIONS FOR PALEOENVIRONMENTAL RECONSTRUCTIONS IN THE CHILEAN LAKE DISTRICT (41°S)

10-03

E. Chapron<sup>(1)</sup>, S. Bertrand<sup>(2)</sup>, F. Charlet<sup>(3)</sup>, X. Boes<sup>(2)</sup>, M. De Batist<sup>(3)</sup>, N. Fagel<sup>(2)</sup>,  
O. Magand<sup>(4)</sup>, F. Arnaud<sup>(5)</sup>, M. A. Mélières<sup>(4)</sup>, M. Pino<sup>(6)</sup>, R. Urrutia<sup>(7)</sup>

(1) *Geological Institute – ETH Zentrum, Sonneggstrasse 5 – 8092 ZURICH Switzerland*

(2) *UR Argiles et Paleoclimats– University of Liège–Belgium*

(3) *Renard Centre of Marine Geology–University of Gent–Belgium*

(4) *Laboratoire de Glaciologie et de Géophysique de l'Environnement–CNRS–Observatoire de Grenoble–France*

(5) *UMR Processus et Bilan en Domaine Sédimentaire – University of Lille 1 – France*

(6) *Instituto de Geociencias – Universidad Austral de Valdivia – Chile*

(7) *Centro EULA – Universidad de Concepción – Chile*

## Summary

The synthesis of the first results of a multidisciplinary study of lake Puyehue sedimentary infill involving high-resolution seismic profiling and multi-proxy analyses of sediment cores is presented. Sub-bottom profiling was essential to optimise the selection of two coring sites, receiving the clastic supply of the main tributary of the lake (the Golgol River). Age-depth models for coring sites PU II and PU I are based on radionuclide measurements and a detailed analysis of the core lithologies (including varve counting on thin sections). These age-depth models are strongly supported by the reconnaissance of historic events such as the sedimentary record of 1960 Valdivia major earthquake

and the eruptions of Puyehue volcano in 1960 and 1929. These two coring sites are characterised by contrasted sedimentary processes and sensitivities to the active geodynamic setting of the SW Andes. This study revealed that detailed, continuous paleo-environmental reconstructions in the study area should be based on coring site PU II.

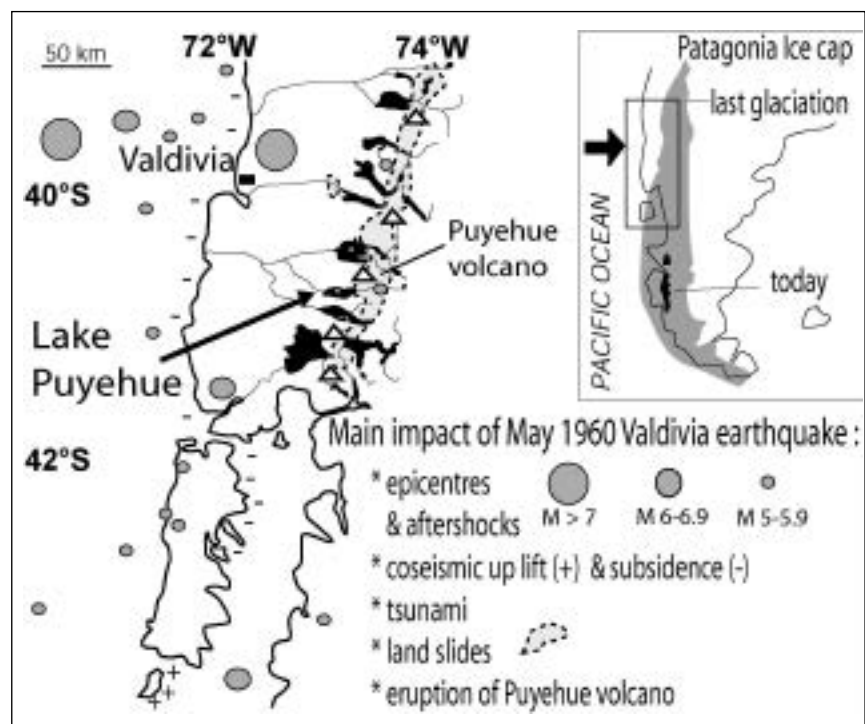
### Abstract text

The middle latitude Chilean coastal range is a key area of our global climate system because the interactions of major oceanic (the Peru-Chile Current, PCC), atmospheric (the Westerlies) and geomorphologic features (the Andes) are responsible for strong precipitation on the continent and for the formation of the third-largest continental ice volume on Earth (the Patagonian Ice Cap). During the last glaciation, the Chilean Lake District was at the North-Western frontier of the Patagonian Ice Cap (Fig. 1), and large piedmont lakes formed as glaciers retreated higher up in the Andes since the early phases of the deglaciation. Furthermore, the glacier retreat in the area coincided -and might have contributed- to the development of some of the most active volcanoes on the American continent (i.e. Llaima and Villarica volcanoes). The growth of these volcanoes, together with major subduction earthquakes (i.e. the 1960 Valdivia event, M 9.5) produced very important geomorphologic changes in the catchments and related drainage basins.

Strong precipitations in the area are related to the strength and latitude of the Westerlies, and favour today an exceptional rainforest (Moreno et al, 2003), strong erosion rates in the Andes and a very large sediment yield. These sediments are partly trapped in the lake systems that characterise the area, but large volumes of nutrients still reach the Pacific coast where, interacting with the PPC, they have triggered exceptional blooms in the recent past resulting in very high sedimentation rates (Lamy et al. 2001). The current knowledge of environmental changes in this key area of the Southern Hemisphere is essentially based on studies on soils, moraines, peat bogs, ponds, small peri-glacial lakes and oceanic sediments, but the sedimentary records of the large glacial lakes characterising the region are yet to be explored.

In this paper, we present the first results of an integrated multidisciplinary study of the historic sedimentary processes in Lake Puyehue, where the regional impact of the volcanism, the seismicity and climate changes is well documented.

Fig. 1 - General location of Lake Puyehue in the Chilean Lake District in front of the Andes. The extension of the Patagonia Ice cap during the last glaciation is also indicated (after Denton et al., 1999). During the 1960 Valdivia earthquake, the eruption of Puyehue volcano together with large land slides all along the front of the Andes and aftershocks largely affected the catchment areas of the lakes (after Oñat, 1960; Rothé, 1961; Gerlach et al., 1988).



High-resolution seismic profiling using sparker (1 KHz) and pinger (3.5 KHz) sources (Charlet et al., 2003) was essential to select the most suitable sites for obtaining long sediment cores in the different depocenters that are presently accumulating the clastic supply of the main tributary of this lake (the Golgol River, Fig. 2). Two sites were sampled using UWITEC piston and short gravity coring devices (Bertrand et al., 2003): PU-I in the deepest basin (-122 m) facing the large Golgol delta and PU-II on top (-48 m) of stratified sediments covering a well-developed sub-aqueous moraine ridge.

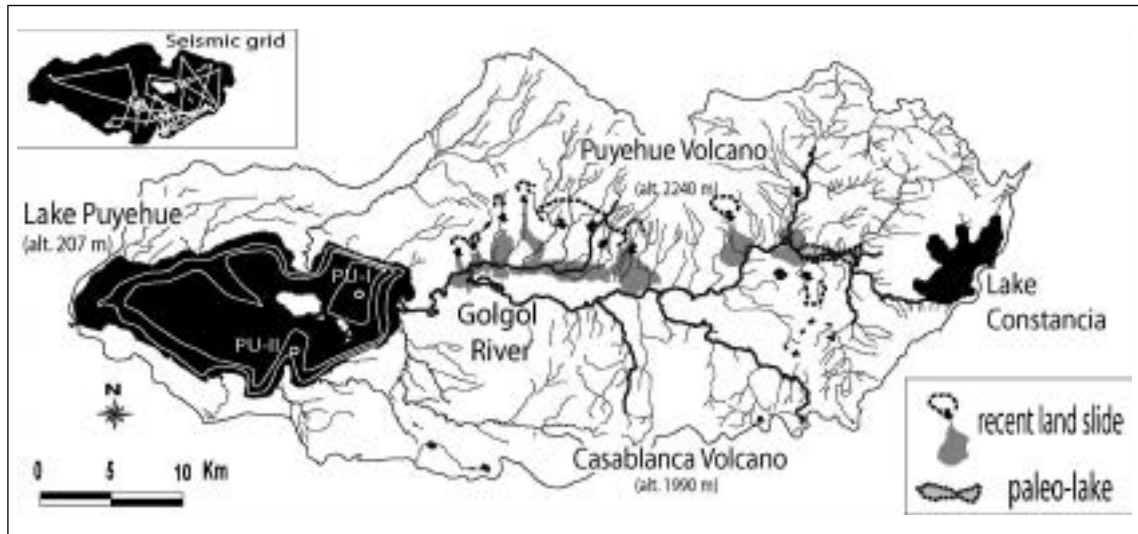


Fig. 2 - The drainage basin of lake Puyehue and location of high-resolution seismic profiles and coring sites. The Golgol river is the main tributary and formed a large delta clearly visible in the bathymetry of the lake (isobaths: 40 m, after Campos et al., 1989). Several large recent land slides affected the southern flank of Puyehue Volcano and the Golgol River. A land slide-dammed paleolake is also indicated in the upper catchment.

On each coring site, multiples short gravity cores were retrieved and then they were logged with a GEOTEK multisensor track (gamma density, P wave velocity, magnetic susceptibility (MS)) before being opened. Once split, the lithologies of these cores were carefully described and digitalized. The best cores were then sampled for  $^{210}\text{Pb}$ ,  $^{137}\text{Cs}$  and  $^{241}\text{Am}$  dating as well as high-resolution multi-proxy measurements (MS, laser grain size, clay mineralogy, tephrostratigraphy, palynology, diatom assemblages and large thin sections; Chapron et al., 2003; De Batist et al., 2003).

Lago Puyehue is an oligotrophic and temperated monomictic lake (Campos et al., 1989) where sedimentation appears to be rather different in our two coring sites:

In site PU II, sediments are finely laminated silts (mean grain size: 20 microns) with few intercalated sandy events (tephra, turbidite). The lamination results from a succession of thin biogenic light lamina (rich in diatoms) and clastic dark lamina (rich in organic matter). PU II site is characterized by a mean sedimentation rate (SR) of 1 mm/yr, deduced from the decay of  $^{210}\text{Pb}$  and from the reconnaissance of the  $^{137}\text{Cs}$  and  $^{241}\text{Am}$  picks produced by atmospheric nuclear tests culminating in 1965. Counting on thin sections revealed an annual lamination (i.e. "biogenic" varves) and confirms the radiogenic measurements till 1960, but then suggest higher SR till the 30'. The age-depth model based on varve counting and on the extrapolation of these SRs down core, is confirmed by the reconnaissance of several sedimentary events and their correlation with historical data: (1) a 2-3 cm thick slope failure deposit can be correlated with the Valdivia 1960 major earthquake; (2) a 0.5 cm thick sandy layer bearing high MS values with Puyehue volcano historic eruption in 1929 and (3) possibly a 0.5 cm thick sandy layer bearing normal MS values with the major subduction earthquake of 1575, which is considered as an equivalent of the Valdivia 1960 event.

Background sedimentation in coring site PU I is coarser (sandy silts with a mean grain size of 30 microns) and contrast with several large flood deposits (1 to 3 cm thick, mean size 15 microns), a coarser mega flood deposit (35 cm thick) and a thin sandy tephra at the base of the short core (Fig. 3). These sedimentary events have different grain size signatures suggesting high flow energies. In



particular, grain size, MS and density profiles of the mega flood deposit are bearing the typical signature of a catastrophic hyperpycnal flow deposit (Syvitski & Schafer, 1994; St Onge et al., in press; Schneider et al., accepted). The mega flood deposit is also clearly visible on 3.5 kHz seismic profiles where it appears associated with sub aqueous slope failure deposits in the deep basin facing the Golgol delta (Fig. 3).

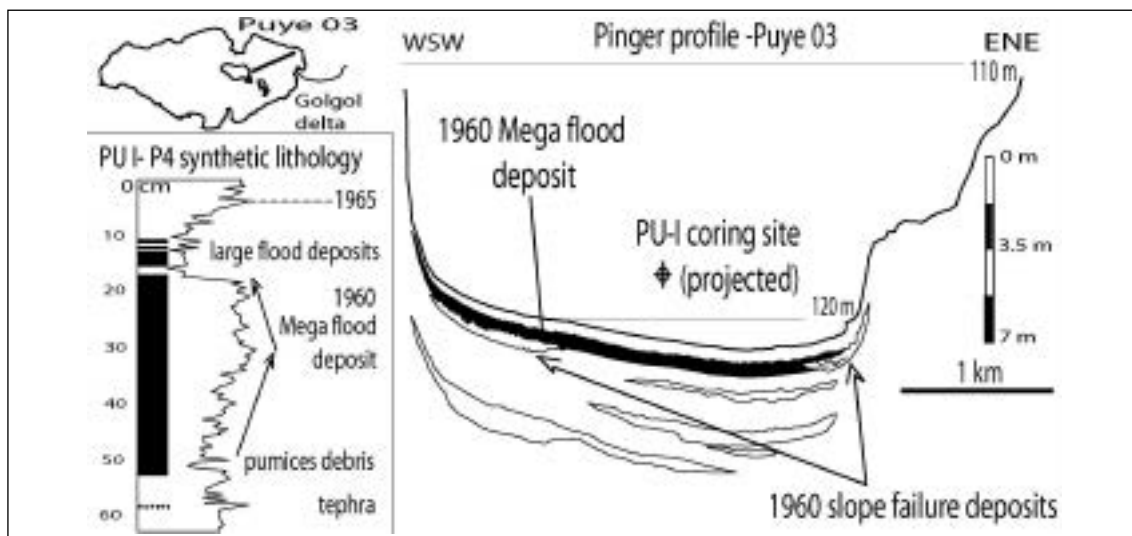


Fig. 3 - Location and interpretation of seismic profile Puye-03 across PU I coring site in the deep basin facing the Golgol delta. The 1960 mega flood deposit is clearly visible and associated with slope failure deposits. The synthetic lithology of short core PU I P4 is also presented and discussed in the text.

In this setting, radionuclide measurements on PU I coring site are largely affected by thick sedimentary events and should be interpreted carefully (c.f. Arnaud et al., 2002). Therefore, based (1) on  $^{137}\text{Cs}$  activity and on the upper measurements of  $^{210}\text{Pb}$ , (2) on historic descriptions of earthquake-triggered land slides in the catchment area of lake Puyehue (Oñat, 1960; Rothé, 1961) and of the formation of pumices during the 1960 Puyehue eruption (Oñat, 1960; Gerlach et al, 1988), (3) on the reconnaissance of pumice debris at the base of the mega flood deposit, and (4) on lamination counting in background sedimentation, we suggest that the mega flood deposit occurred shortly after the 1960 Valdivia event and resulted from the impact of several large land slides on the course of the Golgol River (Fig. 2). We further suggest that the complex succession of large flood deposits together with the detailed evolution of the mean grain size below the 1965 pick in  $^{137}\text{Cs}$  (Fig. 3), can be seen as the progressive recovery of the Golgol fluvial dynamic (i.e. the diffusivity coefficient of sediment load, c.f. Castellort & Van Den Driessche, 2003) from the impact of these land slides. This age-depth model implies a mean continuous SR of  $\sim 3$  mm/yr during the last 70 years, when subtracting the thicknesses of the main sedimentary events (c.f. Chapron et al., 1999; Arnaud et al., 2002), and its extrapolation down core is supported by the correlation of a tephra layer with the eruption of Puyehue volcano in 1929.

These new findings in lake Puyehue have significant implications for paleo-environmental reconstructions in the Chilean Lake District. Concerning the impact of the 1960 Valdivia earthquake (M 9.5), lake Puyehue record highlights a limited slope failure deposit on site PU II, but larger subaqueous slope failure deposits along the slope of the deep basin. These sedimentary features were probably directly triggered by the seismic waves of this major earthquake, together with large land slides documented in the front of the Andes in the study area (Fig. 1). This earthquake also triggered the eruption of the Cordon Caulle-Puyehue volcano (lava flow and pyroclastic flows producing pumices and a large volume of ashes towards the North and the West, according to Oñat (1960) and Gerlach et al, (1988)). Lake Puyehue sedimentary record in coring site PU I provide a key example of the huge impact of this earthquake on the drainage basin of the river Golgol, and can be summarized as follow: land slides along the flanks of Puyehue volcano probably partially damned the river and

triggered, during the winter, a major hyperpycnal flow in the lake. The volume of this major flood deposit can be estimated to be  $\sim 3 \times 10^6$  m<sup>3</sup> based on coring and seismic data. Following this crisis, River Golgol was affected by sediment load and fluvial dynamic during several years.

The sedimentary record of Puyehue volcanic eruptions such as those occurred in 1960 and 1929 in lake Puyehue infill are ranging from direct volcanic fall-out producing thin sandy tephra layers intercalated with background sediments in sites PU II and PU I, to large flood deposits in site PU I, resulting from the erosion and the transport of large volumes of volcanic particles in the drainage basin. These different sedimentary records seem to be essentially depending on the type of volcanic eruptions (Gerlach et al., 1988) and on the influence of the dominating winds during an eruption. For example, during the 1960 eruption of Puyehue volcano, SW winds limited direct and massive ashes fall-out over the lake area (Oñat, 1960), but favoured their accumulation in the upper part of its catchment area. Dominant winds originating from the West in the Chilean Lake District may thus favour the development of thick andosols in this region of the Andes (Bertrand & Fagel, in review) that is characterized by large sediment yields.

Consequently, fluctuation in climate conditions (essentially precipitation regimes associated with the Westerlies) will be recorded in lake Puyehue by a fluctuating clastic supply. Based on its sensitivity to major earthquakes and volcanic eruptions, the most suitable environment to reconstruct climate variability in lake Puyehue is the coring site PU II. Promising proxies in this site involve high-resolution MS and density profiles, together with the reconstruction of varve thicknesses and the evolution of diatoms assemblages. The reconnaissance of <sup>137</sup>Cs and <sup>241</sup>Am picks associated with atmospheric nuclear tests in 1965 might provide new insights for atmospheric circulation models.

## REFERENCES

- Arnaud et al. (2002), *Terra Nova*, 14, 4, 225-232
- Bertrand and Fagel (2004), *Revista Geologica de Chile*, in review
- Bertrand et al. (2003), 10° Congreso Geológico Chileno 2003, Concepcion, Chile
- Castellort & Van Den Driessche (2003), *Sedimentary Geology*, 157, 3-13
- Chapron et al., (1999), *Terra Nova*, 11, 2/3, 86-92
- Chapron et al (2003), IGBP Simposio de Cambio Global: Hacia una vision Sistemática, Punta Arenas, Chile
- Charlet et al. (2003), 10° Congreso Geológico Chileno 2003, Concepcion, Chile
- De Batist et al. (2003), EUG-AGU Joint Assembly, Nice, France
- Denton et al. (1999), *Geografisker Annaler*, 81 A (2), 107-153
- Gerlach et al. (1988), *Journal of Petrology*, 29, 2, 333-382
- Lamy et al (2001), *Earth and Planetary Science Letters*, 185, 369-382
- Moreno et al (2003), *Journal of Quaternary Science*, 18, 1-12
- Oñat C. V. (1960), Reports of Concepcion University, 25 p
- Rothé J. P. (1961), *Revue pour l'Etude des Calamités*, 37, 4-15
- Schneider et al (2004), *Journal of Sedimentary Research*, accepted
- St Onge et al (2004), *Quaternary Science Reviews*, in press
- Syvitski J.P.M. and Schafer C. T. (1994), *Sedimentary Geology*, 104, 127-153

## EOCENE COOLING RECORDED IN THE CHEMISTRY OF LA MESETA FORMATION MOLLUSKS, SEYMOUR ISLAND, ANTARCTIC PENINSULA

10-04

Linda C. Ivany<sup>1</sup>, Daniel B. Blake<sup>2</sup>, Kyger C Lohmann<sup>3</sup>, Richard B. Aronson<sup>4</sup>

<sup>1</sup> Department of Earth Sciences, Syracuse University, Syracuse NY 13244, USA

<sup>2</sup> Department of Geology, University of Illinois, Urbana IL 61801, USA

<sup>3</sup> Department of Geological Sciences, University of Michigan, Ann Arbor MI 48109, USA

<sup>4</sup> Dauphin Island Sea Lab, Dauphin Island AL 32746, USA

### Summary

Seymour Island on the Antarctic Peninsula provides an excellent setting in which to document the timing and magnitude of Eocene-Oligocene cooling and to infer the effects of climate change on the evolution of high latitude shelf biotas. The La Meseta Formation is one of only two places in

Antarctica where Eocene marine shelf sediments are exposed (1). Here, we can generate a record of high latitude shallow water temperature change and tie it directly to co-occurring patterns of temporal change in the diversity and ecology of associated invertebrate macrofaunas. Aronson and Blake (2) have proposed that cooling progressively eliminated the shell-crushing (durophagous) predators of mollusks from Antarctic waters, resulting in a shift in community structure toward a more “Paleozoic” aspect (3) and a decline in defensive architecture of prey species (see abstract by Werner et al., this volume). To evaluate their hypotheses, however, it is critical that temperature history be independently assessed and tied directly to observed patterns of ecological change. Here we present results of a high-resolution,  $\delta^{18}\text{O}$ -derived, temperature curve that is directly tied to the sampling localities and collections reported by Werner et al. (4). When integrated with their faunal data, the temperature record allows the evaluation of evolutionary and ecological observations in a context of changing climate in the Antarctic shallow marine ecosystem. In addition, these data provide valuable constraints on the timing and magnitude of high latitude cooling during the Eocene-Oligocene transition.

### Abstract Text

The La Meseta Formation is a fossiliferous, shallow marine succession comprised of intercalated, locally conglomeratic, sandstones, mudstones, and shell banks (5, 6) that has been ascribed to a variety of inner shelf facies including estuarine, deltaic, and lagoonal environments (5, 7-9). The formation has been separated into seven distinct, mappable units called Telms (acronym for Tertiary Eocene La Meseta; 7), and more recently into three large-scale unconformity-bounded depositional sequences reflecting the interplay of fault-controlled subsidence and eustatic change in sea level (6).  $^{87}\text{Sr}/^{86}\text{Sr}$  ratios of molluscan aragonite from Telms 2, 5, and 7 suggest that sediments span most of the Eocene, with Telm 7 likely being of latest Eocene age (10). This, in combination with its fossiliferous nature, makes the section on Seymour Island an excellent setting within which to investigate relationships between Eocene cooling and ecological and evolutionary change.

Paleontological studies of floral and faunal assemblages from the La Meseta Formation help constrain regional climate during the Eocene, and overall suggest cool to warm-temperate conditions during deposition of the unit (11-15). Paleotemperatures have also been estimated using  $\delta^{18}\text{O}$  values of early marine cements and invertebrate microfossils collected within the Formation (16-18), but these data are difficult to interpret due to limited sampling intensity and combination of results from different taxa. In contrast, Dutton et al. (2002) present a temperature record based on  $\delta^{18}\text{O}$  values of shell carbonate from individuals of a single bivalve genus, *Cucullaea*, for each of Telms 2 through 7. Inferred temperatures average  $\sim 15^\circ\text{C}$  in Telms 2-5 and decrease markedly to  $10.5^\circ\text{C}$  in Telms 6 and 7. These data are consistent with an overall cooling trend through the Eocene, but stratigraphic resolution only to the level of Telm precludes any finer-scale investigation of paleotemperature trends. We have constructed a multi-taxon record of  $\delta^{18}\text{O}$ -derived paleotemperatures through the La Meseta Formation that is stratigraphically resolved to a high degree within Telms. We use mollusk carbonate collected at localities that can be placed with confidence into a regional stratigraphy such that multiple stratigraphic horizons are represented within each Telm. For each horizon, multiple localities along strike were collected when possible. For each collecting locality, we analyzed stable oxygen and carbon isotopic compositions of multiple individuals of two different bivalve taxa, *Cucullaea* and *Eurhomalea*. Individuals were sectioned along the maximum growth axis and polished to reveal growth banding and quality of preservation. Estimates of average annual  $\delta^{18}\text{O}$  are achieved by drilling a path of carbonate across a number of growth bands so as to obtain an average bulk composition across several years of growth. Three to five bulk samples were collected from each individual in this manner. Two individuals of each taxon from a single locality were also sequentially microsampled parallel to growth bands at very high resolution to reveal growth patterns on an intraannual basis, so that the meaning of bulk compositions could be better understood. Shells were drilled on the high-precision micromilling systems at both Syracuse University and the University of Michigan. Resulting powdered samples were roasted and run on the MAT 251 mass spectrometer coupled to an automated carbonate preparation device at the U of M Stable Isotope Laboratory. Paleotemperatures are calculated using the empirically determined paleotemperature equation of Grossman and Ku (1986) for biogenic aragonite. Without better age constraints, we use values of  $\delta^{18}\text{O}_{\text{SW}}$  for an ice-free world,

= -1‰ (19). Note that if other  $\delta^{18}\text{O}_{\text{SEAWATER}}$  values are employed to account for the onset of ice accumulation in Antarctica (i.e., -0.5‰; Lear et al., 2000), estimated temperatures would be somewhat higher.

We employ a hierarchical sampling design in this study to understand the various sources of variation in our isotope data. In addition to comparisons between our two taxa, for each taxon we consider isotopic variation within individuals, between individuals of the same locality, between collecting localities within the same stratigraphic horizon, and across stratigraphic horizons. This approach allows us statistically assess the significance of differences we see among samples at each of these hierarchical levels, so as to be assured of the validity of trends we see through time.

Significant differences were found between the bulk isotopic compositions of the two primary taxa employed in this study. In sets of samples from 11 different collecting localities spanning Telms 3-7, bulk  $\delta^{18}\text{O}$  values for *Cucullaea* were on average, 4‰ more positive than those for *Eurhomalea*, and hence yield paleotemperatures cooler by about 2°C. High-resolution microsampling within and across growth bands of both taxa reveal that *Cucullaea* does not grow during the Austral summer (20), while *Eurhomalea* produces shell carbonate more continuously throughout the year, recording more of the warm season temperatures. This difference in life-history strategy explains the offset in average values between taxa, and emphasizes the importance of understanding the biology of organisms from which geochemical data are extracted if one is to interpret data correctly.

Significant compositional variation exists within individual shells, reflecting intra- and inter-annual temperature variation experienced within the lifespans of individuals, possibly combined with ontogenetic changes in the rate and duration of growth throughout the year. Within taxa, comparisons of shells within collecting localities also revealed some occasionally significant variation, indicating a degree of time-averaging within shell beds that subsumes longer-term inter-annual variation. Comparisons of samples from different collecting localities within the same stratigraphic horizon, however, revealed no significant differences, ensuring that variation within collections is consistent from place to place and will not obscure temporal patterns.

Once variation within and among shells, localities, and horizons is taken into account, the long-term secular trends in  $\delta^{18}\text{O}$  and temperature can be evaluated (Fig. 1). When these values are converted to temperature, assuming normal marine salinity and  $\delta^{18}\text{O}_{\text{SW}} = -1‰$ , temperatures range from about 19°C at the base of Talm 3 (and during the Talm 6 negative excursion), to ~14-15°C through Talm 5, and down to ~11°C in Talm 7. These values are consistent with those reported by Dutton et al. (2002), and the pattern of increasing  $\delta^{18}\text{O}$  (and cooling temperature) upsection mirrors changes seen in foraminifer records from high southern latitude DSDP and ODP sites (21-23).

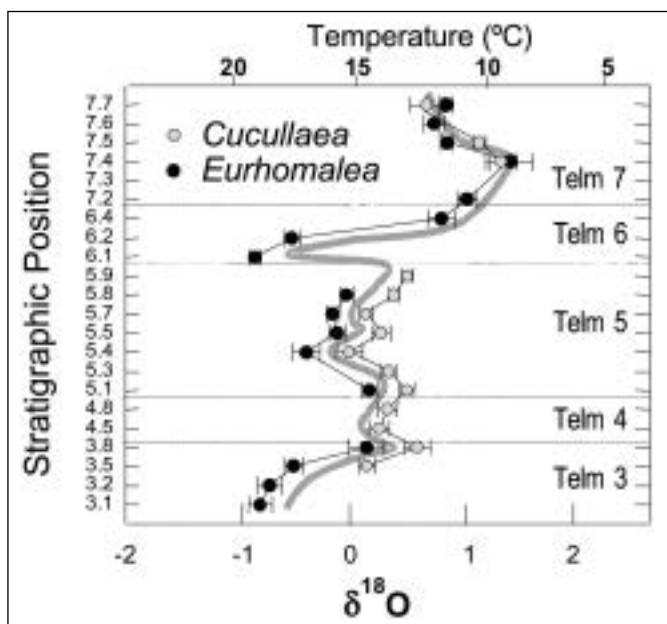


Fig. 1 - Secular change in  $\delta^{18}\text{O}$  of bivalve carbonate from *Cucullaea* and *Eurhomalea* through the La Meseta Formation. Stratigraphic position is relative, dimensions along the y-axis are not intended to reflect section thickness. Thick gray line is interpolated overall trend. Each symbol represents the mean composition of multiple samples within multiple individuals from multiple correlative sampling localities for each stratigraphic horizon. Error bars are indicated by vertical lines on either side of symbols.

Because variation in salinity affects the oxygen isotopic composition of the water and hence of shell carbonate, and because the La Meseta Formation is inferred to have accumulated in an estuarine setting, we need to consider the possibility that the waters were not fully marine during deposition. Any significant fresh-water influx would shift  $\delta^{18}\text{O}$  of shell carbonate toward more negative values, yielding an overestimation of paleotemperatures. We believe that salinity has not substantially biased our paleotemperature estimates for several reasons: 1) the fauna is generally diverse and often includes stenohaline organisms, 2)  $^{87}\text{Sr}/^{86}\text{Sr}$  values are consistent with marine salinity, 3) carbon and oxygen stable isotopes show no covariation, as would be expected with freshwater mixing (e.g., 24), and 4) data from different shells within localities and different localities within horizons do not show significant variation, as would be expected in a brackish environment. The shift toward more negative  $\delta^{18}\text{O}$  values at the base of Tlm 6 is the only potential exception, as there is stratigraphic evidence for very near-shore conditions at this level.

The large shift in  $\delta^{18}\text{O}$  observed in Tlm 6 corresponds in time to the drop in defensive architecture of prey taxa noted by Werner and others (4). These results are consistent with the hypothesis that climate cooling caused a decline in shell-crushing predators and led to the establishment of the unusual "Paleozoic" faunas of today's Antarctic shelf (2,3). Further refinement in their ecological and evolutionary data will allow more detailed comparisons to this temperature trajectory. Our curve reveals a greater level of complexity in  $\delta^{18}\text{O}$  and temperature through the Eocene section on Seymour Island than has been suggested by previous work done at lower resolution. We believe the major aspects of this curve will be shown to reflect the global signal (e.g., ref 19), with early Eocene warmth, middle Eocene relative stability, and a shift toward cooler conditions perhaps superimposed on limited ice growth in the upper Eocene. Additional  $^{87}\text{Sr}/^{86}\text{Sr}$  analyses on select samples from within this section will aid in better constraining age in the trend presented here. Until that time, we refrain from drawing more specific parallels between our curve and the deep-sea record of global change.

## REFERENCES

1. R. M. Feldmann, M. O. Woodburne, Eds., *Geology and Paleontology of Seymour Island, Antarctic Peninsula*, Memoir 169 (Geological Society of America, Boulder, CO, 1988).
2. R. B. Aronson, D. B. Blake, *American Zoologist* 41, 27-39 (2001).
3. R. B. Aronson, D. B. Blake, T. Oji, *Geology* 25, 903-906 (1997).
4. J. E. Werner, D. B. Blake, R. B. Aronson, *GeoSur 2004 Proceedings* in press (2004).
5. D. H. Elliot, T. A. Trautman, in *Antarctic Geosciences* C. Craddock, Ed. (University of Wisconsin Press, 1982) pp. 287-297.
6. S. J. Porebski, *Geology* 28, 147-150 (2000).
7. P. M. Sadler, in *Geology and Paleontology of Seymour Island, Antarctic Peninsula* R. M. Feldmann, M. O. Woodburne, Eds. (Geological Society of America, Boulder, CO, 1988), GSA Memoir 169, pp. 303-320.
8. S. J. Porebski, *Studia Geologica Polonica* 107, 7-97 (1995).
9. J. H. Wrenn, G. F. Hart, in *Geology and Paleontology of Seymour Island, Antarctic Peninsula* R. M. Feldmann, M. O. Woodburne, Eds. (Geological Society of America, Boulder, CO, 1988), Memoir 169, pp. 321-447.
10. A. L. Dutton, K. C. Lohmann, W. J. Zinsmeister, *Paleoceanography* 17, 1-14 (2002).
11. J. A. Case, in *Geology and Paleontology of Seymour Island, Antarctic Peninsula* R. M. Feldmann, M. O. Woodburne, Eds. (Geological Society of America, Boulder, CO, 1988), GSA Memoir 169, pp. 523-530.
12. R. A. Askin, R. F. Fleming, *Antarctic Journal of the United States* 17, 70-71 (1982).
13. M. Doktor, A. Gazdzicki, A. Jerzemska, S. J. Porebski, *Palaeontologica Polonica* 55, 127-146 (1996).
14. L. A. Wiedman, R. M. Feldmann, in *Geology and Paleontology of Seymour Island, Antarctic Peninsula* R. M. Feldmann, M. O. Woodburne, Eds. (Geological Society of America, Boulder, CO, 1988), Memoir 169, pp. 449-457.
15. J. D. Stilwell, W. J. Zinsmeister, *Molluscan Systematics and Biostratigraphy, Lower Tertiary La Meseta Formation, Seymour Island, Antarctic Peninsula*, Antarctic Research Series (American Geophysical Union, Washington D.C., 1992), vol. 55.
16. D. Pirrie, J. D. Marshall, J. A. Crame, *Palaios* 13, 276-286 (1998).
17. A. J. Gazdzicki, et al., *Antarctic Science* 4, 461-468 (1992).
18. P. W. Ditchfield, J. D. Marshall, D. Pirrie, *Palaeogeography, Palaeoclimatology, Palaeoecology* 107, 79-101 (1994).
19. J. C. Zachos, L. D. Stott, K. C. Lohmann, *Paleoceanography* 9, 353-387 (1994).
20. D. P. Buick, L. C. Ivany, *Geology* (in revision).
21. N. J. Shackleton, J. P. Kennett, *Initial Reports of the DSDP* 74, 743-755 (1975).
22. L. D. Stott, J. P. Kennett, N. J. Shackleton, R. M. Corfield, in *Proceedings of the Ocean Drilling Project, Scientific Results Volume 113* P. F. Barker, J. P. Kennett, et al., Eds. (1990), vol. 113, pp. 849-863.
23. A. Mackensen, W. U. Ehrmann, *Marine Geology* 108, 1-27 (1992).
24. B. L. Ingram, J. C. Ingle, M. E. Conrad, *Geology* 24, 331-334 (1996).
25. This research was supported by grants from The US National Science Foundation's Office of Polar Programs to Ivany and Lohmann and to Blake and Aronson.

**FIRST PALEOMAGNETIC RESULTS ON THE SARMIENTO OPHIOLITE, SOUTHERN CHILE: IMPLICATIONS FOR THE PATAGONIAN OROCLINE****10-05**A.E. Rapalini<sup>(1)</sup>, M. Calderón<sup>(2)</sup>, F. Hervé<sup>(2)</sup>, U. Cordani<sup>(3)</sup>, S. Singer<sup>(1)</sup>*(1) INGEODAV, Depto. Cs. Geológicas, F.C.E.yN., Universidad de Buenos Aires, Argentina**(2) Depto. de Geología, Universidad de Chile, Santiago, Chile**(3) Instituto de Geociencias, Universidade de Sao Paulo, Brasil*

The Andean orogen presents a dramatic change of about 90° on its strike around 53°S, where from a dominantly roughly North-South direction to the north turns into an East-West orogen. This bend is known as the Patagonian Orocline, after Carey (1955). As already pointed out by Cunningham et al. (1991), a yet unresolved problem in the evolution of the Southern Andes is whether the Patagonian Orocline formed as a curved orogen, is a non-rotational arc with domains offset by strike-slip faults or it has been produced by orogenic rotation (“oroclinal bending”). Paleomagnetism is a very powerful tool to discriminate between such end-models and to unravel the kinematic evolution of an orocline both in space and time (see for instance Morris and Anderson, eds., 1998). Therefore, reliable paleomagnetic data from outcrops distributed along the whole Andean orogen between 50°S and 56°S would be significant for unravelling the tectonic evolution of this region.

Despite the fact that several different tectonic models have been put forward to explain the late Mesozoic-Cenozoic tectonic evolution of this part of the Andes (e.g. Cunningham, 1993, 1995; Diraison et al., 2000; Kraemer, 2003), very few paleomagnetic studies have been carried out yet in the region (Dalziel et al., 1973; Burns et al., 1980; Cunningham et al., 1991; Rapalini et al., 2001; Baraldo et al., 2002; Iglesia Llanos et al., 2003). Furthermore, the first two quoted above are the only one yet done with a regional distribution of sampling localities but they cannot pass present-day reliability criteria. Nevertheless, they have been widely used in previous tectonic interpretations. The remaining studies are of better experimental quality but are generally restricted to a single locality or relatively far from the oroclinal bend. Therefore, the available database is clearly insufficient to actually test different hypothesis.

In order to obtain new paleomagnetic data to constrain models of the kinematic evolution of the Patagonian orocline a reconnaissance paleomagnetic survey was carried out on the Sarmiento Ophiolite as part of a multidisciplinary project to study this unit (see Calderón et al., 2003).

The Sarmiento Ophiolite constitutes the northern part of the Rocas Verdes marginal basin (Daziel et al., 1974), outcrops which extends discontinuously from about 51°S (Sarmiento Complex) to 55°S (Tortugas Complex). This belt of mafic rocks is composed of pillow-lavas, sheeted dykes, gabros and minor occurrences of plagiogranites. To the west, the belt is flanked by granitic rocks of the Patagonian batholith. The marginal basin developed during the Late Jurassic mainly (Stern et al., 1992) and it was tectonically closed and inverted in several pulses starting in the Mid-Cretaceous (Kraemer, 2003).

In order to obtain a preliminary paleomagnetic pole of the Sarmiento ophiolite, a reconnaissance sampling was carried out on 11 sites (85 samples) regionally distributed (Fig.1). Sampled lithologies comprised both vertical dikes and pillow-lavas. For the latter, bedding attitude was determined from overlying sediments of the Zapata Formation. At several sites, samples were also taken for radiometric datings. K/Ar whole rock ages for several sites is presented in Fig.1.

Preliminary paleomagnetic results from 45 samples from all sites indicate that most are carriers of a characteristic remanence that can be isolated both from alternating field (AF) and thermal demagnetization. This magnetic remanence show good within-site consistency in 8 out of 11 sites. At seven sites the mean site remanence directions correspond to a normal polarity magnetic field, while a single site (S-6) shows reversed polarity. Application of bedding correction to the pillow-lavs sites clearly indicate that the remanence is post-tectonic (Fig.2). Mean preliminary paleomagnetic direction for the Sarmiento Complex is Dec: 286.8°, Inc: -60.1°, a95: 9.7°, N: 8 sites. Age of magnetization is not yet accurately known, although its posttectonic character suggests it is post-Mid Cretaceous. Grouping of K/Ar dates from 4 paleomagnetic sites around 73.5±1.5 Ma, may suggest a Late Cretaceous age for remanence acquisition, coincident with closure of the radioactive system. A dominant normal polarity period between ca. 79 and 72 Ma is consistent with the dominant normal

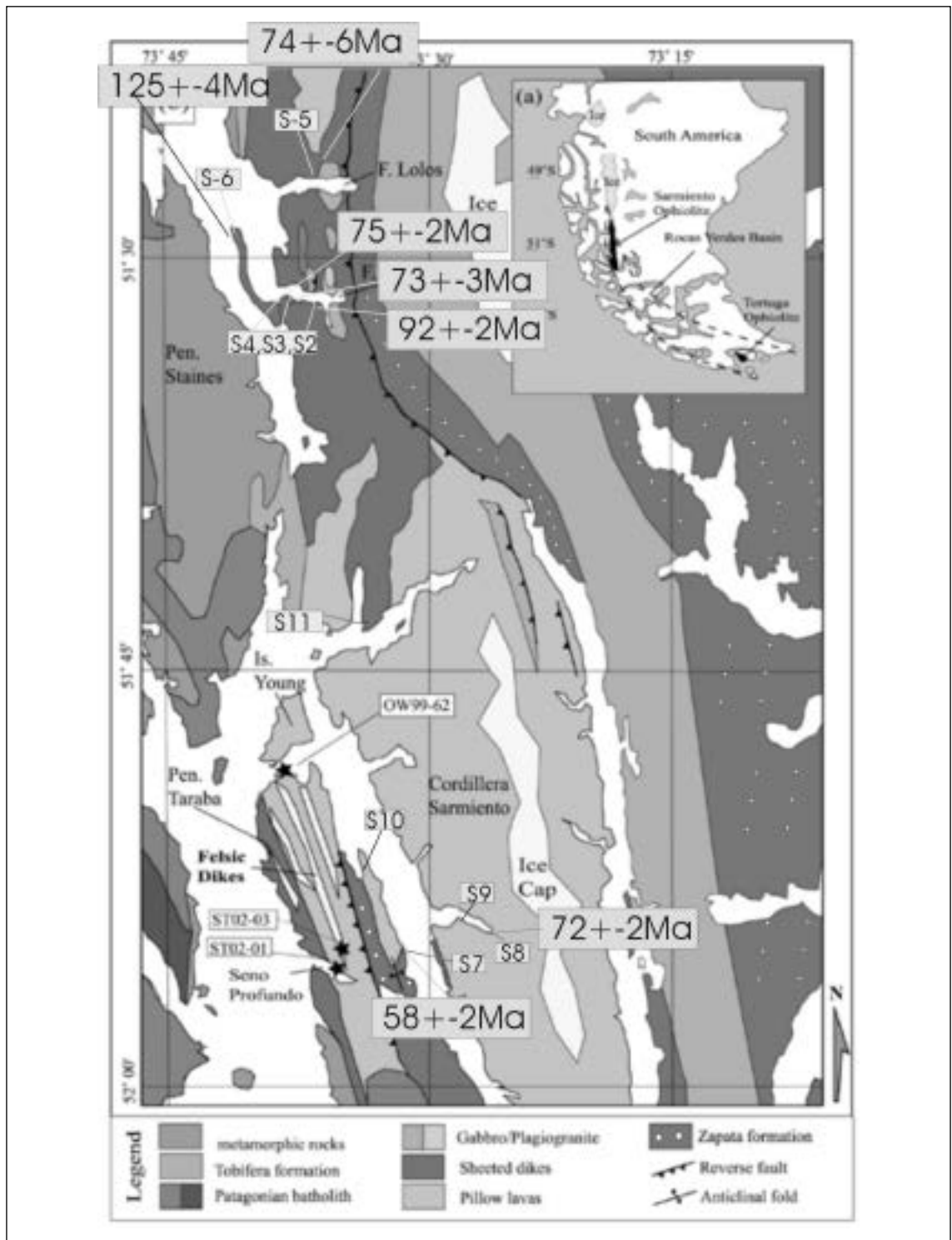


Fig.1 - Simplified geologic map of the Sarmiento ophiolite and distribution of paleomagnetic sampling sites and K/Ar whole rock ages.

polarity found in most sites. Furthermore, the single reverse site yielded a K/Ar age of  $125.2 \pm 3.7$  Ma consistent with the reverse polarity of chron M3r between 123 and 125.5 Ma. Age of magnetization at this site may then be older than in most others.

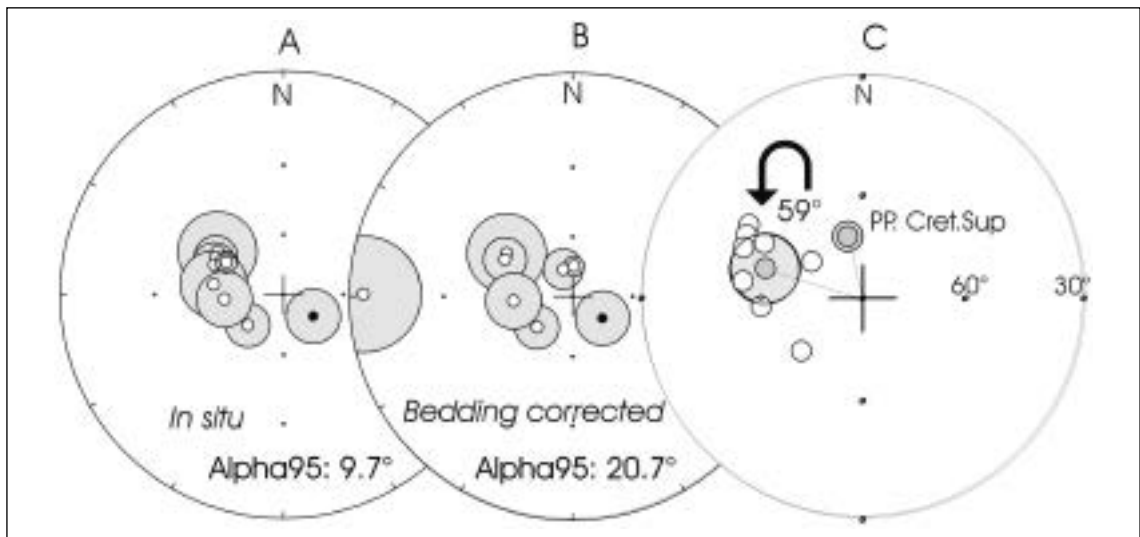


Fig. 2 - Preliminary mean site remanence directions for the Sarmiento ophiolite, before (A) and after (B) bedding correction. C) Mean remanence direction and expected direction for the Late Cretaceous.

Mean preliminary paleomagnetic direction for the Sarmiento Ophiolite is not consistent with that correspondent to the Late Cretaceous reference pole for South America (Somoza, 2002). Its position indicates a counterclockwise rotation of the Sarmiento Ophiolite of  $59.0 \pm 17.0^\circ$  and a less significant flattening (inclination anomaly) of  $11.1 \pm 8.1^\circ$ . The sense of rotation is consistent with the bend of the Andean orogen at this latitude but the amount almost double that expected from the curvature of the orogenic front. Recent paleomagnetic results on Jurassic volcanics of the southern Andes between  $49^\circ$  and  $50^\circ$ S (Iglesia Llanos et al., 2003) obtained nearly identical rotation values, which suggests the existence of a large tectonic domain that experience a large ccw rotation. The interpreted Late Cretaceous age of the remanence of the Sarmiento ophiolite indicates that the rotation must have occurred during the Late Cretaceous and/or Cenozoic.

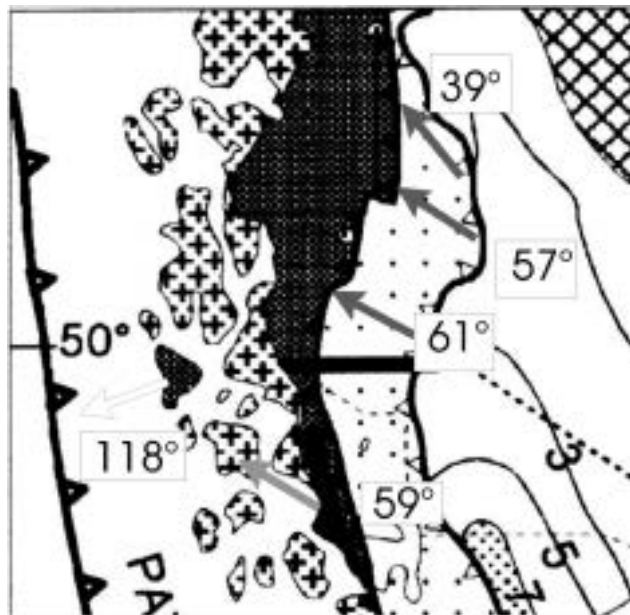


Fig. 3 - Paleomagnetic declinations in the southern Andes between  $49^\circ$ S and  $51^\circ$ S. Data from Iglesia Llanos et al. (2003): dark grey arrows; data from Rapalini et al. (2001): white arrow; this study: light grey arrow.



## REFERENCES

- Baraldo, A.; A. Rapalini; A. Tassone; H. Lippai; M. Menichetti and E. Lodolo; 2002. Estudio paleomagnético del intrusivo del cerro Hewhoepen, Tierra del Fuego, y sus implicancias tectónicas. XV Congreso Geológico Argentino, El Calafate, abril 2002. Actas 1, 285-290
- Burns, K.L., M.J. Rickard, L. Belbin, F. Chamalaun, 1980. Further paleomagnetic confirmation of the Magellanes orocline, *Tectonophysics*, 63, 75-90.
- Calderón, M., Hervé, F., Fildani, A., Cordani, U., Herrera, C., Rapalini, A.E. and Piquer, J.; 2003. Reconnaissance field study of the Sarmiento Ophiolite with emphasis in the petrological meaning of leucocratic dikes at Península Taraba. X Congreso Geol. Chileno, Concepción, Actas en CD: 10 pp.
- Carey, S.W.; 1955. The orocline concept in geotectonics. *Proceedings of the Royal Society of Tasmania*, 89, 255-288.
- Cunningham, W.D., 1993. Strike-slip faults in the southernmost Andes and the development of the Patagonian orocline: *Tectonics*, v. 12, pp. 169-186.
- Cunningham, W. D. 1995. Orogenesis at the southern tip of the Americas: the structural evolution of the Cordillera Darwin metamorphic complex, southernmost Chile. *Tectonophysics*. Vol. 244, p. 197-229.
- Cunningham, W.D., K.A. Klepeis, W.A. Gose, I.W. Dalziel, 1991. The Patagonian Orocline: New paleomagnetic data from the Andean magmatic arc in Tierra del Fuego, Chile, *J. Geophys. Res.*, 96, 16061-16069.
- Dalziel, I.W.D., de Wit, M.J. and Palmer, K.F., 1974. Fossil marginal basin in the Southern Andes: *Nature*, 250, 291-294.
- Dalziel, I.W.D. Kligfield, R. Lowrie, W. Opdyke, N.D., 1973. Paleomagnetic data from the southernmost Andes and the Antarcticandes, in: D.H. Tarling, S.K. Runcorn (Eds.), *Implications of Continental Drift to Earth Sciences*, Academic Press, San Diego, California, 1: 87-101
- Diraison, M., Cobbold, P.R., Gapais, D., Rossello, E., 2000. Cenozoic crustal thickening, wrenching and rifting in the foothills of the southernmost Andes. *Tectonophysics*, 316: 91-119.
- Iglesia Llanos, M.P., Lanza, R., Riccardi, A.C., Geuna, S., Laurenzi, M.A., Ruffini, R., 2003. Palaeomagnetic study of the El Quemado complex and Marifil formation, Patagonian Jurassic igneous province, Argentina. *Geophysical Journal International*, 154: 599-617.
- Kraemer, P.E., 2003. Orogenic shortening and the origin of the Patagonian orocline (56°S. Lat). *J. South Amer. Earth Sci.*, 15: 731-748.
- Morris, A. and Anderson, M.W. (Eds.); 1998. Paleomagnetism and tectonic rotations. *Tectonophysics*, 299, 1-3, 1-253.
- Rapalini, A.E., F.Hervé, V.A. Ramos y S. Singer, 2001. Paleomagnetic evidence of a very large counterclockwise rotation of the Madre de Dios archipelago, southern Chile. *Earth and Planetary Science Letters*, 184 (2): 471-487.
- Somoza, R., 2002. El campo magnético cretácico desde una perspectiva americana. XV Congreso Geológico Argentino, El Calafate, abril 2002. Actas 1, 88-93.
- Stern, C.R., Mukasa, S.B. and Fuenzalida, R., 1992. Age and petrogenesis of the Sarmiento ophiolite complex of southern Chile. *J. South Amer. Earth Sci.*, 6: 97-104.

**VOLCANIC ERUPTION IMPACTS ON PALEOENVIRONMENTAL RECONSTRUCTION: A HIGH-RESOLUTION STUDY OF SEDIMENTOLOGY, GEOCHEMISTRY AND PALEOECOLOGY FROM TWO LAKES OF THE CHILEAN LAKE DISTRICT (SOUTH CENTRAL CHILE)**

10-06

Sabine Volland<sup>1</sup>, Jens Müller<sup>1†</sup>, Mario Pino<sup>2</sup>, Michael Sturm<sup>3</sup>

<sup>1</sup> *Institute of Engineering Geology, Technische Universitaet Muenchen, D-80290 Muenchen, Germany, e-mail: sabine.volland@mytum.de*

<sup>2</sup> *UACH, Universidad Austral de Chile, Valdivia, Chile*

<sup>3</sup> *Swiss Federal Institute for Environmental Science and Technology (EAWAG), CH-8600 Duebendorf, Switzerland*

† *passed away in May 2002*

**Summary**

A high-resolution multidisciplinary study was carried out on surficial bottom sediments and short gravity cores of two lakes in the Chilean Lake District that undergo current continuous ashfall deposition from the volcano Villarrica (South Central Chile). The investigation comprises high-resolution seismic profiling, mineralogical, geochemical, sedimentological and biological parameters, as well as a chronology based on <sup>14</sup>C-AMS and <sup>210</sup>Pb dating and magnetic susceptibility. The sediments show a significant impact from deposition of volcanic tephra into the lake basins that disturb the natural background sedimentation. Volcanic input masks the signals of past environmental change and has to be considered before interpretation of the multiproxy record, to provide suitable results for paleoenvironmental reconstruction.

## Abstract text

During the past decades, lake sediments have been intensively studied in various geological and often extreme geographic settings for the reconstruction of paleoenvironmental and regional paleoclimatic changes, driven by shifts in the atmospheric oscillation patterns and their interhemispheric teleconnections. The regional impact of ENSO patterns in the southern hemisphere along the Chilean Pacific coast has especially been the focus of various multiproxy studies, most of which dealt with large-scale patterns of climate change during the Holocene. In the last decade, high-resolution studies of the late Holocene on a millennium time-scale provided information on tree-ring variability (Villalba, 1994) and lake sediments (Jenny et al., 2002) and dealt with the question, if evidence for abrupt climate changes like the “Little Ice Age” or the “Medieval Warm Period” is also found in terrestrial and lacustrine archives from South America.

As studies of lake sediments have become an important tool to document the variability of environmental systems and climatic changes, the results based on their resolution have to be interpreted carefully. High-resolution studies are only significant for a particular period of time that encompasses variable geological, geochemical and biological parameters. Most of those parameters are very sensitive to terrestrial and atmospheric disturbances, outside the lake system. Such disturbances, like intense volcanic activity, overwhelm the signals of the natural background that reflect e. g. changes in moisture and precipitation rates. The proxies that are used for high-resolution studies on changes in environmental and climatic systems are unique and therefore local, as they differ greatly in nature (Soon & Baliunas, 2003). Consequently, generalization or comparison over extensive regional transects remain difficult and problematic.

The Chilean Lake District is subject to continuous recurring ash-fallout deposition of recent volcanism, primarily due to Villarrica, the most active volcano of South America. A chronology of its highly dangerous and explosive phreatomagmatic eruptions that provide huge amounts of volcanic ash-fallout, as well as pyroclastic surges and flows, accompanied by laharic events, is known since ancient time. However, its effects on the surrounding lakes and ecologic systems have not yet been studied. Until today, a complete sedimentological and paleoenvironmental investigation of the entire lake region is lacking.

The aim of this project is to provide a high-resolution multidisciplinary study of volcanic impacts on the biological, physical and chemical processes that reflect the paleoenvironmental and paleoclimatic signals from the late Holocene until present day.

Lakes Villarrica and Calafquén are located in the northern Chilean Lake District; both are of glacial origin and are situated between the flanks of the active volcano Villarrica. This active geodynamic setting with intensive volcanism and strong earthquakes routinely influences the clastic sedimentation of both lakes by catchment erosion, tephra fall-out deposition and large subaqueous mass movements. Therefore, a high-resolution seismic profiling of both lakes has been carried out to map the sedimentary infill geometries of the lake basins and to select sampling and coring sites for further sedimentological and biological studies. A dense grid of grab samples were taken to study sediment texture, mineralogical composition and geochemistry. Although both lakes are closely located, their watersheds differ significantly. The differences of the drainage system and flushing rate are well recorded in the sediment succession of the short gravity cores but cannot be differentiated by textural patterns of the surficial bottom sediments. The natural background sedimentation recorded in the short cores is disturbed by sequences of tephra layers. A multi-proxy analysis of the short cores collected in Lakes Villarrica and Calafquén provide information about grain-size, mineralogy, geochemistry, magnetic susceptibility, LOI, TC and biogenic fraction. According to <sup>14</sup>C-AMS dating, the cores cover the last 3000 (Lake Calafquén) and 1200 years (Lake Villarrica) of the Holocene. These ages have to be interpreted carefully due to the continuous volcanic impact on plant material in the catchment.

The short cores from both lakes offer the possibility of tracing past changes in the aquatic ecosystem in a time-scale that exceeds long-time monitoring of the natural system. Furthermore, they comprise a number of biotic and abiotic variables (Lotter et al., 1995). Characterisation of micro-scale system behaviour, resulting from direct volcanic fall-out deposition or indirect influence by erosion of the volcanic nappes, seems to be possible. Changes in the lakes are reflected in their well preserved

diatom assemblages. After every tephra input by direct fall-out deposition into the lake, diatom blooms consisting of eutrophic indicator species developed, likely responding to the input of nutrients. No changes in the diatom abundance have been observed, but only displacement of pre-existing species by others.

Although the multiproxy data provide information to perform a detailed environmental reconstruction, interpretations should be made carefully. The response to volcanic influence masks these signals, as there are significant impacts on the physical and biologic processes in the lake basin, as well as erosion of the catchment. Tephra precipitation and input by continuous catchment erosion may last for decades as is reported from the Icelandic lakes (Hardardóttir et al., 2001). Therefore, the influence of tephra deposition has to be separated from the interpretation and its influence has to be considered and evaluated in detail before paleoproductivity and sediment accumulation rates can be taken as a suitable database for the reconstruction of paleoenvironmental changes.

## REFERENCES

- Hardardóttir, J., Geirsdóttir, A. Thórdarson, T. (2001), Tephra layers in a sediment core from Lake Hestvatn, southern Iceland: implications for evaluating sedimentation processes and environmental impacts on a lacustrine system caused by tephra fall deposits in the surrounding watershed. In: White, J.D.L. & Riggs, N.R. (eds.), *Sedimentation in volcanoclastic settings*. Spec. Publ. Int. Ass. Sediment. 30, 225-246.
- Jenny, B., Valero-Garcés, B.L., Urrutia, R., Kelts, K., Veit, H., Appleby, P.G., Geyh, M. (2002), Moisture changes and fluctuations of the Westerlies in Mediterranean Central Chile during the last 2000 years: The Laguna Aculeo record (33°50'). *Quaternary International* 87, 3-18.
- Lotter, A.F., Birks, H.J.B. & Zolitschka, B. (1995), Late glacial pollen and diatom changes in response to two different environmental perturbations: volcanic eruption and Younger Dryas cooling. *Journal of Paleolimnology* 14, 23-47.
- Soon, W. & Baliunas, S. (2003), Proxy climatic and environmental changes of the past 1000 years. *Clim. Res.* 23, 89-110.
- Villalba, R. (1994), Tree-ring and glacial evidence for the medieval warm epoch and the little ice age in southern South America. *Clim. Change* 26, 183-197.



# **Session 11**

---

**PALEONTOLOGY AND  
PALEOECOLOGY**



## MESOZOIC CALCAREOUS NANNOFOSSILS FROM LARSEN BASIN, SOUTHERN ANTARCTIC PENINSULA

11-01

Andrea Concheyro <sup>\*, \*\*, \*\*\*</sup>

(\*) Dept. Ciencias Geológicas. Univ. Buenos Aires. Pabellón II. Ciudad Universitaria. 1428. Buenos Aires. Argentina. E-mail: andrea@gl.fcen.uba.ar

(\*\*) Instituto Antártico Argentino

(\*\*\*) CONICET

### Summary

Calcareous nannofossils from the Upper Jurassic and Upper Cretaceous marine sediments of the west and southeastern sector of James Ross Island, Snow Hill Island, Seymour Island and the Antarctic Peninsula are here presented.

The studied localities comprise Hamilton Point in James Ross Island, Sanctuary Cliffs Nunatak and Refugio Suecia in Snow Hill Island, the proximities to Filo Negro in Seymour Island and Longing Gap in the Antarctic Peninsula. The exposed sedimentary rocks in the area have been assigned to the Ameghino, Santa Marta, Snow Hill Island and López de Bertodano Formations.

The presence of *Polycostella beckmanii*, *Cyclagelosphaera deflandrei*, *Diazomatolithus lehmanii* at Longing Point suggest a Middle to Late Tithonian age. The occurrences of *Misceomarginatus pleniporus*, *Monomarginatus quaternarius*, *Biscutum coronum*, and *Biscutum magnum*, indicate the *Biscutum coronum* and the *Biscutum magnum* Biozones for high austral latitudes (Pospichal and Wise, 1990). The recovered nannofossil associations allow to confirm that the sedimentary sequence has been deposited during Upper Jurassic, and Upper Campanian-Upper Maastrichtian. Nannofossils can be included in the "Falkland Plateau Province" (Wind, 1979), and they show a good correlation with other Campanian-Maastrichtian nannofossil associations from the South Atlantic Ocean and Northern Patagonia.

### Introduction

The Larsen Basin comprises a wide back-arc basin developed in the Southeast Sector of the Antarctic Peninsula between the 65°S and 58°W. This basin has been filled successively by delta, estuarine, shelf and slope deposits, ranging in age from the Upper Jurassic to the Eocene. The basin contains one of the most complete, extended, and best preserved sedimentary records of the Upper Cretaceous from the southern latitudes. An extended ice cap covers the James Ross Island group almost completely, but on the southeast sector of these islands, some snow free outcrops occur on James Ross, Snow Hill, Humps, Cockburn and Seymour islands (Fig. 1).

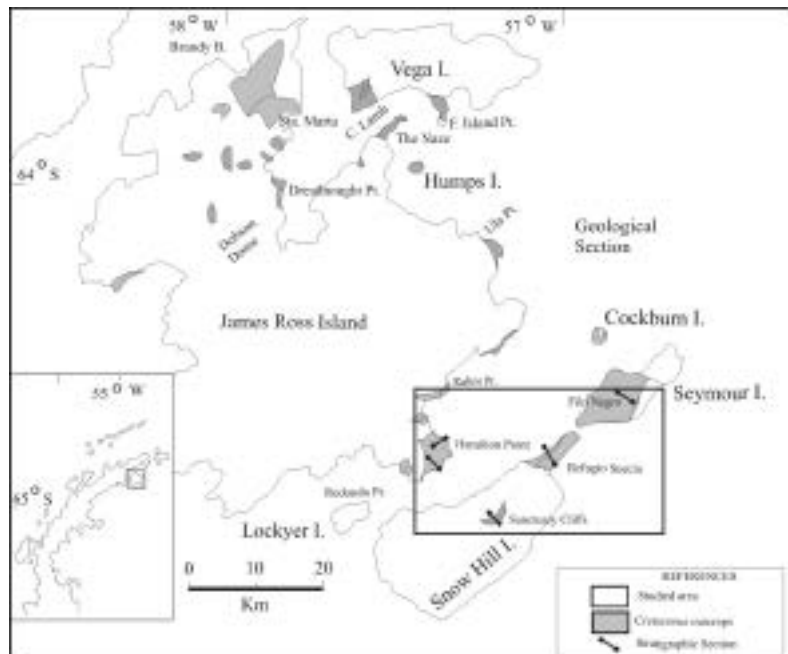


Fig. 1 - Location map of the studied area.

Two different stratigraphic sequences can be separated in the studied region; the first, includes the western sector of James Ross, and it represents the older sediments of the basin (Aptian to Campanian deposits), and the second, the southeastern area of James Ross Island, Snow Hill, Cockburn and Seymour islands, with younger sediments (Upper Campanian to Eocene).

The most relevant investigations have been conducted during the last 25 years by Argentinian, British, American and Polish researchers. Main studies have been focused on establishing the paleoenvironments and the sedimentology of this region. Contemporaneously new advances of invertebrate paleontology have carried out in order to separate different stratigraphic units based upon their fossils.

The aim of this research is to document the currently known Upper Cretaceous Nannofossil Biostratigraphy of James Ross Island Group, and the Upper Jurassic marine deposits in Antarctic Peninsula, updating the existing micropaleontological database, and correlating these results within the previous stratigraphic frame obtained through other fossil groups.

### Lithofacies and Calcareous Nannofossils

At Longing Gap Antarctic Peninsula, the Ameghino Formation contains laminated claystones interbedded with ash layers and tuffs. Carbonatic concretions are frequent and deposited in a dysaerobic marine environment.

At Hamilton Point, Refugio Suecia and Sanctuary Cliffs, the lithofacies consist of silty claystones, silty sandstones, sandy siltstones, lenticular fossiliferous accumulations and fine-bedded tuffs. The lithofacies associations in these areas represent sedimentation below normal wave base, from lower shoreface to offshore settings.

The facies associations at the Refugio Suecia indicate incised valleys systems and estuarine environments followed by transgressive sedimentation. A complete transgressive-regressive cycle within a stable platform in a back-arc basin, with coeval volcanic activity in the Antarctic Peninsula is defined for these localities (Fig. 2).

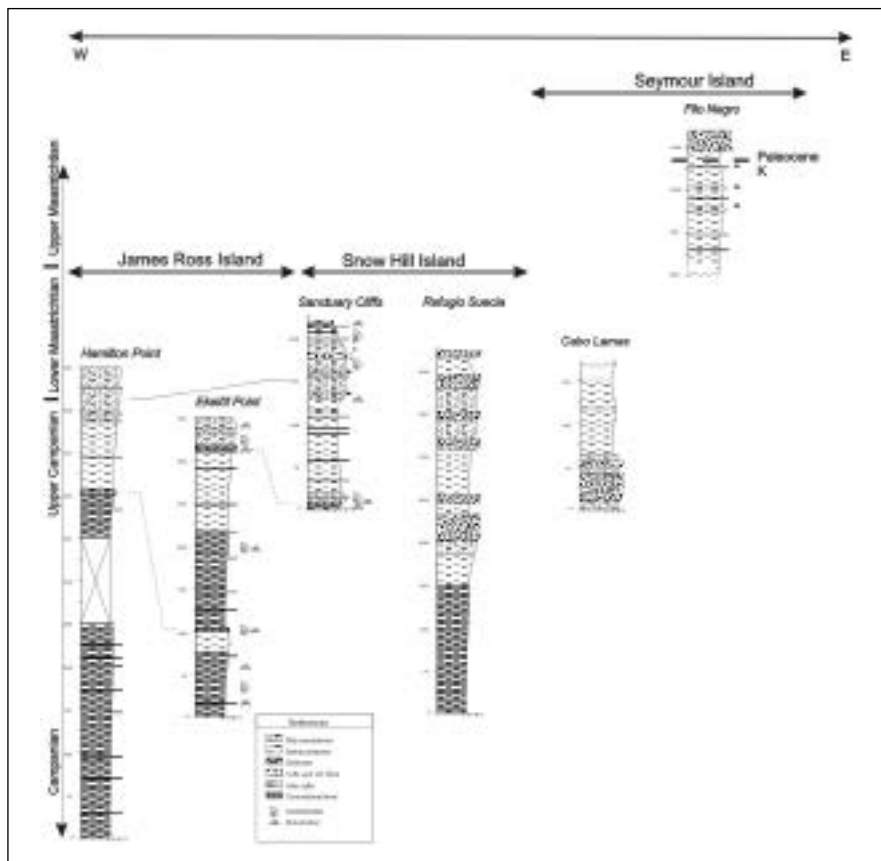


Fig. 2 - Studied Stratigraphic Sections, Larsen basin, Antarctic Peninsula.



At Filo Negro, Seymour Island lithofacies comprise claystones and subordinated sandstones. Facies associations indicate offshore to nearshore environments as part of a regressive cycle near to the Cretaceous/Paleogene boundary.

Calcareous nannofossils have been recovered at Longing Gap, Sharp Valley, Hamilton Point, Sanctuary Cliffs, refugio Suecia and Filo Negro localities. At Longing Gap and Sharp Valley the nannofossil association is poor, low diversified, partially dissolved, with strong evidences of overgrowth as well, and it includes: *Ellipsagelosphaera britannica*, *Watznaueria barnesae*, *Watznaueria ovata*, *Cyclagelosphaera margerelii*, *Cyclagelosphaera deflandrei*, *Diazomatolithus lehmanii*, *Polycostella beckmani* and *Zeughrabdotus erectus*.

*Polycostella beckmani* indicates a Middle to Late Tithonian age, temperate to warm waters and shows Thetyan affinities. *Diazomatolithus lehmanii*, *Cyclagelosphaera deflandrei* and *Zeughrabdotus erectus* are common in Late Jurassic-Early Cretaceous assemblages.

This is the first Late Jurassic calcareous nannofossil record established in the Antarctic Peninsula area. At Hamilton Point, Refugio Suecia and Sanctuary Cliff, nannofossils are partially dissolved, show a low diversity and include: *Ahmuellerella octoradiata*, *Acuturris scotus*, *Arkhangelskiella cymbiformis*, *Biscutum magnum*, *Biscutum coronum*, *Biscutum hattneri*, *Biscutum notaculum*, *Braarudosphaera bigelowi*, *Cribrosphaerella ehrembergii*, *Cyclagelosphaera reinhardtii*, *Eiffellithus turriseiffeli*, *Kamptnerius magnificus*, *Lithraphidites carniolensis*, *Lucianorhabdus cayeuxii*, *Micula concava*, *Micula decussata*, *Microrhabdulus decoratus*, *Misceomarginatus pleniporus*, *Monomarginatus quaternarius*, *Predicosphaera cretacea* and *Predicosphaera spinosa*.

Considering the occurrences of *Misceomarginatus pleniporus*, *Monomarginatus quaternarius*, *Biscutum coronum*, and *Biscutum magnum*, the *Biscutum coronum* and the *Biscutum magnum* Biozones for high austral latitudes (Pospichal and Wise, 1990) are defined (Fig. 3).

	Sissingh 1977	Pospichal & Wise 1990	Watkins et al. 1996	SNOW HILL ISLAND	JAMES ROSS ISLAND	SEYMOUR ISLAND
MAASTRICHTIAN	U	<i>N. oregon</i> <i>M. arvensis</i> <i>Z. clausenii</i>	<i>N. oregon</i> <i>K. magnus</i>			
	L	<i>Z. levi</i> <i>Z. artemesia</i> <i>M. parva</i> <i>C. constricta</i>	<i>K. coronum</i>			
CAMP.	U	<i>Z. artemesia</i> <i>Z. constricta</i>				
	L					

Fig. 3 - Mesozoic Calcareous Nannofossils bioevents in Larsen Basin, Antarctic Peninsula.

At the Filo Negro area, Seymour Island, mostly dissolved calcareous nannofossil has been found, this association is scarce, poorly diversified and composed by *Ahmuellerella octoradiata*, *Acuturris scotus*, *Arkhangelskiella cymbiformis*, *Biscutum magnum*, *B. coronum*, *B. notaculum*, *Braarudosphaera bigelowi*, *Cribrosphaerella ehrembergii*, *Cyclagelosphaera reinhardtii*, *Eiffellithus turriseiffeli*, *Kamptnerius magnificus*, *Lucianorhabdus cayeuxii*, *Micula concava*, *M. decussata*, *Microrhabdulus decoratus*, *Nephrolithus corystus*, *N. frequens*, *Predicosphaera cretacea*, and *P. spinosa*. The nannoflora of Seymour Island confirms a Late to Latest Maastrichtian age for the upper part of López de Bertodano Formation, previously dated by ammonites. The Danian age for the top of this formation is still supported by the planktonic foraminifera, because calcareous nannofossils have been dissolved.

## REFERENCES

- Pospichal, J. and Wise, S. 1990, Proceedings of the ODP, Scientific Results, 113, 465-487.
- Sissingh, W., 1977, Geologie in Mijnbouw, 56, 37-65.
- Watkins et al., 1996. Microfossils and Oceanic Environments (eds. A. Mognilevsky & R. Whatley), University of Wales, Aberystwyth Press, 355-381.
- Wind, F.H., 1979, Results of Deep Sea Drilling in The Atlantic Ocean, American Geophysical Union, Maurice Ewing Series, 3, 124-137.

## EOCENE-PLIOCENE ECOSYSTEMS OF SOUTH SHETLANDS AND ANTARCTIC PENINSULA

11-02

A. Gazdzicki

Institute of Paleobiology, Polish Academy of Sciences, Twarda 51/55, 00-818 Warszawa, Poland  
E-mail: gazdzicki@twarda.pan.pl

### Summary

The South Shetland Islands and the Antarctic Peninsula, contain a significant geological record of Tertiary biota, environments and climates. The paleobiological data from Seymour, King George and Cockburn Islands are important in providing information on the spatio-temporal pattern of paleoenvironmental changes that occurred during the crucial Eocene to Pliocene time interval.

### Abstract text

Seymour Island, initially explored one hundred years ago by the Nordenskjöld's Swedish South Polar Expedition, has proved to be one of the key paleontological localities in Antarctica (Fig. 1). The Eocene La Meseta Formation, exposed in the north-eastern part of Seymour Island, represents about 800 m of nearshore sandstones and siltstones, which preserve an exceptional record of Eocene life (Stilwell and Zinsmeister 1992, Marenssi et al. 1998). Throughout the formation a rich and diverse record of microfossils (palynomorphs, diatoms, foraminifers, ostracods), invertebrates (corals, molluscs, crabs, bryozoans, brachiopods, echinoderms), and vertebrates (fish, birds, marine mammals, primitive marsupials and placentals), as well as plants, occurs in a number of horizons (Feldmann and Woodburne 1988, Gazdzicki 1996, 2001; Dzik and Gazdzicki 2001, Myrcha et al. 2002, Reguero et al. 2002). Many representatives of the above groups have their first fossil occurrences in the La Meseta Formation.

Paleoecological associations with diverse fossil assemblages indicate a temperate marine environment. Paleobotanical studies suggest that the terrestrial environment during the Eocene was heavily vegetated (*Nothofagus*-podocarp forest) and had a humid, temperate, or cold-temperate climate similar to present-day southern South America. The results of geochemical analyses of fossil

shell material from the La Meseta Formation suggest a considerable climatic cooling event during the time of deposition of the upper part of the formation (Gazdzicki *et al.* 1992, see also Dingle *et al.* 1998, Dutton and Lohmann 2002). This cooling event may be correlated with the first phase of the late Eocene-early Oligocene continental glaciation in Antarctica. The La Meseta biota assemblages indicate favourable conditions for life in shallow marine and terrestrial realms during the final stage of the Gondwanaland breakup and the onset of the Paleogene continental glaciation in Antarctica.



Fig. 1 - Location map of King George Island in the South Shetland Island Archipelago and Cockburn and Seymour Islands in the Antarctic Peninsula sector. The arrow shows the represented area in the main map.

The glaciomarine sequences on King George Island (South Shetland Islands) extend from the Oligocene Polonez Cove Formation to the Miocene Cape Melville Formation (Birkenmajer 2001, Troedson and Smellie 2002, Troedson and Riding 2002). The Oligocene Low Head Member (up to 20 m thick) of the Polonez Cove Formation consists of glacio marine strata formed during the Polonez Glaciation, the largest Cenozoic glaciation on the Antarctic Peninsula sector (Birkenmajer and Gazdzicki 1991). At that time, the continental ice-sheet extended across the Bransfield Strait to the South Shetlands Archipelago. The marine paleoenvironment controlled by calving ice-sheets hosted a cold-water invertebrate fauna. The pectinid lumachelles, which are common here, are especially rich in fossils of sessile and vagile benthos (Gazdzicki 1984). In addition to pectinids, the biota includes calcareous nannoplankton (partly recycled), diatoms, benthic and planktonic foraminifera, polychaete worms, bryozoans, brachiopods, gastropods, ostracods, echinoderms (Gazdzicki and Pugaczewska 1984) as well as isolated, abioforic stromatolites (up to 8 cm in diameter). The occurrence of such coquinoid beds, interbedded with shales and fine-grained sandstones, indicates frequent, sudden changes from low- to high-energy environments and these beds may be interpreted as proximal shelly tempestites. This sequence can be dated as Early Oligocene on the basis of a suite of planktonic foraminifera including *Globigerina angiporoides* and *Chiloguembelina cubensis* as well as calcareous nannoplankton (*Reticulofenestra umbilica* and *Chiasmolithus altus*).

The Miocene glaciomarine strata of the Cape Melville Formation (~200 m thick) contain a rich and predominantly invertebrate fauna (Birkenmajer et al. 1983, Gazdzicki 1987). Microfossils include abundant diatoms, silicoflagellates, chryomonad cysts, calcareous and arenaceous foraminifera, sponge spicules and polychaete jaws. Macrofossils are represented by solitary corals, usually occurring in life orientation, abundant infaunal bivalves, gastropods, as well as homolodromiid crabs, nephropid lobsters, bryozoans, brachiopods and echinoderms. Vertebrates are represented by fish fragments. The fossil assemblage has a relatively deep-water, outer-shelf character, making it one of the most significant Miocene biotas known from Antarctica.

The Pliocene Cockburn Island Formation (more than 10 m thick), previously referred informally as the *Pecten* Conglomerate, has its type locality on Cockburn Island (Fig. 1), a small island situated between James Ross and Seymour Islands. The unit was first named and described by Andersson (1906; see also Gazdzicki and Webb, 1996; Stilwell, 2002; Jonkers, 2003) and is interpreted as representing an interglacial environment. The rich and diverse assemblages of macro- and microfauna/flora composed of more than 100 species, indicate that the environment was near a coastline, in water no deeper than 50 meters. The pectinid *Austrochlamys anderssoni* is the most abundant bivalve at the type locality. The calcareous benthic foraminiferal assemblage, dominated by *Cassidulina crassa* and *Ammoelphidiella antarctica*, share many features with Pliocene assemblages from southwestern Ross Sea–Transantarctic Mountains and Larseman Hills. The Cockburn Island Formation contains the most paleontologically diverse Pliocene sequence known from Antarctica and provides an important biogeographic link between the shallow marine assemblages of South America and other parts of Antarctica. The paleoclimate at the coastline in the Cockburn Island area and in other coastal regions of Pliocene Antarctica appears to have been polar but mild, –indicating an interval of deglaciation.

The paleoecosystems presented above provide exciting information on the Tertiary evolutionary history of Antarctica. Changes in the Tertiary Antarctic environments and climates are reflected in the paleontological record. Knowledge of the events leading to the isolation and cooling of Antarctica in the Cenozoic is necessary to the understanding of the evolution of both the fossil and the modern-day Antarctic biota.

## REFERENCES

- Andersson J.G. 1906. On the geology of Graham Land. Bulletin of the Geological Institute, University of Upsala 7: 19-71.
- Birkenmajer K. 2001. Mesozoic and Cenozoic stratigraphic units in parts of the South Shetland Islands and Northern Antarctic Peninsula (as used by the Polish Antarctic Programmes). In: K. Birkenmajer (ed.) Geological Results of the Polish Antarctic Expeditions. Part XIII. Studia Geologica Polonica 118: 5-188.
- Birkenmajer K. and Gazdzicki A. (1991). Cenozoic palaeoenvironments and biota, Bransfield Strait area, West Antarctica. International Conference Antarctic Science-Global Concerns. Scientific Poster Abstracts. Bremen, Germany, 23-27 Sept. 1991: 16-17.

- Birkenmajer K., Gazdzicki A. and Wrona R. 1983. Cretaceous and Tertiary fossils in glacio-marine strata at Cape Melville, Antarctica. *Nature* 303 (5912): 56-59.
- Dingle S.A., Marenssi S.A. and Lavelle M. 1998. High latitude Eocene climate deterioration: evidence from the northern Antarctic Peninsula. *Journal of South American Earth Sciences* 11: 571-579.
- Dutton A.L. and Lohmann K.C. 2002. Stable isotope and minor element proxies for Eocene climate of Seymour Island. *Paleoceanography* 17, 2: 6-1 – 6-13.
- Dzik, J. and Gazdzicki A. 2001. The Eocene expansion of nautilids to high latitudes. *Palaeogeography, Palaeoclimatology, Palaeoecology* 172: 279–312.
- Feldmann R.M. and Woodburne M.O. 1988. Geology and Paleontology of Seymour Island, Antarctic Peninsula. Geological Society of America, *Memoir* 169: 1-566.
- Gazdzicki A. 1984. The Chlamys coquinas in glacio-marine sediments (Pliocene) of King George Island, West Antarctica.

## **SOUTHERN OCEAN EOCENE-OLIGOCENE CALCAREOUS NANNOFOSSIL: PALAEOECOLOGY AND PALAEOCEANOGRAPHIC IMPLICATIONS** **11-03**

G. Villa(\*), D. Persico(\*), Steven M. Bohaty(\*\*), Fabio Florindo(\*\*\*)

(\*) *Dipartimento di Scienze della Terra –Università di Parma, Parco Area delle Scienze 157/A  
43100 Parma - Italy*

(\*\*) *Earth Sciences Department, University of California - Santa Cruz, Santa Cruz, California, 95064*

(\*\*\*) *Istituto Nazionale di Geofisica e Vulcanologia, Via di Vigna Murata, 605 - 00143 Roma - Italy*

### **Summary**

Earth's climate has undergone significant transformations, recording the passage from the "greenhouse" climates of the Cretaceous and Early Paleogene to the "ice-house" conditions of the Oligocene to Recent. A gradual, but stepwise cooling trend through the Eocene is inferred from well-dated deep-sea sediments. Several transient warming events, however, are documented during the cooling trend prior to the drastic earliest Oligocene cooling event (33.54 Ma). Also, in Oligocene time, characterized by generally cool conditions, a prominent warming event occurred in the latest Oligocene. This prominent warming event has been previously shown by means of oxygen stable isotope (Zachos et al., 2001) and corresponds to the re-establishment of moderately warm conditions, following the Oligocene cooling phase.

### **Abstract text**

Recent studies on calcareous nannofossil palaeoecology in key-areas of the Southern Ocean confirmed the important role of these microfossils for palaeoclimatic and palaeoceanographic reconstructions (Bralower, 2002, Persico and Villa, in press). Detailed investigation of calcareous nannofossil assemblages has been conducted on several Eocene and Oligocene sequences drilled in the Southern Ocean (Maud Rise and Kerguelen Plateau) to attempt correlations between palaeoecological groups and the major sea surface temperature (SST) variations. Quantitative analyses data allowed subdivision of the calcareous nannofossil assemblages into groups with different palaeoecological behaviour, especially with respect to sea surface temperature. The following palaeoecological groups are recognized: warm-water taxa, temperate-water taxa, cool-water taxa, and no temperature affinity taxa.

On the basis of the interpretation of the palaeoecological groups as climate proxy, we could identify the main mid-Eocene to late Oligocene climatic events:

- MIDDLE EOCENE WARMING EVENT (~41 Ma)
- LATE EOCENE COOLING PHASES (36 to 34 Ma)
- ABRUPT COOLING EVENT IN THE EARLIEST OLIGOCENE (33.54 Ma)
- WARMING PHASE IN THE LATEST OLIGOCENE (26 to about 24 Ma)

a) Recently, high-resolution stable isotope records, from several Southern Ocean sites, document a clear middle Eocene warming event. Foraminiferal  $\delta^{18}\text{O}$  values show a significant short-term warming event in the Southern Ocean during the middle Eocene at about 41.5 Ma, designated as the

Middle Eocene Climatic Optimum (MECO) (Bohaty and Zachos, 2003). During the MECO, the fine fraction  $\delta^{18}\text{O}$  data indicate that surface waters warmed  $4^\circ\text{C}$  on both the Kerguelen Plateau (Indian sector of the Southern Ocean) and Maud Rise (Atlantic sector of the Southern Ocean). By means of calcareous nannofossils we investigated the Eocene successions from the Kerguelen Plateau (ODP Leg 120, Site 748, and ODP Leg 119, Site 738). The middle Eocene sections of Hole 748B and Hole 738B were sampled at short spacing distance (8-10 cm), to obtain high-resolution calcareous nannofossil biostratigraphy and palaeoecology and to evaluate the response of the assemblage to climatic variations. The abundance variation of the main palaeoecological groups are correlated with stable isotope data and inferred as palaeoecological and palaeoclimatic signals.

In an interval nearly coinciding with the MECO, the nannofossil assemblage, dominated by temperate-water taxa and the presence of warm-water taxa, suggests a water temperature compatible with that indicated by the isotope data. At the same time, we cannot discount the possibility that other factors, such as the nutrient availability and stratification, may have influenced the assemblage variation.

b) During the late Eocene, at Sites 744 and 689, we have identified for the first time by means of the nannofossil assemblage fluctuations, four cooling phases in the time interval between 36 and 34 Ma, from Chrons C16 2n to C13n (Florindo and Roberts, in press). Several lines of evidence are consistent with the interpretation of cooling phases, here identified by the nannofossil assemblages. In particular foraminiferal assemblage studies (Quilty, 2001), high-resolution  $\delta^{18}\text{O}$  data from Site 689 (Wilson et al., 2001), environmental magnetic record from CRP3, (Sagnotti et al., 2001) and from Massignano (Jovane et al., submitted), clay minerals distributions (Diester-Haass et al., 1996), are indicative of cool climate influxes.

c) A sharp cooling event, detected at both Sites 689 and 744, is dated at 33.54 Ma (earliest Oligocene), and occurred about 160 kyr after the E/O boundary, which is dated at 33.7 Ma. At Site 744, Salamy and Zachos (1999) obtained a detailed characterisation of the Oi-1 oxygen isotope excursion from benthic foraminifera, and showed two short, prominent maxima, just after the main cooling shift, restricted to Chron C13n, termed Oi-1a and Oi-1b. High-resolution nannofossil quantitative analysis at Site 744 found matching peaks in the cool-water taxa curve. Relatively stable and cool conditions are interpreted to persist until the latest Oligocene.

d) The upper Oligocene sections of Holes 689D and 748B were sampled at high resolution. Quantitative analyses allowed us to detect distinct changes in abundance of the main floral groups, interpreted as palaeoclimatic signals, both at Maud Rise and Kerguelen Plateau. In the late Oligocene from about 26 to about 24 Ma, an increase of warm-water taxa is detected and interpreted as a significant warming event around the entire Antarctic margin. Rare warm-water taxa are present only at Site 748, and not at Site 689, this could be related to the more northerly latitude of the Site 748 which, in addition, lies to the north of a deep water passage that separates Kerguelen Plateau from Antarctica. The beginning of this warming phase at Site 744 was out of phase by ca. 1 m.y. with Site 689, this difference could be tied to the latitudinal location and to the palaeoceanographic setting at the Oligocene time, or due to the difficulty to interpret the magnetostratigraphic signal at Site 744 (Roberts et al., 2003).

This prominent warming event has been previously shown by means of oxygen stable isotope (Zachos et al., 2001) and corresponds to the re-establishment to moderately warm-temperate conditions, following the Oligocene cooling phase.

Our nannofossil results corroborate a palaeoceanographic scenario for the late Eocene to late Oligocene in which the sharp climatic response of the nannofossil assemblages at 33.54 Ma (just after the E/O boundary) is due to a SST decrease.

A leading hypothesis is that the tectonic opening of seaways permitted unrestricted latitudinal flow of the Antarctic Circumpolar Current (ACC), which progressively thermally isolated Antarctica by decoupling the warmer subtropical gyres from the Antarctic continent (e.g., Kennett, et al., 1975; Kennett, 1977; Exon et al., 2001). The breakup of Gondwanaland caused expansion of the Southern Ocean during the Cenozoic through northward movement of Australia and its southern continental extension, the South Tasman Rise, and through opening of Drake Passage between Patagonia and the Antarctic Peninsula (e.g. Exon et al., 2001; Lawver and Gahagan, 2003). Marine magnetic anomalies

and fracture zone and transform fault lineations constrain the age of both these seaways to ~31-32 Ma (Lawver and Gahagan, 2003). An important alternative hypothesis is that global cooling resulted from decreasing concentrations of atmospheric CO<sub>2</sub> (Pearson and Palmer, 2000), and that tectonic opening of deep-sea gateways was of secondary importance (DeConto and Pollard, 2003). On the basis of our dating, the cooling event was seen as the response to the concomitant openings of the Tasmanian Gateway and Drake Passage. Our results suggest, therefore, that the beginning of Drake Passage opening could have occurred, allowing shallow-water circulation, as early as 33.54 Ma, earlier than the 33 Ma postulated by Lawver and Gahagan (2003), while the establishment of deep-water connections through the Tasmanian Gateway occurred at 33 Ma, as suggested by Exxon et al. (2001).

## REFERENCES

- Bohaty S.M. and Zachos J., 2003. Significant Southern Ocean warming event in the late middle Eocene Geology: Vol. 31, No. 11, pp. 1017–1020.
- Bralower, T.J., 2002. Evidence of surface water oligotrophy during the Paleocene-Eocene thermal maximum: Nannofossil assemblage data from Ocean Drilling Program Site 690, Maud Rise, Weddell Sea. *Paleoceanography* 17, 13.1-13.13.
- DeConto, R.M., Pollard, D., 2003. Rapid Cenozoic glaciation of Antarctica induced by declining atmospheric CO<sub>2</sub> *Nature* 421, 245-247.
- Diester-Haass, L., Zahn, R., 1996. The Eocene-Oligocene transition in the Southern Ocean: history of water masses, circulation, and biological productivity inferred from high resolution records of stable isotopes and benthic foraminiferal abundances (ODP Site 689). *Geology* 26, 163-166
- Exxon, N.F., et al., 2001. The Tasmanian Gateway: Cenozoic Climatic and Oceanographic Development Sites 1168-1172. *Proc. ODP, Init. Rep.* 189, 1-149.
- Florindo F., Roberts A.P., in press. Eocene-Oligocene magnetobiochronology of ODP Sites 689 and 690, Maud Rise, Weddell Sea, Antarctica. *Geol. Soc. of America Bull.*
- Jovane L. et al., submitted. Environmental magnetic record of paleoclimate change: revisiting the Eocene-Oligocene stratotype section, Massignano, Italy
- Kennett, J. P., 1977. Cenozoic Evolution of Antarctic Glaciation, the Circum-Antarctic Ocean, and Their Impact on Global Paleoceanography. *Journal of Geophysical Research* 82, 27 3843-3860.
- Kennett, J.P., et al., 1975. Cenozoic paleoceanography in the southwest Pacific Ocean, Antarctic glaciation, and the development of the Circum-Antarctic Current. In: Kennett, J.P., Houtz, R.E. et al. (Eds.), *Init. Reports DSDP 29*, 1155-1169.
- Lawver, L.A., Gahagan, L.M., 2003. Evolution of Cenozoic seaways in the circum-Antarctic region. *Palaeo., Palaeo., Palaeo.* 198, 11-37.
- Pearson, P.N., Palmer, M.R. 2000. Atmospheric carbon dioxide concentrations over the past 60 million years. *Nature*, 406, 695-699.
- Persico and Villa, 2004. Eocene-Oligocene calcareous nannofossils from Maud rise and Kerguelen Plateau (Antarctica): paleoecological and paleoceanographic implications. *Mar. Micropaleontol.* Special issue (in press).
- Quilty, P. G., 2001. Late Eocene foraminifers and palaeoenvironment, Cascade Seamount, southwest Pacific Ocean: implications for seamount subsidence and Australia-Antarctica Eocene correlation. *Australian J. of Earth Sc.* 48, 633-641.
- Roberts, A.P., et al., 2003. Magnetostratigraphic calibration of Southern Ocean diatom datums from the Eocene - Oligocene of Kerguelen Plateau (Ocean Drilling Program Sites 744 and 748). *Palaeo., Palaeo., Palaeo.* 198 145-168.

## EFFECTS OF LATE EOCENE COOLING ON ANTARCTIC MARINE COMMUNITIES

11-04

John E. Werner(\*), Daniel B. Blake(\*\*), Richard B. Aronson(\*\*\*)

(\*) *Department of Physical Sciences, Seminole Community College, 100 Weldon Blvd., Sanford FL 32773, USA*

(\*\*) *Department of Geology, University of Illinois, 1301 W. Green St., Urbana IL 61801, USA*

(\*\*\*) *Dauphin Island Sea Lab, 101 Bienville Blvd., Dauphin Island AL 36528, USA*

### Summary

Isotopic evidence implies a late Eocene cooling event between the deposition of the middle and upper parts of the La Meseta Formation (Seymour Island, Antarctic Peninsula). In response, the La Meseta molluscan fauna changes through the disappearance of gastropods bearing defensive architectural features. This decline in defensive architecture upsection is likely related to a reduced frequency of

attacks by durophagous predators and the thermodynamic costs of calcification in cold water. Additionally, a reduced frequency of molluscan shells upsection bear evidence of drilling predation by *Polinices*.

### Abstract text

The thermal and ecological isolation that characterize modern Antarctica are rooted in the Eocene/Oligocene cooling event that initiated deterioration of early Cenozoic greenhouse climate and the buildup of polar ice. Mechanisms that might have contributed to climatic deterioration at this time include the restriction of southward flow of warm surface water toward Antarctica (Diester-Haass and Zahn, 1996) and a sharp decline in atmospheric carbon dioxide concentration (DeConto and Pollard, 2003). Stable isotope studies indicate that Antarctic seawater temperatures decreased from 4-9 °C degrees during the late Eocene to early Oligocene transition (Gazdzicki et al., 1992; Kennet and Warnke, 1992; Dutton et al., 2003).

Shallow water in the modern antarctic sea harbors a number of taxa that are otherwise generally restricted to deep water; these groups retreated from temperate and tropical shallow-water environments with the radiation of durophagous predators in the Mesozoic (Clarke and Crame, 1992; Aronson and Blake, 2001). Antarctic faunal turnover associated with the onset of colder conditions in the late Eocene is evident in the fossil record of the La Meseta Formation on Seymour Island, Antarctic Peninsula. Abundant isocrinid crinoids and dense assemblages of ophiuroids (Aronson et al., 1997) occur in shallow-water deposits (Sadler, 1998; Porebski, 1995,2000). This unusual ophiuroid and crinoid occurrence is found in Telm7, the uppermost member of the formation (Sadler, 1988). Evidence of sublethal predation upon these echinoderms is scarce, suggesting that antarctic durophagous predators were rare during the late Eocene (Aronson et al., 1997). Though intriguing, this occurrence does not necessarily imply ecosystem-wide upheaval; as with most Cenozoic assemblages, La Meseta fossils are dominated by gastropod and bivalve mollusks. Change in the molluscan fauna upsection, though not as striking as for the echinoderms, does feature the replacement of cool-temperate mollusks by those characteristic of colder water (Stilwell and Zinsmeister, 1992).

Understanding the effects of global climate change upon fossil communities is becoming paramount given the likelihood of global warming and an increased frequency of El Niño events in the near future. The last major long-term (tens of millions of years) change in global climate was the onset of the late Cenozoic icehouse conditions during the Eocene/Oligocene transition, the effects of which were pronounced in the antarctic, where the eponymous ice accumulated. The La Meseta Formation on Seymour Island represents one of the few ice-free settings in the antarctic where it is possible to obtain large-scale collections of abundant Eocene fossils. Because of their overwhelming abundance, molluscan fossil populations provide the most accurate available assessment of the Eocene antarctic paleocommunity. The present study assesses morphological and ecological aspects of molluscan faunal change during the Eocene deposition of the La Meseta on Seymour Island. The La Meseta is divided here into lower, middle, and upper portions, corresponding to Telm2 and Telm3, Telm4 and Telm5, and Telm6 and Telm7 of Sadler (1988), respectively. Late Eocene cooling has been detected in the transition from the middle to the upper La Meseta (Gazdzicki et al., 1992; Dutton et al., 2002). Changes in molluscan morphology upsection are thus expected primarily to show contrast between the upper La Meseta mollusks and those from the lower and middle parts of the formation.

Previous work has documented that shells produced by living gastropods in cold-temperate and polar seas bear few defensive architectural features; this pattern has been explained as being due to a low frequency of attacks by shell-breaking durophagous predators and the thermodynamic cost of calcification in cold water (Vermeij, 1978, 1987 and references therein). Fossil evidence indicates that architecturally defended shells became commonplace in shallow, tropical settings in the Jurassic in response to the radiation of shell-breaking durophagous predators that characterized the Mesozoic Marine Revolution (Vermeij, 1978, 1987). Examples of such defensive architecture frequently observed in living gastropods found in shallow, warm-water settings include large shells, tall spires, numerous or tall spines, ribs or tubercles, elongate but narrow apertures, multiple columellar folds, and thickened or alate outer lips (Vermeij, 1987 and refs. therein). Due in part to the cold water, shell-

breaking predatory groups are excluded from the modern antarctic. In response to late Eocene cooling, the expectation is thus that the frequency of architecturally defensive features in La Meseta gastropods should decline upsection. A synoptic overview of La Meseta mollusks (Stilwell and Zinsmeister, 1992) qualitatively supports this hypothesis; here we test it quantitatively (as our Hypothesis I).

The naticid *Polinices* is the most abundant gastropod in the La Meseta Formation and of special ecological importance as a predator of other mollusks. Predatory attacks by *Polinices*, including examples of cannibalism, are recorded in shells bearing boreholes with characteristic beveled edges. Most borehole examples completely pierce the shell, suggesting successful predatory encounters, but others are incomplete, implying aborted attacks. *Polinices* is expected to have experienced a declining frequency of predatory attacks from shell-breakers through the Eocene, and it is thus hypothesized that the release of shell-breaking predation pressure might have brought naticids greater success in their own hunting forays. Presumably, in the absence of durophagous predators, members of *Polinices* would have time to choose suitable victims and manipulate their prey so as to drill into a region of the shell that would maximize the probability of lethality. A second hypothesis (Hypothesis II) of ecological change associated with late Eocene cooling is thus that both the frequency and degree of stereotypy in naticid attacks upon mollusks should increase upsection.

Preliminary results from the testing of Hypothesis I confirm that defensive architecture in gastropods declines upsection. Gastropod genera were evaluated for eight morphological traits correlated with architectural defense: size (product of length and width), height of spire, thickness of outer lip, presence/absence of an alate outer lip, abundance of sculptural relief (number of spines, ribs, or tubercles on the last whorl), height of sculptural relief, number of columellar folds, and the ratio of apertural length to width. Given the discordant nature of these measures of form, data corresponding to each variable were reduced to ordinal states, with 0 scored for the state corresponding to a minimum of defensive value in each case. Each ordinal variable was then standardized to reduce the effects of single characters that occur in a multitude of states (such as numbers of spines). For the set of eight variables, the La Meseta gastropods exhibit 26 unique morphotypes. Patterns of morphological distance among morphotypes were assessed using nonmetric multidimensional scaling. The resultant two-dimensional rendering of the eight-dimensional morphospace contrasts three outlying morphotypes with the remainder, which inhabit a central cluster. Genera corresponding to these outlying morphotypes (*Antarctodarwinella*, *Conomitra*, and *Struthioptera*) are architecturally better defended than the gastropods of the central cluster ( $p < 0.001$ ; two sample  $t$ -test of the sum of standardized scores over the eight variables). All three of these genera are restricted to the lower and middle members of the La Meseta Formation. Similarly, only four of the 26 observed morphotypes have a sum of standardized defense scores that is greater than unity, and all four of the genera corresponding to these states (*Antarctodarwinella*, *Eoscapella*, *Struthioptera*, and *Taioma*) occur in the middle La Meseta but not the upper portion. Finally, of 31 gastropod genera collected from the middle La Meseta, the 16 found in the upper part of the formation are significantly less defended than are the 15 genera that do not cross the boundary ( $p < 0.05$ ,  $t$ -test of sum of standardized scores for the eight variables). These results suggest that a majority of gastropod genera in the La Meseta are not architecturally well defended, but the few that are well defended are excluded from the upper part of the formation.

Unlike the case with Hypothesis I, observations do not support Hypothesis II. Contrary to expectation, the proportion of both gastropods (Table 1) and bivalves (Table 2) bearing a naticid borehole declines significantly upsection ( $p < 0.0001$  in both cases;  $\chi^2$ ). Although results are not supportive of prior expectation, previous work (Hansen and Kelley, 1995) on the predatory ecology of Eocene naticids has shown that temporal patterns in drilling predation can elude facile explanation. Ongoing analysis includes evaluation of the degree of drilling stereotypy through time evidenced in predatory attacks and evaluation of microevolution within a few of the more abundant molluscan lineages. The authors thank the U. S. National Science Foundation; this study was made possible by NSF grants OPP-9908828 to R.B.A. and OPP-9908856 to D.B.B.



Table 1 - Proportion of gastropod shells bearing a borehole indicative of attack by *Polinices*.

Unit	# lethal boreholes	# sublethal boreholes	Total gastropods	% bearing a borehole
upper La Meseta	8	0	818	1.0
middle La Meseta	63	12	3421	2.2
lower La Meseta	89	18	2028	5.3

Table 2 - Proportion of bivalve shells bearing a borehole indicative of attack by *Polinices*.

Unit	# lethal boreholes	# sublethal boreholes	Total bivalves	% bearing a borehole
upper La Meseta	43	1	1855	2.4
middle La Meseta	56	1	1263	4.5
lower La Meseta	79	3	1397	5.9

## REFERENCES

- Aronson, R. B., and D. B. Blake. 2001. Global climate change and the origin of modern benthic communities in Antarctica. *American Zoologist* 41:27-39.
- Aronson, R. B., D. B. Blake, and T. Oji. 1997. Retrograde community structure in the late Eocene of Antarctica. *Geology* 25:903-906.
- Clarke, A. and J. A. Crame. 1992. The southern Ocean benthic fauna and climate change: a historical perspective. *Philosophical Transactions of the Royal Society of London, Series B* 338:299-309.
- DeConto, R. M. and D. Pollard. 2003. Rapid Cenozoic glaciation of Antarctica induced by declining atmospheric CO<sub>2</sub>. *Nature* 421:245-249.
- Diester-Haass, L. and R. Zahn. 1996. Eocene-Oligocene transition in the Southern Ocean: History of water mass circulation and biological productivity. *Geology* 24:163-166.
- Dutton, A. L., K. C. Lohmann, and W. J. Zinsmeister. 2002. Stable isotope and minor element proxies for Eocene climate of Seymour Island Antarctica. *Paleoceanography* 17(2). doi:10.1029/2000PA000593.
- Gazdzicki, A., M. Gruszczynski, A. Hoffman, K. Malkowski, S. A. Marensi, S. Halas, and A. Tatur. 1992. Stable carbon and oxygen isotope record in the Paleogene La Meseta Formation, Seymour Island, Antarctica. *Antarctic Science* 4:461-468.
- Kennett, J. P. and D. A. Warnke (eds.). 1992. *The Antarctic Paleoenvironment: A Perspective on Global Change, Part I*. Antarctic Research Series 56, American Geophysical Union, Washington, D. C.
- Porebski, S. J. 1995. Facies architecture in a tectonically-controlled incised-valley estuary: La Meseta Formation (Eocene) of Seymour Island, Antarctic Peninsula. *Studia Geologica Polonica* 107:7-97
- Porebski, S. J. 2000. Shelf-valley compound fill produced by fault subsidence and eustatic sea-level changes, Eocene La Meseta
- Sadler, P. M. 1988. Geometry and stratification of uppermost Cretaceous and Paleogene units on Seymour Island, northern Antarctic Peninsula. Pp. 303-320 in R. M. Feldman and M. O. Woodburne, eds. *Geology and Paleontology of Seymour Island, Antarctic Peninsula*. Geological Society of America Memoir 169, Boulder, Co.
- Stilwell, J. D. and W. J. Zinsmeister. 1992. *Molluscan Systematics and Biostratigraphy: Lower Tertiary La Meseta Formation, Seymour Island, Antarctic Peninsula*. Antarctic Research Series 55, American Geophysical Union, Washington, D.C.
- Vermeij, G. J. 1978. *Biogeography and Adaptation: Patterns of Marine Life*. Harvard University Press, Cambridge, Mass.
- Vermeij, G. J. 1987. *Evolution and Escalation: an Ecological History of Life*. Princeton University Press, Princeton, N.J.



# **Session 12**

---

## **HYDRODYNAMICS**



## **HYDROLOGICAL MEASUREMENTS COLLECTED ON BOARD THE R/V OGS-EXPLORA IN THE WESTERN SECTOR OF THE STRAIT OF MAGELLAN AND IN THE PACIFIC MARGIN DURING APRIL 2004**

12-01

A. Giorgetti, R. Laterza

*Istituto Nazionale di Oceanografia e di Geofisica Sperimentale – OGS,  
Borgo Grotta Gigante 42c – 34010 SGONICO -TS, Italy*

### **Abstract**

First results on the hydrological survey undertaken in the framework of the geophysical SCP04 cruise on board the R/V OGS-Explora are here presented. The synoptic oceanographic measurements include ship-borne ADCP and TS continuous recordings as well as high resolution CTD and XBT vertical profiles. The intensive current measurements and hydrological sampling program was carried out on a continuous basis from the 3<sup>rd</sup> to the 7<sup>th</sup> of April, 2004. The investigation area was the Strait of Magellan and the Southernmost Chilean margin (54° - 52° S, 77° - 70° W). The data acquisition methods and the used instrument are also described. The thermohaline properties of the water masses over the Strait of Magellan are analysed by means of  $\theta$ -S diagrams, including also a comparison with other measurements available from the same region. In order to follow the spatial variability of the hydrological characteristics, temperature vertical profiles in the Pacific slope are considered as well. A good agreement in the thermohaline characteristics of the new observations with respect to historical data is highlighted. The spatial distribution of the hydrological parameters considered so far is briefly discussed.

### **Introduction**

The oceanographic observations in the Strait of Magellan were collected in the framework of the “Antarctic/Scotia Plate convergence off southern Chile” Project, sponsored by the Programma Nazionale di Ricerche in Antartide (PNRA). The research program addresses the mechanisms of subduction accretion of the Antarctic plate sediments along the Southernmost Chilean margin (Polonia et al., 1999; Polonia et al., In preparation), through the acquisition of high resolution morpho-bathymetric data using the multi-beam bathymetric system as well as side scan sonar data, together with sub-bottom chirp data. In this context, the oceanographic survey aimed to determine the sound velocity field for the interpretation of the high-resolution multi-beam bathymetric measurements collected underway. Besides, the new oceanographic equipment on board of R/V OGS-Explora allowed to obtain a real-time continuous sampling of the surface and intermediate hydrological parameters.

The Strait of Magellan, extending over about 570 km from the South Pacific and the South Atlantic Ocean, is characterized by a significant spatial variability in the hydrographic features (Panella et al., 1991), in the climatic and weather conditions, as well as in the geographical, morphological and geological setting (Brambati et al., 1991; Marinoni et al., 1997), contributing to the development of widely differing oceanographic characteristics. The central part of the Strait is occupied by the wide Paso Ancho Basin, reaching depths of 400 m. The western sector, where this hydrographic survey was conducted, extends in a NW-SE direction from Cabo Froward to the Pacific Ocean with narrow and elongated shape. The passage width varies from 2 to 15 km, with water depths increasing to 1000 m as far as NW of Carlos III Island, then decreasing to 50 m near the Pacific entrance (Cabo Deseado) and suddenly abruptly facing the open ocean. Tides and surface currents are particularly strong in the Atlantic entrance (with spring tide ranges of 9 m and currents reaching 4.5 m/s, respectively) with decreasing values towards the Pacific sector (about 1.5 m of spring tide range), as described in Medeiros and Kjerfve (1988).

This paper is concerned with the description of the instrumental set-up on board of R/V OGS-Explora and with the preliminary analyses conducted on the collected CTD and XBT data. It may provide a first picture of the variability of the thermohaline properties recorded in the Strait of Magellan during April 2004 with respect to the conditions found in 1989 and 1991 (Magellano cruises, Brambati et al., 1991) and in 1993 (WOD01, Conkright et al., 2002).

## Data and methods

The R/V OGS-Explora is equipped with an Ocean Surveyor Vessel-Mounted 75kHz ADCP, a Sea-Bird SEACAT SBE 21 Thermosalinograph, a couple of high precision thermometers Sea-Bird SBE 38 and an AWS (Automated Weather Station).

The Doppler current profiler (the transducer has four 30° beam, phased array) has been installed close to the central part of the keel, about 4.5 m below sea surface, in a sea chest filled with sea water and separated from the sea by a Polycarbonate acoustic window. Data of heading, roll, pitch and heave come from an inertial navigation system through a navigation software together with position data provided by a GPS. The range of the profiler in this configuration is about 750 m (not very affected by the speed of the ship), and the blank after transmission is of 2 m. The thermosalinograph takes seawater samples from an intake positioned very close to the ship bow. This assures a not contaminated sample but bad weather conditions could prevent data acquisition. A pump provides a flow rate of about 1 l/s, allowing the collection of near real-time data. Navigation information are appended to temperature and salinity acquisitions via NMEA 0183 interface port. In order to monitor the sea surface temperature and minimize the thermal contamination by the ship's hull, a couple of high precision thermometers have been positioned outside the hull, supplying data to the weather station, and close to the valve of the seawater thermosalinograph intake, respectively. The AWS is formed by a controller (developed at OGS) and a double sensor system (R.M.Young), mounted at about 22.5 m above sea level. It collects data of wind speed and direction, air temperature, atmospheric pressure, relative humidity, sea surface temperature (thanks to one of the above mentioned temperature probe), in addition to GPS and time data.

During the hydrological survey, current profiling and surface thermohaline data were collected over nearly all the Austral autumn SCP04 cruise, along the ship track. Besides, four high resolution CTD casts and ten different types of XBT probes were lowered (Fig.1). The overall length of the current and thermohaline data records is about 75 and 74 hours, respectively (from 03.04.04 at 15.40 and 16.00 GMT to 07.04.04 at 11.15 GMT, with a forced stop over the 06.04.04 from 02.00 to 18.40 and 19.05 GMT, respectively). The starting acquisition time delay in temperature and salinity measurements was necessary to ensure conductivity sensor stabilisation. In the Strait of Magellan, up to 700 m bottom depth, the ADCP acquisition set-up used was in highest precision (broad bandwidth) with bottom tracking. In the deepest part of the Strait and in the Pacific coastal area, the lowest precision (narrow bandwidth) configuration was used, with positioning provided by GPS through NMEA Com Port. The vertical resolution was always settled to 16 m. Unfortunately, the positioning data were not included in the data files during the acquisition phase and further data reprocessing are needed.

A self-recording, self-powered, multiparametric probe (Sea-Bird MICROCAT model SBE37-SM) equipped with standard pressure, temperature and conductivity sensors was used for four CTD casts (Table 1). Two of these were carried out in the Strait of Magellan and two in the Pacific coastal area. Unfortunately, due to rough weather conditions, the third cast was interrupted at 36 m depth and, because of not reliable values, cannot be considered. The CTD probe was lowered at a velocity of 0.8-0.9 m/s, with a sampling interval of 5 sec. CTD raw data were processed on board, inspected and corrected for rough errors (spikes). Final data were averaged over one-dbar pressure interval, considering both down-casting and up-casting, and converted to physical units. Pressure is used as a vertical coordinate, whereas the temperature is given as potential temperature ( $\theta$ ), salinity (S) is expressed according to the practical salinity scale, and sea water density ( $\gamma_{\theta} = \gamma_{S,\theta,0}$ ) is presented as potential density excess at atmospheric pressure. Ten Sippican T7, T5 and Fast Deep expendable bathythermograph (XBT) probes were launched during the cruise, three in the Strait of Magellan and 7 in the Pacific slope, respectively (Table 2). XBT data were obtained by using a Sippican MK-12 read-out card. Sound velocity was computed on board for each cast, assuming an indicative salinity of 30 psu in the Strait of Magellan, 34 psu in the Pacific entrance and 34.30 psu for the more distal stations. These values were fixed taking into consideration the Thermosalinograph real-time surface observations as well as the salinity values in the entire water column obtained with the CTD casts.

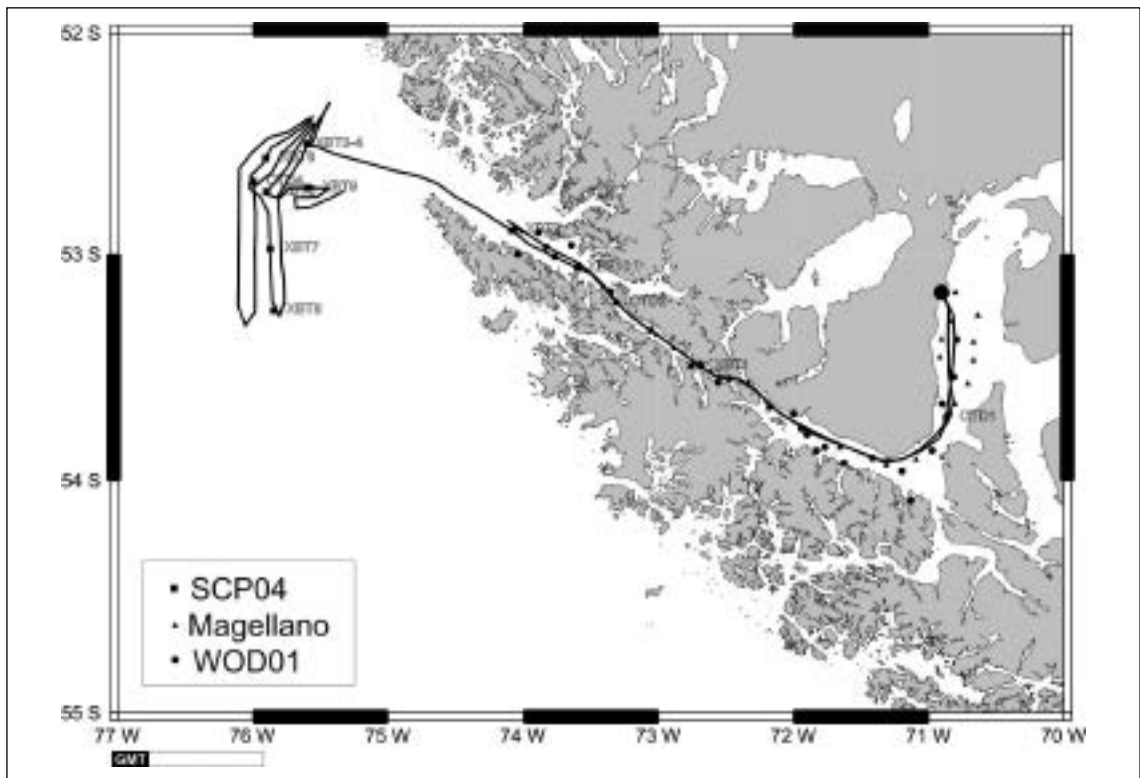


Fig. 1. Map showing the R/V OGS-Explora ship track covered during the SCP04 cruise combined with the locations of CTD and XBT casts (full squares), as well as the WOD01 (Conkright et al., 2002, full circle) and Magellano (Brambati et al., 1991, full triangle) CTD profiles.

Table 1 - Location of CTD station collected by R/V OGS-Explora during SCP04 cruise

Station	Date	Lat. S	Lon. W	Bottom Depth (m)
CTD1	3 April 04	53°43.43'	70° 52.02'	510
CTD2	4 April 04	53° 12.83'	73° 18.54'	1130
CTD3	4 April 04	52° 30.35'	75° 35.30'	1150
CTD4	5 April 04	52° 40.44'	75° 59.91'	2800

Table 2 - Location and type of XBT probes launched by R/V OGS-Explora during SCP04 cruise

Station	Date	Lat. S	Lon. W	Probe Type / Terminal Depth (m)
XBT1	3 April 04	53° 29.84'	72° 41.17'	T-7 / 760 m
XBT2	4 April 04	52° 53.49'	74° 05.04'	T-7 / 760 m
XBT3	4 April 04	52° 30.24'	75° 35.94'	T-5 / 1830 m
XBT4	4 April 04	52° 30.24'	75° 35.94'	Fast Deep / 1000 m
XBT5	4 April 04	52° 43.11'	75° 53.99'	T-5 / 1830 m
XBT6	5 April 04	52° 34.03'	75° 54.36'	Fast Deep / 1000 m
XBT7	5 April 04	52° 58.51'	75° 52.41'	T-7 / 760 m
XBT8	5 April 04	53° 14.99'	75° 51.27'	T-7 / 760 m
XBT9	5 April 04	52° 42.03'	75° 35.54'	T-7 / 760 m
XBT10	6 April 04	53° 02.14'	75° 35.25'	T-7 / 760 m

## Results

The temperature and salinity properties in the Strait of Magellan are studied by examining the  $\theta$ -S diagram obtained with the CTD data collected during the SCP04 cruise. They have been combined with the CTD measurements extracted from World Ocean Data 2001 (WOD01, Conkright et al., 2002), in the same area, as well as CTD profiles collected as part of the Magellano Project (Brambati et al., 1991) (Fig. 2). CTD1 and CTD2 casts show similar  $\theta$ -S distributions in the surface and bottom layer with respect to WOD01 data set, while the Magellano Project profiles present lower temperature values ( $\theta = 7.2$ - $8^{\circ}\text{C}$ ) in the surface layer. It has to be noted that during the surveyed period, in the Strait of Magellan mean dry air temperature was approximately  $10.4^{\circ}\text{C}$ , while during the 1989 cruise values of  $9.2 \pm 1.7^{\circ}\text{C}$  were recorded (Panella et al., 1991). A well developed halocline is observed in CTD2 cast, consistent with both WOD01 and Magellano data set values, and this is ascribed to the freshwater run off of the complex system of fjords and channels characterizing this region. Higher salinity values in the underlying layer ( $S = 33.27$  psu) suggest the influence of saltier Pacific water. CTD1 cast, deployed in Paso Ancho Basin, shows lower salinity values with homogeneous vertical distribution, reflecting the strong vertical mixing in the inner basin water with fresh water from several *rios* flowing into the bay. CTD4 cast shows, as expected, a big discrepancy in the  $\theta$ -S properties. It was collected in the Pacific margin (see Fig. 1), spanning over a wide temperature range ( $\theta = 8.8^{\circ}\text{C}$  at surface and  $\theta = 2.4^{\circ}\text{C}$  at 1700 m depth) and with rather constant high salinity values.

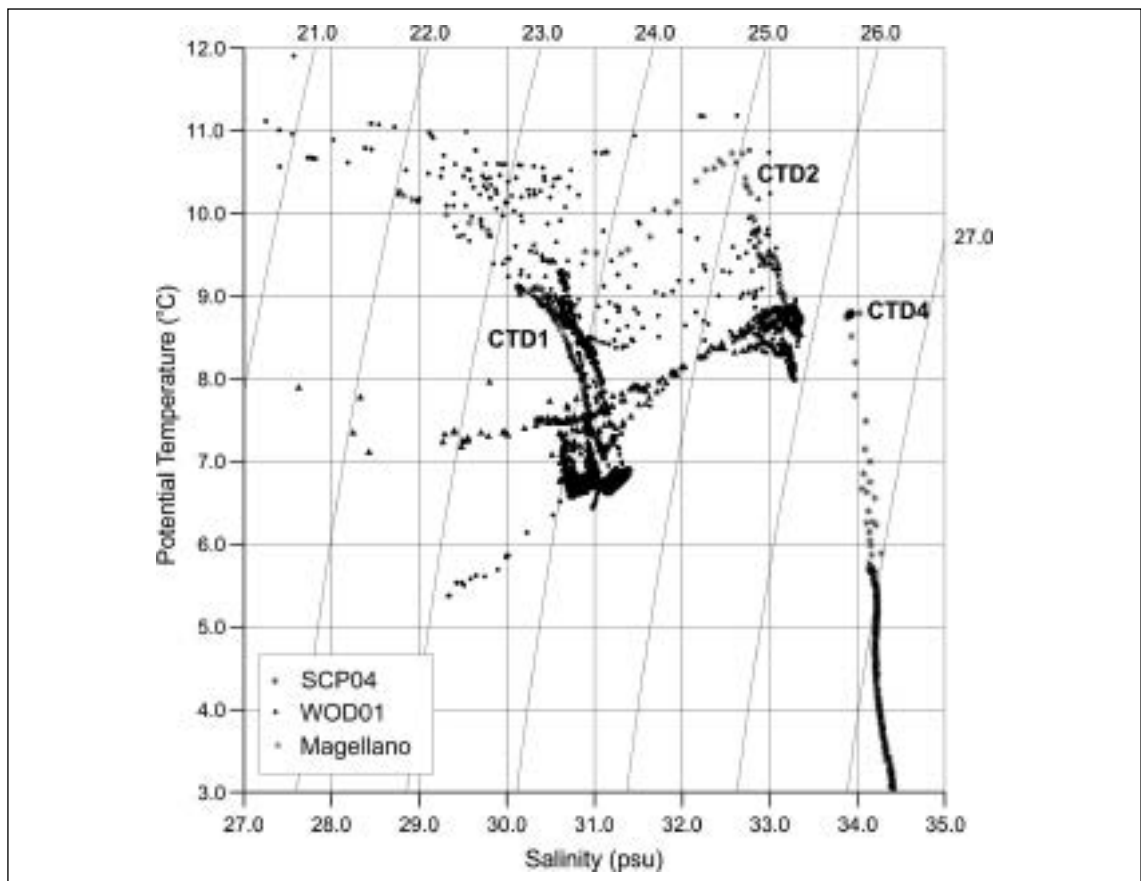


Fig. 2 - Potential temperature and salinity diagrams constructed with SCP04 data (stars) and WOD01 data (Conkright et al., 2002, full circles) and Magellano data (Brambati, 1991, full triangles) averaged over 5 dbar.

Potential temperature vertical profiles collected in Strait of Magellan and in the Pacific slope by means of XBT probes are shown in Fig. 3. The three profiles in the Strait of Magellan (dashed lines in Fig. 3) evidence a double stratification with thermal inversion in the surface layer (at 0-50 m and



50-100 m) and a thick nucleus of warmer (and saltier) water in the underlying layer down to 300 m. These variations in upper water column could reflect the advective processes of temperature changes, mainly dictated by water masses intrusions from the network inlets as well as the northward propagation of Pacific waters. Below the 300 m, the temperature profiles exhibit fairly constant distributions, with values of 8.7-8.8 °C, along the entire western passage. The profiles in the Pacific slope (full lines in Fig. 3), present a well defined thermocline, with higher surface temperature values in the in-shore stations. Similar temperature values were already recorded in the same area (Silva and Neshyba, 1977) and interpreted as representing to Sub-Antarctic water, carried towards the Chilean coast by the West Drift Current. Further analyses of this data set combined with continuous surface thermohaline measurements and currents can help to clarify ocean environmental variability in the Strait and in the surrounding Pacific area.

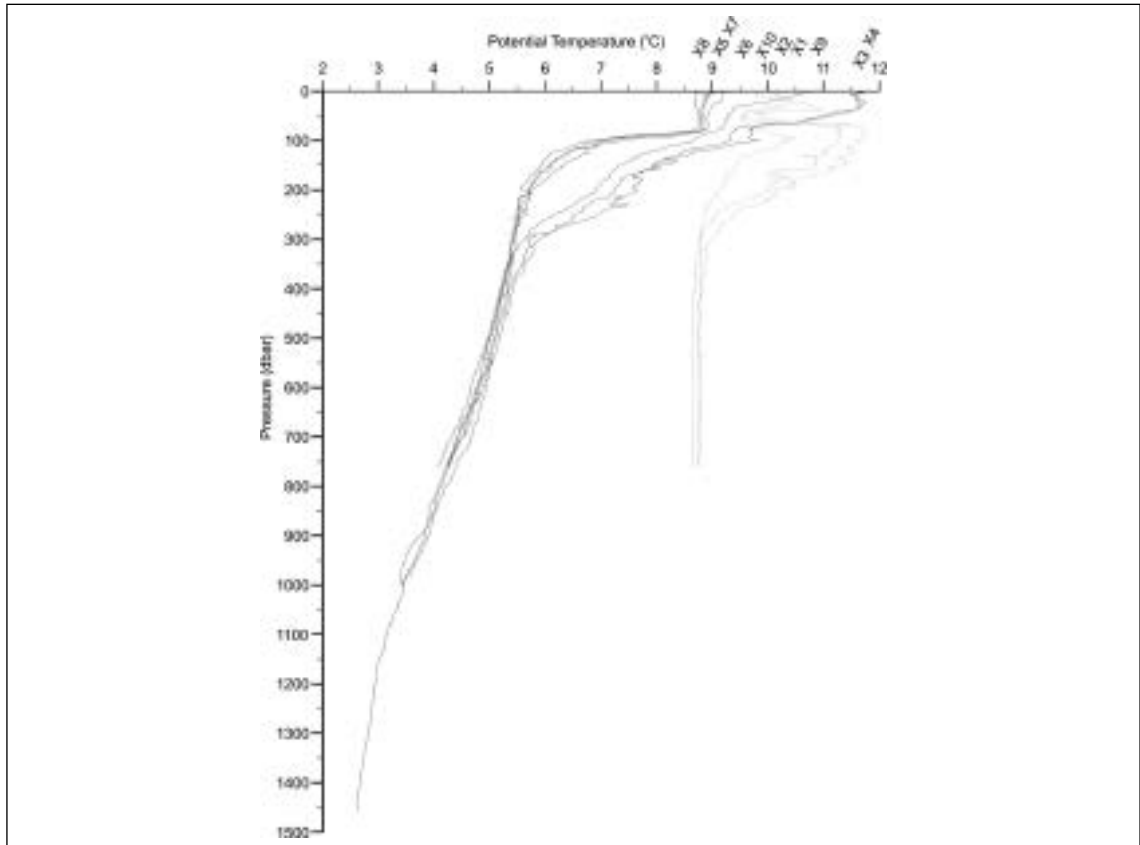


Fig. 3 - Potential temperature vertical profiles as obtained from ten XBT probes launched during SCP04 cruise in the Strait of Magellan (dashed lines, casts X10, X2 and X1 indicated on the top) and in the Pacific slope (full lines, casts X3-X9).

### Acknowledgements

This study take part of the Antarctic/Scotia Plate convergence off southern Chile Project, funded by the Programma Nazionale di Ricerche in Antartide (PNRA). Funding from the European Union (grant ENV1-CT-2001-20005) are also acknowledged. Bruno Della Vedova is acknowledged for providing the CTD equipment. We wish to thank the crew of R/V OGS-Explora for their assistance on board, Alina Polonia, Giovanni Bortoluzzi and his staff for providing information on the multidisciplinary research. Thanks also to Isabella Tomini and Franco Arena for their support and co-operation. Fabrizio Zgur, Dario Antonaz, Diego Cotterle, Andrea Cova, Carmine D'Amicantonio have contributed to the success of the oceanographic data acquisition with their constant support on board of R/V OGS-Explora.

## REFERENCES

- Brambati A., 1991. Introduction to the Magellan Project. *Boll. Ocean. Teor. Appl.*, 9, 83-92.
- Conkright M.E., Antonov J., Baranova O., Boyer T.B., Garcia H.E., Gelfed R., Johnson D., Locarnini R.A., Murphy P.P., O'Brien T.D., Smolyar I. and Stephens C., 2002. *World Ocean Database 2001, Vol. 1: Introduction*. S. Levitus (Ed.), NOAA Atlas NESDIS 42, U. S. Gov. Print. Off., Washington D.C., 167 pp.
- Marinoni L., Setti M. and Soggetti F., 1997. Mineralogy of sea-bottom sediments of the Strait of Magellan. *Boll. Ocean. Teor. Appl.*, 38 (3-4), 281-292.
- Medeiros C. and Kjerfve B., 1988. Tidal characteristics of the Strait of Magellan. *Cont. Shelf Res.*, 8, 947-960.
- Panella S., Michelato A., Perdicaro R., Magazzù G., Decembrini S. and Scarazzato P., 1991. A preliminary contribution to understanding the hydrological characteristics of the Strait of Magellan: Austral string 1989. *Boll. Ocean. Teor. Appl.*, 9, 107-126.
- Polonia A., Brancolini G., and Torelli L., 1999. Structural variability at the active continental margin off Southern Chile. *Journ. of Geodynamics*, 27, 289-307.
- Polonia A., Brancolini G., and Torelli L. Architecture of the oblique convergent margin off Southern Chile. In preparation for *Tectonophysics*.

## HYDRODYNAMICS OF LAGO FAGNANO, TIERRA DEL FUEGO

12-02

A. Richter<sup>1</sup>, R. Dietrich<sup>1</sup>, J.L. Hormaechea<sup>2</sup>, D. Del Cogliano<sup>3</sup>,  
R. Perdomo<sup>3</sup>, G. Liebsch<sup>11</sup>, M. Fritsche<sup>1</sup>

<sup>1</sup> Technische Universität Dresden, Institut für Planetare Geodäsie, Germany

<sup>11</sup> now: Bundesamt für Kartographie und Geodäsie, Außenstelle Leipzig, Germany

<sup>2</sup> Estacion Astronomica Rio Grande, Tierra del Fuego, Argentina

<sup>3</sup> Universidad Nacional de La Plata, Facultad de Astronomicas y Geofisicas, Argentina

contact: richter@ipg.geo.tu-dresden.de

Lake level observations with pressure gauges have been carried out in Lago Fagnano, Tierra del Fuego.

This narrow lake extends over 105 km in an East-West direction, and particular hydrodynamic conditions result from local meteorology characterized by predominant western winds. The measurements are performed at three locations spaced roughly along the lake's longitudinal axis in distances of 25 and 55 km apart. At these positions, Aanderaa WLR7 pressure tide gauges have been deployed. The operations were supported by the local Prefectura Naval Argentina.



Fig. 1 - Deployment of a pressure tide gauge in Lago Fagnano.

The instruments work continuously and autonomously on the lake bottom in depths of 4 to 7 metres. The measurements began in February 2003 and are still continuing. At present, about 15 days long time series of tide gauge data with sampling intervals of 2 and 5 minutes are available for the determination of water level heights and their variations. Another record covers an entire year with a sampling rate of one hour.

Based on the resulting time series of relative lake level heights, the variability of the lake's water level is analysed.

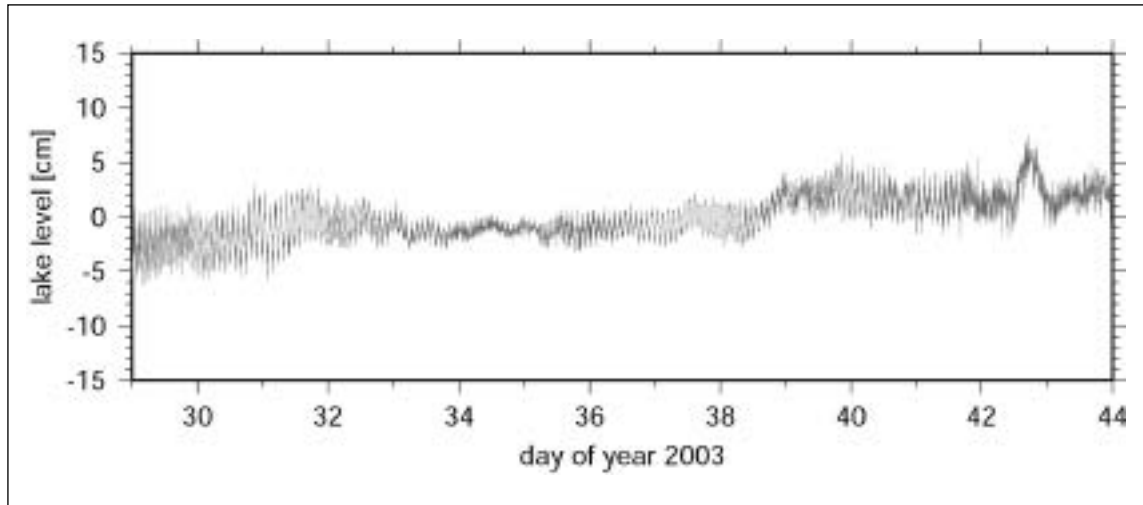


Fig. 2 - Example of a lake level record obtained from pressure tide gauge measurements in Lago Fagnano.

In the presentation, the observed variations are quantified and different dynamical forcings are studied. Special attention is paid to meteorologically forced changes, seiches and lake tides. Possible impacts and the significance of the identified lake-level changes for the determination of other local phenomena are investigated.

#### **HYDROLOGIC CHARACTERISTICS OF MELTING CREEKS IN POTTER COVE, (KING GEORGE ISLAND, ANTARCTICA) 12-03**

L. Varela (\*), E. Kruse(\*), M. Bonardi (\*\*), L. Tosi(\*\*), A. Mazzoldi(\*\*)

(\*) *Universidad Nacional de La Plata (UNLP), Paseo del Bosque, 1900 La Plata (Argentina)*

(\*\*) *Istituto di Scienze Marine (ISMAR) Consiglio Nazionale delle Ricerche (CNR), San Polo 1364, 30125 Venezia (Italy)*

#### **Summary**

This paper reports a preliminary study aiming to characterize the hydrological dynamics of the two main streams (Matias and Potter Creeks) that drain towards Potter Cove (King George Island, South Shetland Islands, Antarctica). It includes a description of the geologic characteristics of the study area with emphasis on the drainage network. The analysis of the variability of the two streamflows was based on data recorded in 1993-1994 and 1996-1997. This variability, which was identified by the distribution of the two discharges as a function of time, is the effect of temperature and precipitation changes. The data indicate that the values of the discharge amplitude and variability of Potter Creek are greater than those of Matias Creek. It is important to mention that the streamflow starts in December and ends in February and is controlled by snow melting. The hydrological behaviour of

these streams is important to the region because it controls the ecosystems' development in the Antarctic terrestrial environment.

### Abstract text

The streamflow of Antarctic streams is very variable on all time scales (Chinn, 1981). Discharges are directly related to climatic variations. Summer air temperatures fluctuate around 0°C with small changes in cloud coverage; this influences the radiation balance that can create significant changes in water discharge. Extreme cold and dryness characterize the Antarctic environment, deeply influencing the hydrological properties of rivers and streams along the South Polar Region. These bodies of water are distributed around the Antarctica margins in proximity to the sea and influence the ecosystems in this zone, which are important due to their high biologic productions (higher than those of oceanic environments).

Studies and specific informations regarding the hydrological characteristics of the Antarctic region are relatively few. Worth mentioning are the studies of Antiguëdad et al., 1991 and Inbar, 1992.

The main objective of this paper is to present a preliminary characterization of the hydrological dynamics of the two main streams (Matias and Potter creeks) draining towards Potter Cove (King George Island, South Shetland Islands, Antarctica) (Fig 1).

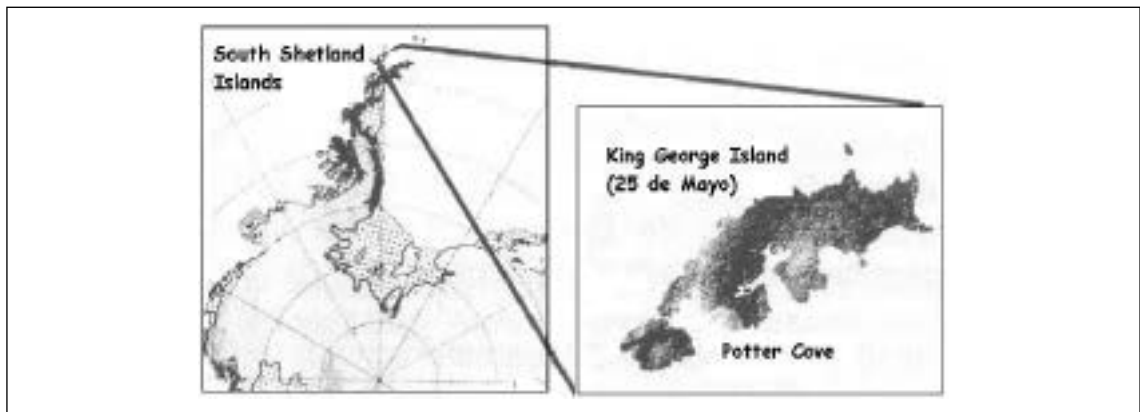


Fig 1 – King George Island location

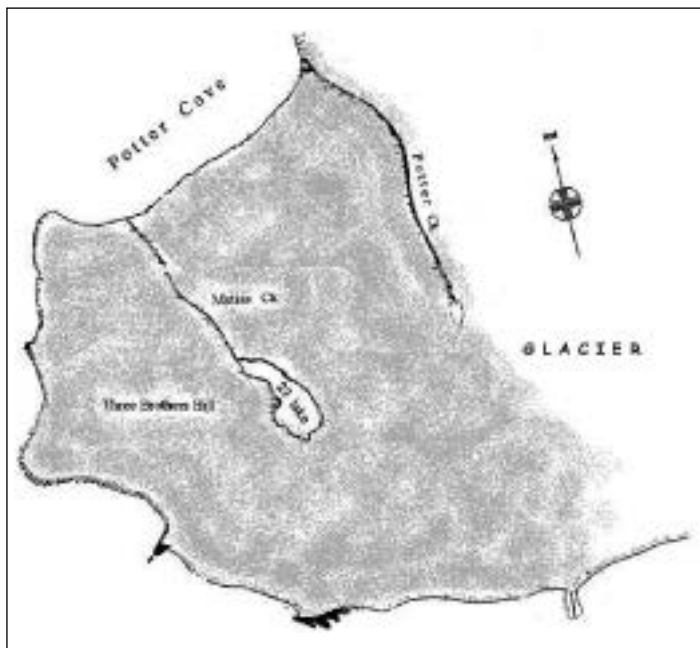


Fig 2 – Study area location (Matias and Potter Creeks)

It is important to mention that most of the studies performed in Antarctica have taken place in the Dry Valleys south of Tierra Victoria (Green et al., 1988; Vincent, 1987), which are polar deserts without ice different from the coastal maritime environment characterizing Potter Cove.

The study area includes the drainage basins of Matías and Potter creeks (Fig 2). They both discharge directly into the south coast of the cove. The geological composition (Fourcade, 1960) is characterized by isolated outcrops of volcanic rocks (andesites, basalts), sedimentary rocks (conglomerates, tuffs, clays), debris slope material and glacial sediments. The last group is made up of cryoclastic volcanic rocks and tilly deposits and forms moraines that cover most of the internal zones. The shallow zone is covered mainly by sediments of volcanic origin. Their particle sizes are sandy - psephitic, except in the outlet stream zones, which are characterized by pelitic sediments.

The maritime climate experiences strong winds from the east and west sectors and wind gusts of more than 100 km/h. Either snow or rain falls in the summer season and evaporation is very limited. Relative humidity is comparatively high (90% in summer) and summer temperatures vary between -4°C and 10°C.

Many lakes, different in size and shape, spread out on beach sectors as well as on the moraines. The most remarkable one is the 23 Lake that constitutes the largest water body and forms the Matías Creek headwaters.

In springtime, streams start flowing through incipient streambeds within small valleys dissecting the area. Matías Creek has its source in the 23 Lake. Its main trunk runs from SSE to NNW through a glen of about 1 km long. It has a single channel drainage pattern and only one tributary channel adjacent to the outlet. Its upper area has a slope of approximately 8%. In this area, Matías Creek runs through a narrow channel. Creep from the Three Brothers hillside forms the creek's left bank. The lower area (approximate slope 5%) has a concrete man-made dam 80 m from the outlet and drains into the cove through a small streambed. At the beginning of the runoff period, the water flow originates from melting snow accumulated during winter and from water of the 23 Lake. When the snow disappears, water flow is maintained by the lake and groundwater seepage.

Potter Creek also has a pattern of single drainage. Along its right bank there is a glacier tongue. Its upper streambed has gorges larger than 2 m, which become smaller downstream. The lower streambed is defined by a slope change ranging from 20% at the headwater to 3% in the lower zone. The latter develops a deltaic drainage pattern. This is due to a minor transport capacity of the water and/or to an excessive increase of sedimentary load. The water flow is fed from the melting of the glacier and the snow accumulated during winter and also from groundwater seepage, which flows through morainic sediments.

Streamflows of these creeks were analyzed, based on data obtained from measurement stations located on both streams and according to observations performed during 1993-94 and 1996-97 summer samplings (December-February). At these stations, flow characteristics such as depth and width, current velocity, current meter, temperature and water conductivity were measured. Measurements were made manually every day and always at the same time. Proper discharge and sediment transport estimations were also performed.

Daily discharge for the 1993-94 period, from Matías Creek fluctuated between 0.03 and 0.11 m<sup>3</sup>/sec, with water velocity oscillating between 0.31 and 0.76 m/sec. Conductivity values varied between 75 and 110 microS/cm, showing a tendency to increase towards the end of the period (Varela, 1994).

For the 1993-94 period, the Potter streamflow was higher than the Matías streamflow since it oscillated between 0.04 m<sup>3</sup>/s and 1.86 m<sup>3</sup>/s. Distribution of streamflow as a function of time allowed the identification of variations related to the effect of temperatures and precipitations.

Average streamflow for Potter Creek (1996-97) at the outlet was 1.1 m<sup>3</sup>/sec, while the discharge volume during the recording period (60 days) was of 5.7 hm<sup>3</sup>. The lowest and highest values registered were 0.08 m<sup>3</sup>/sec and 3.8 m<sup>3</sup>/sec, respectively (Varela, 1997).

Water samplings were also taken in order to evaluate the discharge and concentration of the suspended material in Potter Creek (1996-97). Regarding the concentration, values between 0.04 and 15 g/l were registered, with an average value of 0.14 g/l. Suspended material discharges showed values between 5 g/sec and 60,000 g/sec; the most frequent values were lower than 5000 g/sec.

The results indicate that the temporal distribution of suspended material in Potter Creek coincides with discharges, being more evident when these are above the average values.

Recorded streamflow data have indicated that Potter Creek shows a greater amplitude and variability of its discharge values than Matías Creek.

According to acquired data, the melting of snow banks and ice fields controls the streamflow. This continues for only few months every year before re-freezing, starting generally in December and ending in February.

Since the waters of these streams provide the greatest biologic activity concentration in the Antarctic terrestrial environment, it is highly recommended that the record of hydrological data can be continued and applied to the interpretation of processes developed by the biological communities in these ecosystems that are widely distributed all over on Antarctica.

## REFERENCES

- Antigüedad, I., Eraso, A., Mangin A., Fernandez Rubio, R., 1991. Características del hidrograma en función de los datos meteorológicos y elaboración de la curva de gastos del río de la base antártica española (Isla Livingstone, Shetland del Sur). Tercer Simposio Español de Estudios Antárticos: 327-322. Madrid.
- Chinn, T., 1981. Hydrology and climate in the Ross Sea area. *Journal of the Royal Society of New Zealand*. 11:373-386.
- Fourcade, N., 1960. Estudio geológico-petrográfico de caleta Potter, Isla 25 de Mayo. Islas Shetland del Sur. Instituto Antártico Argentino. Publicación N° 8: 17-119. Buenos Aires.
- Green, W., Angle, M. and Chave, K., 1988. The geochemistry of Antarctic streams and their role in the evolution of four lakes of the McMurdo Dry Valleys. *Geochimica et Cosmochimica, Acta* 52:1265-1274.
- Inbar, M., 1992. Hidrología y geometría hidráulica en litología volcánica y clima antártico, estudio cuantitativo morfológico en la isla Decepción, Islas Shetland del Sur. En: JL López Martínez (ed) III Congreso Geológico de España y VIII Congreso Latinoamericano de Geología de Salamanca, Geología de la Antártida occidental.) Simposios Tomo 3:337-346. España.
- Varela, L., 1994. Régimen fluvial en el arroyo Matías (península Potter, Isla 25 de Mayo). 3ª Reunión de Comunicaciones Científicas sobre Investigaciones Antárticas: 439-442. Buenos Aires
- Varela, L., 1997. Estimación del caudal sólido en el Arroyo Potter. Caleta Potter. Isla 25 de Mayo, Shetland del Sur. IV Jornadas sobre Investigaciones Antárticas. Buenos Aires
- Vincent, W.F., 1987. Antarctic Limnology. Inland waters of New Zealand. (Ed.) A. Viner. DSIR Bulletin 241: 379-412.

---

## AUTHOR INDEX

---

*The code after the name indicates the session and the place in the book.*

Accaino F.	6-08	Celeda A.	4-11
Acevedo R.D.	4-01, 4-02, 4-11	Cenni M.	1-09
Agarwal S.	9-01	Chapron E.	7-02, 10-03
Amore F.O.	7-03	Charlet F.	7-02, 10-03
Arnaud F.	10-03	Chávez R.E.	9-03
Aronson R.B.	10-04, 11-04	Choe M.Y.	4-07, 7-06
Arriagada C.	4-04	Colautti W.	6-02
Backman E.	6-03	Colizza E.	6-02, 7-03
Barbero L.	3-01	Comínguez A.H.	1-03, 9-04
Barriga R.	5-05	Concheyro A.	11-01
Bartole R.	6-01, 6-02, 7-03	Connon G.	3-01
Bataille K.	9-05	Cordani U.	10-05
Ben-Avraham Z.	2-01	Coronato A.	8-04, 10-02
Bengoa C.	4-03	Creixell C.	4-04
Bertrand S.	7-02, 10-03	Cuppari A.	6-01
Bevis M.G.	5-05	Dalziel I.W.D.	1-04, 5-05
Blake D.B.	10-04, 11-04	De Batist M.	7-02, 10-03
Boes X.	10-03	De Donatis M.	6-07
Bohaty S.M.	11-03	Dean A.	1-05
Bonardi M.	12-03	Del Cogliano D.	5-01, 5-02, 12-02
Botelho M.A.B.	9-02	Del Negro E.	9-06
Brambati A.	10-01	Della Vedova B.	6-08
Bratus A.	9-06	DeMuro S.	10-01
Bujalesky G.G.	8-04, 10-02	Dietrich R.	2-02, 5-01, 5-02, 12-02
Bukchin B.G.	3-03	Domack E.W.	6-03
Calderón M.	1-01, 4-05, 4-09, 4-10, 10-05	Eagles G.	2-07
Camacho H.H.	1-02	Fagel N.	10-03
Canals M.	8-01	Fanning C.M.	1-01, 4-06
Carcione J.M.	9-02	Fazio A.M.	7-01
Carrera Gómez P.	8-04	Ferraccioli F.	1-05
Casassa G.	5-05	Ferrer C.	3-01
Caselli A.T.	4-03	Flores-Márquez E.L.	6-06, 9-03
Castro L.N.	7-01	Florindo F.	11-03
		Flüh E.	9-05

Franzese J.R.	1-03	Kruse E.	12-03
Fritsche M.	5-01, 5-02, 12-02	Larter R.D.	2-05, 7-04
Fuentealba J.	7-05	Laterza R.	12-01
Gahagan L.M.	2-03, 2-06	Lauría E.	5-05
Galindo-Zaldivar J.	6-06, 9-03	Lawver L.A.	2-03, 2-06
Gallegos E.	4-08	le Broq A.	8-02
Gattini D.	1-09	Leat P.T.	1-05
Gaudio A.	1-09	Lee J.I.	4-07, 7-06
Gazdzicki A.	11-02	Lenzano L.E.	5-03
Gei D.	9-02	Liebsch G.	5-01, 5-02, 12-02
Geletti R.	6-08, 9-06	Lippai H.	5-04
Ghidella M.E.	2-03	Livermore R.	2-07
Ghiglione M.C.	2-04	Lodolo E.	1-11, 2-01, 2-08, 5-04, 6-05, 9-04
Giorgetti A.	12-01	Lohmann K.C.	10-04
Giunta G.	1-06	Loreto M.-F.	2-10
Godoy E.	4-06, 7-05	Lüth S.	9-05
Gonzalez O.	1-07	Mackern M.V.	5-03
Guidarelli M.	1-07, 3-02, 3-03, 3-04	Magand O.	10-03
Helm V.	6-04	Maldonado A.	6-06, 7-04, 9-03
Hernández-Molina F.J.	7-04	Marchand C.	7-02
Hervé F.	1-01, 4-05, 4-06, 4-09, 4-10, 7-05, 10-05	Marensi S.A.	1-08
Hormaechea J.L.	3-01, 5-01, 5-02, 5-04, 12-02	Marsella E.	8-03
Hubbard A.	8-02	Martínez Dopico C.I.	4-08
Hur S.D.	4-07, 7-06	Massonne H.-J.	4-05, 4-09
Introcaso A.	5-03	Mattioli M.	1-09
Iorio M.	8-03	Mazzoldi A.	12-03
Ivany L.C.	10-04	Mechie J.	9-05
Jin Y.K.	7-06	Mélières M.A.	10-03
Jo H.R.	7-06	Menichetti M.	1-09, 1-11, 2-09, 5-04
Jokat W.	6-04	Morabito S.	7-03
Jones P.	1-05	Morata D.	4-04
Kendrick E.	5-05	Morelli D.	6-01
Kim S.B.	4-07	Morris P.	2-07
Kim Y.	7-06	Mpodozis C.	4-06
Krawczyk C.	9-05	Müller J.	10-06
Krocker R.	6-04	Nankivell A.	2-07



Nardi G.	8-03	Smalley Jr. R.	5-05
Nieto Yabar D.	9-06	Sohn Y.K.	4-07, 7-06
Olivero E.B.	2-04, 5-05	Solari M.	7-05
Panza G.F.	1-07, 3-02, 3-03	Somoza R.	2-11, 2-12
Parada M.A.	4-04	SPOC Research Group	9-05
Perdomo R.	5-01, 5-02, 12-02	Stiller M.	9-05
Pérez Alberti A.	8-04	Sturm M.	10-06
Persico D.	11-03	Suriñach E.	6-06, 9-03
Petruccione E.	8-03	Susini S.	6-07
Piana E.	5-05	Tassone A.	1-11, 5-04, 6-05, 9-04
Pinat T.	1-07	Taylor F.	5-05
Pincioli R.	3-01	Taylor G.	2-12
Pino M.	7-02, 10-03, 10-06	TESAC Party	5-04
Plasencia Linares M.P.	3-01, 3-02, 3-03, 3-04	Theye T.	4-05
Poletto F.	9-02	Tinivella U.	6-08
Polonia A.	2-10, 6-05	Tiwari S.	9-01
Rabassa J.	8-04, 10-02	Torelli L.	2-10
Ramos V.A.	1-10, 2-04	Tosi L.	12-03
Rapalini A.E.	4-10, 10-05	Tosoratti F.	6-02
Rastelli C.	3-01	Tourn S.M.	4-03
Raykova R.	1-07	Urrutia R.	7-02, 10-03
Redondo Vega J.M.	8-04	Valcárcel Díaz M.	8-04
Reichert C.	9-05	Valín-Alberdi M.L.	4-02
Richter A.	5-01, 5-02, 12-02	Varela L.	12-03
Robin A.M.	5-03	Vattuone M.E.	4-08
Rodríguez-Fernández J.	9-03	Vaughan A.P.M.	1-05
Roig C.	4-02, 10-02	Vera E.	2-10
Romano A.	4-11	Vilas J.F.	1-11, 5-04
Roperch P.	4-04	Villa G.	11-03
Rülke A.	2-02	Villar L.	4-11
Russi M.	3-02, 3-03, 3-04	Vizán H.	2-12
Sabbione N.	3-01	Volland S.	10-06
Salvi C.	6-02, 7-03	Wardell N.	6-05
Sánchez A.	7-05	Werner J.E.	11-04
Sauli C.	6-05	Wigger P.	9-05
Schreider A.A.	2-08	Yagupsky D.	1-11
Segal S.	4-11	Zakrajsek A.	5-05
Singer S.	4-10, 10-05	Zappettini E.	4-11
		Zitellini N.	6-07





